

Autogenic and climate-driven shifts in mid- to high-latitude peatlands

Thomas George Sim

**Submitted in accordance with the requirements for
the degree of Doctor of Philosophy**

School of Geography

University of Leeds

June 2022

Intellectual Property and Publication Statements

Declaration

The candidate confirms that the work submitted is his/her/their own, except where work which has formed part of jointly authored publications has been included. The contribution of the candidate and the other authors to this work has been explicitly indicated below. The candidate confirms that appropriate credit has been given within the thesis where reference has been made to the work of others.

Attribution of work to others

Work creditable to others is included in the following Chapters:

Chapter 2: Ecology of peatland testate amoebae in Svalbard and the development of transfer functions for reconstructing past water-table depth and pH

Based on the published paper:

Sim, T.G., Swindles, G.T., Morris, P.J., Baird, A.J., Charman, D.J., Amesbury, M.J., Beilman, D., Channon, A., Gallego-Sala, A.V., 2021. Ecology of peatland testate amoebae in Svalbard and the development of transfer functions for reconstructing past water-table depth and pH. *Ecol. Indic.* 131, 108122. <https://doi.org/10.1016/j.ecolind.2021.108122>

Work attribution:

Graeme Swindles, Dan Charman, Matt Amesbury, Dave Beilman, Angela Gallego-Sala and I undertook fieldwork and sampling in 2019. I performed data analysis in discussion with Graeme Swindles and Matt Amesbury. I wrote the manuscript with supervision from Graeme Swindles, Paul Morris and Andy Baird. Alex Channon performed peat bulk density and C/N analysis and all authors provided manuscript feedback.

Chapter 3: Divergent responses of permafrost peatlands to recent climate change

Based on the published paper:

Sim, T.G., Swindles, G.T., Morris, P.J., Baird, A.J., Cooper, C.L., Gallego-Sala, A.V., Charman, D.J., Roland, T.P., Borke, W., Mullan, D.J., Aquino-López, M.A., Gałka, M., 2021. Divergent responses of permafrost peatlands to recent climate change. *Environ. Res. Lett.* 16, 034001. <https://doi.org/10.1088/1748-9326/abe00b>

Work attribution:

Fieldwork was carried out by Graeme Swindles in 2012 to sample peat profiles in northern Sweden. I undertook testate amoebae analysis, Mariusz Gałka conducted plant macrofossil

analysis and Claire Cooper performed tephra analysis. Angela Gallego-Sala and I carried out bulk density determinations. Angela Gallego-Sala analysed C and N content of peat samples and Dan Charman and Tom Roland carried out ^{210}Pb dating, while Werner Borken dated a number of ^{14}C samples. I analysed the climatic data with supervision from Paul Morris and in discussion with Donal Mullan. I wrote the manuscript with supervision from Graeme Swindles, Paul Morris and Andy Baird. Marco Aquino-López processed age-depth modelling of the peat profiles and all authors provided manuscript feedback.

Chapter 4: Regional variability in peatland burning at mid- to high-latitudes during the Holocene

Based on the submitted paper:

Sim, T.G., Swindles, G.T., Morris, P.J., Baird, A.J., Gallego-Sala, A.V., Wang, Y., Blaauw, M., Camill, P., Garneau, M., Hardiman, M., Loisel, J., Väliranta, M., Anderson, L., Apolinarska, K., Augustijns, F., Aunina, L., Beaulne, J., Bobek, P., Borken, W., Broothaerts, N., Cui, Q.Y., Davies, M. A., Ejarque, A., Farrell, M., Feeser, I., Feurdean, A., Fewster, R., Finkelstein, S.A., Gaillard, M.J., Gałka, M., Heffernan, L., Hoovers, R., Jones, M., Juselius, T., Karofeld, E., Knorr, K.H., Korhola, A., Kupriyanov, D., Kylander, M.E., Lacourse, T., Lamentowicz, M., Lavoie, M., Lemdahl, G., Łuców, D., Magnan, G., Maksims, A., Mansilla, C.A., Marcisz, K., Marinova, E., Mathijssen, P.J.H., Mauquoy, D., Mazei, Y., Mazei, N., McCarroll, J., McCulloch, R., Milner, A., Miras, Y., Mitchell, F.J.G., Novenko, E., Pelletier, N., Peros, M., Piilo, S.R., Pilote, L.M., Primeau, G., Rius, D., Robin, V., Robitaille, M., Roland, T.P., Ryberg, E., Sannel, A.B.K., Schitteck, K., Servera-Vives, G., Shotyk, W., Słowiński, M., Stivrins, N., Swinnen, W., Thompson, G., Tiunov, A., Tsyganov, A.N., Tuittila, E.S., Verstraeten, G., Wallenius, T., Webb, J., Willard, D., Yu, Z., Zaccone, C., Zhang, H. In review. Regional variability in peatland burning at mid- to high-latitudes during the Holocene. *Global Change Biology*.

Work attribution:

I, Graeme Swindles, Paul Morris and Andy Baird designed the study. I conducted the compilation, standardisation and analysis of charcoal records. I wrote the manuscript, under supervision of Graeme Swindles, Paul Morris and Andy Baird. All other authors contributed data to the analyses and/or provided input to the manuscript.

Rationale for submission using alterative thesis style

From the outset of my PhD I have sought to report my research in the form of journal articles and at the time of submission have two manuscripts accepted and published, with a third drafted for submission. My thesis has been completed in three clear stages that have built on the findings of each previous stage, while expanding in temporal and spatial scale. The introduction/background section for each publication contains some overlap due to the similar themes throughout the project, which is required to provide proper context to the reader.

This thesis has the following structure: an introduction chapter providing a background/rationale for the overall research aim and objectives; three results chapters as outlined above; and finally a chapter synthesising the findings of the three results chapters and their implications, followed by overall conclusions.

Copyright statement

This copy has been supplied on the understanding that it is copyright material and that no quotation from the thesis may be published without proper acknowledgement

Assertion of moral rights

The right of Thomas G. Sim to be identified as Author of this work has been asserted by Thomas G. Sim in accordance with the Copyright, Designs and Patents Act 1988.

© 2022 The University of Leeds and Thomas G. Sim

Acknowledgements

The journey to finishing this thesis has been far from straightforward, but it has also been greatly enjoyable, greatly challenging and greatly rewarding. It would not have been possible without the support of my supervisors. I would like to thank Graeme for his constant enthusiasm and valuable advice, I would like to thank Paul for his support, feedback and encouragement, and I would like to thank Andy for his guidance, attention to detail and assurance. The time you all invested in discussing ideas, trouble shooting and providing feedback on my work has been invaluable – your optimism and humour kept me going throughout the process.

I am grateful to Angela Gallego-Sala, Dan Charman, Matt Amesbury, Dave Beilman and Xavier Comas for their support during my fieldwork in Svalbard back in August 2019. Additionally, thank you to Yuwan Wang and Angela – both from the University of Exeter – for discussing ideas about past peatland fire. I would like to thank Mariusz Gałka for completing the plant macrofossil analysis for the northern Swedish records and for the collaborative opportunities that he has afforded me alongside my thesis. At Leeds, thanks to: Richard Fewster for talking all things peat over a beer, Michael Grimes for the many runs and rides, and Josh Chambers for his terrible jokes and wisdom. I am grateful to Mark Smith, Jonathan Carrivick and Megan Klaar who always had time to offer advice and encouragement, and I appreciate the support, advice and friendship I received from many others in the department.

I am incredibly grateful to my wife Kristen for her constant support, for being there through the ups and downs and for helping me have fun throughout the PhD process. I would also like to thank those at Leodiensian RUFC and my tag rugby team for offering an outlet during times of stress. Finally, I would like to thank my Mum, Dad, Jonny and Ed for taking an interest (or at least trying to) in my research, for their support and for their continual encouragement.

Abstract

Peatlands are a globally-important terrestrial carbon store, provide a range of ecosystem services and are valuable archives of information regarding past environmental change. Reconstructions of past ecohydrological dynamics in peatlands can help improve understanding about the response and vulnerability of these carbon-rich ecosystems to ongoing and future climate change. In this thesis, I use palaeoenvironmental techniques to investigate trends in ecohydrology and fire regime in mid- to high-latitude peatlands during the Holocene. My findings highlight the importance of not only climate but also autogenic mechanisms in driving change in peatland ecosystems. I show that water-table depth and pH exhibit a strong control over modern distributions of peatland testate amoeba communities in Svalbard, and that statistical transfer functions can be successfully used to quantitatively reconstruct past hydrological and hydrochemical conditions from downcore assemblages. From a multiproxy palaeoecological investigation of 10 permafrost peatland records in northern Sweden, I found a divergent ecohydrological response to recent warming. Whether a peatland became wetter or drier was due to autogenic and local factors relating to permafrost thaw, vegetation dynamics, decomposition and productivity. Composite analysis of 221 macrocharcoal records from across North America, Europe and Patagonia highlights regional variability in peatland burning trends during the Holocene. Climate was the main driver of peatland fire, yet human activities appear to become more important in the late Holocene – predominantly in Europe. Peatlands show lower susceptibility to burning than the wider landscape, likely in relation to autogenic processes helping to maintain high moisture levels. Overall, this thesis shows that alongside the overarching influence of climate, autogenic processes play an important role in controlling ecohydrological and fire dynamics in peatlands. Under future climate change, autogenic feedbacks may help some peatlands – particularly those less modified – maintain sufficient moisture, but overall the stability of the peatland carbon store will likely reduce.

Table of contents

Chapter 1 – Introduction	1
1.1. Background and rationale.....	2
1.1.1. Peatlands as palaeoenvironmental archives	7
1.1.2. Testate amoebae	8
1.1.3. Plant macrofossils	9
1.1.4. Charcoal	10
1.2. Research aim and objectives.....	11
1.3. Thesis structure.....	11
References	13
Chapter 2 – Ecology of peatland testate amoebae in Svalbard and the development of transfer functions for reconstructing past water-table depth and pH.....	24
Abstract.....	26
2.1. Introduction	27
2.2. Study region	28
2.3. Method	30
2.3.1. Sampling.....	30
2.3.2. Surface vegetation and peat properties	31
2.3.3. Age-depth modelling.....	32
2.3.4. Testate amoebae	32
2.3.5. Statistical analyses	33
2.4. Results.....	34
2.4.1. Relationship between species distribution and environmental variables.....	34
2.4.2. Transfer function development	40
2.4.3. Transfer function application.....	48
2.5. Discussion.....	50
2.5.1. Testate amoebae and water-table depth	51
2.5.2. Testate amoebae and trophic status (pH)	51
2.5.3. Application of transfer functions	52
2.5.4. Future research	54
2.6. Conclusions	55
References	56
Chapter 3 – Divergent responses of permafrost peatlands to recent climate change	64
Abstract.....	66
3.1. Introduction	67
3.2. Methods.....	68

3.2.1. Study region and sampling	68
3.2.2. Age modelling.....	69
3.2.3. Peat properties	70
3.2.4. Carbon accumulation	70
3.2.5. Water-table reconstructions	70
3.2.6. Plant macrofossils.....	71
3.2.7. Climatic data	71
3.2.8. Theil-sen regression.....	72
3.3. Results and discussion.....	72
3.3.1. Response of permafrost peatlands to recent warming.....	72
3.3.2. Climatic and autogenic drivers of ecosystem change	78
3.3.3. Implications for ecohydrological and carbon dynamics in global permafrost peatlands	82
3.4. Conclusions.....	83
References.....	85
Chapter 4 – Regional variability in peatland burning at mid- to high-latitudes during the Holocene	94
Abstract	99
4.1. Introduction.....	100
4.2. Materials and methods	100
4.2.1. Study region.....	101
4.2.2. Charcoal data.....	103
4.2.3. Age-depth modelling	103
4.2.4. Resampling and transformation	104
4.2.4.1. Proportional relative scaling and presence/absence	104
4.2.4.2. Comparison of local peatland and regional biomass burning.....	105
4.3. Result and discussion	105
4.3.1. North America	107
4.3.2. Europe	110
4.3.3. Patagonia.....	114
4.3.4. Peatland burning and bioclimatic space.....	117
4.3.5. Controls on peatland burning and wider implications.....	119
4.4. Conclusions.....	119
References.....	122
Chapter 5 – Discussion and conclusions.....	134
5. Discussion and conclusions	135

5.1. Research synthesis	136
5.2. Implications and future work.....	140
5.3. Conclusions	141
References	143
Appendices.....	147
Appendix A. Supporting information for Chapter 2: Ecology of peatland testate amoebae in Svalbard and the development of transfer functions for reconstructing past water-table depth and pH.....	148
Appendix B. Supporting information for Chapter 3: Divergent responses of permafrost peatlands to recent climate change	157
Appendix C. Supporting information for Chapter 4: Regional variability in peatland burning at mid- to high-latitudes during the Holocene.....	189

List of figures

Figure 1.1. Distribution of northern peatlands and extent of ice, glaciers and permafrost... 3	3
Figure 1.2. Simplified conceptual model of processes affecting the peatland carbon balance	5
Figure 1.3. Examples of peatland testate amoebae photographed at 200-400 times magnification.	9
Figure 2.1. Site map showing locations for surface sampling and the coring site, alongside glacier coverage.	31
Figure 2.2. CCA of species, samples and environmental variables for a) all taxa and b) with WISTs removed.	37
Figure 2.3. NMDS of species, samples and environmental variables for a) all taxa and b) with WISTs removed.	38
Figure 2.4. Abundance of selected testate amoeba taxa (at least 10 occurrences) ranked by observed water-table depth (WTD) indicating a range of WTD conditions.....	43
Figure 2.5. Abundance of selected testate amoeba taxa (at least 10 occurrences) ranked by observed pH indicating a range of pH conditions.	44
Figure 2.6. Transfer function performance.	45
Figure 2.7. Water-table depth (WTD) optima and tolerance calculated through weighted averaging for taxa at least five occurrences.	46
Figure 2.8. pH optima and tolerance calculated through weighted averaging for taxa at least five occurrences.	47
Figure 2.9. Stratigraphic diagram of testate amoeba abundance in the Colesdalen core and best reconstructions for WTD and pH.....	49
Figure 2.10. Comparison of WTD reconstructions for the Colesdalen core from different regional transfer functions.	50
Figure 3.1. Location map of study sites, weather stations and regional climatic data.....	69
Figure 3.2. Palaeoecological summary diagrams from all ten peat profiles, across eight sites..	74
Figure 3.3. Water-table depth (WTD) data from all peat profiles since 1500 CE..	76
Figure 3.4. Relationship between climatic variables and water-table depth (WTD) across all sites	80
Figure 4.1. Site map of peatland record locations and their sub-region	102
Figure 4.2. Peatland and wider landscape burning trends by region	107
Figure 4.3. Peatland and wider landscape burning trends by North American sub-region..	109
Figure 4.4. Peatland and wider landscape burning trends by European sub-region.....	113
Figure 4.5. Peatland burning trends in Patagonia.....	116
Figure 4.6. Distribution of proportional relatively scaled (PRS) charcoal values (cubic root transformed) for 2000 cal. BP to present by region and sub-region	118
Figure 4.7. Bioclimatic space by sub-region and charcoal values.	118

List of tables

Table 2.1. Site overview and environmental conditions.	31
Table 2.2. Overview of 60 testate amoebae taxa identified	35
Table 2.3. Ordination statistics of environmental variables, both including and excluding taxa with weak idiosomic siliceous tests (WISTs)	39
Table 2.4. Transfer function performance metrics for pruned WTD and pH models with WIST taxa removed.....	42

Abbreviations

ACAR – Apparent carbon accumulation rate

AICc – Corrected Akaike information criterion

AMS – Accelerator mass spectrometer

BD – Bulk density

C – Carbon

CCA – Canonical correspondence analysis

CH₄ – Methane

CO₂ – Carbon dioxide

CRS – Constant rate of supply

DCA – Detrended correspondence analysis

DIC – Dissolved inorganic carbon

DOC – Dissolved organic carbon

EC – Electrical conductivity

ET – Evapotranspiration

GCD – Global charcoal database

GDD₀ – Growing degree days above 0°C

GHG – Greenhouse gas

HTM – Holocene thermal maximum

LIA – Little Ice Age

LOESS – Locally estimated scatterplot smoothing

LOI – Loss-on-ignition

LOO – Leave-one-out

LOSO – Leave-one-site-out

MC – Moisture content

MCA – Medieval Climate Anomaly

MCMC – Markov Chain Monte Carlo

ML – Maximum likelihood

N – Nitrogen

NMDS – Non-metric multidimensional scaling

Abbreviations (continued)

P – Phosphorus

PAR – Photosynthetically active radiation

P-E – Precipitation minus evaporation

POC – Particulate organic carbon

PRS – Proportional relative scaling

RMSEP – Root mean squared error of prediction

SCPs – Spheroidal carbonaceous particles

SW – Segment-wise

SWWs – South westerly winds

TA – Testate amoeba

UOM – Unidentified organic matter

WA.tol – Weighted averaging tolerance downweighting

WA.tol.cla – Weighted averaging tolerance downweighting with classical deshrinking

WA.tol.inv – Weighted averaging tolerance downweighting with inverse deshrinking

WAPLS – Weighted averaging partial least squares

WIST – Weak idiosomic siliceous test

WTD – Water-table depth

Chapter 1 – Introduction

1.1. Background and rationale

Peatlands cover ~3% of global land area (>4 million km²), they are distributed in both northern and southern hemispheres across tropical, temperate, boreal and arctic regions, but the majority are located at mid- to high-latitudes (Xu et al., 2018a). Despite this limited geographic extent, they store an estimated 600 Gt C accounting for ~25% of global soil carbon storage (Yu et al., 2010). The peatland carbon store is equivalent to over half the carbon in the atmosphere (Houghton, 2007) and over twice that stored in global forests (Pan et al., 2011). It is therefore important to understand the vulnerability of the peatland carbon store in the face of climate change and intensifying human modification of these ecosystems. Peat consists of partially decomposed plant material. To classify as peat the material has to contain at least 30% (Joosten and Clarke, 2002) or 50% (Burton and Hodgson, 1987) organic matter at dry mass. In many classifications a minimum peat depth has to be attained before an ecosystem can be defined as a peatland; there is general agreement that a depth of 30-45 cm is sufficient (Hammond, 1981; Hånell, 1991; Zoltai and Pollett, 1983).

The accumulation of peat occurs when the formation of plant litter outweighs losses to decomposition, combustion or erosion over timescales of centuries to millennia. Net gains usually require waterlogged, anoxic conditions which greatly slow decomposition (Charman et al., 2013; Gorham, 1991). A large proportion of peatland extent is coincident with permafrost areas (Figure 1.1), where the cold conditions further limit decomposition losses – with an estimated 277 Gt C stored in permafrost regions (Tarnocai et al., 2009). Permafrost occurs in the cold regions of the world where rock or soil remains below 0°C for two or more consecutive years (French, 2017). At mid- to high-latitudes in temperate, boreal and arctic regions the cool temperatures keep rates of decomposition low and peat forming vegetation consists of mosses, grasses, sedges, shrubs and sometimes trees (Page and Baird, 2016).

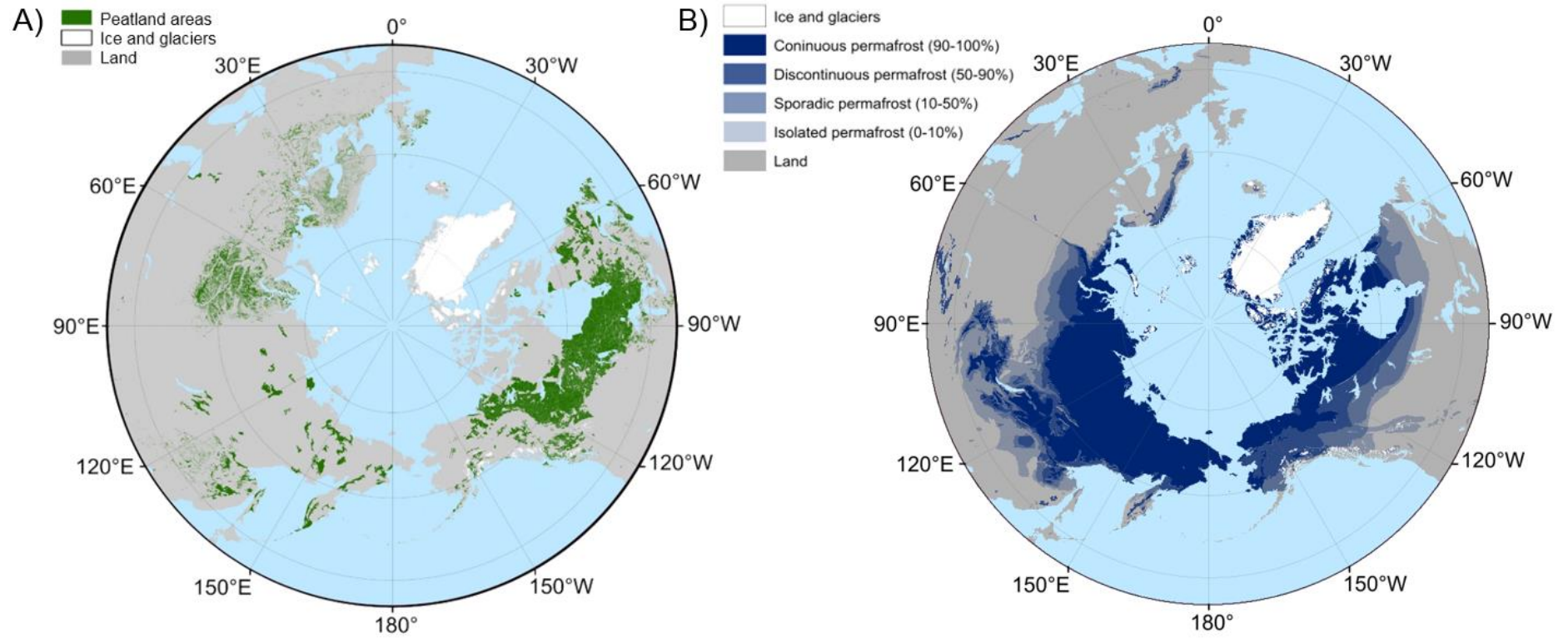


Figure 1.1. A) Distribution of northern peatlands (Xu et al., 2018a) and B) extent of ice, glaciers and permafrost (Brown et al., 2002). Map extent is >40 °N.

Not only do peatlands act as globally important carbon stores, they provide a range of ecosystem services that include biodiversity protection, water purification/regulation, importance as cultural landscapes and excellent archives of past environmental change. Specifically, peatlands provide a habitat for highly specialised plant species and are important for certain stages in the life cycle of other organisms; for example they are refuges for migrating or breeding birds (Minayeva et al., 2016). The presence of even small wetland habitats has been shown to be important for the maintenance of vertebrate biodiversity (Gibbs, 1993). Peatlands are a key source of drinking water in the UK (Holden et al., 2007; Xu et al., 2018b), with atmospheric pollutants immobilised and retained in the peat (Smith et al., 2013). Similarly, intact peatlands with abundant *Sphagnum* coverage can slow the flow of water across the surface and influence the timing of flood hydrograph peaks (Evans et al., 2014; Holden et al., 2008). Culturally, peatlands have spiritual associations and provide the opportunity for recreational activities such as shooting or walking and can be harvested for fuel; however, mismanagement of these activities can lead to degradation (Waylen et al., 2016). The anoxic conditions found in peatlands that allow for the build-up of organic carbon, are also ideal for the preservation of cultural artefacts (or even bodies) and of sub-fossil material that provides information about past environmental change (Gearey and Fyfe, 2016).

In the presence of anoxic waterlogged conditions and the associated low decomposition rates, productivity can remain higher than decomposition (Gallego-Sala et al., 2016) (Figure 1.2). Similarly, near-surface water-tables encourage the growth of decomposition resistant vegetation, e.g. *Sphagnum* mosses (Rydin and Jeglum, 2006). Peatlands can be broadly categorised into bogs and fens. Bogs are ombrotrophic ecosystems that receive their water and nutrients solely from precipitation, while fens are more minerotrophic and receive additional water and nutrients from groundwater or runoff from the surrounding catchment (Rydin and Jeglum, 2006). *Sphagnum* is a key peat forming species and its productivity has been shown to increase with levels of photosynthetically active radiation (PAR) and the length of the growing season (Loisel et al., 2012). Mid- to high-latitude peatlands have formed and grown since the last glacial maximum (Gorham et al., 2007; Yu et al., 2010), with the majority initiating as growing seasons became warmer and longer in the early-Holocene (Morris et al., 2018). Therefore, the productivity of peatland ecosystems may be more important than decomposition for long term carbon storage (Charman et al., 2013). The flow of water through a peatland transports carbon to nearby watercourses in the form of dissolved organic carbon (DOC), particulate organic carbon (POC) and dissolved inorganic carbon (DIC) (Billett et al., 2006; Olefeldt et al., 2013). These fluvial carbon losses typically account for 10-30% of total losses in a peatland (Limpens et al., 2008; Worrall et al.,

2003). On a less frequent timescale, but with a greater severity are losses of peatland carbon to fire. Peatland fire occurs on a centennial to millennial timescale and is particularly important in boreal regions, yet intact peatlands with high moisture content have some protection from burning (Harden et al., 2000; Turetsky et al., 2015).

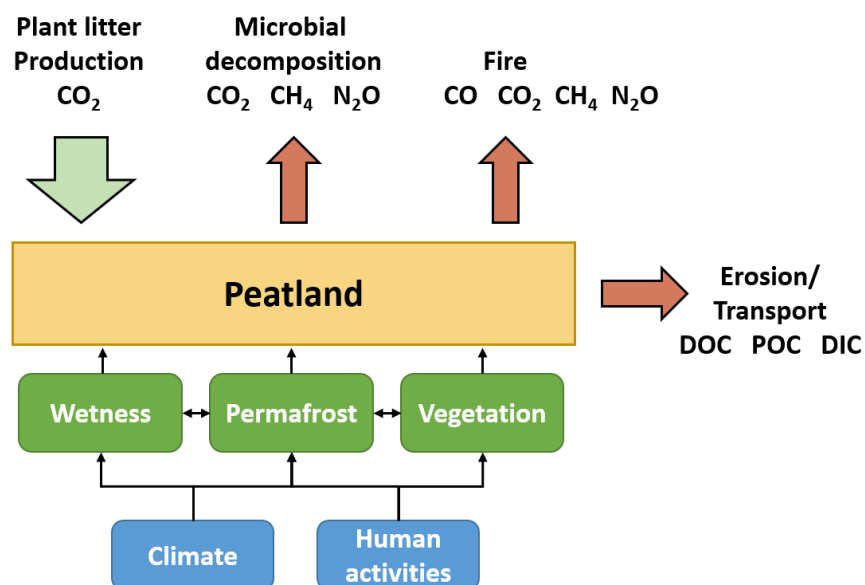


Figure 1.2. Simplified conceptual model of processes affecting the peatland carbon balance. Green arrows signify carbon gains, while red arrows indicate losses. Green boxes represent local scale autogenic factors and blue boxes are allogenic factors.

With climate warming in the twenty-first century – where adequate moisture can be maintained – there is the potential at high latitudes for increased peatland productivity that may outweigh losses to microbial decomposition (Gallego-Sala et al., 2018). However, while climate directly influences both plant productivity and decomposition rates, climate also indirectly influences hydrological conditions, vegetation, permafrost thaw and fire that can complicate the relationship (Åkerman and Johansson, 2008; Turetsky et al., 2015; Yu et al., 2009). Therefore, there is considerable uncertainty on future carbon sink capacity of peatlands (Hugelius et al., 2020) – particularly at high-latitudes where peatlands have shown an inconsistent carbon accumulation response to recent warming (Zhang et al., 2018). Climate remains the primary control on peatland accumulation, but the direct modification of peatlands by humans (e.g. drainage, afforestation, grazing) is having an increasing impact (Page and Baird, 2016).

In Europe, increasing temperatures and human activities have greatly contributed to recent widespread peatland drying (Swindles et al., 2019). Climatic drying in boreal and temperate regions has been linked with increased aerobic decomposition and losses of CO₂ to the atmosphere (Helbig et al., 2020; Zhang et al., 2020). At high-latitudes, warming conditions have led to permafrost thaw and thickening of the active layer (Åkerman and Johansson, 2008; Burn

and Kokelj, 2009; Christensen et al., 2004), which has influenced peatland hydrology, vegetation and biogeochemical cycling (Liljedahl et al., 2016; Väiranta et al., 2021; Zhang et al., 2017). By 2100, it is likely that human induced warming will dramatically reduce the climatic-space suitable for permafrost peatlands in northern Europe and Western Siberia (Fewster et al., 2022). Although not yet modelled, the climate-space for permafrost peatlands in North America is also likely to decrease massively. With the thawing of permafrost, previously inert carbon is exposed to decomposition and emission to the atmosphere, potentially leading to a feedback with climate (Schuur et al., 2015). Permafrost thaw commonly leads to thermokarst subsidence and localised wetting (Johansson et al., 2006; Swindles et al., 2015b; Zoltai, 1993), where the pooling of water at the surface of a peatland can lead to increased anaerobic microbial respiration and carbon losses in the form of CH₄ (Christensen et al., 2004; Gorham, 1991). Alternatively, peatlands undergoing permafrost thaw can experience localised drying with increased hydrological connectivity and drainage (Connon et al., 2014). There is some evidence to suggest that permafrost peatlands may experience increased carbon accumulation where hydrological extremes are avoided (Swindles et al., 2015b). Consequently, there is uncertainty in how permafrost peatland hydrology, vegetation and carbon balance will respond to climate change.

Peatland surface moisture is an important factor in limiting the risk of fire (Thompson et al., 2019). Consequently, with warmer and drier conditions peatland fire frequency and extent may increase – particularly in boreal regions – emitting large quantities of carbon to the atmosphere (Flannigan et al., 2009; Turetsky et al., 2015). There is evidence to suggest peatland burning has increased in recent decades in Alaskan forests and peatlands (Turetsky et al., 2010). Moreover, increasingly frequent or extensive peatland fire may increase permafrost thaw by raising soil temperature (Gibson et al., 2018). There are a number of autogenic feedbacks within peatland ecosystems such as the moisture retention abilities of *Sphagnum* moss communities and hydrological connectivity, that are likely to only partially mitigate greater peatland fire with warming (Nelson et al., 2021). Additionally, permafrost thaw may lead to greater erosion and losses of DOC (Olefeldt and Roulet, 2012). Ultimately, the influence of climate change on peatland carbon storage is likely to be detrimental, but to what extent remains uncertain. This uncertainty is largely in relation to peatland autogenic processes and the interaction between hydrological conditions, fire, vegetation and permafrost thaw (Abbott et al., 2016; Loisel et al., 2021; Veraverbeke et al., 2021; Waddington et al., 2015).

1.1.1. Peatlands as palaeoenvironmental archives

The study of peatland ecosystems can broadly be categorised into monitoring, experimental, modelling and palaeoenvironmental approaches. All approaches contribute to the advancement of the discipline and have their various strengths and weaknesses, which I consider briefly below before focusing on the use of peatlands as palaeoenvironmental archives in more detail. In this thesis, I adopt a palaeoenvironmental approach, using the information preserved in peatlands about past environmental change to better understand these ecosystems on a centennial to millennial timescale.

Contemporary monitoring studies generally measure variables directly in the field, with a prominent example being the use of flux towers or chambers to measure CO₂ and/or CH₄ emissions from a peatland (Billett et al., 2010). Here the influence upon peatland carbon fluxes of an intact vs. restored peatland (Jauhiainen et al., 2016) or of differing hydrological conditions (Christensen et al., 2004) can be investigated. The main advantage here is that the measurements are taken in situ; however, studies are limited in the temporal extent to decades at most. For example for permafrost peatlands in northern Sweden, continuous active layer depth monitoring stretches back to 1978 (Christensen et al., 2004), while extensive monitoring of CO₂ and CH₄ fluxes began no earlier than the 1990s (Johansson et al., 2006). An experimental study can modify variables by for example increasing soil temperature or raising the water-table in the field (Turetsky et al., 2008) or in a laboratory setting (Moore and Dalva, 1993). Therefore, an experimental approach attempts to isolate the influence of specific variables, but again is limited in temporal extent by resource availability. The use of satellite imagery to study peatland processes straddles both monitoring and modelling approaches and is generally termed remote sensing. Optical data from satellites allow the study of large spatial extents and can be used to drive models of peatland carbon flux, but records only date back to the 1970s and these early records are of reduced spatiotemporal resolution (Lees et al., 2018). Modelling is excellent for implementing the knowledge gained from monitoring and experimental studies, applying it on a greater spatiotemporal extent and in developing new research hypotheses. Yet, all models are wrong to some extent, so it is important to understand their limitations during interpretation (Box, 1976). Prominent examples of models for peatland development are DigiBog (Baird et al., 2012; Morris et al., 2012) and the Holocene Peat Model (Frolking et al., 2010; Quillet et al., 2013).

A palaeoenvironmental approach uses information preserved in peat to reconstruct past environmental conditions. This usually involves extracting cores or monoliths, producing an age-depth model and analysing sections of the core for the physical properties of peat or

environmental proxies (Chambers et al., 2011). Methods for dating a peat profile include ^{14}C and ^{210}Pb isotope dating, tephrochronology and spheroidal carbonaceous particles (SCPs) (Gearey and Fyfe, 2016). Common environmental proxies include testate amoebae for past moisture conditions (Booth et al., 2010), plant macrofossils or pollen for past vegetation (Birks and Berglund, 2018; Mauquoy et al., 2010) and charcoal as an indicator of past fire (Mooney and Tinner, 2011). These proxies provide a snapshot of the environmental conditions at the time a particular layer of peat formed (Amesbury et al., 2011) and are reviewed in greater detail in the following sections. The advantage of a palaeoenvironmental approach is that it can reconstruct environmental change on the decadal to millennial timescale that peatland ecosystems develop on and account for any potential lag times to external forcing (Swindles et al., 2016). Similarly, this approach can provide an early warning of future changes (Finlayson et al., 2016) and even inform current conservation practices (McCarroll et al., 2016). However, in certain situations the signal in a peat archive can be degraded, for example, extreme drying may expose older peat to secondary decomposition and distort carbon accumulation rates (Morris et al., 2015; Swindles et al., 2012; Young et al., 2021). Therefore, the factors that may degrade peatland palaeoenvironmental archives need to be considered in their interpretation.

1.1.2. Testate amoebae

Testate amoebae are single celled eukaryotic organisms universally found on the surface of peatlands (Figure 1.3) and are commonly used as indicators of past hydrological conditions owing to their sensitivity to moisture and resistance to decomposition (Booth et al., 2010; Charman et al., 2000). Testate amoebae are limited to the surface of peatlands by moisture availability, light, temperature and nutrients (Charman et al., 2000; Mieczan, 2010; Roe et al., 2017). Therefore, subfossil testate amoebae can be used to infer past environmental conditions from the time they were deposited in the peat record. Transfer functions to reconstruct past environmental conditions can be developed by measuring contemporary testate amoeba species distribution across an environmental gradient, most commonly for a range of water-table depths (WTDs). Certain species of testate amoebae with weak idiosomic siliceous tests (WISTs) – such as *Euglypha* spp. – preserve less favourably down core. WISTs do not typically introduce discernible bias in WTD reconstruction, but it is recommended they are excluded to ensure robust reconstructions (Swindles et al., 2020).

A number of testate amoeba transfer functions for peatland hydrological conditions have been developed in temperate (Booth, 2008; Charman et al., 2007; Lamentowicz et al., 2008; Wilmshurst et al., 2003; Woodland et al., 1998), boreal (Amesbury et al., 2013; Lamarre et al., 2013) and

subarctic regions (Swindles et al., 2015a; Taylor et al., 2019; Zhang et al., 2017). These transfer functions for hydrological conditions have been primarily developed for ombrotrophic peatlands; in more minerotrophic settings pH and nutrient levels become a more important factor in testate amoeba species distribution (Lamentowicz et al., 2013; Payne, 2011). Additionally, there are regional WTD transfer functions for Europe (Amesbury et al., 2016), North America (Amesbury et al., 2018) and Asia (Qin et al., 2021). The European transfer function has been applied in a regional synthesis of 31 testate amoeba records across continental Europe, Scandinavia and Britain and Ireland by Swindles et al. (2019). Yet, the Swindles et al. (2019) study includes few records from subarctic Europe. In fact, there are areas towards the northern limits of peatland distribution across Eurasia and North America (e.g. High Arctic Canada, Svalbard or Western Siberia) where the potential for developing testate amoeba transfer functions to reconstruct past WTD is yet to be fully explored. This is an important research gap to address because of the rapid rate of change that high latitude ecosystems are experiencing and the importance of hydrological conditions for the peatland carbon balance (Evans et al., 2021; Loisel et al., 2021). For this reason, the first aim of this thesis is to develop and apply a testate amoeba transfer function for peatland WTD and pH in Svalbard.

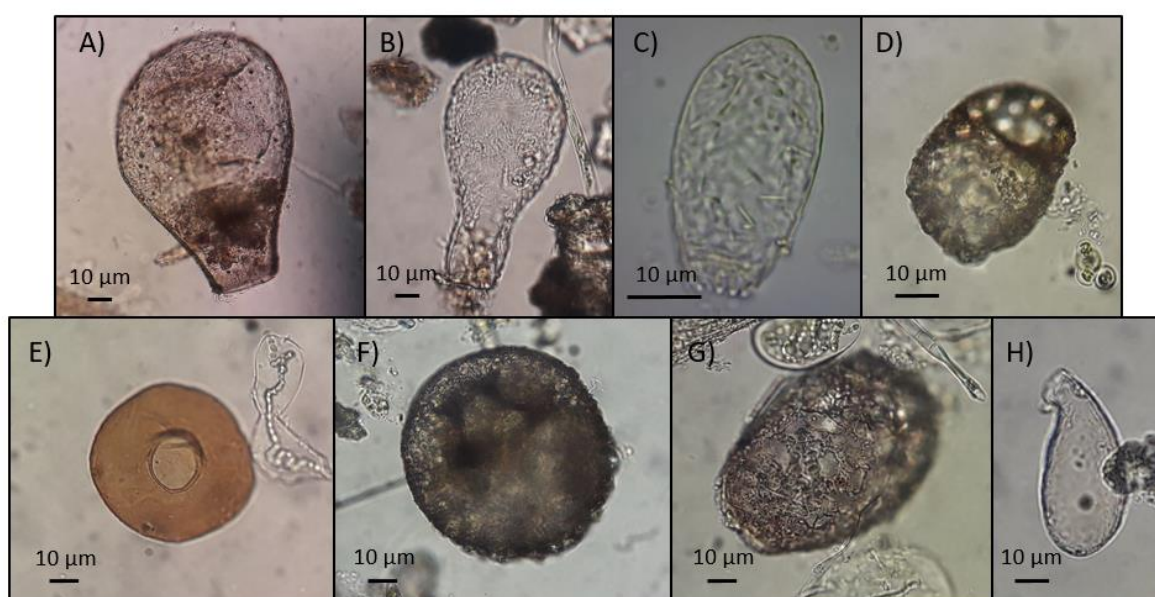


Figure 1.3. Examples of peatland testate amoebae photographed at 200-400 times magnification. Scale bar is approximate. A) *Gibbocarina galeata*, B) *Padaungiella lageniformis*, C) *Euglypha strigosa*, D) *Centropyxis aerophila*, E) *Arcella discoidea*, F) *Centropyxis gasparella*, G) *Heleopera rosea* and H) *Campascus minutus*.

1.1.3. Plant macrofossils

Plant macrofossils are the partially decomposed remains (e.g. fruit, seeds, leaves, stems) of plants, generally 0.5 to 2 mm in size (Birks, 2017). Unlike pollen that can be transported a great distance, plant macrofossils provide evidence of past changes in vegetation in the immediate vicinity of the

coring location (Birks and Birks, 2000) and have been widely used to reconstruct past peatland vegetation (e.g. Gafka et al., 2014; Piilo et al., 2019; Väiliranta et al., 2017). Furthermore, plant macrofossils have been used to estimate the timing of permafrost aggradation/thaw and fen/bog transitions during the Holocene (Treat et al., 2016; Treat and Jones, 2018). However, this approach assumes a direct relationship between vegetation and permafrost or nutrient conditions, whereas in reality a variety of biochemical and hydrological factors influence vegetation composition. Plant macrofossil remains (excluding roots) are ideal for ^{14}C dating because they are deposited in situ at the time of death (Birks, 2017; Mauquoy et al., 2010). Plant macrofossils can be used to quantitatively reconstruct past hydrological change in peatlands using modern calibration data (Väiliranta et al., 2007). However, unlike testate amoeba plant macrofossils are perennial and spread slowly. Reconstructions of peatland surface moisture from plant macrofossils may be less sensitive than reconstructions using testate amoebae (Väiliranta et al., 2012). This differential response strengthens the case for multiproxy palaeoenvironmental studies, particularly when autogenic ecohydrological processes are so important for understanding the resistance, resilience and vulnerability of mid- to high-latitude peatlands (Waddington et al., 2015). Consequently, the second aim of this thesis is to investigate the ecohydrological and carbon dynamics response of permafrost peatlands in a rapidly warming region of subarctic Sweden across multiple sites using multiple proxies.

1.1.4. Charcoal

Charcoal is the product of incomplete combustion of organic matter that has undergone charring due to oxygen limitation and once formed, is extremely resistant to decomposition (Mooney and Tinner, 2011). Since the pioneering work of Iversen (1941), sedimentary charcoal records primarily in lacustrine settings (Clark, 1988; Earle et al., 1996; MacDonald et al., 1991) have long been used as a proxy for past fire. Particles are generally separated into macrocharcoal (>100 μm) and microcharcoal (<100 μm), with larger macrocharcoal particles dispersing a shorter distance and reflecting more localised burning than microcharcoal particles (Conedera et al., 2009; Mooney and Tinner, 2011). Similarly, larger charcoal particles are generally associated with more intense fires (Clark et al., 1998). A number of studies suggest that macrocharcoal records from peatlands reflects localised peatland burning (Florescu et al., 2018; Ohlson et al., 2006; Rius et al., 2011). Similarly, peatland charcoal records are less likely to be subject reworking or secondary deposition than lacustrine records (Clark and Patterson, 1997; Conedera et al., 2009). Yet on occasion, an intense smouldering peatland fire may destroy part of the record (Davies et al., 2013). In the last two decades there have been a number of syntheses that reconstruct global or continental biomass burning from sedimentary charcoal records (Daniau et al., 2012; Marlon et al., 2016,

2008; Power et al., 2008; Vanni re et al., 2016). However, currently no such syntheses exist specifically for peatland ecosystems. Therefore, the third aim of this thesis was to synthesise and examine existing Holocene peatland biomass burning records from North America, Europe and Patagonia.

1.2. Research aim and objectives

The overall aim of the thesis is:

“To investigate trends in ecohydrology and fire regime in mid- to high-latitude peatlands during the Holocene using palaeoecological techniques, with a focus on better understanding autogenic and climate-driven ecosystem shifts.”

I developed three objectives to achieve this overall aim, which inform the structure of the results chapters:

1. Develop and apply testate amoeba transfer functions for water-table depth and pH for high-latitude peatlands in Svalbard (Chapter 2).
2. Investigate the ecohydrological and carbon dynamics response of permafrost peatlands in a rapidly warming region of subarctic Sweden across multiple sites (Chapter 3).
3. Examine peatland biomass burning trends and controls in North America, Europe and Patagonia during the Holocene (Chapter 4).

Initially, this project was to focus on reconstructing the ecohydrological response of permafrost peatlands to late Holocene climatic warming. However, there was a slight change of direction with the final results chapter owing to COVID-19 related laboratory delays. Instead of investigating the late Holocene ecohydrological dynamics of peatlands on Svalbard, the last results chapter collates existing macrocharcoal records to analyse trends in peatland burning in North America, Europe and Patagonia during the Holocene. Ultimately, this enabled me to consider peatland environmental change more comprehensively on a broader temporal and spatial scale.

1.3. Thesis structure

This thesis is presented largely in a traditional format, but the three individual results chapters are comprised of published journal articles, or drafted for publication in the case of Chapter 4. Each of the following results chapters (Chapters 2, 3 and 4) takes the form of a manuscript that has a specific research focus relating to one of the research objectives stated above. Each manuscript is separated into an introduction, methods, results, discussion (or a combined results and

discussion) and conclusion section. Each chapter contained a separate reference list. Contributions to each manuscript are listed on pages iii to iv. Chapter 5 brings together the findings of each results chapter and provides an overall discussion and synthesis of the work presented in this thesis. Finally, the Appendices (A-C) includes the supporting information for each of the results chapters.

References

- Abbott, B.W., Jones, J.B., Schuur, E.A.G., Chapin III, F.S., Bowden, W.B., Bret-Harte, M.S., Epstein, H.E., Flannigan, M.D., Harms, T.K., Hollingsworth, T.N., Mack, M.C., McGuire, A.D., Natali, S.M., Rocha, A. V, Tank, S.E., Turetsky, M.R., Vonk, J.E., Wickland, K.P., Aiken, G.R., Alexander, H.D., Amon, R.M.W., Benscoter, B.W., Bergeron, Y., Bishop, K., Blarquez, O., Ben Bond-Lamberty, B., Breen, A.L., Buffam, I., Cai, Y., Carcaillet, C., Carey, S.K., Chen, J.M., Chen, H.Y.H., Christensen, T.R., Cooper, L.W., Cornelissen, J.H.C., de Groot, W.J., DeLuca, T.H., Dorrepaal, E., Fetcher, N., Finlay, J.C., Forbes, B.C., French, N.H.F., Gauthier, S., Girardin, M.P., Goetz, S.J., Goldammer, J.G., Gough, L., Grogan, P., Guo, L., Higuera, P.E., Hinzman, L., Hu, F.S., Hugelius, G., Jafarov, E.E., Jandt, R., Johnstone, J.F., Jan Karlsson, J., Kasischke, E.S., Kattner, G., Kelly, R., Keuper, F., Kling, G.W., Kortelainen, P., Kouki, J., Kuhry, P., Laudon, H., Laurion, I., Macdonald, R.W., Mann, P.J., Martikainen, P.J., McClelland, J.W., Molau, U., Oberbauer, S.F., Olefeldt, D., Paré, D., Parisien, M.-A., Payette, S., Peng, C., Pokrovsky, O.S., Rastetter, E.B., Raymond, P.A., Reynolds, M.K., Rein, G., Reynolds, J.F., Robards, M., Rogers, B.M., Schädel, C., Schaefer, K., Schmidt, I.K., Shvidenko, A., Sky, J., Spencer, R.G.M., Starr, G., Striegl, R.G., Teisserenc, R., Tranvik, L.J., Virtanen, T., Welker, J.M., Zimov, S., 2016. Biomass offsets little or none of permafrost carbon release from soils, streams, and wildfire: an expert assessment. *Environ. Res. Lett.* 11, 034014. <https://doi.org/10.1088/1748-9326/11/3/034014>
- Åkerman, H.J., Johansson, M., 2008. Thawing permafrost and thicker active layers in sub-arctic Sweden. *Permafr. Periglac. Process.* 19, 279–292. <https://doi.org/10.1002/ppp.626>
- Amesbury, M.J., Barber, K.E., Hughes, P.D.M., 2011. The methodological basis for fine-resolution, multi-proxy reconstructions of ombrotrophic peat bog surface wetness. *Boreas* 40, 161–174. <https://doi.org/10.1111/j.1502-3885.2010.00152.x>
- Amesbury, M.J., Booth, R.K., Roland, T.P., Bunbury, J., Clifford, M.J., Charman, D.J., Elliot, S., Finkelstein, S., Garneau, M., Hughes, P.D.M., Lamarre, A., Loisel, J., Mackay, H., Magnan, G., Markel, E.R., Mitchell, E.A.D., Payne, R.J., Pelletier, N., Roe, H., Sullivan, M.E., Swindles, G.T., Talbot, J., van Bellen, S., Warner, B.G., 2018. Towards a Holarctic synthesis of peatland testate amoeba ecology: Development of a new continental-scale palaeohydrological transfer function for North America and comparison to European data. *Quat. Sci. Rev.* 201, 483–500. <https://doi.org/10.1016/J.QUASCIREV.2018.10.034>
- Amesbury, M.J., Mallon, G., Charman, D.J., Hughes, P.D.M., Booth, R.K., Daley, T.J., Garneau, M., 2013. Statistical testing of a new testate amoeba-based transfer function for water-table depth reconstruction on ombrotrophic peatlands in north-eastern Canada and Maine, United States. *J. Quat. Sci.* 28, 27–39. <https://doi.org/10.1002/jqs.2584>
- Amesbury, M.J., Swindles, G.T., Bobrov, A., Charman, D.J., Holden, J., Lamentowicz, M., Mallon, G., Mazei, Y., Mitchell, E.A.D., Payne, R.J., Roland, T.P., Turner, T.E., Warner, B.G., 2016. Development of a new pan-European testate amoeba transfer function for reconstructing peatland palaeohydrology. *Quat. Sci. Rev.* 152, 132–151. <https://doi.org/10.1016/J.QUASCIREV.2016.09.024>
- Baird, A.J., Morris, P.J., Belyea, L.R., 2012. The DigiBog peatland development model 1: rationale, conceptual model, and hydrological basis. *Ecohydrology* 5, 242–255. <https://doi.org/10.1002/ECO.230>
- Billett, M.F., Charman, D.J., Clark, J.M., Evans, C.D., Evans, M.G., Ostle, N.J., Worrall, F., Burden, A., Dinsmore, K.J., Jones, T., McNamara, N.P., Parry, L., Rowson, J.G., Rose, R., 2010. Carbon balance of UK peatlands: Current state of knowledge and future research challenges. *Clim.*

- Res. 45, 13–29. <https://doi.org/10.3354/cr00903>
- Billett, M.F., Deacon, C.M., Palmer, S.M., Dawson, J.J.C., Hope, D., 2006. Connecting organic carbon in stream water and soils in a peatland catchment. *J. Geophys. Res. Biogeosciences* 111, 2010. <https://doi.org/10.1029/2005JG000065>
- Birks, H.H., 2017. Plant Macrofossil Introduction, Reference Module in Earth Systems and Environmental Sciences. Elsevier Inc. <https://doi.org/10.1016/b978-0-12-409548-9.10499-3>
- Birks, H.H., Birks, H.J.B., 2000. Future uses of pollen analysis must include plant macrofossils. *J. Biogeogr.* 27. <https://doi.org/10.1046/j.1365-2699.2000.00375.x>
- Birks, H.J.B., Berglund, B.E., 2018. One hundred years of Quaternary pollen analysis 1916–2016, Vegetation History and Archaeobotany. Springer Berlin Heidelberg. <https://doi.org/10.1007/s00334-017-0630-2>
- Booth, R.K., 2008. Testate amoebae as proxies for mean annual water-table depth in Sphagnum-dominated peatlands of North America. *J. Quat. Sci.* 23, 43–57. <https://doi.org/10.1002/jqs.1114>
- Booth, R.K., Lamentowicz, M., Charman, D.J., 2010. Preparation and analysis of testate amoebae in peatland palaeoenvironmental studies. *Mires Peat* 7, 1–7.
- Box, G.E.P., 1976. Science and statistics. *J. Am. Stat. Assoc.* 71. <https://doi.org/10.1080/01621459.1976.10480949>
- Brown, J., Ferrians, O., Heginbottom, J.A., Melnikov, E., 2002. Circum-Arctic Map of Permafrost and Ground-Ice Conditions, Version 2. <https://doi.org/https://doi.org/10.7265/skbg-kf16>
- Burn, C.R., Kokelj, S. V., 2009. The environment and permafrost of the Mackenzie Delta area. *Permafr. Periglac. Process.* 20, 83–105. <https://doi.org/10.1002/ppp.655>
- Burton, R.G.O., Hodgson, J.M., 1987. Lowland peat in England and Wales. Soil Survey of England and Wales, Harpenden.
- Chambers, F.M., Beilman, D.W., Yu, Z., 2011. Methods for determining peat humification and for quantifying peat bulk density, organic matter and carbon content for palaeostudies of climate and peatland carbon dynamics. *Mires Peat* 7, 1–10.
- Charman, D.J., Beilman, D.W., Blaauw, M., Booth, R.K., Brewer, S., Chambers, F.M., Christen, J.A., Gallego-Sala, A., Harrison, S.P., Hughes, P.D.M., Jackson, S.T., Korhola, A., Mauquoy, D., Mitchell, F.J.G., Prentice, I.C., van der Linden, M., De Vleeschouwer, F., Yu, Z.C., Alm, J., Bauer, I.E., Corish, Y.M.C., Garneau, M., Hohl, V., Huang, Y., Karofeld, E., Le Roux, G., Loisel, J., Moschen, R., Nichols, J.E., Nieminen, T.M., MacDonald, G.M., Phadtare, N.R., Rausch, N., Sillasoo, Ü., Swindles, G.T., Tuittila, E.-S., Ukonmaanaho, L., Väliranta, M., van Bellen, S., van Geel, B., Vitt, D.H., Zhao, Y., 2013. Climate-related changes in peatland carbon accumulation during the last millennium. *Biogeosciences* 10, 929–944. <https://doi.org/10.5194/bg-10-929-2013>
- Charman, D.J., Blundell, A., Abrupt Climate Change Over the European Land Mass project members, 2007. A new European testate amoebae transfer function for palaeohydrological reconstruction on ombrotrophic peatlands. *J. Quat. Sci.* 22, 209–221. <https://doi.org/10.1002/jqs.1026>
- Charman, D.J., Hendon, D., Woodland, W.A., 2000. The identification of testate amoebae (Protozoa: Rhizopoda) in peats: QRA Technical Guide No. 9, Quaternary Research Association. Quaternary Research Association, London. <https://doi.org/10.1016/j.quascirev.2004.02.012>

- Christensen, T.R., Johansson, T., Åkerman, H.J., Mastepanov, M., Malmer, N., Friberg, T., Crill, P., Svensson, B.H., 2004. Thawing sub-arctic permafrost: Effects on vegetation and methane emissions. *Geophys. Res. Lett.* 31, L04501. <https://doi.org/10.1029/2003GL018680>
- Clark, J.S., 1988. Stratigraphic charcoal analysis on petrographic thin sections: Application to fire history in northwestern Minnesota. *Quat. Res.* 30. [https://doi.org/10.1016/0033-5894\(88\)90089-0](https://doi.org/10.1016/0033-5894(88)90089-0)
- Clark, J.S., Lynch, J., Stocks, B.J., Goldammer, J.G., 1998. Relationships between charcoal particles in air and sediments in west-central Siberia. *Holocene* 8. <https://doi.org/10.1191/095968398672501165>
- Clark, J.S., Patterson, W.A., 1997. Background and Local Charcoal in Sediments: Scales of Fire Evidence in the Paleorecord, in: *Sediment Records of Biomass Burning and Global Change*. Springer Berlin Heidelberg, pp. 23–48. https://doi.org/10.1007/978-3-642-59171-6_3
- Conedera, M., Tinner, W., Neff, C., Meurer, M., Dickens, A.F., Krebs, P., 2009. Reconstructing past fire regimes: methods, applications, and relevance to fire management and conservation. *Quat. Sci. Rev.* 28, 555–576. <https://doi.org/10.1016/j.quascirev.2008.11.005>
- Connon, R.F., Quinton, W.L., Craig, J.R., Hayashi, M., 2014. Changing hydrologic connectivity due to permafrost thaw in the lower Liard River valley, NWT, Canada. *Hydrol. Process.* 28, 4163–4178. <https://doi.org/10.1002/hyp.10206>
- Daniau, A.L., Bartlein, P.J., Harrison, S.P., Prentice, I.C., Brewer, S., Friedlingstein, P., Harrison-Prentice, T.I., Inoue, J., Izumi, K., Marlon, J.R., Mooney, S., Power, M.J., Stevenson, J., Tinner, W., Andrič, M., Atanassova, J., Behling, H., Black, M., Blarquez, O., Brown, K.J., Carcaillet, C., Colhoun, E.A., Colombaroli, D., Davis, B.A.S., D’Costa, D., Dodson, J., Dupont, L., Eshetu, Z., Gavin, D.G., Genries, A., Haberle, S., Hallett, D.J., Hope, G., Horn, S.P., Kassa, T.G., Katamura, F., Kennedy, L.M., Kershaw, P., Krivonogov, S., Long, C., Magri, D., Marinova, E., McKenzie, G.M., Moreno, P.I., Moss, P., Neumann, F.H., Norström, E., Paitre, C., Rius, D., Roberts, N., Robinson, G.S., Sasaki, N., Scott, L., Takahara, H., Terwilliger, V., Thevenon, F., Turner, R., Valsecchi, V.G., Vannière, B., Walsh, M., Williams, N., Zhang, Y., 2012. Predictability of biomass burning in response to climate changes. *Global Biogeochem. Cycles* 26, 4007. <https://doi.org/10.1029/2011GB004249>
- Earle, C.J., Brubaker, L.B., Anderson, P.M., 1996. Charcoal in northcentral Alaskan lake sediments: Relationships to fire and late-Quaternary vegetation history. *Rev. Palaeobot. Palynol.* 92. [https://doi.org/10.1016/0034-6667\(95\)00095-X](https://doi.org/10.1016/0034-6667(95)00095-X)
- Evans, C.D., Bonn, A., Holden, J., Reed, M.S., Evans, M.G., Worrall, F., Couwenberg, J., Parnell, M., 2014. Relationships between anthropogenic pressures and ecosystem functions in UK blanket bogs: Linking process understanding to ecosystem service valuation. *Ecosyst. Serv.* 9, 5–19. <https://doi.org/10.1016/j.ecoser.2014.06.013>
- Evans, C.D., Peacock, M., Baird, A.J., Artz, R.R.E., Burden, A., Callaghan, N., Chapman, P.J., Cooper, H.M., Coyle, M., Craig, E., Cumming, A., Dixon, S., Gauci, V., Grayson, R.P., Helfter, C., Heppell, C.M., Holden, J., Jones, D.L., Kaduk, J., Levy, P., Matthews, R., McNamara, N.P., Misselbrook, T., Oakley, S., Page, S.E., Rayment, M., Ridley, L.M., Stanley, K.M., Williamson, J.L., Worrall, F., Morrison, R., 2021. Overriding water table control on managed peatland greenhouse gas emissions. *Nature* 593, 548–552. <https://doi.org/10.1038/s41586-021-03523-1>
- Fewster, R.E., Morris, P.J., Ivanovic, R.F., Swindles, G.T., Peregon, A.M., Smith, C.J., 2022. Imminent loss of climate space for permafrost peatlands in Europe and Western Siberia. *Nat. Clim. Chang.* 12, 373–379. <https://doi.org/10.1038/s41558-022-01296-7>

- Finlayson, C.M., Clarke, S.J., Davidson, N.C., Gell, P., 2016. Role of palaeoecology in describing the ecological character of wetlands. *Mar. Freshw. Res.* 67, 687–694. <https://doi.org/10.1071/MF15293>
- Flannigan, M., Stocks, B., Turetsky, M., Wotton, M., 2009. Impacts of climate change on fire activity and fire management in the circumboreal forest. *Glob. Chang. Biol.* 15, 549–560. <https://doi.org/10.1111/j.1365-2486.2008.01660.x>
- Florescu, G., Vanni re, B., Feurdean, A., 2018. Exploring the influence of local controls on fire activity using multiple charcoal records from northern Romanian Carpathians. *Quat. Int.* 488, 41–57. <https://doi.org/10.1016/j.quaint.2018.03.042>
- French, H.M., 2017. *The Periglacial Environment*, 4th ed. John Wiley & Sons.
- Frolking, S., Roulet, N.T., Tuittila, E., Bubier, J.L., Quillet, A., Talbot, J., Richard, P.J.H., 2010. A new model of Holocene peatland net primary production, decomposition, water balance, and peat accumulation. *Earth Syst. Dyn.* 1, 1–21. <https://doi.org/10.5194/esd-1-1-2010>
- Ga ka, M., Tobolski, K., G rska, A., Milecka, K., Fia kiewicz-Kozie , B., Lamentowicz, M., 2014. Disentangling the drivers for the development of a Baltic bog during the Little Ice Age in northern Poland. *Quat. Int.* 328–329, 323–337. <https://doi.org/10.1016/J.QUAINT.2013.02.026>
- Gallego-Sala, A. V., Charman, D.J., Brewer, S., Page, S.E., Prentice, I.C., Friedlingstein, P., Moreton, S., Amesbury, M.J., Beilman, D.W., Bj rck, S., Blyakharchuk, T., Bochicchio, C., Booth, R.K., Bunbury, J., Camill, P., Carless, D., Chimner, R.A., Clifford, M., Cressey, E., Courtney-Mustaphi, C., De Vleeschouwer, F., de Jong, R., Fialkiewicz-Koziel, B., Finkelstein, S.A., Garneau, M., Githumbi, E., Hribljan, J., Holmquist, J., Hughes, P.D.M., Jones, C., Jones, M.C., Karofeld, E., Klein, E.S., Kokfelt, U., Korhola, A., Lacourse, T., Le Roux, G., Lamentowicz, M., Large, D., Lavoie, M., Loisel, J., Mackay, H., MacDonald, G.M., Makila, M., Magnan, G., Marchant, R., Marcisz, K., Mart nez Cortizas, A., Massa, C., Mathijssen, P., Mauquoy, D., Mighall, T., Mitchell, F.J.G., Moss, P., Nichols, J., Oksanen, P.O., Orme, L., Packalen, M.S., Robinson, S., Roland, T.P., Sanderson, N.K., Sannel, A.B.K., Silva-S nchez, N., Steinberg, N., Swindles, G.T., Turner, T.E., Uglow, J., V liranta, M., van Bellen, S., van der Linden, M., van Geel, B., Wang, G., Yu, Z., Zaragoza-Castells, J., Zhao, Y., 2018. Latitudinal limits to the predicted increase of the peatland carbon sink with warming. *Nat. Clim. Chang.* 1. <https://doi.org/10.1038/s41558-018-0271-1>
- Gallego-Sala, A. V., Booth, R.K., Charman, D., Prentice, I.C., Yu, Z., 2016. Peatlands and Climate Change, in: Bonn, A., Allott, T., Evans, M., Joosten, H., Stoneman, R. (Eds.), *Peatland Restoration and Ecosystem Services: Science, Policy and Practice*. Cambridge University Press, Cambridge, UK, pp. 129–150.
- Gearey, B., Fyfe, R., 2016. Peatlands as knowledge archives, in: Bonn, A., Allott, T., Evans, M., Joosten, H., Stoneman, R. (Eds.), *Peatland Restoration and Ecosystem Services: Science, Policy and Practice*. Cambridge University Press, pp. 95–113. <https://doi.org/10.1017/CBO9781139177788.007>
- Gibbs, J.P., 1993. Importance of small wetlands for the persistence of local populations of wetland-associated animals. *Wetlands* 13, 25–31. <https://doi.org/10.1007/BF03160862>
- Gibson, C.M., Chasmer, L.E., Thompson, D.K., Quinton, W.L., Flannigan, M.D., Olefeldt, D., 2018. Wildfire as a major driver of recent permafrost thaw in boreal peatlands. *Nat. Commun.* 9, 3041. <https://doi.org/10.1038/s41467-018-05457-1>
- Gorham, E., 1991. *Northern Peatlands: Role in the Carbon Cycle and Probable Responses to*

Climatic Warming. *Ecol. Appl.* 1, 182–195. <https://doi.org/10.2307/1941811>

- Gorham, E., Lehman, C., Dyke, A., Janssens, J., Dyke, L., 2007. Temporal and spatial aspects of peatland initiation following deglaciation in North America. *Quat. Sci. Rev.* 26. <https://doi.org/10.1016/j.quascirev.2006.08.008>
- Hammond, R.F., 1981. *The Peatlands of Ireland: Soil Survey Bulletin No. 35*, 2nd ed. An Foras Taluntais, Dublin, Ireland.
- Hånell, U., 1991. *Forest classification of peatlands in Sweden - a field guide*, Forest classification of peatlands in Sweden - a field guide. Swedish University of Agricultural Sciences, Department of Silviculture, Umeå, Sweden.
- Harden, J.W., Trumbore, S.E., Stocks, B.J., Hirsch, A., Gower, S.T., O’Neill, K.P., Kasischke, E.S., 2000. The role of fire in the boreal carbon budget. *Glob. Chang. Biol.* 6, 174–184. <https://doi.org/10.1046/j.1365-2486.2000.06019.x>
- Helbig, M., Waddington, J.M., Alekseychik, P., Amiro, B.D., Aurela, M., Barr, A.G., Black, T.A., Blanken, P.D., Carey, S.K., Chen, J., Chi, J., Desai, A.R., Dunn, A., Euskirchen, E.S., Flanagan, L.B., Forbrich, I., Friborg, T., Grelle, A., Harder, S., Heliasz, M., Humphreys, E.R., Ikawa, H., Isabelle, P.E., Iwata, H., Jassal, R., Korkiakoski, M., Kurbatova, J., Kutzbach, L., Lindroth, A., Löfvenius, M.O., Lohila, A., Mammarella, I., Marsh, P., Maximov, T., Melton, J.R., Moore, P.A., Nadeau, D.F., Nicholls, E.M., Nilsson, M.B., Ohta, T., Peichl, M., Petrone, R.M., Petrov, R., Prokushkin, A., Quinton, W.L., Reed, D.E., Roulet, N.T., Runkle, B.R.K., Sonntag, O., Strachan, I.B., Taillardat, P., Tuittila, E.S., Tuovinen, J.P., Turner, J., Ueyama, M., Varlagin, A., Wilkening, M., Wofsy, S.C., Zyrianov, V., 2020. Increasing contribution of peatlands to boreal evapotranspiration in a warming climate. *Nat. Clim. Chang.* 10, 555–560. <https://doi.org/10.1038/s41558-020-0763-7>
- Holden, J., Kirkby, M.J., Lane, S.N., Milledge, D.G., Brookes, C.J., Holden, V., McDonald, A.T., 2008. Overland flow velocity and roughness properties in peatlands. *Water Resour. Res.* 44, 1–11. <https://doi.org/10.1029/2007WR006052>
- Holden, J., Shotbolt, L., Bonn, A., Burt, T.P., Chapman, P.J., Dougill, A.J., Fraser, E.D.G., Hubacek, K., Irvine, B., Kirkby, M.J., Reed, M.S., Prell, C., Stagl, S., Stringer, L.C., Turner, A., Worrall, F., 2007. Environmental change in moorland landscapes. *Earth-Science Rev.* <https://doi.org/10.1016/j.earscirev.2007.01.003>
- Houghton, R.A., 2007. Balancing the Global Carbon Budget. *Annu. Rev. Earth Planet. Sci.* 35, 313–347. <https://doi.org/10.1146/annurev.earth.35.031306.140057>
- Hugelius, G., Loisel, J., Chadburn, S., Jackson, R.B., Jones, M., Macdonald, G., 2020. Large stocks of peatland carbon and nitrogen are vulnerable to permafrost thaw. *Proc. Natl. Acad. Sci.* 117, 20438–20446. <https://doi.org/10.1073/pnas.1916387117>
- Iversen, J., 1941. Land occupation in Denmark’s Stone Age. *Danmarks Geol. Undersogelse II* 66, 1–68.
- Jauhiainen, J., Page, S.E., Vasander, H., 2016. Greenhouse gas dynamics in degraded and restored tropical peatlands. *Mires Peat* 17, 1–12. <https://doi.org/10.19189/MaP.2016.OMB.229>
- Johansson, T., Malmer, N., Crill, P.M., Friborg, T., Åkerman, J.H., Mastepanov, M., Christensen, T.R., 2006. Decadal vegetation changes in a northern peatland, greenhouse gas fluxes and net radiative forcing. *Glob. Chang. Biol.* 12, 2352–2369. <https://doi.org/10.1111/j.1365-2486.2006.01267.x>
- Joosten, H., Clarke, D., 2002. *Wise Use of Mires and Peatlands — Background Principles including*

a Framework for Decision-Making. International Mire Conservation Group and International Peat Society, Saarijärvi, Finland.

- Lamarre, A., Magnan, G., Garneau, M., Boucher, É., 2013. A testate amoeba-based transfer function for paleohydrological reconstruction from boreal and subarctic peatlands in northeastern Canada. *Quat. Int.* 306, 88–96. <https://doi.org/10.1016/J.QUAINT.2013.05.054>
- Lamentowicz, Ł., Lamentowicz, M., Gąbka, M., 2008. Testate amoebae ecology and a local transfer function from a peatland in western Poland. *Wetlands* 28, 164–175. <https://doi.org/10.1672/07-92.1>
- Lamentowicz, M., Lamentowicz, Ł., Payne, R.J., 2013. Towards quantitative reconstruction of peatland nutrient status from fens. *The Holocene* 23, 1661–1665. <https://doi.org/10.1177/0959683613508162>
- Lees, K.J., Quaife, T., Artz, R.R.E., Khomik, M., Clark, J.M., 2018. Potential for using remote sensing to estimate carbon fluxes across northern peatlands – A review. *Sci. Total Environ.* 615, 857–874. <https://doi.org/10.1016/j.scitotenv.2017.09.103>
- Liljedahl, A.K., Boike, J., Daanen, R.P., Fedorov, A.N., Frost, G. V., Grosse, G., Hinzman, L.D., Iijima, Y., Jorgenson, J.C., Matveyeva, N., Necsoiu, M., Reynolds, M.K., Romanovsky, V.E., Schulla, J., Tape, K.D., Walker, D.A., Wilson, C.J., Yabuki, H., Zona, D., 2016. Pan-Arctic ice-wedge degradation in warming permafrost and its influence on tundra hydrology. *Nat. Geosci.* 9, 312–318. <https://doi.org/10.1038/ngeo2674>
- Limpens, J., Berendse, F., Blodau, C., Canadell, J.G., Freeman, C., Holden, J., Roulet, N., Rydin, H., Schaepman-Strub, G., 2008. Peatlands and the carbon cycle: from local processes to global implications - a synthesis, *Biogeosciences*.
- Loisel, J., Gallego-Sala, A. V., Amesbury, M.J., Magnan, G., Anshari, G., Beilman, D.W., Benavides, J.C., Blewett, J., Camill, P., Charman, D.J., Chawchai, S., Hedgpeth, A., Kleinen, T., Korhola, A., Large, D., Mansilla, C.A., Müller, J., van Bellen, S., West, J.B., Yu, Z., Bubier, J.L., Garneau, M., Moore, T., Sannel, A.B.K., Page, S., Väiliranta, M., Bechtold, M., Brovkin, V., Cole, L.E.S., Chanton, J.P., Christensen, T.R., Davies, M.A., De Vleeschouwer, F., Finkelstein, S.A., Frothingham, S., Gałka, M., Gandois, L., Girkin, N., Harris, L.I., Heinemeyer, A., Hoyt, A.M., Jones, M.C., Joos, F., Juutinen, S., Kaiser, K., Lacourse, T., Lamentowicz, M., Larmola, T., Leifeld, J., Lohila, A., Milner, A.M., Minkinen, K., Moss, P., Naafs, B.D.A., Nichols, J., O'Donnell, J., Payne, R., Philben, M., Piilo, S., Quillet, A., Ratnayake, A.S., Roland, T.P., Sjögersten, S., Sonntag, O., Swindles, G.T., Swinnen, W., Talbot, J., Treat, C., Valach, A.C., Wu, J., 2021. Expert assessment of future vulnerability of the global peatland carbon sink. *Nat. Clim. Chang.* 11. <https://doi.org/10.1038/s41558-020-00944-0>
- Loisel, J., Gallego-Sala, A. V., Yu, Z., 2012. Global-scale pattern of peatland Sphagnum growth driven by photosynthetically active radiation and growing season length. *Biogeosciences* 9, 2737–2746. <https://doi.org/10.5194/bg-9-2737-2012>
- MacDonald, G.M., Larsen, C.P.S., Szeicz, J.M., Moser, K.A., 1991. The reconstruction of boreal forest fire history from lake sediments: A comparison of charcoal, pollen, sedimentological, and geochemical indices. *Quat. Sci. Rev.* 10. [https://doi.org/10.1016/0277-3791\(91\)90030-X](https://doi.org/10.1016/0277-3791(91)90030-X)
- Marlon, J.R., Bartlein, P.J., Carcaillet, C., Gavin, D.G., Harrison, S.P., Higuera, P.E., Joos, F., Power, M.J., Prentice, I.C., 2008. Climate and human influences on global biomass burning over the past two millennia. *Nat. Geosci.* 1, 697–702. <https://doi.org/10.1038/ngeo313>
- Marlon, J.R., Kelly, R., Daniiau, A.L., Vanni ere, B., Power, M.J., Bartlein, P., Higuera, P., Blarquez, O., Brewer, S., Br ucher, T., Feurdean, A., Romera, G.G., Iglesias, V., Yoshi Maezumi, S., Magi,

- B., Mustaphi, C.J.C., Zhihai, T., 2016. Reconstructions of biomass burning from sediment-charcoal records to improve data-model comparisons. *Biogeosciences* 13, 3225–3244. <https://doi.org/10.5194/bg-13-3225-2016>
- Mauquoy, D., Hughes, P.D.M., Geel, B. Van, 2010. A protocol for plant macrofossil analysis of peat deposits. *Mires Peat* 7, 1–5.
- McCarroll, J., Chambers, F.M., Webb, J.C., Thom, T., 2016. Using palaeoecology to advise peatland conservation: An example from West Arkengarthdale, Yorkshire, UK. *J. Nat. Conserv.* 30, 90–102. <https://doi.org/10.1016/J.JNC.2016.02.002>
- Mieczan, T., 2010. Vertical Micro-Zonation of Testate Amoebae and Ciliates in Peatland Waters in Relation to Potential Food Resources and Grazing Pressure. *Int. Rev. Hydrobiol.* 95, 86–102. <https://doi.org/10.1002/iroh.200911188>
- Minayeva, T., Bragg, O., Sirin, A., 2016. Peatland biodiversity and its restoration, in: Bonn, A., Allott, T., Evans, M., Joosten, H., Stoneman, R. (Eds.), *Peatland Restoration and Ecosystem Services: Science, Policy and Practice*. Cambridge University Press, pp. 44–62. <https://doi.org/10.1017/CBO9781139177788.004>
- Mooney, S.D., Tinner, W., 2011. The analysis of charcoal in peat and organic sediments. *Mires Peat* 7, 1–18.
- Moore, T.R., Dalva, M., 1993. The influence of temperature and water table position on carbon dioxide and methane emissions from laboratory columns of peatland soils. *J. Soil Sci.* 44, 651–664. <https://doi.org/10.1111/j.1365-2389.1993.tb02330.x>
- Morris, P.J., Baird, A.J., Belyea, L.R., 2012. The DigiBog peatland development model 2: ecohydrological simulations in 2D. *Ecohydrology* 5, 256–268. <https://doi.org/10.1002/eco.229>
- Morris, P.J., Baird, A.J., Young, D.M., Swindles, G.T., 2015. Untangling climate signals from autogenic changes in long-term peatland development. *Geophys. Res. Lett.* 42, 10,788–10,797. <https://doi.org/10.1002/2015GL066824>
- Morris, P.J., Swindles, G.T., Valdes, P.J., Ivanovic, R.F., Gregoire, L.J., Smith, M.W., Tarasov, L., Haywood, A.M., Bacon, K.L., 2018. Global peatland initiation driven by regionally asynchronous warming. *Proc. Natl. Acad. Sci. U. S. A.* 115, 4851–4856. <https://doi.org/10.1073/pnas.1717838115>
- Nelson, K., Thompson, D., Hopkinson, C., Petrone, R., Chasmer, L., 2021. Peatland-fire interactions: A review of wildland fire feedbacks and interactions in Canadian boreal peatlands. *Sci. Total Environ.* 769, 145212. <https://doi.org/10.1016/j.scitotenv.2021.145212>
- Ohlson, M., Korbøl, A., Økland, R.H., 2006. The macroscopic charcoal record in forested boreal peatlands in southeast Norway. *Holocene* 16, 731–741. <https://doi.org/10.1191/0959683606h1955rp>
- Olefeldt, D., Roulet, N., Giesler, R., Persson, A., 2013. Total waterborne carbon export and DOC composition from ten nested subarctic peatland catchments-importance of peatland cover, groundwater influence, and inter-annual variability of precipitation patterns. *Hydrol. Process.* 27, 2280–2294. <https://doi.org/10.1002/hyp.9358>
- Olefeldt, D., Roulet, N.T., 2012. Effects of permafrost and hydrology on the composition and transport of dissolved organic carbon in a subarctic peatland complex. *J. Geophys. Res. Biogeosciences* 117. <https://doi.org/10.1029/2011JG001819>

- Page, S.E., Baird, A.J., 2016. Peatlands and Global Change: Response and Resilience. *Annu. Rev. Environ. Resour.* 41, 35–57. <https://doi.org/10.1146/annurev-environ-110615-085520>
- Pan, Y., Birdsey, R.A., Fang, J., Houghton, R., Kauppi, P.E., Kurz, W.A., Phillips, O.L., Shvidenko, A., Lewis, S.L., Canadell, J.G., Ciais, P., Jackson, R.B., Pacala, S.W., McGuire, A.D., Piao, S., Rautiainen, A., Sitch, S., Hayes, D., 2011. A large and persistent carbon sink in the world's forests. *Science* (80-.). 333. <https://doi.org/10.1126/science.1201609>
- Payne, R.J., 2011. Can testate amoeba-based palaeohydrology be extended to fens? *J. Quat. Sci.* 26, 15–27. <https://doi.org/10.1002/jqs.1412>
- Piilo, S.R., Zhang, H., Garneau, M., Gallego-Sala, A., Amesbury, M.J., Väliranta, M.M., 2019. Recent peat and carbon accumulation following the Little Ice Age in northwestern Québec, Canada. *Environ. Res. Lett.* 14. <https://doi.org/10.1088/1748-9326/ab11ec>
- Power, M.J., Marlon, J., Ortiz, N., Bartlein, P.J., Harrison, S.P., Mayle, F.E., Ballouche, A., Bradshaw, R.H.W., Carcaillet, C., Cordova, C., Mooney, S., Moreno, P.I., Prentice, I.C., Thonicke, K., Tinner, W., Whitlock, C., Zhang, Y., Zhao, Y., Ali, A.A., Anderson, R.S., Beer, R., Behling, H., Briles, C., Brown, K.J., Brunelle, A., Bush, M., Camill, P., Chu, G.Q., Clark, J., Colombaroli, D., Connor, S., Daniau, A.L., Daniels, M., Dodson, J., Doughty, E., Edwards, M.E., Finsinger, W., Foster, D., Frechette, J., Gaillard, M.J., Gavin, D.G., Gobet, E., Haberle, S., Hallett, D.J., Higuera, P., Hope, G., Horn, S., Inoue, J., Kaltenrieder, P., Kennedy, L., Kong, Z.C., Larsen, C., Long, C.J., Lynch, J., Lynch, E.A., McGlone, M., Meeks, S., Mensing, S., Meyer, G., Minckley, T., Mohr, J., Nelson, D.M., New, J., Newnham, R., Noti, R., Oswald, W., Pierce, J., Richard, P.J.H., Rowe, C., Sanchez Goñi, M.F., Shuman, B.N., Takahara, H., Toney, J., Turney, C., Urrego-Sanchez, D.H., Umbanhowar, C., Vandergoes, M., Vanniere, B., Vescovi, E., Walsh, M., Wang, X., Williams, N., Wilmshurst, J., Zhang, J.H., 2008. Changes in fire regimes since the last glacial maximum: An assessment based on a global synthesis and analysis of charcoal data. *Clim. Dyn.* <https://doi.org/10.1007/s00382-007-0334-x>
- Qin, Y., Li, H., Mazei, Y., Kurina, I., Swindles, G.T., Bobrov, A., Tsyganov, A.N., Gu, Y., Huang, X., Xue, J., Lamentowicz, M., Marcisz, K., Roland, T., Payne, R.J., Mitchell, E.A.D., Xie, S., 2021. Developing a continental-scale testate amoeba hydrological transfer function for Asian peatlands. *Quat. Sci. Rev.* 258, 106868. <https://doi.org/10.1016/j.quascirev.2021.106868>
- Quillet, A., Garneau, M., Froking, S., 2013. Sobol' sensitivity analysis of the Holocene Peat Model: What drives carbon accumulation in peatlands? *J. Geophys. Res. Biogeosciences* 118, 203–214. <https://doi.org/10.1029/2012JG002092>
- Rius, D., Vannière, B., Galop, D., Richard, H., 2011. Holocene fire regime changes from multiple-site sedimentary charcoal analyses in the Lourdes basin (Pyrenees, France). *Quat. Sci. Rev.* 30, 1696–1709. <https://doi.org/10.1016/j.quascirev.2011.03.014>
- Roe, H.M., Elliott, S.M., Patterson, R.T., 2017. Re-assessing the vertical distribution of testate amoeba communities in surface peats: Implications for palaeohydrological studies. *Eur. J. Protistol.* 60, 13–27. <https://doi.org/10.1016/J.EJOP.2017.03.006>
- Rydin, H., Jeglum, J.K., 2006. *The Biology of Peatlands*. Oxford University Press, Oxford, UK. <https://doi.org/10.1093/acprof:oso/9780198528722.001.0001>
- Schuur, E.A.G., McGuire, A.D., Schädel, C., Grosse, G., Harden, J.W., Hayes, D.J., Hugelius, G., Koven, C.D., Kuhry, P., Lawrence, D.M., Natali, S.M., Olefeldt, D., Romanovsky, V.E., Schaefer, K., Turetsky, M.R., Treat, C.C., Vonk, J.E., 2015. Climate change and the permafrost carbon feedback. *Nature* 520, 171–179. <https://doi.org/10.1038/nature14338>
- Smith, P., Ashmore, M.R., Black, H.I.J., Burgess, P.J., Evans, C.D., Quine, T.A., Thomson, A.M., Hicks,

- K., Orr, H.G., 2013. The role of ecosystems and their management in regulating climate, and soil, water and air quality. *J. Appl. Ecol.* 50, 812–829. <https://doi.org/10.1111/1365-2664.12016>
- Swindles, G.T., Amesbury, M.J., Turner, T.E., Carrivick, J.L., Woulds, C., Raby, C., Mullan, D., Roland, T.P., Galloway, J.M., Parry, L., Kokfelt, U., Garneau, M., Charman, D.J., Holden, J., 2015a. Evaluating the use of testate amoebae for palaeohydrological reconstruction in permafrost peatlands. *Palaeogeogr. Palaeoclimatol. Palaeoecol.* 424, 111–122. <https://doi.org/10.1016/J.PALAEO.2015.02.004>
- Swindles, G.T., Morris, P.J., Baird, A.J., Blaauw, M., Plunkett, G., 2012. Ecohydrological feedbacks confound peat-based climate reconstructions. *Geophys. Res. Lett.* 39, L11401. <https://doi.org/10.1029/2012GL051500>
- Swindles, G.T., Morris, P.J., Mullan, D., Watson, E.J., Turner, T.E., Roland, T.P., Amesbury, M.J., Kokfelt, U., Schoning, K., Pratte, S., Gallego-Sala, A., Charman, D.J., Sanderson, N., Garneau, M., Carrivick, J.L., Woulds, C., Holden, J., Parry, L., Galloway, J.M., 2015b. The long-term fate of permafrost peatlands under rapid climate warming. *Sci. Rep.* 5, 17951. <https://doi.org/10.1038/srep17951>
- Swindles, G.T., Morris, P.J., Mullan, D.J., Payne, R.J., Roland, T.P., Amesbury, M.J., Lamentowicz, M., Turner, T.E., Gallego-Sala, A., Sim, T., Barr, I.D., Blaauw, M., Blundell, A., Chambers, F.M., Charman, D.J., Feurdean, A., Galloway, J.M., Gałka, M., Green, S.M., Kajukalo, K., Karofeld, E., Korhola, A., Lamentowicz, Ł., Langdon, P., Marcisz, K., Mauquoy, D., Mazei, Y.A., McKeown, M.M., Mitchell, E.A.D., Novenko, E., Plunkett, G., Roe, H.M., Schoning, K., Sillasoo, Ü., Tsyganov, A.N., van der Linden, M., Väliranta, M., Warner, B., 2019. Widespread drying of European peatlands in recent centuries. *Nat. Geosci.* 12, 922–928. <https://doi.org/10.1038/s41561-019-0462-z>
- Swindles, G.T., Morris, P.J., Wheeler, J., Smith, M.W., Bacon, K.L., Edward Turner, T., Headley, A., Galloway, J.M., 2016. Resilience of peatland ecosystem services over millennial timescales: evidence from a degraded British bog. *J. Ecol.* 104, 621–636. <https://doi.org/10.1111/1365-2745.12565>
- Swindles, G.T., Roland, T.P., Amesbury, M.J., Lamentowicz, M., McKeown, M.M., Sim, T.G., Fewster, R.E., Mitchell, E.A.D., 2020. Quantifying the effect of testate amoeba decomposition on peat-based water-table reconstructions. *Eur. J. Protistol.* 125693. <https://doi.org/10.1016/j.ejop.2020.125693>
- Tarnocai, C., Canadell, J.G., Schuur, E.A.G., Kuhry, P., Mazhitova, G., Zimov, S., 2009. Soil organic carbon pools in the northern circumpolar permafrost region. *Global Biogeochem. Cycles* 23, GB2023. <https://doi.org/10.1029/2008GB003327>
- Taylor, L.S., Swindles, G.T., Morris, P.J., Gałka, M., 2019. Ecology of peatland testate amoebae in the Alaskan continuous permafrost zone. *Ecol. Indic.* 96, 153–162. <https://doi.org/10.1016/J.ECOLIND.2018.08.049>
- Thompson, D.K., Simpson, B.N., Whitman, E., Barber, Q.E., Parisien, M.A., 2019. Peatland hydrological dynamics as a driver of landscape connectivity and fire activity in the Boreal plain of Canada. *Forests* 10. <https://doi.org/10.3390/f10070534>
- Treat, C.C., Jones, M.C., 2018. Near-surface permafrost aggradation in Northern Hemisphere peatlands shows regional and global trends during the past 6000 years. *The Holocene* 28, 998–1010. <https://doi.org/10.1177/0959683617752858>
- Treat, C.C., Jones, M.C., Camill, P., Gallego-Sala, A., Garneau, M., Harden, J.W., Hugelius, G., Klein,

- E.S., Kokfelt, U., Kuhry, P., Loisel, J., Mathijssen, P.J.H., O'Donnell, J.A., Oksanen, P.O., Ronkainen, T.M., Sannel, A.B.K., Talbot, J., Tarnocai, C., Väliranta, M., 2016. Effects of permafrost aggradation on peat properties as determined from a pan-Arctic synthesis of plant macrofossils. *J. Geophys. Res. Biogeosciences* 121, 78–94. <https://doi.org/10.1002/2015JG003061>
- Turetsky, M., Benscoter, B., Page, S., Rein, G., van der Werf, G.R., Watts, A., 2015. Global vulnerability of peatlands to fire and carbon loss. *Nat. Geosci.* 8, 11–14. <https://doi.org/10.1038/ngeo2325>
- Turetsky, M.R., Kane, E.S., Harden, J.W., Ottmar, R.D., Manies, K.L., Hoy, E., Kasischke, E.S., 2010. Recent acceleration of biomass burning and carbon losses in Alaskan forests and peatlands. *Nat. Geosci.* 2010 41 4, 27–31. <https://doi.org/10.1038/ngeo1027>
- Turetsky, M.R., Treat, C.C., Waldrop, M.P., Waddington, J.M., Harden, J.W., McGuire, A.D., 2008. Short-term response of methane fluxes and methanogen activity to water table and soil warming manipulations in an Alaskan peatland. *J. Geophys. Res. Biogeosciences* 113, G00A10. <https://doi.org/10.1029/2007JG000496>
- Väliranta, M., Blundell, A., Charman, D.J., Karofeld, E., Korhola, A., Sillasoo, Ü., Tuittila, E.-S., 2012. Reconstructing peatland water tables using transfer functions for plant macrofossils and testate amoebae: A methodological comparison. *Quat. Int.* 268, 34–43. <https://doi.org/10.1016/J.QUAINT.2011.05.024>
- Väliranta, M., Korhola, A., Seppä, H., Tuittila, E.S., Sarmaja-Korjonen, K., Laine, J., Alm, J., 2007. High-resolution reconstruction of wetness dynamics in a southern boreal raised bog, Finland, during the late Holocene: A quantitative approach. *Holocene* 17, 1093–1107. <https://doi.org/10.1177/0959683607082550>
- Väliranta, M., Marushchak, M.E., Tuovinen, J.-P., Lohila, A., Biasi, C., Voigt, C., Zhang, H., Piilo, S., Virtanen, T., Räsänen, A., Kaverin, D., Pastukhov, A., Sannel, A.B.K., Tuittila, E.-S., Korhola, A., Martikainen, P.J., 2021. Warming climate forcing impact from a sub-arctic peatland as a result of late Holocene permafrost aggradation and initiation of bare peat surfaces. *Quat. Sci. Rev.* 264, 107022. <https://doi.org/10.1016/j.quascirev.2021.107022>
- Väliranta, M., Salojärvi, N., Vuorsalo, A., Juutinen, S., Korhola, A., Luoto, M., Tuittila, E.S., 2017. Holocene fen–bog transitions, current status in Finland and future perspectives. *Holocene* 27, 752–764. <https://doi.org/10.1177/0959683616670471>
- Vannièrè, B., Blarquez, O., Rius, D., Doyen, E., Brücher, T., Colombaroli, D., Connor, S., Feurdean, A., Hickler, T., Kaltenrieder, P., Lemmen, C., Leys, B., Massa, C., Olofsson, J., 2016. 7000-year human legacy of elevation-dependent European fire regimes. *Quat. Sci. Rev.* 132, 206–212. <https://doi.org/10.1016/j.quascirev.2015.11.012>
- Veraverbeke, S., Delcourt, C.J.F., Kukavskaya, E., Mack, M., Walker, X., Hessilt, T., Rogers, B., Scholten, R.C., 2021. Direct and longer-term carbon emissions from arctic-boreal fires: A short review of recent advances. *Curr. Opin. Environ. Sci. Heal.* 23, 100277. <https://doi.org/10.1016/j.coesh.2021.100277>
- Waddington, J.M., Morris, P.J., Kettridge, N., Granath, G., Thompson, D.K., Moore, P.A., 2015. Hydrological feedbacks in northern peatlands. *Ecohydrology* 8, 113–127. <https://doi.org/10.1002/eco.1493>
- Waylen, K.A., van de Noort, R., Blackstock, K.L., 2016. Peatlands and cultural ecosystem services, in: Bonn, A., Allott, T., Evans, M., Joosten, H., Stoneman, R. (Eds.), *Peatland Restoration and Ecosystem Services: Science, Policy and Practice*. Cambridge University Press, pp. 114–128.

<https://doi.org/10.1017/CBO9781139177788.008>

- Wilmshurst, J.M., Wisser, S.K., Charman, D.J., 2003. Reconstructing Holocene water tables in New Zealand using testate amoebae: differential preservation of tests and implications for the use of transfer functions. *The Holocene* 13, 61–72. <https://doi.org/10.1191/0959683603hl595rp>
- Woodland, W.A., Charman, D.J., Sims, P.C., 1998. Quantitative estimates of water tables and soil moisture in Holocene peatlands from testate amoebae. *The Holocene* 8, 261–273. <https://doi.org/10.1191/095968398667004497>
- Worrall, F., Reed, M., Warburton, J., Burt, T., 2003. Carbon budget for a British upland peat catchment. *Sci. Total Environ.* 312, 133–146. [https://doi.org/10.1016/S0048-9697\(03\)00226-2](https://doi.org/10.1016/S0048-9697(03)00226-2)
- Xu, J., Morris, P.J., Liu, J., Holden, J., 2018a. PEATMAP: Refining estimates of global peatland distribution based on a meta-analysis. *CATENA* 160, 134–140. <https://doi.org/10.1016/J.CATENA.2017.09.010>
- Xu, J., Morris, P.J., Liu, J., Holden, J., 2018b. Hotspots of peatland-derived potable water use identified by global analysis. *Nat. Sustain.* 1, 246–253. <https://doi.org/10.1038/s41893-018-0064-6>
- Young, D.M., Baird, A.J., Gallego-Sala, A. V., Loisel, J., 2021. A cautionary tale about using the apparent carbon accumulation rate (aCAR) obtained from peat cores. *Sci. Rep.* 11, 9547. <https://doi.org/10.1038/s41598-021-88766-8>
- Yu, Z., Beilman, D.W., Jones, M.C., 2009. Sensitivity of Northern Peatland Carbon Dynamics to Holocene Climate Change. *Carbon Cycling in Northern Peatlands. Carbon Cycl. North. Peatlands* 184, 55–69. <https://doi.org/10.1029/2008GM000822>
- Yu, Z., Loisel, J., Brosseau, D.P., Beilman, D.W., Hunt, S.J., 2010. Global peatland dynamics since the Last Glacial Maximum. *Geophys. Res. Lett.* 37, L13402. <https://doi.org/10.1029/2010GL043584>
- Zhang, H., Amesbury, M.J., Ronkainen, T., Charman, D.J., Gallego-Sala, A. V., Välliranta, M., 2017. Testate amoeba as palaeohydrological indicators in the permafrost peatlands of north-east European Russia and Finnish Lapland. *J. Quat. Sci.* 32, 976–988. <https://doi.org/10.1002/jqs.2970>
- Zhang, H., Gallego-Sala, A. V., Amesbury, M.J., Charman, D.J., Piilo, S.R., Välliranta, M.M., 2018. Inconsistent response of Arctic permafrost peatland carbon accumulation to warm climate phases. *Global Biogeochem. Cycles* 32, 1605–1620. <https://doi.org/10.1029/2018GB005980>
- Zhang, H., Välliranta, M., Piilo, S., Amesbury, M.J., Aquino-López, M.A., Roland, T.P., Salminen-Paatero, S., Paatero, J., Lohila, A., Tuittila, E., 2020. Decreased carbon accumulation feedback driven by climate-induced drying of two southern boreal bogs over recent centuries. *Glob. Chang. Biol.* 26, 2435–2448. <https://doi.org/10.1111/gcb.15005>
- Zoltai, S.C., 1993. Cyclic Development of Permafrost in the Peatlands of Northwestern Alberta. *Arct. Alp. Res.* 25, 240–246. <https://doi.org/10.1080/00040851.1993.12003011>
- Zoltai, S.C., Pollett, F.C., 1983. Wetlands in Canada: Their Classification, Distribution, and Use, in: Gore, A.J.P. (Ed.), *Mires: Swamp, Bog, Fen and Moor*. Elsevier, Amsterdam, pp. 245–268.

**Chapter 2 – Ecology of peatland
testate amoebae in Svalbard and
the development of transfer
functions for reconstructing past
water-table depth and pH**

Ecology of peatland testate amoebae in Svalbard and the development of transfer functions for reconstructing past water-table depth and pH

Thomas G. Sim¹, Graeme T. Swindles^{2,3}, Paul J. Morris¹, Andy J. Baird¹, Dan J. Charman⁴, Matthew J. Amesbury⁴, Dave Beilman⁵, Alex Channon⁴ and Angela V. Gallego-Sala⁴

¹School of Geography, University of Leeds, Leeds, UK

²Geography, School of Natural and Built Environment, Queen's University Belfast, Belfast, UK

³Ottawa-Carleton Geoscience Centre and Department of Earth Sciences, Carleton University, Ottawa, Ontario, Canada

⁴Geography, College of Life and Environmental Sciences, University of Exeter, Exeter, UK

⁵Department of Geography and Environment, University of Hawaii Manoa, Honolulu, USA

Citation:

Sim, T.G., Swindles, G.T., Morris, P.J., Baird, A.J., Charman, D.J., Amesbury, M.J., Beilman, D., Channon, A., Gallego-Sala, A.V., 2021. Ecology of peatland testate amoebae in Svalbard and the development of transfer functions for reconstructing past water-table depth and pH. *Ecol. Indic.* 131, 108122. <https://doi.org/10.1016/j.ecolind.2021.108122>

Abstract

Peatlands are valuable archives of information about past environmental conditions and represent a globally-important carbon store. Robust proxy methods are required to reconstruct past ecohydrological dynamics in high-latitude peatlands to improve our understanding of change in these carbon-rich ecosystems. The High Arctic peatlands in Svalbard are at the northern limit of current peatland distribution and have experienced rapidly rising temperatures of 0.81°C per decade since 1958. We examine the ecology of peatland testate amoebae in surface vegetation samples from permafrost peatlands on Spitsbergen, the largest island of the Svalbard archipelago, and develop new transfer functions to reconstruct water-table depth (WTD) and pH that can be applied to understand past peatland ecosystem dynamics in response to climate change. These transfer functions are the first of their kind for peatlands in Svalbard and the northernmost developed to date. Multivariate statistical analysis shows that WTD and pore water pH are the dominant controls on testate amoeba species distribution. This finding is consistent with results from peatlands in lower latitudes with regard to WTD and supports work showing that when samples are taken across a long enough trophic gradient, peatland trophic status is an important control on the distribution of testate amoebae. No differences were found between transfer functions including and excluding the taxa with weak idiosomic siliceous tests (WISTs) that are most susceptible to decay. The final models for application to fossil samples therefore excluded these taxa. The WTD transfer function demonstrates the best performance ($R^2_{\text{LOO}} = 0.719$, $\text{RMSEP}_{\text{LOO}} = 3.2$ cm), but the pH transfer function also performs well ($R^2_{\text{LOO}} = 0.690$, $\text{RMSEP}_{\text{LOO}} = 0.320$). The transfer functions were applied to a core from western Spitsbergen and suggest drying conditions ~1750 CE, followed by a trend of recent wetting and increasing pH from ~1920 CE. These new transfer functions allow the reconstruction of past peatland WTD and pH in Svalbard, thereby enabling a greater understanding of long-term ecohydrological dynamics in these rapidly changing ecosystems.

2.1. Introduction

Peatlands and wetlands are widespread across the non-glaciated areas of the High Arctic (Walker et al., 2005) and represent a substantial carbon store, with soils holding an estimated 34 ± 16 Pg C (Hugelius et al., 2014). High-latitude regions in general are now warming at two to three times the global average rate (Masson-Delmotte et al., 2018) and High Arctic areas are especially vulnerable to Arctic amplification feedbacks (Serreze and Barry, 2011). There are growing concerns that warming temperatures will expose greater amounts of soil carbon to decomposition via deeper permafrost thaw and that warming will increase rates of microbial decomposition, leading to a positive feedback with climate (Koven et al., 2015; Schuur et al., 2015). Conversely, increases in productivity associated with longer and warmer growing seasons may result in greater carbon accumulation in peatlands at mid-latitudes and in particular at high-latitudes (Gallego-Sala et al., 2018). Hydrological conditions are likely to be crucial factors influencing the balance of decomposition and productivity in peatlands, with excessive drying linked to increased CO₂ production from aerobic decomposition and inundation associated with elevated CH₄ production and flux to the atmosphere (Evans et al., 2021; Lawrence et al., 2015; Olefeldt et al., 2013). Nonetheless, comparatively less is known about High Arctic peatland processes compared with those in Boreal and Subarctic regions. Improved understanding of autogenic factors relating to permafrost thaw, hydrological change, productivity and decomposition are crucial for better quantifying future peatland carbon dynamics (Sim et al., 2021; Waddington et al., 2015). It is therefore important that proxy methods for reconstructing past ecohydrological dynamics in High Arctic peatlands are developed and rigorously tested to increase understanding of ecosystem change and to inform future predictions.

Testate amoebae are single-celled protists found on the surface of peatlands and are routinely used as palaeoenvironmental indicators because of the rapid response they demonstrate to hydrological conditions and the resistance they show to decomposition (Booth et al., 2010; Charman et al., 2000). Transfer functions to reconstruct past hydrological conditions have been developed for a range of regions and peatland types (e.g. Amesbury et al., 2018, 2016; Charman et al., 2007; Qin et al., 2021). More specifically, a number of transfer functions have now been developed in discontinuous (Lamarre et al., 2013; Swindles et al., 2015; Zhang et al., 2017) and continuous (Taylor et al., 2019a) permafrost peatlands. Taylor et al. (2019a) also developed a transfer function for electrical conductivity as a proxy for trophic status. In addition, certain species with weak idiosomic siliceous tests (WISTs) preserve less well (Payne, 2007; Swindles and Roe, 2007). This differential preservation needs to be considered by researchers because it can

introduce taphonomic bias into transfer function reconstructions when WISTs are present in high abundance (Swindles et al., 2020).

Species diversity of testate amoebae is lower in High Arctic communities than lower latitude regions and there is thought to be a degree of regionalised distribution in taxa (Beyens and Bobrov, 2016). Previous studies have recorded the presence of testate amoebae in the contemporary and fossil records across the High Arctic (Beyens and Chardez, 1995; Sim et al., 2019) and specifically in Svalbard (Balik, 1994; Beyens et al., 1986c, 1986b, 1986a; Beyens and Chardez, 1987). However, the potential to use testate amoebae to reconstruct past hydrological conditions and/or trophic status for High Arctic peatlands with the development of transfer functions has yet to be fully explored.

In this paper we:

- i. Examine the contemporary ecology of testate amoebae in continuous permafrost peatlands in Svalbard.
- ii. Test the hypothesis that the contemporary distribution of testate amoeba species in Svalbard is primarily controlled by hydrological conditions.
- iii. Develop transfer functions that can be used to reconstruct the most important controls on testate amoeba distribution.
- iv. Examine the influence of excluding taxa with weak idiosomic siliceous tests (WISTs) on transfer function performance.
- v. Apply the transfer function(s) to an independent subfossil testate amoeba record from a peat profile in Svalbard.

2.2. Study region

Svalbard is a Norwegian archipelago in the Arctic Ocean between 74°N and 81°N, of which the largest island of Spitsbergen is our study region. The climate is moderated by the West Spitsbergen Current (Walczowski and Piechura, 2011). It is therefore considerably warmer than comparable latitudes in Canada and Russia, with a mean annual temperature of -4.6°C (averaging period 1981-2010) at Svalbard Airport near Longyearbyen (78.25°N, 15.47°E, 28 metres above sea level; Førland et al., 2011). Records for mean annual precipitation vary on a local scale with a mean annual precipitation (averaging period 1971-2000) of 196 mm at Svalbard Airport and 409 mm ~108 km north northwest at Ny-Ålesund (Hanssen-Bauer et al., 2019). Reanalysis temperature and precipitation data suggests our predominantly low-altitude sampling sites (Figure 2.1; Table 2.1) are likely to experience similar climatic conditions to those at Svalbard Airport (Vikhamar Schuler

and Østby, 2020). Ice-free areas in Svalbard are characterised by tundra with vegetation types including sedge, grass and brown-moss wetlands and dwarf-shrub and herbs (Walker et al., 2005). Soil cover in Svalbard is estimated to be around 10% with the majority of the landscape cover being ice (70%) or exposed rock (20%) (Hugelius et al., 2013). Despite this limited soil cover, ~5% of the land area of Svalbard (equivalent to ~50% of total soil cover) is estimated to be accumulating peat (Tanneberger et al., 2017) and long-term carbon accumulation rates of 9–19.2 g m⁻² yr⁻¹ have been recorded (Nakatsubo et al., 2015).

Composite temperature data from Svalbard Airport between 1899 and 2017 show a linear increase of 3.1°C per century despite cooler periods in the 1910s and 1960s, while reanalysis data for the whole of Svalbard show warming of 0.81°C per decade from 1958 to 2017 (Hanssen-Bauer et al., 2019; Vikhamar Schuler and Østby, 2020). Furthermore, ice-core temperature reconstructions suggest twentieth century warming is the greatest experienced in the past 600 years (Isaksson et al., 2003). The rapid nature of recent warming makes Svalbard an interesting area to study recent changes in peatland vegetation, hydrology and carbon dynamics. Moreover, under medium to high greenhouse gas emission scenarios the future climate of Svalbard (1971-2000 to 2071-2100) is projected to show an increase of 7-10°C in median annual temperature and a 45-65% increase in median annual precipitation (Hanssen-Bauer et al., 2019), potentially creating more favourable conditions for peat formation.

Scientists have studied testate amoebae in Svalbard since as early as the ninetieth century (Ehrenberg, 1870; Scourfield, 1897). Since then, pioneering researchers have investigated testate amoebae in a largely exploratory and descriptive manner (Awerinzew, 1907; Balik, 1994; Bonnet, 1965; Opravilova, 1989; Penard, 1903; Schönborn, 1966). More ecology-focused research in the 1980s found moisture content to be a key control on species distribution in lichens and mosses on Northwest Spitsbergen, with notable taxa including: *Corythion dubium*, *Centropyxis aerophila*, *Trinema lineare*, *Assulina muscorum*, *Phryganella acropodia* and *Euglypha rotunda* (Beyens et al., 1986c). In aquatic environments on Northwest Spitsbergen, *C. aerophila* and *Paraquadrula irregularis* were the most common species observed, with the former associated with more acid waters and the latter more alkaline (Beyens et al., 1986b). Additionally, samples from mosses and pools on Edgeøya documented the first occurrence on the Svalbard archipelago of the predominantly Arctic taxon *Conicocassis pontigulasiformis* (Beyens et al., 1986a). Changes in local hydrological conditions between ~5000 and 3800 BP have been inferred from testate amoeba preserved in peat layers on Edgeøya (Beyens and Chardez, 1987); however, the number of testate amoebae counted were extremely low and no statistical transfer function was used. More recent ecological work in Svalbard (Mazei et al., 2018) suggests a reduced abundance of *P. acropodia* and

C. aerophila in soils enriched with guano, tentatively linked with changing nutrient supply and the availability of fungal food sources.

2.3. Method

2.3.1. Sampling

In August 2019 we collected 103 surface vegetation samples from five permafrost peatland areas in Svalbard, encompassing a representative range of environmental conditions (Figure 2.1 and Table 2.1). Surface vegetation samples mainly comprised bryophytes, but also included sedges such as *Eriophorum* spp. and *Carex* spp. in hummock areas. Around 70% of Svalbard is covered by glaciers or permanent ice (Hugelius et al., 2013); therefore our study sampled a representative range of environments from the main ice-free area in Svalbard. The geology of the study region is predominantly characterised by the sandstones, siltstones and shales of the Central Tertiary Basin of Svalbard, with a shift to a limestone and dolostone bedrock towards the east in Sassendalen (Elvevold et al., 2007). Water-table depth (WTD) was determined by augering a well and measuring the water-table at regular intervals until it had stabilised. Both pH and electrical conductivity (EC) of the pore water in each augered well were measured using calibrated field meters. A peat core was extracted from a permafrost peatland of approximately 0.25 km² located on the valley floor towards the southern margin of the U-shaped valley of Colesdalen, Svalbard (78.09131°N, 14.98783°E). Analysis of this core provided a palaeo dataset of subfossil testate amoebae upon which to apply transfer functions. The core was sampled from a lawn area where the surface vegetation was characterised by Cyperaceae and brown mosses, including *Tomentypnum nitens* and *Aulacomnium palustre*. The core was extracted using a box corer to the base of the active layer (45 cm) and with a permafrost drill corer down to 91 cm.

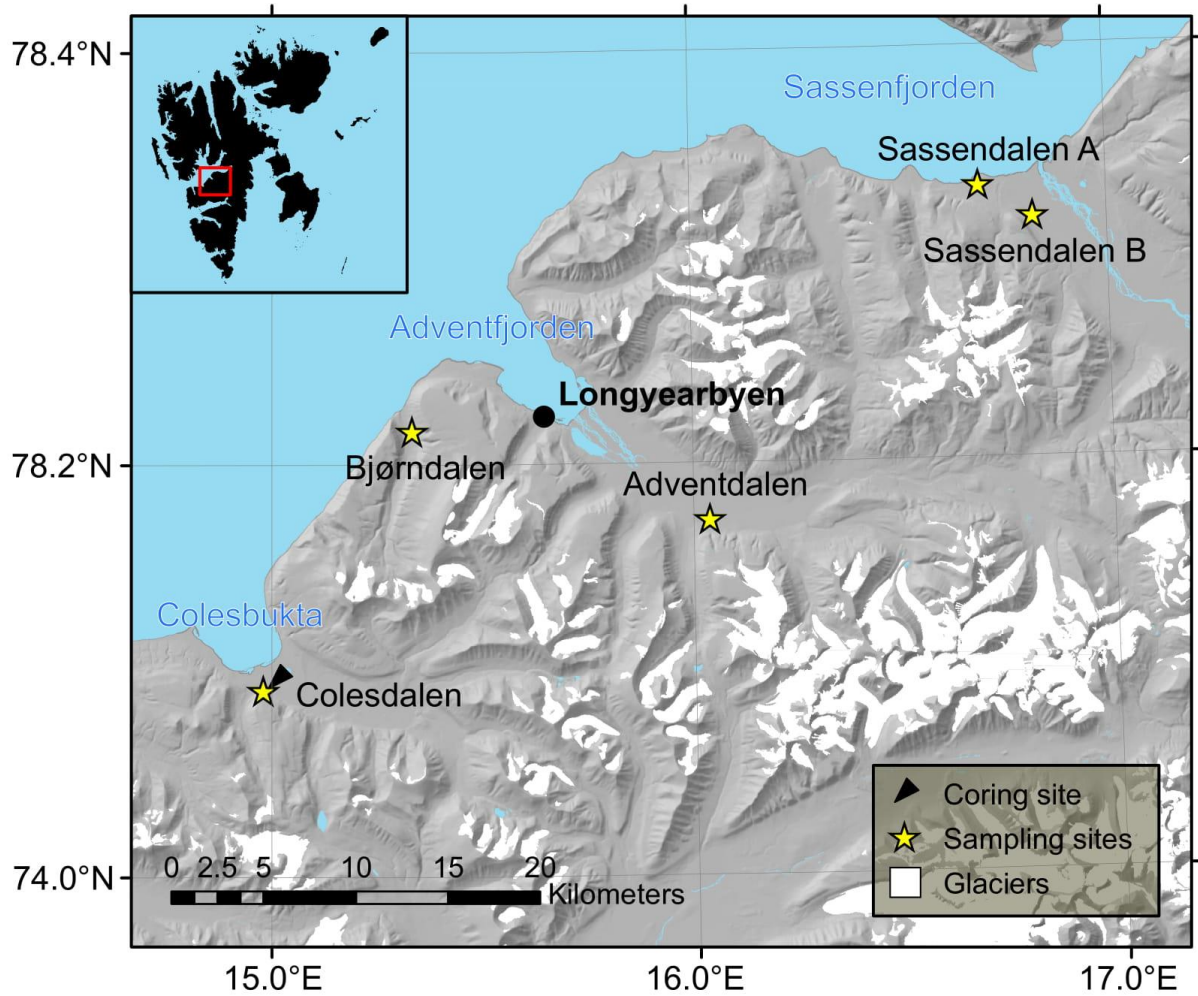


Figure 2.1. Site map showing locations for surface sampling and the coring site, alongside glacier coverage. Digital elevation model data and glacier coverage sourced from the Norwegian Polar Institute (2014a, 2014b).

Table 2.1. Site overview and environmental conditions. Coordinates are averaged for all surface samples taken at each site. Negative WTD values means surface inundation.

Site	Latitude (°N)	Longitude (°E)	Altitudinal range (m)	WTD range (cm)	MC range (%)	pH range	EC range ($\mu\text{S cm}^{-1}$)
Colesdalen	78.09099	14.97843	47-51	-2 to 22	60.1-95.8	5.15-6.75	108-360
Sassendalen A	78.33262	16.69365	11-14	-3 to 22	80.6-97.1	6.49-7.03	249-519
Sassendalen B	78.31682	16.82241	16-20	-1 to 34	63.7-89.1	6.72-8.22	237-1088
Bjørndalen	78.21644	15.33184	50-226	3 to 23	80.2-92.7	5.24-6.48	83-344
Adventdalen	78.17288	16.03754	27-28	-2 to 15	74.4-95.0	6.18-7.12	561-790

2.3.2. Surface vegetation and peat properties

From the surface vegetation samples, ~5 g of material for each sample was weighed, dried overnight at 105°C and then reweighed to calculate gravimetric moisture content (MC) (Chambers et al., 2011). The Colesdalen core was sub-sampled into 1-cm slices and pH measurements

were made of dry bulk density, loss-on-ignition (LOI) and concentrations of carbon (C) and nitrogen (N). Dry bulk density (g cm^{-3}) was calculated by dividing dry mass of peat (g; dried overnight at 105°C) by the total sample volume (cm^3), while LOI (%) was calculated by subtracting ash mass (g; after 8 hours in a 550°C furnace) from dry mass (g), before dividing this by dry mass and multiplying the product by 100 (Chambers et al., 2011). C and N contents were measured on a ThermoScientific Flash (2000) Series CHNS/O analyser.

2.3.3. Age-depth modelling

The chronology of the Colesdalen peat profile was determined using ^{210}Pb and ^{14}C dating methods. The ^{14}C dates ($n = 3$) were analysed from above ground plant macrofossils on a 3MV accelerator mass spectrometer (AMS) at the André E. Lalonde AMS Laboratory, University of Ottawa, Canada (Table A.1). The dates were calibrated using the IntCal20 calibration curve (Reimer et al., 2020) and an age-depth profile (Figure A.1) was constructed using the R package Plum (Aquino-López et al., 2018). Plum assumes a constant rate of supply (CRS) of ^{210}Pb within samples. However, unlike previous CRS models (Appleby, 2001; Appleby and Oldfield, 1978) Plum separates the age-depth modelling process from the ^{210}Pb decay equation and implements a Bayesian modelling approach using a self-adjusting Markov Chain Monte Carlo (MCMC) algorithm. This Bayesian modelling approach allows for better quantification of uncertainty in modelled dates and more robust integration of ^{210}Pb and ^{14}C dates. See Aquino-López et al. (2018) for full details.

2.3.4. Testate amoebae

Testate amoebae were prepared for analysis following Booth et al. (2010) for surface vegetation and peat core samples – palaeo-samples were analysed every other centimetre down core; i.e. a 1-cm layer, every 2 cm. Approximately 5 cm^3 of each surface vegetation sample and around 2 cm^3 for each palaeo-sample was boiled in water for 10 minutes, passed through a $300 \mu\text{m}$ sieve and then back-sieved through a $15 \mu\text{m}$ mesh. These processed samples were then stored at 4°C prior to examination under a high-powered, transmitted-light microscope at between 200 and $400\times$ magnification. A minimum of 100 individuals of taxa without weak idiosomic siliceous tests (WISTs) were counted per sample, with any WIST taxa recorded in addition. WISTs have been shown to preserve less favourably in peat as subfossils down core (Swindles et al., 2020) and within our study included: *Euglypha* spp., *Trinema* spp., *Corythion* spp., *Placocista spinosa* type, *Sphenodenria lenta* and *Tracheleuglypha denta*. In order to examine the influence of excluding WISTs, we conducted multivariate statistical analysis and developed transfer functions for the entire dataset including WISTs and then separately excluding WISTs. Testate amoebae were

identified where possible to species level, with reference to standard taxonomic materials (Charman et al., 2000; Siemensma, 2021).

2.3.5. Statistical analyses

Multivariate statistical analysis was undertaken in R version 3.6.3 (R Core Team, 2020) with the packages *vegan* (Oksanen et al., 2020) and *analogue* (Simpson and Oksanen, 2020) to explore the dataset and to examine the relationships between testate amoebae and environmental conditions. Taxa with a maximum abundance of less than 2% and fewer than five occurrences were excluded from multivariate analyses to reduce the influence of rare taxa (see Swindles et al., 2009). We performed ordination with Non-metric Multidimensional Scaling (NMDS) using the Bray-Curtis dissimilarity index. Additionally, Detrended Correspondence Analysis (DCA) showed that the data had a long axis length (DCA1 all taxa = 4.15; DCA1 WISTs removed = 4.71) suggesting heterogeneity in the data, high beta diversity and predominantly unimodal species distributions – consequently Canonical Correspondence Analysis (CCA) was then performed. CCA allowed us to partial out the amount of variance explained by specific environmental variables and to test the significance of each variable.

Transfer functions for WTD and pH were developed using the R package *rioja* (Juggins, 2020). The following common model types were applied: Weighted Averaging with tolerance downweighting (WA.tol) and without (WA), with the option for classical (cla) or inverse (inv) deshrinking, Weighted Averaging Partial Least Squares (WAPLS) and Maximum Likelihood (ML). These transfer function models were developed and cross-validated using the leave-one-out (LOO) method for the entire dataset and then with WIST taxa removed. The metrics $RMSEP_{LOO}$, R^2_{LOO} , average bias and maximum bias were used to evaluate transfer function performance. Model predictions generally had higher residual values towards the ends of the environmental gradients, especially for WTD. Therefore, in a second model run transfer functions were pruned of high residual values greater than 20% of the total range of measured WTD (> 7.4 cm) and pH (> 0.617). This cut-off point has been shown to strike a good balance between improving model performance and preserving the range of the environmental gradient for which a transfer function has predictive power (Amesbury et al., 2018, 2016, 2013; Booth, 2008; Charman et al., 2007; Payne et al., 2006; Swindles et al., 2015; Taylor et al., 2019a). Leave-one-site-out ($RMSEP_{LOSO}$) and segment-wise ($RMSEP_{SW}$) cross validation methods were applied to the pruned WTD and pH transfer function models with WISTs removed to further evaluate performance (Table 2.4; Figure A.2). Spatial autocorrelation analysis was not performed due to the limited geographical range of our sampling

region and the minimal effect this typically has on model performance (see Amesbury et al., 2018). Tolerance and optima statistics for WTD and pH were calculated for all taxa using WA.

The best performing transfer function models for WTD and pH were applied to a palaeo dataset of subfossil testate amoebae from the Colesdalen core. We compared our WTD reconstruction for the Colesdalen core with the outputs from other regional transfer function models: Subarctic Sweden (Swindles et al., 2015), pan-European (Amesbury et al., 2016), Arctic Alaska (Taylor et al., 2019a) and Subarctic Finland and West Russia (Zhang et al., 2017).

2.4. Results

2.4.1. Relationship between species distribution and environmental variables

A total of 60 testate amoeba taxa from 30 genera were identified in the surface vegetation samples from peatlands in Svalbard (Table 2.2), with a total count of 15,475 individuals. The species occurring in the most samples were *Centropyxis aerophila*, *Euglypha rotunda*, *Euglypha tuberculata*, *Trinema lineare*, *Euglypha strigosa*, *Diffflugia lucida* and *Diffflugia lithophila*. Other notable species occurring in fewer samples, but at a high maximum abundance were *Nebela tinctoria* (73.6%), *Cryptodiffugia oviformis* (68.6%), *Campascus minutus* (67%) and *Valkanovia elegans* (50.4%). CCA shows that pH, WTD and EC are the most important controls of testate amoeba distribution (Figure 2.2; Table 2.3). Partial CCAs when run for all taxa show pH explained 29.04% of variance ($p < 0.001$), WTD explained 24.99% ($p = 0.002$), EC explained 15.96% ($p < 0.001$) and MC explained 6.67% ($p = 0.344$). When WISTs are removed the amount of variance explained by environmental variables increased slightly, with pH explaining 33.06% ($p < 0.001$), WTD explaining 26.44% ($p < 0.001$), EC explaining 16.96% ($p < 0.001$) and MC explaining 5.92% ($p = 0.406$). NMDS analysis supports these findings, with all environmental variables – including MC – shown to be important controls on species distribution, both when run for all taxa and then with WISTs removed ($p < 0.001$; Figure 2.3; Table 2.3). NMDS suggests the most important environmental controls are WTD (all taxa $R^2 = 0.51$; WISTs removed $R^2 = 0.54$) and pH (all taxa $R^2 = 0.41$; WISTs removed $R^2 = 0.39$). Figure 2.3 highlights the association of the Sassendalen sites – underlain by a limestone bedrock – with a higher pH and Colesdalen – underlain by sandstones, siltstones and shales – with a slightly lower pH (Table 2.1).

Table 2.2. Overview of 60 testate amoebae taxa identified, type (testate amoeba = TA; taxa with a weak idiosomic siliceous test = WIST), number, max abundance and authority.

Taxon	Type	Code	In n samples	Max (%)	Authority
<i>Alabasta militaris</i>	TA	ALMI	2	0.6	Penard 1890; Duckert, Blandenier, Kosakyan and Singer 2018
<i>Arcella arenania</i>	TA	ARAR	8	5.5	Greef 1866
<i>Arcella catinus</i>	TA	ARCA	34	24.4	Penard 1890
<i>Arcella discooides</i>	TA	ARDI	49	46.6	Ehrenberg 1843
<i>Arcella hemisphaerica</i>	TA	ARHE	13	10.5	Perty 1852
<i>Archerella flavum</i>	TA	ARFL	23	45.4	Archer 1877; Loeblich and Tappan 1961
<i>Assulina muscorum</i>	TA	ASMU	35	35.6	Greeff 1888
<i>Assulina scandinavica</i>	TA	ASSC	3	1.4	Penard 1890
<i>Bullinularia indica</i>	TA	BUIN	1	1.7	Penard 1907
<i>Campascus minutus</i>	TA	CAMI	32	67.0	Penard 1902
<i>Centropyxis aculeata</i>	TA	CEAC	6	3.7	Ehrenberg 1838
<i>Centropyxis aerophila</i>	TA	CEAE	95	59.3	Deflandre 1929
<i>Centropyxis constricta</i>	TA	CECO	26	7.1	Ehrenberg 1841; Penard 1890
<i>Centropyxis gasparella</i>	TA	CEGA	5	2.8	Chardez, Beyens and De Bock 1988
<i>Centropyxis orbicularis</i>	TA	CEOR	9	3.7	Deflandre 1929
<i>Centropyxis plagiostoma</i>	TA	CEPLAG	11	1.6	Bonnet and Thomas 1955
<i>Centropyxis platystoma</i>	TA	CEPLAT	6	3.0	Penard 1890
<i>Centropyxis sylvatica</i>	TA	CESY	3	1.9	Deflandre 1929; Bonnet and Thomas 1955
<i>Coniococassis pontigulasiformis</i>	TA	COPO	28	22.3	Beyens, Chardez and De Bock 1986; Nasser and Anderson 2015
<i>Corythion constricta</i>	WIST	COCO	5	6.8	Certes 1889; Jung 1942
<i>Corythion dubium</i>	WIST	CODU	37	47.5	Taranek 1871
<i>Cryptodifflugia ovaliformis</i>	TA	CROV	55	68.6	Penard 1890
<i>Cyclopyxis arcelloides</i>	TA	CYAR	1	4.7	Penard 1902; Deflandre 1929
<i>Cyclopyxis eurostoma</i>	TA	CYEU	20	8.9	Deflandre 1929
<i>Cyclopyxis kahli</i>	TA	CYKA	1	1.3	Deflandre 1929
<i>Difflugia acuminata</i>	TA	DIAC	18	3.8	Ehrenberg 1838
<i>Difflugia globulosa</i>	TA	DIGL	26	29.0	Dujardin 1837; Penard 1902
<i>Difflugia lithophila</i>	TA	DILI	66	32.7	Penard 1902
<i>Difflugia lucida</i>	TA	DILU	70	34.5	Penard 1890
<i>Difflugia oblonga</i>	TA	DIOB	52	11.2	Ehrenberg 1838
<i>Difflugia penardi</i>	TA	DIPE	35	30.9	Hopkinson 1909
<i>Difflugia pristis type</i>	TA	DIPR	29	9.3	Penard 1902
<i>Difflugia pulex</i>	TA	DIPU	36	8.6	Penard 1902
<i>Difflugia pyriformis</i>	TA	DIPY	7	5.9	Perty 1849
<i>Difflugia rubescens</i>	TA	DIRU	12	8.4	Penard 1891
<i>Difflugia urceolata</i>	TA	DIUR	9	6.2	Carter 1864
<i>Euglyphya degraded</i>	WIST	EUDE	15	5.8	N/A
<i>Euglyphya laevis</i>	WIST	EULA	21	3.7	Ehrenberg 1845
<i>Euglyphya rotunda</i>	WIST	EURO	95	42.7	Ehrenberg 1845; Wailes and Penard 1911
<i>Euglyphya strigosa</i>	WIST	EUST	74	24.4	Ehrenberg 1848
<i>Euglyphya tuberculata</i>	WIST	EUTU	76	40.0	Dujardin 1841
<i>Gibbocarina galeata</i>	TA	GIGA	21	11.8	Penard 1890; Kosakyan et al. 2016
<i>Gibbocarina gracilis</i>	TA	GIGR	43	14.3	Penard 1910

<i>Heleopera petricola</i>	TA	HEPE	31	4.8	Leidy 1879
<i>Heleopera rosea</i>	TA	HERO	31	11.8	Penard 1890
<i>Heleopera sphagni</i>	TA	HESP	1	0.6	Leidy 1874
<i>Heleopera sylvatica</i>	TA	HESY	1	3.0	Penard 1890
<i>Hyalosphenia elegans</i>	TA	HYEL	1	0.9	Leidy 1874
<i>Hyalosphenia ovalis</i>	TA	HYOV	13	22.0	Wailes 1912
<i>Nebela collaris</i>	TA	NECO	36	15.8	Ehrenberg 1848; Kosakyan and Gomaa 2013
<i>Nebela tincta</i>	TA	NETI	48	73.6	Leidy 1979; Awerintzew 1906; Kosakyan et al. 2012
<i>Netzelia walesi</i>	TA	NEWA	5	8.4	Ogden 1980; Meisterfeld 1984
<i>Padaungiella lageniformis</i>	TA	PALA	38	17.3	Penard 1890
<i>Paraquadrula irregularis</i>	TA	PAIR	48	41.7	Wallich 1863
<i>Phryganella acropodia</i> type	TA	PHAC	53	20.5	Hertwig and Lesser 1874; Cash and Hopkinson 1909
<i>Placocista spinosa</i> type	WIST	PLSP	3	1.5	Penard 1899
<i>Planocarina marginata</i>	TA	PLMA	1	2.9	Penard 1902
<i>Pseudodiffugia fulva</i> type	TA	PSFU	3	0.9	Archer 1870
<i>Quadrullella symmetrica</i>	TA	QUSY	1	0.8	Wallich 1863; Schulze 1875; Kosakyan et al. 2016
<i>Sphenoderia lenta</i>	WIST	SPLE	1	0.8	Schlumberger 1845
<i>Tracheleuglypha denta</i>	WIST	TRDE	7	11.1	Vejdovsky 1882; Deflandre 1928
<i>Trigonopyxis arcula</i>	TA	TRGA	4	1.7	Penard 1912
<i>Trigonopyxis minuta</i>	TA	TRGM	2	1.0	Schönborn and Peschke 1988
<i>Trinema complanatum</i>	WIST	TRCO	5	2.4	Penard 1890
<i>Trinema enchelys</i>	WIST	TREN	19	4.4	Leidy 1878
<i>Trinema lineare</i>	WIST	TRLI	76	12.2	Penard 1890
<i>Valkanovia elegans</i>	TA	VAEL	53	50.4	Schönborn 1964
<i>Wailesella eboracensis</i>	TA	WAEB	17	21.0	Wailes and Penard 1911

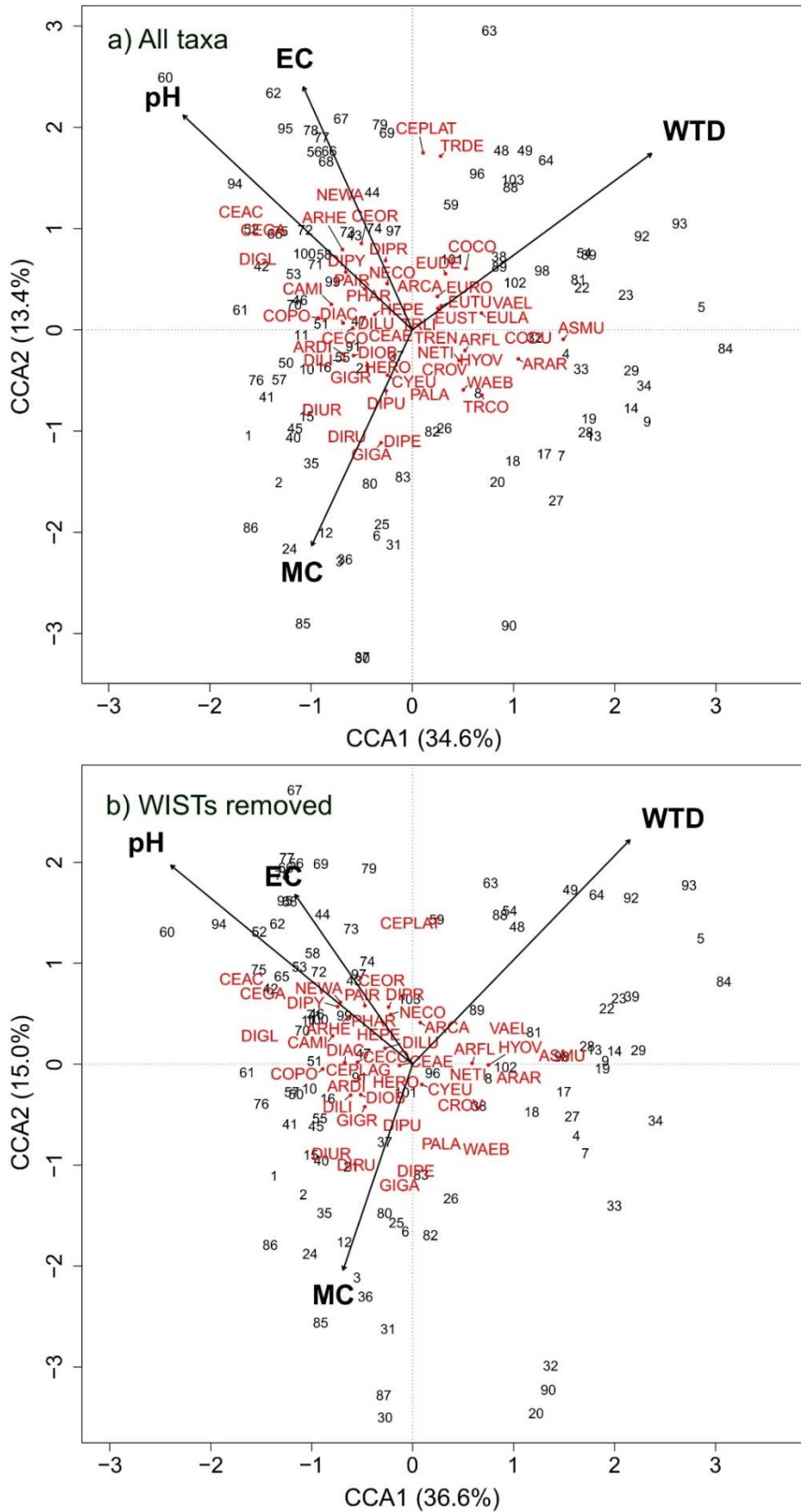


Figure 2.2. CCA of species, samples and environmental variables for a) all taxa and b) with WISTs removed. Species with fewer than five occurrences and a maximum abundance < 2% were removed. See Table 2.2 for species codes.

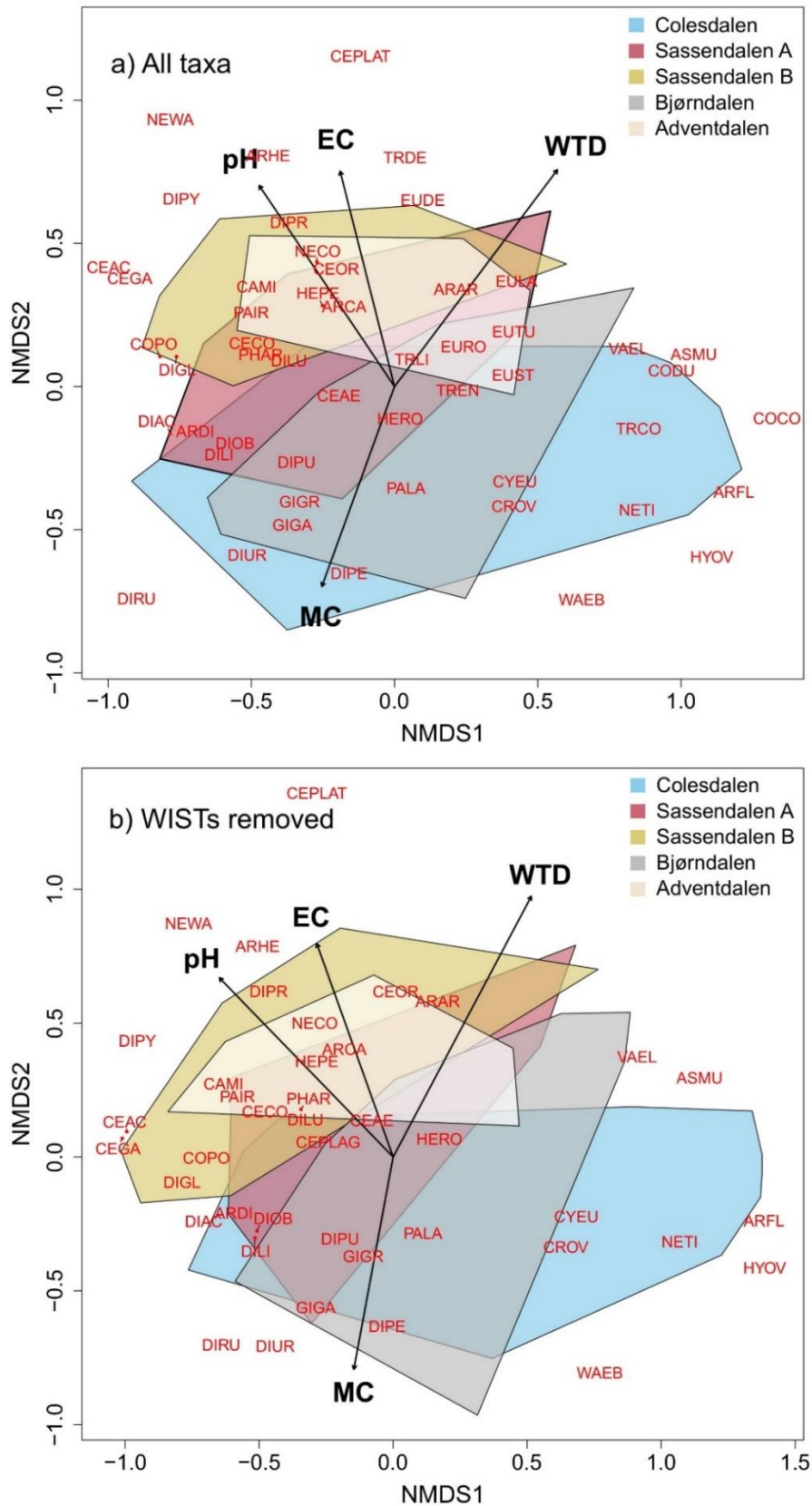


Figure 2.3. NMDS of species, samples and environmental variables for a) all taxa and b) with WISTs removed. Species with fewer than five occurrences and a maximum abundance < 2% removed. See Table 2.2 for species codes.

Table 2.3. Ordination statistics of environmental variables, both including and excluding taxa with weak idiosomic siliceous tests (WISTs).

<i>Environmental variables</i>	<i>pCCA</i>				<i>NMDS</i>							
	<i>pCCA all taxa</i>		<i>pCCA no WISTs</i>		<i>NMDS all taxa</i>				<i>NMDS no WISTs</i>			
	Variance explained (%)	Significance	Variance explained (%)	Significance	NMDS1	NMDS2	R ²	Significance	NMDS1	NMDS2	R ²	Significance
<i>EC</i>	15.96	p < 0.001	16.96	p < 0.001	-0.24482	0.96957	0.3446	p < 0.001	-0.33694	0.94153	0.3213	p < 0.001
<i>pH</i>	29.04	p < 0.001	33.06	p < 0.001	-0.55835	0.82961	0.4102	p < 0.001	-0.69611	0.71794	0.3896	p < 0.001
<i>MC</i>	6.67	p = 0.344	5.92	p = 0.406	-0.34161	-0.93984	0.3159	p < 0.001	-0.18209	-0.98328	0.2918	p < 0.001
<i>WTD</i>	24.99	p = 0.002	26.44	p < 0.001	0.60047	0.79965	0.5135	p < 0.001	0.46814	0.88366	0.5445	p < 0.001

2.4.2. Transfer function development

Transfer functions were developed for both WTD (TF_{WTD}) and pH (TF_{pH}) as both variables were highly significant environmental controls on testate amoeba species distribution in the ordination analysis. R^2_{LOO} and $RMSEP_{LOO}$ were used as the primary metrics to identify the best performing models. Models were run including all taxa (TF_{ALL}) and again with WISTs removed ($TF_{NO.WIST}$) and produced models of comparable performance (Table A.2). The $TF_{NO.WIST}$ iteration of the models for both TF_{WTD} and TF_{pH} was used because of concerns over the preservation of WISTs down core (Swindles et al., 2020), compounded by a complete absence of WISTs in our entire independent palaeo dataset of testate amoeba abundance analysed from Colesdalen core (see Figure 2.9). For $TF_{WTD-NO.WIST}$ with high residual values removed (residuals > 7.4 cm), all models showed lower $RMSEP_{LOSO}$ and $RMSEP_{SW}$ when compared to $RMSEP_{LOO}$, with the exception of ML (Table 2.4). All WA based models performed worse in wet (WTD < 0 cm) segments, while WA.cla and WA.cla.tol also performed poorly in the driest segment (WTD > 20 cm) (Figure A.2). The best performing model was component 2 of the WAPLS model ($R^2_{LOO} = 0.719$, $RMSEP_{LOO} = 3.20$ cm, $RMSEP_{LOSO} = 3.53$ cm, $RMSEP_{SW} = 3.39$ cm, average bias = 0.04 cm, maximum bias = 5.29 cm, $n = 85$; Table 2.4; Figure 2.6). ML models for $TF_{WTD-NO.WIST}$ demonstrated slightly higher R^2_{LOO} -values. However, the ML model had a greater number of high residual values (> 7.4 cm) in initial model runs and demonstrated slightly higher $RMSEP_{LOO}$ values (Table 2.4) – therefore the WAPLS model was preferred. $TF_{WTD-NO.WIST}$ performs well, but with a slight over prediction of low WTD values and slight under prediction of high WTD values. For the $TF_{WTD-NO.WIST}$ model three species with low maximum abundances (*Heleopera sylvatica* = 3%, *Hyalosphenia elegans* = 0.9% and *Pseudodiffugia fulva* type = 0.9%) were removed owing to high residual values. Clear dry indicator species include *Assulina muscorum*, *Corythion dubium* (WIST taxon), *Valkanovia elegans*, *Hyalosphenia ovalis* and *Archerella flavum*, while important wet indicator species include *Diffflugia rubescens*, *Diffflugia globulosa*, *Gibbocarina galeata*, *Arcella hemisphaerica* and *Diffflugia acuminata* (Figure 2.4). WTD optima and tolerance statistics for individual species are presented in Figure 2.7.

For $TF_{pH-NO.WIST}$ with high residual values removed (> 0.617), all models showed lower $RMSEP_{LOO}$ when compared to $RMSEP_{LOSO}$ and $RMSEP_{SW}$ (Table 2.4). The WA.inv, WA.inv.tol, WAPLS and ML models performed slightly worse in lowest pH segment (i.e. 5-5.49), yet the WA.cla and WA.cla.tol models were more consistent across a range of pH values (Figure A.2). The preferred model was WA with classical deshrinking and tolerance downweighting (WA.cla.tol) ($R^2_{LOO} = 0.690$, $RMSEP_{LOO} = 0.320$, $RMSEP_{LOSO} = 0.439$, $RMSEP_{SW} = 0.331$, average bias = 0.018, maximum bias = 0.316, $n = 70$; Table 2.4; Figure 2.6). WA with classical deshrinking (WA.cla) demonstrated a higher R^2_{LOO}

(0.771); however, WA.cl.tol required the removal of fewer high residual (> 0.617) values and was therefore preferred. For the $TF_{pH-NO.WIST}$ model two species with low maximum abundances (*Heleopera sylvatica* = 3% and *Quadrullella symmetrica* = 0.8%) were also removed due to high residual values. Peatland pH is generally linked with trophic status (Gorham et al., 1987; Lamentowicz et al., 2013) and is something considered further in the discussion section. High pH (more minerotrophic) indicator species include *Campascus minutus*, *Arcella catinus* and *Paraquadrula irregularis*, while lower pH (less minerotrophic) indicator species include *Wailesella eboracensis*, *Assulina muscorum* and *Hyalosphenia ovalis* (Figure 2.5). For pH some species demonstrate bimodal peaks in abundance at low and high pH levels; e.g., *Assulina muscorum* and *Corythion dubium* (Figure 2.5)

Table 2.4. Transfer function performance metrics for pruned WTD and pH models with WIST taxa removed. Root mean squared error of prediction (RMSEP) statistics are based on leave-one-out (RMSEP_{LoO}), leave-one-site-out (RMSEP_{LoSo}) and segment-wise (RMSEP_{Sw}) cross validation methods. Changes in model performance from RMSEP_{LoO} to both RMSEP_{LoSo} and RMSEP_{Sw} are given in parentheses.

TF _{WTD-NO.WIST}							
<i>Model</i>	RMSEP _{LoO}	RMSEP _{LoSo}	RMSEP _{Sw}	R ² _{LoO}	Avg. Bias	Max. Bias	<i>n</i>
<i>WA.inv</i>	3.697	4.617 (0.920)	4.027 (0.330)	0.634	0.001	6.028	88
<i>WA.cla</i>	4.303	4.740 (0.437)	4.782 (0.479)	0.652	0.074	8.633	67
<i>WA.inv.tol</i>	3.565	4.495 (0.930)	3.860 (0.295)	0.669	0.073	5.774	88
<i>WA.cla.tol</i>	4.299	5.110 (0.811)	4.596 (0.297)	0.653	0.217	9.551	70
<i>WAPLS.C2</i>	3.198	3.526 (0.328)	3.392 (0.194)	0.719	0.036	5.293	85
<i>ML</i>	3.776	3.669 (-0.107)	3.740 (-0.036)	0.721	0.276	3.05	74
TF _{pH-NO.WIST}							
<i>Model</i>	RMSEP _{LoO}	RMSEP _{LoSo}	RMSEP _{Sw}	R ² _{LoO}	Avg. Bias	Max. Bias	<i>n</i>
<i>WA.inv</i>	0.278	0.408 (0.131)	0.340 (0.062)	0.541	-0.002	0.553	85
<i>WA.cla</i>	0.271	0.347 (0.075)	0.279 (0.007)	0.771	0.002	0.343	61
<i>WA.inv.tol</i>	0.271	0.448 (0.177)	0.340 (0.069)	0.577	0.007	0.539	86
<i>WA.cla.tol</i>	0.32	0.439 (0.119)	0.331 (0.011)	0.69	0.018	0.316	70
<i>WAPLS.C2</i>	0.284	0.392 (0.107)	0.333 (0.049)	0.595	0	0.412	88
<i>ML</i>	0.3	0.521 (0.221)	0.357 (0.058)	0.619	-0.036	0.401	80

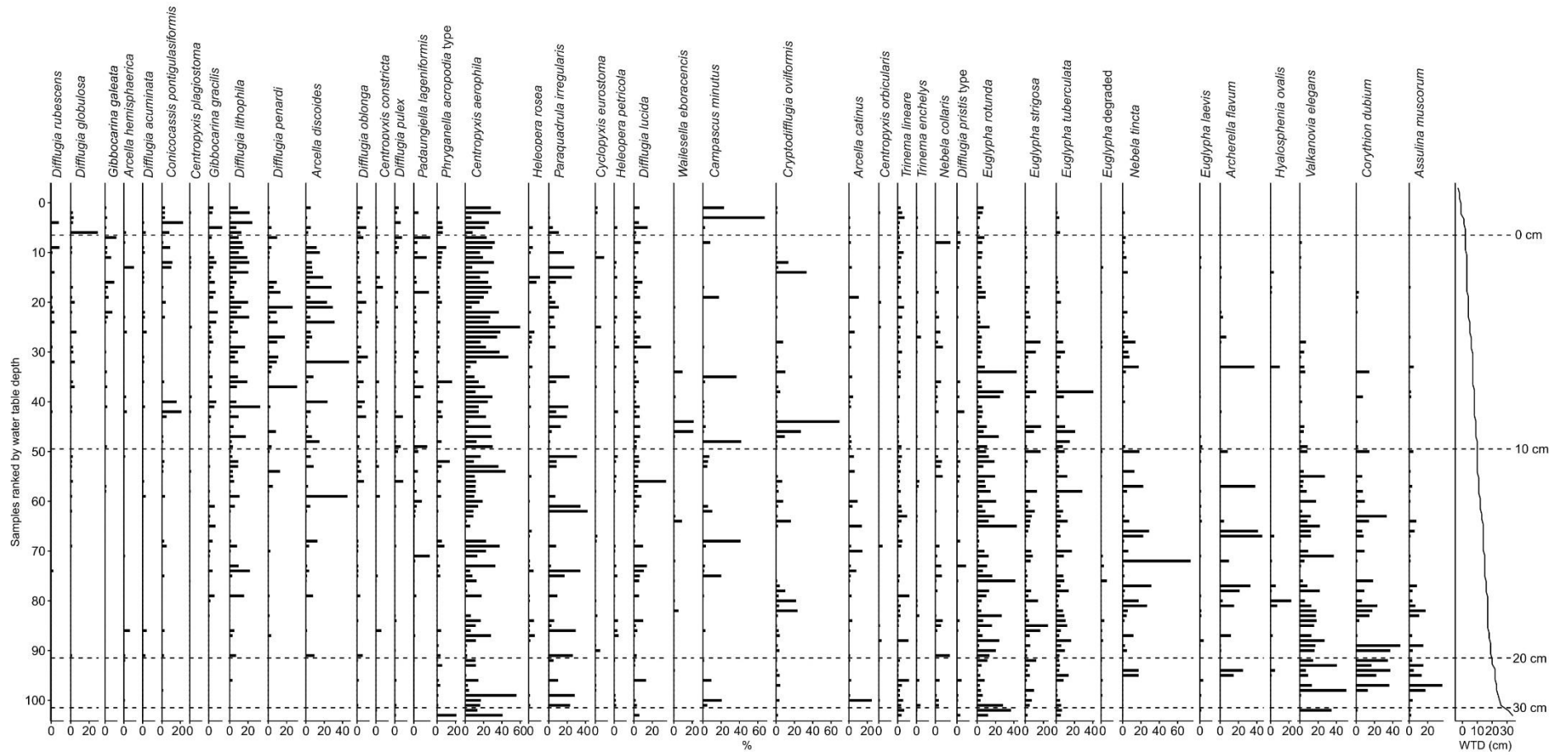


Figure 2.4. Abundance of selected testate amoeba taxa (at least 10 occurrences) ranked by observed water-table depth (WTD) indicating a range of WTD conditions. Dotted lines denote 10 cm intervals in measured WTD.

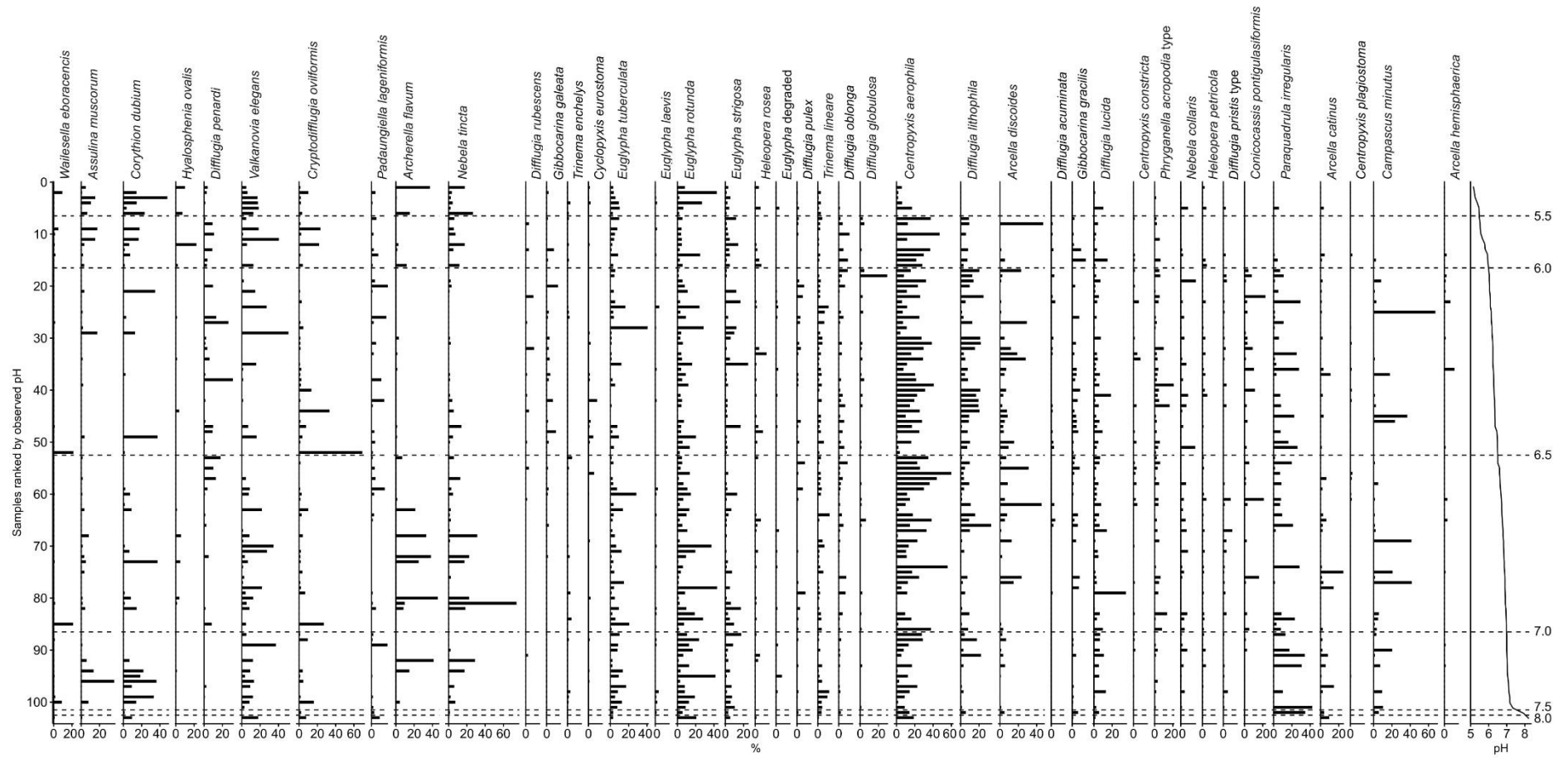


Figure 2.5. Abundance of selected testate amoeba taxa (at least 10 occurrences) ranked by observed pH indicating a range of pH conditions. Dotted lines denote 0.5 intervals in measured pH.

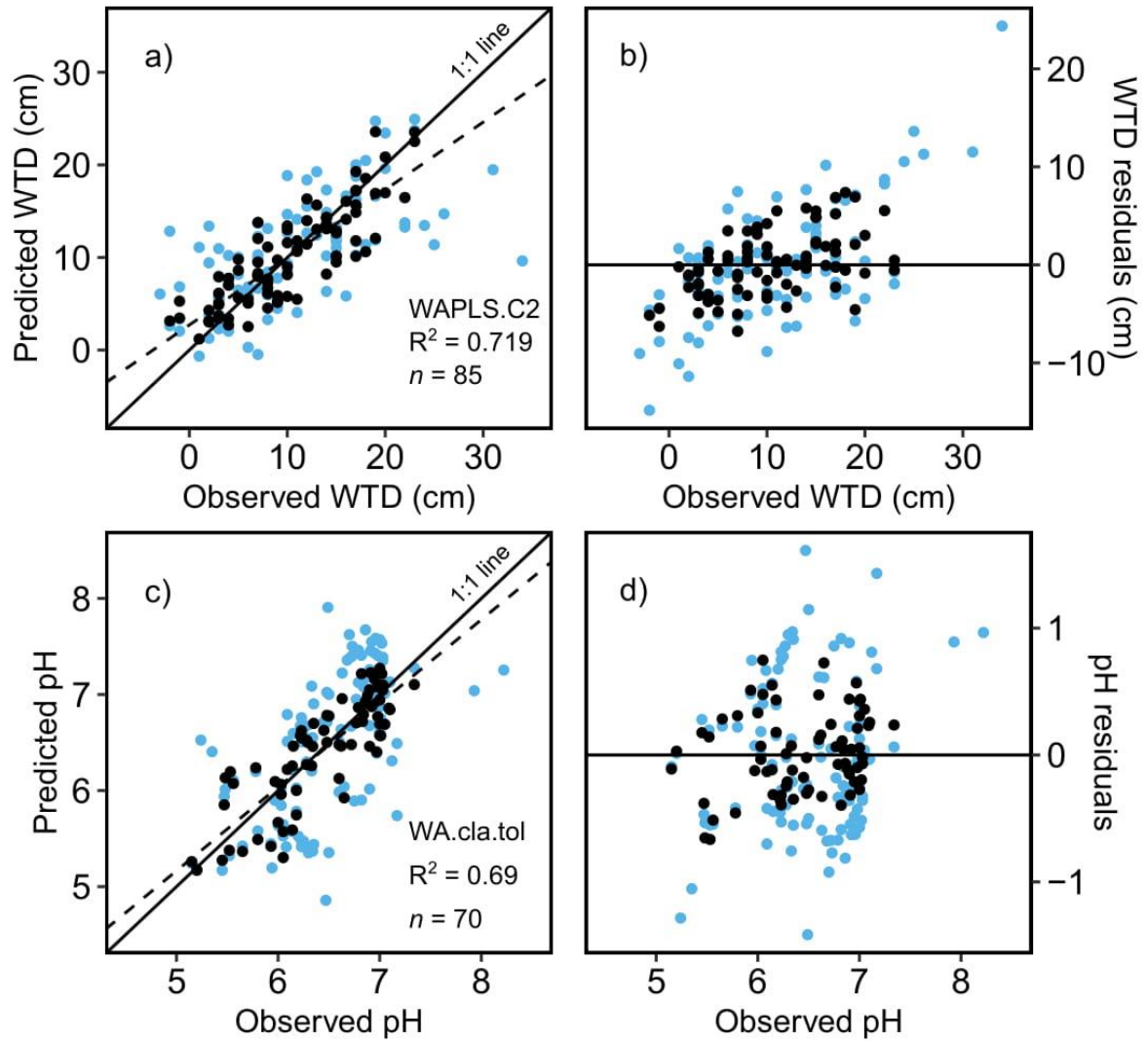


Figure 2.6. Transfer function performance. a) Observed and predicted water-table depth (WTD) for each site using the WAPLS.C2 model (WIST taxa removed) and b) residuals for each site against observed WTD. c) Observed and predicted pH for each site using the WA.cla.tol model (WIST taxa removed) and d) residuals for each site against observed pH. Blue-coloured points are model runs with all data and black-coloured points are model runs after the removal of samples with high residual values. Dotted lines represent the linear trends of the data points and solid lines represent 1:1 lines.

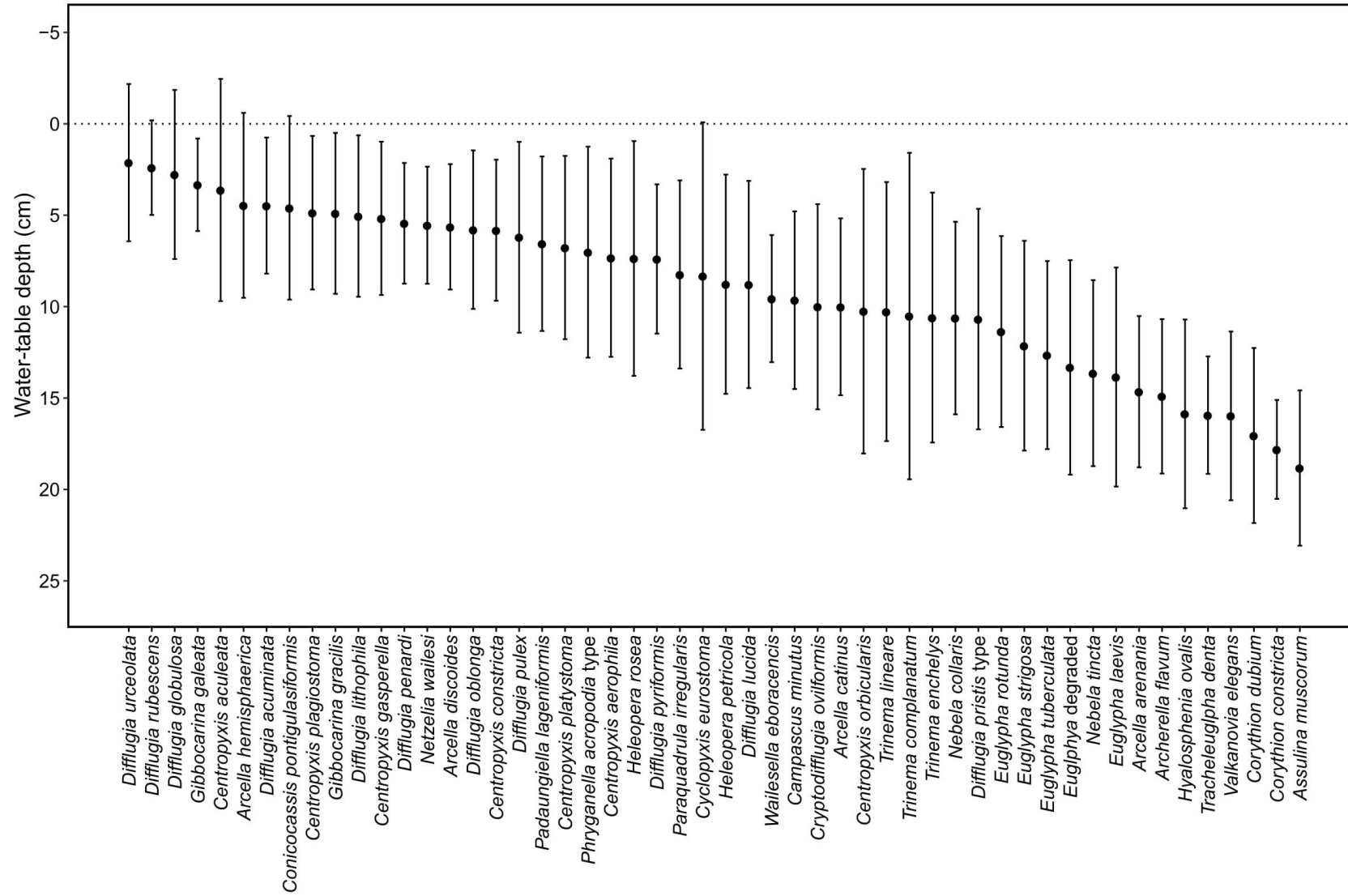


Figure 2.7. Water-table depth (WTD) optima and tolerance calculated through weighted averaging for taxa at least five occurrences.

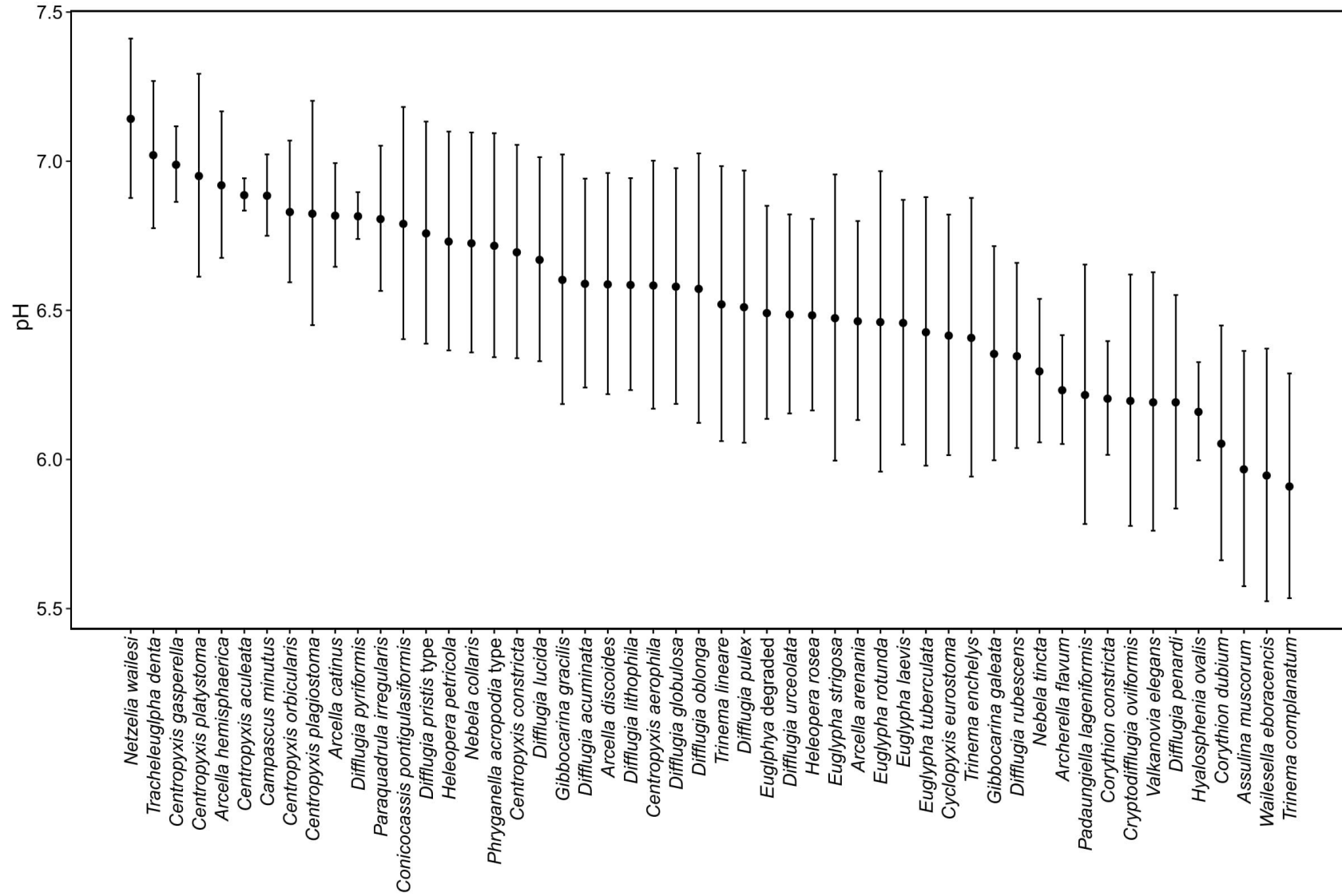


Figure 2.8. pH optima and tolerance calculated through weighted averaging for taxa at least five occurrences.

2.4.3. Transfer function application

The $TF_{WTD-NO.WIST}$ and $TF_{pH-NO.WIST}$ models (Figure 2.6) were applied to a peat core sampled in Colesdalen to reconstruct past WTD and pH from ~800 CE to present (Figure 2.9). The most common subfossil taxa present in the core include *Gibbocarina galeata*, *Gibbocarina gracilis*, *Conicocassis pontigulasiformis*, *Nebela tincta* and *Centropyxis aerophila*. Notably, there was a complete absence of WISTs in the palaeo record. Both $TF_{WTD-NO.WIST}$ and $TF_{pH-NO.WIST}$ transfer functions were applied with no missing analogues. The quality of analogues was tested by comparing maximum relative abundances of species in the palaeo and calibration datasets (Figure A.3). The majority of taxa demonstrate well constrained species optima (Hill's $N2 > 5$), including all taxa (with the exception of *Alablasta militaris*) showing a higher maximum abundance in the palaeo dataset than the calibration dataset.

The $TF_{WTD-NO.WIST}$ reconstruction shows a relatively stable WTD from the base of the core at ~800 CE to ~1500 CE cm, where there is a period of drying, followed by another dry period at ~1750 CE (Figure 2.9). This spike in WTD ~1750 CE is associated with increased abundance of *Nebela tincta* and a decrease in *Gibbocarina galeata*. From ~1750 CE onwards there is a general wetting trend, particularly from ~1920 CE. The $TF_{pH-NO.WIST}$ reconstruction shows a shift to lower pH conditions ~1400 CE, with the lowest pH value coinciding with the dry phase ~1750 CE. From ~1750 CE to present, pH fluctuates but demonstrates a general trend of an increasing pH with a slight lowering of pH from ~2000 CE onwards. There is a significant inverse relationship between WTD and pH ($p < 0.01$), with dry conditions associated with a lower pH and vice versa. Axis 1 scores from a DCA and NMDS analysis of the fossil data from the Colesdalen core correlate significantly with both WTD (DCA $p < 0.001$; NMDS $p < 0.001$) and pH (DCA $p < 0.001$; NMDS $p < 0.001$), suggesting both our reconstructions are good representations of changes in the structure of the fossil data (Figure A.4).

We compared the $TF_{WTD-NO.WIST}$ reconstruction of the Colesdalen core with transfer functions originally developed for other regions (Figure 2.10). There were a number of missing analogues for the Colesdalen core in the Subarctic Sweden ($n = 12$), pan-European ($n = 3$), Arctic Alaska ($n = 9$) and Subarctic Finland and West Russia ($n = 10$) calibration datasets (See Table A.3). The range in reconstructed WTD values is greater in transfer functions from other regions, in particular for Arctic Alaska (Figure 2.10a), yet reconstructed z-scores for the Svalbard transfer function are very similar to those from other regions (Figure 2.10b). In fact, WTD z-scores produced by $TF_{WTD-NO.WIST}$ correlate significantly with z-scores produced by the Subarctic Sweden ($p = 0.002$), pan-European ($p < 0.001$), Arctic Alaska ($p < 0.001$) and Subarctic Finland and West Russia ($p < 0.001$) models.

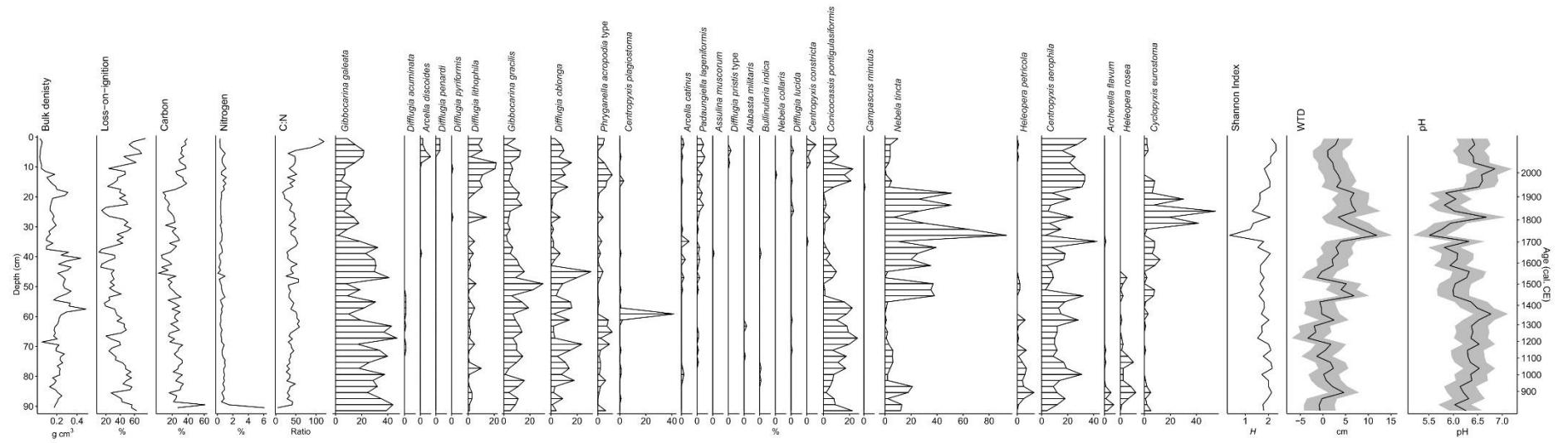


Figure 2.9. Stratigraphic diagram of testate amoeba abundance in the Colesdale core and best reconstructions for WTD and pH. Taxa ordered left (wetter) to right (drier) by WTD optima. Error based on 999 bootstrap cycles.

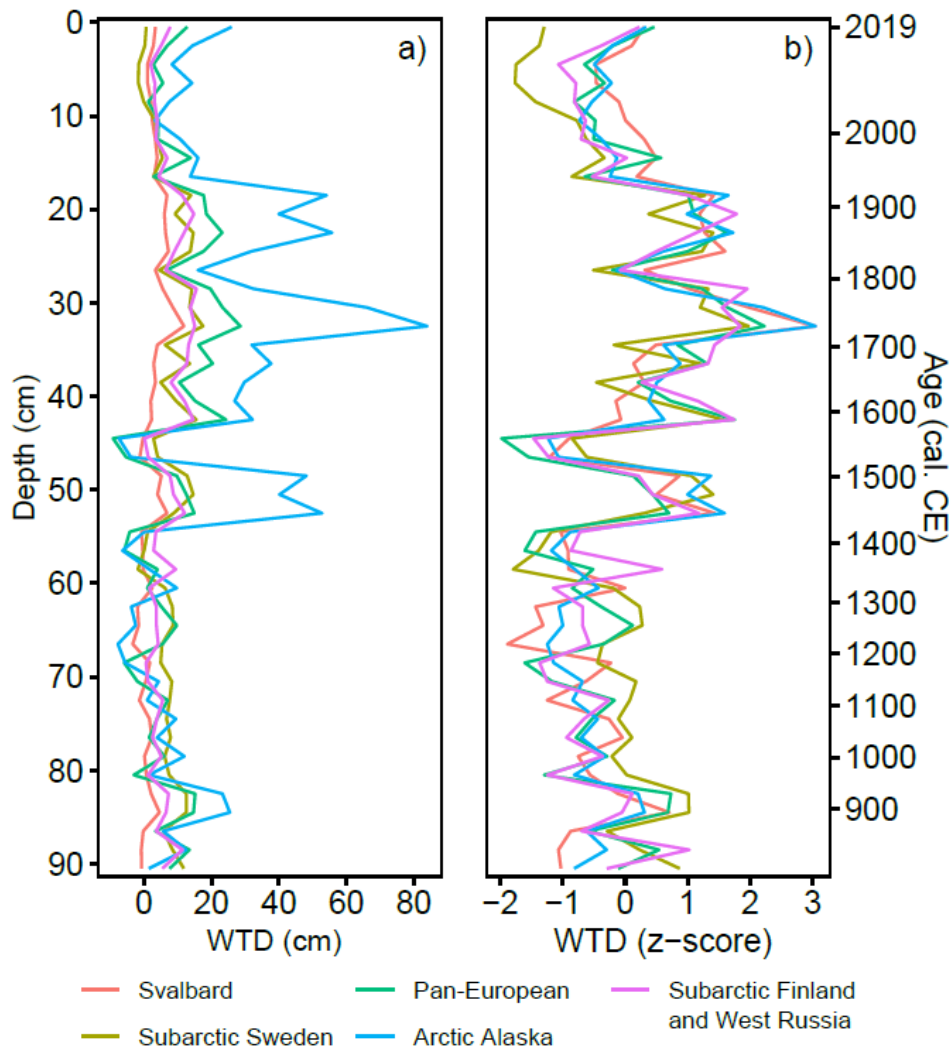


Figure 2.10. Comparison of WTD reconstructions for the Colesdalen core from different regional transfer functions: Svalbard (this study), Subarctic Sweden (Swindles et al., 2015), pan-European (Amesbury et al., 2016), Arctic Alaska (Taylor et al., 2019a) and Subarctic Finland and West Russia (Zhang et al., 2017). a) WTD reconstructions in cm, b) WTD reconstruction z-scores. Note – the year of sampling (2019) has been added to Age (cal. CE) y-axis to highlight the non-linearity of age-depth relationship.

2.5. Discussion

We developed the first testate amoeba transfer functions for peatlands in Svalbard, the northernmost study of its kind to date. Despite lower testate amoeba diversity being observed in the High Arctic (Beyens and Bobrov, 2016), we identified 60 testate amoeba taxa in surface vegetation samples (Table 2.2) – including the regionalised High Arctic taxa of *Centropyxis gasparella* and *Conicocassis pontigulasiformis*. In the palaeo core from Colesdalen spanning the period ~800 CE to present, 27 taxa were identified and species diversity was relatively stable down core (Figure 2.9). Furthermore, testate amoeba were abundant enough for the minimum count of 100 individuals in all palaeo samples. This diversity and abundance in both contemporary and palaeo samples is uncharacteristic of other High Arctic regions (e.g. Sim et al., 2019) and may be

as a result of the unusual climate of Svalbard for its latitude, which is moderated by the West Spitsbergen Current (Walczowski and Piechura, 2011).

2.5.1. Testate amoebae and water-table depth

We found that peatland WTD was a key control on testate amoeba species distribution in Svalbard (Figures 2.2 and 2.3; Table 2.3) and developed a palaeohydrological transfer function. The majority of taxa occupy WTD niches as expected from lower latitude peatlands (e.g. Amesbury et al., 2018, 2016; Charman et al., 2007; Qin et al., 2021) and other permafrost peatlands (e.g. Lamarre et al., 2013; Swindles et al., 2015a; Taylor et al., 2019a; Zhang et al., 2017). Nonetheless, we were able to better quantify the hydrological niches of High Arctic testate amoeba in Svalbard, building on initial pioneering studies from the twentieth century. We corroborate previous suggestions that *Assulina muscorum* prefers drier habitats in Svalbard (Beyens et al., 1986c) and that *Arcella hemisphaerica* is a predominantly wet taxon (Schönborn, 1966). Similarly, our data confirm previous observations from Svalbard suggesting *Centropyxis aerophila* occurs across both wet and dry habitats (Beyens et al., 1986c, 1986b). The predominantly Arctic taxa *Conicocassis pontigulasiformis* and *Centropyxis gasparella* (Beyens and Bobrov, 2016; Bobrov and Wetterich, 2012) were observed in our surface samples, both with a wet WTD optimum of ~5 cm (Figure 2.7). This WTD optimum for *C. pontigulasiformis* in Svalbard agrees with transfer function data from Arctic Alaska (Taylor et al., 2019a). Similarly, *C. gasparella* has been observed in standing water and wet mosses (Beyens et al., 1986b; Chardez and Beyens, 1988), but we present the first inclusion of this species in a transfer function.

2.5.2. Testate amoebae and trophic status (pH)

We found that pore water pH was an important control on testate amoeba species distribution (Figures 2.2 and 2.3; Table 2.3) and developed a transfer function to reconstruct past pH. Peatland pH has a strong relationship with trophic status; oligotrophic bogs are acidic, while minerotrophic poor fens and rich fens demonstrate an increasing alkalinity and concentration of dissolved minerals (see Gorham et al., 1987; Lamentowicz et al., 2013). In contrast to lower-latitudes, there are few true low pH bogs in the High Arctic (Woo and Young, 2006) and in Svalbard. Our contemporary sampling data showed a strong oligotrophic to minerotrophic gradient both within and between sampling sites, from poor fen to extremely rich fen conditions (Table 2.1). Poor fens are generally dominated by *Sphagnum* mosses and shrubs; moderately rich fens are characterised by brown mosses (e.g. *Drepanocladus* sp.) and sedges; while extremely rich fens also exhibit brown mosses (e.g. *Scorpidium* sp.) and sedges (Warner and Rubec, 1997). However, nutrient levels and pH will not always be coincident along a fen-bog gradient (Bridgham et al., 1996). For

example, phosphorus (P) concentrations are typically higher in fens than bogs, but rapid microbial mineralisation can result in similar levels of available P (Kellogg and Bridgham, 2003). Nonetheless, pH is a key control on bryophyte vegetation (Vitt and Chee, 1990) and an important characteristic used in the classification of wetland type (e.g. Tiner, 2016) – therefore, we suggest it is appropriate to use pH as a proxy for trophic status in the context of changing permafrost dynamics and shifting hydrological patterns.

The response of individual testate amoeba species to changing trophic conditions is predominantly in line with previous studies. Similarly to Taylor et al. (2019a), we found that *Gibbocarina galeata* and *Archerella flavum* were indicative of more oligotrophic conditions (Figure 2.8). We found that *Assulina muscorum* is abundant in more oligotrophic conditions supporting earlier work by Beyens et al. (1986c) and Mitchell (2004), but the taxon was also present in minerotrophic conditions (Figure 2.5) as was observed by Taylor et al. (2019a). *A. muscorum* has a clearly defined unimodal WTD optima and only appeared with more than 5% abundance in samples with a WTD over 13 cm (Figure 2.4), therefore suggesting hydrological conditions were the primary control on the distribution of this taxon. *Paraquadula irregularis* was more abundant in the more minerotrophic samples (Figures 2.5 and 2.8), corroborating previous observations from Svalbard (Beyens et al., 1986b). Nonetheless, *P. irregularis* occurred across a broad range of WTDs (Figure 2.4), suggesting species distribution is primarily driven by pH. It has been suggested that modification of surface soils by sea birds in Svalbard, linked partly to nutrient addition, may reduce the abundance of *Phyragrenella acropodia* and *Centropyxis aerophila* (Mazei et al., 2018). Nutrient levels were not directly measured in our study, but no clear abnormalities in abundance were observed. Both *P. acropodia* type ($n = 53$, max abundance = 20.5%) and *C. aerophila* ($n = 95$, max abundance = 59.3%) were common taxa in the surface samples (Table 2.2) and present across a broad range of both WTD and pH values (Figures 2.4 and 2.5).

2.5.3. Application of transfer functions

The pan-Europe (Amesbury et al., 2016), Subarctic Sweden (Swindles et al., 2015), Arctic Alaska (Taylor et al., 2019a) and Subarctic Finland and West Russia (Zhang et al., 2017) transfer functions were also applied to Colesdalen core and produced WTD reconstructions of higher magnitude shifts than the $TF_{WTD-NO.WIST}$ model (Figure 2.10a). The higher magnitude reconstructed WTD shifts in transfer functions from other regions was likely a result of a wider range of sampled WTD than those experienced in Svalbard, effectively stretching the gradient. When z-scores were standardised for each regional transfer function they all produced comparable reconstructions that correlated significantly with our reconstruction (Figure 2.10b). Nonetheless, there were a

number of missing modern analogues for the palaeo dataset in the transfer functions from other regions that were relatively abundant in peatlands in Svalbard (Table A.3). Notably, *C. pontigulasiformis* is absent from the Subarctic Sweden, pan-European and Subarctic Finland and West Russia transfer functions, while *Centropyxis plagiostoma* is absent across all other regional transfer functions. These are both relatively wet taxa (optima ~5 cm) and therefore when present in greater abundance in the fossil record, transfer functions experiencing missing analogues showed noticeable discrepancies in standardised values to our reconstruction, e.g. ~1200 CE (67 cm; Figure 2.10b). However, *C. plagiostoma* was not abundant in our calibration dataset ($n = 11$, max = 1.6%) and optima for both WTD and pH would likely be better defined with further sampling. Nonetheless, we suggest that WTD transfer function models from other regions are less applicable to peatlands in Svalbard, highlighting the importance of developing regional transfer functions – particularly in relatively unexplored environments.

The absence of taxa with weak idiosomic siliceous tests (WISTs) down core (Figure 2.9) and prevalence of degraded *Euglypha* spp. in surface samples (Table 2.1) evidences the poor preservation of these tests and echoes previous taphonomic concerns over the long-term preservations of WISTs in older peats (Payne, 2007; Swindles et al., 2020; Swindles and Roe, 2007). Removing WISTs had minimal impact on transfer function performance statistics (Table A.2) and actually slightly improved the degree of variance in species abundance explained by WTD and pH (Figure 2.2; Table 2.3). Therefore, we chose to use transfer functions excluding WISTs and can have confidence that the removal of WISTs retains the effectiveness of our transfer function models, while avoiding potential taphonomic issues. Testate amoebae diversity (Shannon Index) remains relatively consistent down the core (Figure 2.9), evidencing good preservation of non-WIST taxa. There is a drop in testate amoeba diversity ~1750 CE (33 cm), corresponding to a dominance of *Nebela tinctoria* (Figure 2.9). Yet, this period of reduced diversity does not correspond to any shift in peat physical or chemical properties (e.g. bulk density, C, N, LOI) that might indicate increased decomposition – suggesting genuine changes in WTD and pH are driving the shift in testate amoeba populations.

Peatland pH is strongly linked with trophic status (Gorham et al., 1987; Lamentowicz et al., 2013), therefore $TF_{\text{pH-NO.WIST}}$ is likely to be an effective proxy for interpreting past trophic conditions, particularly when paired with plant macrofossil analysis (see Väliranta et al., 2017). Payne (2011) raised concerns over the application of palaeohydrological transfer functions through periods of fen-bog transition in Mediterranean peatlands. However, in High Arctic Svalbard there is a narrower trophic gradient from poor to rich fen systems (Table 2.1) and WTD remains a significant control on species distribution across the entire pH range (Figures 2.2 and 2.3; Table 2.3),

therefore WTD reconstructions in Svalbard are likely to be more robust. Furthermore, RMSEP_{sw} analysis suggests $TF_{\text{pH-NO}_3\text{WIST}}$ (WA.cla.tol) performs consistently across a range of pH values (Figure A.2). Thus, application of $TF_{\text{pH-NO}_3\text{WIST}}$ and $TF_{\text{WTD-NO}_3\text{WIST}}$ enables the reconstruction of peatland dynamics during the Holocene, including indications of changing trophic status – echoing similar findings from peatlands in Arctic Alaska (Taylor et al., 2019b).

The significant inverse correlation between reconstructed WTD and pH for the Colesdalen core ($p < 0.01$; Figure 2.9) raises interesting questions over ecosystem and catchment dynamics. Specifically, recent wetting from ~1920 CE in the Colesdalen core corresponds to a shift to more minerotrophic conditions. Increases in precipitation across Svalbard in the twentieth century (Førland et al., 2011) may partially explain recent wetting. Similarly, the reorganisation of drainage systems caused by glacial retreat is associated with increased chemical weathering and higher meltwater pH in Svalbard (Nowak and Hodson, 2014). The Colesdalen core is located towards the edge of a U-shaped valley (Figure 2.1) and can be expected to receive both surface and groundwater flow from the surrounding catchment. Sandstones of the Central Tertiary Basin underlying Colesdalen are rich in feldspar and have a carbonate cement (Schlegel et al., 2013). Consequently, greater chemical weathering in the Colesdalen catchment as a result of changing drainage patterns linked to ice retreat, and increases in precipitation, offer potential explanations for recent increases in peatland wetness and pH.

2.5.4. Future research

The development of these transfer functions for WTD and pH opens up the possibility for comprehensive multiproxy palaeoecological reconstructions in Svalbard. Moreover, application of these transfer function models will be useful in examining the response of Svalbard's peatlands to rapid climate change during the twentieth century. Other avenues for future research could work to better quantify the influence of birds on soil nutrients and testate amoeba species in Svalbard (see Mazei et al., 2018), investigate the influence of increased salinity from salt spray or storm inundation on testate amoebae diversity and richness (see Swindles et al., 2018) and look to add regional transfer function data from higher-latitude peatlands to an updated pan-European transfer function model (Amesbury et al., 2016). Improved ecohydrological understanding of these ecosystems in recent decades, centuries and millennia will enable more thorough testing of hypotheses relating to increased productivity and expansion of high-latitude peatlands with warming (e.g. Gallego-Sala et al., 2018). Therefore, a study across multiple sites focusing on peatland ecohydrological and carbon dynamics in Svalbard during the Holocene would be particularly valuable.

2.6. Conclusions

1. We present the first testate amoebae transfer functions for reconstructing WTD and pH in peatlands in Svalbard, the northernmost study of its kind to date.
2. The majority of testate amoebae occupy WTD niches as expected from lower-latitude studies, although we were able to better quantify the hydrological niches of regionalised High Arctic taxa, e.g. *Centropyxis gasparella* and *Conicocassis pontigulasiformis*.
3. Pore water pH was a significant control on testate amoeba species distribution and a proxy for trophic status – therefore our transfer function can be used to reliably reconstruct changes in past peatland pH in the context of changing permafrost dynamics and shifting hydrological patterns.
4. WISTs appear to preserve poorly in these peatlands, yet removal of WISTs from our transfer function models had minimal impact upon their performance. Therefore, we were able to confidently remove WISTs from our models to avoid potential taphonomic problems and recommend excluding them from minimum sample counts.
5. These transfer functions are valuable tools for multiproxy reconstructions investigating the response of peatlands in Svalbard to Holocene climate change and have the potential to improve understanding of long-term ecohydrological dynamics in these rapidly changing carbon-rich ecosystems.

Acknowledgments

T.G.S. is in receipt of a UK Natural Environment Research Council Training Grant, NE/L002574/1. A.G.S., D.C. and A.C. acknowledge funding support from a UK Natural Environment Research Council Grant, NE/S001166/1 (ICAAP: Increasing Carbon Accumulation in Arctic Peatlands). We thank Macro Aquino-López and Maarten Blaauw for useful discussions regarding age-depth modelling. We also thank Xavier Comas for valuable assistance with fieldwork.

References

- Amesbury, M.J., Booth, R.K., Roland, T.P., Bunbury, J., Clifford, M.J., Charman, D.J., Elliot, S., Finkelstein, S., Garneau, M., Hughes, P.D.M., Lamarre, A., Loisel, J., Mackay, H., Magnan, G., Markel, E.R., Mitchell, E.A.D., Payne, R.J., Pelletier, N., Roe, H., Sullivan, M.E., Swindles, G.T., Talbot, J., van Bellen, S., Warner, B.G., 2018. Towards a Holarctic synthesis of peatland testate amoeba ecology: Development of a new continental-scale palaeohydrological transfer function for North America and comparison to European data. *Quat. Sci. Rev.* 201, 483–500. <https://doi.org/10.1016/j.quascirev.2018.10.034>
- Amesbury, M.J., Mallon, G., Charman, D.J., Hughes, P.D.M., Booth, R.K., Daley, T.J., Garneau, M., 2013. Statistical testing of a new testate amoeba-based transfer function for water-table depth reconstruction on ombrotrophic peatlands in north-eastern Canada and Maine, United States. *J. Quat. Sci.* 28, 27–39. <https://doi.org/10.1002/jqs.2584>
- Amesbury, M.J., Swindles, G.T., Bobrov, A., Charman, D.J., Holden, J., Lamentowicz, M., Mallon, G., Mazei, Y., Mitchell, E.A.D., Payne, R.J., Roland, T.P., Turner, T.E., Warner, B.G., 2016. Development of a new pan-European testate amoeba transfer function for reconstructing peatland palaeohydrology. *Quat. Sci. Rev.* 152, 132–151. <https://doi.org/10.1016/J.QUASCIREV.2016.09.024>
- Appleby, P.G., 2001. Chronostratigraphic Techniques in Recent Sediments, in: *Tracking Environmental Change Using Lake Sediments*. Kluwer Academic Publishers, pp. 171–203. https://doi.org/10.1007/0-306-47669-x_9
- Appleby, P.G., Oldfield, F., 1978. The calculation of lead-210 dates assuming a constant rate of supply of unsupported ^{210}Pb to the sediment. *Catena* 5, 1–8. [https://doi.org/10.1016/S0341-8162\(78\)80002-2](https://doi.org/10.1016/S0341-8162(78)80002-2)
- Aquino-López, M.A., Blaauw, M., Christen, J.A., Sanderson, N.K., 2018. Bayesian Analysis of ^{210}Pb Dating. *J. Agric. Biol. Environ. Stat.* 23, 317–333. <https://doi.org/10.1007/s13253-018-0328-7>
- Awerinzew, S., 1907. Über einige Süßwasser-Protozoen der Bäreninsel. *Zool. Anz.* 31, 243–247.
- Balik, V., 1994. On the Soil Testate Amoebae Fauna (Protozoa: Rhizopoda) of the Spitsbergen Islands (Svalbard). *Arch. für Protistenkd.* 144, 365–372. [https://doi.org/10.1016/S0003-9365\(11\)80239-3](https://doi.org/10.1016/S0003-9365(11)80239-3)
- Beyens, L., Bobrov, A., 2016. Evidence supporting the concept of a regionalized distribution of testate amoebae in the Arctic. *Acta Protozool.* 55, 197–209. <https://doi.org/10.4467/16890027AP.16.019.6006>
- Beyens, L., Chardez, D., 1995. An Annotated List of Testate Amoebae Observed in the Arctic between the Longitudes 27° E and 168° W. *Arch. für Protistenkd.* 146, 219–233. [https://doi.org/10.1016/S0003-9365\(11\)80114-4](https://doi.org/10.1016/S0003-9365(11)80114-4)
- Beyens, L., Chardez, D., 1987. Evidence from testate amoebae for changes in some local hydrological conditions between c. 5000 BP and c. 3800 BP on Edgeøya (Svalbard). *Polar Res.* 5, 165–169. <https://doi.org/10.3402/polar.v5i2.6873>
- Beyens, L., Chardez, D., De Bock, P., 1986a. Some new and rare testate amoebae from the Arctic.

- Acta Protozool. 25, 81–91.
- Beyens, L., Chardez, D., De Landtsheer, R., De Baere, D., 1986b. Testate amoebae communities from aquatic habitats in the Arctic. *Polar Biol.* 6, 197–205. <https://doi.org/10.1007/BF00443396>
- Beyens, L., Chardez, D., De Landtsheer, R., De Bock, P., Jacques, E., 1986c. Testate amoebae populations from moss and lichen habitats in the Arctic. *Polar Biol.* 5, 165–173. <https://doi.org/10.1007/BF00441696>
- Bobrov, A.A., Wetterich, S., 2012. Testate amoebae of Arctic tundra landscapes. *Protistology* 7, 51–58.
- Bonnet, L., 1965. Sur le peuplement thécamoebien de quelques sols du Spitsberg. *Bull. la Société d'Histoire Nat. Toulouse* 100, 281–293.
- Booth, R.K., 2008. Testate amoebae as proxies for mean annual water-table depth in Sphagnum-dominated peatlands of North America. *J. Quat. Sci.* 23, 43–57. <https://doi.org/10.1002/jqs.1114>
- Booth, R.K., Lamentowicz, M., Charman, D.J., 2010. Preparation and analysis of testate amoebae in peatland palaeoenvironmental studies. *Mires Peat* 7, 1–7.
- Bridgham, S.D., Pastor, J., Janssens, J.A., Chapin, C., Malterer, T.J., 1996. Multiple limiting gradients in peatlands: A call for a new paradigm. *Wetlands* 16, 45–65. <https://doi.org/10.1007/BF03160645>
- Chambers, F.M., Beilman, D.W., Yu, Z., 2011. Methods for determining peat humification and for quantifying peat bulk density, organic matter and carbon content for palaeostudies of climate and peatland carbon dynamics. *Mires Peat* 7, 1–10.
- Chardez, D., Beyens, L., 1988. *Centropyxis gasparella* sp.nov. and *Parmulina lousi* sp.nov., New Testate Amoebae from the Canadian High Arctic (Devon Island, NWT). *Arch. fur Protistenkd.* 136, 337–344. [https://doi.org/10.1016/S0003-9365\(88\)80014-9](https://doi.org/10.1016/S0003-9365(88)80014-9)
- Charman, D.J., Blundell, A., Abrupt Climate Change Over the European Land Mass project members, 2007. A new European testate amoebae transfer function for palaeohydrological reconstruction on ombrotrophic peatlands. *J. Quat. Sci.* 22, 209–221. <https://doi.org/10.1002/jqs.1026>
- Charman, D.J., Hendon, D., Woodland, W.A., 2000. The identification of testate amoebae (Protozoa: Rhizopoda) in peats: QRA Technical Guide No. 9, Quaternary Research Association. Quaternary Research Association, London. <https://doi.org/10.1016/j.quascirev.2004.02.012>
- Ehrenberg, C.G., 1870. Die Mikroskopischen Lebensverhältnisse auf der Oberfläche der Insel Spitzbergen, *Monatber. Akad. Berlin* 254–264.
- Elvevold, S., Dallmann, W., Blomeier, D., 2007. *Geology of Svalbard*. Norwegian Polar Institute, Tromsø, Norway.
- Evans, C.D., Peacock, M., Baird, A.J., Artz, R.R.E., Burden, A., Callaghan, N., Chapman, P.J., Cooper, H.M., Coyle, M., Craig, E., Cumming, A., Dixon, S., Gauci, V., Grayson, R.P., Helfter, C., Heppell, C.M., Holden, J., Jones, D.L., Kaduk, J., Levy, P., Matthews, R., McNamara, N.P., Misselbrook, T., Oakley, S., Page, S.E., Rayment, M., Ridley, L.M., Stanley, K.M., Williamson, J.L., Worrall,

- F., Morrison, R., 2021. Overriding water table control on managed peatland greenhouse gas emissions. *Nature* 593, 548–552. <https://doi.org/10.1038/s41586-021-03523-1>
- Førland, E.J., Benestad, R., Hanssen-Bauer, I., Haugen, J.E., Skaugen, T.E., 2011. Temperature and Precipitation Development at Svalbard 1900–2100. *Adv. Meteorol.* 2011, 1–14. <https://doi.org/10.1155/2011/893790>
- Gallego-Sala, A. V., Charman, D.J., Brewer, S., Page, S.E., Prentice, I.C., Friedlingstein, P., Moreton, S., Amesbury, M.J., Beilman, D.W., Björck, S., Blyakharchuk, T., Bochicchio, C., Booth, R.K., Bunbury, J., Camill, P., Carless, D., Chimner, R.A., Clifford, M., Cressey, E., Courtney-Mustaphi, C., De Vleeschouwer, F., de Jong, R., Fialkiewicz-Koziel, B., Finkelstein, S.A., Garneau, M., Githumbi, E., Hribljan, J., Holmquist, J., Hughes, P.D.M., Jones, C., Jones, M.C., Karofeld, E., Klein, E.S., Kokfelt, U., Korhola, A., Lacourse, T., Le Roux, G., Lamentowicz, M., Large, D., Lavoie, M., Loisel, J., Mackay, H., MacDonald, G.M., Makila, M., Magnan, G., Marchant, R., Marcisz, K., Martínez Cortizas, A., Massa, C., Mathijssen, P., Mauquoy, D., Mighall, T., Mitchell, F.J.G., Moss, P., Nichols, J., Oksanen, P.O., Orme, L., Packalen, M.S., Robinson, S., Roland, T.P., Sanderson, N.K., Sannel, A.B.K., Silva-Sánchez, N., Steinberg, N., Swindles, G.T., Turner, T.E., Uglow, J., Väliranta, M., van Bellen, S., van der Linden, M., van Geel, B., Wang, G., Yu, Z., Zaragoza-Castells, J., Zhao, Y., 2018. Latitudinal limits to the predicted increase of the peatland carbon sink with warming. *Nat. Clim. Chang.* 1. <https://doi.org/10.1038/s41558-018-0271-1>
- Gorham, E., Janssens, J.A., Wheeler, G.A., Glaser, P.H., 1987. The natural and anthropogenic acidification of peatlands, in: Hutchinson, T.C., Meema, K.M. (Eds.), *Effects of Atmospheric Pollutants on Forests, Wetlands and Agricultural Ecosystems*. NATO ASI Series (Series G: Ecological Sciences). Springer Berlin Heidelberg, pp. 493–512. https://doi.org/10.1007/978-3-642-70874-9_36
- Hanssen-Bauer, I., Førland, E.J., Hisdal, H., Mayer, S., Sandø, A.B., Sorteberg, A., Adakudlu, M., Andresen, J., Bakke, J., Beldring, S., Benestad, R., Bilt, W., Bogen, J., Borstad, C., Breili, K., Breivik, Ø., Børshem, K.Y., Christiansen, H.H., Dobler, A., Engeset, R., Frauenfelder, R., Gerland, S., Gjeltén, H.M., Gundersen, J., Isaksen, K., Jaedicke, C., Kierulf, H., Kohler, J., Li, H., Lutz, J., Melvold, K., Mezghani, A., Nilsen, F., Nilsen, I.B., Nilsen, J.E.Ø., Pavlova, O., Ravndal, O., Risebrobakken, B., Saloranta, T., Sandven, S., Schuler, T. V, Simpson, M.J.R., Skogen, M., Smedsrud, L.H., Sund, M., Vikhamar-Schuler, D., Westermann, S., Wong, W.K., 2019. Climate in Svalbard 2100 - a knowledge base for climate adaptation. Norwegian Environment Agency (Miljødirektoratet).
- Hugelius, G., Strauss, J., Zubrzycki, S., Harden, J.W., Schuur, E.A.G., Ping, C.-L., Schirrmeister, L., Grosse, G., Michaelson, G.J., Koven, C.D., O'Donnell, J.A., Elberling, B., Mishra, U., Camill, P., Yu, Z., Palmtag, J., Kuhry, P., 2014. Estimated stocks of circumpolar permafrost carbon with quantified uncertainty ranges and identified data gaps. *Biogeosciences* 11, 6573–6593. <https://doi.org/10.5194/bg-11-6573-2014>
- Hugelius, G., Tarnocai, C., Broll, G., Canadell, J.G., Kuhry, P., Swanson, D.K., 2013. Earth System Science Data The Northern Circumpolar Soil Carbon Database: spatially distributed datasets of soil coverage and soil carbon storage in the northern permafrost regions. *Earth Syst. Sci. Data* 5, 3–13. <https://doi.org/10.5194/essd-5-3-2013>
- Isaksson, E., Hermanson, M., Hicks, S., Igarashi, M., Kamiyama, K., Moore, J., Motoyama, H., Muir, D., Pohjola, V., Vaikmäe, R., van de Wal, R.S., Watanabe, O., 2003. Ice cores from Svalbard–

- useful archives of past climate and pollution history. *Phys. Chem. Earth, Parts A/B/C* 28, 1217–1228. <https://doi.org/10.1016/J.PCE.2003.08.053>
- Juggins, S., 2020. rioja: Analysis of Quaternary Science Data. R package version 0.9-26.
- Kellogg, L.E., Bridgham, S.D., 2003. Phosphorus retention and movement across an ombrotrophic-minerotrophic peatland gradient. *Biogeochemistry* 63, 299–315. <https://doi.org/10.1023/A:1023387019765>
- Koven, C.D., Schuur, E.A.G., Schädel, C., Bohn, T.J., Burke, E.J., Chen, G., Chen, X., Ciais, P., Grosse, G., Harden, J.W., Hayes, D.J., Hugelius, G., Jafarov, E.E., Krinner, G., Kuhry, P., Lawrence, D.M., MacDougall, A.H., Marchenko, S.S., McGuire, A.D., Natali, S.M., Nicolosky, D.J., Olefeldt, D., Peng, S., Romanovsky, V.E., Schaefer, K.M., Strauss, J., Treat, C.C., Turetsky, M., 2015. A simplified, data-constrained approach to estimate the permafrost carbon–climate feedback. *Philos. Trans. R. Soc. A Math. Phys. Eng. Sci.* 373, 20140423. <https://doi.org/10.1098/rsta.2014.0423>
- Lamarre, A., Magnan, G., Garneau, M., Boucher, É., 2013. A testate amoeba-based transfer function for paleohydrological reconstruction from boreal and subarctic peatlands in northeastern Canada. *Quat. Int.* 306, 88–96. <https://doi.org/10.1016/J.QUAINT.2013.05.054>
- Lamentowicz, M., Lamentowicz, Ł., Payne, R.J., 2013. Towards quantitative reconstruction of peatland nutrient status from fens. *The Holocene* 23, 1661–1665. <https://doi.org/10.1177/0959683613508162>
- Lawrence, D.M., Koven, C.D., Swenson, S.C., Riley, W.J., Slater, A.G., 2015. Permafrost thaw and resulting soil moisture changes regulate projected high-latitude CO₂ and CH₄ emissions. *Environ. Res. Lett.* 10, 094011. <https://doi.org/10.1088/1748-9326/10/9/094011>
- Masson-Delmotte, V., Zhai, P., Pörtner, H.-O., Roberts, D., Skea, J., Shukla, P.R., Pirani, A., Moufouma-Okia, W., Péan, C., Pidcock, R., Connors, S., Matthews, J.B.R., Chen, Y., Zhou, X., Gomis, M.I., Lonnoy, E., Maycock, T., Tignor, M., Waterfield, T., 2018. Intergovernmental Panel on Climate Change, 2018: Summary for Policymakers, in: *Global Warming of 1.5°C. An IPCC Special Report on the Impacts of Global Warming of 1.5°C above Pre-Industrial Levels and Related Global Greenhouse Gas Emission Pathways, in the Context of Strengthening the Global Response to the Threat of Climate Change*, pp. 3–24. <https://doi.org/10.1017/CBO9781107415324>
- Mazej, Y.A., Lebedeva, N. V., Taskaeva, A.A., Ivanovsky, A.A., Chernyshov, V.A., Tsyganov, A.N., Payne, R.J., 2018. Potential influence of birds on soil testate amoebae in the Arctic. *Polar Sci.* 16, 78–85. <https://doi.org/10.1016/j.polar.2018.03.001>
- Mitchell, E.A.D., 2004. Response of Testate Amoebae (Protozoa) to N and P Fertilization in an Arctic Wet Sedge Tundra. *Arctic, Antarct. Alp. Res.* 36, 78–83. [https://doi.org/10.1657/1523-0430\(2004\)036\[0078:ROTAPT\]2.0.CO;2](https://doi.org/10.1657/1523-0430(2004)036[0078:ROTAPT]2.0.CO;2)
- Nakatsubo, T., Uchida, M., Sasaki, A., Kondo, M., Yoshitake, S., Kanda, H., 2015. Carbon accumulation rate of peatland in the High Arctic, Svalbard: Implications for carbon sequestration. *Polar Sci.* 9, 267–275. <https://doi.org/10.1016/J.POLAR.2014.12.002>
- Norwegian Polar Institute, 2014a. Terrengmodell Svalbard (S0 Terrengmodell, Svalbard-mosaikker). <https://doi.org/https://doi.org/10.21334/npolar.2014.dce53a47>

- Norwegian Polar Institute, 2014b. Kartdata Svalbard 1:100 000 (S100 Kartdata, ESRI Shapefile). <https://doi.org/https://doi.org/10.21334/npolar.2014.645336c7>
- Nowak, A., Hodson, A., 2014. Changes in meltwater chemistry over a 20-year period following a thermal regime switch from polythermal to cold-based glaciation at Austre Brøggerbreen, Svalbard. *Polar Res.* 33, 22779. <https://doi.org/10.3402/polar.v33.22779>
- Oksanen, J., Blanchet, F.G., Friendly, M., Kindt, R., Legendre, P., McGlenn, D., Minchin, P.R., O'Hara, R.B., Simpson, G.L., Solymos, P., Stevens, M.H.H., Szoecs, E., Wagner, H., 2020. *vegan*: Community Ecology Package. R package version 2.5-7.
- Olefeldt, D., Turetsky, M.R., Crill, P.M., McGuire, A.D., 2013. Environmental and physical controls on northern terrestrial methane emissions across permafrost zones. *Glob. Chang. Biol.* 19, 589–603. <https://doi.org/10.1111/gcb.12071>
- Opravilova, V., 1989. Some Information on the Testate Amoebae from Spitsbergen. *Fauna Norv. Ser. A10*, 33–37.
- Payne, R., 2007. Laboratory Experiments on Testate Amoebae Preservation in Peats: Implications for Palaeoecology and Future Studies. *Acta Protozool.* 46, 325–332.
- Payne, R.J., 2011. Can testate amoeba-based palaeohydrology be extended to fens? *J. Quat. Sci.* 26, 15–27. <https://doi.org/10.1002/jqs.1412>
- Payne, R.J., Kishaba, K., Blackford, J.J., Mitchell, E.A.D., 2006. Ecology of testate amoebae (protista) in south-central Alaska peatlands: Building transfer-function models for palaeoenvironmental studies. *Holocene* 16, 403–414. <https://doi.org/10.1191/0959683606hl936rp>
- Penard, E., 1903. Notice sur les rhizopodes du Spitsberg. *Arch. für Protistenkd.* 2, 238–282.
- Qin, Y., Li, H., Mazei, Y., Kurina, I., Swindles, G.T., Bobrov, A., Tsyganov, A.N., Gu, Y., Huang, X., Xue, J., Lamentowicz, M., Marcisz, K., Roland, T., Payne, R.J., Mitchell, E.A.D., Xie, S., 2021. Developing a continental-scale testate amoeba hydrological transfer function for Asian peatlands. *Quat. Sci. Rev.* 258, 106868. <https://doi.org/10.1016/j.quascirev.2021.106868>
- R Core Team, 2020. R: a language and environment for statistical computing. Version 3.6.3.
- Reimer, P.J., Austin, W.E.N., Bard, E., Bayliss, A., Blackwell, P.G., Bronk Ramsey, C., Butzin, M., Cheng, H., Edwards, R.L., Friedrich, M., Grootes, P.M., Guilderson, T.P., Hajdas, I., Heaton, T.J., Hogg, A.G., Hughen, K.A., Kromer, B., Manning, S.W., Muscheler, R., Palmer, J.G., Pearson, C., Van Der Plicht, J., Reimer, R.W., Richards, D.A., Scott, E.M., Southon, J.R., Turney, C.S.M., Wacker, L., Adolphi, F., Büntgen, U., Capano, M., Fahrni, S.M., Fogtmann-Schulz, A., Friedrich, R., Köhler, P., Kudsk, S., Miyake, F., Olsen, J., Reinig, F., Sakamoto, M., Sookdeo, A., Talamo, S., 2020. The IntCal20 Northern Hemisphere Radiocarbon Age Calibration Curve (0–55 cal kBP). *Radiocarbon* 62, 725–757. <https://doi.org/10.1017/RDC.2020.41>
- Schlegel, A., Lisker, F., Dörr, N., Jochmann, M., Schubert, K., Spiegel, C., 2013. Petrography and geochemistry of siliciclastic rocks from the Central Tertiary Basin of Svalbard - implications for provenance, tectonic setting and climate. *Zeitschrift der Dtsch. Gesellschaft für Geowissenschaften* 164, 173–186. <https://doi.org/10.1127/1860-1804/2013/0012>
- Schönborn, W., 1966. Beitrag zur Ökologie and Systematik der Testaceen Spitsbergens. *Limnologica* 4, 463–470.

- Schuur, E.A.G., McGuire, A.D., Schädel, C., Grosse, G., Harden, J.W., Hayes, D.J., Hugelius, G., Koven, C.D., Kuhry, P., Lawrence, D.M., Natali, S.M., Olefeldt, D., Romanovsky, V.E., Schaefer, K., Turetsky, M.R., Treat, C.C., Vonk, J.E., 2015. Climate change and the permafrost carbon feedback. *Nature* 520, 171–179. <https://doi.org/10.1038/nature14338>
- Scourfield, D.J., 1897. Contributions to the non-marine fauna of Spitsbergen. Part I. Preliminary notes, and reports on the Rhizopoda, Tardigrada, Entomostraca, & c. *Proc. Zool. Soc. London* 65, 784–792.
- Serreze, M.C., Barry, R.G., 2011. Processes and impacts of Arctic amplification: A research synthesis. *Glob. Planet. Change* 77, 85–96. <https://doi.org/10.1016/J.GLOPLACHA.2011.03.004>
- Siemensma, F.J., 2021. Microworld, world of amoeboid organisms [WWW Document]. *World-wide Electron. Publ.* URL <http://www.arcella.nl>
- Sim, T.G., Swindles, G.T., Morris, P.J., Baird, A.J., Cooper, C.L., Gallego-Sala, A. V, Charman, D.J., Roland, T.P., Borken, W., Mullan, D.J., Aquino-López, M.A., Gałka, M., 2021. Divergent responses of permafrost peatlands to recent climate change. *Environ. Res. Lett.* 16, 034001. <https://doi.org/10.1088/1748-9326/abe00b>
- Sim, T.G., Swindles, G.T., Morris, P.J., Gałka, M., Mullan, D., Galloway, J.M., 2019. Pathways for Ecological Change in Canadian High Arctic Wetlands Under Rapid Twentieth Century Warming. *Geophys. Res. Lett.* 46, 4726–4737. <https://doi.org/10.1029/2019GL082611>
- Simpson, G.L., Oksanen, J., 2020. analogue: Analogue and Weighted Averaging Methods for Palaeoecology.
- Swindles, G.T., Amesbury, M.J., Turner, T.E., Carrivick, J.L., Woulds, C., Raby, C., Mullan, D., Roland, T.P., Galloway, J.M., Parry, L., Kokfelt, U., Garneau, M., Charman, D.J., Holden, J., 2015. Evaluating the use of testate amoebae for palaeohydrological reconstruction in permafrost peatlands. *Palaeogeogr. Palaeoclimatol. Palaeoecol.* 424, 111–122. <https://doi.org/10.1016/J.PALAEO.2015.02.004>
- Swindles, G.T., Baird, A.J., Kilbride, E., Low, R., Lopez, O., 2018. Testing the relationship between testate amoeba community composition and environmental variables in a coastal tropical peatland. *Ecol. Indic.* 91, 636–644. <https://doi.org/10.1016/j.ecolind.2018.03.021>
- Swindles, G.T., Charman, D.J., Roe, H.M., Sansum, P.A., 2009. Environmental controls on peatland testate amoebae (Protozoa: Rhizopoda) in the North of Ireland: Implications for Holocene palaeoclimate studies. *J. Paleolimnol.* <https://doi.org/10.1007/s10933-008-9266-7>
- Swindles, G.T., Roe, H.M., 2007. Examining the dissolution characteristics of testate amoebae (Protozoa: Rhizopoda) in low pH conditions: Implications for peatland palaeoclimate studies. *Palaeogeogr. Palaeoclimatol. Palaeoecol.* 252, 486–496. <https://doi.org/10.1016/J.PALAEO.2007.05.004>
- Swindles, G.T., Roland, T.P., Amesbury, M.J., Lamentowicz, M., McKeown, M.M., Sim, T.G., Fewster, R.E., Mitchell, E.A.D., 2020. Quantifying the effect of testate amoeba decomposition on peat-based water-table reconstructions. *Eur. J. Protistol.* 125693. <https://doi.org/10.1016/j.ejop.2020.125693>
- Tanneberger, F., Tegetmeyer, C., Busse, S., Barthelmes, A., Shumka, S., Moles Mariné, A.,

- Jenderedjian, K., Steiner, G.M., Essl, F., Etzold, J., Mendes, C., Kozulin, A., Frankard, P., Milanović, Đ., Ganeva, A., Apostolova, I., Alegro, A., Delipetrou, P., Navrátilová, J., Risager, M., Leivits, A., Fosaa, A.M., Tuominen, S., Muller, F., Bakuradze, T., Sommer, M., Christanis, K., Szurdoki, E., Oskarsson, H., Brink, S.H., Connolly, J., Bragazza, L., Martinelli, G., Aleksāns, O., Priede, A., Sungaila, D., Melovski, L., Belous, T., Saveljić, D., De Vries, F., Moen, A., Dembek, W., Mateus, J., Hanganu, J., Sirin, A., Markina, A., Napreenko, M., Lazarević, P., Stanová, V.Š., Skoberne, P., Heras Pérez, P., Pontevedra-Pombal, X., Lonnstad, J., Kuchler, M., Wüst-Galley, C., Kirca, S., Mykytiuk, O., Lindsay, R., Joosten, H., 2017. The peatland map of Europe. *Mires peat* 19, 1–17. <https://doi.org/10.19189/MaP.2016.OMB.264>
- Taylor, L.S., Swindles, G.T., Morris, P.J., Gařka, M., 2019a. Ecology of peatland testate amoebae in the Alaskan continuous permafrost zone. *Ecol. Indic.* 96, 153–162. <https://doi.org/10.1016/J.ECOLIND.2018.08.049>
- Taylor, L.S., Swindles, G.T., Morris, P.J., Gařka, M., Green, S.M., 2019b. Evidence for ecosystem state shifts in Alaskan continuous permafrost peatlands in response to recent warming. *Quat. Sci. Rev.* 207, 134–144. <https://doi.org/10.1016/j.quascirev.2019.02.001>
- Tiner, R.W., 2016. *Wetland indicators: A guide to wetland formation, identification, delineation, classification, and mapping*, 2nd ed. Taylor & Francis, Boca Raton.
- Väliranta, M., Salojärvi, N., Vuorsalo, A., Juutinen, S., Korhola, A., Luoto, M., Tuittila, E.-S., 2017. Holocene fen–bog transitions, current status in Finland and future perspectives. *The Holocene* 27, 752–764. <https://doi.org/10.1177/0959683616670471>
- Vikhamar Schuler, T., Østby, T. rn I., 2020. Sval-Imp: A gridded forcing dataset for climate change impact research on Svalbard. *Earth Syst. Sci. Data* 12, 875–885. <https://doi.org/10.5194/essd-12-875-2020>
- Vitt, D.H., Chee, W.-L., 1990. The relationships of vegetation to surface water chemistry and peat chemistry in fens of Alberta, Canada. *Vegetatio* 89, 87–106. <https://doi.org/10.1007/BF00032163>
- Waddington, J.M., Morris, P.J., Kettridge, N., Granath, G., Thompson, D.K., Moore, P.A., 2015. Hydrological feedbacks in northern peatlands. *Ecohydrology* 8, 113–127. <https://doi.org/10.1002/eco.1493>
- Walczowski, W., Piechura, J., 2011. Influence of the West Spitsbergen Current on the local climate. *Int. J. Climatol.* 31, 1088–1093. <https://doi.org/10.1002/joc.2338>
- Walker, D.A., Raynolds, M.K., Daniëls, F.J.A., Einarsson, E., Elvebakk, A., Gould, W.A., Katenin, A.E., Kholod, S.S., Markon, C.J., Melnikov, E.S., Moskalenko, N.G., Talbot, S.S., Yurtsev, B.A., The other members of the CAVM Team, T. other members of the C., 2005. The Circumpolar Arctic vegetation map. *J. Veg. Sci.* 16, 267–282. <https://doi.org/10.1111/j.1654-1103.2005.tb02365.x>
- Warner, B.G., Rubec, C.D.A., 1997. *The Canadian Wetland Classification System (Second Edition)*, 2nd ed. Wetlands Research Centre, Waterloo, Ontario, Canada.
- Woo, M., Young, K.L., 2006. High Arctic wetlands: Their occurrence, hydrological characteristics and sustainability. *J. Hydrol.* 320, 432–450. <https://doi.org/10.1016/J.JHYDROL.2005.07.025>
- Zhang, H., Amesbury, M.J., Ronkainen, T., Charman, D.J., Gallego-Sala, A. V., Väliranta, M., 2017.

Testate amoeba as palaeohydrological indicators in the permafrost peatlands of north-east European Russia and Finnish Lapland. *J. Quat. Sci.* 32, 976–988.
<https://doi.org/10.1002/jqs.2970>

**Chapter 3 – Divergent responses
of permafrost peatlands to
recent climate change**

Divergent responses of permafrost peatlands to recent climate change

Thomas G. Sim¹, Graeme T. Swindles², Paul J. Morris¹, Andy J. Baird¹, Claire L. Cooper³, Angela V. Gallego-Sala⁴, Dan J. Charman⁴, Thomas P. Roland⁴, Werner Borke⁵, Donal J. Mullan², Marco A. Aquino-López⁶ and Mariusz Gałka⁷

¹School of Geography, University of Leeds, Leeds, UK

²Geography, School of Natural and Built Environment, Queen's University Belfast, Belfast, UK

³School of Geography, University of Lincoln, UK

⁴Geography, College of Life and Environmental Sciences, University of Exeter, Exeter, UK

⁵Soil Ecology, University of Bayreuth, Bayreuth Center of Ecology and Environmental Research (BayCEER), Dr.-Hans-Frisch-Str. 1-3, 95448 Bayreuth, Germany

⁶Centro de Investigacion en Matemáticas, Guanajuato, MX

⁷University of Łódź, Faculty of Biology and Environmental Protection, Department of Biogeography, Paleoecology and Nature Protection, 12/16 Banacha Str., Łódź, Poland

Citation:

Sim, T.G., Swindles, G.T., Morris, P.J., Baird, A.J., Cooper, C.L., Gallego-Sala, A.V., Charman, D.J., Roland, T.P., Borke, W., Mullan, D.J., Aquino-López, M.A., Gałka, M., 2021. Divergent responses of permafrost peatlands to recent climate change. *Environ. Res. Lett.* 16, 034001. <https://doi.org/10.1088/1748-9326/abe00b>

Abstract

Permafrost peatlands are found in high-latitude regions and store globally-important amounts of soil organic carbon. These regions are warming at over twice the global average rate, causing permafrost thaw, and exposing previously inert carbon to decomposition and emission to the atmosphere as greenhouse gases. However, it is unclear how peatland hydrological behaviour, vegetation structure and carbon balance, and the linkages between them, will respond to permafrost thaw in a warming climate. Here we show that permafrost peatlands follow divergent ecohydrological trajectories in response to recent climate change within the same rapidly warming region (northern Sweden). Whether a site becomes wetter or drier depends on local factors and the autogenic response of individual peatlands. We find that bryophyte-dominated vegetation demonstrates resistance, and in some cases resilience, to climatic and hydrological shifts. Drying at four sites is clearly associated with reduced carbon sequestration, while no clear relationship at wetting sites is observed. We highlight the complex dynamics of permafrost peatlands and warn against an overly-simple approach when considering their ecohydrological trajectories and role as C sinks under a warming climate.

3.1. Introduction

Permafrost peatlands have developed in cold regions during the Holocene and store a disproportionate amount of organic carbon (C) for their extent, estimated to total ~277 Gt C (Tarnocai et al., 2009) – making up around a fifth of all permafrost soil C (Hugelius et al., 2014). These ecosystems experience a short growing season where a seasonal active layer thaws (French, 2017), and C accumulates when the addition of plant litter exceeds losses from decomposition (Yu et al., 2011). The maintenance of a near-surface water-table by seasonal active layer thaw, snow melt and summer precipitation (Woo and Winter, 1993) limits C losses from microbial decomposition (Heffernan et al., 2020) and encourages the growth of decomposition-resistant plants such as *Sphagnum* mosses (Rydin et al., 2006).

High-latitude regions of the Northern Hemisphere are now experiencing warming at a rate two to three times the global average (Masson-Delmotte et al., 2018). Permafrost extent is shifting northwards with warming, evidenced by the thawing of peatlands in the discontinuous permafrost zones of North America (Camill, 2005) and Eurasia (Åkerman and Johansson, 2008; Payette et al., 2004). Deeper thaw increases the amount of soil organic matter vulnerable to decomposition, while rising temperatures simultaneously increase the rate of microbial decomposition; both contribute to increased greenhouse gas (GHG) emissions and a positive feedback with climate (Jeong et al., 2018). In addition, climate-driven drying may expose peat to increased aerobic decomposition, leading to increases in carbon dioxide (CO₂) emissions (Ise et al., 2008), while thaw-induced wetting has been associated with elevated methane (CH₄) emissions (Christensen et al., 2004). However, these C losses may be partially offset or even reversed by improved plant productivity during longer growing seasons (Gallego-Sala et al., 2018; Heffernan et al., 2020; Taylor et al., 2019).

Although studies of degrading permafrost peatlands have established a relationship between GHG fluxes, permafrost thaw and hydrological conditions, intensive monitoring in most areas began no earlier than the 1990s (Johansson et al., 2006). Therefore, a palaeoecological approach using proxies – such as testate amoebae (Jones et al., 2013; Lamarre et al., 2012; Pelletier et al., 2017; Swindles et al., 2015a; Taylor et al., 2019) and plant macrofossils (Fritz et al., 2016; Gałka et al., 2017a) – provides a valuable longer-term perspective. A recent palaeohydrological study of European peatlands in mainly temperate latitudes showed widespread twentieth century drying (Swindles et al., 2019); however, permafrost peatlands are subject to processes that are unique to cold regions. Gradual permafrost thaw increases active layer thickness and can lead to evaporation-driven drying (Zhang et al., 2018a, van Bellen et al., 2018). If a threshold point in

permafrost thaw is reached structural collapse and wetting can occur, often linked to deep C losses (Jones et al., 2017; O'Donnell et al., 2012; Turetsky et al., 2020), but there is evidence that in some instances abrupt permafrost thaw can lead to increased post-thaw C accumulation that partially or completely offsets deep C losses (Jones et al., 2013, Swindles et al., 2015b, Heffernan et al., 2020). This non-linear response suggests ecological thresholds and autogenic feedbacks may be important, but these are not yet fully understood.

The uncertainty over the future of permafrost peatland C stocks mirrors that of the entire permafrost zone, arising from limited understanding of feedbacks between changes in hydrological regime, vegetation shifts, and permafrost thaw (Abbott et al., 2016). In this study we investigate the ecohydrological and carbon dynamics response of permafrost peatlands in a rapidly warming region of subarctic Sweden. We conduct multi-proxy palaeoecological reconstructions from 10 peat profiles across eight sites that are reliably dated at high-resolution using ^{210}Pb , ^{14}C and tephrochronology. More specifically we aim to (i) reconstruct changes in peatland vegetation, moisture conditions and carbon dynamics over at least the last 300 years, (ii) determine the relationship between any important changes and measured climatic variables and (iii) better quantify autogenic ecohydrological feedbacks operating in permafrost peatlands.

3.2. Methods

3.2.1. Study region and sampling

Our study region near Abisko in northern Sweden (Figure 3.1) is in the discontinuous permafrost zone and is characterised by extensive palsas, peat plateaus, bogs, and fens, many of which are currently experiencing permafrost degradation (Åkerman and Johansson, 2008) and are no longer in equilibrium with climate (Olvmo et al., 2020). Therefore, our study region may indicate how peatland areas currently with more extensive permafrost may respond to future warming. In total, we sampled ten peat profiles across eight sites within a ~60 km radius of each other. All sites were underlain by permafrost and were sampled to the base of the active layer, excluding Maunuvuoma fen where no permafrost was present. Monoliths were cut out from the peat at all sites, with the exception of Stordalen palsa and Maunuvuoma fen, that were sampled using a Russian corer (De Vleeschouwer et al., 2010). Refer to Figures B.31-B.33 for imagery of sampling site locations.

The peatlands in our study region formed as early as ~9,500 yr BP following the retreat of the Fennoscandian Ice Sheet (Sannel et al., 2018), with peatland initiation linked to warming growing seasons and potentially increased precipitation (Morris et al., 2018). Yet, permafrost may only have started forming in Fennoscandia from ~1500 yr BP (Treat and Jones, 2018), perhaps as late

as the Little Ice Age. Abisko has warmed by 1.59°C in the last century (Figure 3.1), far above the mean global increase of 0.91°C (GISTEMP Team, 2020) (averages for 1913-1922 against 2003-2012), with annual temperatures in some areas of our study region now above 0°C – a key threshold for permafrost and ecological dynamics (Callaghan et al., 2010).

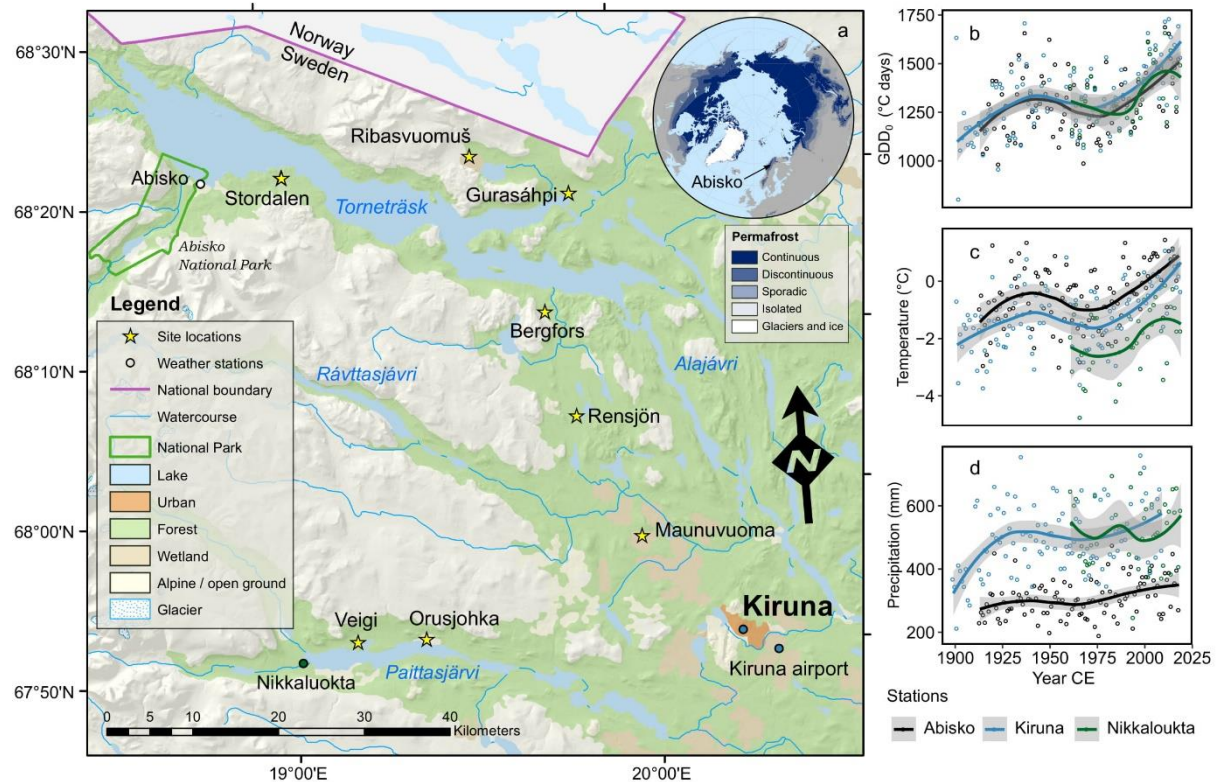


Figure 3.1. Location map of study sites, weather stations and regional climatic data. a) Study sites and weather stations near Abisko in the Kiruna Municipality, northern Sweden and location of study region in the context of pan-Arctic permafrost extent (Brown et al., 2002). Climatic station data are shown for b) growing degree days above 0°C (GDD₀); c) mean annual temperature; and d) total precipitation. Points represent annual averages and lines are locally estimated scatterplot smoothing (loess) models, with grey shading indicating the 95% confidence range of the loess function. Topographic, watercourse and land-cover data sourced from: <https://www.lantmateriet.se/>

3.2.2. Age modelling

The chronology of these peat profiles was determined from ²¹⁰Pb, ¹⁴C and tephra layers. ¹⁴C dates were calibrated using the IntCal13 calibration curve (Reimer et al., 2013) and the northern hemisphere zone 1 post-bomb calibration curve (Hua et al., 2013). Annually-resolved tephra layers found in Stordalen palsa (Hekla 1158 at 23 cm; Hekla 1104 at 30 cm) – see Cooper et al., (2019) – were included in the age-depth model. Age-depth profiles (Figures B.21-B.30) were constructed using PLUM (Aquino-López et al., 2018), which is a Bayesian modelling approach, for a more robust integration of ²¹⁰Pb, ¹⁴C and tephra dates.

3.2.3. Peat properties

Peat was stored at 4°C before bulk density and loss-on-ignition (LOI; %) analyses were completed in the laboratory following Chambers et al., (2011). Bulk density was measured for contiguous 0.5-cm thick layers, while LOI was determined for 1-cm thick layers. Bulk density (g cm^{-3}) was calculated by dividing dry mass of peat (g; dried overnight at 105°C) by the total sample volume (cm^3). LOI was calculated by subtracting ash mass (g; after 8 hours in 550°C furnace) from dry mass (g), dividing this by dry mass and multiplying the product by 100. C and nitrogen (N) content was measured for 0.5-cm layers in each peat profile on a Thermo Scientific Flash (2000) Series CHNS/O analyser.

3.2.4. Carbon accumulation

Apparent C accumulation rate (ACAR; $\text{g C m}^{-2} \text{ yr}^{-1}$) was calculated for each peat profile by multiplying the accumulation rate of peat ($\text{g m}^{-2} \text{ yr}^{-1}$), determined from respective age-depth models, by the proportion of C in each sample. Peat decay modelling (Clymo, 1984) has been successfully used in other studies to calculate C accumulation under constant conditions – i.e. partially accounting for incomplete decomposition of surface peats – and to interpret the influence of allogenic (external) forcing (Zhang et al., 2018b, 2020). However, here subjectivity in determining the transition of oxic to anoxic peat in these permafrost peatland sites, confounded by uncertainties associated with fitting exponential curves to data (Belyea and Baird, 2006), made use of such an approach inappropriate. Therefore, we have used a case-by-case discursive approach to interpret the relationship between ACAR and ecohydrological or climatic variables.

3.2.5. Water-table reconstructions

Testate amoebae were prepared and analysed following a modified version of Booth et al. (2010), peat samples of 2 cm^3 were boiled in water for 10 minutes and stirred with a glass rod. This solution was rinsed through a $300 \mu\text{m}$ sieve, back-sieved through a $15 \mu\text{m}$ mesh and left to settle. Slides were made up for microscopy and a minimum of 100 individual testate amoebae were counted per sample at $200\text{-}400 \times$ magnification. In 10.5% (24 out of 228) of the samples a minimum of 50 individuals were counted owing to low abundance. Testate amoebae species identification was aided by reference to relevant literature (Charman et al., 2000; Siemensma, 2021). Refer to Swindles et al. (2015b) for information on counting of testate amoebae in Stordalen palsa and Maunuvuoma fen (an additional 54 samples).

Taxonomies were harmonised to that of the Amesbury et al. (2016) European-wide transfer function which was then applied to testate amoeba abundance data to reconstruct past water-

table depth (WTD). This transfer function uses a weighted average tolerance-down weighted model with inverse de-shrinking. Errors are based on 999 bootstrap cycles. Full testate amoeba abundance data are presented in Figures B.1-B.10. Standardised z-scores of WTD reconstructions were calculated following Swindles et al. (2015c) for the periods 1500 CE to present (see Figure 3.3) and 1913 CE to present (see Figure 3.4).

Testate amoeba species were grouped by k-means clustering into three groups (wet, intermediate and dry indicators - see Figure 3.2) based upon their water-table optima values in the transfer function (Amesbury et al., 2016). The testate amoeba indicator percentages allow for an assessment of the homogeneity of WTD optima values within each sample – high heterogeneity could in theory indicate seasonal variation in hydrological regime or that wet and dry periods are captured within a single sample.

3.2.6. *Plant macrofossils*

Plant macrofossils were analysed for contiguous 1-cm thick layers in all peat profiles. Samples of 5 cm³ were washed under a warm-water spray and sieved using a 0.2 mm mesh. Initially, the entire sample was examined with a stereomicroscope to obtain volume percentages of individual subfossils of vascular plants and mosses. The subfossil carpological remains and vegetative fragments (leaves, rootlets, epidermis) were identified using identification keys (Hadenäs, 2003; Mauquoy and van Geel, 2007; Smith, 2004). Identification of *Sphagnum* to species level was carried out separately based upon analyses of stem leaves using specialist keys (Hölzer, 2010; Laine et al., 2011). See Gałka et al. (2017b) for a more detailed methodology for plant macrofossil analysis. Entire plant macrofossil records are presented in Figures B.11-B.20, along with the species groupings used for presentation in Figure 3.2. Refer to Gałka et al. (2017a) regarding the plant macrofossil analysis of Stordalen palsa and Maunuvuoma fen.

3.2.7. *Climatic data*

Temperature and precipitation data for regional weather stations were downloaded from the Swedish Meteorological and Hydrological Institute (<https://www.smhi.se/en>). Climate data were also provided by Abisko Scientific Research Station. Growing degree days (GDD₀) were calculated annually by summing daily temperature values above 0°C.

For the Abisko station Penman-Monteith potential evapotranspiration (mm day⁻¹) was calculated for the period July 1984 CE to December 2002 CE, where data of sufficient climatic variables were available. For this period, gaps made up 6.04% of the data, therefore gaps (up to 20 days) were filled using linear interpolation – following this process gaps made up only 0.34% of the data. This

interpolation was based upon the average of 5 days prior to and after a gap. If there were no data for 5 days prior to or after the gap, then data from 15 days before or after respectively was extrapolated to fill the gap. For the Penman-Monteith calculations, roughness length (z_0) values measured at a boreal Swedish peatland (Alekseychik et al., 2017) and albedo values from a study at Stordalen (Stiegler et al., 2016) were used.

The period for which there is Penman-Monteith evapotranspiration data is limited in timespan, although temperature, GDD_0 and sunlight hours data – related to evapotranspiration rates - are available from 1913 to present. Therefore multiple linear regression models using these variables were fitted to the Penman-Monteith evapotranspiration data at a monthly resolution for the period July 1984 to December 2002 in R v.3.6.1 (R Core Team, 2021). The relative quality of these models was assessed by comparing corrected Akaike information criterion (AICc) values in the R package “MuMIn” v.43.6 (Bartoń, 2019). The best performing model with a zero intercept had GDD_0 , temperature and sunlight hours as explanatory variables and had an adjusted R-squared of 0.87. This multiple linear regression model was then used to model monthly evapotranspiration at Abisko from 1913-2017 CE.

3.2.8. Theil-sen regression

The relationship between climate variables (GDD_0 , evapotranspiration and precipitation) at Abisko and WTD from 1913-2012 CE was explored using Theil-Sen robust regression in the R package “deming” v.1.4 (Therneau, 2018). WTD data was standardised following Swindles et al., (2015c) for the time period 1913-2012 CE. Climatic data were averaged for the time period each WTD sample represented in the age-depth model to make data comparable. The testate amoebae subfossil assemblage has accumulated over the time period represented by each sample slice (typically 1 cm) and therefore provides a WTD reconstruction averaged to this timeframe. Theil-sen regression coefficients were then standardised to produce beta coefficients.

3.3. Results and discussion

3.3.1. Response of permafrost peatlands to recent warming

Our palaeoecological reconstructions span at least the last 500 years and show a varied ecohydrological response to recent warming (Figure 3.2). In terms of hydrological regime, local regression (loess) models highlight a divergent response to recent warming (Figure 3.3). Stordalen palsa, Stordalen bog, Ribasvuomuš bog, Bergfors bog and Rensjön palsa have all undergone clear drying since the mid-twentieth century. In contrast, Gurasáhi palsa 1 and 2 and Maunuvuoma fen have experienced a period of twentieth century drying, followed by rapid wetting from ~1990

CE. Meanwhile, Veigi bog and Orusjohka palsa in Paittasjärvi valley to the south record asynchronously fluctuating wet and dry periods in recent decades. Individual sites have undergone wet or dry shifts earlier in the record (e.g. Stordalen palsa and Stordalen bog), but it is only within the last century that high-magnitude shifts in hydrological regime have occurred across all sites.

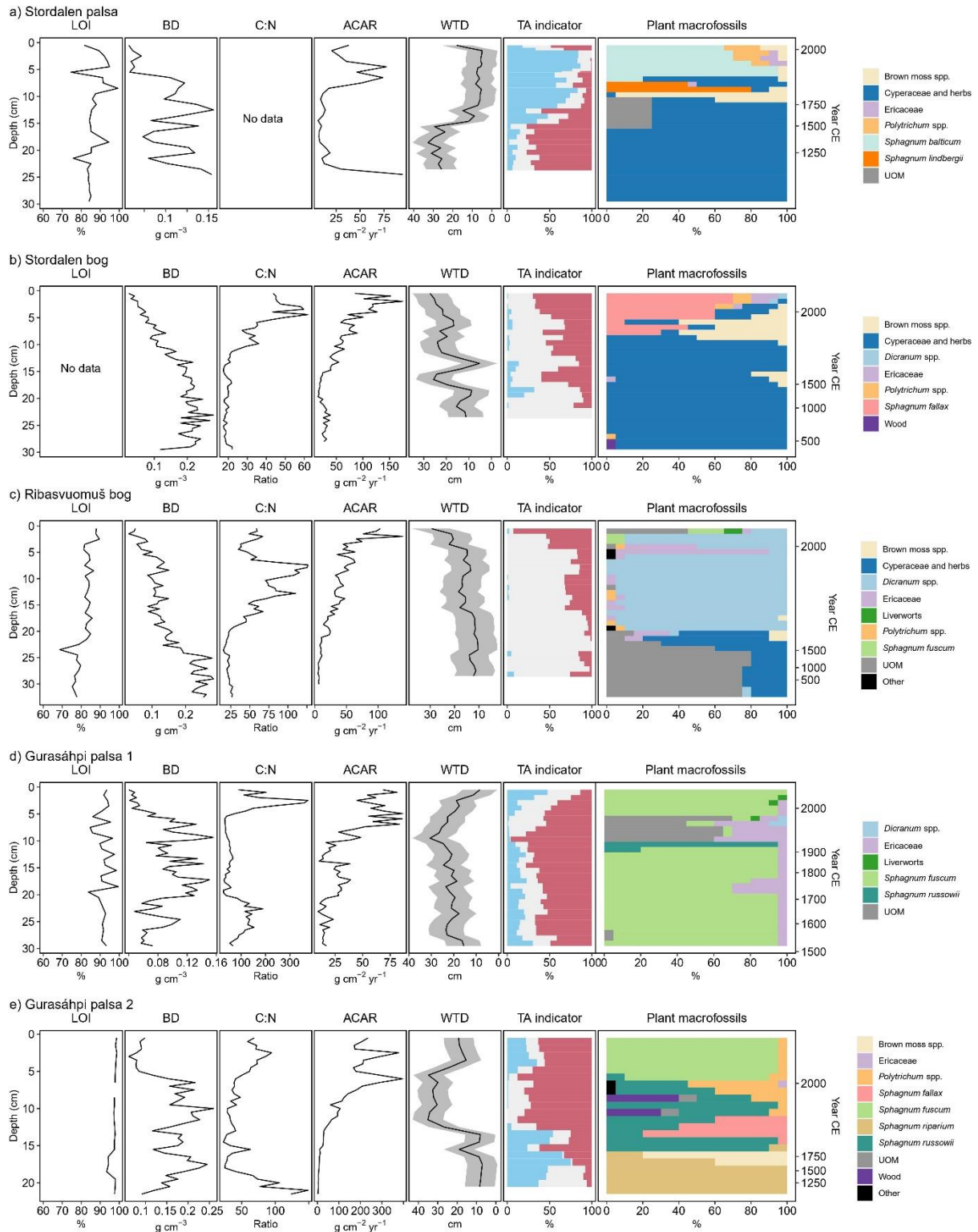


Figure 3.2. Palaeoecological summary diagrams from all ten peat profiles, across eight sites. Data shown are: i) loss on ignition (LOI; organic matter), ii) dry bulk density (BD), iii) C to N quotient, iv) apparent carbon accumulation rate (ACAR), v) water-table depth (WTD) reconstructions using a testate amoeba transfer function (Amesbury et al., 2016) (grey shading represents error based on 999 bootstrap cycles), vi) proportion wet (blue), intermediate (grey) and dry (red) testate amoeba (TA) indicators and vii) plant macrofossil remains (volume percentages). See Figures B.11-B.20 for full plant macrofossil data and Table B.1 for groupings.

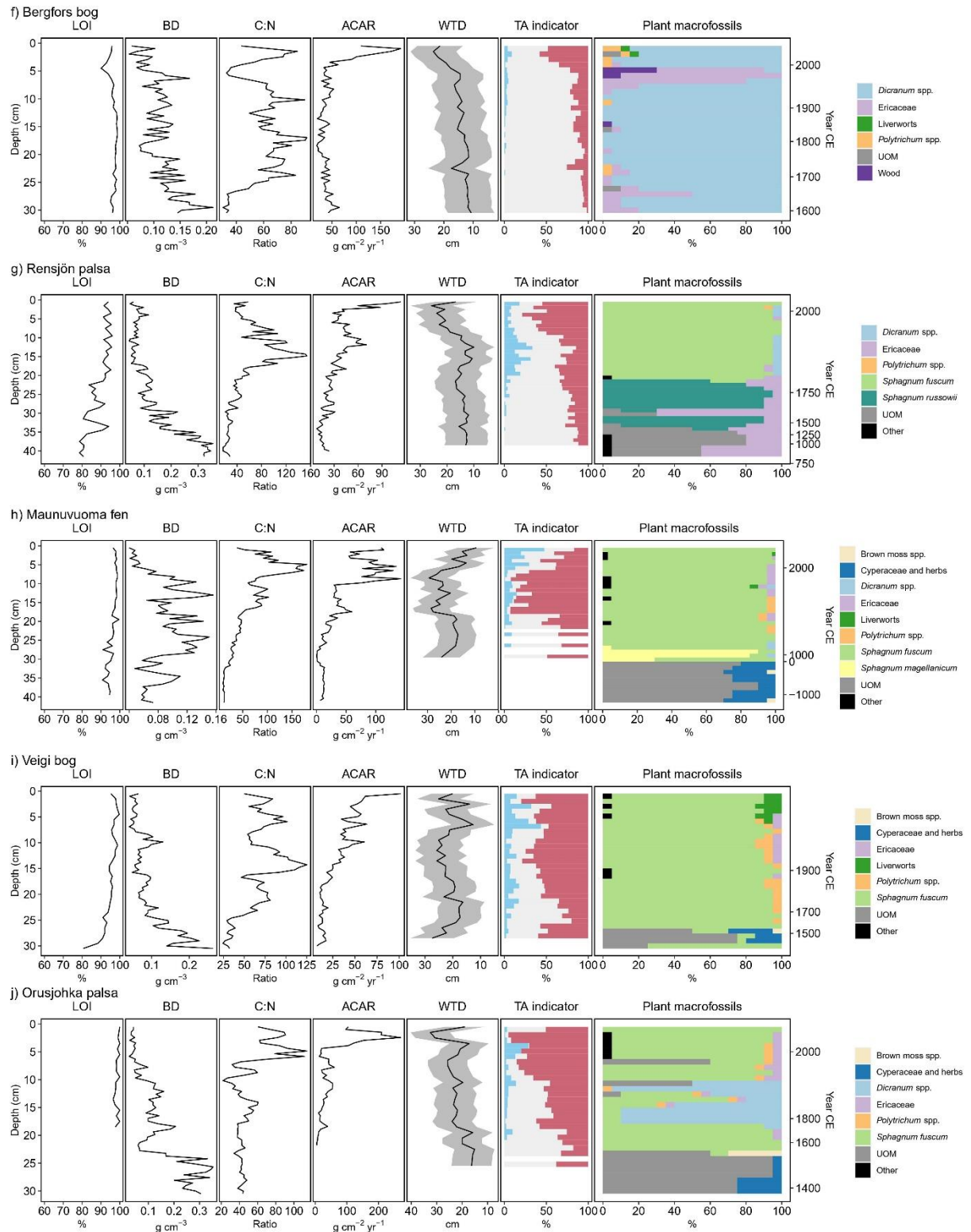


Figure 3.2. Continued.

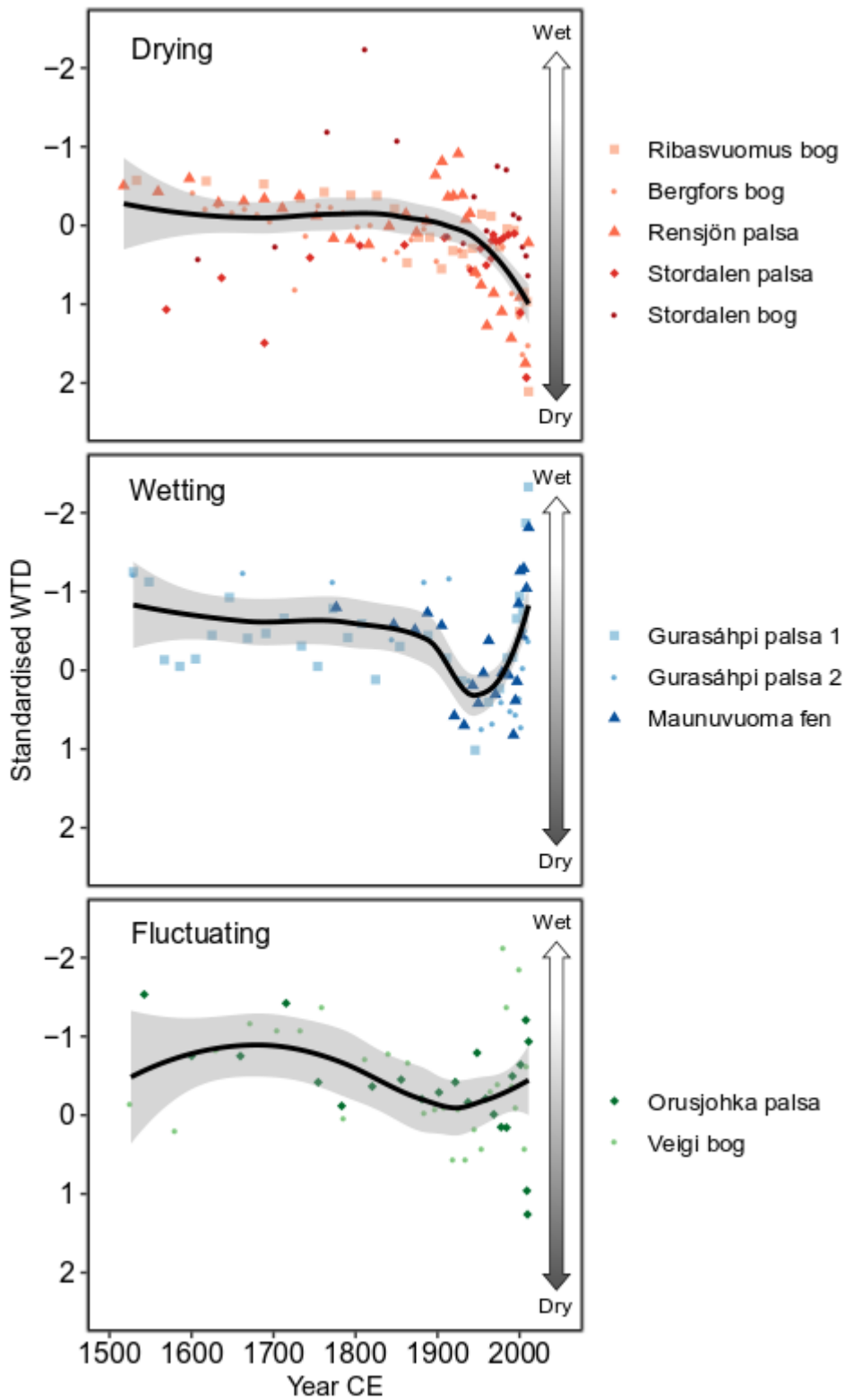


Figure 3.3. Water-table depth (WTD) data from all peat profiles since 1500 CE. WTD data are standardised for all peat profiles from 1500 CE. Results are divided into peat profiles exhibiting recent drying, wetting (preceded by drying) and asynchronously fluctuating WTD trends. For each panel a locally estimated scatterplot smoothing (loess) model is shown in black, with grey shading indicating the 95% confidence range of the loess function.

Vegetation across all sites demonstrates a degree of resistance (the ability of a population to avoid displacement during a period of stress; Harrison 1979), and in some cases resilience (the ability of a population to recover from change or disturbance when a period of stress has subsided; Harrison 1979) to recent hydrological shifts and climate change (Figure 3.2). In Rensjön palsa, Maunuvuoma fen and Veigi bog, *Sphagnum fuscum* populations remain stable during the last century, demonstrating resistance to warming and changing hydrological regimes, probably because of its broad hydrological tolerance (Rydin and McDonald, 1985). In Gurasáhpi palsa 1, *S. fuscum* demonstrates resilience with populations recovering following a period of intense drying – inferred from WTD reconstructions and high presence of unidentified organic matter (UOM) – in the mid-twentieth century. The resilience and resistance of *S. fuscum* may have been aided by its forming dense carpets and its increased growth rate with warming; however, a reduced bulk density with faster growth could hamper moisture retention capabilities in the long-term and limit future productivity (Dorrepaal et al., 2004). Both Ribasvuomuš bog and Bergfors bog have been dominated by *Dicranum* spp. – predominantly the hummock species *Dicranum elongatum* (Figures B.11 and B.17) – since ~1600 CE, with a period of Ericaceae dominance in the late twentieth century. Initially, drying may have allowed Ericaceae to outcompete *D. elongatum*, but further drying appears to have favoured *D. elongatum* – which can tolerate extreme dry habitats (Sonesson et al., 2002) – allowing the species to re-emerge as dominant. Stordalen palsa and Stordalen bog experience a shift from ~1950 CE to more ombrotrophic conditions, from sedge (Cyperaceae) and herbs to bryophyte dominance. From ~1800 CE to ~2000 CE, Stordalen palsa experiences a stable WTD of ~6 cm, while exhibiting shifts in plant communities (Figure 3.2a). From ~1800 CE, brown moss (*Drepanocladus* sp.) dominates, from ~1900 CE there is a period of *Sphagnum lindbergii* and sedge and herb dominance before a transition in recent decades to *Sphagnum balticum*. In the absence of clear hydrological change during this period, a reduction in available nutrients could be driving the shift from *S. lindbergii* to *S. balticum* (Gunnarsson et al., 2004). *S. balticum* is a species typical of moderately-wet conditions (Johansson and Linder, 1980), yet demonstrates resistance to considerable drying since ~2000 CE. Similarly, in Stordalen bog the typically wet hollow species *Sphagnum fallax* demonstrates resistance to drying in recent decades, likely owing to its tolerance to desiccation (Wagner and Titus, 1984).

All sample locations – excluding Maunuvuoma fen – are currently underlain by permafrost. A transition from Cyperaceae and herb and UOM dominated assemblages to *Sphagnum* spp. or *Dicranum* spp. dominance may represent the aggradation of permafrost in Maunuvuoma fen ~2150 cal. BP, in Orusjohka palsa ~400 cal. BP and ~200 cal. BP in Ribasvuomus bog (Figure 3.2). In general permafrost is thought to have begun aggrading in Fennoscandia ~450 cal. BP (Treat and

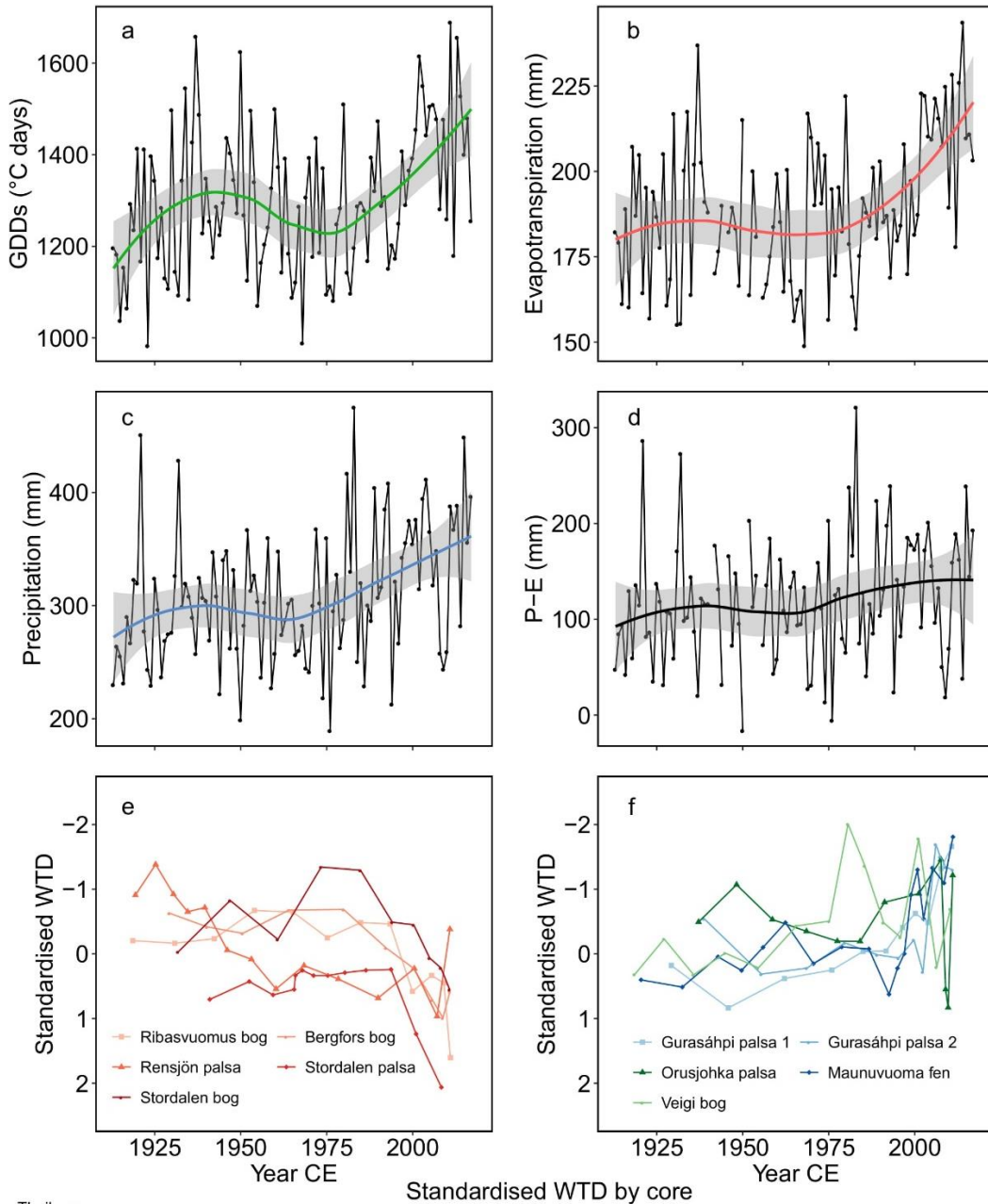
Jones, 2018), with evidence that permafrost aggradation may have been occurred in Stordalen mire as early as 2650 cal BP and late as 120 cal BP (Kokfelt et al., 2010). Greater certainty in the reconstruction of permafrost dynamics would likely be obtained through the study of subfossil oribatid mite communities (Markkula and Kuhry, 2020).

Any increases in C accumulation owing to improved productivity with warming or hydrological changes are difficult to distinguish from the artefact of incomplete decomposition in recent peats (Young et al., 2019) – characterised by an uptick in recent apparent C accumulation rate (ACAR; see Figure 3.2). Nonetheless, it is clear there is a decrease in C accumulation in Stordalen palsa, Rensjön palsa, Ribasvuomuš bog and Gurasáhpi palsa 1 during drying periods in the last century. A decrease in ACAR from the late-twentieth century in Stordalen palsa (Figure 3.2a) indicates a reduction in C accumulation great enough to overcome any artefact of incomplete decomposition, likely responsible for the increase in ACAR during the mid-twentieth century. We suggest this decreased C accumulation in the surface peat is probably because of high levels of aerobic decomposition associated with drying from ~2000 CE. This drying appears to be to such an extent as to have caused decomposition further down the profile (secondary decomposition) and consequently a reduced ACAR in the late-twentieth century (Frolking et al., 2014, Morris et al., 2015a). In Rensjön palsa, there is a decrease in ACAR coincident with drying prior to the recent uptick in ACAR (Figure 3.2g). Similarly, increased UOM – associated with high levels of decomposition – is observed alongside drying at the surface of Ribasvuomuš bog (Figure 3.2c) and at ~1950 CE in Gurasáhpi palsa 1 (Figure 3.2d). The UOM layer in both of these sites is stratigraphically above older, better preserved peat, suggesting an increase in the rate of decomposition that led to poorer preservation of more recent plant material. The subsequent replacement of UOM by a dominance of *S. fuscum* from ~1990 CE alongside wetting in Gurasáhpi palsa 1 suggests lower decomposition due to wetting and may indicate an increase in C sequestration. A complete lack of macrocharcoal in all our peat profiles shows fire has not been important in affecting C dynamics, in contrast to the importance of fire in some North American permafrost peatlands (Camill et al., 2009; Gibson et al., 2018; Jones et al., 2013; Robinson and Moore, 2000).

3.3.2. Climatic and autogenic drivers of ecosystem change

Abisko instrumental records show an increase in temperature, growing degree days (GDD₀), evapotranspiration and precipitation during the early- and late-twentieth century, while precipitation minus evaporation (P-E) experiences a slight increase since the late twentieth century (Figures 3.1 and 3.4). Precipitation observed at Abisko is lower than that of other local

stations (Figure 3.1). Sites experiencing drying show a positive relationship between WTD and climatic variables, while sites experiencing wetting or fluctuating WTD trends exhibit a negative relationship (Figure 3.4). This suggests that autogenic processes and site-specific factors play a key role in the hydrological response to climatic forcing. Under a steady-state climate, models of cyclic palsa formation and degradation associated with vegetation and snow accumulation feedbacks have been proposed, with drying during permafrost aggradation and wetting during degradation (Zuidhoff and Kolstrup, 2005). However, recent and continued warming in our study region makes further permafrost aggradation and palsa formation all but impossible.



Theil-sen beta slope		Standardised WTD by core										
		g	SP	SB	RB	BB	RP	GP1	GP2	MF	VB	OP
1	GDD (°C days)	Coefficient	0.002	0.004	0.003	0.006	0.002	-0.005	-0.005	-0.006	-0.004	0.000
	Beta	0.29	0.55	0.42	0.69	0.27	-0.68	-0.85	-0.78	-0.45	-0.01	
0.5	Evaporation (mm)	Coefficient	0.005	0.028	0.027	0.048	0.017	-0.029	-0.042	-0.025	-0.018	-0.012
	Beta	0.10	0.52	0.45	0.85	0.26	-0.52	-0.87	-0.45	-0.35	-0.17	
0	Precipitation (mm)	Coefficient	0.001	0.006	0.009	0.010	0.002	-0.011	-0.005	-0.011	-0.013	-0.012
	Beta	0.04	0.26	0.40	0.48	0.06	-0.44	-0.27	-0.59	-0.63	-0.44	
-0.5	P-E (mm)	Coefficient	0.002	0.001	0.005	0.011	-0.007	-0.013	0.001	-0.012	-0.011	-0.011
		Beta	0.08	0.04	0.25	0.51	-0.21	-0.53	0.06	-0.66	-0.63	-0.35
-1												

Figure 3.4. Relationship between climatic variables and water-table depth (WTD) across all sites. Annual a) growing degree days above 0°C (GDD₀; °C days), b) evapotranspiration (ET; mm) and c) precipitation (mm); d) precipitation minus evapotranspiration (P-E; mm) for Abisko, 1913 CE to present. Standardised WTD data from e) drying and f) wetting or fluctuating peat profiles since 1913 CE, and g) Theil-sen regression matrix (coefficients and betas) of standardised WTD by peat profile against each climatic variable. SP = Stordalen palsa, SB = Stordalen bog, RB = Ribasvuomuš bog, BB = Bergfors bog, RP = Rensjön palsa, GP1 = Gurasáhpi palsa 1, GP2= Gurasáhpi palsa 2, MF = Maunuvuoma fen, VB = Veigi bog and OP = Orusjohka palsa.

Greater winter snow depth, combined with rising summer temperatures, are thought to be the cause of thaw in the permafrost peatlands of northern Sweden (Sannel et al., 2016). Therefore, permafrost thaw, combined with increased growing season moisture from precipitation and snowmelt, provide a plausible explanation for sites experiencing recent wetting (Figure 3.4). Wetting from ~1990 CE in Gurasáhpi palsa 1 and 2 and Maunuvuoma fen was preceded by a period of drying (Figure 3.3). Here, a threshold point in drying and permafrost thaw may have been reached causing surface collapse and associated rewetting (Swindles et al., 2015b), suggesting the state of localised permafrost degradation is an important control on hydrological regime. Additionally, increases in decomposition with drying – as evidenced by a high mid-twentieth century concentration of UOM (~60%) in Gurasáhpi palsa 1 (Figure 3.2d) – may have reduced peatland surface hydraulic conductivity and drainage enough to facilitate recent wetting (Morris et al., 2015b).

Recent drying in Stordalen palsa, Stordalen bog, Ribasvuomuš bog, Bergfors bog, Rensjön palsa (and drying prior to wetting in Gurasáhpi palsa 1 and 2 and Maunuvuoma fen; Figure 3.3) is likely driven by increases in evapotranspiration and potentially productivity (i.e. GDD_0 ; Figure 3.4). Evaporation-driven drying with recent warming has also been observed in other Fennoscandian and northwest Russian permafrost peatlands (Zhang et al., 2018a). The lower precipitation experienced at Stordalen palsa and Stordalen bog (Figure 3.1) has perhaps made these sites more susceptible to drying. The slight recent increase in P-E appears to be of lesser importance to WTD in drying sites, but shows a stronger relationship with WTD at wetting sites (Figure 3.4g). A potential explanation for this is differences in permafrost structure affecting runoff rate and drainage. For example, localised permafrost collapse could create a topographic depression more favourable for retention of surplus precipitation. In other studies (Sonesson et al., 2002), greater *S. fuscum* or *D. elongatum* growth has been associated with increases in temperature and precipitation, and this increased productivity may be the cause of a deepening of the water-table as the peat surface grows rapidly upwards (van Bellen et al., 2018). However, this explanation could only apply where there is no clear decrease in C accumulation associated with drying, e.g. Bergfors bog with recent *D. elongatum* growth (Figure 3.2). The insulating properties of dry bryophyte layers are likely to have reduced the amplitude of soil temperatures and conversely may have acted to slow the rate of permafrost thaw (Soudzilovskaia et al., 2013). Nevertheless, increased connectivity of drainage pathways with permafrost thaw could be increasing runoff, leading to drying (Haynes et al., 2018) – here local topographic setting is likely to be important. Comparison of imagery of our study sites from 1959-1960 CE and 2012-2019 CE provides some

evidence of changes in permafrost peatland structure and drainage (Figures B.31-B.33). These structural changes associated with permafrost thaw have the potential to cause both wetting (e.g. surface collapse) and drying (e.g. drainage of surface water features).

Both Orusjohka palsa and Veigi bog experience fluctuations in wetness since the mid-twentieth century that are asynchronous to each other and the other sites (Figure 3.3). This fluctuating WTD may represent a flickering of ecosystem state (Wang et al., 2012), with negative autogenic feedbacks moderating the response to recent climate forcing (Swindles et al., 2012, Morris et al., 2015a, Waddington et al., 2015). Despite comparable growing season conditions, colder annual temperatures recorded near these sites at Nikkaloukta station (Figure 3.1) may be slowing rates of localised permafrost thaw, allowing autogenic feedbacks to dominate. For example, increases in bryophyte productivity with higher GDD_0 may facilitate rapid vertical growth and an increase in relative WTD (i.e. deeper water-tables). Higher aerobic decomposition with drying – evidenced in Orusjohka palsa ~1985 CE by a high UOM concentration (60%) and fungal remains count (Figure 3.2j; Figure B.25) – may cause a decrease in hydraulic conductivity of upper peats that then reduces water loss, inducing wetting. These more favourable (wetter) hydrological conditions may then again allow for greater bryophyte productivity as GDD_0 rise – continuing to drive fluctuations in hydrological conditions.

3.3.3. Implications for ecohydrological and carbon dynamics in global permafrost peatlands

Here we show a divergent response of permafrost peatland ecohydrological regimes to climate change over the last century (Figures 3.2, 3.3 and 3.4) and highlight the importance of internal autogenic and site-specific factors in these ecosystems. We link climate-driven drying with reduced C accumulation at four sites, but observe no clear relationship between wetting sites and C accumulation (Figure 3.2). Our data provide multi-proxy high-resolution evidence to substantiate previous suggestions of a heterogeneous response to recent warming in permafrost peatlands from longer Holocene archives in Fennoscandia (Zhang et al., 2018b) and late Holocene reconstructions in High Arctic Canada (Sim et al., 2019). Our findings illustrate how localised climatic variations between sites and autogenic processes linked to permafrost thaw, peatland structure, productivity and decomposition can combine in many ways to determine the future trajectory of permafrost peatlands, exemplified by the potential to cause both wetting and drying. Consequently, models of catastrophic C loss associated with drying (e.g. Ise et al., 2008) do not capture the complex ecological and hydrological dynamics of permafrost peatlands. Models incorporating permafrost, vegetation and hydrological dynamics (e.g. Chaudhary et al., 2020) are likely to provide a truer representation of reality and here we provide empirical data to inform

and test such models. Future research may be better able to disentangle the relative importance of autogenic and site-specific factors by: (i) collating existing palaeoecological records coupled with climatic data from a variety of permafrost peatlands; and (ii) combining a palaeoecological approach with models of peatland ecosystem development (e.g. Morris et al., 2015a), specifically adapted for permafrost conditions.

We show that bryophyte populations have demonstrated resistance and in some cases, resilience to climatic and hydrological changes over the last century (Figure 3.2). Bryophytes are abundant across high-latitude ecosystems, with *Sphagnum* spp. – such as *S. fuscum* - dominating boreal and tundra permafrost peatlands (Treat et al., 2016). This bryophyte resistance and resilience may allow for widespread increases in productivity with warming (Charman et al., 2013), perhaps to an extent where post-thaw surface C accumulation offsets C losses from deeper peat (Heffernan et al., 2020). However, bryophyte populations may be vulnerable to replacement by vascular plants with a greater availability of near-surface nitrogen (N) (Berendse et al., 2001) associated with permafrost thaw (Keuper et al., 2012) and increasing atmospheric N deposition (Galloway et al., 2004). Nonetheless, despite levels of N deposition being greater in Fennoscandia than other permafrost regions in recent centuries (Galloway et al., 2004), our data show stable bryophyte populations. This resistance and resilience suggests a degree of long-term bryophyte sustainability in global permafrost peatlands and through their insulating properties (Soudzilovskaia et al., 2013) they may help slow rates of inevitable permafrost thaw.

The divergent response to recent warming seen here in peatland ecosystems on the limits of discontinuous permafrost extent, may act as an indication for the future trajectory of more northerly or continental ecosystems currently exhibiting continuous permafrost (Brown et al., 2002). Moreover, these areas of extensive permafrost peatlands – such as northern Canada, Alaska and northern Russia – are likely to experience greater increases in temperature and precipitation than Fennoscandia in the twenty-first century (Christensen et al., 2013). Furthermore, there is likely to be regional variation in the importance of certain ecological processes, such as fire frequency – for which our findings suggest has a limited role, currently, in northern Sweden. Therefore, we can likely expect a degree of heterogeneity between Arctic regions in the future trajectory of permafrost peatlands.

3.4. Conclusions

Our findings suggest that: (i) permafrost peatlands have the potential to exhibit both wetting and drying under future climate change, owing to autogenic processes linked to permafrost thaw, peatland structure, productivity and decomposition; (ii) although ACAR should be interpreted

cautiously, hydrological conditions appear to be an important control on C dynamics; (iii) models of catastrophic C loss associated with drying do not capture the complex ecological and hydrological dynamics of permafrost peatlands; and (iv) bryophyte populations – specifically *S. fuscum* and *Dicranum* spp. – demonstrate resistance and in some cases resilience to recent climatic and hydrological changes. Our study provides a detailed insight into the recent response of permafrost peatlands to climate change in Fennoscandia and warns against an overly-simple approach to considering their future ecohydrological dynamics and role in the global C cycle.

Acknowledgements

T.G.S. is in receipt of a UK Natural Environment Research Council Training Grant (NE/ L002574/1). G.T.S. acknowledges the support of a Worldwide University Network (WUN) grant which helped fund the fieldwork (Project: Arctic Environments, Vulnerabilities and Opportunities). C.L.C. acknowledges a Leeds Anniversary Research Scholarship at the University of Leeds, in addition to support from the Climate Research Bursary Fund awarded by the Priestley International Centre for Climate. A.V.G-S. and D.J.C. were funded by the Natural Environment Research Council (NERC standard grant number NE/I012915/1). Staff from the Abisko Scientific Research Station assisted with field logistics and provided climatic data. Kallax Flyg AB provided helicopter support. We thank Matt Amesbury for useful discussions on testate amoeba transfer functions.

References

- Abbott, B.W., Jones, J.B., Schuur, E.A.G., Chapin III, F.S., Bowden, W.B., Bret-Harte, M.S., Epstein, H.E., Flannigan, M.D., Harms, T.K., Hollingsworth, T.N., Mack, M.C., McGuire, A.D., Natali, S.M., Rocha, A.V., Tank, S.E., Turetsky, M.R., Vonk, J.E., Wickland, K.P., Aiken, G.R., Alexander, H.D., Amon, R.M.W., Benscoter, B.W., Bergeron, Y., Bishop, K., Blarquez, O., Ben Bond-Lamberty, B., Breen, A.L., Buffam, I., Cai, Y., Carcaillet, C., Carey, S.K., Chen, J.M., Chen, H.Y.H., Christensen, T.R., Cooper, L.W., Cornelissen, J.H.C., de Groot, W.J., DeLuca, T.H., Dorrepaal, E., Fetcher, N., Finlay, J.C., Forbes, B.C., French, N.H.F., Gauthier, S., Girardin, M.P., Goetz, S.J., Goldammer, J.G., Gough, L., Grogan, P., Guo, L., Higuera, P.E., Hinzman, L., Hu, F.S., Hugelius, G., Jafarov, E.E., Jandt, R., Johnstone, J.F., Jan Karlsson, J., Kasischke, E.S., Kattner, G., Kelly, R., Keuper, F., Kling, G.W., Kortelainen, P., Kouki, J., Kuhry, P., Laudon, H., Laurion, I., Macdonald, R.W., Mann, P.J., Martikainen, P.J., McClelland, J.W., Molau, U., Oberbauer, S.F., Olefeldt, D., Paré, D., Parisien, M.-A., Payette, S., Peng, C., Pokrovsky, O.S., Rastetter, E.B., Raymond, P.A., Reynolds, M.K., Rein, G., Reynolds, J.F., Robards, M., Rogers, B.M., Schädel, C., Schaefer, K., Schmidt, I.K., Shvidenko, A., Sky, J., Spencer, R.G.M., Starr, G., Striegl, R.G., Teisserenc, R., Tranvik, L.J., Virtanen, T., Welker, J.M., Zimov, S., 2016. Biomass offsets little or none of permafrost carbon release from soils, streams, and wildfire: an expert assessment. *Environ. Res. Lett.* 11, 034014. <https://doi.org/10.1088/1748-9326/11/3/034014>
- Åkerman, H.J., Johansson, M., 2008. Thawing permafrost and thicker active layers in sub-arctic Sweden. *Permafr. Periglac. Process.* 19, 279–292. <https://doi.org/10.1002/ppp.626>
- Alekseychik, P.K., Korrensalo, A., Mammarella, I., Vesala, T., Tuittila, E.S., 2017. Relationship between aerodynamic roughness length and bulk sedge leaf area index in a mixed-species boreal mire complex. *Geophys. Res. Lett.* 44, 5836–5843. <https://doi.org/10.1002/2017GL073884>
- Amesbury, M.J., Swindles, G.T., Bobrov, A., Charman, D.J., Holden, J., Lamentowicz, M., Mallon, G., Mazei, Y., Mitchell, E.A.D., Payne, R.J., Roland, T.P., Turner, T.E., Warner, B.G., 2016. Development of a new pan-European testate amoeba transfer function for reconstructing peatland palaeohydrology. *Quat. Sci. Rev.* 152, 132–151. <https://doi.org/10.1016/J.QUASCIREV.2016.09.024>
- Aquino-López, M.A., Blaauw, M., Christen, J.A., Sanderson, N.K., 2018. Bayesian Analysis of 210 Pb Dating. *J. Agric. Biol. Environ. Stat.* 23, 317–333. <https://doi.org/10.1007/s13253-018-0328-7>
- Bartoń, K., 2019. MuMIn: Multi-Model Inference, Version 1.43.6. R Packag.
- Belyea, L.R., Baird, A.J., 2006. Beyond “The Limits to Peat Bog Growth”: Cross-Scale Feedback in Peatland Development. *Ecol. Monogr.* 76, 299–322. [https://doi.org/10.1890/0012-9615\(2006\)076\[0299:BTLPB\]2.0.CO;2](https://doi.org/10.1890/0012-9615(2006)076[0299:BTLPB]2.0.CO;2)
- Berendse, F., Van Breemen, N., Rydin, H., Buttler, A., Heijmans, M., Hoosbeek, M.R., Lee, J.A., Mitchell, E., Saarinen, T., Vasander, H., Wallén, B., 2001. Raised atmospheric CO₂ levels and increased N deposition cause shifts in plant species composition and production in Sphagnum bogs. *Glob. Chang. Biol.* 7, 591–598. <https://doi.org/10.1046/j.1365-2486.2001.00433.x>

- Booth, R.K., Lamentowicz, M., Charman, D.J., 2010. Preparation and analysis of testate amoebae in peatland palaeoenvironmental studies. *Mires Peat* 7, 1–7.
- Brown, J., Ferrians, O., Heginbottom, J.A., Melnikov, E., 2002. Circum-Arctic Map of Permafrost and Ground-Ice Conditions, Version 2. <https://doi.org/https://doi.org/10.7265/skbg-kf16>
- Callaghan, T. V., Bergholm, F., Christensen, T.R., Jonasson, C., Kokfelt, U., Johansson, M., 2010. A new climate era in the sub-Arctic: Accelerating climate changes and multiple impacts. *Geophys. Res. Lett.* 37, L14705. <https://doi.org/10.1029/2009GL042064>
- Camill, P., 2005. Permafrost Thaw Accelerates in Boreal Peatlands During Late-20th Century Climate Warming. *Clim. Change* 68, 135–152. <https://doi.org/10.1007/s10584-005-4785-y>
- Camill, P., Barry, A., Williams, E., Andreassi, C., Limmer, J., Solick, D., 2009. Climate-vegetation-fire interactions and their impact on long-term carbon dynamics in a boreal peatland landscape in northern Manitoba, Canada. *J. Geophys. Res.* 114, G04017. <https://doi.org/10.1029/2009JG001071>
- Chambers, F.M., Beilman, D.W., Yu, Z., 2011. Methods for determining peat humification and for quantifying peat bulk density, organic matter and carbon content for palaeostudies of climate and peatland carbon dynamics. *Mires Peat* 7, 1–10.
- Charman, D.J., Beilman, D.W., Blaauw, M., Booth, R.K., Brewer, S., Chambers, F.M., Christen, J.A., Gallego-Sala, A., Harrison, S.P., Hughes, P.D.M., Jackson, S.T., Korhola, A., Mauquoy, D., Mitchell, F.J.G., Prentice, I.C., van der Linden, M., De Vleeschouwer, F., Yu, Z.C., Alm, J., Bauer, I.E., Corish, Y.M.C., Garneau, M., Hohl, V., Huang, Y., Karofeld, E., Le Roux, G., Loisel, J., Moschen, R., Nichols, J.E., Nieminen, T.M., MacDonald, G.M., Phadtare, N.R., Rausch, N., Sillasoo, Ü., Swindles, G.T., Tuittila, E.-S., Ukonmaanaho, L., Väliranta, M., van Bellen, S., van Geel, B., Vitt, D.H., Zhao, Y., 2013. Climate-related changes in peatland carbon accumulation during the last millennium. *Biogeosciences* 10, 929–944. <https://doi.org/10.5194/bg-10-929-2013>
- Charman, D.J., Hendon, D., Woodland, W.A., 2000. The identification of testate amoebae (Protozoa: Rhizopoda) in peats: QRA Technical Guide No. 9, Quaternary Research Association. Quaternary Research Association, London. <https://doi.org/10.1016/j.quascirev.2004.02.012>
- Chaudhary, N., Westermann, S., Lamba, S., Shurpali, N., Sannel, A.B.K., Schurgers, G., Miller, P.A., Smith, B., 2020. Modelling past and future peatland carbon dynamics across the pan-Arctic. *Glob. Chang. Biol.* 26, 4119–4133. <https://doi.org/10.1111/gcb.15099>
- Christensen, J.H., Kumar, K.K., Aldrian, E., An, S.-I., Cavalcanti, I.F.A., de Castro, M., Dong, W., Goswami, P., Hall, A., Kanyanga, J.K., Kitoh, A., Kossin, J., Lau, N.-C., Renwick, J., Stephenson, D., Xie, S.-P., Zhou, T., 2013. Climate Phenomena and their Relevance for Future Regional Climate Change, in: Stocker, T.F., Qin, D., Plattner, G.-K., Tignor, M., Allen, S.K., Boschung, J., Nauels, A., Xia, Y., Bex, V., Midgley, P.M. (Eds.), *The Physical Science Basis. Contribution of Working Group I to the Fifth Assessment Report of the Intergovernmental Panel on Climate Change*. Cambridge University Press, Cambridge, United Kingdom and New York, NY, USA, pp. 1217–1310.
- Christensen, T.R., Johansson, T., Åkerman, H.J., Mastepanov, M., Malmer, N., Friborg, T., Crill, P., Svensson, B.H., 2004. Thawing sub-arctic permafrost: Effects on vegetation and methane emissions. *Geophys. Res. Lett.* 31, L04501. <https://doi.org/10.1029/2003GL018680>

- Clymo, R.S., 1984. The Limits to Peat Bog Growth. *Philos. Trans. R. Soc. B Biol. Sci.* 303, 605–654. <https://doi.org/10.1098/rstb.1984.0002>
- Cooper, C.L., Swindles, G.T., Watson, E.J., Savov, I.P., Gałka, M., Gallego-Sala, A., Borken, W., 2019. Evaluating tephrochronology in the permafrost peatlands of northern Sweden. *Quat. Geochronol.* 50, 16–28. <https://doi.org/10.1016/J.QUAGEO.2018.11.001>
- De Vleeschouwer, F., Chambers, F.M., Swindles, G.T., 2010. Coring and sub-sampling of peatlands for palaeoenvironmental research. *Mires Peat* 7, 1–10.
- Dorrepaal, E., Aerts, R., Cornelissen, J.H.C., Callaghan, T. V., Van Logtestijn, R.S.P., 2004. Summer warming and increased winter snow cover affect *Sphagnum fuscum* growth, structure and production in a sub-arctic bog. *Glob. Chang. Biol.* 10, 93–104. <https://doi.org/10.1111/j.1365-2486.2003.00718.x>
- French, H.M., 2017. *The Periglacial Environment*, 4th ed. John Wiley & Sons Ltd, Chichester, UK.
- Fritz, M., Wolter, J., Rudaya, N., Palagushkina, O., Nazarova, L., Obu, J., Rethemeyer, J., Lantuit, H., Wetterich, S., 2016. Holocene ice-wedge polygon development in northern Yukon permafrost peatlands (Canada). *Quat. Sci. Rev.* 147, 279–297. <https://doi.org/10.1016/J.QUASCIREV.2016.02.008>
- Frolking, S., Talbot, J., Subin, Z.M., 2014. Exploring the relationship between peatland net carbon balance and apparent carbon accumulation rate at century to millennial time scales. *The Holocene* 24, 1167–1173. <https://doi.org/10.1177/0959683614538078>
- Gałka, M., Szal, M., Watson, E.J., Gallego-Sala, A., Amesbury, M.J., Charman, D.J., Roland, T.P., Edward Turner, T., Swindles, G.T., 2017a. Vegetation Succession, Carbon Accumulation and Hydrological Change in Subarctic Peatlands, Abisko, Northern Sweden. *Permafr. Periglac. Process.* 28, 589–604. <https://doi.org/10.1002/ppp.1945>
- Gałka, M., Tobolski, K., Lamentowicz, Ł., Ersek, V., Jassey, V.E.J., van der Knaap, W.O., Lamentowicz, M., 2017b. Unveiling exceptional Baltic bog ecohydrology, autogenic succession and climate change during the last 2000 years in CE Europe using replicate cores, multi-proxy data and functional traits of testate amoebae. *Quat. Sci. Rev.* 156, 90–106. <https://doi.org/10.1016/J.QUASCIREV.2016.11.034>
- Gallego-Sala, A. V., Charman, D.J., Brewer, S., Page, S.E., Prentice, I.C., Friedlingstein, P., Moreton, S., Amesbury, M.J., Beilman, D.W., Björck, S., Blyakharchuk, T., Bochicchio, C., Booth, R.K., Bunbury, J., Camill, P., Carless, D., Chimner, R.A., Clifford, M., Cressey, E., Courtney-Mustaphi, C., De Vleeschouwer, F., de Jong, R., Fialkiewicz-Kozziel, B., Finkelstein, S.A., Garneau, M., Githumbi, E., Hribljan, J., Holmquist, J., Hughes, P.D.M., Jones, C., Jones, M.C., Karofeld, E., Klein, E.S., Kokfelt, U., Korhola, A., Lacourse, T., Le Roux, G., Lamentowicz, M., Large, D., Lavoie, M., Loisel, J., Mackay, H., MacDonald, G.M., Makila, M., Magnan, G., Marchant, R., Marcisz, K., Martínez Cortizas, A., Massa, C., Mathijssen, P., Mauquoy, D., Mighall, T., Mitchell, F.J.G., Moss, P., Nichols, J., Oksanen, P.O., Orme, L., Packalen, M.S., Robinson, S., Roland, T.P., Sanderson, N.K., Sannel, A.B.K., Silva-Sánchez, N., Steinberg, N., Swindles, G.T., Turner, T.E., Uglow, J., Väliranta, M., van Bellen, S., van der Linden, M., van Geel, B., Wang, G., Yu, Z., Zaragoza-Castells, J., Zhao, Y., 2018. Latitudinal limits to the predicted increase of the peatland carbon sink with warming. *Nat. Clim. Chang.* 1. <https://doi.org/10.1038/s41558-018-0271-1>

- Galloway, J.N., Dentener, F.J., Capone, D.G., Boyer, E.W., Howarth, R.W., Seitzinger, S.P., Asner, G.P., Cleveland, C.C., Green, P.A., Holland, E.A., Karl, D.M., Michaels, A.F., Porter, J.H., Townsend, A.R., Vörösmarty, C.J., 2004. Nitrogen cycles: Past, present, and future. *Biogeochemistry* 70, 153–226. <https://doi.org/10.1007/s10533-004-0370-0>
- Gibson, C.M., Chasmer, L.E., Thompson, D.K., Quinton, W.L., Flannigan, M.D., Olefeldt, D., 2018. Wildfire as a major driver of recent permafrost thaw in boreal peatlands. *Nat. Commun.* 9, 3041. <https://doi.org/10.1038/s41467-018-05457-1>
- GISTEMP Team, 2020. GISS Surface Temperature Analysis (GISTEMP) [WWW Document]. NASA Goddard Inst. Sp. Stud. <https://doi.org/10.1029/2010RG000345>
- Gunnarsson, U., Granberg, G., Nilsson, M., 2004. Growth, production and interspecific competition in Sphagnum: effects of temperature, nitrogen and sulphur treatments on a boreal mire. *New Phytol.* 163, 349–359. <https://doi.org/10.1111/j.1469-8137.2004.01108.x>
- Hadenäs, L., 2003. The European species of the Calliergon–Scorpidium–Drepanocladus complex, including some related or similar species. *Meylania* 28, 1–116.
- Harrison, G.W., 1979. Stability under Environmental Stress: Resistance, Resilience, Persistence, and Variability. *Am. Nat.* 113, 659–669. <https://doi.org/10.1086/283424>
- Haynes, K.M., Connon, R.F., Quinton, W.L., 2018. Permafrost thaw induced drying of wetlands at Scotty Creek, NWT, Canada. *Environ. Res. Lett.* 13. <https://doi.org/10.1088/1748-9326/aae46c>
- Heffernan, L., Estop-Aragónés, C., Knorr, K., Talbot, J., Olefeldt, D., 2020. Long-term impacts of permafrost thaw on carbon storage in peatlands: deep losses offset by surficial accumulation. *J. Geophys. Res. Biogeosciences* 125, e2019JG005501. <https://doi.org/10.1029/2019JG005501>
- Hölzer, A., 2010. Die Torfmoose Südwestdeutschlands und der Nachbargebiete. Weissdorn-Verlag, Jena, Germany.
- Hua, Q., Barbetti, M., Rakowski, A.Z., 2013. Atmospheric Radiocarbon for the Period 1950–2010. *Radiocarbon* 55, 2059–2072. https://doi.org/10.2458/azu_js_rc.v55i2.16177
- Hugelius, G., Strauss, J., Zubrzycki, S., Harden, J.W., Schuur, E.A.G., Ping, C.-L., Schirmermeister, L., Grosse, G., Michaelson, G.J., Koven, C.D., O'Donnell, J.A., Elberling, B., Mishra, U., Camill, P., Yu, Z., Palmtag, J., Kuhry, P., 2014. Estimated stocks of circumpolar permafrost carbon with quantified uncertainty ranges and identified data gaps. *Biogeosciences* 11, 6573–6593. <https://doi.org/10.5194/bg-11-6573-2014>
- Ise, T., Dunn, A.L., Wofsy, S.C., Moorcroft, P.R., 2008. High sensitivity of peat decomposition to climate change through water-table feedback. *Nat. Geosci.* 1, 763–766. <https://doi.org/10.1038/ngeo331>
- Jeong, S.-J., Bloom, A.A., Schimel, D., Sweeney, C., Parazoo, N.C., Medvigy, D., Schaepman-Strub, G., Zheng, C., Schwalm, C.R., Huntzinger, D.N., Michalak, A.M., Miller, C.E., 2018. Accelerating rates of Arctic carbon cycling revealed by long-term atmospheric CO₂ measurements. *Sci. Adv.* 4, eaao1167. <https://doi.org/10.1126/sciadv.aao1167>
- Johansson, L.G., Linder, S., 1980. Photosynthesis of Sphagnum in Different Microhabitats on a Subarctic Mire. *Ecol. Bull.*

- Johansson, M., Christensen, T.R., Akerman, H.J., Callaghan, T. V., 2006. What Determines the Current Presence or Absence of Permafrost in the Torneträsk Region, a Sub-arctic Landscape in Northern Sweden? [https://doi.org/10.1579/0044-7447\(2006\)35\[190:WDTCP0\]2.0.CO;2](https://doi.org/10.1579/0044-7447(2006)35[190:WDTCP0]2.0.CO;2), 190–197. [https://doi.org/10.1579/0044-7447\(2006\)35\[190:WDTCP0\]2.0.CO;2](https://doi.org/10.1579/0044-7447(2006)35[190:WDTCP0]2.0.CO;2)
- Jones, M.C., Booth, R.K., Yu, Z., Ferry, P., 2013. A 2200-Year Record of Permafrost Dynamics and Carbon Cycling in a Collapse-Scar Bog, Interior Alaska. *Ecosystems* 16, 1–19. <https://doi.org/10.1007/s10021-012-9592-5>
- Jones, M.C., Harden, J., O'Donnell, J., Manies, K., Jorgenson, T., Treat, C., Ewing, S., 2017. Rapid carbon loss and slow recovery following permafrost thaw in boreal peatlands. *Glob. Chang. Biol.* 23, 1109–1127. <https://doi.org/10.1111/gcb.13403>
- Keuper, F., van Bodegom, P.M., Dorrepaal, E., Weedon, J.T., van Hal, J., van Logtestijn, R.S.P., Aerts, R., 2012. A frozen feast: Thawing permafrost increases plant-available nitrogen in subarctic peatlands. *Glob. Chang. Biol.* 18, 1998–2007. <https://doi.org/10.1111/j.1365-2486.2012.02663.x>
- Kokfelt, U., Reuss, N., Struyf, E., Sonesson, M., Rundgren, M., Skog, G., Rosén, P., Hammarlund, D., 2010. Wetland development, permafrost history and nutrient cycling inferred from late Holocene peat and lake sediment records in subarctic Sweden. *J. Paleolimnol.* 44, 327–342. <https://doi.org/10.1007/s10933-010-9406-8>
- Laine, J., Harju, P., Timonen, T., Laine, A., Tuittila, E.-S., Minkkinen, K., Vasander, H., 2011. The Intricate Beauty of Sphagnum Mosses: A Finnish Guide to Identification. Department of Forest Sciences, University of Helsinki.
- Lamarre, A., Garneau, M., Asnong, H., 2012. Holocene paleohydrological reconstruction and carbon accumulation of a permafrost peatland using testate amoeba and macrofossil analyses, Kuujuarapik, subarctic Québec, Canada. *Rev. Palaeobot. Palynol.* 186, 131–141. <https://doi.org/10.1016/J.REVPALBO.2012.04.009>
- Markkula, I., Kuhry, P., 2020. Subfossil oribatid mite communities indicate Holocene permafrost dynamics in Canadian mires. *Boreas* bor.12444. <https://doi.org/10.1111/bor.12444>
- Masson-Delmotte, V., Zhai, P., Pörtner, H.-O., Roberts, D., Skea, J., Shukla, P.R., Pirani, A., Moufouma-Okia, W., Péan, C., Pidcock, R., Connors, S., Matthews, J.B.R., Chen, Y., Zhou, X., Gomis, M.I., Lonnoy, E., Maycock, T., Tignor, M., Waterfield, T., 2018. Intergovernmental Panel on Climate Change, 2018: Summary for Policymakers, in: *Global Warming of 1.5°C. An IPCC Special Report on the Impacts of Global Warming of 1.5°C above Pre-Industrial Levels and Related Global Greenhouse Gas Emission Pathways, in the Context of Strengthening the Global Response to the Threat of Climate Change,* pp. 3–24. <https://doi.org/10.1017/CBO9781107415324>
- Mauquoy, D., van Geel, B., 2007. Mire and peat macros, in: Elias, S.A. (Ed.), *Encyclopedia of Quaternary Science*. Elsevier, Amsterdam, pp. 2315–2336.
- Morris, P.J., Baird, A.J., Belyea, L.R., 2015a. Bridging the gap between models and measurements of peat hydraulic conductivity. *Water Resour. Res.* 51, 5353–5364. <https://doi.org/10.1002/2015WR017264>
- Morris, P.J., Baird, A.J., Young, D.M., Swindles, G.T., 2015b. Untangling climate signals from autogenic changes in long-term peatland development. *Geophys. Res. Lett.* 42, 10,788–

10,797. <https://doi.org/10.1002/2015GL066824>

- Morris, P.J., Swindles, G.T., Valdes, P.J., Ivanovic, R.F., Gregoire, L.J., Smith, M.W., Tarasov, L., Haywood, A.M., Bacon, K.L., 2018. Global peatland initiation driven by regionally asynchronous warming. *Proc. Natl. Acad. Sci. U. S. A.* 115, 4851–4856. <https://doi.org/10.1073/pnas.1717838115>
- O'Donnell, J.A., Jorgenson, M.T., Harden, J.W., McGuire, A.D., Kanevskiy, M.Z., Wickland, K.P., 2012. The Effects of Permafrost Thaw on Soil Hydrologic, Thermal, and Carbon Dynamics in an Alaskan Peatland. *Ecosystems* 15, 213–229. <https://doi.org/10.1007/s10021-011-9504-0>
- Olvmo, M., Holmer, B., Thorsson, S., Reese, H., Lindberg, F., 2020. Sub-arctic palsa degradation and the role of climatic drivers in the largest coherent palsa mire complex in Sweden (Vissátvuopmi), 1955–2016. *Sci. Rep.* 10, 1–10. <https://doi.org/10.1038/s41598-020-65719-1>
- Payette, S., Delwaide, A., Caccianiga, M., Beauchemin, M., 2004. Accelerated thawing of subarctic peatland permafrost over the last 50 years. *Geophys. Res. Lett.* 31, L18208. <https://doi.org/10.1029/2004GL020358>
- Pelletier, N., Talbot, J., Olefeldt, D., Turetsky, M., Blodau, C., Sonnentag, O., Quinton, W.L., 2017. Influence of Holocene permafrost aggradation and thaw on the paleoecology and carbon storage of a peatland complex in northwestern Canada. *The Holocene* 27, 1391–1405. <https://doi.org/10.1177/0959683617693899>
- R Core Team, 2021. R: a language and environment for statistical computing. Version 4.0.5.
- Reimer, P.J., Bard, E., Bayliss, A., Beck, J.W., Blackwell, P.G., Ramsey, C.B., Buck, C.E., Cheng, H., Edwards, R.L., Friedrich, M., Grootes, P.M., Guilderson, T.P., Hafliðason, H., Hajdas, I., Hatté, C., Heaton, T.J., Hoffmann, D.L., Hogg, A.G., Hughen, K.A., Kaiser, K.F., Kromer, B., Manning, S.W., Niu, M., Reimer, R.W., Richards, D.A., Scott, E.M., Southon, J.R., Staff, R.A., Turney, C.S.M., van der Plicht, J., 2013. IntCal13 and Marine13 Radiocarbon Age Calibration Curves 0–50,000 Years cal BP. *Radiocarbon* 55, 1869–1887. https://doi.org/10.2458/azu_js_rc.55.16947
- Robinson, S.D., Moore, T.R., 2000. The Influence of Permafrost and Fire upon Carbon Accumulation in High Boreal Peatlands, Northwest Territories, Canada. *Arctic, Antarct. Alp. Res.* 32, 155–166. <https://doi.org/10.1080/15230430.2000.12003351>
- Rydin, H., Gunnarsson, U., Sundberg, S., 2006. The Role of Sphagnum in Peatland Development and Persistence, in: Wieder, R.K., Vitt, D.H. (Eds.), *Boreal Peatland Ecosystems*. Springer Berlin Heidelberg, pp. 47–65. https://doi.org/10.1007/978-3-540-31913-9_4
- Rydin, H., McDonald, A.J.S., 1985. Tolerance of Sphagnum to water level. *J. Bryol.* 13, 571–578. <https://doi.org/10.1179/jbr.1985.13.4.571>
- Sannel, A.B.K., Hempel, L., Kessler, A., Prėskienis, V., 2018. Holocene development and permafrost history in sub-arctic peatlands in Tavvavuoma, northern Sweden. *Boreas* 47, 454–468. <https://doi.org/10.1111/bor.12276>
- Sannel, A.B.K., Hugelius, G., Jansson, P., Kuhry, P., 2016. Permafrost Warming in a Subarctic Peatland – Which Meteorological Controls are Most Important? *Permafr. Periglac. Process.* 27, 177–188. <https://doi.org/10.1002/ppp.1862>

- Siemensma, F.J., 2021. Microworld, world of amoeboid organisms [WWW Document]. World-wide Electron. Publ. URL <http://www.arcella.nl>
- Sim, T.G., Swindles, G.T., Morris, P.J., Gałka, M., Mullan, D., Galloway, J.M., 2019. Pathways for Ecological Change in Canadian High Arctic Wetlands Under Rapid Twentieth Century Warming. *Geophys. Res. Lett.* 46, 4726–4737. <https://doi.org/10.1029/2019GL082611>
- Smith, A.J.E., 2004. *The Moss Flora of Britain and Ireland*, 2nd ed. Cambridge University Press, Cambridge, United Kingdom.
- Sonesson, M., Carlsson, B.Å., Callaghan, T. V., Halling, S., Björn, L.O., Bertgren, M., Johanson, U., 2002. Growth of two peat-forming mosses in subarctic mires: Species interactions and effects of simulated climate change. *Oikos* 99, 151–160. <https://doi.org/10.1034/j.1600-0706.2002.990115.x>
- Soudzilovskaia, N.A., van Bodegom, P.M., Cornelissen, J.H.C., 2013. Dominant bryophyte control over high-latitude soil temperature fluctuations predicted by heat transfer traits, field moisture regime and laws of thermal insulation. *Funct. Ecol.* 27, 1442–1454. <https://doi.org/10.1111/1365-2435.12127>
- Stiegler, C., Johansson, M., Christensen, T.R., Mastepanov, M., Lindroth, A., 2016. Tundra permafrost thaw causes significant shifts in energy partitioning. *Tellus B Chem. Phys. Meteorol.* 68, 30467. <https://doi.org/10.3402/tellusb.v68.30467>
- Swindles, G.T., Amesbury, M.J., Turner, T.E., Carrivick, J.L., Woulds, C., Raby, C., Mullan, D., Roland, T.P., Galloway, J.M., Parry, L., Kokfelt, U., Garneau, M., Charman, D.J., Holden, J., 2015a. Evaluating the use of testate amoebae for palaeohydrological reconstruction in permafrost peatlands. *Palaeogeogr. Palaeoclimatol. Palaeoecol.* 424, 111–122. <https://doi.org/10.1016/J.PALAEO.2015.02.004>
- Swindles, G.T., Holden, J., Raby, C.L., Turner, T.E., Blundell, A., Charman, D.J., Menberu, M.W., Kløve, B., 2015b. Testing peatland water-table depth transfer functions using high-resolution hydrological monitoring data. *Quat. Sci. Rev.* 120, 107–117. <https://doi.org/10.1016/J.QUASCIREV.2015.04.019>
- Swindles, G.T., Morris, P.J., Baird, A.J., Blaauw, M., Plunkett, G., 2012. Ecohydrological feedbacks confound peat-based climate reconstructions. *Geophys. Res. Lett.* 39, L11401. <https://doi.org/10.1029/2012GL051500>
- Swindles, G.T., Morris, P.J., Mullan, D., Watson, E.J., Turner, T.E., Roland, T.P., Amesbury, M.J., Kokfelt, U., Schoning, K., Pratte, S., Gallego-Sala, A., Charman, D.J., Sanderson, N., Garneau, M., Carrivick, J.L., Woulds, C., Holden, J., Parry, L., Galloway, J.M., 2015c. The long-term fate of permafrost peatlands under rapid climate warming. *Sci. Rep.* 5, 17951. <https://doi.org/10.1038/srep17951>
- Swindles, G.T., Morris, P.J., Mullan, D.J., Payne, R.J., Roland, T.P., Amesbury, M.J., Lamentowicz, M., Turner, T.E., Gallego-Sala, A., Sim, T., Barr, I.D., Blaauw, M., Blundell, A., Chambers, F.M., Charman, D.J., Feurdean, A., Galloway, J.M., Gałka, M., Green, S.M., Kajukalo, K., Karofeld, E., Korhola, A., Lamentowicz, Ł., Langdon, P., Marcisz, K., Mauquoy, D., Mazei, Y.A., McKeown, M.M., Mitchell, E.A.D., Novenko, E., Plunkett, G., Roe, H.M., Schoning, K., Sillasoo, Ü., Tsyganov, A.N., van der Linden, M., Väliranta, M., Warner, B., 2019. Widespread drying of European peatlands in recent centuries. *Nat. Geosci.* 12, 922–928.

<https://doi.org/10.1038/s41561-019-0462-z>

- Tarnocai, C., Canadell, J.G., Schuur, E.A.G., Kuhry, P., Mazhitova, G., Zimov, S., 2009. Soil organic carbon pools in the northern circumpolar permafrost region. *Global Biogeochem. Cycles* 23, GB2023. <https://doi.org/10.1029/2008GB003327>
- Taylor, L.S., Swindles, G.T., Morris, P.J., Gałka, M., Green, S.M., 2019. Evidence for ecosystem state shifts in Alaskan continuous permafrost peatlands in response to recent warming. *Quat. Sci. Rev.* 207, 134–144. <https://doi.org/10.1016/j.quascirev.2019.02.001>
- Therneau, T., 2018. deming, Version 1.4. R Packag.
- Treat, C.C., Jones, M.C., 2018. Near-surface permafrost aggradation in Northern Hemisphere peatlands shows regional and global trends during the past 6000 years. *The Holocene* 28, 998–1010. <https://doi.org/10.1177/0959683617752858>
- Treat, C.C., Jones, M.C., Camill, P., Gallego-Sala, A., Garneau, M., Harden, J.W., Hugelius, G., Klein, E.S., Kokfelt, U., Kuhry, P., Loisel, J., Mathijssen, P.J.H., O'Donnell, J.A., Oksanen, P.O., Ronkainen, T.M., Sannel, A.B.K., Talbot, J., Tarnocai, C., Väliranta, M., 2016. Effects of permafrost aggradation on peat properties as determined from a pan-Arctic synthesis of plant macrofossils. *J. Geophys. Res. Biogeosciences* 121, 78–94. <https://doi.org/10.1002/2015JG003061>
- Turetsky, M.R., Abbott, B.W., Jones, M.C., Anthony, K.W., Olefeldt, D., Schuur, E.A.G., Grosse, G., Kuhry, P., Hugelius, G., Koven, C., Lawrence, D.M., Gibson, C., Sannel, A.B.K., McGuire, A.D., 2020. Carbon release through abrupt permafrost thaw. *Nat. Geosci.* 13, 138–143. <https://doi.org/10.1038/s41561-019-0526-0>
- van Bellen, S., Magnan, G., Davies, L., Froese, D., Mullan-Boudreau, G., Zaccone, C., Garneau, M., Shotyk, W., 2018. Testate amoeba records indicate regional 20th-century lowering of water tables in ombrotrophic peatlands in central-northern Alberta, Canada. *Glob. Chang. Biol.* 24, 2758–2774. <https://doi.org/10.1111/gcb.14143>
- Waddington, J.M., Morris, P.J., Kettridge, N., Granath, G., Thompson, D.K., Moore, P.A., 2015. Hydrological feedbacks in northern peatlands. *Ecohydrology* 8, 113–127. <https://doi.org/10.1002/eco.1493>
- Wagner, D.J., Titus, J.E., 1984. Comparative desiccation tolerance of two Sphagnum mosses. *Oecologia* 62, 182–187. <https://doi.org/10.1007/BF00379011>
- Wang, R., Dearing, J.A., Langdon, P.G., Zhang, E., Yang, X., Dakos, V., Scheffer, M., 2012. Flickering gives early warning signals of a critical transition to a eutrophic lake state. *Nature* 492, 419–422. <https://doi.org/10.1038/nature11655>
- Woo, M.-K., Winter, T.C., 1993. The role of permafrost and seasonal frost in the hydrology of northern wetlands in North America. *J. Hydrol.* 141, 5–31. [https://doi.org/10.1016/0022-1694\(93\)90043-9](https://doi.org/10.1016/0022-1694(93)90043-9)
- Young, D.M., Baird, A.J., Charman, D.J., Evans, C.D., Gallego-Sala, A. V., Gill, P.J., Hughes, P.D.M., Morris, P.J., Swindles, G.T., 2019. Misinterpreting carbon accumulation rates in records from near-surface peat. *Sci. Rep.* 9, 1–8. <https://doi.org/10.1038/s41598-019-53879-8>
- Yu, Z., Beilman, D.W., Frohking, S., MacDonald, G.M., Roulet, N.T., Camill, P., Charman, D.J., 2011. Peatlands and Their Role in the Global Carbon Cycle. *Eos, Trans. Am. Geophys. Union* 92, 97–

98. <https://doi.org/10.1029/2011EO120001>

- Zhang, H., Gallego-Sala, A. V., Amesbury, M.J., Charman, D.J., Piilo, S.R., Väliranta, M.M., 2018a. Inconsistent response of Arctic permafrost peatland carbon accumulation to warm climate phases. *Global Biogeochem. Cycles* 32, 1605–1620. <https://doi.org/10.1029/2018GB005980>
- Zhang, H., Piilo, S.R., Amesbury, M.J., Charman, D.J., Gallego-Sala, A. V., Väliranta, M.M., 2018b. The role of climate change in regulating Arctic permafrost peatland hydrological and vegetation change over the last millennium. *Quat. Sci. Rev.* 182, 121–130. <https://doi.org/10.1016/J.QUASCIREV.2018.01.003>
- Zhang, H., Väliranta, M., Piilo, S., Amesbury, M.J., Aquino-López, M.A., Roland, T.P., Salminen-Paatero, S., Paatero, J., Lohila, A., Tuittila, E., 2020. Decreased carbon accumulation feedback driven by climate-induced drying of two southern boreal bogs over recent centuries. *Glob. Chang. Biol.* 26, 2435–2448. <https://doi.org/10.1111/gcb.15005>
- Zuidhoff, F.S., Kolstrup, E., 2005. Palsa Development and Associated Vegetation in Northern Sweden Palsa Development and Associated Vegetation in Northern Sweden. *Arctic, Antarct. Alp. Res.* 37, 49–60. [https://doi.org/10.1657/1523-0430\(2005\)037\[0049:PDAAVI\]2.0.CO;2](https://doi.org/10.1657/1523-0430(2005)037[0049:PDAAVI]2.0.CO;2)

Chapter 4 – Regional variability in peatland burning at mid- to high- latitudes during the Holocene

Regional variability in peatland burning at mid- to high-latitudes during the Holocene

Thomas G. Sim^{1,2}, Graeme T. Swindles^{3,4}, Paul J. Morris¹, Andy J. Baird¹, Angela V. Gallego-Sala², Yuwan Wang^{2,5}, Maarten Blaauw⁶, Philip Camill⁷, Michelle Garneau⁸, Mark Hardiman⁹, Julie Loisel¹⁰, Minna Väliranta¹¹, Lysanna Anderson¹², Karina Apolinarska¹³, Femke Augustijns¹⁴, Liene Aunina¹⁵, Joannie Beaulne⁸, Přemysl Bobek¹⁶, Werner Borken¹⁷, Nils Broothaerts¹⁴, Qiao-Yu Cui^{18,19}, Marissa A. Davies²⁰, Ana Ejarque²¹, Michelle Farrell²², Ingo Feeser²³, Angelica Feurdean^{24,25}, Richard Fewster¹, Sarah A. Finkelstein²⁰, Marie-José Gaillard¹⁹, Mariusz Gałka²⁶, Liam Heffernan²⁷, Renske Hoever¹⁴, Miriam Jones²⁸, Teemu Juselius¹¹, Edgar Karofeld²⁹, Klaus Holger Knorr³⁰, Atte Korhola¹¹, Dmitri Kupriyanov³¹, Malin E. Kylander³², Terri Lacourse³³, Mariusz Lamentowicz³⁴, Martin Lavoie³⁵, Geoffrey Lemdahl¹⁹, Dominika Łuców³⁶, Gabriel Magnan⁸, Alekss Maksims³⁷, Claudia A. Mansilla³⁸, Katarzyna Marcisz³⁴, Elena Marinova³⁹, Paul J.H. Mathijssen^{30,40}, Dmitri Mauquoy⁴¹, Yuri Mazei^{31,42}, Natalia Mazei³¹, Julia McCarroll⁴³, Robert McCulloch⁴⁴, Alice Milner⁴⁵, Yannick Miras⁴⁶, Fraser J.G. Mitchell⁴⁷, Elena Novenko^{31,48}, Nicolas Pelletier⁴⁹, Matthew Peros⁵⁰, Sanna R. Piilo¹¹, Louis-Martin Pilote⁸, Guillaume Primeau⁸, Damien Rius⁵¹, Vincent Robin⁵², Mylène Robitaille⁸, Thomas P. Roland², Eleonor Ryberg^{32,52}, A. Britta K. Sannel⁵⁴, Karsten Schitteck⁵⁵, Gabriel Servera-Vives^{56,57}, William Shotyk²⁷, Michał Słowiński³⁶, Normunds Stivrins^{58,59}, Ward Swinnen^{14,60}, Gareth Thompson², Alexei Tiunov⁶¹, Andrey N. Tsyganov^{31,61}, Eeva-Stiina Tuittila⁶², Gert Verstraeten¹⁴, Tuomo Wallenius¹¹, Julia Webb⁴³, Debra Willard²⁸, Zicheng Yu^{63, 64}, Claudio Zaccone⁶⁵ and Hui Zhang^{11,66}

¹School of Geography, University of Leeds, Leeds, UK

²Geography, College of Life and Environmental Sciences, University of Exeter, Exeter, UK

³Geography, School of Natural and Built Environment, Queen's University Belfast, Belfast, UK

⁴Ottawa-Carleton Geoscience Centre and Department of Earth Sciences, Carleton University, Ottawa, Ontario, Canada

⁵School of Earth and Environmental Sciences, University of Queensland, Australia

⁶Archaeology and Palaeoecology, School of Natural and Built Environment, Queen's University Belfast, Belfast, UK

⁷Bowdoin College, Earth and Oceanographic Science Dept., 6800 College Station, Brunswick, Maine, 04011, USA

⁸Geotop-Université du Québec à Montréal, C.P. 8888, Succ. Centre-Ville, Montréal, QC, H3C 3P8, Canada

⁹School of the Environment, Geography and Geosciences, University of Portsmouth, Buckingham Building, Lion Terrace, Portsmouth, PO1 3HE, UK

¹⁰Department of Geography, Texas A&M University, College Station, TX 77843, USA

¹¹Environmental Change Research Unit (ECRU), Ecosystems, Environment Research Programme, Faculty of Biological and Environmental Sciences, and Helsinki Institute of Sustainability Science (HELSUS), University of Helsinki, Viikinkaari 1, P.O. Box 65, 00014, Helsinki, Finland

¹²U.S. Geological Survey, GEMEG-SC, Menlo Park, CA 94025, USA

¹³Institute of Geology, Adam Mickiewicz University, Krygowskiego 12, 61-680 Poznań, Poland

- ¹⁴Division of Geography and Tourism, Department of Earth and Environmental Sciences, KU Leuven, Celestijnenlaan 200E, 3001 Heverlee, Belgium
- ¹⁵University of Latvia, Institute of Biology, Laboratory of Geobotany, Riga, Latvia
- ¹⁶Institute of Botany, Czech Academy of Sciences, Zámek 1, 25243, Průhonice, Czech Republic
- ¹⁷Soil Ecology, University of Bayreuth, Bayreuth Center of Ecology and Environmental Research (BayCEER), Dr.-Hans-Frisch-Str. 1-3, 95448 Bayreuth, Germany
- ¹⁸Key Laboratory of Land Surface Pattern and Simulation, Institute of Geographical Sciences and Natural Resources Research, Chinese Academy of Sciences, Beijing 100101, China
- ¹⁹Department of Biology and Environmental Science, Linnaeus University, Kalmar, Sweden
- ²⁰Department of Earth Sciences, University of Toronto, 22 Ursula Franklin Street, Toronto, Ontario, M5S 3B1, Canada
- ²¹ISEM, Univ Montpellier, CNRS, IRD, France
- ²²Centre for Agroecology, Water and Resilience, Coventry University, Wolston Lane, Ryton-on-Dunsmore, Coventry, CV8 3LG, UK
- ²³Institute of Pre- and Protohistoric Archaeology, University of Kiel, D-24098 Kiel, Germany
- ²⁴Department of Physical Geography, Goethe University, Altenhöferallee 1, 60438 Frankfurt am Main, Germany
- ²⁵STAR-UBB Institute, Babeş-Bolyai University, Kogălniceanu 1, 400084, Cluj-Napoca, Romania
- ²⁶University of Łódź, Faculty of Biology and Environmental Protection, Department of Biogeography, Paleoecology and Nature Protection, Banacha 1/3, 90-237, Łódź, Poland
- ²⁷Department of Renewable Resources, University of Alberta, Edmonton, AB, Canada
- ²⁸U.S. Geological Survey, Florence Bascom Geoscience Center, Reston, VA, USA
- ²⁹Institute of Ecology and Earth Sciences, University of Tartu, Tartu, Estonia
- ³⁰University of Münster, Institute of Landscape Ecology, Ecohydrology and Biogeochemistry Group, Heisenbergstr. 2, 48149 Münster, Germany
- ³¹Lomonosov Moscow State University, Leninskiye gory, 1, Moscow, 119991, Russia
- ³²Department of Geological Sciences, Stockholm University, SE-106 91 Stockholm, Sweden
- ³³Department of Biology and Centre for Forest Biology, University of Victoria, Victoria, BC V8W 2Y2, Canada
- ³⁴Climate Change Ecology Research Unit, Faculty of Geographical and Geological Sciences, Adam Mickiewicz University, Bogumiła Krygowskiego 10, 61-680, Poznań, Poland
- ³⁵Département de géographie and Centre d'études nordiques, Université Laval, Québec, Canada
- ³⁶Institute of Geography and Spatial Organization, Polish Academy of Sciences, Twarda 51/55, 00-818 Warsaw, Poland
- ³⁷Department of Geology, University of Latvia, Jelgavas iela 1, LV-1004, Riga, Latvia
- ³⁸Centro de Investigación GAIA/Antártica, Universidad de Magallanes. Punta Arenas 6210427, Chile
- ³⁹Laboratory for Archaeobotany, Baden-Württemberg State Office for Cultural Heritage, Fischersteig 9, 78343 Gaienhofen-Hemmenhofen, Germany
- ⁴⁰Vegetation, Forest and Landscape Ecology, Wageningen Environmental Research, Wageningen University & Research, PO Box 47, NL-6700 AA, Wageningen, The Netherlands
- ⁴¹School of Geosciences, University of Aberdeen, AB24 3UF, UK

- ⁴²Shenzhen MSU-BIT University, International University Park Road, Dayun New Town, Longgang District, Shenzhen 517182, China
- ⁴³Centre for Environmental Change and Quaternary Research, School of Natural and Social Sciences, University of Gloucestershire, UK
- ⁴⁴Centro de Investigación en Ecosistemas de la Patagonia, Coyhaique, Aysén, Chile
- ⁴⁵Department of Geography, Royal Holloway University of London, Egham, TW20 0EX, UK
- ⁴⁶CNRS, HNHP UMR 7194, Muséum National d'Histoire Naturelle, Institut de Paléontologie Humaine, Paris, France
- ⁴⁷Botany Department, School of Natural Sciences, Trinity College Dublin, Dublin, Ireland
- ⁴⁸Institute of Geography Russian Academy of Science, Staromonetny lane, Moscow, 119017, Russia
- ⁴⁹Department of Geography and Environmental Studies, Carleton University, 1125 Colonel By Dr, Ottawa, ON K1S 5B6, Canada
- ⁵⁰Bishop's University, Department of Environment and Geography, Sherbrooke, Quebec, J1M 1Z7, Canada
- ⁵¹Chrono-environnement UMR6249, CNRS, Université Bourgogne Franche-Comté, F-25000, Besançon, France
- ⁵²Interdisciplinary Laboratory for Continental Environments, University of Lorraine, Campus Bridoux, 57070 Metz, France
- ⁵³Bolin Centre for Climate Research, Stockholm University, SE-106 91 Stockholm, Sweden
- ⁵⁴Department of Physical Geography, Stockholm University, SE-106 91 Stockholm, Sweden
- ⁵⁵Institut für Geographiedidaktik, Universität zu Köln, Gronewaldstr. 2. 50931 Köln, Germany
- ⁵⁶Laboratory of Palynology and Paleobotany, Department of Life Sciences, Università degli Studi di Modena e Reggio Emilia, Italy
- ⁵⁷ArqueoUIB, Department of Historical Sciences and Theory of Art, University of the Balearic Islands, Palma, Spain
- ⁵⁸Department of Geography, University of Latvia, Jelgavas iela 1, LV-1004, Riga, Latvia
- ⁵⁹Department of Geology, Tallinn University of Technology, Ehitajate tee 5, EE-19086, Tallinn, Estonia
- ⁶⁰Research Foundation Flanders (FWO), Brussels, 1000, Belgium
- ⁶¹A.N. Severtsov Institute of Ecology and Evolution, Russian Academy of Sciences, Moscow, 119071, Russia
- ⁶²University of Eastern Finland, Faculty of Science and Forestry, School of Forest Sciences. P. O. Box 111. FI- 80101 Joensuu, Finland
- ⁶³Key Laboratory of Geographical Processes & Ecological Security in Changbai Mountains, Ministry of Education, School of Geographical Sciences, Northeast Normal University, Changchun, Jilin 130024, China
- ⁶⁴Key Laboratory of Wetland Ecology and Environment, Northeast Institute of Geography and Agroecology, Chinese Academy of Sciences, Changchun, Jilin 130102, China
- ⁶⁵Department of Biotechnology, University of Verona, Strada Le Grazie 15, 37134 Verona, Italy
- ⁶⁶Key Laboratory of Cenozoic Geology and Environment, Institute of Geology and Geophysics, Chinese Academy of Sciences, Beijing 100029, China

Citation:

Sim, T.G., Swindles, G.T., Morris, P.J., Baird, A.J., Gallego-Sala, A.V., Wang, Y., Blaauw, M., Camill, P., Garneau, M., Hardiman, M., Loisel, J., Väliranta, M., Anderson, L., Apolinarska, K., Augustijns, F., Aunina, L., Beaulne, J., Bobek, P., Borke, W., Broothaerts, N., Cui, Q.Y., Davies, M. A., Ejarque, A., Farrell, M., Feeser, I., Feurdean, A., Fewster, R., Finkelstein, S.A., Gaillard, M.J., Gałka, M., Heffernan, L., Hoovers, R., Jones, M., Juselius, T., Karofeld, E., Knorr, K.H., Korhola, A., Kupriyanov, D., Kylander, M.E., Lacourse, T., Lamentowicz, M., Lavoie, M., Lemdahl, G., Łuców, D., Magnan, G., Maksims, A., Mansilla, C.A., Marcisz, K., Marinova, E., Mathijssen, P.J.H., Mauquoy, D., Mazei, Y., Mazei, N., McCarroll, J., McCulloch, R., Milner, A., Miras, Y., Mitchell, F.J.G., Novenko, E., Pelletier, N., Peros, M., Piilo, S.R., Pilote, L.M., Primeau, G., Rius, D., Robin, V., Robitaille, M., Roland, T.P., Ryberg, E., Sannel, A.B.K., Schitteck, K., Servera-Vives, G., Shotyk, W., Słowiński, M., Stivrins, N., Swinnen, W., Thompson, G., Tiunov, A., Tsyganov, A.N., Tuittila, E.S., Verstraeten, G., Wallenius, T., Webb, J., Willard, D., Yu, Z., Zaccone, C., Zhang, H. In review. Regional variability in peatland burning at mid- to high-latitudes during the Holocene. *Global Change Biology*.

Abstract

Northern peatlands store globally-important amounts of carbon in the form of partly-decomposed plant detritus. Drying associated with climate and land-use change may lead to increased fire frequency and severity in peatlands and the rapid loss of carbon – accumulated over centuries to millennia – to the atmosphere. We synthesise existing peatland macrocharcoal records across North America, Europe and Patagonia to reveal regional variation in peatland burning during the Holocene. We also used an existing database of proximal sedimentary charcoal to represent regional burning trends in the wider landscape for each region. Peatlands demonstrate lower susceptibility to burning than the wider landscape, possibly because of autogenic processes that maintain high levels of near-surface wetness even during drought. Warmer conditions during the Holocene Thermal Maximum were associated with greater peatland burning in central Canada, North America's Atlantic coast, southern Scandinavia and the Baltics, and Patagonia. Long-term trends in peatland burning appear to be largely climate driven, with human activities having an increasing influence in the late Holocene, particularly in Europe. Peatland burning has declined in some areas of Europe and across North America since the Little Ice Age. This decline mirrors trends in global biomass burning linked to fire-suppression policies, and landscape fragmentation caused by agricultural expansion. Nonetheless, widespread drying and degradation of peatlands, particularly in Europe, has likely increased their vulnerability to burning in recent centuries. Consequently, peatland restoration efforts are important to mitigate the risk of peatland fire under a changing climate.

4.1. Introduction

Peatlands cover only ~3% of global land area (Xu et al., 2018), but the carbon they store is equivalent to around twice that of global forests (Pan et al., 2011). Peatlands have accumulated ~600 Gt of carbon during the Holocene, primarily at mid- to high-latitudes in the Northern Hemisphere (Yu et al., 2010). Increasingly deeper peatland water tables associated with climate change and human activities (e.g. agriculture, forestry, peat harvesting or road construction) will likely increase the frequency and extent of fires (Flannigan et al., 2009; Turetsky et al., 2015). Furthermore, greater incidence of lightning with warming will increase the frequency of naturally ignited wildfire, particularly in high-latitude ecosystems (He et al., 2022; McCarty et al., 2021). The burning of deep peat releases carbon into the atmosphere that has not been an active part of the carbon cycle for centuries or millennia, and may therefore contribute to positive feedbacks influencing climate warming (Davies et al., 2013; Lin et al., 2021). Similarly, burning influences peatland vegetation dynamics, surface moisture and plant productivity – all of which influence the carbon balance (Nelson et al. 2021).

Peatlands are subject to both smouldering and flaming combustion; smouldering combustion has the potential to cause greater direct carbon losses (Rein, 2013), while burning of peatland vegetation may lead to indirect carbon losses via modification of the thermal regime (Brown et al., 2015) or hydrology (Wilkinson et al., 2020). Peatlands store large amounts of biomass, but typically have high surface moisture content, which limits the chance of ignition and fire propagation (Frandsen, 1997). Furthermore, wildfire can drive permafrost thaw in boreal peatlands, leading to surface wetting (Gibson et al., 2018). Drying caused by the aggradation of permafrost during the Holocene has been shown to have increased the susceptibility of peatlands to fire in North America (Zoltai et al., 1998). Contemporary climatic warming and human disturbance are thought to be increasing peatland vulnerability to wildfire (Nelson et al., 2021). The composition of vegetation cover is an important influence on peatland fire dynamics. Forested peatlands generally burn more frequently than open peatlands (Kuhry, 1994; Magnan et al., 2012), as these ecosystems have increased above-ground fuel availability (Thompson et al., 2019).

Patterns in peatland burning vary among biomes and can differ from the fire regime at a landscape scale. For example, boreal peatlands in Canada exhibit mean fire return intervals of 624-2930 years compared to 200-1141 years in upland forests (Camill et al., 2009). In Europe, a mean fire interval of ~475 years has been estimated from peatland areas in boreal Norway (Ohlson et al., 2006), while a temperate peatland area in continental Europe showed a frequency of 0-2 fires per

1000 years (Marcisz et al., 2019). The complex ecohydrological dynamics of peatlands interact with changes in local and extra-local vegetation composition, climate and human activities to affect the frequency and severity of peatland fires (Feurdean et al., 2022; Morris et al., 2015; Słowiński et al., 2022).

The long timescales involved in peatland development, climatic change, vegetation dynamics and fire regimes mean that contemporary monitoring studies may not provide a full picture of peatland fire dynamics. A number of continental and global syntheses have used sedimentary charcoal records to reconstruct biomass burning on millennial timescales (e.g. Daniau et al., 2012; Marlon et al., 2008, 2016), but no such studies currently exist specifically for peatlands. Consequently, uncertainties remain regarding the long-term ecology of peatland fires on a continental scale. Here, we use a palaeoenvironmental approach to explore regional variability in peatland burning trends at mid- to high-latitudes in North America, Europe and Patagonia on a timescale that provides a baseline for peatland fire dynamics and to elucidate the past controls on peatland fire.

4.2. Materials and methods

4.2.1. Study region

We compiled and quality checked macrocharcoal records (we defined macrocharcoal as particles with a diameter $>100\ \mu\text{m}$ (Mooney and Tinner, 2011)) spanning 10,000 cal. yr BP to the present day from mid- to high-latitude peatlands in North America (sites = 68, records = 108), Europe (sites = 95, records = 103), and Patagonia (sites = 9, records = 10). The Patagonian region also includes a record from the Falkland Islands. Chronological quality control criteria are outlined in Section 2.3. These data provide good spatial coverage of peatland areas in North America and Europe (Figure 4.1; Table C.1). We divided North America and Europe into sub-regions to account for spatial differences in modern climate, human occupation and key peatland areas. Only basic analyses were possible for Patagonia due to the low number of sites there. We characterised the average modern climatic space of peatland sites and sub-regions using monthly climate data from the CRU TS 4.04 dataset for the 1981-2010 period (Harris et al., 2020). These data have been interpolated from climate stations to a 0.5° latitude by 0.5° longitude spatial resolution.

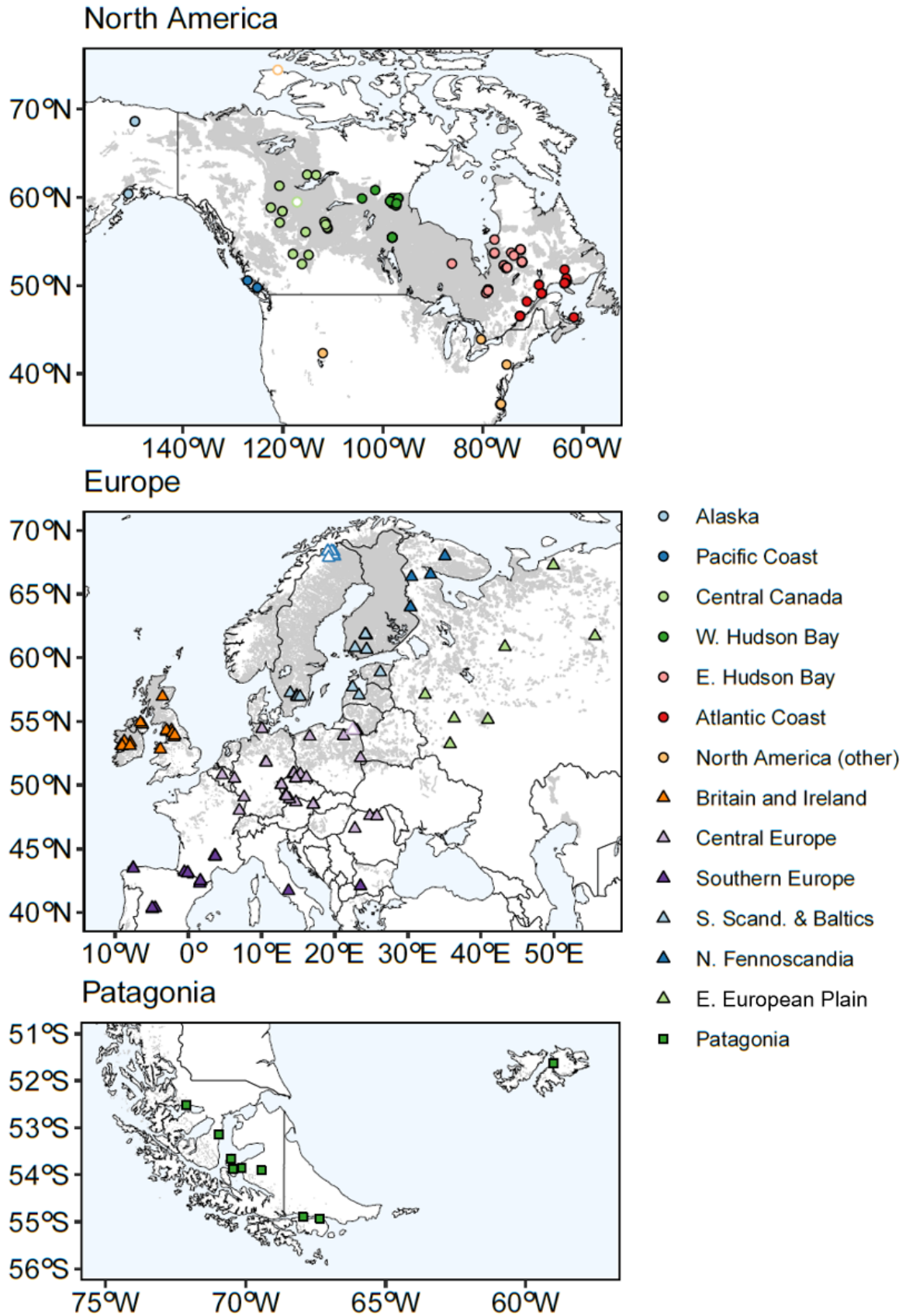


Figure 4.1. Site map of peatland record locations and their sub-region. Symbols with a white fill indicate that no charcoal was present throughout a record. Grey shading denotes peatland areas sourced from PEATMAP (Xu et al., 2018).

4.2.2. Charcoal data

Theoretical models suggest that the dispersal distance of charcoal decreases with particle size (Clark, 1988; Clark et al., 1998; Clark and Patterson, 1997; Higuera et al., 2007). Many studies provide evidence of macrocharcoal records (>100-200 μm) representing local scale fires within a few hundred meters (Carcaillet et al., 2001; Clark and Royall, 1996, 1995) or within several kilometres (Feurdean et al., 2020a, 2022; Tinner et al., 2006) of a coring location. Source areas of macrocharcoal across Europe may be up to 40 km, but these findings are in relatively open landscapes and specifically for lacustrine settings (Adolf et al., 2018). Peatlands are thought to provide a more localised record of past fire occurrences than lakes because they experience limited secondary deposition by fluvial transport (Florescu et al., 2018; Remy et al., 2018). Furthermore, the peatland records may provide higher resolution information because they are not subjected to the same sediment reworking as in lakes (Clark and Patterson, 1997; Conedera et al., 2009; Oswald et al., 2005).

For these reasons, we assume that our peatland macrocharcoal records (>100 μm) are primarily a proxy for burning of peatland aboveground vegetation or burning of the peat itself. However, we cannot rule out the influence of some charcoal input from vegetation in immediate vicinity of the peatland and in some instances from a regional source – especially from intense crown fires or those occurring during high winds (Gardner and Whitlock, 2001; Peters and Higuera, 2007). Similarly, particularly serve in-situ smouldering fires can consume much of the charcoal they produce and cause some loss of the peatland archive (Zaccone et al., 2014).

To enable a comparison of localised peatland burning to that in the wider regional landscape, we selected records that were proximal to our peatland sites (see Figure C.1) from the Global Charcoal Database (GCD) v.4.0.7 using the Paleofire package v.1.2.4 (Blarquez et al., 2014) in R v.4.0.5 (R Core Team, 2021). These records from the GCD include microcharcoal and macrocharcoal and are from a variety of sedimentary archives, excluding those listed as a bog, fen or mire. These records are assumed to provide a record of regional biomass burning (e.g. Marlon et al., 2016). We ensured that the wider landscape sites that pertained to each sub-region were within a convex hull defined by the loci of the peatland sites in that sub-region, or no more than 200 km outside it (150 km in central Europe to avoid duplication of sites). Further details of the wider landscape records selected from the GCD can be found in Figure C.1 and Table C.2. Where peatland macrocharcoal records from the GCD met our quality control criteria, we included them in our peatland burning dataset (see Table C.1).

4.2.3. Age-depth modelling

In order to standardise the methodology used for age-depth modelling, we produced new Bayesian age-depth models (Figures C.2-C.38) for each peatland record from chronological information such as ^{14}C , ^{210}Pb , tephra layers and spheroidal carbonaceous particles (SCPs), using the rbacon package v.2.5.7 (Blaauw et al., 2021) in R (R Core Team, 2021). We established quality control criteria that required cores to comprise at least ten sample depths, to have a chronology spanning at least 500 years, and to have a date (e.g. ^{210}Pb , ^{14}C or tephra) at least every 2500 years on average. Prior information on accumulation rate and its memory or variability can be found for each age-depth model in Figures C.2-C.38.

4.2.4. Resampling and transformation

The peatland macrocharcoal records that we used have been compiled using a variety of methods (e.g. particle counts, area measurements and relative abundances) and a range of particle size fractions (e.g. $>125\ \mu\text{m}$, $>150\ \mu\text{m}$ and $>0.5\ \text{mm}$). This variability in measurement approach can result in values that differ by orders of magnitude and therefore data standardisation is required to compare relative changes between records over time (Power et al., 2010). Furthermore, owing to varying accumulation rates within and among cores, standardisation of temporal resolution via binning or smoothing is required to avoid an inflated influence of high-resolution samples on any subsequent analyses. Macrocharcoal occurs in 47.8% (12,321 out of 25,758) of pre-binned peat samples. We used proportional relative scaling (PRS) - developed specifically for systems where fire is rare (McMichael et al., 2021) - and presence/absence analyses to standardise our peatland records (see below).

4.2.4.1. Proportional relative scaling and presence/absence

For the PRS and presence/absence analyses, we developed a new method to resample the temporal resolution of raw charcoal data proportionally into equal 50-year time bins using depth intervals calculated from age-depth models (Figure C.39). This approach minimises potential distortion from non-contiguous sampling, particularly for records with infrequent sampling (Figure C.40). The proportion of samples containing charcoal is important for calculating both PRS and presence/absence; therefore, we applied the depth binning approach to resample the data prior to calculation of PRS and presence/absence. We calculated presence/absence for each resampled record, and the percentage of sites containing charcoal for each 50-year period in North America, Europe, Patagonia and sub-regions of interest. To calculate PRS for each record, we divided individual resampled charcoal values (C_i) by the maximum resampled charcoal value from that

record (C_{max}) and multiplied by 100. We then scaled this value by the proportion of resampled values containing charcoal. The PRS formula applied to our resampled charcoal data is as follows:

$$char_{pscaled} = \left(\frac{c_i}{C_{max}} \times 100 \right) \frac{f}{N}$$

Where $char_{pscaled}$ is proportionally relatively scaled charcoal values, C_i is a singular resampled charcoal value within a record, C_{max} is the maximum resampled charcoal value within that same record, f is the number of resampled values containing charcoal (value > 0) within that same record and N is the total number of resampled values within that same record. We subsequently applied a cubic root transformation to PRS values to aid data visualisation and reduce positive skew.

PRS adjusts the magnitude of charcoal records by the frequency of charcoal occurrence, down-weighting records with infrequent charcoal. This scaling is based on observations from tropical lake records collected using the same method, where a low frequency of samples containing charcoal was related to a lower maximum abundance of charcoal (McMichael et al., 2021). We assessed the effect of PRS on our data by comparing records from the three most common particle sizes (>150 μm , >0.5 mm and >1 mm) that expressed charcoal quantity as a concentration (particles cm^{-3}). This comparison tested whether, for peatland records analysed in a similar fashion, a greater maximum charcoal value was associated with a higher proportion of samples containing charcoal. We found that the maximum charcoal value (C_{max}) of a record increased across the three particle sizes when a greater proportion of resampled values contained charcoal (Figure C.41). This relationship suggests the down-weighting in PRS of sites exhibiting a low proportion of total samples containing charcoal is an appropriate approach for inter-site comparisons of peatland macrocharcoal data.

4.2.4.2. Comparison of local peatland and regional biomass burning

Sufficient chronological information was not available from the GCD to apply our depth binning approach to sites representing biomass burning in the wider landscape. Therefore, we used an established method from major composite analyses of sedimentary charcoal records from the GCD that involves a Box-Cox, a min-max and a z-score transformation (Daniau et al., 2012; Marlon et al., 2016, 2008). We applied the Box-Cox, min-max and z-score transformations to our peatland dataset (Table C.1) and the wider landscape dataset from the GCD (Table C.2) using the paleofire package (Blarquez et al., 2014) in R. Peatland records with a complete absence of charcoal were excluded from the analysis. We pre-binned the data in 50-year non-overlapping bins and used a

500-year smoothing window to produce charcoal composite curves for North America, Europe and sub-regions of interest. There were too few sites in the GCD to produce a robust z-score reconstruction for Patagonia. Similarly, there were too few peatland records to produce sub-region composite curves for Alaska, the Pacific Coast, East European Plain and Northern Fennoscandia – although these data are included in the continental scale composite curves.

4.3. Results and discussion

North America, Europe and Patagonia exhibited distinct spatiotemporal patterns of peatland burning from 10 ka (thousands of year before 1950 CE) to the present (Figure 4.2). In North America, there was a general increase in peatland burning from 10 to ~0.5 ka (Figure 4.2A-B), but there is a high degree of regional variability (Figure 4.3). These burning trends largely correspond with changing climatic conditions and/or vegetation dynamics in the wider landscape, but peatland autogenic processes may be important. From ~0.5 ka to the present we see a widespread decrease in peatland burning that may have been initiated by the Little Ice Age (LIA) cooling. The tendency of peatlands to retain high surface moisture content even during drought (Kettridge and Waddington, 2014; Morris and Waddington, 2011), and a general policy of fire suppression since the early-twentieth century, may be in part responsible for this recent downturn in burning. Our European composite record shows more peatland burning in the early Holocene from 10 to 8 ka, a period during which our database is composed primarily of records from central Europe and southern Scandinavia and the Baltics (Figure 4.2). Relatively constant levels of peatland burning are observed after 8 ka, but with marked increases at ~5 ka and from 1.5 to 0.5 ka (Figure 4.2). Burning in the wider landscape increases conspicuously from 6.5 to 5.5 ka and, unlike the peat record, shows an overall increase in recent centuries.

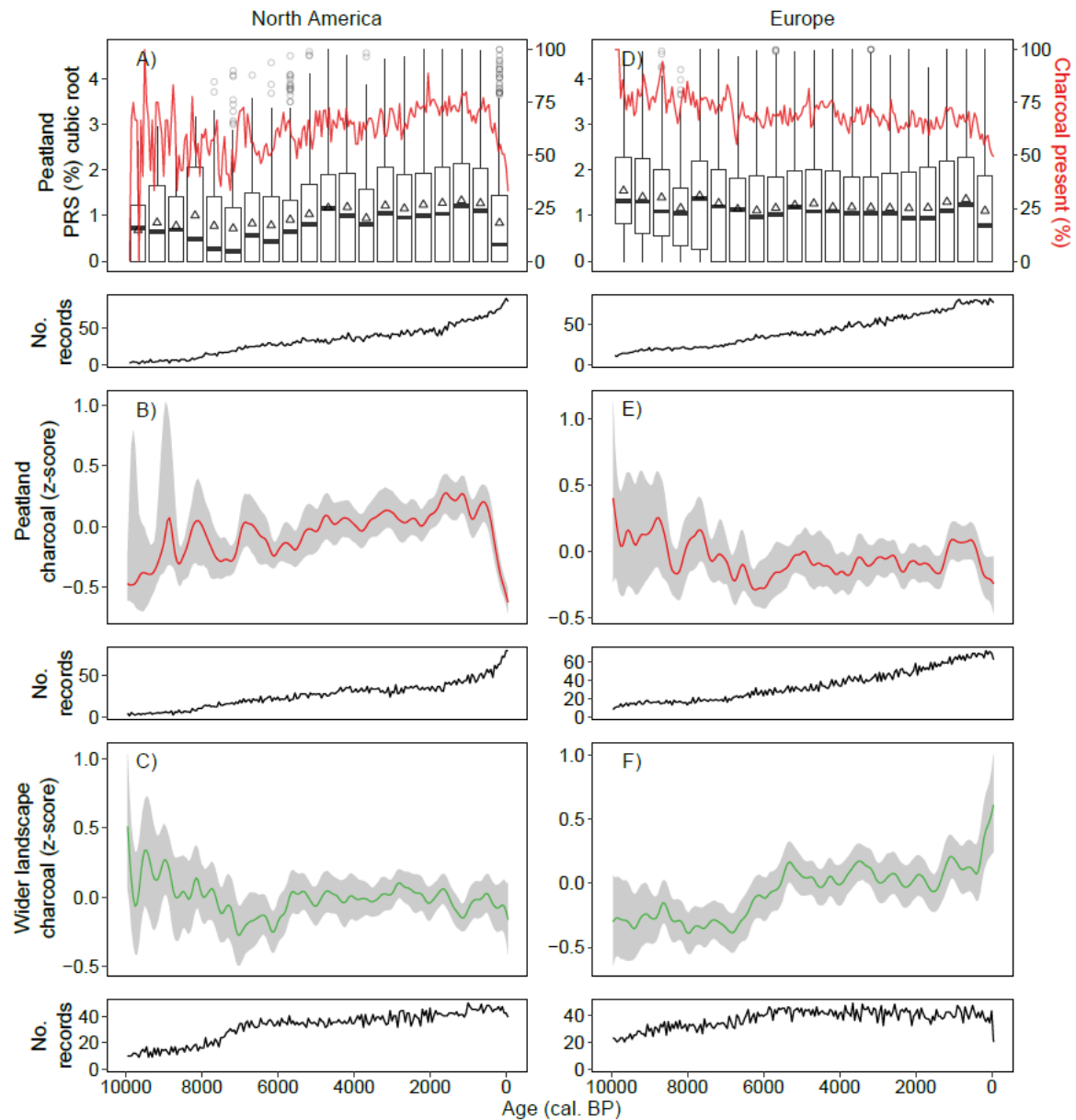


Figure 4.2. Peatland and wider landscape burning trends by region. The distribution of proportionally relatively scaled (PRS) charcoal values (cubic root transformed) in 500-year bins for A) North America and D) Europe; box heights represent the upper and lower quartiles, centerlines indicate medians, hollow triangles represent means, whiskers extend to 1.5 times the interquartile range beyond the upper and lower quartiles, and hollow circles show the remaining observations. Trends in the proportion of samples (%) with charcoal present within 50-year bins indicated by the red line. Biomass burning trends for peatlands in B) North America and E) Europe and wider landscape biomass burning for C) North America and F) Europe – all with a 500-year smoothing window and showing 95% bootstrap confidence intervals (1000 cycles). For each panel the number of sites corresponds to 50-year time steps.

4.3.1. North America

From 10 to 8 ka our records show a slight increase in burning in both peatlands and the wider landscape that is coincident with rising summer temperatures at a continental scale (Viau et al., 2006). However, we have a dearth of records in the early Holocene from 10 to 8 ka in North America and therefore cannot make detailed inferences about burning trends for this time. During

the early Holocene growing seasons became gradually longer and warmer, driving widespread peatland initiation in western and eastern North America from ~14.5 ka, with initiation in central Canada and the Hudson Bay lowlands from ~8.5 ka onwards following increasing temperatures and ice sheet retreat (Gorham et al., 2007; Morris et al., 2018).

Warmer and drier conditions during the Holocene Thermal Maximum (HTM) were likely responsible for greater peatland burning from 8 to 7 ka in central Canada (Edwards et al., 1996; Kuhry, 1994). Similarly, increased burning in the wider landscape from 8 to 7 ka (Figure 4.3C) coincides with the northward expansion of conifer forests (Williams, 2003) and this may also be a factor in increased peatland burning. Decreased peatland burning in central Canada during the mid-Holocene (7 to ~3 ka) corresponds to warmer and more humid climatic conditions (Edwards et al., 1996; Viau and Gajewski, 2009). However, our findings from central Canada prior to ~3 ka should be treated with a degree of caution because of a small number of records span this time. Between 3 and 0 ka summer cooling and higher annual precipitation (Viau and Gajewski, 2009) correspond with decreased burning in the wider landscape, but peatland burning did not consistently decrease until ~0.5 ka (Figure 4.3A-C). Many peatlands in central Canada show evidence of permafrost aggradation linked to late-Holocene cooling, particularly during the LIA (Treat and Jones, 2018). Drier peatland conditions caused by surface uplift during permafrost aggradation may have contributed to sustained levels of peatland burning until 0.5 ka. Similarly, permafrost thaw driven by twentieth century warming (Pelletier et al., 2017) offers a plausible explanation for a recent decrease in peatland burning, although wetting from permafrost thaw can be short-lived (Magnan et al., 2018).

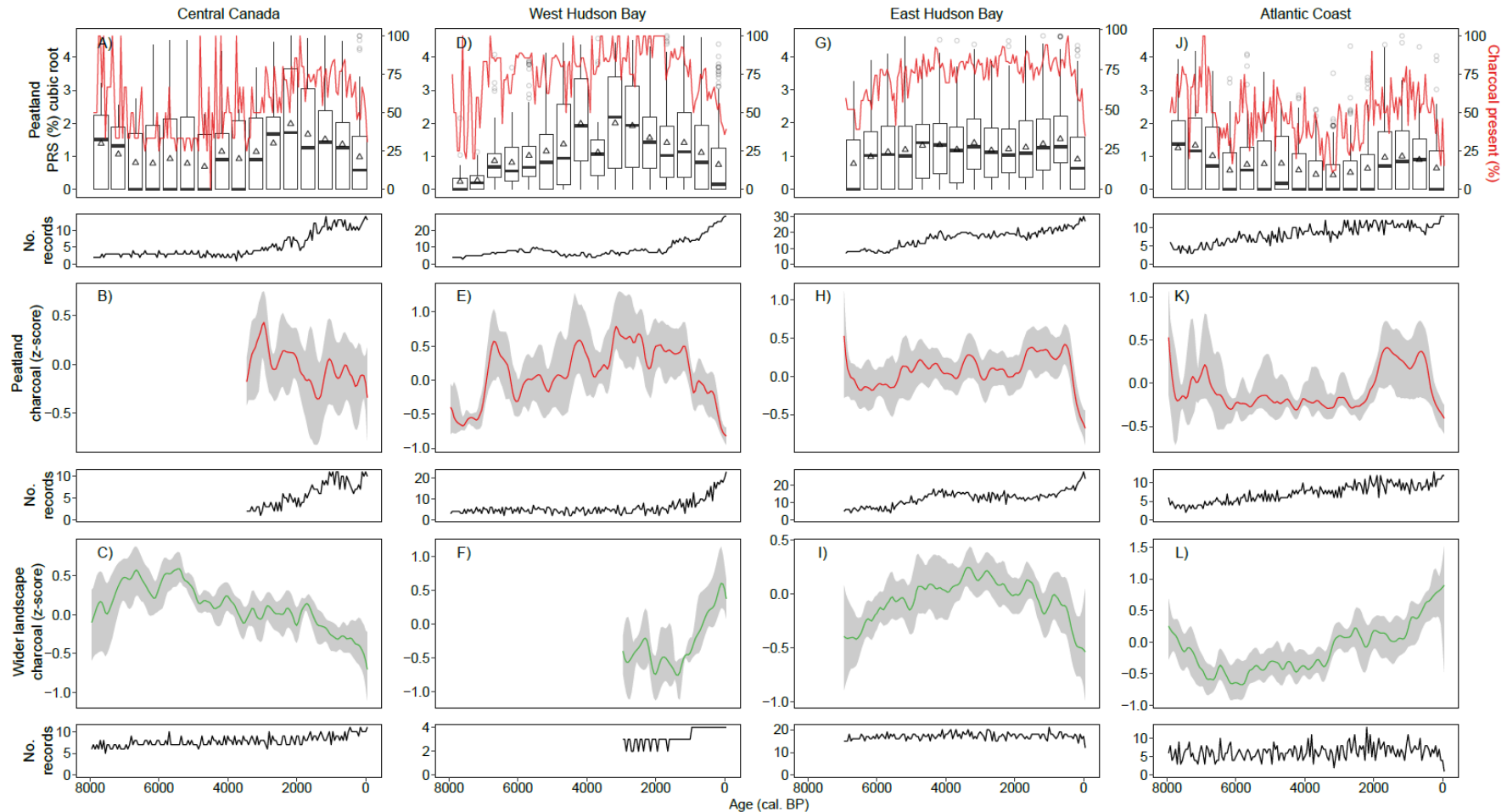


Figure 4.3. Peatland and wider landscape burning trends by North American sub-region. The distribution of proportionally relatively scaled (PRS) charcoal values (cubic root transformed) in 500-year bins for A) Central Canada, D) West Hudson Bay, G) East Hudson Bay and J) Atlantic coast; box heights represent the upper and lower quartiles, centerlines indicate medians, hollow triangles represent means, whiskers extend to 1.5 times the interquartile range beyond the upper and lower quartiles, and hollow circles show the remaining observations. Trends in the proportion of samples (%) with charcoal present within 50-year bins indicated by the red line. Biomass burning trends for peatlands in B) Central Canada, E) West Hudson Bay, H) East Hudson Bay and K) Atlantic coast and wider landscape biomass burning for C) Central Canada, F) West Hudson Bay, I) East Hudson Bay and L) Atlantic coast – all with a 500-year smoothing window and showing 95% bootstrap confidence intervals (1000 cycles). For each panel the number of sites corresponds to 50-year time steps.

During the mid-Holocene, warm and moist climatic conditions existed across the Hudson Bay region, prior to cooler and generally moist conditions during the Neoglacial from around 2.5 ka onwards (Camill et al., 2012; Hargan et al., 2020; Hobbs et al., 2017). These warmer conditions in the mid-Holocene were associated with less frequent intrusions of cool, dry Pacific or Arctic air masses, resulting in fewer periods of late-spring or summer drought that are conducive to fire activity (Carcaillet and Richard, 2000; Edwards et al., 1996). We observe increasing levels of peatland burning from 8 to 4.5 ka in the western Hudson Bay, along with increased burning in peatlands and the wider landscape in the eastern Hudson Bay from 7 to 4.5 ka (Figure 4.3). However, it should be noted that there are spatial gaps in our dataset with few records from Hudson Bay Lowlands and to the west of James Bay (Figure 4.1). During the mid-Holocene many peatlands in the Hudson Bay region were transitioning from wet fens to drier bogs and this reduction in surface wetness and increased potential for the build-up of woody biomass likely made peatlands more susceptible to fire (Camill et al., 2009; Davies et al., 2021; Hokanson et al., 2016; Magnan et al., 2012). However, the timing of fen to bog transitions in the Hudson Bay region exhibits a spatial gradient that mirrors the patterns of isostatic uplift (e.g. Glaser, Hansen, Siegel, Reeve, & Morin, 2004). Peatland productivity may have decreased during the Neoglacial, leading to increased surface wetness, and in some instances bog to fen transitions (van Bellen et al., 2013). A clear decline in peatland burning occurred from 0.5 ka to present across the Hudson Bay region, possibly initiated by LIA cooling.

On the Atlantic coast of Canada and the northeastern United States, increased burning in the wider landscape and peatlands from 8 to 7 ka (Figure 4.3J-L) is associated with dry summers during a period of low annual precipitation (Carcaillet and Richard, 2000; Viau and Gajewski, 2009). Increases in peatland burning from around 2 to 0.5 ka are at odds with cooling summer temperatures and increasing annual precipitation in northern Quebec (Viau and Gajewski, 2009). From ~4 ka (and especially from 2 ka) a reduction in broadleaf tree species and a shift to more flammable conifers has been linked to summer cooling (Blarquez et al., 2015), which appears to have driven increased landscape burning (Figure 4.3L). Similarly in southern Quebec, a shift to less regular and more intense biomass burning from ~1.5 ka has been linked to indigenous burning practices (Blarquez et al., 2018), but the extent of these practices are widely contested (Barrett et al., 2005). Nonetheless, despite increased burning in the wider landscape from ~4 ka onwards, fire in peatlands only increased modestly from 2 to 0.5 ka (Figure 4.3J-K). The typically more open and *Sphagnum*-dominated maritime bogs of the Atlantic coast rarely experience fire (Lavoie et al., 2009; Magnan et al., 2014) and fire frequencies in open peatlands are lower than those with greater tree density (Camill et al., 2009; Kuhry, 1994). The fire regime in southern Quebec shifted

to less frequent but more severe fires in the last 1000 years following the spread of native agriculture and particularly following European colonisation (Blarquez et al., 2018; Shiller et al., 2014). These human impacts likely explain the increase in wider landscape burning from 0.5 ka to present. Distance to forest and the presence of conifer trees have been linked to fire susceptibility and intensity in ombrotrophic peatlands (Magnan et al., 2012). Therefore, the contrasting decrease in peatland burning from 0.5 ka to present may be related to the reduced susceptibility of open peatlands to fire as they increased in spatial extent (Payette et al., 2013).

Peatlands of the mid-Atlantic Coastal Plain in the United States differ in the timing of peak burning from boreal peatlands farther north. Minimal burning occurred prior to ~6.5 ka, but frequent mid-Holocene fires from 6.5 to ~3.7 ka, coincided with warm and dry conditions in the region and marsh hydroperiods shortened due to slowing rates of sea-level rise (Willard et al., in prep). Low levels of fire characterize the late Holocene, when mid-Atlantic winters were cooler and wetter (Watts, 1979; Webb III et al., 1987) and the site had transitioned from a marsh to a forested wetland. Since European colonization, drainage of the peatland and logging activities resulted in periodic severe fires (Spieran and Wurster, 2020).

4.3.2. Europe

Peatlands in Britain and Ireland broadly initiated in the early Holocene, from 10 to 8 ka (Morris et al., 2018), but we were only able to reconstruct peatland burning from 4 ka to present owing to a lack of data prior to this. Peatland sites showed consistently low PRS and presence/absence values throughout, despite changes in wider landscape burning (Figure 4.4A-C). The comparatively humid climate of Britain and Ireland (Figure 4.7) likely mitigated peatland fire. From the mid-Holocene, burning in the wider landscape appears to be primarily influenced by human activity rather than generally cooling summer temperatures from ~6 ka onwards (Davis et al., 2003; Mauri et al., 2015). Increased burning in the wider landscape ~5 ka (Figure 4.4C) may be linked to the human use of fire to clear woodland (Ryan and Blackford, 2010). Similarly, Neolithic population growth from ~5.5 ka is clear in the archaeological record and is associated with a trend of reduced forest cover that has continued to the present (Woodbridge et al., 2014). Decreased burning in the wider landscape from ~2 ka onwards may be linked to the conversion of forest to agricultural land, resulting in landscape fragmentation and a loss of fuel for wildfires (Fyfe et al., 2003; Marlon et al., 2013). PRS charcoal values decrease from 0.5 ka to present, whereas z-score and presence/absence values drop initially, before increasing slightly in recent centuries (Figure 4.4A-B). Cooler, wetter conditions in Britain and Ireland during the LIA (Swindles et al., 2013; Webb et al., 2022) likely contributed to reduced burning in peatlands and the wider landscape ~0.5 ka.

Shifting land management practices, including peatland drainage and prescribed burning of moorlands from ~AD 1850 (Holden et al., 2007), are coincident with widespread peatland drying across Britain and Ireland since ~AD 1800 (Swindles et al., 2019). These recent human impacts may explain the uptick in the proportion of sites burning in the last century (Figure 4.4A).

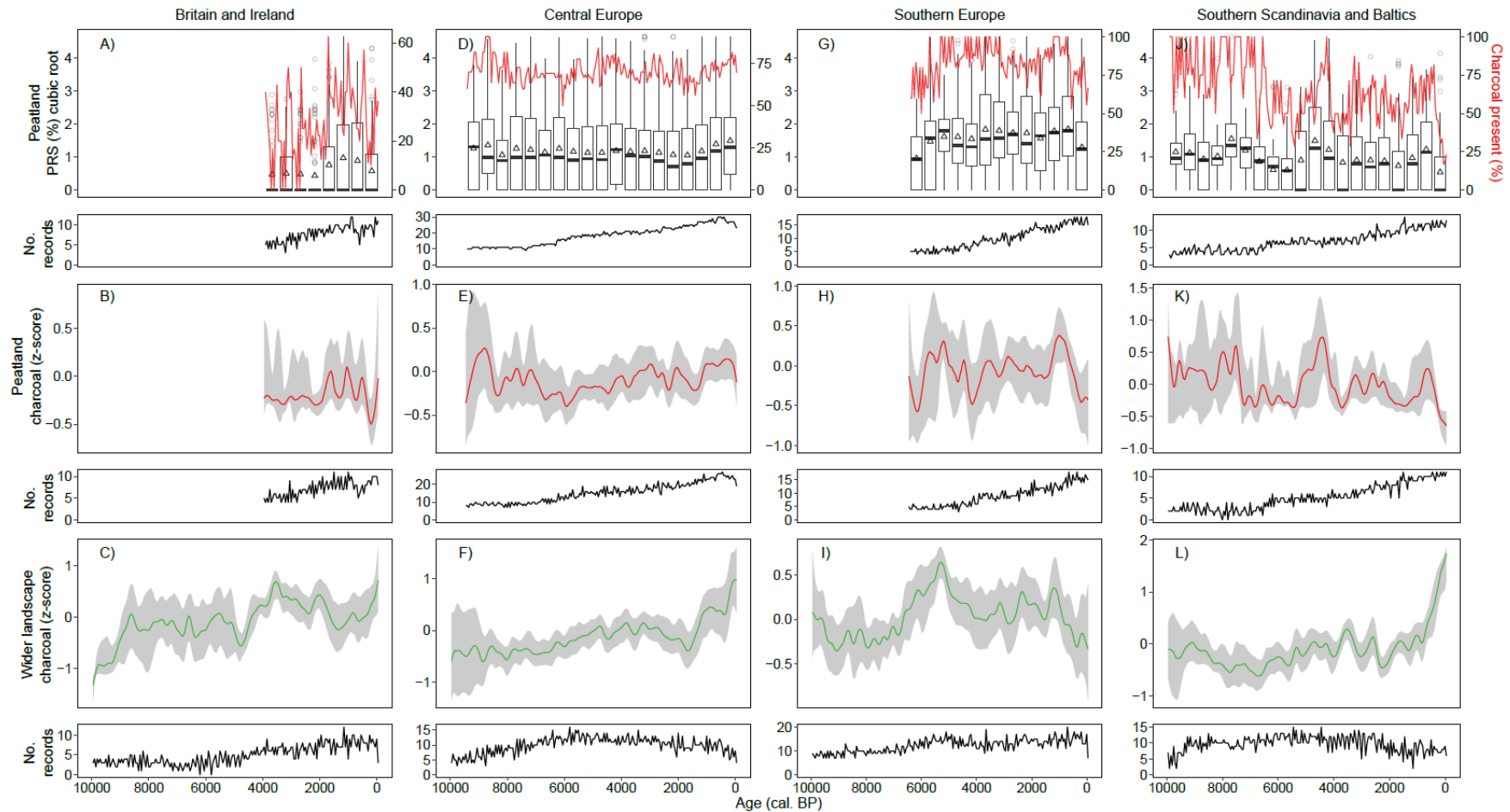


Figure 4.4. Peatland and wider landscape burning trends by European sub-region. The distribution of proportionally relatively scaled (PRS) charcoal values (cubic root transformed) in 500-year bins for A) Britain and Ireland, D) Central Europe, G) Southern Europe and J) Southern Scandinavia and Baltics; box heights represent the upper and lower quartiles, centerlines indicate medians, hollow triangles represent means, whiskers extend to 1.5 times the interquartile range beyond the upper and lower quartiles, and hollow circles show the remaining observations. Trends in the proportion of samples (%) with charcoal present within 50-year bins indicated by the red line. Biomass burning trends for peatlands in B) Britain and Ireland, E) Central Europe, H) Southern Europe and K) Southern Scandinavia and Baltics and wider landscape biomass burning for C) Britain and Ireland, F) Central Europe, I) Southern Europe and L) Southern Scandinavia and Baltics – all with a 500-year smoothing window and showing 95% bootstrap confidence intervals (1000 cycles). For each panel the number of sites corresponds to 50-year time steps.

Central European sites in our database are characterised by greater peatland burning ~ 9 ka, before relatively constant levels of burning until the late Holocene, with decreased burning ~ 2 ka and an increase from 1 ka to present (Figure 4.4D-E). Burning in the wider landscape during the Holocene generally showed a slow increase before 1.5 ka, followed by a steeper increase to present (Figure 4.4F). Summer temperatures increased until ~ 8 ka, before stabilising and showing a general decrease from ~ 6 ka for the majority of the Holocene (Davis et al., 2003; Mauri et al., 2015). The abundance of flammable conifer species in continental Europe decreases from ~ 10 ka to ~ 8 ka and remained relatively consistent until ~ 1.5 ka before decreasing further to the present (Feurdean et al., 2020b). These cool, wet conditions and a stable or decreasing abundance of flammable coniferous trees from the mid-Holocene onwards, suggests that increased burning in the wider landscape may be because of changing human activity. There is some evidence of hunter-gatherer initiated forest fires from as early as 8.5 ka, with human-related fires intensified during the Bronze Age (~ 4 to 3 ka) and again from 1 ka to present (Bobek et al., 2018; Dietze et al., 2018). Peatlands did not show this same clear increase in burning at this time, suggesting that they were less affected by fires in the wider landscape and/or less targeted by anthropogenic fires. Decreased peatland burning at ~ 2 ka coincides with more humid conditions across central Europe (Fohlmeister et al., 2012). Wetter climatic conditions may have increased surface wetness in peatlands (Pleskot et al., 2022), reducing susceptibility to burning in the wider landscape linked to human activity. However, peatland burning from ~ 1 ka onwards coincides with a pronounced uptick in wider landscape burning (Figure 4.4E-F), suggesting that human use of fire has exceeded the ability of peatlands to resist burning. During the LIA from \sim AD 1400 to AD 1700, a cool humid maritime climate in western Europe helped maintain wetter peatlands, but many continental peatlands in central Europe experienced drying (Marcisz et al., 2020), likely increasing peatland vulnerability to fire. Similarly, peatland water table reconstructions suggest many peatlands in central Europe have become significantly drier in the last 400 years as a result of human and climatic factors (Swindles et al., 2019).

Summer temperatures in southern Europe have generally increased since ~ 8 ka until present (Davis and Brewer, 2009). In addition, summer precipitation decreased throughout the Holocene (Peyron et al., 2011). The pattern of burning is more complex and cannot be explained by climate change alone. Burning increased in peatlands and the wider landscape from ~ 7 ka to a peak ~ 5.5 ka (Figure 4.4G-I), which coincided with the onset of the Neolithic and may have been driven by increased slash and burn activities to clear forest for agriculture (Gilck and Poschlod, 2021; Rius et al., 2011, 2012). A peak in peatland and wider landscape burning ~ 1 ka may have been partially linked to increased farming and settlement following Christian conquest of the Pyrenees (Ejarque

et al., 2009), or an increased build-up of woody biomass with a return to previous fire practices following the Roman period (Vanni re et al., 2016). A marked decrease in peatland and wider landscape burning from ~1 ka until present is likely linked to landscape fragmentation and reduced fuel for wildfires with the expansion of agriculture (Marlon et al., 2013), and the onset of cooler conditions ~AD 1400 to AD 1700 during the LIA (Mann et al., 2009). Fire suppression policies have been widespread across southern Europe in recent decades (Brotons et al., 2013; Moreira et al., 2011). However, peatland burning remains relatively high in comparison to other regions, which may be attributed to comparatively warm and dry summer conditions (Figures 4.6 and 4.7). Similarly, burning in southern European peatlands shows good correspondence with burning in the wider landscape from 8 ka until present, suggesting that these typically smaller peatlands (Payne, 2018) are more vulnerable to burning.

Southern Scandinavia and the Baltics exhibit more peatland burning from 10 ka to ~7.5 ka in terms of PRS, presences/absence and z-score values (Figure 4.4J-K). This early Holocene trend is more subtle in burning of the wider landscape, with slightly elevated burning 10 to ~8.5 ka (Figure 4.4L). These higher levels of burning are likely linked to climate and perhaps changes in vegetation. Pollen reconstructions suggest this region was warming during this period, with the HTM ~8 to 6 ka (Davis et al., 2003; Mauri et al., 2015). However, aquatic plant macrofossil evidence suggests an earlier onset of the summer HTM in Fennoscandia not captured in pollen reconstructions (V liranta et al., 2015). In terms of vegetation, an increased abundance of flammable coniferous taxa in the early Holocene may have contributed to greater burning, while a transition to broadleaf dominance in the mid-Holocene may have mitigated burning during the HTM (Brown and Giesecke, 2014; Feurdean et al., 2020b). An increase in peatland burning from 5 to 4 ka may have been influenced by a brief warm, dry phase prior to a general cooling trend from 4 to 2.6 ka in the Baltic region (Hammarlund et al., 2003; Heikkil  and Sepp , 2010), yet there is no corresponding increase in burning of the wider landscape. Therefore, the peak in peatland burning around 4.5 ka may have been driven by increasing abundance of woody plants (e.g. *Calluna vulgaris*) under drier conditions (Sillasoo et al., 2011). Increased burning from 1 to 0.5 ka in peatlands and the wider landscape may be linked to warmer conditions during the Medieval Climate Anomaly (MCA) (Mann et al., 2009), alongside increasing intensity of agricultural grazing and burning practices (Olsson et al., 2010). However, from 0.5 ka to present peatland burning decreased, perhaps initiated by LIA cooling; while wider landscape burning continued to increase (Figure 4.4J-L). This divergent burning trend may be explained by slash-and-burn agricultural practices that were widespread in southern Scandinavia and the Baltics from ~AD 1650 to AD 1850 (J aats et al., 2010; Lehtonen and Huttunen, 1997). These burning practices were typically low intensity and small

scale (Parviainen, 2015) and may have kept fuel loads low in the wider landscape and allowed peatlands to be less susceptible to ignition.

4.3.3. Patagonia

In Patagonia, biomass burning in lowland peatland sites appears to be strongly linked to climate. From 10.5 to 7.5 ka, southern Patagonia experienced a warm and dry period during a time of weaker South Westerly Winds (SWWs) (Moreno et al., 2018). This warm, dry period corresponds to greater burning of lowland peatlands from 10 to 6 ka (Figure 4.5). From ~6 ka onwards there was a general wetting and cooling of climate due to the equatorial migration of the SWWs and a reduction in summer drought (Markgraf and Huber, 2010; McCulloch et al., 2020). These cooler, wetter conditions in the mid to late Holocene may explain the extremely low levels of burning in southern Patagonian peatlands from 6 ka to present (Figure 4.5). Similarly, there is evidence of persistent *Sphagnum* communities in lowland peatlands from ~5.5 ka coincident with reduced summer drought and fire activity (Markgraf and Huber, 2010). The absence of high severity peatland fires was probably favourable to *Sphagnum* mosses in this region (Nelson et al., 2021). Huber & Markgraf (2003) suggest that increased fire activity in a southern Patagonian peatland from ~AD 1600 onwards may be linked to changing indigenous hunting practices, following the introduction of horses upon European contact. However, any such increases in recent centuries are not well represented in our regional analysis, suggesting that climate remains the main control on lowland peatland burning in southern Patagonia.

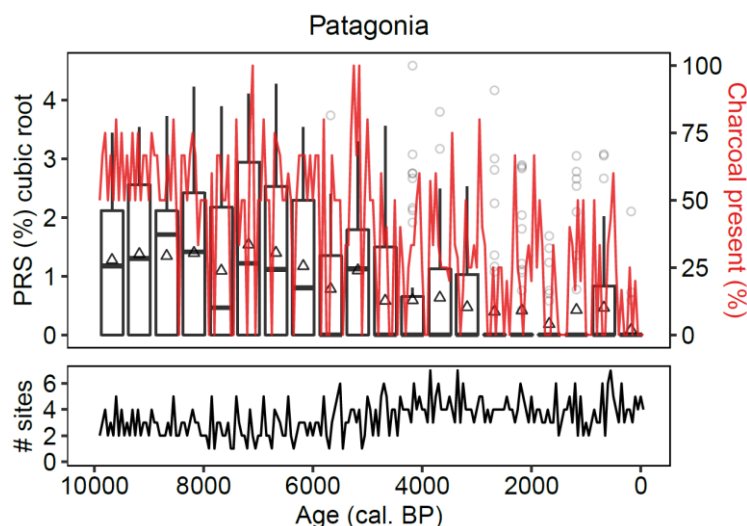


Figure 4.5. Peatland burning trends in Patagonia. The distribution of proportionally relatively scaled (PRS) charcoal values (cubic root transformed) in 500-year bins. Box heights represent the upper and lower quartiles, centerlines indicate medians, hollow triangles represent the mean, whiskers extend to 1.5 times the interquartile range and hollow circles show the remaining observations. Trends in the proportion of samples (%) with charcoal present within 50-year bins indicated by the red line. The number of sites corresponds to 50-year time steps.

4.3.4. Peatland burning and climatic space

Our sub-regions show some clear differences in the magnitude of burning (Figure 4.6), which may be explained in part by regional differences in climate (Figure 4.7). Gridded modern climate data provide good context for the relative differences between sub-regions. We focused on the last 2 ka because this period is long enough to capture meaningful temporal patterns of burning and has the best spatial coverage.

Patagonia, Northern Fennoscandia, and Britain and Ireland demonstrated a median PRS value of zero since 2 ka, while southern Europe and the East European Plain exhibited the highest burning values (Figure 4.6). The warmest months in our Patagonian and Northern Fennoscandian sites have relatively low precipitation, but are relatively cool compared to the other sub-regions (Figure 4.7). Although, an annual precipitation of ~1000 to 1500 mm has been recorded at a number of our Patagonia sites (Broder et al., 2012; Schneider et al., 2003), suggesting our gridded climate data may not be capturing some local variation in rainfall. Nevertheless, low summer temperatures may be allowing peatlands – especially those dominated by *Sphagnum* – to retain surface moisture and to avoid the desiccated conditions that promote fire propagation (Turetsky et al., 2011; Waddington et al., 2015). The high levels of precipitation during the warmest month in Britain and Ireland may prevent conditions favourable to fire. In contrast, southern Europe is characterised by sites with high temperatures and low precipitation for the warmest month, which likely contribute to greater burning (Figure 4.7). The East European Plain does not have the hottest or driest summers, on average, yet experiences greater burning than other sub-regions. In this instance, the summary variables presented in Figure 4.7 may be less important than short-term climatic and weather variability that may foster peatland fire in the East European Plain. Additionally, the relatively few peatland sites from the East European Plain in comparison to other sub-regions appear to have undergone changes in vegetation structure related to recent slash-and-burn agriculture (Barhoumi et al., 2019) and shifts from minerotrophic to ombrotrophic conditions (Mazei et al., 2020). Future analyses would benefit from a greater number of records from the East European Plain and the West Siberian Lowlands. Nevertheless, there are some clear links between burning and climatic extremes, but our findings suggest that peatland fire regimes are influenced by a combination of factors.

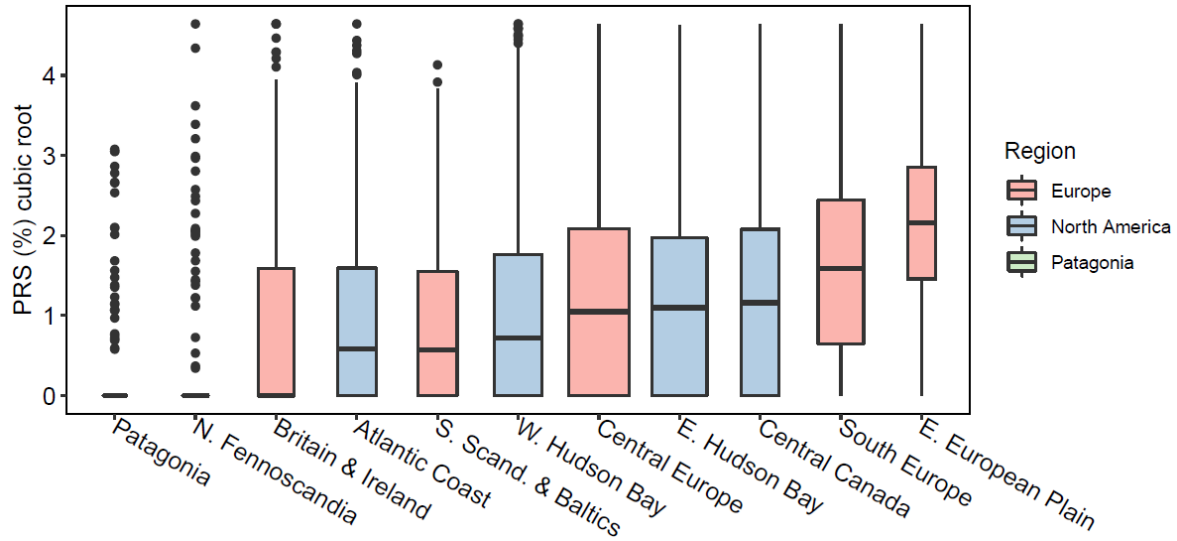


Figure 4.6. Distribution of proportionally relatively scaled (PRS) charcoal values (cubic root transformed) for 2000 cal. BP to present by region and sub-region. PRS values are cubic root transformed owing to the skewed distribution of the data. Box heights represent the upper and lower quartiles, centerlines indicate medians, whiskers extend to 1.5 times the interquartile range and black circles show the remaining observations. Box width is proportional to the square root of the number of samples per sub-region.

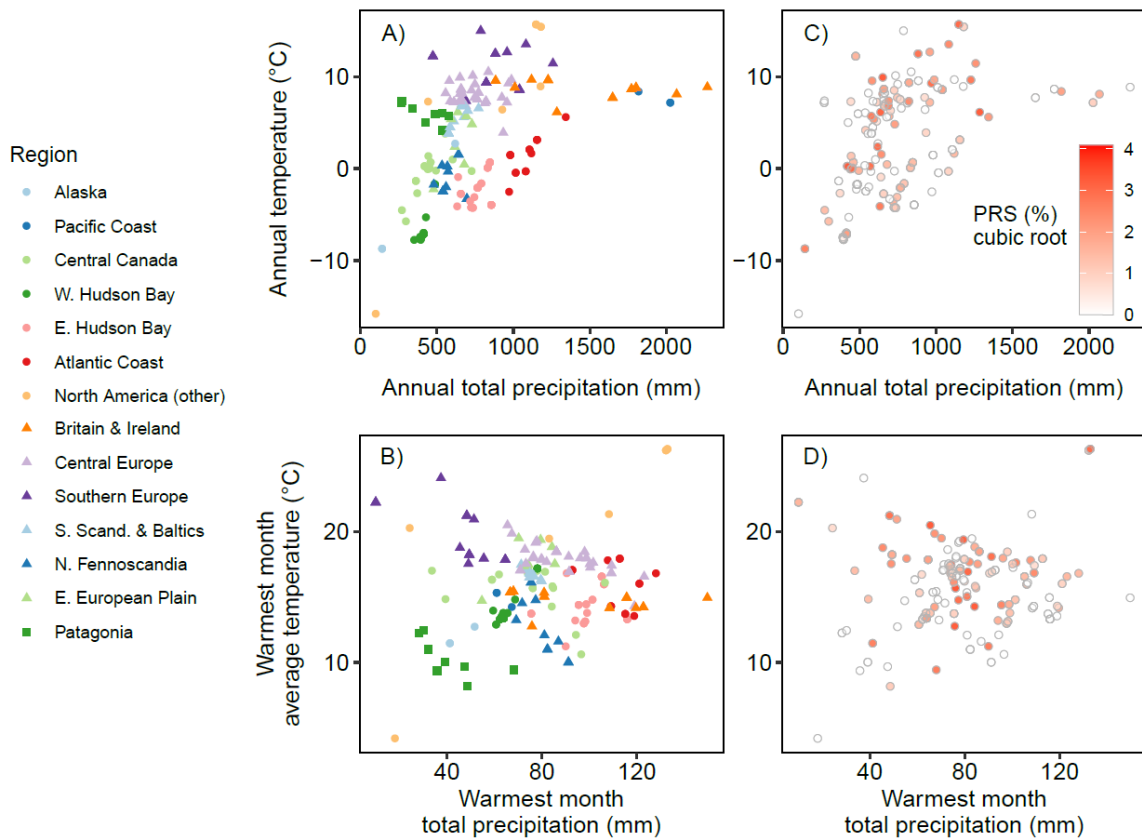


Figure 4.7. Climatic space by sub-region and charcoal values. Modern bioclimatic space for peatland records averaged for 1981-2010 (Harris et al., 2020) by sub-region for average temperature (°C) and total precipitation (mm) A) annually and B) for the warmest month. Median proportionally relatively scaled (PRS) charcoal values (cubic root transformed) for each record within the last 2000 years in modern bioclimatic space for average temperature (°C) and total precipitation (mm) C) annually and D) for the warmest month.

4.3.5. Controls on peatland burning and wider implications

Our composite analysis of peatland macrocharcoal records from mid- to high-latitude peatlands in North America, Europe and Patagonia highlights regional variability in peatland burning during the Holocene. Warmer and drier climatic conditions during the HTM were associated with greater peatland burning in central Canada, North America's Atlantic coast, southern Scandinavia and the Baltics, and Patagonia (Figures 4.3, 4.4 and 4.5). Cooler or wetter climatic conditions during the Neoglacial coincided with reduced peatland burning in central Canada and the western Hudson Bay (Figure 4.3). Similarly, there were widespread decreases in burning linked to the LIA across Europe and North America (Figures 4.3 and 4.4). Therefore, climate appears to be the overarching control on peatland fire until the late Holocene in Europe and perhaps until the present day in North America and Patagonia. This echoes findings by Marlon et al. (2013), who suggested that climate is the main influence on global biomass burning for the majority of the Holocene.

Human impacts upon the landscape became more prevalent from the Neolithic onwards in Europe, and increased burning was generally associated with clearance of land for agriculture (Dietze et al., 2018; Gilck and Poschlod, 2021; Olsson et al., 2010; Rösch et al., 2017; Ryan and Blackford, 2010). In particular, human-induced fire may have led to increased peatland burning from 7 to 5.5 ka in southern Europe, and from 1 to 0.5 ka in southern Scandinavia and the Baltics (Figure 4.4). Paradoxically, there have been widespread reductions in global biomass burning from the late nineteenth century onwards, associated with fire suppression policies and the expansion of agriculture, despite increasing temperatures and rising global population (Marlon et al., 2008). The conversion of land to agricultural uses has reduced fuel for wildfires and decreased landscape connectivity (Arora and Melton, 2018). These processes are probably responsible for recent decreases in burning in the wider landscape in central Canada, eastern Hudson Bay and southern Europe (Figures 4.3 and 4.4). A key uncertainty is whether land-use and fire-suppression policies in the 21st century will be able to offset the influence of warming. A modelling study by Kloster, Mahowald, Randerson, & Lawrence (2012) suggests that management could largely mitigate future carbon emissions from fire, although important uncertainties remain, partly because they did not account for peatland ecosystems.

Differences in burning trends between peatlands and the wider landscape may be a result of autogenic processes that are specific to peatlands, including retention of near-surface moisture even during drought (Waddington et al., 2015) and ecosystem state shifts such as fen-bog transitions (Väliranta et al., 2017). There are a number of occasions when peatland burning has remained stable or even decreased, while burning in the wider landscape has increased. The most

prominent examples are from ~0.5 ka to present in the Atlantic coast area of North America, and in southern Scandinavia and the Baltics (Figures 4.3 and 4.4). In both instances, increased burning in the wider landscape was likely driven by human activities (Blarquez et al., 2018; Parviainen, 2015). The lower susceptibility of peatlands to burning may be linked to cooler conditions during the LIA ~AD 1400 to AD 1700 (Mann et al., 2009) in combination with internal mechanisms. More specifically, the mostly extensive, open and *Sphagnum*-dominated peatlands of the Atlantic coast region of North America are generally resistant to fire (Lavoie et al., 2009; Magnan et al., 2014). Here, a lower peatland edge-to-area ratio reduces rates of subsurface losses of water to adjacent forests, and lowers the risk of deep burning of peat (Hokanson et al., 2016; Nelson et al., 2021). Similarly, larger peatland complexes in northern Poland have been shown to be more resistant to disturbances (Marcisz et al., 2019). In contrast, fire records from the smaller and more fragmented peatlands of southern Europe (Payne, 2018) correlated closely with burning in the wider landscape (Figure 4.4), suggesting a greater vulnerability of these ecosystems.

Both future climate change and human activities may increase the susceptibility of peatlands to burning. Increased evapotranspiration associated with warmer temperatures, and drainage from human activities are both expected to increase peatland drying, leading to greater peatland burning and carbon emissions (Flannigan et al., 2009; Turetsky et al., 2015). In Europe, extensive peatland drying has already been observed in recent centuries (Swindles et al., 2019). However, our results predominantly show recent decreases in peatland burning from ~0.5 ka to present, especially in North America (Figures 4.2, 4.3 and 4.4). A number of factors may be contributing to this trend. Large areas of peatlands in North America remain relatively intact – just 1.5% of peatlands there are estimated to be degraded, in comparison to 18% in Europe (Urák et al., 2017). Therefore, less modified peatlands in North America may be more resilient to burning (see Nelson et al., 2021). Peatland fires commonly initiate elsewhere in the landscape before spreading onto peatlands (Hokanson et al., 2016). Therefore, a reduction in wider landscape burning from ~0.5 ka in some regions likely reduced the potential for peatland vegetation to ignite. Furthermore, the resolution of our analyses (50 years per sample) is unlikely to detect any increased burning in recent decades. The centennial to millennial timescales of peatland fires mean that even if the risk of peatland fire has increased with recent climate change and human activities, the impact on peatland fire may not yet be manifest in palaeoenvironmental records. Similarly, peatland ecosystems are generally resilient to disturbance and often exhibit a delayed response to external forcing (Page and Baird, 2016).

We find ample evidence for increased peatland burning during previous warm periods, and in warmer and drier regions (e.g. southern Europe). The vulnerability of peatlands to fire is likely to have been increased by recent climatic warming and anthropogenic management, particularly in Europe where ecosystems have been more heavily modified. For these reasons, policies are needed to enhance peatland resistance and resilience to fire. Rewetting of degraded peatlands has been shown to reduce the risk of deep burns (Granath et al., 2016). Consequently, peatland restoration will be an important strategy to mitigate the impact of climate change and human activities (Baird et al., 2019).

4.4. Conclusions

Our composite analysis of peatland macrocharcoal records from mid- to high-latitudes in North America, Europe and Patagonia highlights regional variability in peatland burning during the Holocene. Peatlands are generally much less susceptible to fire than the wider landscape, likely due to the persistence of high surface moisture levels and a lower density of woody biomass. Climate appears to be the overarching control on peatland fire until the mid-Holocene in Europe, and perhaps until the present day in North America and Patagonia. Our analysis suggests that peatland burning is generally higher during warm or dry periods of the Holocene and the magnitude of burning is greater in warmer and drier regions, i.e. southern Europe. Lower anthropogenic disturbance of peatlands in North America compared to Europe likely makes them less susceptible to burning and may partially explain the clear decline in North American peatland burning since the Little Ice Age. Going forwards, peatland restoration will be an important tool in reducing the susceptibility of peatlands to fire.

Acknowledgements

This work developed from the PAGES (Past Global Changes) C-PEAT (Carbon in Peat on Earth through Time) working group. PAGES is supported by the US National Science Foundation and the Swiss Academy of Sciences. T.G.S. and R.F. are in receipt of the UK Natural Environment Research Council Training Grants NE/ L002574/1 and NE/S007458/1 respectively. C.A.M. acknowledges funding from PAI/SIA 77180002 - ANID and FONDECYT Iniciación 11220705 - ANID, Gobierno de Chile. Records from the Global Charcoal Database supplemented this work and therefore we would like to thank the contributors and managers of this open source resource. We also thank Annica Greisman, Jennifer Shriller, Fredrik Olsson and Simon van Bellen for contributing charcoal data to our analyses. Any use of trade, firm, or product name is for descriptive purposes only and does not imply endorsement by the U.S. Government.

References

- Adolf, C., Wunderle, S., Colombaroli, D., Weber, H., Gobet, E., Heiri, O., van Leeuwen, J.F.N., Bigler, C., Connor, S.E., Gałka, M., La Mantia, T., Makhortykh, S., Svitavská-Svobodová, H., Vannièrè, B., Tinner, W., 2018. The sedimentary and remote-sensing reflection of biomass burning in Europe. *Glob. Ecol. Biogeogr.* 27, 199–212. <https://doi.org/10.1111/geb.12682>
- Arora, V.K., Melton, J.R., 2018. Reduction in global area burned and wildfire emissions since 1930s enhances carbon uptake by land. *Nat. Commun.* 9, 1–10. <https://doi.org/10.1038/s41467-018-03838-0>
- Baird, A.J., Evans, C.D., Mills, R., Morris, P.J., Page, S.E., Peacock, M., Reed, M., Robroek, B.J.M., Stoneman, R., Swindles, G.T., Thom, T., Waddington, J.M., Young, D.M., 2019. Validity of managing peatlands with fire. *Nat. Geosci.* 12, 884–885. <https://doi.org/10.1038/s41561-019-0477-5>
- Barhoumi, C., Peyron, O., Joannin, S., Subetto, D., Kryshen, A., Drobyshev, I., Girardin, M.P., Brossier, B., Paradis, L., Pastor, T., Alleaume, S., Ali, A.A., 2019. Gradually increasing forest fire activity during the Holocene in the northern Ural region (Komi Republic, Russia): The Holocene 29, 1906–1920. <https://doi.org/10.1177/0959683619865593>
- Barrett, S.W., Swetnam, T.W., Baker, W.L., 2005. Indian Fire Use: Deflating the Legend. *Fire Manag. Today* 65, 31–34.
- Blaauw, M., Christen, J.A., Marco A. Aquino, L., Vazquez, J.E., Gonzalez, O.M., Belding, T., Theiler, J., Gough, B., Karney, C., 2021. rbacon: Age-depth modelling using Bayesian statistics. R package version 2.5.7.
- Blarquez, O., Ali, A.A., Girardin, M.P., Grondin, P., Fréchet, B., Bergeron, Y., Hély, C., 2015. Regional paleofire regimes affected by non-uniform climate, vegetation and human drivers. *Sci. Rep.* 5, 13356. <https://doi.org/10.1038/srep13356>
- Blarquez, O., Talbot, J., Paillard, J., Lapointe-Elmrabti, L., Pelletier, N., Gates St-Pierre, C., 2018. Late Holocene influence of societies on the fire regime in southern Québec temperate forests. *Quat. Sci. Rev.* 180, 63–74. <https://doi.org/10.1016/J.QUASCIREV.2017.11.022>
- Blarquez, O., Vannièrè, B., Marlon, J.R., Daniau, A.L., Power, M.J., Brewer, S., Bartlein, P.J., 2014. Paleofire: An R package to analyse sedimentary charcoal records from the Global Charcoal Database to reconstruct past biomass burning. *Comput. Geosci.* 72, 255–261. <https://doi.org/10.1016/j.cageo.2014.07.020>
- Bobek, P., Svobodová, H.S., Werchan, B., Švarcová, M.G., Kuneš, P., 2018. Human-induced changes in fire regime and subsequent alteration of the sandstone landscape of Northern Bohemia (Czech Republic). *The Holocene* 28, 427–443. <https://doi.org/10.1177/0959683617729443>
- Broder, T., Blodau, C., Biester, H., Knorr, K.H., 2012. Peat decomposition records in three pristine ombrotrophic bogs in southern Patagonia. *Biogeosciences* 9, 1479–1491. <https://doi.org/10.5194/bg-9-1479-2012>
- Brotons, L., Aquilué, N., de Cáceres, M., Fortin, M.J., Fall, A., 2013. How Fire History, Fire Suppression Practices and Climate Change Affect Wildfire Regimes in Mediterranean Landscapes. *PLoS One* 8, e62392. <https://doi.org/10.1371/journal.pone.0062392>

- Brown, K.J., Giesecke, T., 2014. Holocene fire disturbance in the boreal forest of central Sweden. *Boreas* 43, 639–651. <https://doi.org/10.1111/bor.12056>
- Brown, L.E., Palmer, S.M., Johnston, K., Holden, J., 2015. Vegetation management with fire modifies peatland soil thermal regime. *J. Environ. Manage.* 154, 166–176. <https://doi.org/10.1016/j.jenvman.2015.02.037>
- Camill, P., Barry, A., Williams, E., Andreassi, C., Limmer, J., Solick, D., 2009. Climate-vegetation-fire interactions and their impact on long-term carbon dynamics in a boreal peatland landscape in northern Manitoba, Canada. *J. Geophys. Res.* 114, G04017. <https://doi.org/10.1029/2009JG001071>
- Camill, P., Umbanhowar, C.E., Geiss, C., Hobbs, W.O., Edlund, M.B., Shinneman, A.C., Dorale, J.A., Lynch, J., 2012. Holocene climate change and landscape development from a low-Arctic tundra lake in the western Hudson Bay region of Manitoba, Canada. *J. Paleolimnol.* 48, 175–192. <https://doi.org/10.1007/s10933-012-9619-0>
- Carcaillet, C., Bouvier, M., Fréchette, B., Larouche, A.C., Richard, P.J.H., 2001. Comparison of pollen-slide and sieving methods in lacustrine charcoal analyses for local and regional fire history. *The Holocene* 11, 467–476. <https://doi.org/10.1191/095968301678302904>
- Carcaillet, C., Richard, P.J.H., 2000. Holocene changes in seasonal precipitation highlighted by fire incidence in eastern Canada. *Clim. Dyn.* 16, 549–559. <https://doi.org/10.1007/s003820000062>
- Clark, J.S., 1988. Particle motion and the theory of charcoal analysis: Source area, transport, deposition, and sampling. *Quat. Res.* 30, 67–80. [https://doi.org/10.1016/0033-5894\(88\)90088-9](https://doi.org/10.1016/0033-5894(88)90088-9)
- Clark, J.S., Lynch, J., Stocks, B.J., Goldammer, J.G., 1998. Relationships between charcoal particles in air and sediments in west-central Siberia. *Holocene* 8, 19–29. <https://doi.org/10.1191/095968398672501165>
- Clark, J.S., Patterson, W.A., 1997. Background and Local Charcoal in Sediments: Scales of Fire Evidence in the Paleorecord, in: *Sediment Records of Biomass Burning and Global Change*. Springer Berlin Heidelberg, pp. 23–48. https://doi.org/10.1007/978-3-642-59171-6_3
- Clark, J.S., Royall, P.D., 1996. Local and Regional Sediment Charcoal Evidence for Fire Regimes in Presettlement North-Eastern North America. *J. Ecol.* 84, 365–382. <https://doi.org/10.2307/2261199>
- Clark, J.S., Royall, P.D., 1995. Particle-size evidence for source areas of charcoal accumulation in late holocene sediments of eastern north american lakes. *Quat. Res.* 43, 80–89. <https://doi.org/10.1006/qres.1995.1008>
- Conedera, M., Tinner, W., Neff, C., Meurer, M., Dickens, A.F., Krebs, P., 2009. Reconstructing past fire regimes: methods, applications, and relevance to fire management and conservation. *Quat. Sci. Rev.* 28, 555–576. <https://doi.org/10.1016/j.quascirev.2008.11.005>
- Daniau, A.L., Bartlein, P.J., Harrison, S.P., Prentice, I.C., Brewer, S., Friedlingstein, P., Harrison-Prentice, T.I., Inoue, J., Izumi, K., Marlon, J.R., Mooney, S., Power, M.J., Stevenson, J., Tinner, W., Andrič, M., Atanassova, J., Behling, H., Black, M., Blarquez, O., Brown, K.J., Carcaillet, C., Colhoun, E.A., Colombaroli, D., Davis, B.A.S., D'Costa, D., Dodson, J., Dupont, L., Eshetu, Z.,

- Gavin, D.G., Genries, A., Haberle, S., Hallett, D.J., Hope, G., Horn, S.P., Kassa, T.G., Katamura, F., Kennedy, L.M., Kershaw, P., Krivonogov, S., Long, C., Magri, D., Marinova, E., McKenzie, G.M., Moreno, P.I., Moss, P., Neumann, F.H., Norström, E., Paitre, C., Rius, D., Roberts, N., Robinson, G.S., Sasaki, N., Scott, L., Takahara, H., Terwilliger, V., Thevenon, F., Turner, R., Valsecchi, V.G., Vannièrè, B., Walsh, M., Williams, N., Zhang, Y., 2012. Predictability of biomass burning in response to climate changes. *Global Biogeochem. Cycles* 26, GB4007. <https://doi.org/10.1029/2011GB004249>
- Davies, G.M., Gray, A., Rein, G., Legg, C.J., 2013. Peat consumption and carbon loss due to smouldering wildfire in a temperate peatland. *For. Ecol. Manage.* 308, 169–177. <https://doi.org/10.1016/j.foreco.2013.07.051>
- Davies, M.A., McLaughlin, J.W., Packalen, M.S., Finkelstein, S.A., 2021. Using Water Table Depths Inferred From Testate Amoebae to Estimate Holocene Methane Emissions From the Hudson Bay Lowlands, Canada. *J. Geophys. Res. Biogeosciences* 126, 1–20. <https://doi.org/10.1029/2020JG005969>
- Davis, B.A.S., Brewer, S., 2009. Orbital forcing and role of the latitudinal insolation/temperature gradient. *Clim. Dyn.* 32, 143–165. <https://doi.org/10.1007/s00382-008-0480-9>
- Davis, B.A.S., Brewer, S., Stevenson, A.C., Guiot, J., Allen, J., Almquist-Jacobson, H., Ammann, B., Andreev, A.A., Argant, J., Atanassova, J., Balwierz, Z., Barnosky, C.D., Bartley, D.D., De Beaulieu, J.L., Beckett, S.C., Behre, K.E., Bennett, K.D., Berglund, B.E.B., Beug, H.J., Bezusko, L., Binka, K., Birks, H.H., Birks, H.J.B., Björck, S., Bliakheartchouk, T., Bogdel, I., Bonatti, E., Bottema, S., Bozilova, E.D.B., Bradshaw, R., Brown, A.P., Brugiapaglia, E., Carrion, J., Chernavskaya, M., Clerc, J., Clet, M., Coûteaux, M., Craig, A.J., Cserny, T., Cwynar, L.C., Dambach, K., De Valk, E.J., Digerfeldt, G., Diot, M.F., Eastwood, W., Elina, G., Filimonova, L., Filipovitch, L., Gaillard-Lemdhall, M.J., Gauthier, A., Göransson, H., Guenet, P., Gunova, V., Hall, V.A.H., Harmata, K., Hicks, S., Huckerby, E., Huntley, B., Huttunen, A., Hyvärinen, H., Ilves, E., Jacobson, G.L., Jahns, S., Jankovská, V., Jóhansen, J., Kabailiene, M., Kelly, M.G., Khomutova, V.I., Königsson, L.K., Kremenetski, C., Kremenetskii, K. V., Krisai, I., Krisai, R., Kvavadze, E., Lamb, H., Lazarova, M.A., Litt, T., Lotter, A.F., Lowe, J.J., Magyari, E., Makohonienko, M., Mamakowa, K., Mangerud, J., Mariscal, B., Markgraf, V., McKeever, Mitchell, F.J.G., Munuera, M., Nicol-Pichard, S., Noryskiewicz, B., Odgaard, B. V., Panova, N.K., Pantaleon-Cano, J., Paus, A.A., Pavel, T., Peglar, S.M., Penalba, M.C., Pennington, W., Perez-Obiol, R., Pushenko, M., Ralska-Jasiewiczowa, M., Ramfjord, H., Regnell, J., Rybnickova, E., Rybnickova, M., Sarse, L., Sanchez Gomez, M.F., Sarmaja-Korjonen, K., Sarv, A., Seppä, H., Sivertsen, S., Smith, A.G., Spiridonova, E.A., Stancikaite, M., Stefanova, J., Stewart, D.A., Suc, J.P., Svobodova, H., Szczepanek, K., Tarasov, P., Tobolski, K., Tonkov, S.P., Turner, J., Van der Knaap, W.O., Van Leeuwen, J.F.N., Vasari, A., Vasari, Y., Verbruggen, C., Vergne, V., Veski, S., Visset, L., Vuorela, I., Wacnik, A., Walker, M.J.C., Waller, M.P., Watson, C.S., Watts, W.A., Whittington, G., Willis, K.J., Willutzki, H., Yelovicheva, Y., Yli, E.I., Zelikson, E.M., Zernitskaya, V.P., 2003. The temperature of Europe during the Holocene reconstructed from pollen data. *Quat. Sci. Rev.* 22, 1701–1716. [https://doi.org/10.1016/S0277-3791\(03\)00173-2](https://doi.org/10.1016/S0277-3791(03)00173-2)
- Dietze, E., Theuerkauf, M., Bloom, K., Brauer, A., Dörfler, W., Feeser, I., Feurdean, A., Gedminienė, L., Giesecke, T., Jahns, S., Karpińska-Kończek, M., Kończek, P., Lamentowicz, M., Latałowa, M., Marcisz, K., Obremaska, M., Pędziszewska, A., Poska, A., Rehfeld, K., Stančikaitė, M., Stivrins, N., Święta-Musznicka, J., Szal, M., Vassiljev, J., Veski, S., Wacnik, A., Weisbrodt, D., Wiethold, J., Vannièrè, B., Słowiński, M., 2018. Holocene fire activity during low-natural

- flammability periods reveals scale-dependent cultural human-fire relationships in Europe. *Quat. Sci. Rev.* 201, 44–56. <https://doi.org/10.1016/j.quascirev.2018.10.005>
- Edwards, T.W.D., Wolfe, B.B., Macdonald, G.M., 1996. Influence of changing atmospheric circulation on precipitation $\delta^{18}\text{O}$ -temperature relations in Canada during the Holocene. *Quat. Res.* 46, 211–218. <https://doi.org/10.1006/qres.1996.0061>
- Ejarque, A., Julià, R., Riera, S., Palet, J.M., Orengo, H.A., Miras, Y., Gascón, C., 2009. Tracing the history of highland human management in the eastern Pre-Pyrenees: An interdisciplinary palaeoenvironmental study at the Pradell fen, Spain. *The Holocene* 19, 1241–1255. <https://doi.org/10.1177/0959683609345084>
- Feurdean, A., Diaconu, A.-C., Pfeiffer, M., Gałka, M., Hutchinson, S.M., Butiseaca, G., Gorina, N., Tonkov, S., Niamir, A., Tantau, I., Zhang, H., Kirpotin, S., 2022. Holocene wildfire regimes in western Siberia: interaction between peatland moisture conditions and the composition of plant functional types. *Clim. Past* 18, 1255–1274. <https://doi.org/10.5194/CP-18-1255-2022>
- Feurdean, A., Florescu, G., Tanțău, I., Vannièrè, B., Diaconu, A.C., Pfeiffer, M., Warren, D., Hutchinson, S.M., Gorina, N., Gałka, M., Kirpotin, S., 2020a. Recent fire regime in the southern boreal forests of western Siberia is unprecedented in the last five millennia. *Quat. Sci. Rev.* 244, 106495. <https://doi.org/10.1016/j.quascirev.2020.106495>
- Feurdean, A., Vannièrè, B., Finsinger, W., Warren, D., Connor, S.C., Forrest, M., Liakka, J., Panait, A., Werner, C., Andrič, M., Bobek, P., Carter, V.A., Davis, B., Diaconu, A.C., Dietze, E., Feeser, I., Florescu, G., Gałka, M., Giesecke, T., Jahns, S., Jamrichová, E., Kajukalo, K., Kaplan, J., Karpińska-Kołaczek, M., Kołaczek, P., Kuneš, P., Kupriyanov, D., Lamentowicz, M., Lemmen, C., Magyari, E.K., Marcisz, K., Marinova, E., Niamir, A., Novenko, E., Obremaska, M., Pędziszewska, A., Pfeiffer, M., Poska, A., Rösch, M., Słowiński, M., Stančikaite, M., Szal, M., Święta-Musznicka, J., Tanțău, I., Theuerkauf, M., Tonkov, S., Valkó, O., Vassiljev, J., Veski, S., Vincze, I., Wacnik, A., Wiethold, J., Hickler, T., 2020b. Fire hazard modulation by long-term dynamics in land cover and dominant forest type in eastern and central Europe. *Biogeosciences* 17, 1213–1230. <https://doi.org/10.5194/BG-17-1213-2020>
- Flannigan, M., Stocks, B., Turetsky, M., Wotton, M., 2009. Impacts of climate change on fire activity and fire management in the circumboreal forest. *Glob. Chang. Biol.* 15, 549–560. <https://doi.org/10.1111/j.1365-2486.2008.01660.x>
- Florescu, G., Vannièrè, B., Feurdean, A., 2018. Exploring the influence of local controls on fire activity using multiple charcoal records from northern Romanian Carpathians. *Quat. Int.* 488, 41–57. <https://doi.org/10.1016/j.quaint.2018.03.042>
- Fohlmeister, J., Schröder-Ritzrau, A., Scholz, D., Spötl, C., Riechelmann, D.F.C., Mudelsee, M., Wackerbarth, A., Gerdes, A., Riechelmann, S., Immenhauser, A., Richter, D.K., Mangini, A., 2012. Bunker Cave stalagmites: An archive for central European Holocene climate variability. *Clim. Past* 8, 1751–1764. <https://doi.org/10.5194/cp-8-1751-2012>
- Frandsen, W.H., 1997. Ignition probability of organic soils. *Can. J. For. Res.* 27, 1471–1477. <https://doi.org/10.1139/x97-106>
- Fyfe, R.M., Brown, A.G., Rippon, S.J., 2003. Mid- to late-Holocene vegetation history of Greater Exmoor, UK: Estimating the spatial extent of human-induced vegetation change. *Veg. Hist. Archaeobot.* 12, 215–232. <https://doi.org/10.1007/s00334-003-0018-3>

- Gardner, J.J., Whitlock, C., 2001. Charcoal accumulation following a recent fire in the Cascade Range, northwestern USA, and its relevance for fire-history studies. *The Holocene* 11, 541–549. <https://doi.org/10.1191/095968301680223495>
- Gibson, C.M., Chasmer, L.E., Thompson, D.K., Quinton, W.L., Flannigan, M.D., Olefeldt, D., 2018. Wildfire as a major driver of recent permafrost thaw in boreal peatlands. *Nat. Commun.* 9, 3041. <https://doi.org/10.1038/s41467-018-05457-1>
- Gilck, F., Poschlod, P., 2021. The history of human land use activities in the Northern Alps since the Neolithic Age. A reconstruction of vegetation and fire history in the Mangfall Mountains (Bavaria, Germany). *The Holocene* 31, 579–591. <https://doi.org/10.1177/0959683620981701>
- Glaser, P.H., Hansen, B.C.S., Siegel, D.I., Reeve, A.S., Morin, P.J., 2004. Rates, pathways and drivers for peatland development in the Hudson Bay Lowlands, northern Ontario, Canada. *J. Ecol.* 92, 1036–1053. <https://doi.org/10.1111/J.0022-0477.2004.00931.X>
- Gorham, E., Lehman, C., Dyke, A., Janssens, J., Dyke, L., 2007. Temporal and spatial aspects of peatland initiation following deglaciation in North America. *Quat. Sci. Rev.* 26, 300–311. <https://doi.org/10.1016/j.quascirev.2006.08.008>
- Granath, G., Moore, P.A., Lukenbach, M.C., Waddington, J.M., 2016. Mitigating wildfire carbon loss in managed northern peatlands through restoration. *Sci. Rep.* 6, 28498. <https://doi.org/10.1038/srep28498>
- Hammarlund, D., Björck, S., Buchardt, B., Israelson, C., Thomsen, C.T., 2003. Rapid hydrological changes during the Holocene revealed by stable isotope records of lacustrine carbonates from Lake Igelsjön, southern Sweden. *Quat. Sci. Rev.* 22, 353–370. [https://doi.org/10.1016/S0277-3791\(02\)00091-4](https://doi.org/10.1016/S0277-3791(02)00091-4)
- Hargan, K.E., Finkelstein, S.A., Rühland, K.M., Packalen, M.S., Dalton, A.S., Paterson, A.M., Keller, W., Smol, J.P., 2020. Post-glacial lake development and paleoclimate in the central Hudson Bay Lowlands inferred from sediment records. *J. Paleolimnol.* 64, 25–46. <https://doi.org/10.1007/s10933-020-00119-z>
- Harris, I., Osborn, T.J., Jones, P., Lister, D., 2020. Version 4 of the CRU TS monthly high-resolution gridded multivariate climate dataset. *Sci. Data* 7, 1–18. <https://doi.org/10.1038/s41597-020-0453-3>
- He, J., Loboda, T. V., Chen, D., French, N.H.F., 2022. Cloud-to-Ground Lightning and Near-Surface Fire Weather Control Wildfire Occurrence in Arctic Tundra. *Geophys. Res. Lett.* 49, e2021GL096814. <https://doi.org/10.1029/2021GL096814>
- Heikkilä, M., Seppä, H., 2010. Holocene climate dynamics in Latvia, eastern Baltic region: A pollen-based summer temperature reconstruction and regional comparison. *Boreas* 39, 705–719. <https://doi.org/10.1111/j.1502-3885.2010.00164.x>
- Higuera, P.E., Peters, M.E., Brubaker, L.B., Gavin, D.G., 2007. Understanding the origin and analysis of sediment-charcoal records with a simulation model. *Quat. Sci. Rev.* 26, 1790–1809. <https://doi.org/10.1016/j.quascirev.2007.03.010>
- Hobbs, W.O., Edlund, M.B., Umbanhowar, C.E., Camill, P., Lynch, J.A., Geiss, C., Stefanova, V., 2017. Holocene evolution of lakes in the forest-tundra biome of northern Manitoba, Canada.

- Quat. Sci. Rev. 159, 116–138. <https://doi.org/10.1016/j.quascirev.2017.01.014>
- Hokanson, K.J., Lukenbach, M.C., Devito, K.J., Kettridge, N., Petrone, R.M., Waddington, J.M., 2016. Groundwater connectivity controls peat burn severity in the boreal plains. *Ecohydrology* 9, 574–584. <https://doi.org/10.1002/ECO.1657>
- Holden, J., Shotbolt, L., Bonn, A., Burt, T.P., Chapman, P.J., Dougill, A.J., Fraser, E.D.G., Hubacek, K., Irvine, B., Kirkby, M.J., Reed, M.S., Prell, C., Stagl, S., Stringer, L.C., Turner, A., Worrall, F., 2007. Environmental change in moorland landscapes. *Earth-Science Rev.* 82, 75–100. <https://doi.org/10.1016/j.earscirev.2007.01.003>
- Huber, U.M., Markgraf, V., 2003. European impact on fire regimes and vegetation dynamics at the steppe-forest ecotone of southern Patagonia. *The Holocene* 13, 567–579. <https://doi.org/10.1191/0959683603hl647rp>
- Jääts, L., Kihno, K., Tomson, P., Konsa, M., 2010. Tracing fire cultivation in Estonia. *For. Stud. / Metsanduslikud Uurim.* 53, 53–65. <https://doi.org/10.2478/v10132-011-0089-3>
- Kettridge, N., Waddington, J.M., 2014. Towards quantifying the negative feedback regulation of peatland evaporation to drought. *Hydrol. Process.* 28, 3728–3740. <https://doi.org/10.1002/hyp.9898>
- Kloster, S., Mahowald, N.M., Randerson, J.T., Lawrence, P.J., 2012. The impacts of climate, land use, and demography on fires during the 21st century simulated by CLM-CN. *Biogeosciences* 9, 509–525. <https://doi.org/10.5194/bg-9-509-2012>
- Kuhry, P., 1994. The Role of Fire in the Development of Sphagnum-Dominated Peatlands in Western Boreal Canada. *J. Ecol.* 82, 899–910.
- Lavoie, M., Filion, L., Robert, É.C., 2009. Boreal peatland margins as repository sites of long-term natural disturbances of balsam fir/spruce forests. *Quat. Res.* 71, 295–306. <https://doi.org/10.1016/J.YQRES.2009.01.005>
- Lehtonen, H., Huttunen, P., 1997. History of forest fires in eastern Finland from the fifteenth century AD - The possible effects of slash-and-burn cultivation. *The Holocene* 7, 223–228. <https://doi.org/10.1177/095968369700700210>
- Lin, S., Liu, Y., Huang, X., 2021. Climate-induced Arctic-boreal peatland fire and carbon loss in the 21st century. *Sci. Total Environ.* 796, 148924. <https://doi.org/10.1016/j.scitotenv.2021.148924>
- Magnan, G., Garneau, M., Payette, S., 2014. Holocene development of maritime ombrotrophic peatlands of the St. Lawrence North Shore in eastern Canada. *Quat. Res.* 82, 96–106. <https://doi.org/10.1016/j.yqres.2014.04.016>
- Magnan, G., Lavoie, M., Payette, S., 2012. Impact of fire on long-term vegetation dynamics of ombrotrophic peatlands in northwestern Québec, Canada. *Quat. Res.* 77, 110–121. <https://doi.org/10.1016/J.YQRES.2011.10.006>
- Magnan, G., van Bellen, S., Davies, L., Froese, D., Garneau, M., Mullan-Boudreau, G., Zaccone, C., Shotyk, W., 2018. Impact of the Little Ice Age cooling and 20th century climate change on peatland vegetation dynamics in central and northern Alberta using a multi-proxy approach and high-resolution peat chronologies. *Quat. Sci. Rev.* 185, 230–243. <https://doi.org/10.1016/j.quascirev.2018.01.015>

- Mann, M.E., Zhang, Z., Rutherford, S., Bradley, R.S., Hughes, M.K., Shindell, D., Ammann, C., Faluvegi, G., Ni, F., 2009. Global signatures and dynamical origins of the Little Ice Age and Medieval Climate Anomaly. *Science* (80-). 326, 1256–1260. <https://doi.org/10.1126/science.1177303>
- Marcisz, K., Kołaczek, P., Gałka, M., Diaconu, A.C., Lamentowicz, M., 2020. Exceptional hydrological stability of a Sphagnum-dominated peatland over the late Holocene. *Quat. Sci. Rev.* 231, 106180. <https://doi.org/10.1016/J.QUASCIREV.2020.106180>
- Marcisz, K., Lamentowicz, M., Gałka, M., Colombaroli, D., Adolf, C., Tinner, W., 2019. Responses of vegetation and testate amoeba trait composition to fire disturbances in and around a bog in central European lowlands (northern Poland). *Quat. Sci. Rev.* 208, 129–139. <https://doi.org/10.1016/J.QUASCIREV.2019.02.003>
- Markgraf, V., Huber, U.M., 2010. Late and postglacial vegetation and fire history in Southern Patagonia and Tierra del Fuego. *Palaeogeogr. Palaeoclimatol. Palaeoecol.* 297, 351–366. <https://doi.org/10.1016/J.PALAEO.2010.08.013>
- Marlon, J.R., Bartlein, P.J., Carcaillet, C., Gavin, D.G., Harrison, S.P., Higuera, P.E., Joos, F., Power, M.J., Prentice, I.C., 2008. Climate and human influences on global biomass burning over the past two millennia. *Nat. Geosci.* 1, 697–702. <https://doi.org/10.1038/ngeo313>
- Marlon, J.R., Bartlein, P.J., Daniau, A.L., Harrison, S.P., Maezumi, S.Y., Power, M.J., Tinner, W., Vanni ere, B., 2013. Global biomass burning: A synthesis and review of Holocene paleofire records and their controls. *Quat. Sci. Rev.* 65, 5–25. <https://doi.org/10.1016/j.quascirev.2012.11.029>
- Marlon, J.R., Kelly, R., Daniau, A.L., Vanni ere, B., Power, M.J., Bartlein, P., Higuera, P., Blarquez, O., Brewer, S., Br ucher, T., Feurdean, A., Romera, G.G., Iglesias, V., Yoshi Maezumi, S., Magi, B., Mustaphi, C.J.C., Zhihai, T., 2016. Reconstructions of biomass burning from sediment-charcoal records to improve data-model comparisons. *Biogeosciences* 13, 3225–3244. <https://doi.org/10.5194/bg-13-3225-2016>
- Mauri, A., Davis, B.A.S., Collins, P.M., Kaplan, J.O., 2015. The climate of Europe during the Holocene: A gridded pollen-based reconstruction and its multi-proxy evaluation. *Quat. Sci. Rev.* 112, 109–127. <https://doi.org/10.1016/j.quascirev.2015.01.013>
- Mazei, Y.A., Tsyganov, A.N., Bobrovsky, M. V., Mazei, N.G., Kupriyanov, D.A., Gałka, M., Rostanets, D. V., Khazanova, K.P., Stoiko, T.G., Pastukhova, Y.A., Fatynina, Y.A., Komarov, A.A., Babeshko, K. V., Makarova, A.D., Saldaev, D.A., Zazovskaya, E.P., Dobrovolskaya, M. V., Tiunov, A. V., 2020. Peatland development, vegetation history, climate change and human activity in the valdai uplands (Central european Russia) during the holocene: A multi-proxy palaeoecological study. *Diversity* 12, 1–25. <https://doi.org/10.3390/d12120462>
- McCarty, J.L., Aalto, J., Paunu, V.-V., Arnold, S.R., Eckhardt, S., Klimont, Z., Fain, J.J., Evangelidou, N., Ven al inen, A., Tchebakova, N.M., Parfenova, E.I., Kupiainen, K., Soja, A.J., Huang, L., Wilson, S., 2021. Reviews and syntheses: Arctic fire regimes and emissions in the 21st century. *Biogeosciences* 18, 5053–5083. <https://doi.org/10.5194/BG-18-5053-2021>
- McCulloch, R.D., Blaikie, J., Jacob, B., Mansilla, C.A., Morello, F., De Pol-Holz, R., San Rom an, M., Tisdall, E., Torres, J., 2020. Late glacial and Holocene climate variability, southernmost Patagonia. *Quat. Sci. Rev.* 229, 106131. <https://doi.org/10.1016/J.QUASCIREV.2019.106131>

- McMichael, C.N.H., Heijink, B.M., Bush, M.B., Gosling, W.D., 2021. On the scaling and standardization of charcoal data in paleofire reconstructions. *Front. Biogeogr.* <https://doi.org/10.21425/F5FBG49431>
- Mooney, S.D., Tinner, W., 2011. The analysis of charcoal in peat and organic sediments. *Mires Peat* 7, 1–18.
- Moreira, F., Viedma, O., Arianoutsou, M., Curt, T., Koutsias, N., Rigolot, E., Barbati, A., Corona, P., Vaz, P., Xanthopoulos, G., Mouillot, F., Bilgili, E., 2011. Landscape - wildfire interactions in southern Europe: Implications for landscape management. *J. Environ. Manage.* 92, 2389–2402. <https://doi.org/10.1016/j.jenvman.2011.06.028>
- Moreno, P.I., Vilanova, I., Villa-Martínez, R., Dunbar, R.B., Mucciarone, D.A., Kaplan, M.R., Garreaud, R.D., Rojas, M., Moy, C.M., De Pol-Holz, R., Lambert, F., 2018. Onset and Evolution of Southern Annular Mode-Like Changes at Centennial Timescale. *Sci. Rep.* 8, 3458. <https://doi.org/10.1038/s41598-018-21836-6>
- Morris, J.L., Välranta, M., Sillasoo, Ü., Tuittila, E.S., Korhola, A., 2015. Re-evaluation of late Holocene fire histories of three boreal bogs suggest a link between bog fire and climate. *Boreas* 44, 60–67. <https://doi.org/10.1111/bor.12086>
- Morris, P.J., Swindles, G.T., Valdes, P.J., Ivanovic, R.F., Gregoire, L.J., Smith, M.W., Tarasov, L., Haywood, A.M., Bacon, K.L., 2018. Global peatland initiation driven by regionally asynchronous warming. *Proc. Natl. Acad. Sci. U. S. A.* 115, 4851–4856. <https://doi.org/10.1073/pnas.1717838115>
- Morris, P.J., Waddington, J.M., 2011. Groundwater residence time distributions in peatlands: Implications for peat decomposition and accumulation. *Water Resour. Res.* 47, W02511. <https://doi.org/10.1029/2010WR009492>
- Nelson, K., Thompson, D., Hopkinson, C., Petrone, R., Chasmer, L., 2021. Peatland-fire interactions: A review of wildland fire feedbacks and interactions in Canadian boreal peatlands. *Sci. Total Environ.* 769, 145212. <https://doi.org/10.1016/j.scitotenv.2021.145212>
- Ohlson, M., Korbøl, A., Økland, R.H., 2006. The macroscopic charcoal record in forested boreal peatlands in southeast Norway. *The Holocene* 16, 731–741. <https://doi.org/10.1191/0959683606hl955rp>
- Olsson, F., Gaillard, M.J., Lemdahl, G., Greisman, A., Lanos, P., Marguerie, D., Marcoux, N., Skoglund, P., Wäglind, J., 2010. A continuous record of fire covering the last 10,500 calendar years from southern Sweden - The role of climate and human activities. *Palaeogeogr. Palaeoclimatol. Palaeoecol.* 291, 128–141. <https://doi.org/10.1016/j.palaeo.2009.07.013>
- Oswald, W.W., Anderson, P.M., Brown, T.A., Brubaker, L.B., Feng, S.H., Lozhkin, A. V., Tinner, W., Kaltenrieder, P., 2005. Effects of sample mass and macrofossil type on radiocarbon dating of arctic and boreal lake sediments. *The Holocene* 15, 758–767. <https://doi.org/10.1191/0959683605hl849rr>
- Page, S.E., Baird, A.J., 2016. Peatlands and Global Change: Response and Resilience. *Annu. Rev. Environ. Resour.* 41, 35–57. <https://doi.org/10.1146/annurev-environ-110615-085520>
- Pan, Y., Birdsey, R.A., Fang, J., Houghton, R., Kauppi, P.E., Kurz, W.A., Phillips, O.L., Shvidenko, A., Lewis, S.L., Canadell, J.G., Ciais, P., Jackson, R.B., Pacala, S.W., McGuire, A.D., Piao, S.,

- Rautiainen, A., Sitch, S., Hayes, D., 2011. A large and persistent carbon sink in the world's forests. *Science* (80-.). 333. <https://doi.org/10.1126/science.1201609>
- Parviainen, J., 2015. Cultural heritage and biodiversity in the present forest management of the boreal zone in Scandinavia. *J. For. Res.* 20, 445–452. <https://doi.org/10.1007/s10310-015-0499-9>
- Payette, S., Garneau, M., Delwaide, A., Schaffhauser, A., 2013. Forest soil paludification and mid-Holocene retreat of jack pine in easternmost North America: Evidence for a climatic shift from fire-prone to peat-prone conditions. *The Holocene* 23, 494–503. <https://doi.org/10.1177/0959683612463099>
- Payne, R., 2018. Peatlands of the Mediterranean region, in: *The Wetland Book II: Distribution, Description, and Conservation*. pp. 1–12. https://doi.org/10.1007/978-94-007-4001-3_111
- Pelletier, N., Talbot, J., Olefeldt, D., Turetsky, M., Blodau, C., Sonntag, O., Quinton, W.L., 2017. Influence of Holocene permafrost aggradation and thaw on the paleoecology and carbon storage of a peatland complex in northwestern Canada. *The Holocene* 27, 1391–1405. <https://doi.org/10.1177/0959683617693899>
- Peters, M.E., Higuera, P.E., 2007. Quantifying the source area of macroscopic charcoal with a particle dispersal model. *Quat. Res.* 67, 304–310. <https://doi.org/10.1016/j.yqres.2006.10.004>
- Peyron, O., Goring, S., Dormoy, I., Kotthoff, U., Pross, J., de Beaulieu, J.L., Drescher-Schneider, R., Vanni re, B., Magny, M., 2011. Holocene seasonality changes in the central Mediterranean region reconstructed from the pollen sequences of Lake Accessa (Italy) and Tenaghi Philippon (Greece). *The Holocene* 21, 131–146. <https://doi.org/10.1177/0959683610384162>
- Pleskot, K., Apolinarska, K., Cwynar, L.C., Kotrys, B., Lamentowicz, M., 2022. The late-Holocene relationship between peatland water table depth and summer temperature in northern Poland. *Palaeogeogr. Palaeoclimatol. Palaeoecol.* 586, 110758. <https://doi.org/10.1016/J.PALAEO.2021.110758>
- Power, M.J., Marlon, J.R., Bartlein, P.J., Harrison, S.P., 2010. Fire history and the global charcoal database: A new tool for hypothesis testing and data exploration. *Palaeogeogr. Palaeoclimatol. Palaeoecol.* 291, 52–59. <https://doi.org/10.1016/j.palaeo.2009.09.014>
- R Core Team, 2021. R: a language and environment for statistical computing. Version 4.0.5.
- Rein, G., 2013. Smouldering Fires and Natural Fuels, in: Belcher, C.M. (Ed.), *Fire Phenomena and the Earth System: An Interdisciplinary Guide to Fire Science*. John Wiley and Sons, pp. 15–33. <https://doi.org/10.1002/9781118529539.ch2>
- Remy, C.C., Fouquemberg, C., Asselin, H., Andrieux, B., Magnan, G., Brossier, B., Grondin, P., Bergeron, Y., Talon, B., Girardin, M.P., Blarquez, O., Bajolle, L., Ali, A.A., 2018. Guidelines for the use and interpretation of palaeofire reconstructions based on various archives and proxies. *Quat. Sci. Rev.* 193, 312–322. <https://doi.org/10.1016/j.quascirev.2018.06.010>
- Rius, D., Vanni re, B., Galop, D., 2012. Holocene history of fire, vegetation and land use from the central Pyrenees (France). *Quat. Res.* 77, 54–64. <https://doi.org/10.1016/J.YQRES.2011.09.009>
- Rius, D., Vanni re, B., Galop, D., Richard, H., 2011. Holocene fire regime changes from multiple-

- site sedimentary charcoal analyses in the Lourdes basin (Pyrenees, France). *Quat. Sci. Rev.* 30, 1696–1709. <https://doi.org/10.1016/j.quascirev.2011.03.014>
- Rösch, M., Biester, H., Bogenrieder, A., Eckmeier, E., Ehrmann, O., Gerlach, R., Hall, M., Hartkopf-Fröder, C., Herrmann, L., Kury, B., Lechterbeck, J., Schier, W., Schulz, E., 2017. Late Neolithic agriculture in temperate Europe—a long-term experimental approach. *Land* 6, 1–17. <https://doi.org/10.3390/land6010011>
- Ryan, P.A., Blackford, J.J., 2010. Late Mesolithic environmental change at Black Heath, south Pennines, UK: A test of Mesolithic woodland management models using pollen, charcoal and non-pollen palynomorph data. *Veg. Hist. Archaeobot.* 19, 545–558. <https://doi.org/10.1007/s00334-010-0263-1>
- Schneider, C., Glaser, M., Kilian, R., Santana, A., Casassa, G., 2003. Weather observations across the southern andes at 53°S. *Phys. Geogr.* 24, 97–119. <https://doi.org/10.2747/0272-3646.24.2.97>
- Shiller, J.A., Finkelstein, S.A., Cowling, S.A., 2014. Relative importance of climatic and autogenic controls on Holocene carbon accumulation in a temperate bog in southern Ontario, Canada. *The Holocene* 24, 1105–1116. <https://doi.org/10.1177/0959683614538070>
- Sillasoo, Ü., Väliiranta, M., Tuittila, E.S., 2011. Fire history and vegetation recovery in two raised bogs at the Baltic Sea. *J. Veg. Sci.* 22, 1084–1093. <https://doi.org/10.1111/j.1654-1103.2011.01307.x>
- Słowiński, M., Obremska, M., Avirmed, D., Woszczyk, M., Adiya, S., Łuców, D., Mroczkowska, A., Halaś, A., Szczuciński, W., Kruk, A., Lamentowicz, M., Stańczak, J., Rudaya, N., 2022. Fires, vegetation, and human—The history of critical transitions during the last 1000 years in Northeastern Mongolia. *Sci. Total Environ.* 838, 155660. <https://doi.org/10.1016/j.scitotenv.2022.155660>
- Spietan, G.K., Wurster, F.C., 2020. Hydrology and water quality of the Great Dismal Swamp, Virginia and North Carolina, and implications for hydrologic-management goals and strategies, U.S. Geological Survey Scientific Investigations Report, 2020-5100. <https://doi.org/https://doi.org/10.3133/sir20205100>
- Swindles, G.T., Lawson, I.T., Matthews, I.P., Blaauw, M., Daley, T.J., Charman, D.J., Roland, T.P., Plunkett, G., Schettler, G., Gearey, B.R., Turner, T.E., Rea, H.A., Roe, H.M., Amesbury, M.J., Chambers, F.M., Holmes, Jonathan, Mitchell, F.J.G., Blackford, J., Blundell, A., Branch, N., Holmes, Jane, Langdon, P., McCarroll, J., McDermott, F., Oksanen, P.O., Pritchard, O., Stastney, P., Stefanini, B., Young, D., Wheeler, J., Becker, K., Armit, I., 2013. Centennial-scale climate change in Ireland during the Holocene. *Earth-Science Rev.* 126, 300–320. <https://doi.org/10.1016/j.earscirev.2013.08.012>
- Swindles, G.T., Morris, P.J., Mullan, D.J., Payne, R.J., Roland, T.P., Amesbury, M.J., Lamentowicz, M., Turner, T.E., Gallego-Sala, A., Sim, T., Barr, I.D., Blaauw, M., Blundell, A., Chambers, F.M., Charman, D.J., Feurdean, A., Galloway, J.M., Gałka, M., Green, S.M., Kajukało, K., Karofeld, E., Korhola, A., Lamentowicz, Ł., Langdon, P., Marcisz, K., Mauquoy, D., Mazei, Y.A., McKeown, M.M., Mitchell, E.A.D., Novenko, E., Plunkett, G., Roe, H.M., Schoning, K., Sillasoo, Ü., Tsyganov, A.N., van der Linden, M., Väliiranta, M., Warner, B., 2019. Widespread drying of European peatlands in recent centuries. *Nat. Geosci.* 12, 922–928. <https://doi.org/10.1038/s41561-019-0462-z>

- Thompson, D.K., Simpson, B.N., Whitman, E., Barber, Q.E., Parisien, M.A., 2019. Peatland hydrological dynamics as a driver of landscape connectivity and fire activity in the Boreal plain of Canada. *Forests* 10, 1–21. <https://doi.org/10.3390/f10070534>
- Tinner, W., Hofstetter, S., Zeugin, F., Conedera, M., Wohlgemuth, T., Zimmermann, L., Zweifel, R., 2006. Long-distance transport of macroscopic charcoal by an intensive crown fire in the Swiss Alps - Implications for fire history reconstruction. *Holocene* 16, 287–292. <https://doi.org/10.1191/0959683606hl925rr>
- Treat, C.C., Jones, M.C., 2018. Near-surface permafrost aggradation in Northern Hemisphere peatlands shows regional and global trends during the past 6000 years. *The Holocene* 28, 998–1010. <https://doi.org/10.1177/0959683617752858>
- Turetsky, M., Benscoter, B., Page, S., Rein, G., van der Werf, G.R., Watts, A., 2015. Global vulnerability of peatlands to fire and carbon loss. *Nat. Geosci.* 8, 11–14. <https://doi.org/10.1038/ngeo2325>
- Turetsky, M., Donahue, W.F., Benscoter, B.W., 2011. Experimental drying intensifies burning and carbon losses in a northern peatland. *Nat. Commun.* 2, 1–5. <https://doi.org/10.1038/ncomms1523>
- Urák, I., Hartel, T., Gallé, R., Balog, A., 2017. Worldwide peatland degradations and the related carbon dioxide emissions: the importance of policy regulations. *Environ. Sci. Policy* 69, 57–64. <https://doi.org/10.1016/j.envsci.2016.12.012>
- Väliranta, M., Salojärvi, N., Vuorsalo, A., Juutinen, S., Korhola, A., Luoto, M., Tuittila, E.S., 2017. Holocene fen–bog transitions, current status in Finland and future perspectives. *Holocene* 27, 752–764. <https://doi.org/10.1177/0959683616670471>
- Väliranta, M., Salonen, J.S., Heikkilä, M., Amon, L., Helmens, K., Klimaschewski, A., Kuhry, P., Kultti, S., Poska, A., Shala, S., Veski, S., Birks, H.H., 2015. Plant macrofossil evidence for an early onset of the Holocene summer thermal maximum in northernmost Europe. *Nat. Commun.* 6, 1–8. <https://doi.org/10.1038/ncomms7809>
- van Bellen, S., Garneau, M., Ali, A.A., Lamarre, A., Robert, É.C., Magnan, G., Asnong, H., Pratte, S., 2013. Poor fen succession over ombrotrophic peat related to late Holocene increased surface wetness in subarctic Quebec, Canada. *J. Quat. Sci.* 28, 748–760. <https://doi.org/10.1002/jqs.2670>
- Vannièrè, B., Blarquez, O., Rius, D., Doyen, E., Brücher, T., Colombaroli, D., Connor, S., Feurdean, A., Hickler, T., Kaltenrieder, P., Lemmen, C., Leys, B., Massa, C., Olofsson, J., 2016. 7000-year human legacy of elevation-dependent European fire regimes. *Quat. Sci. Rev.* 132, 206–212. <https://doi.org/10.1016/j.quascirev.2015.11.012>
- Viau, A.E., Gajewski, K., 2009. Reconstructing Millennial-Scale, Regional Paleoclimates of Boreal Canada during the Holocene. *J. Clim.* 22, 316–330. <https://doi.org/10.1175/2008JCLI2342.1>
- Viau, A.E., Gajewski, K., Sawada, M.C., Fines, P., 2006. Millennial-scale temperature variations in North America during the Holocene. *J. Geophys. Res. Atmos.* 111, D09102. <https://doi.org/10.1029/2005JD006031>
- Waddington, J.M., Morris, P.J., Kettridge, N., Granath, G., Thompson, D.K., Moore, P.A., 2015. Hydrological feedbacks in northern peatlands. *Ecohydrology* 8, 113–127.

<https://doi.org/10.1002/eco.1493>

- Wallenius, T., 2011. Major decline in fires in coniferous forests - reconstructing the phenomenon and seeking for the cause. *Silva Fenn.* 45, 139–155. <https://doi.org/10.14214/sf.36>
- Watts, W.A., 1979. Late Quaternary vegetation of central Appalachia and the New Jersey coastal plain. *Ecol. Monogr.* 49, 427–469. <https://doi.org/10.2307/1942471>
- Webb III, T., Bartlein, P.J., Kutzbach, J.E., 1987. Climatic change in eastern North America during the past 18,000 years; comparisons of pollen data with model results, in: Ruddiman, W.R., Wright Jr., H.E. (Eds.), *North America and Adjacent Oceans During the Last Deglaciation*. Geological Society of America, Boulder, Colorado USA, pp. 447–462.
- Webb, J.C., McCarroll, J., Chambers, F.M., Thom, T., 2022. Evidence for the Little Ice Age in upland northwestern Europe: Multiproxy climate data from three blanket mires in northern England. *The Holocene* 32, 451–467. <https://doi.org/10.1177/09596836221074036>
- Wilkinson, S.L., Verkaik, G.J., Moore, P.A., Waddington, J.M., 2020. Threshold peat burn severity breaks evaporation-limiting feedback. *Ecohydrology* 13, 1–11. <https://doi.org/10.1002/eco.2168>
- Williams, J.W., 2003. Variations in tree cover in North America since the last glacial maximum. *Glob. Planet. Change* 35, 1–23. [https://doi.org/10.1016/S0921-8181\(02\)00088-7](https://doi.org/10.1016/S0921-8181(02)00088-7)
- Woodbridge, J., Fyfe, R.M., Roberts, N., Downey, S., Edinborough, K., Shennan, S., 2014. The impact of the Neolithic agricultural transition in Britain: A comparison of pollen-based land-cover and archaeological 14C date-inferred population change. *J. Archaeol. Sci.* 51, 216–224. <https://doi.org/10.1016/j.jas.2012.10.025>
- Xu, J., Morris, P.J., Liu, J., Holden, J., 2018. PEATMAP: Refining estimates of global peatland distribution based on a meta-analysis. *CATENA* 160, 134–140. <https://doi.org/10.1016/J.CATENA.2017.09.010>
- Yu, Z., Loisel, J., Brosseau, D.P., Beilman, D.W., Hunt, S.J., 2010. Global peatland dynamics since the Last Glacial Maximum. *Geophys. Res. Lett.* 37, L13402. <https://doi.org/10.1029/2010GL043584>
- Zaccone, C., Rein, G., D’Orazio, V., Hadden, R.M., Belcher, C.M., Miano, T.M., 2014. Smouldering fire signatures in peat and their implications for palaeoenvironmental reconstructions. *Geochim. Cosmochim. Acta* 137, 134–146. <https://doi.org/10.1016/j.gca.2014.04.018>
- Zoltai, S.C., Morrissey, L.A., Livingston, G.P., De Groot, W.J., 1998. Effects of fires on carbon cycling in North American boreal peatlands. *Environ. Rev.* 6, 13–24. <https://doi.org/10.1139/a98-002>

Chapter 5 – Discussion and conclusions

5. Discussion and conclusions

In this chapter, the findings of each previous results chapter will be discussed in relation to each other and placed in context of the wider literature. I will first summarise the key findings from Chapters 2, 3 and 4 to show how they meet the thesis objectives. I will then synthesise the findings between each results chapter in the context of the wider literature (Section 5.1). The implications of these findings for the field of peatland environmental change and ideas for future work will then be discussed (Section 5.2) and finally the overall conclusions of the thesis will be stated (Section 5.3). For clarity, the overall aim of this thesis was:

“To investigate trends in ecohydrology and fire regime in mid- to high-latitude peatlands during the Holocene using palaeoecological techniques, with a focus on better understanding autogenic and climate-driven ecosystem shifts.”

To fulfil this aim, three objectives were devised with each objective relating to an individual results chapter. To meet this overall aim:

1. I developed and applied testate amoeba-based transfer functions for water-table depth and pH for high-latitude peatlands in Svalbard (Chapter 2). Testate amoebae included in these transfer functions preserved well and maintain diversity down core, suggesting changing species assemblages reflect genuine shifts in WTD and pH. These reconstructions showed increases in pH and wetness in the last century that may be linked to recent climate change.
2. I investigated the ecohydrological and carbon dynamics response of permafrost peatlands in a rapidly warming region of subarctic Sweden across multiple sites (Chapter 3). Here I found that permafrost peatlands demonstrated a divergent ecohydrological response to recent climate change. Whether a peatland becomes wetter or drier under a particular external forcing may depend on local and autogenic factors relating to vegetation dynamics, permafrost thaw, productivity and decomposition.
3. I examined peatland biomass burning trends and controls in North America, Europe and Patagonia during the Holocene (Chapter 4). This analysis shows that there was a degree of regional variability in peatland burning during the Holocene, largely linked to changes in climate, although human activities exert a greater influence in the late Holocene and there is evidence to suggest that autogenic processes have been important.

5.1. Research synthesis

Over the course of this thesis the scope and spatial extent have increased between the three results chapters. I have moved from testate amoeba transfer function methodological development for the understudied region of Svalbard (Chapter 2), to implementation of multiple palaeoecological proxies across multiple sites within the rapidly changing region of northern Sweden (Chapter 3). Then finally, I undertook a synthesis of existing data to explore continental-level trends in the emerging field of peatland palaeofire reconstruction (Chapter 4). This has given me a valuable, cross-scale perspective of peatland environmental change in terms of ecohydrology and fire regime, using multiple palaeoecological techniques and ultimately contributed to a greater understanding of autogenic and climate-driven shifts in mid- to high-latitude peatlands.

In Chapter 2, I developed testate amoeba-based transfer functions for WTD and pH for peatlands in Svalbard and applied these both to a peat core from Colesdalen to address Objective 1. The primary control on the distribution of testate amoebae in these High Arctic peatlands was WTD, as seen at lower latitudes (e.g. Amesbury et al., 2016). Furthermore, I was able to better quantify the WTD niches of the Arctic specific taxa *Centropyxis gasparella* and *Conicocassis pontigulasiformis* (Beyens and Bobrov, 2016) (Section 2.4.2; Figure 2.7) – the former of which has never been included in a transfer function and to my knowledge the latter only appears in Taylor et al. (2019). The influence of pore water pH upon populations of testate amoebae was marginally secondary to that of WTD (Section 2.4.1; Table 2.3), but development of a transfer function for pH allows for a more comprehensive understanding of past ecosystem change, although the relative importance of WTD and pH is likely to vary temporally down core (Markel et al., 2010). Swindles et al. (2015) found that, in the Abisko region of northern Sweden (the area studied in Chapter 3), where peatlands were less nutrient rich than those in Svalbard, pH had a more limited influence on the species distribution of testate amoebae – highlighting spatial variation in the relative importance of WTD and pH.

Weak idiosomic siliceous test (WIST) taxa showed poor preservation down core and their exclusion from transfer functions slightly improved model performance (Table A.2). In Chapter 3, WIST taxa were not excluded from our WTD reconstructions on the basis that limited decomposition would have occurred on the short active layer monoliths. Across 30 European sites, Swindles et al. (2020) have shown that differential preservation of WISTs has a minimal impact upon WTD reconstruction, yet the authors recommend removing WIST taxa from WTD reconstructions and excluding them from minimum count thresholds. Nonetheless, additional analyses of the records used in Chapter 3 suggest that the exclusion of WISTs does not greatly

affect WTD values (Figure B.34). I applied the Svalbard non-WIST transfer functions for both WTD and pH to a core from Colesdalen, with non-WIST taxa showing good preservation and consistent levels of diversity down core (Section 2.4.3; Figure 2.9). Of the testate amoebae found in the Colesdalen core, three species had missing modern analogues (*Campascus minutus*, *Centropyxis plagiostoma* and *Conicocassis pontigulasiformis*) from the pan-European transfer function (Amesbury et al., 2016) that was used to reconstruct WTD for core in Chapter 3. Similarly, transfer functions for Arctic Alaska (Taylor et al., 2019), subarctic Sweden (Swindles et al., 2015a) and subarctic Finland and West Russia (Zhang et al., 2017) had 9, 12 and 10 missing modern analogues respectively for the Colesdalen core (see Table A.3). Yet, these missing modern analogues were generally in low abundance in the Colesdalen core and therefore the three subarctic/Arctic and the pan-European transfer functions all performed quite well in terms of indicating relative shifts in WTD (Section 2.4.3; Figure 2.10). This good performance by extra-regional transfer functions suggests that their application can be effective to regions where local transfer functions are not available, particularly when missing modern analogue species are in low abundance and have minimal influence of reconstructions.

In Chapter 3, I investigated how the ecohydrology and carbon dynamics of permafrost peatlands respond to rapid warming across multiple sites in subarctic Sweden. My findings suggest that permafrost peatlands can exhibit both wetting and drying responses to climate change within the same region (Section 3.3.1; Figure 3.3). The reason for this divergent ecohydrological response may be autogenic processes relating to permafrost thaw, peatland structure, vegetation dynamics, productivity and decomposition. More specifically, permafrost thaw could lead to wetting through thermokarst collapse (Swindles et al., 2015b), as was the case in Gurasáhpí palsa 1 and 2. Alternatively, greater connectivity of drainage pathways with thaw could increase runoff and drainage, leading to drying (Haynes et al., 2018). Furthermore, I found that bryophyte populations in the Abisko region (especially *Sphagnum fuscum* and *Dicranum* spp.) showed resistance and sometimes resilience to hydrological changes indicated by testate amoeba WTD reconstructions (Section 3.3.1; Figure 3.2). Here, the persistence of bryophytes could actually work to slow permafrost thaw through their insulating properties (Soudzilovskaia et al., 2013).

The results of Chapter 3 emphasise the importance of sampling multiple sites/locations in palaeoecological studies, which is a considerable strength of my work in Chapter 4 that includes data from 221 records. Conversely in Chapter 2, the focus was transfer function development and therefore only one palaeo core was analysed to test the applicability of the transfer function and testate amoeba preservation. Reconstructions for the Colesdalen core show increases in pH and wetness in the last century that may be linked to greater chemical weathering as a result of

changing drainage patterns with ice retreat (Nowak and Hodson, 2014), alongside increases in precipitation (Førland et al., 2011). Yet, Juselius et al. (2022) suggest drying in recent decades across multiple soil cores in Svalbard, but they do not apply the open source transfer function I published in relation to Chapter 2 (Sim et al., 2021). Nevertheless, this discrepancy in recent hydrological trends in Svalbard emphasises the likely importance of autogenic processes and local factors in Svalbard, as has been demonstrated for subarctic peatlands in northern Sweden (Chapter 3) and for High Arctic peatlands in Canada (Sim et al., 2019).

Analysis of ACAR in Chapter 2 showed that drying in the last century could be tentatively linked with reduced carbon accumulation at four sites (Section 3.3.1; Figure 3.2). However, incomplete decomposition of recent peat and secondary decomposition of peat during drought can degrade and overwrite the ACAR record (Morris et al., 2015; Young et al., 2019). Therefore, interpretation of ACAR requires caution. In Stordalen palsa, a recent decrease in carbon accumulation was great enough to overcome the artefact of incomplete decomposition and is therefore likely to be genuine. Similarly, the presence of UOM (identified by plant macrofossil analyses) in Gurasáhpí palsa 1 prior to recent wetting suggests high levels of decomposition that may be masked by incomplete decomposition – reinforcing the idea that multiproxy studies offer a higher level of understanding. In terms of carbon accumulation going forwards, Young et al. (2019) suggest fitting carbon balance models (e.g. Clymo, 1984) to age-depth curves to estimate peatland carbon balance over centuries and millennia (see Zhang et al., 2018).

There is potential for increases in productivity with climate change in high-latitude peatlands to outpace increases in decomposition (Gallego-Sala et al., 2018). Therefore, a study investigating peatland carbon accumulation across Svalbard alongside integration with ecohydrological proxies (e.g. plant macrofossils and testate amoeba) would be extremely useful. Yet, peatland carbon accumulation was not considered in Chapter 2. This is because the original thesis plan was to investigate carbon accumulation as part of a multiproxy study in Svalbard in the final results chapter, but this was not possible owing to COVID-19 related laboratory delays. Juselius et al. (2022) document the recent initiation of new organic soils in Svalbard despite testate amoeba records indicating recent drying, suggesting further investigation is required to more fully understand the carbon accumulation response of these ecosystems. Additionally, considering the impact of peatland fire upon carbon accumulation in Chapter 4 would have been extremely useful – particularly in relation to smouldering fire dynamics – but unfortunately was not possible due to data availability.

In Chapter 4, I collated and synthesised 221 peatland macrocharcoal records from mid- to high-latitude peatlands in North America, Europe and Patagonia. This analysis is the first to examine peatland fire on a continental scale and highlighted regional variability in peatland burning during the Holocene (Sections 4.3.1 to 4.3.3; Figures 4.2 to 4.5). A warmer and drier climate during the HTM in central Canada, the Atlantic coast of North America, southern Scandinavia and the Baltics, and Patagonia, was associated with greater peatland burning (Sections 4.3.1 to 4.3.3; Figures 4.3 to 4.5). Similarly, the magnitude of burning appears to be greater in warmer and drier regions such as southern Europe (Section 4.3.4; Figures 4.6 and 4.7). Climate appears to be the overall control on peatland fire until at least the mid-Holocene in Europe and perhaps to this day in North America and Patagonia – echoing findings from a global syntheses of biomass burning across ecosystems, which included but did not differentiate peatlands (Marlon et al., 2013). Nevertheless, peatlands appear to be less susceptible to burning than the wider landscape, probably because of ecohydrological feedbacks that help maintain surface moisture (Nelson et al., 2021; Waddington et al., 2015). There are a number of occasions when peatland burning has remained constant or decreased when wider landscape burning has increased, e.g. ~0.5 ka to present in southern Scandinavia and the Baltics (Section 4.3.2; Figure 4.4). Some of the autogenic processes explored in Chapter 3 are likely to be relevant to the lower susceptibility of peatlands to burning demonstrated in Chapter 4. In fact, the cores from northern Sweden analysed in Chapter 3 are included in the Chapter 4 analyses. The resistance demonstrated by bryophytes to hydrological change (Section 3.3.1; Figure 3.2) in combination with their superior moisture retention capacity (Nelson et al., 2021) likely contributed to the absence of charcoal in the records from northern Sweden (Chapter 3). Charcoal was not analysed for the Colesdalen core in Svalbard in Chapter 2 but, in general, tundra ecosystems experience less fire than those at lower boreal latitudes (Flannigan et al., 2009). Nonetheless, with climate change there is evidence to suggest Arctic tundra fires may increase and lead to large-scale carbon losses (Mack et al., 2011).

In contrast to my findings in Chapters 2 and 3, in Chapter 4 I find that direct human impact may have had a profound impact upon my results. In Europe, with the onset of the Neolithic the use of fire for land clearance became more prevalent and may for example have contributed to increased peatland burning 7 to 5.5 ka in southern Europe (Section 4.3.2; Figure 4.4). However, in the last century or so there have been widespread decreases in global biomass burning contrary to increases in human population and rising temperatures that are linked to fire suppression policies and the conversion of land to agriculture (Arora and Melton, 2018; Marlon et al., 2008). I observe a similar recent decrease in peatland burning since the end of the LIA, especially in North America (Sections 4.3.1 and 4.2.2; Figures 4.3 and 4.4). The less extensive degradation of

peatlands in North America in comparison to Europe (Urák et al., 2017) may reduce susceptibility to burning. Nevertheless, the combination of climate change and direct human activities may lead to ecosystem shifts that reduce the resilience of peatlands to burning.

5.2. Implications and future work

The findings from my thesis can be used to guide the development of a number of further questions that could provide a focus for future research, which I will summarise in this section.

The testate amoeba transfer functions developed in Chapter 2 for peatland WTD and pH reconstruction in Svalbard are among the few models developed in marginal Arctic systems. These transfer functions are currently the northernmost peatland testate amoeba transfer functions and the first for peatlands in Svalbard. This work provides a valuable tool for conducting multiproxy palaeoecological investigations of Svalbard wetlands to better understand the ecohydrological dynamics of these carbon-rich and rapidly changing ecosystems. It would be valuable to conduct similar research in other understudied Arctic regions, such as the Canadian High Arctic and across Arctic Eurasia. Ultimately, this work could lead to the development of a pan-Arctic testate amoeba transfer function as have been developed for WTD at lower latitudes, for example across North America (Amesbury et al., 2018). Similarly, my data from Svalbard could be included in an updated version of the pan-European transfer function (Amesbury et al., 2016). Another direction for future research could focus on better quantifying the influence of other environmental variables on testate amoeba diversity and richness, such as salinity and nutrient addition from birds. Better quantification of temporal variation in the relative importance of pH and WTD in reconstruction would also be useful (see Markel et al., 2010). All these steps would solidify the relationship between testate amoeba species and environmental variables at high-latitudes and have major implications for palaeoecological studies, especially when hydrological conditions are of such importance for peatland carbon and fire dynamics (Chapters 3 and 4).

The divergent ecohydrological response to recent warming demonstrated in the permafrost peatlands of northern Sweden reported in Chapter 3 highlights the importance of autogenic and local factors in the behaviour of these ecosystems. My findings build on those from similar studies in High Arctic Canada and Fennoscandia (Sim et al., 2019; Zhang et al., 2018b) with high resolution and multiproxy data from 10 records. In particular, I provide robust evidence that permafrost peatlands may exhibit either a drying or wetting response to warming suggesting that simplistic models of massive carbon loss with peatland drying (see Ise et al., 2008) fail to capture the complexity of these ecosystems. Moreover, my results provide empirical data to inform models of peatland carbon dynamics, such as Chaudhary et al. (2020). Further research should look to

conduct more multiproxy palaeoecological studies in high-latitude peatlands, such as those in Svalbard. Combining a modelling and palaeoecological approach (e.g. Morris et al., 2015; Swindles et al., 2012) specifically for permafrost peatland ecosystems would also be highly useful. There is the potential to collate existing palaeoecological records across permafrost peatlands, as has been done at lower latitudes in Europe with testate amoeba records (Swindles et al., 2019). In fact, I am a co-author on a project currently in review that does exactly this (Zhang et al., in review) – where we collated 98 testate amoeba records from high latitudes and found that 54% show drying and 32% have been wetting in recent centuries.

In Chapter 4, I collated peatland burning records on a continental scale for the first time, which showed a degree of regional variability during the Holocene. This work is a step forward in terms of understanding the climatic and human controls on peatland fire and the importance of ecohydrological autogenic processes within intact peatlands for resisting fire. Nonetheless, it would be valuable to combine that analysis with a collation of existing peatland environmental change data that encompass multiple proxies (e.g. testate amoebae, plant macrofossils and charcoal). Doing so would contribute to understanding the role of autogenic processes in determining fire dynamics. Specifically, a multiproxy approach could allow for a fuller understanding of the influence of permafrost thaw and peatland successional stage on burning. Coupling of past fire data with climatic data and human population/land-use data (e.g. Klein Goldewijk et al., 2011) would allow for a more in-depth analysis of the drivers of peatland fire. The widespread recent decrease in peatland burning across much of North America and to a lesser extent in Europe may be a somewhat unexpected finding for many peatland scientists. This recent decrease in peatland burning may be associated with fire suppression policies and the expansion of agriculture reducing the prevalence of fire in the wider landscape (Arora and Melton, 2018; Marlon et al., 2008). A high-resolution analysis (e.g. 20-year time bins) focusing on the last millennium would improve spatiotemporal understanding of these recent trends. Finally, it would be extremely useful to investigate how peatland biomass burning and fire return intervals have varied on a continental scale. Such analysis is possible to some extent with CharAnalysis when records have been prepared using the same methodology (Higuera, 2009) and has previously been applied to sedimentary charcoal records across Europe (Vanni re et al., 2016), but not specifically to peatlands.

5.3. Conclusions

In this thesis, I have developed and used palaeoecological techniques to investigate trends in ecohydrology and fire regime in mid- to high-latitude peatlands during the Holocene. My findings

have highlighted the importance of autogenic factors alongside climate in driving shifts in peatland ecosystems. In Chapter 2, I showed that water-table depth (WTD) and pH had a strong control over peatland testate amoeba species distributions in Svalbard and I developed a statistical transfer function to quantitatively reconstruct past WTD and pH dynamics. In Chapter 3, I conducted a multiproxy palaeoecological investigation across eight permafrost peatland sites (10 records) in northern Sweden and found a divergent ecohydrological response to recent warming. Whether a peatland became wetter or drier was related to autogenic and local factors including permafrost thaw, vegetation dynamics, decomposition and productivity. In Chapter 4, I undertook a composite analysis of 221 macrocharcoal records from across North America, Europe and Patagonia that highlighted regional variability in peatland burning trends during the Holocene. Here, climate was the main driver of peatland fire, while human activities appear to become more important in the late Holocene – particularly in Europe. Autogenic processes operating within peatlands that help to maintain high moisture levels may explain the reduced susceptibility peatlands showed to burning than that in the wider landscape. The findings of this thesis suggest that alongside the overarching influence of climate, autogenic processes play an important role in controlling both ecohydrological and fire dynamics in peatlands. Future climate change will likely increase the vulnerability of the peatland carbon store at mid- to high-latitudes, yet autogenic processes may help maintain moisture in less modified ecosystems and mitigate some losses.

References

- Amesbury, M.J., Booth, R.K., Roland, T.P., Bunbury, J., Clifford, M.J., Charman, D.J., Elliot, S., Finkelstein, S., Garneau, M., Hughes, P.D.M., Lamarre, A., Loisel, J., Mackay, H., Magnan, G., Markel, E.R., Mitchell, E.A.D., Payne, R.J., Pelletier, N., Roe, H., Sullivan, M.E., Swindles, G.T., Talbot, J., van Bellen, S., Warner, B.G., 2018. Towards a Holarctic synthesis of peatland testate amoeba ecology: Development of a new continental-scale palaeohydrological transfer function for North America and comparison to European data. *Quat. Sci. Rev.* 201, 483–500. <https://doi.org/10.1016/J.QUASCIREV.2018.10.034>
- Amesbury, M.J., Swindles, G.T., Bobrov, A., Charman, D.J., Holden, J., Lamentowicz, M., Mallon, G., Mazei, Y., Mitchell, E.A.D., Payne, R.J., Roland, T.P., Turner, T.E., Warner, B.G., 2016. Development of a new pan-European testate amoeba transfer function for reconstructing peatland palaeohydrology. *Quat. Sci. Rev.* 152, 132–151. <https://doi.org/10.1016/J.QUASCIREV.2016.09.024>
- Arora, V.K., Melton, J.R., 2018. Reduction in global area burned and wildfire emissions since 1930s enhances carbon uptake by land. *Nat. Commun.* 9. <https://doi.org/10.1038/s41467-018-03838-0>
- Beyens, L., Bobrov, A., 2016. Evidence supporting the concept of a regionalized distribution of testate amoebae in the Arctic. *Acta Protozool.* 55, 197–209. <https://doi.org/10.4467/16890027AP.16.019.6006>
- Chaudhary, N., Westermann, S., Lamba, S., Shurpali, N., Sannel, A.B.K., Schurgers, G., Miller, P.A., Smith, B., 2020. Modelling past and future peatland carbon dynamics across the pan-Arctic. *Glob. Chang. Biol.* 26, 4119–4133. <https://doi.org/10.1111/gcb.15099>
- Clymo, R.S., 1984. The Limits to Peat Bog Growth. *Philos. Trans. R. Soc. B Biol. Sci.* 303, 605–654. <https://doi.org/10.1098/rstb.1984.0002>
- Flannigan, M., Krawchuk, M.A., De Groot, W.J., Wotton, B.M., Gowman, L.M., 2009. Implications of changing climate for global wildland fire. *Int. J. Wildl. Fire* 18, 483–507. <https://doi.org/10.1071/WF08187>
- Gallego-Sala, A. V., Charman, D.J., Brewer, S., Page, S.E., Prentice, I.C., Friedlingstein, P., Moreton, S., Amesbury, M.J., Beilman, D.W., Björck, S., Blyakharchuk, T., Bochicchio, C., Booth, R.K., Bunbury, J., Camill, P., Carless, D., Chimner, R.A., Clifford, M., Cressey, E., Courtney-Mustaphi, C., De Vleeschouwer, F., de Jong, R., Fialkiewicz-Kozziel, B., Finkelstein, S.A., Garneau, M., Githumbi, E., Hribljan, J., Holmquist, J., Hughes, P.D.M., Jones, C., Jones, M.C., Karofeld, E., Klein, E.S., Kokfelt, U., Korhola, A., Lacourse, T., Le Roux, G., Lamentowicz, M., Large, D., Lavoie, M., Loisel, J., Mackay, H., MacDonald, G.M., Makila, M., Magnan, G., Marchant, R., Marcisz, K., Martínez Cortizas, A., Massa, C., Mathijssen, P., Mauquoy, D., Mighall, T., Mitchell, F.J.G., Moss, P., Nichols, J., Oksanen, P.O., Orme, L., Packalen, M.S., Robinson, S., Roland, T.P., Sanderson, N.K., Sannel, A.B.K., Silva-Sánchez, N., Steinberg, N., Swindles, G.T., Turner, T.E., Uglow, J., Väliranta, M., van Bellen, S., van der Linden, M., van Geel, B., Wang, G., Yu, Z., Zaragoza-Castells, J., Zhao, Y., 2018. Latitudinal limits to the predicted increase of the peatland carbon sink with warming. *Nat. Clim. Chang.* 1. <https://doi.org/10.1038/s41558-018-0271-1>
- Haynes, K.M., Connon, R.F., Quinton, W.L., 2018. Permafrost thaw induced drying of wetlands at Scotty Creek, NWT, Canada. *Environ. Res. Lett.* 13. <https://doi.org/10.1088/1748-9326/aae46c>
- Higuera, P., 2009. CharAnalysis 0.9 : Diagnostic and analytical tools for sediment-charcoal analysis.

Mont. State Univ. Bozeman, MT.

- Ise, T., Dunn, A.L., Wofsy, S.C., Moorcroft, P.R., 2008. High sensitivity of peat decomposition to climate change through water-table feedback. *Nat. Geosci.* 1, 763–766. <https://doi.org/10.1038/ngeo331>
- Juselius, T., Ravolainen, V., Zhang, H., Piilo, S., Müller, M., Gallego-Sala, A., Väliiranta, & M., 2022. Newly initiated carbon stock, organic soil accumulation patterns and main driving factors in the High Arctic Svalbard, Norway. *Sci. Rep.* 12, 4679. <https://doi.org/10.1038/s41598-022-08652-9>
- Klein Goldewijk, K., Beusen, A., Van Drecht, G., De Vos, M., 2011. The HYDE 3.1 spatially explicit database of human-induced global land-use change over the past 12,000 years. *Glob. Ecol. Biogeogr.* 20, 73–86. <https://doi.org/10.1111/j.1466-8238.2010.00587.x>
- Mack, M.C., Bret-Harte, M.S., Hollingsworth, T.N., Jandt, R.R., Schuur, E.A.G., Shaver, G.R., Verbyla, D.L., 2011. Carbon loss from an unprecedented Arctic tundra wildfire. *Nature* 475, 489–492. <https://doi.org/10.1038/nature10283>
- Markel, E.R., Booth, R.K., Qin, Y., 2010. Testate amoebae and $\delta^{13}C$ of Sphagnum as surface-moisture proxies in Alaskan peatlands. *Holocene* 20, 463–475. <https://doi.org/10.1177/0959683609354303>
- Marlon, J.R., Bartlein, P.J., Carcaillet, C., Gavin, D.G., Harrison, S.P., Higuera, P.E., Joos, F., Power, M.J., Prentice, I.C., 2008. Climate and human influences on global biomass burning over the past two millennia. *Nat. Geosci.* 1, 697–702. <https://doi.org/10.1038/ngeo313>
- Marlon, J.R., Bartlein, P.J., Daniau, A.L., Harrison, S.P., Maezumi, S.Y., Power, M.J., Tinner, W., Vanni re, B., 2013. Global biomass burning: A synthesis and review of Holocene paleofire records and their controls. *Quat. Sci. Rev.* <https://doi.org/10.1016/j.quascirev.2012.11.029>
- Morris, P.J., Baird, A.J., Young, D.M., Swindles, G.T., 2015. Untangling climate signals from autogenic changes in long-term peatland development. *Geophys. Res. Lett.* 42, 10,788–10,797. <https://doi.org/10.1002/2015GL066824>
- Nelson, K., Thompson, D., Hopkinson, C., Petrone, R., Chasmer, L., 2021. Peatland-fire interactions: A review of wildland fire feedbacks and interactions in Canadian boreal peatlands. *Sci. Total Environ.* 769, 145212. <https://doi.org/10.1016/j.scitotenv.2021.145212>
- Sim, T.G., Swindles, G.T., Morris, P.J., Baird, A.J., Charman, D.J., Amesbury, M.J., Beilman, D., Channon, A., Gallego-Sala, A. V., 2021. Ecology of peatland testate amoebae in Svalbard and the development of transfer functions for reconstructing past water-table depth and pH. *Ecol. Indic.* 131, 108122. <https://doi.org/10.1016/j.ecolind.2021.108122>
- Sim, T.G., Swindles, G.T., Morris, P.J., Ga ka, M., Mullan, D., Galloway, J.M., 2019. Pathways for Ecological Change in Canadian High Arctic Wetlands Under Rapid Twentieth Century Warming. *Geophys. Res. Lett.* 46, 4726–4737. <https://doi.org/10.1029/2019GL082611>
- Soudzilovskaia, N.A., van Bodegom, P.M., Cornelissen, J.H.C., 2013. Dominant bryophyte control over high-latitude soil temperature fluctuations predicted by heat transfer traits, field moisture regime and laws of thermal insulation. *Funct. Ecol.* 27, 1442–1454. <https://doi.org/10.1111/1365-2435.12127>
- Swindles, G.T., Holden, J., Raby, C.L., Turner, T.E., Blundell, A., Charman, D.J., Menberu, M.W., Kl ve, B., 2015a. Testing peatland water-table depth transfer functions using high-resolution hydrological monitoring data. *Quat. Sci. Rev.* 120, 107–117. <https://doi.org/10.1016/J.QUASCIREV.2015.04.019>

- Swindles, G.T., Morris, P.J., Baird, A.J., Blaauw, M., Plunkett, G., 2012. Ecohydrological feedbacks confound peat-based climate reconstructions. *Geophys. Res. Lett.* 39, L11401. <https://doi.org/10.1029/2012GL051500>
- Swindles, G.T., Morris, P.J., Mullan, D., Watson, E.J., Turner, T.E., Roland, T.P., Amesbury, M.J., Kokfelt, U., Schoning, K., Pratte, S., Gallego-Sala, A., Charman, D.J., Sanderson, N., Garneau, M., Carrivick, J.L., Woulds, C., Holden, J., Parry, L., Galloway, J.M., 2015b. The long-term fate of permafrost peatlands under rapid climate warming. *Sci. Rep.* 5, 17951. <https://doi.org/10.1038/srep17951>
- Swindles, G.T., Morris, P.J., Mullan, D.J., Payne, R.J., Roland, T.P., Amesbury, M.J., Lamentowicz, M., Turner, T.E., Gallego-Sala, A., Sim, T., Barr, I.D., Blaauw, M., Blundell, A., Chambers, F.M., Charman, D.J., Feurdean, A., Galloway, J.M., Gałka, M., Green, S.M., Kajukała, K., Karofeld, E., Korhola, A., Lamentowicz, Ł., Langdon, P., Marcisz, K., Mauquoy, D., Mazei, Y.A., McKeown, M.M., Mitchell, E.A.D., Novenko, E., Plunkett, G., Roe, H.M., Schoning, K., Sillasoo, Ü., Tsyganov, A.N., van der Linden, M., Väliranta, M., Warner, B., 2019. Widespread drying of European peatlands in recent centuries. *Nat. Geosci.* 12, 922–928. <https://doi.org/10.1038/s41561-019-0462-z>
- Swindles, G.T., Roland, T.P., Amesbury, M.J., Lamentowicz, M., McKeown, M.M., Sim, T.G., Fewster, R.E., Mitchell, E.A.D., 2020. Quantifying the effect of testate amoeba decomposition on peat-based water-table reconstructions. *Eur. J. Protistol.* 125693. <https://doi.org/10.1016/j.ejop.2020.125693>
- Taylor, L.S., Swindles, G.T., Morris, P.J., Gałka, M., 2019. Ecology of peatland testate amoebae in the Alaskan continuous permafrost zone. *Ecol. Indic.* 96, 153–162. <https://doi.org/10.1016/J.ECOLIND.2018.08.049>
- Urák, I., Hartel, T., Gallé, R., Balog, A., 2017. Worldwide peatland degradations and the related carbon dioxide emissions: the importance of policy regulations. *Environ. Sci. Policy* 69, 57–64. <https://doi.org/10.1016/j.envsci.2016.12.012>
- Vannièrè, B., Blarquez, O., Rius, D., Doyen, E., Brücher, T., Colombaroli, D., Connor, S., Feurdean, A., Hickler, T., Kaltenrieder, P., Lemmen, C., Leys, B., Massa, C., Olofsson, J., 2016. 7000-year human legacy of elevation-dependent European fire regimes. *Quat. Sci. Rev.* 132, 206–212. <https://doi.org/10.1016/j.quascirev.2015.11.012>
- Waddington, J.M., Morris, P.J., Kettridge, N., Granath, G., Thompson, D.K., Moore, P.A., 2015. Hydrological feedbacks in northern peatlands. *Ecohydrology* 8, 113–127. <https://doi.org/10.1002/eco.1493>
- Young, D.M., Baird, A.J., Charman, D.J., Evans, C.D., Gallego-Sala, A. V., Gill, P.J., Hughes, P.D.M., Morris, P.J., Swindles, G.T., 2019. Misinterpreting carbon accumulation rates in records from near-surface peat. *Sci. Rep.* 9, 1–8. <https://doi.org/10.1038/s41598-019-53879-8>
- Zhang, H., Amesbury, M.J., Ronkainen, T., Charman, D.J., Gallego-Sala, A. V., Väliranta, M., 2017. Testate amoeba as palaeohydrological indicators in the permafrost peatlands of north-east European Russia and Finnish Lapland. *J. Quat. Sci.* 32, 976–988. <https://doi.org/10.1002/jqs.2970>
- Zhang, H., Gallego-Sala, A. V., Amesbury, M.J., Charman, D.J., Piilo, S.R., Väliranta, M.M., 2018a. Inconsistent response of Arctic permafrost peatland carbon accumulation to warm climate phases. *Global Biogeochem. Cycles* 32, 1605–1620. <https://doi.org/10.1029/2018GB005980>
- Zhang, H., Piilo, S.R., Amesbury, M.J., Charman, D.J., Gallego-Sala, A. V., Väliranta, M.M., 2018b. The role of climate change in regulating Arctic permafrost peatland hydrological and

vegetation change over the last millennium. *Quat. Sci. Rev.* 182, 121–130.
<https://doi.org/10.1016/J.QUASCIREV.2018.01.003>

Zhang, H., Väliranta, M., Swindles, G.T., Lopez, M.A., Mullan, D., Tan, N., Amesbury, M., Andrei-Cosmin, D., Babeshko, K., Bao, K., Bobrov, A., Chernyshov, V., Davies, M., Feurdean, A., Finkelstein, S.A., Garneau, M., Guo, Z., Jones, M.C., Kay, M., Klein, E., Lamarre, A., Lamentowicz, M., Magnan, G., Marcisz, K., Mazei, N., Mazei, Y., Payne, R., Pelletier, N., Piilo, S., Pratte, S., Primeau, G., Robitaille, M., Roland, T., Saldaev, D., Shotyk, W., Sim, T.G., Sloan, T.J., Talbot, J., Taylor, L., Tsyganov, A., Bellen, S. van, Wetterich, S., Xing, W., Zhao, Y., In review. Recent climate change has driven divergent hydrological shifts in high-latitude peatlands. *Nat. Commun.* 1–10.

Appendices

Appendix A. Supporting information for Chapter 2: Ecology of peatland testate amoebae in Svalbard and the development of transfer functions for reconstructing past water-table depth and pH

Contents of this section:

1. Table A.1: Radiocarbon dates from the Colesdalen core.
2. Table A.2: Transfer function performance metrics for both WTD and pH models.
3. Table A.3: Missing modern analogues for the Colesdalen core from different regional transfer functions.
4. Figure A.1: Age-depth model for the Colesdalen core.
5. Figure A.2: Summary results for segment-wise RMSEP for pruned transfer function models.
6. Figure A.3: Maximum abundance of testate amoeba taxa in the fossil and modern calibration datasets for the chosen transfer functions.
7. Figure A.4: NMDS axis 1 scores and DCA axis 1 scores for testate amoeba abundance data from the Colesdalen core, plotted against WTD and pH reconstructions.

Table A.1. Radiocarbon dates from the Colesdalen core. Parentheses following calibrated age refers to the probability for that age range. † = Seuss effect. See Figure A.1 for age-depth model.

Lab ID	Depth (cm)	Material	Age (14C yr BP)	1 σ error	Calibrated age, 2 σ range (yr BP)
<i>UOC-15017</i>	30	Peat	46	34	257 - 224 (26.9%), 140 - 33 (68.5%) †
<i>UOC-15018</i>	60	Peat	565	34	645 - 586 (53.5%), 567 - 522 (41.9%)
<i>UOC-15019</i>	90	Peat	1205	34	1261 - 1209 (9.9%), 1180 - 1056 (83.0%), 1024 - 1003 (2.6%)

Table A.2. Transfer function performance metrics for both WTD and pH models, with all taxa included and then with WIST taxa removed.

		All taxa									
		TF _{WTD}					TF _{pH}				
<i>Original model (n = 103)</i>		RMSEP _{Loo}	R ² _{Loo}	Avg. Bias	Max. Bias	<i>n</i>	RMSEP _{Loo}	R ² _{Loo}	Avg. Bias	Max. Bias	<i>n</i>
	<i>WA.inv</i>	5.899	0.384	-0.010	20.367	103	0.445	0.363	0.005	1.154	103
	<i>WA.cla</i>	8.176	0.394	-0.032	18.547	103	0.624	0.376	0.008	0.632	103
	<i>WA.inv.tol</i>	5.629	0.439	0.027	19.398	103	0.434	0.392	0.003	1.259	103
	<i>WA.cla.tol</i>	7.388	0.447	0.041	17.147	103	0.586	0.403	0.005	0.917	103
	<i>WAPLS.C2</i>	5.818	0.413	0.042	19.036	103	0.436	0.401	0.013	1.054	103
	<i>ML</i>	7.198	0.346	1.479	19.446	103	0.628	0.255	0.046	0.893	103
<i>Model residuals removed (> 20%)</i>		RMSEP _{Loo}	R ² _{Loo}	Avg. Bias	Max. Bias	<i>n</i>	RMSEP _{Loo}	R ² _{Loo}	Avg. Bias	Max. Bias	<i>n</i>
	<i>WA.inv</i>	3.555	0.677	-0.013	5.661	86	0.291	0.499	-0.001	0.614	85
	<i>WA.cla</i>	3.628	0.704	0.014	4.296	63	0.329	0.709	0.005	0.915	65
	<i>WA.inv.tol</i>	3.633	0.670	0.042	5.468	88	0.296	0.550	0.010	0.612	90
	<i>WA.cla.tol</i>	3.948	0.686	0.115	3.748	70	0.308	0.717	0.019	0.437	72
	<i>WAPLS.C2</i>	3.226	0.730	-0.005	5.669	84	0.285	0.575	-0.002	0.455	90
	<i>ML</i>	3.453	0.763	0.269	2.599	75	0.304	0.614	-0.011	0.474	82
		WISTs removed									
		TF _{WTD-NO.WIST}					TF _{pH-NO.WIST}				
<i>Original model (n = 103)</i>		RMSEP _{Loo}	R ² _{Loo}	Avg. Bias	Max. Bias	<i>n</i>	RMSEP _{Loo}	R ² _{Loo}	Avg. Bias	Max. Bias	<i>n</i>
	<i>WA.inv</i>	5.891	0.386	0.015	19.293	103	0.443	0.368	0.002	1.187	103
	<i>WA.cla</i>	8.074	0.396	0.013	16.335	103	0.622	0.381	0.004	0.700	103
	<i>WA.inv.tol</i>	5.661	0.433	0.120	18.294	103	0.440	0.375	0.001	1.271	103
	<i>WA.cla.tol</i>	7.267	0.441	0.198	15.079	103	0.601	0.388	0.002	0.928	103
	<i>WAPLS.C2</i>	5.647	0.443	0.069	17.944	103	0.434	0.402	0.007	1.071	103
	<i>ML</i>	7.724	0.293	2.108	22.168	103	0.574	0.340	0.020	0.884	103
<i>Model residuals removed (> 20%)</i>		RMSEP _{Loo}	R ² _{Loo}	Avg. Bias	Max. Bias	<i>n</i>	RMSEP _{Loo}	R ² _{Loo}	Avg. Bias	Max. Bias	<i>n</i>
	<i>WA.inv</i>	3.697	0.634	0.001	6.028	88	0.278	0.541	-0.002	0.553	85
	<i>WA.cla</i>	4.303	0.652	0.074	8.633	67	0.271	0.771	0.002	0.343	61
	<i>WA.inv.tol</i>	3.565	0.669	0.073	5.774	88	0.271	0.577	0.007	0.539	86

<i>WA.c/a.tol</i>	4.299	0.653	0.217	9.551	70	0.320	0.690	0.018	0.316	70
<i>WAPLS.C2</i>	3.198	0.719	0.036	5.293	85	0.284	0.595	0.000	0.412	88
<i>ML</i>	3.776	0.721	0.276	3.050	74	0.300	0.619	-0.036	0.401	80

Table A.3. Missing modern analogues for the Colesdalen core from different regional transfer functions: Arctic Alaska (Taylor et al., 2019a), Europe (Amesbury et al., 2016) and Subarctic Sweden (Swindles et al., 2015). See Table 2.2 for species codes, “x” indicates missing taxa.

<i>Species</i>	<i>Transfer function</i>			
	Arctic Alaska	Pan- European	Subarctic Sweden	Subarctic Finland and West Russia
<i>ARDI</i>	x			
<i>CAMI</i>	x	x	x	x
<i>CEPLAG</i>	x	x	x	x
<i>COPO</i>		x	x	x
<i>CYEU</i>			x	x
<i>DIAC</i>	x		x	
<i>DILI</i>			x	x
<i>DILU</i>	x			
<i>DIPE</i>	x		x	x
<i>DIPR</i>	x			
<i>DIPY</i>			x	x
<i>GIGR</i>	x		x	x
<i>GIGA</i>			x	x
<i>HEPE</i>	x			
<i>HERO</i>			x	
<i>PALA</i>			x	x

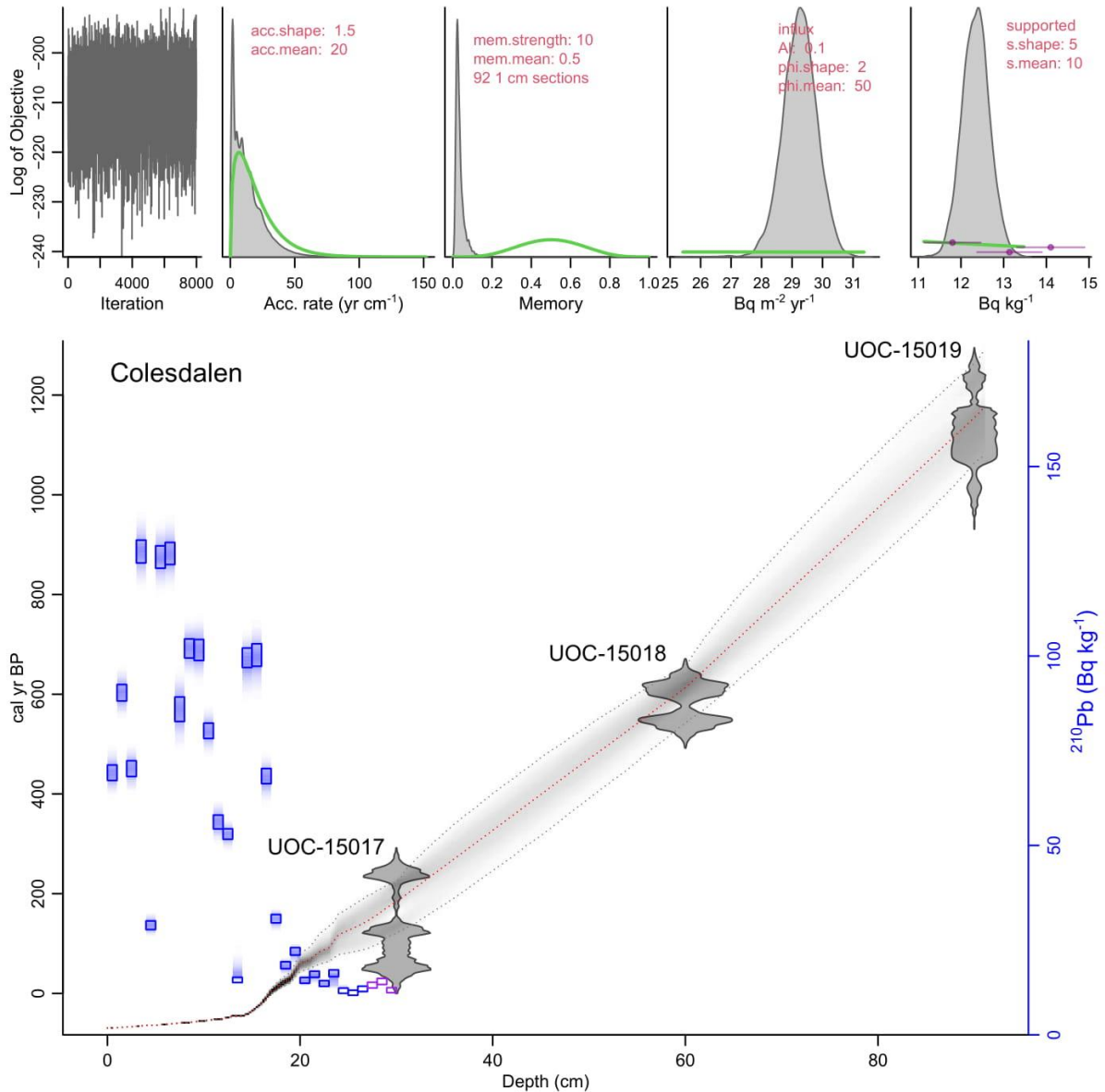


Figure A.1. Age-depth model for the Colesdalen core, produced using PLUM (Aquino-López et al., 2018). Upper panels depicted from left to right: the log of the objective function of the MCMC iterations, accumulation rate (yr cm^{-1}), Memory, influx of ^{210}Pb ($\text{Bq m}^{-2} \text{yr}^{-1}$) and supported ^{210}Pb (Bq kg^{-1}). The log of the objective function panel is used for interpreting the convergence of the MCMC model: good runs show a stationary distribution with little structure among neighbouring iterations. Bottom panel shows the calibrated ^{14}C dates (transparent grey), ^{210}Pb (Bq kg^{-1}) concentrations (blue lines with reference to the blue scale on the right), bottom three ^{210}Pb (Bq kg^{-1}) values used to estimate supported values (purple lines) and the age-depth model (darker greys indicate more likely calendar ages; grey stippled lines show 95% confidence intervals; red stippled line shows single 'best' model based on the mean age for each depth). Lab codes for the ^{14}C dates are labelled. See Table A.1 for full radiocarbon dating information.

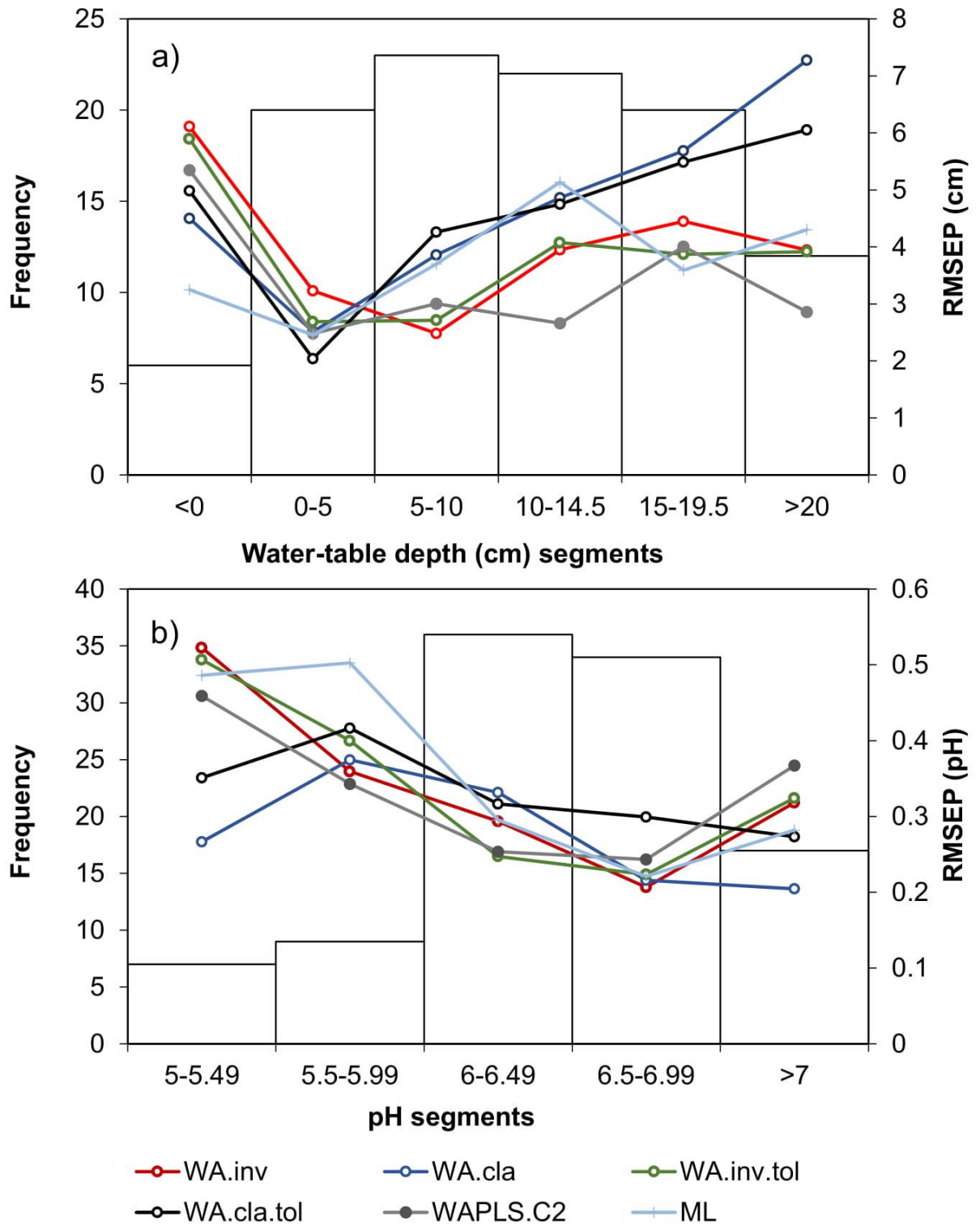


Figure A.2. Summary results for segment-wise RMSEP for pruned transfer function models with WIST taxa removed for a) WTD and b) pH. Histograms show sampling distribution for WTD (6 segments) and pH (5 segments) for all samples ($n = 103$). The coloured lines show RMSEP values for specific segments for different model types.

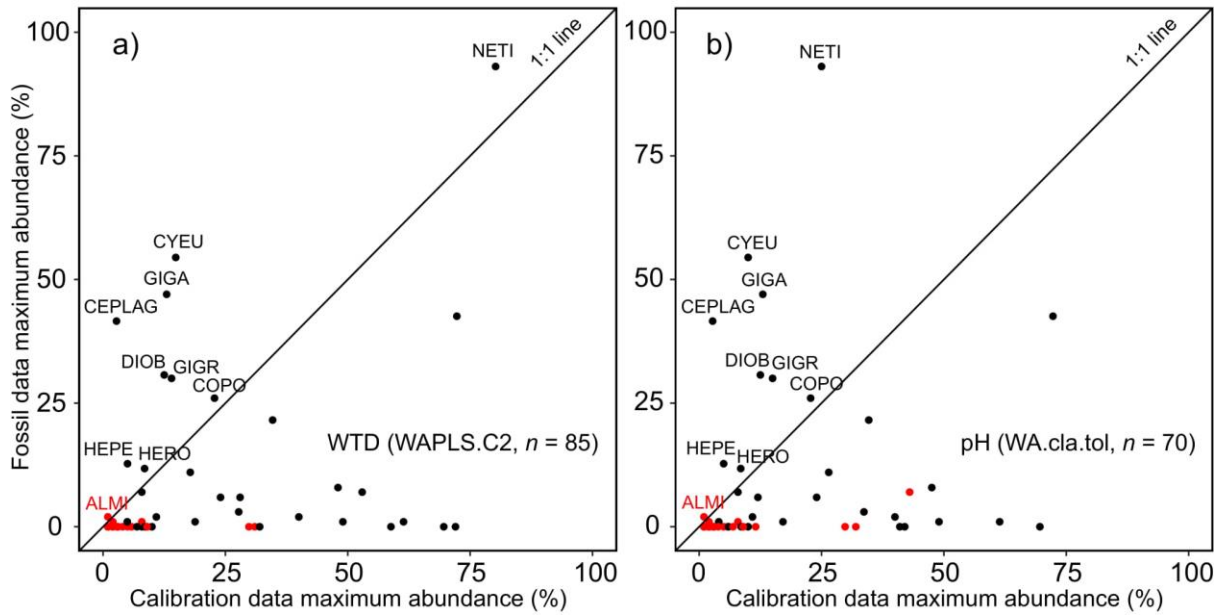


Figure A.3. Maximum abundance of testate amoeba taxa in the fossil and modern calibration datasets for the chosen transfer functions: a) $TF_{WTD-NO.WIST}$ (WAPLS.C2, $n = 85$) and b) $TF_{pH-NO.WIST}$ (WA.cla.tol, $n = 70$). Taxa with Hill's $N_2 \leq 5$ are highlight in red, this suggests a poorly constrained species optima. See Table 2.2 for species codes.

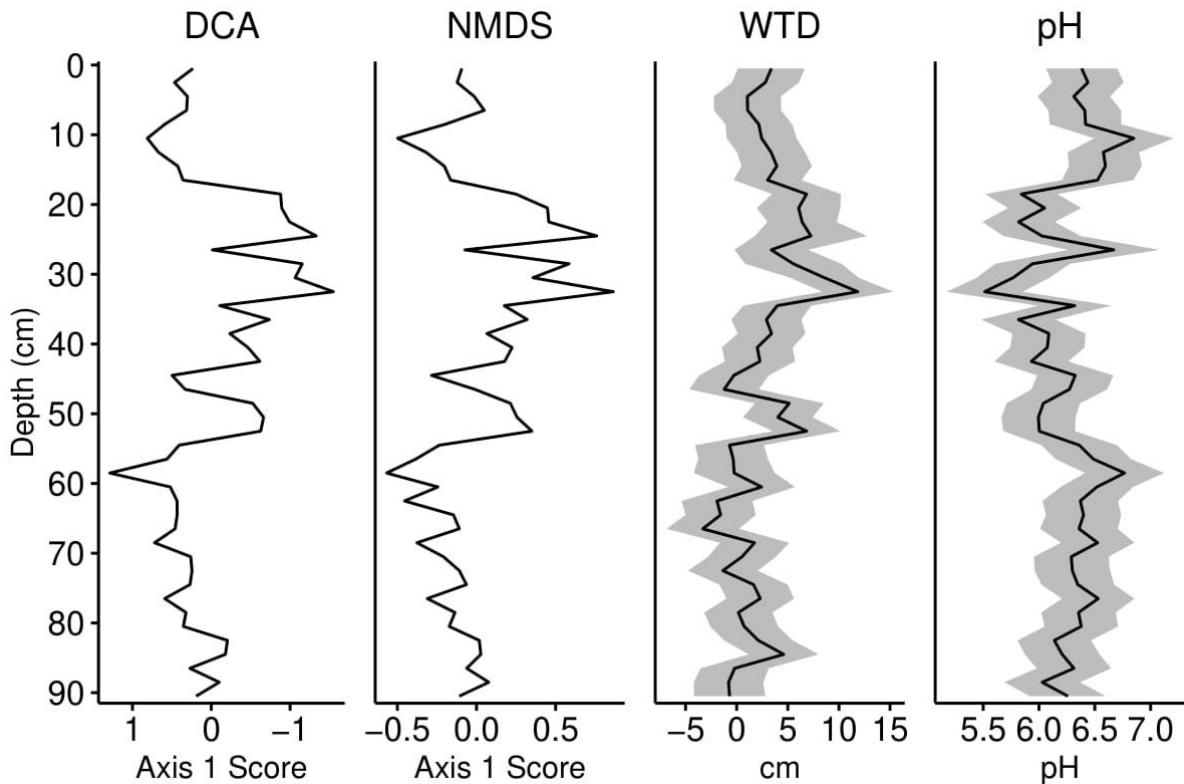


Figure A.4. NMDS axis 1 scores and DCA axis 1 scores for testate amoeba abundance data from the Colesdalen core, plotted against WTD and pH reconstructions using the transfer functions from this study.

Appendix B. Supporting information for Chapter 3: Divergent responses of permafrost peatlands to recent climate change

Contents of this section:

1. Figure B.1: Testate amoeba abundance data (%) for Bergfors bog.
2. Figure B.2: Testate amoeba abundance data (%) for Gurasáhpi palsa 1.
3. Figure B.3: Testate amoeba abundance data (%) for Gurasáhpi palsa 2.
4. Figure B.4: Testate amoeba abundance data (%) for Maunuvuoma fen.
5. Figure B.5: Testate amoeba abundance data (%) for Orusjohka palsa.
6. Figure B.6: Testate amoeba abundance data (%) for Rensjön palsa.
7. Figure B.7: Testate amoeba abundance data (%) for Ribasvuomuš bog.
8. Figure B.8: Testate amoeba abundance data (%) for Stordalen bog.
9. Figure B.9: Testate amoeba abundance data (%) for Stordalen palsa.
10. Figure B.10: Testate amoeba abundance data (%) for Veigi bog.
11. Figure B.11: Plant macrofossil diagrams for Bergfors bog.
12. Figure B.12: Plant macrofossil diagrams for Gurasáhpi palsa 1.
13. Figure B.13: Plant macrofossil diagrams for Gurasáhpi palsa 2.
14. Figure B.14: Plant macrofossil diagrams for Maunuvuoma fen.
15. Figure B.15: Plant macrofossil diagrams for Orusjohka palsa.
16. Figure B.16: Plant macrofossil diagrams for Rensjön palsa.
17. Figure B.17: Plant macrofossil diagrams for Ribasvuomuš bog.
18. Figure B.18: Plant macrofossil diagrams for Stordalen bog.
19. Figure B.19: Plant macrofossil diagrams for Stordalen palsa.
20. Figure B.20: Plant macrofossil diagrams for Veigi bog.
21. Figure B.21: Age-depth model for Bergfors bog.
22. Figure B.22: Age-depth model for Gurasáhpi palsa 1.
23. Figure B.23: Age-depth model for Gurasáhpi palsa 2.
24. Figure B.24: Age-depth model for Maunuvuoma fen.
25. Figure B.25: Age-depth model for Orusjohka palsa.
26. Figure B.26: Age-depth model for Rensjön palsa.
27. Figure B.27: Age-depth model for Ribasvuomuš bog.
28. Figure B.28: Age-depth model for Stordalen bog.
29. Figure B.29: Age-depth model for Stordalen palsa.
30. Figure B.30: Age-depth model for Veigi bog.
31. Figure B.31: Comparative historic and recent imagery of the Stordalen, Ribasvuomuš bog and Gurasáhpi sites.
32. Figure B.32: Comparative historic and recent imagery of the Bergfors bog, Rensjön palsa and Maunuvuoma fen sites.
33. Figure B.33: Comparative historic and recent imagery of the Veigi bog and Orusjohka palsa sites.
34. Table B.1: Plant macrofossil taxa groupings used in Figure 3.2.

Bergfors bog – Testate amoebae

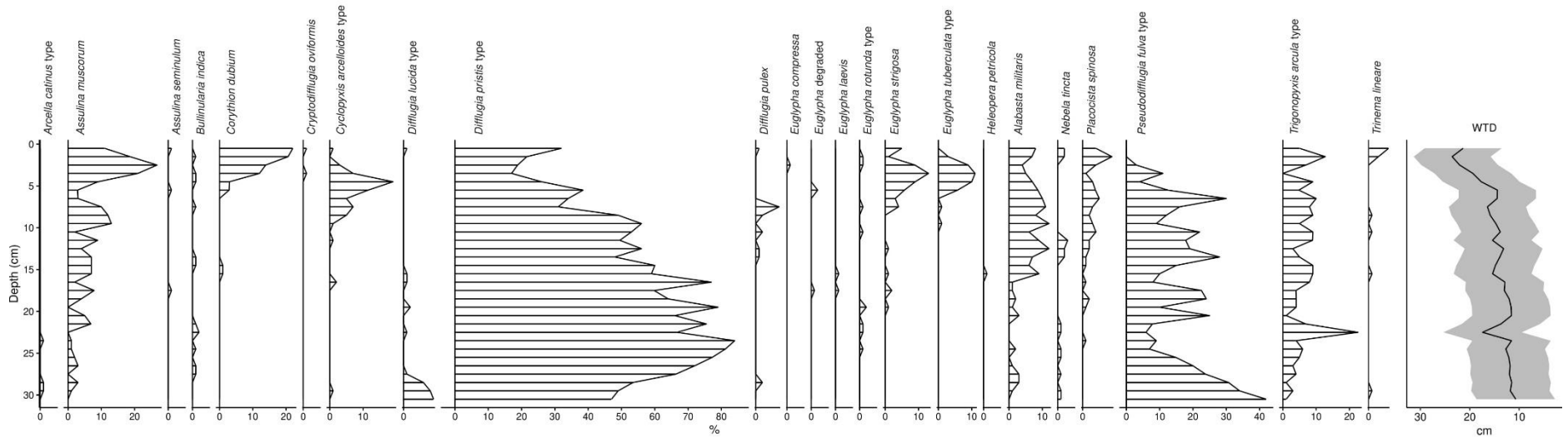


Figure B.1. Testate amoeba abundance data (%) for Bergfors bog peat profile and water-table depth (WTD; cm) reconstructions based on the Amesbury et al (2016) transfer function. Grey shading represents error based on 999 bootstrap cycles.

Gurasáhpí palsa 1 – Testate amoebae

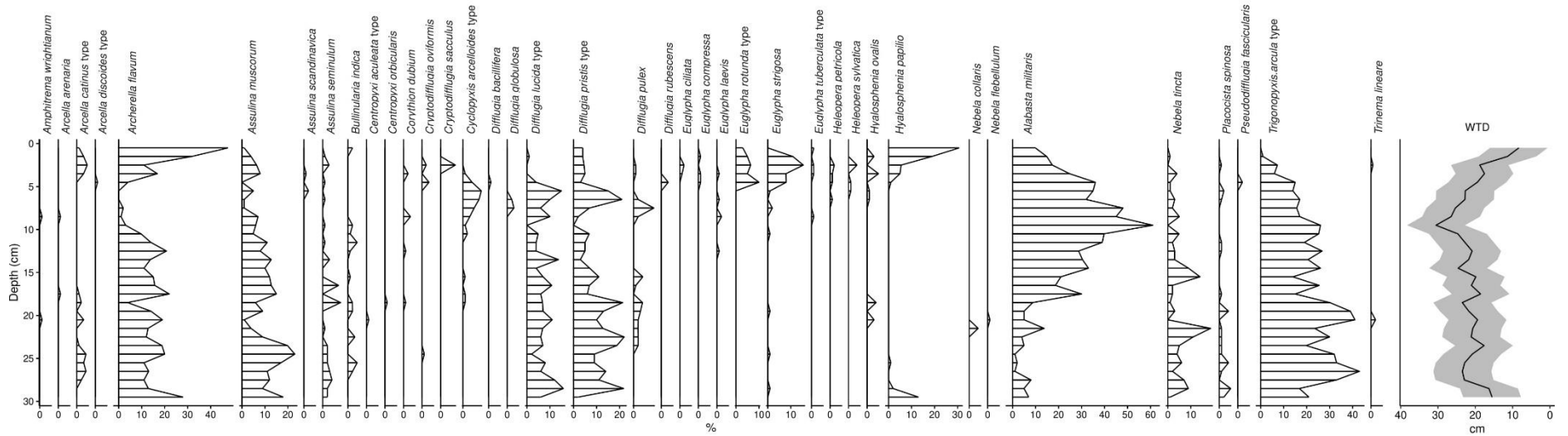


Figure B.2. Testate amoeba abundance data (%) for Gurasáhpí palsa 1 peat profile and water-table depth (WTD; cm) reconstructions based on the Amesbury et al (2016) transfer function. Grey shading represents error based on 999 bootstrap cycles.

Gurasáphi palsa 2 – Testate amoebae

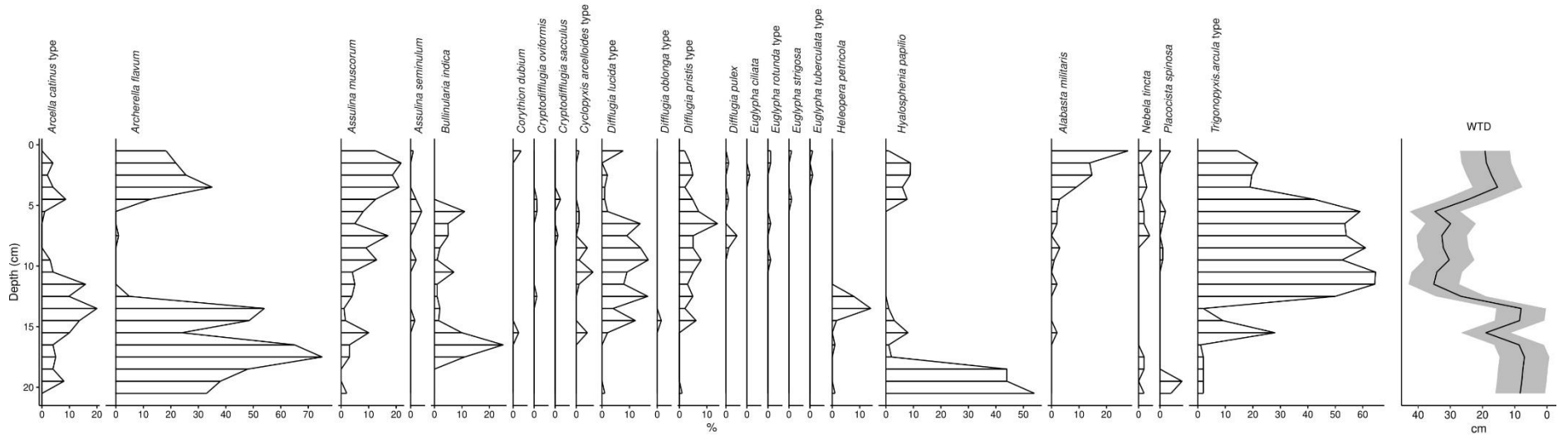


Figure B.3. Testate amoeba abundance data (%) for Gurasáphi palsa 2 peat profile and water-table depth (WTD; cm) reconstructions based on the Amesbury et al (2016) transfer function. Grey shading represents error based on 999 bootstrap cycles.

Maunuvuoma fen – Testate amoebae

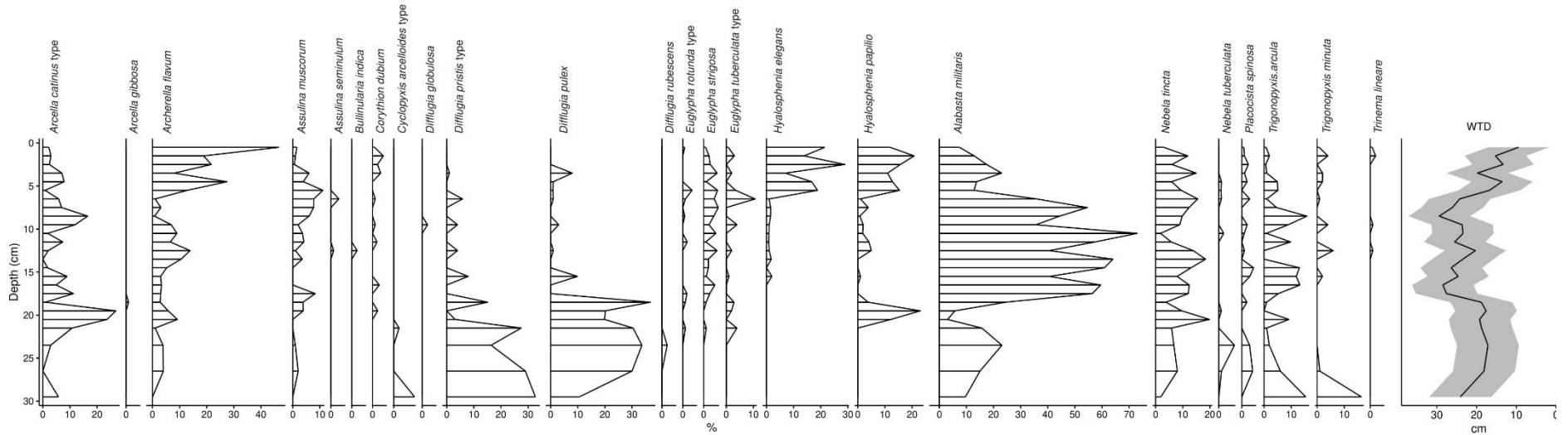


Figure B.4. Testate amoeba abundance data (%) for Maunuvuoma fen peat profile and water-table depth (WTD; cm) reconstructions based on the Amesbury et al (2016) transfer function. Grey shading represents error based on 999 bootstrap cycles.

Orusjohka palsa – Testate amoebae

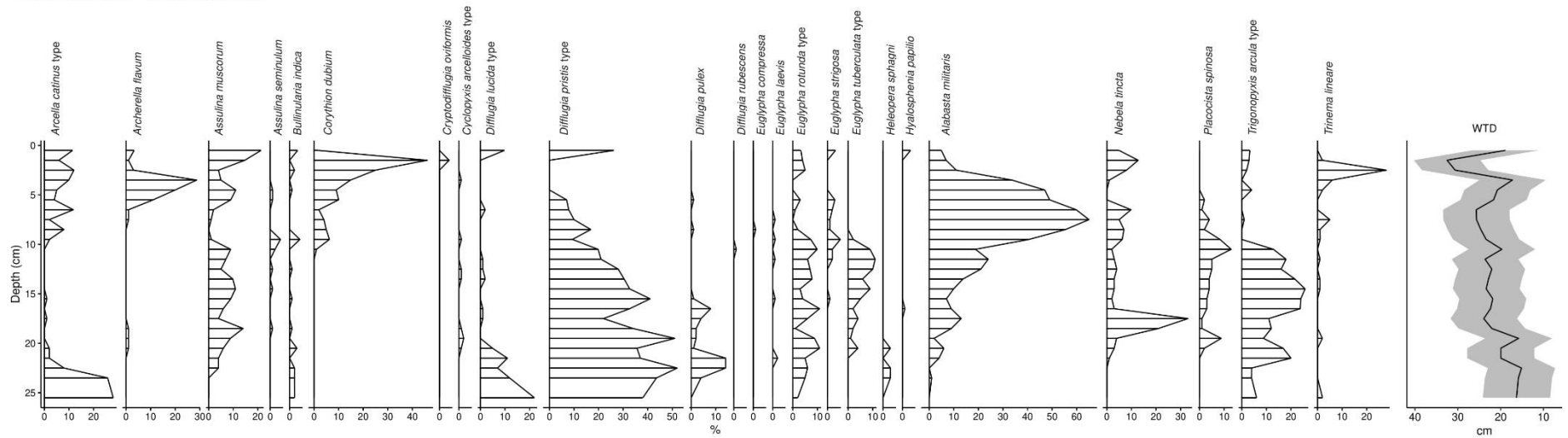


Figure B.5. Testate amoeba abundance data (%) for Orusjohka palsa peat profile and water-table depth (WTD; cm) reconstructions based on the Amesbury et al (2016) transfer function. Grey shading represents error based on 999 bootstrap cycles.

Rensjön palsa – Testate amoebae

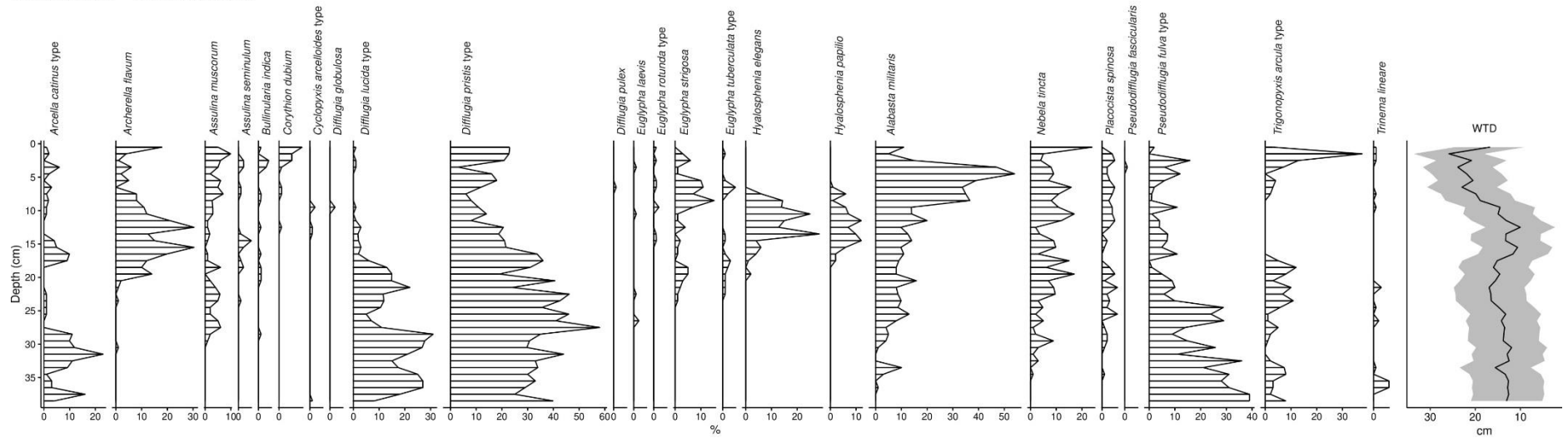


Figure B.6. Testate amoeba abundance data (%) for Rensjön palsa peat profile and water-table depth (WTD; cm) reconstructions based on the Amesbury et al (2016) transfer function. Grey shading represents error based on 999 bootstrap cycles.

Ribasvuomuš bog – Testate amoebae

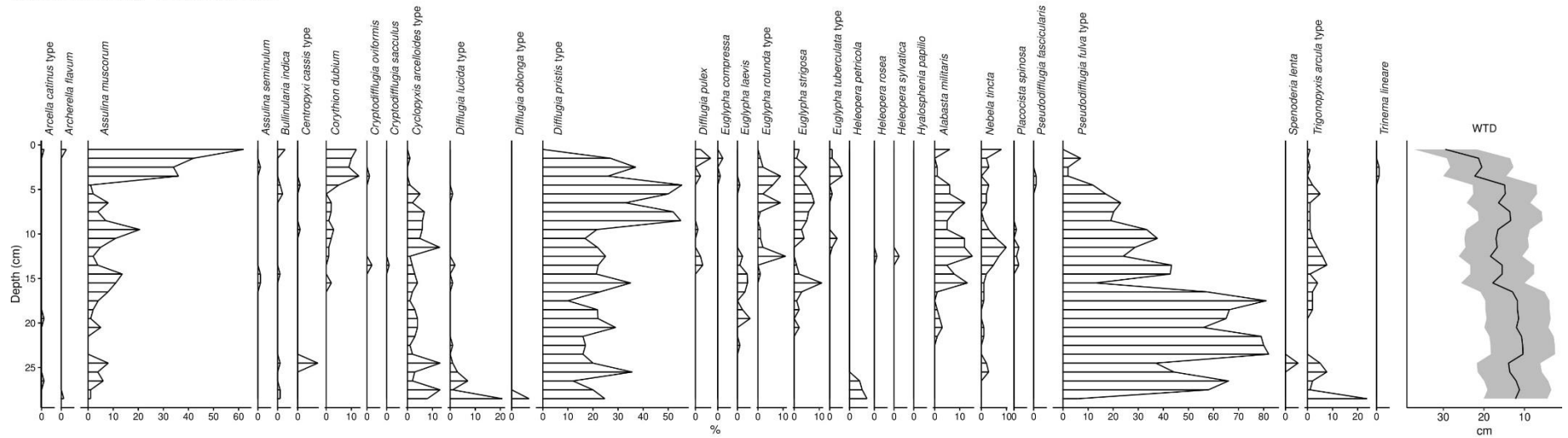


Figure B.7. Testate amoeba abundance data (%) for Ribasvuomuš bog peat profile and water-table depth (WTD; cm) reconstructions based on the Amesbury et al (2016) transfer function. Grey shading represents error based on 999 bootstrap cycles.

Stordalen palsa – Testate amoebae

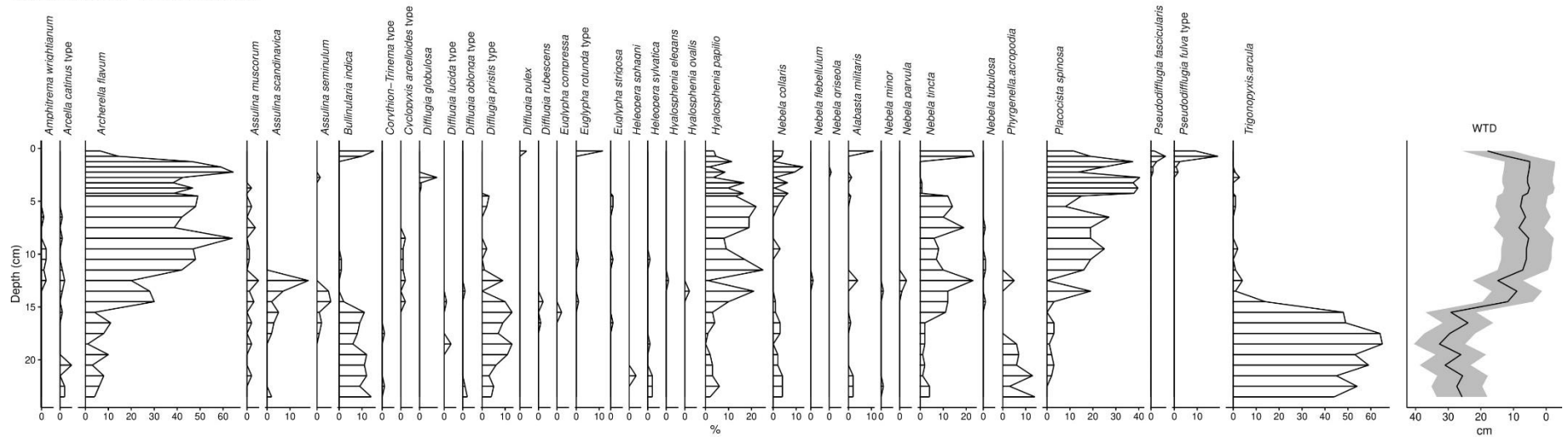


Figure B.9. Testate amoeba abundance data (%) for Stordalen palsa peat profile and water-table depth (WTD; cm) reconstructions based on the Amesbury et al (2016) transfer function. Grey shading represents error based on 999 bootstrap cycles.

Veigi bog – Testate amoebae

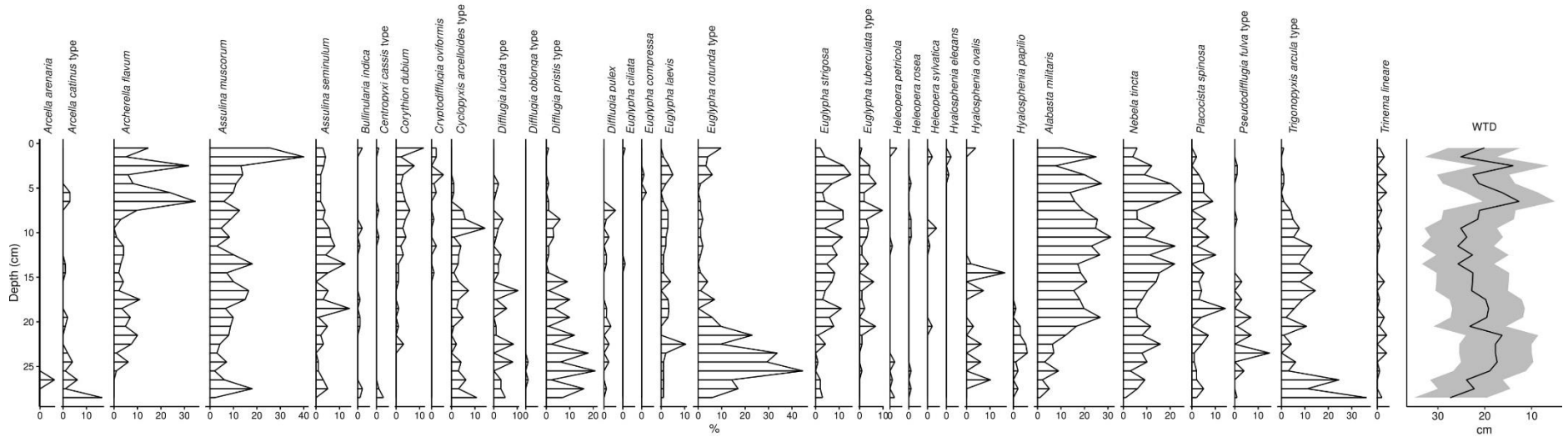


Figure B.10. Testate amoeba abundance data (%) for Veigi bog peat profile and water-table depth (WTD; cm) reconstructions based on the Amesbury et al (2016) transfer function. Grey shading represents error based on 999 bootstrap cycles.

Bergfors bog – Plant macrofossils

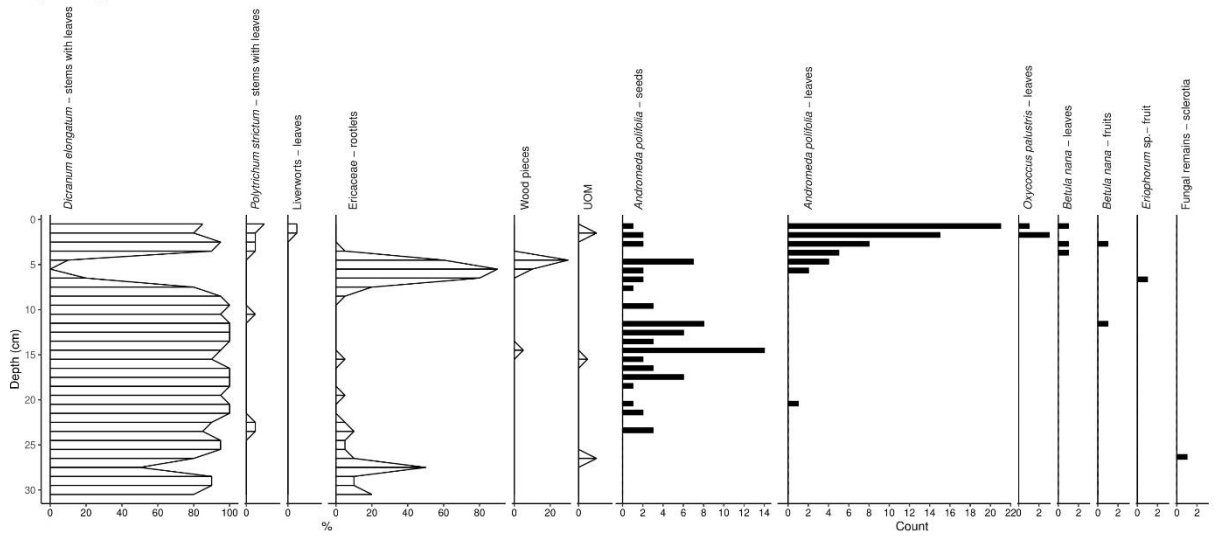


Figure B.11. Plant macrofossil diagrams for Bergfors bog peat profile, both volume percentages (lines) and count data (bars).

Gurasáhpí palsa 1 – Plant macrofossils

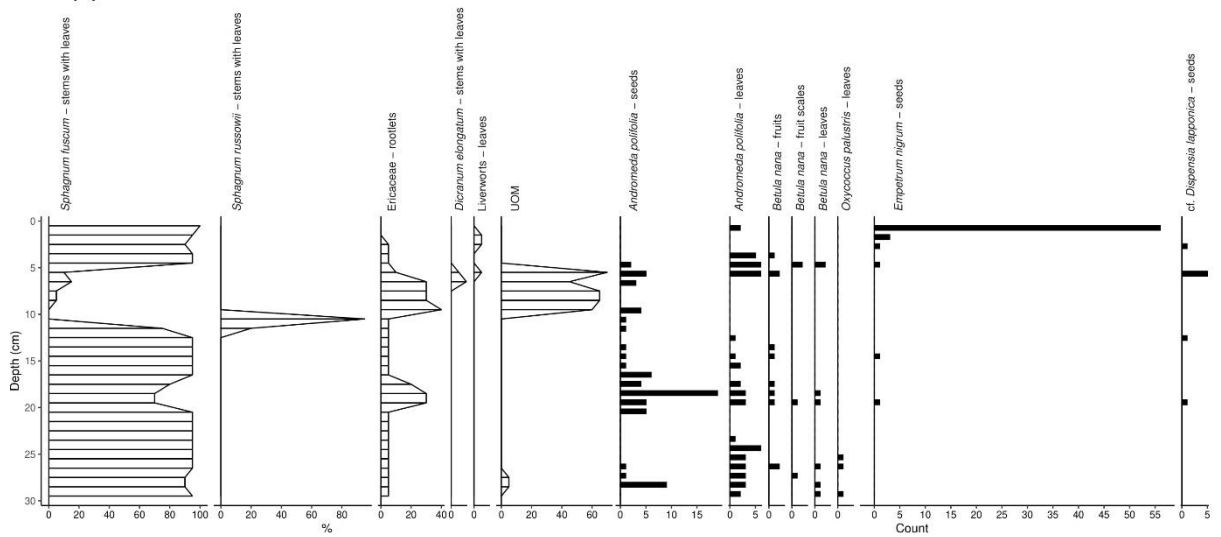


Figure B.12. Plant macrofossil diagrams for Gurasáhpí palsa 1 peat profile, both volume percentages (lines) and count data (bars).

Gurasáhi palsa 2 – Plant macrofossils

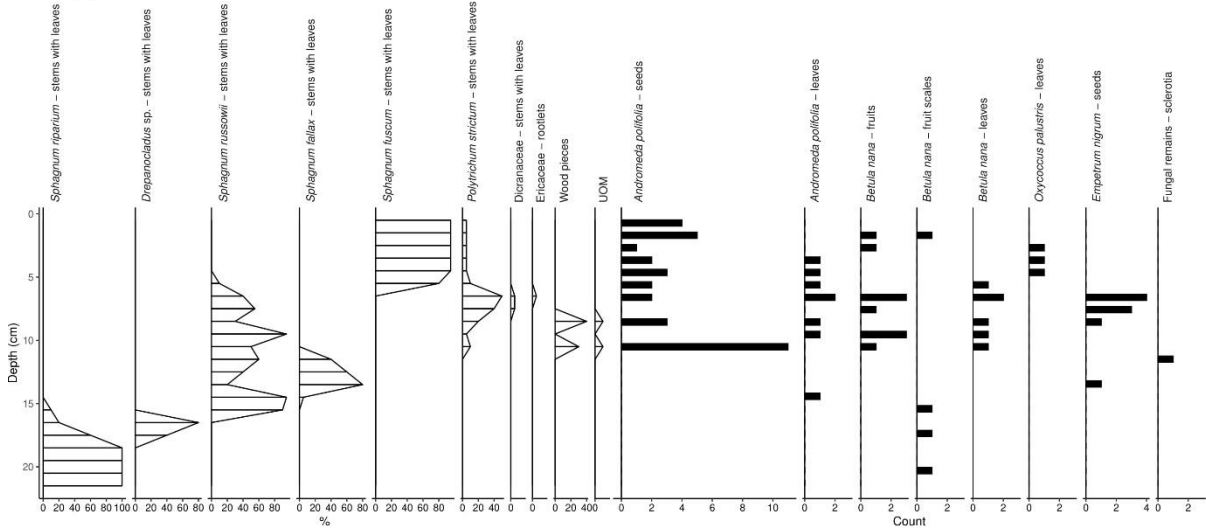


Figure B.13. Plant macrofossil diagrams for Gurasáhi palsa 2 peat profile, both volume percentages (lines) and count data (bars).

Maunuvuoma fen – Plant macrofossils

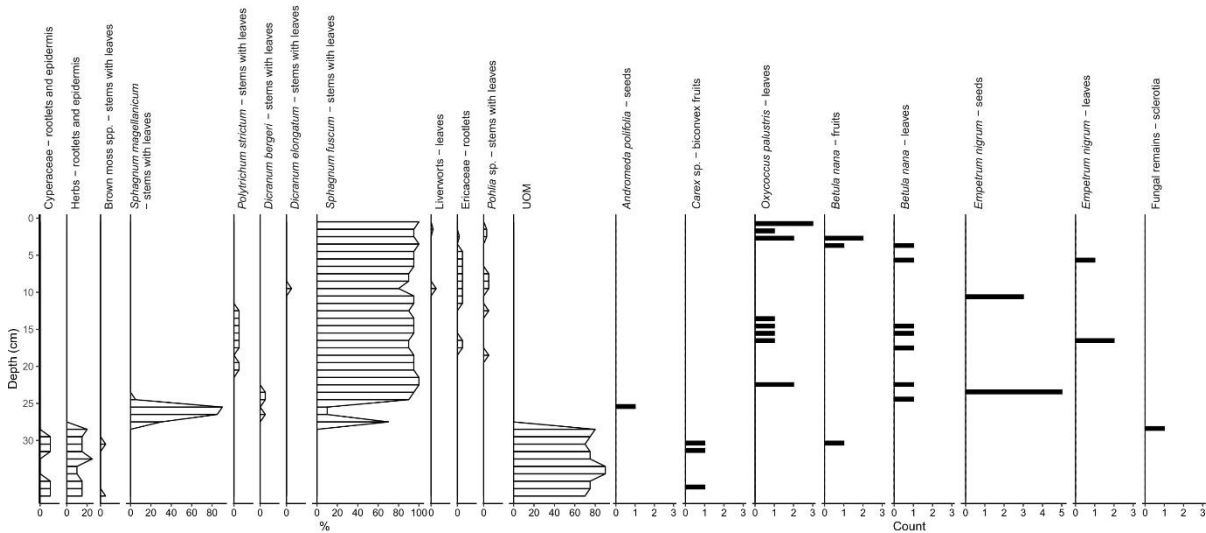


Figure B.14. Plant macrofossil diagrams for Maunuvuoma fen peat profile, both volume percentages (lines) and count data (bars).

Orusjohka palsa – Plant macrofossils

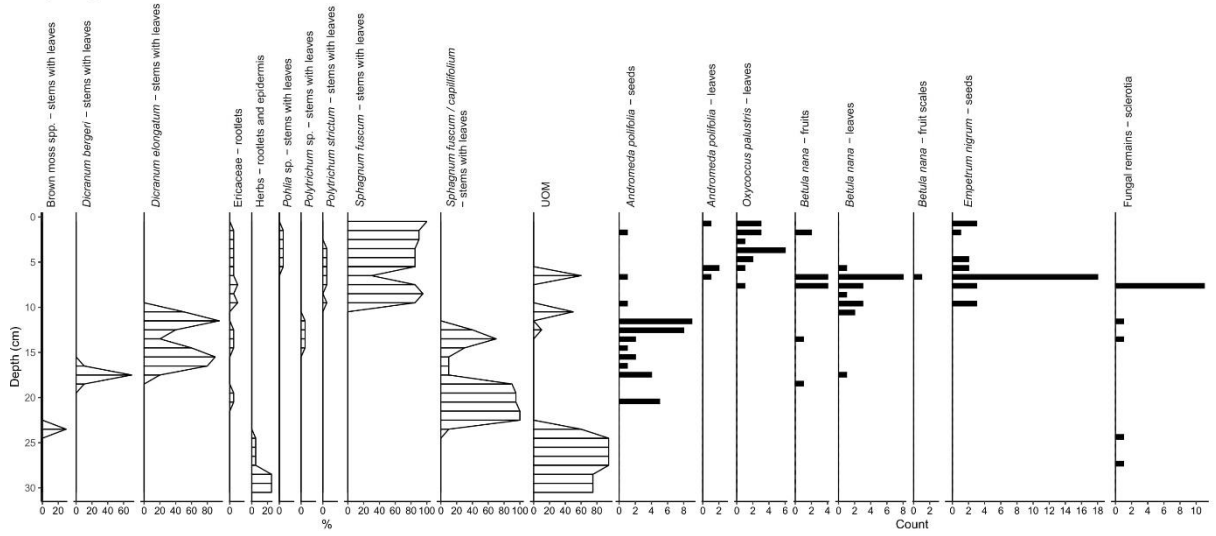


Figure B.15. Plant macrofossil diagrams for Orusjohka palsa peat profile, both volume percentages (lines) and count data (bars).

Rensjön palsa – Plant macrofossils

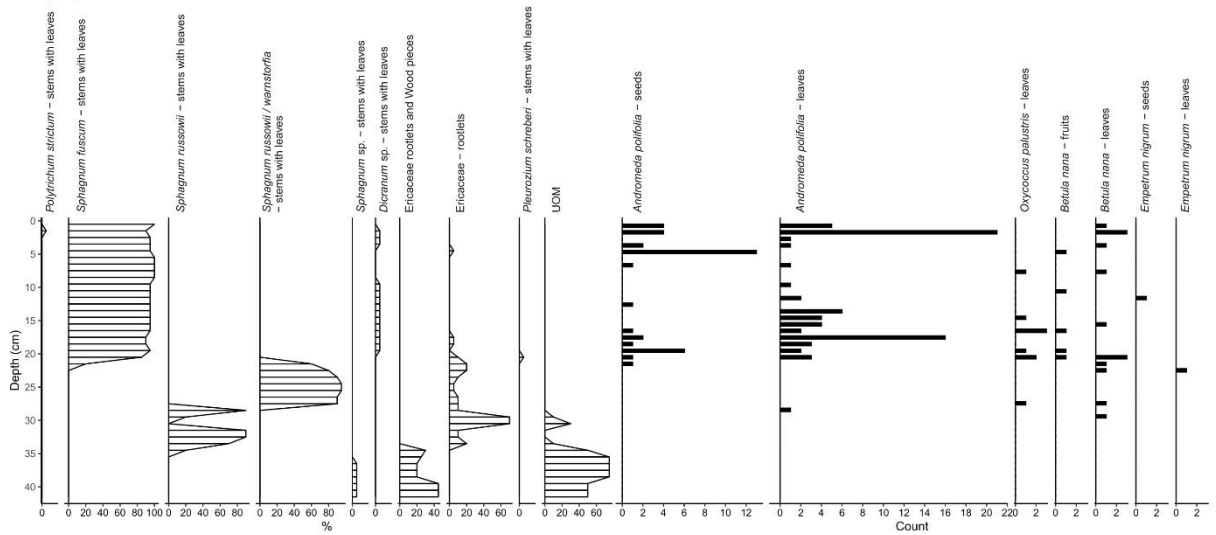


Figure B.16. Plant macrofossil diagrams for Rensjön palsa peat profile, both volume percentages (lines) and count data (bars).

Ribasvuomuš bog – Plant macrofossils

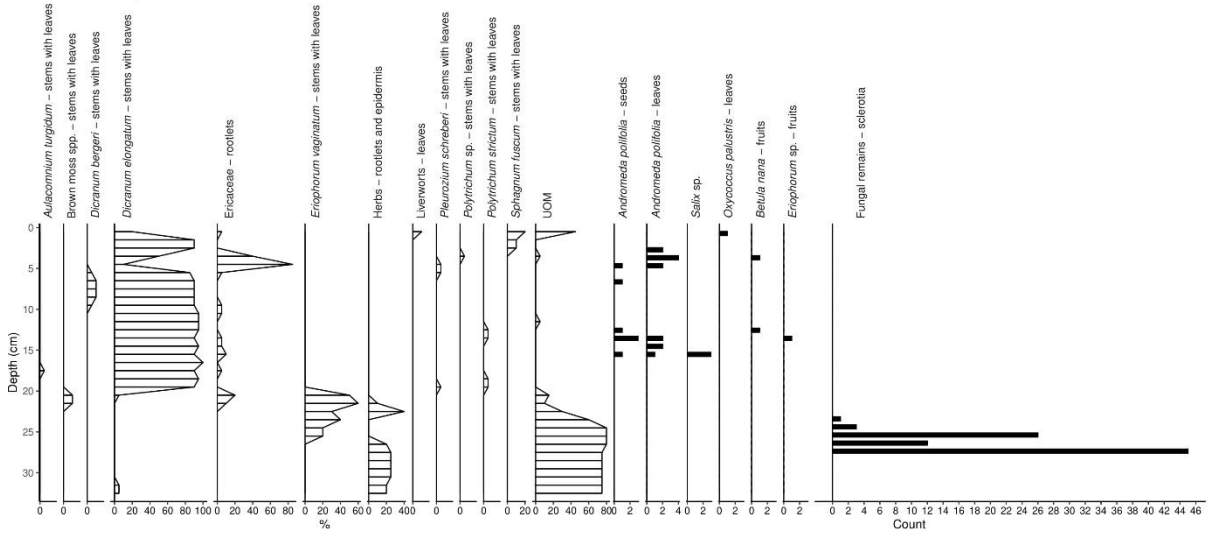


Figure B.17. Plant macrofossil diagrams for Ribasvuomuš bog peat profile, both volume percentages (lines) and count data (bars).

Stordalen bog – Plant macrofossils

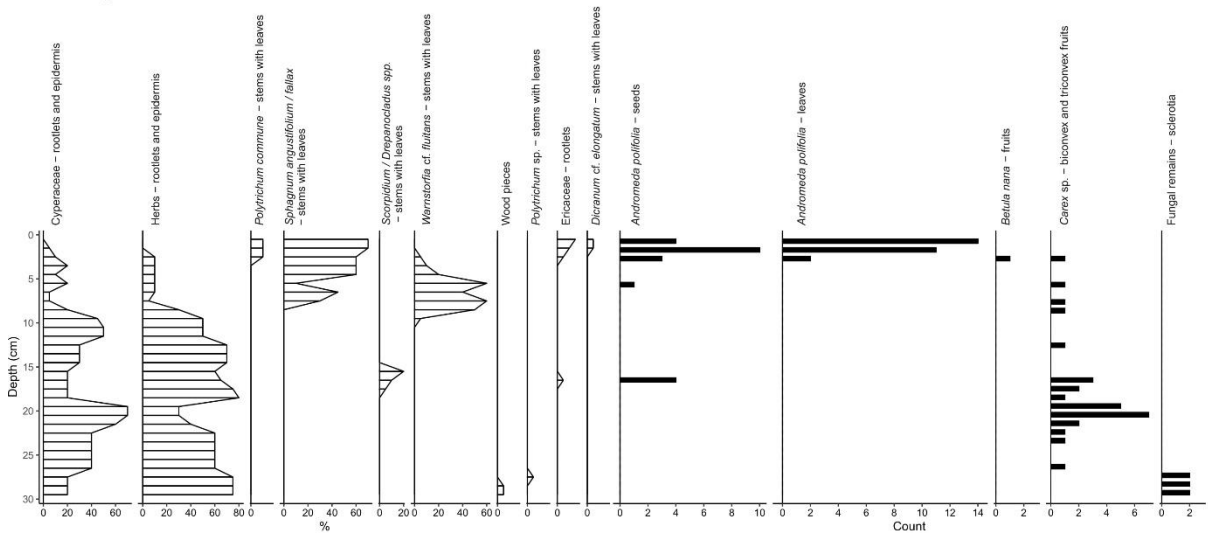


Figure B.18. Plant macrofossil diagrams for Stordalen bog peat profile, both volume percentages (lines) and count data (bars).

Stordalen palsa – Plant macrofossils

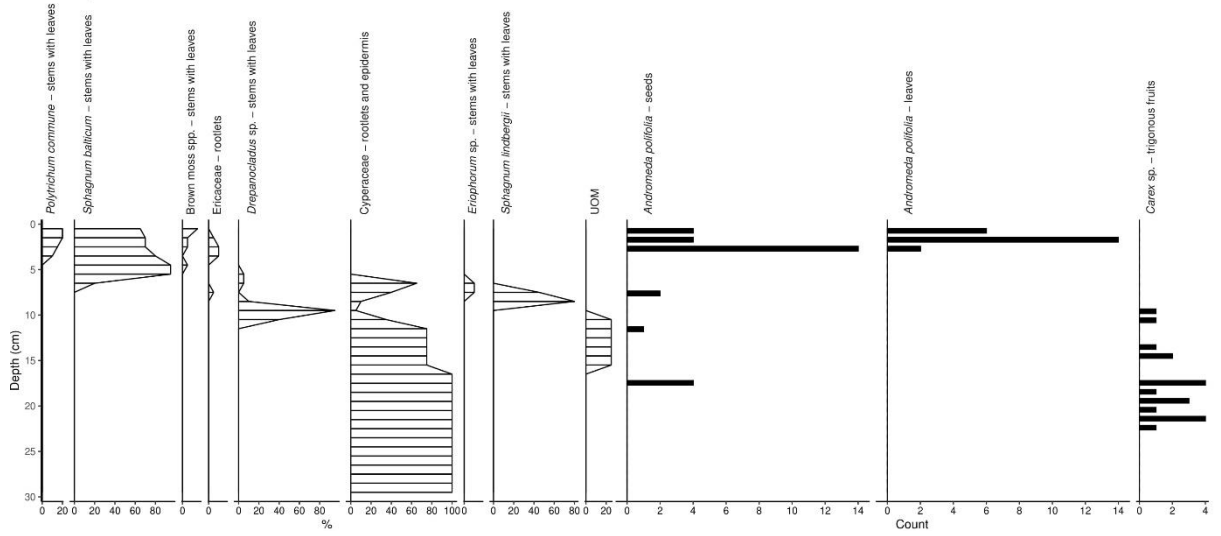


Figure B.19. Plant macrofossil diagrams for Stordalen palsa peat profile, both volume percentages (lines) and count data (bars).

Veigi bog – Plant macrofossils

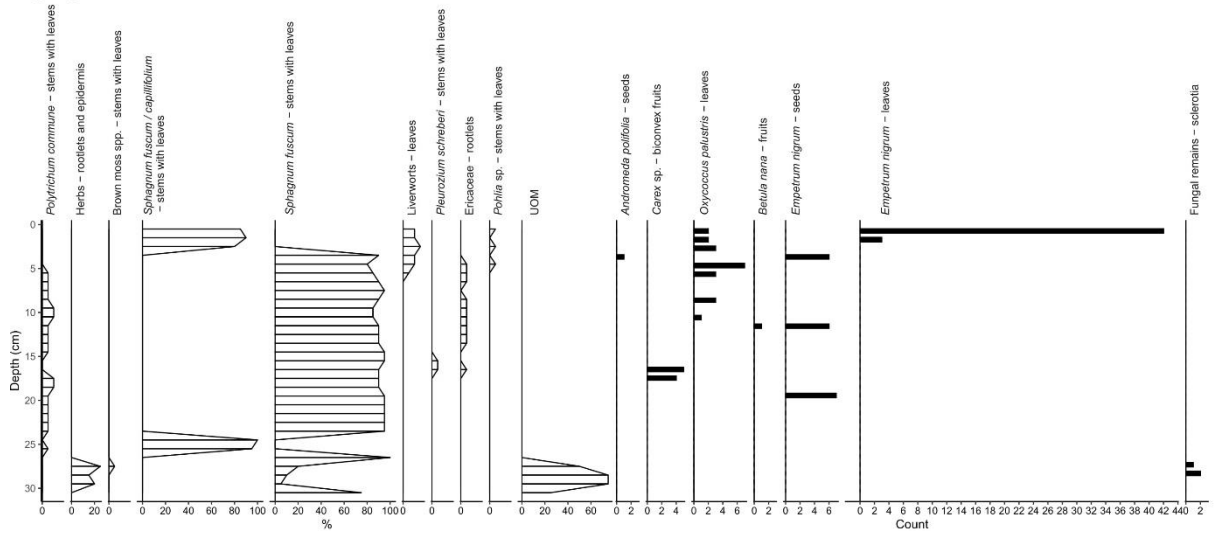


Figure B.20. Plant macrofossil diagrams for Veigi bog peat profile, both volume percentages (lines) and count data (bars).

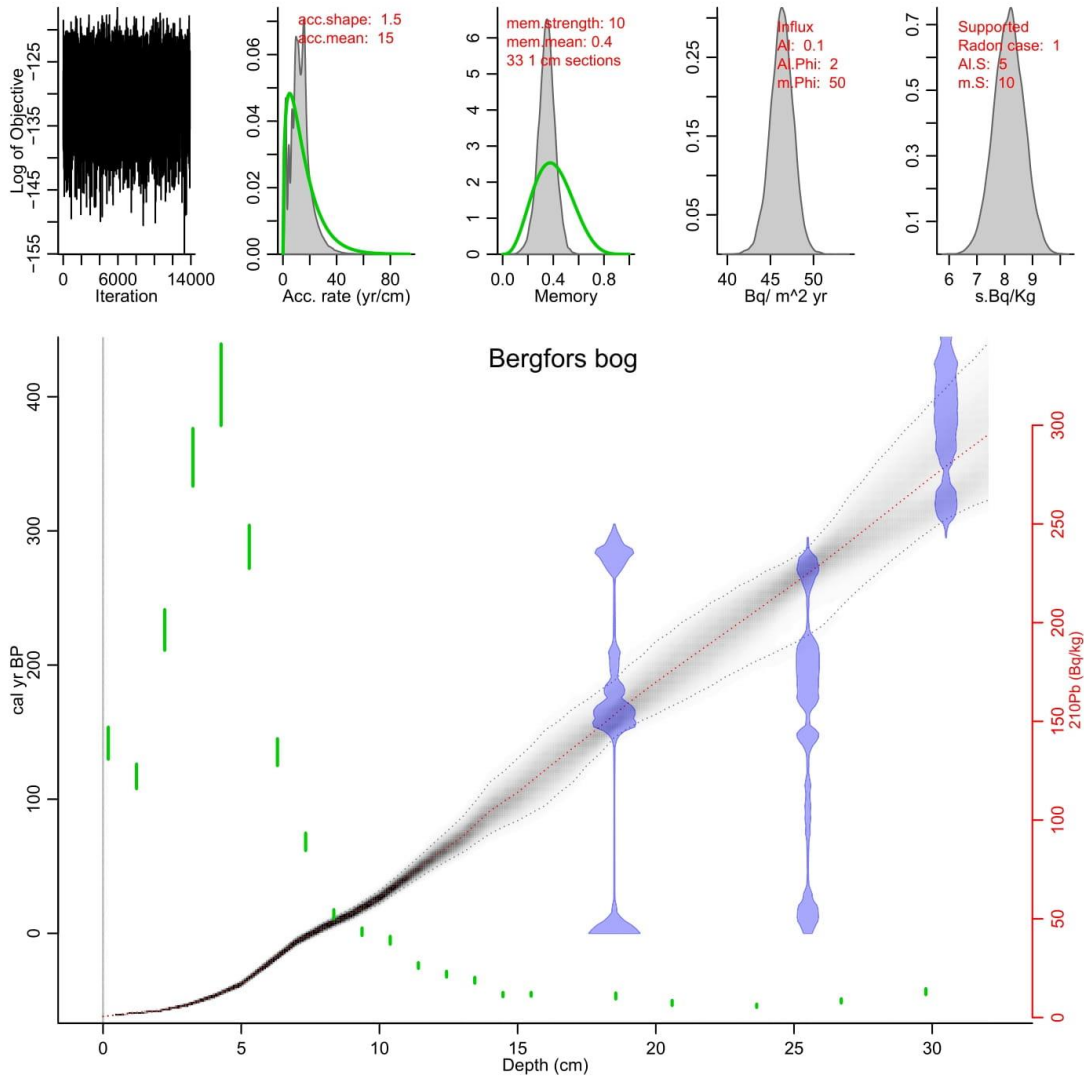


Figure B.21. Age-depth model for Bergfors bog peat profile. Upper panels depicted from left to right: the log of the objective function of the MCMC iterations, accumulation rate (yr cm^{-1}), Memory, influx of ^{210}Pb ($\text{Bq cm}^{-2} \text{yr}^{-1}$) and supported ^{210}Pb (Bq kg^{-1}). The log of the objective function panel is used for interpreting the convergence of the MCMC model: good runs show a stationary distribution with little structure among neighbouring iterations. Bottom panel shows the calibrated ^{14}C dates (transparent blue), ^{210}Pb (Bq/kg) concentrations (green lines with reference to the red scale on the right) and the age-depth model (darker greys indicate more likely calendar ages; grey stippled lines show 95% confidence intervals; red stippled line shows single 'best' model based on the mean age for each depth).

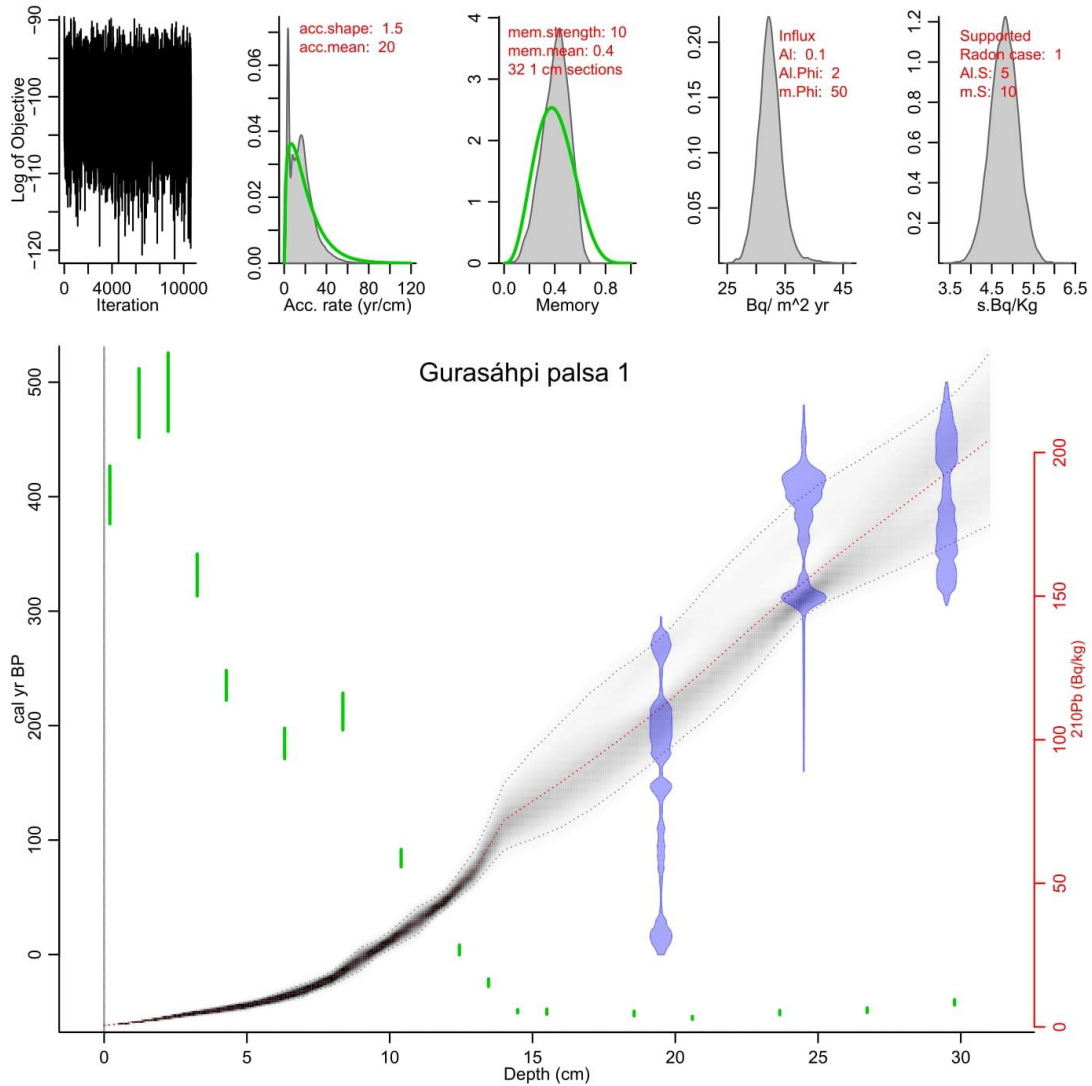


Figure B.22. Age-depth model for Gurasáhi palsa 1 peat profile. Upper panels depicted from left to right: the log of the objective function of the MCMC iterations, accumulation rate (yr cm^{-1}), Memory, influx of ^{210}Pb ($\text{Bq cm}^{-2} \text{ yr}^{-1}$) and supported ^{210}Pb (Bq kg^{-1}). The log of the objective function panel is used for interpreting the convergence of the MCMC model: good runs show a stationary distribution with little structure among neighbouring iterations. Bottom panel shows the calibrated ^{14}C dates (transparent blue), ^{210}Pb (Bq/kg) concentrations (green lines with reference to the red scale on the right) and the age-depth model (darker greys indicate more likely calendar ages; grey stippled lines show 95% confidence intervals; red stippled line shows single 'best' model based on the mean age for each depth).

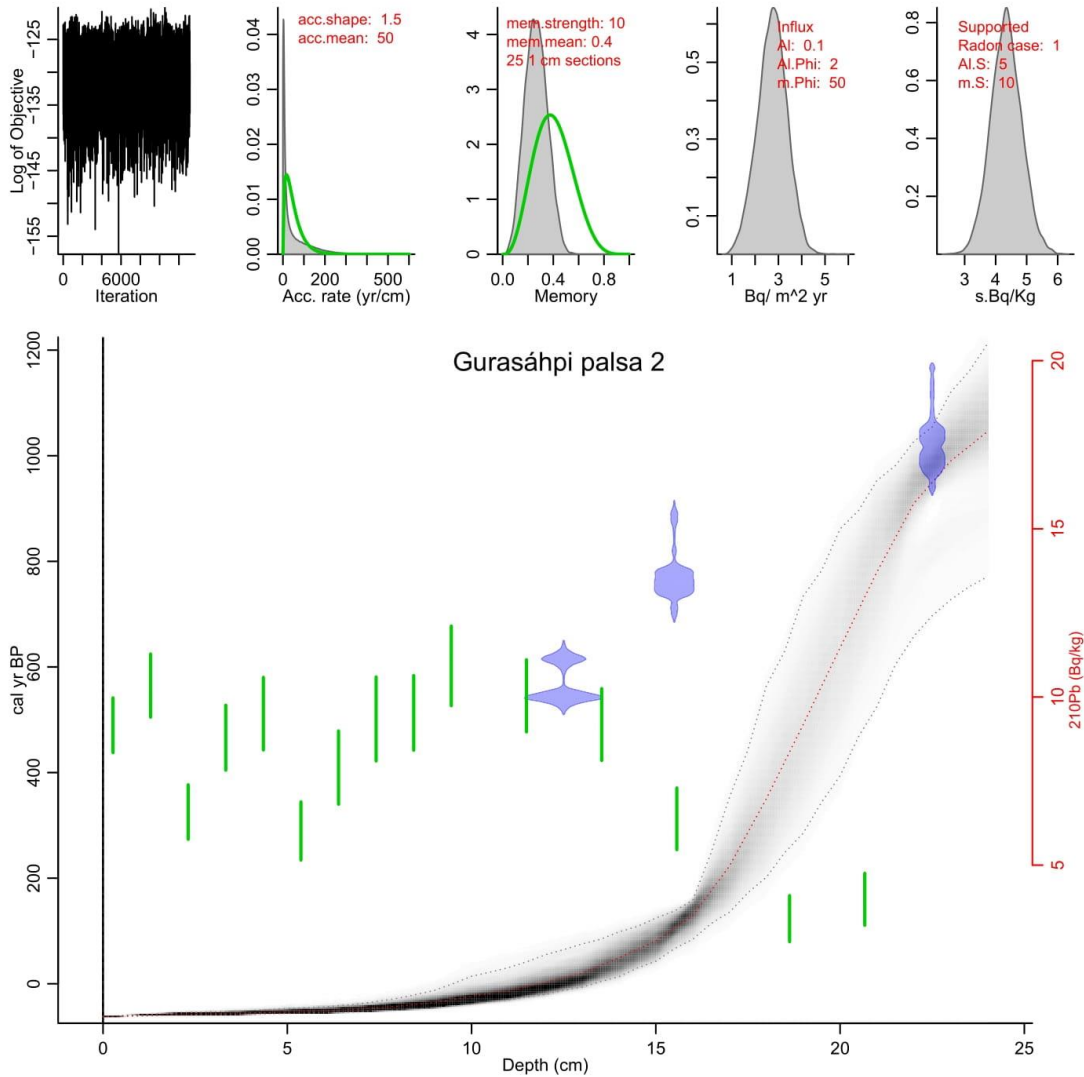


Figure B.23. Age-depth model for Gurasáhi palsa 2 peat profile. Upper panels depicted from left to right: the log of the objective function of the MCMC iterations, accumulation rate (yr cm^{-1}), Memory, influx of ^{210}Pb ($\text{Bq cm}^{-2} \text{yr}^{-1}$) and supported ^{210}Pb (Bq kg^{-1}). The log of the objective function panel is used for interpreting the convergence of the MCMC model: good runs show a stationary distribution with little structure among neighbouring iterations. Bottom panel shows the calibrated ^{14}C dates (transparent blue), ^{210}Pb (Bq/kg) concentrations (green lines with reference to the red scale on the right) and the age-depth model (darker greys indicate more likely calendar ages; grey stippled lines show 95% confidence intervals; red stippled line shows single 'best' model based on the mean age for each depth).

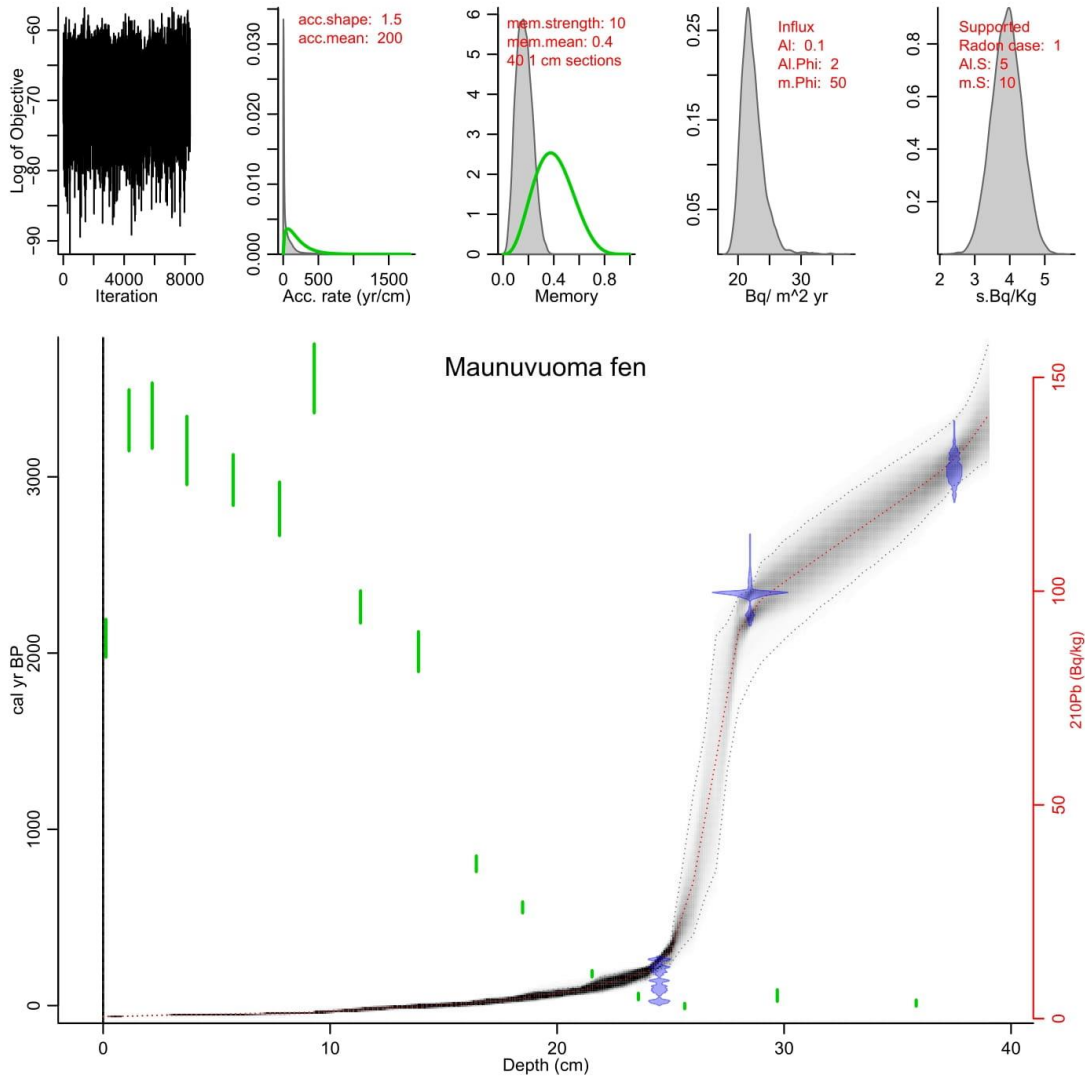


Figure B.24. Age-depth model for Maunuvuoma fen peat profile. Upper panels depicted from left to right: the log of the objective function of the MCMC iterations, accumulation rate (yr cm^{-1}), Memory, influx of ^{210}Pb ($\text{Bq cm}^{-2} \text{ yr}^{-1}$) and supported ^{210}Pb (Bq kg^{-1}). The log of the objective function panel is used for interpreting the convergence of the MCMC model: good runs show a stationary distribution with little structure among neighbouring iterations. Bottom panel shows the calibrated ^{14}C dates (transparent blue), ^{210}Pb (Bq/kg) concentrations (green lines with reference to the red scale on the right) and the age-depth model (darker greys indicate more likely calendar ages; grey stippled lines show 95% confidence intervals; red stippled line shows single 'best' model based on the mean age for each depth).

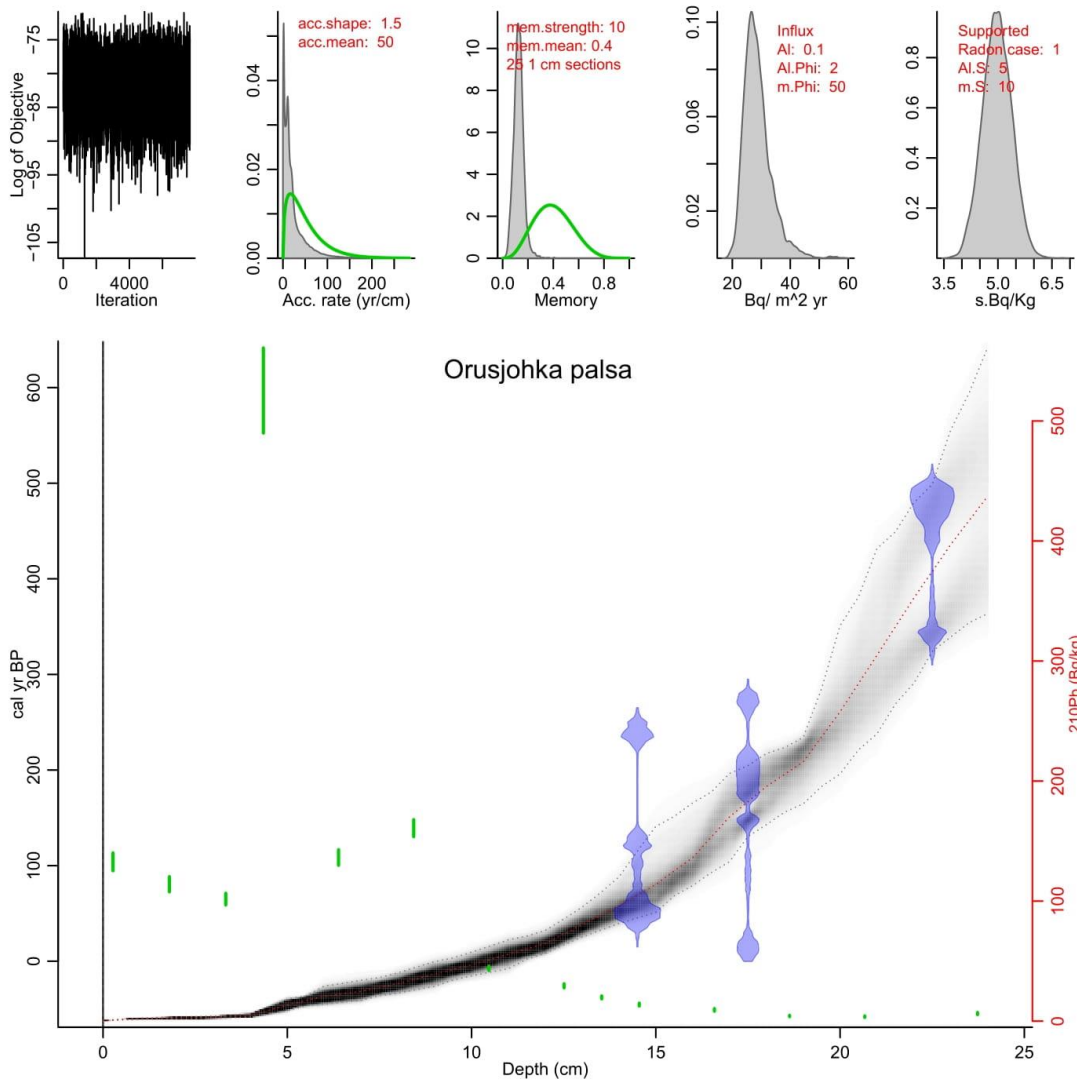


Figure B.25. Age-depth model for Orusjohka palsa peat profile. Upper panels depicted from left to right: the log of the objective function of the MCMC iterations, accumulation rate (yr cm^{-1}), Memory, influx of ^{210}Pb ($\text{Bq cm}^{-2} \text{yr}^{-1}$) and supported ^{210}Pb (Bq kg^{-1}). The log of the objective function panel is used for interpreting the convergence of the MCMC model: good runs show a stationary distribution with little structure among neighbouring iterations. Bottom panel shows the calibrated ^{14}C dates (transparent blue), ^{210}Pb (Bq/kg) concentrations (green lines with reference to the red scale on the right) and the age-depth model (darker greys indicate more likely calendar ages; grey stippled lines show 95% confidence intervals; red stippled line shows single 'best' model based on the mean age for each depth).

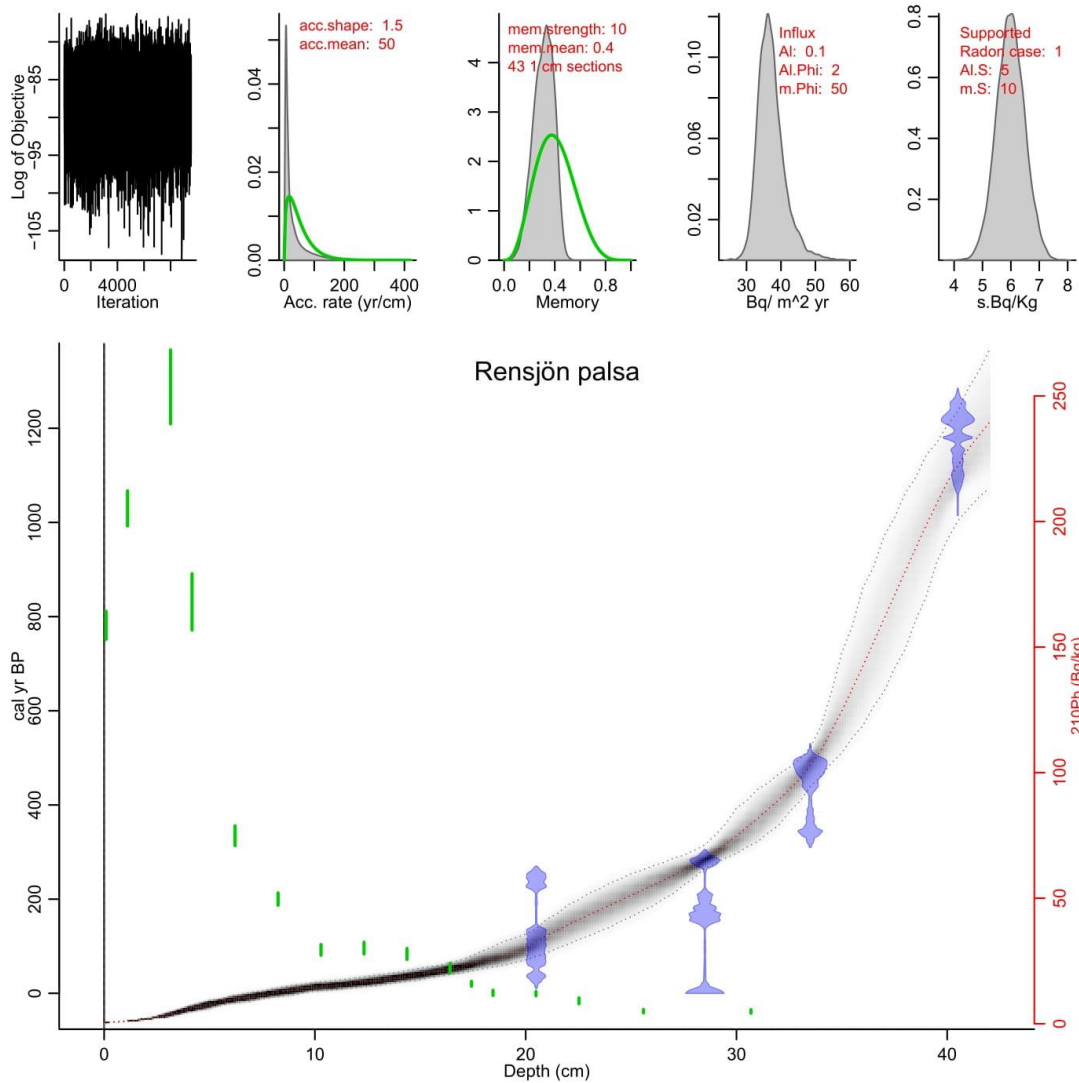


Figure B.26. Age-depth model for Rensjön palsa peat profile. Upper panels depicted from left to right: the log of the objective function of the MCMC iterations, accumulation rate (yr cm^{-1}), Memory, influx of ^{210}Pb ($\text{Bq cm}^{-2} \text{yr}^{-1}$) and supported ^{210}Pb (Bq kg^{-1}). The log of the objective function panel is used for interpreting the convergence of the MCMC model: good runs show a stationary distribution with little structure among neighbouring iterations. Bottom panel shows the calibrated ^{14}C dates (transparent blue), ^{210}Pb (Bq/kg) concentrations (green lines with reference to the red scale on the right) and the age-depth model (darker greys indicate more likely calendar ages; grey stippled lines show 95% confidence intervals; red stippled line shows single 'best' model based on the mean age for each depth).

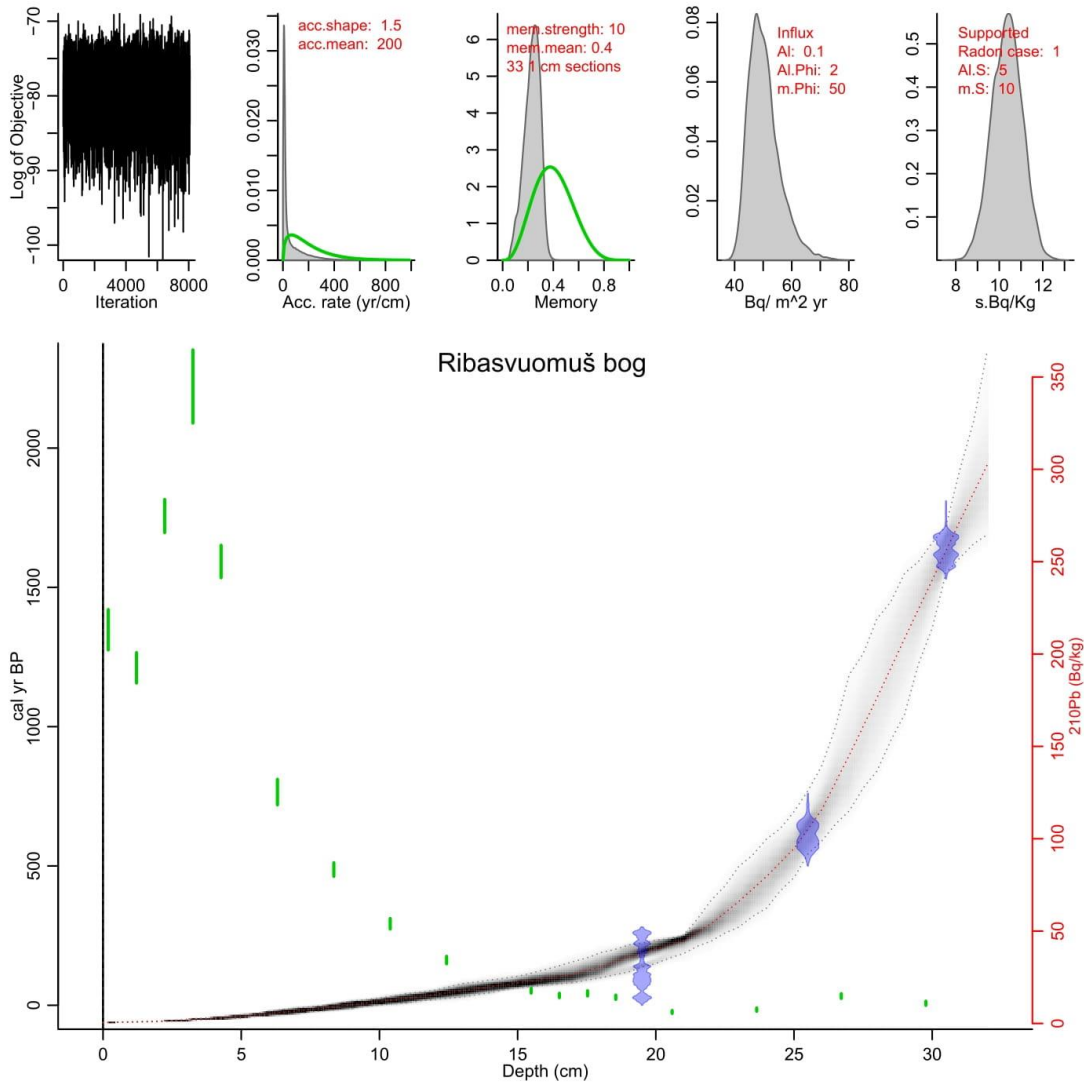


Figure B.27. Age-depth model for Ribasvuomuš bog peat profile. Upper panels depicted from left to right: the log of the objective function of the MCMC iterations, accumulation rate (yr cm^{-1}), Memory, influx of ^{210}Pb ($\text{Bq cm}^{-2} \text{ yr}^{-1}$) and supported ^{210}Pb (Bq kg^{-1}). The log of the objective function panel is used for interpreting the convergence of the MCMC model: good runs show a stationary distribution with little structure among neighbouring iterations. Bottom panel shows the calibrated ^{14}C dates (transparent blue), ^{210}Pb (Bq/kg) concentrations (green lines with reference to the red scale on the right) and the age-depth model (darker greys indicate more likely calendar ages; grey stippled lines show 95% confidence intervals; red stippled line shows single 'best' model based on the mean age for each depth).

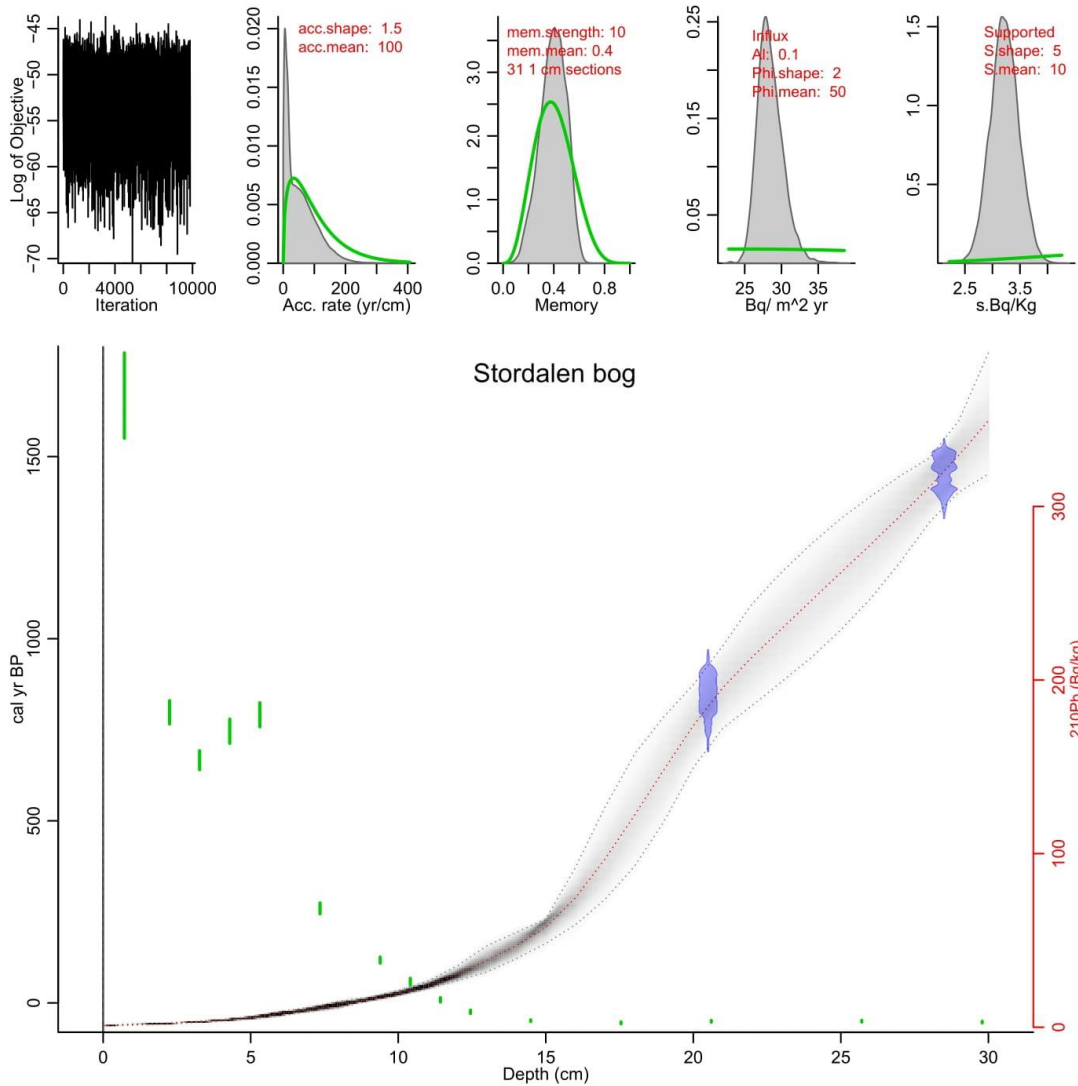


Figure B.28. Age-depth model for Stordalen bog peat profile. Upper panels depicted from left to right: the log of the objective function of the MCMC iterations, accumulation rate (yr cm^{-1}), Memory, influx of ^{210}Pb ($\text{Bq cm}^{-2} \text{yr}^{-1}$) and supported ^{210}Pb (Bq kg^{-1}). The log of the objective function panel is used for interpreting the convergence of the MCMC model: good runs show a stationary distribution with little structure among neighbouring iterations. Bottom panel shows the calibrated ^{14}C dates (transparent blue), ^{210}Pb (Bq/kg) concentrations (green lines with reference to the red scale on the right) and the age-depth model (darker greys indicate more likely calendar ages; grey stippled lines show 95% confidence intervals; red stippled line shows single 'best' model based on the mean age for each depth).

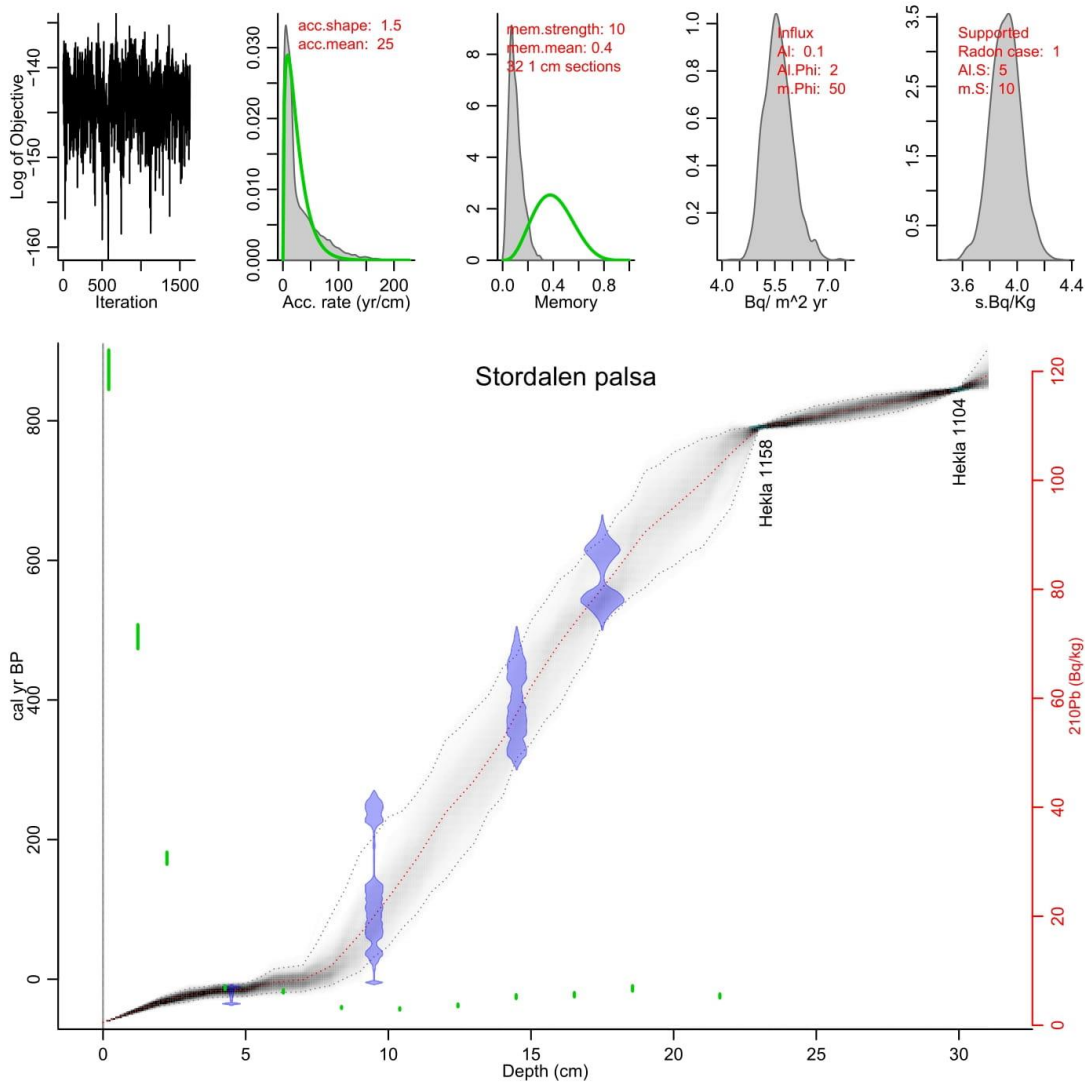


Figure B.29. Age-depth model for Stordalen palsa peat profile. Upper panels depicted from left to right: the log of the objective function of the MCMC iterations, accumulation rate (yr cm^{-1}), Memory, influx of ^{210}Pb ($\text{Bq cm}^{-2} \text{yr}^{-1}$) and supported ^{210}Pb (Bq kg^{-1}). The log of the objective function panel is used for interpreting the convergence of the MCMC model: good runs show a stationary distribution with little structure among neighbouring iterations. Bottom panel shows the calibrated ^{14}C dates (transparent blue), ^{210}Pb (Bq/kg) concentrations (green lines with reference to the red scale on the right) and the age-depth model (darker greys indicate more likely calendar ages; grey stippled lines show 95% confidence intervals; red stippled line shows single 'best' model based on the mean age for each depth).

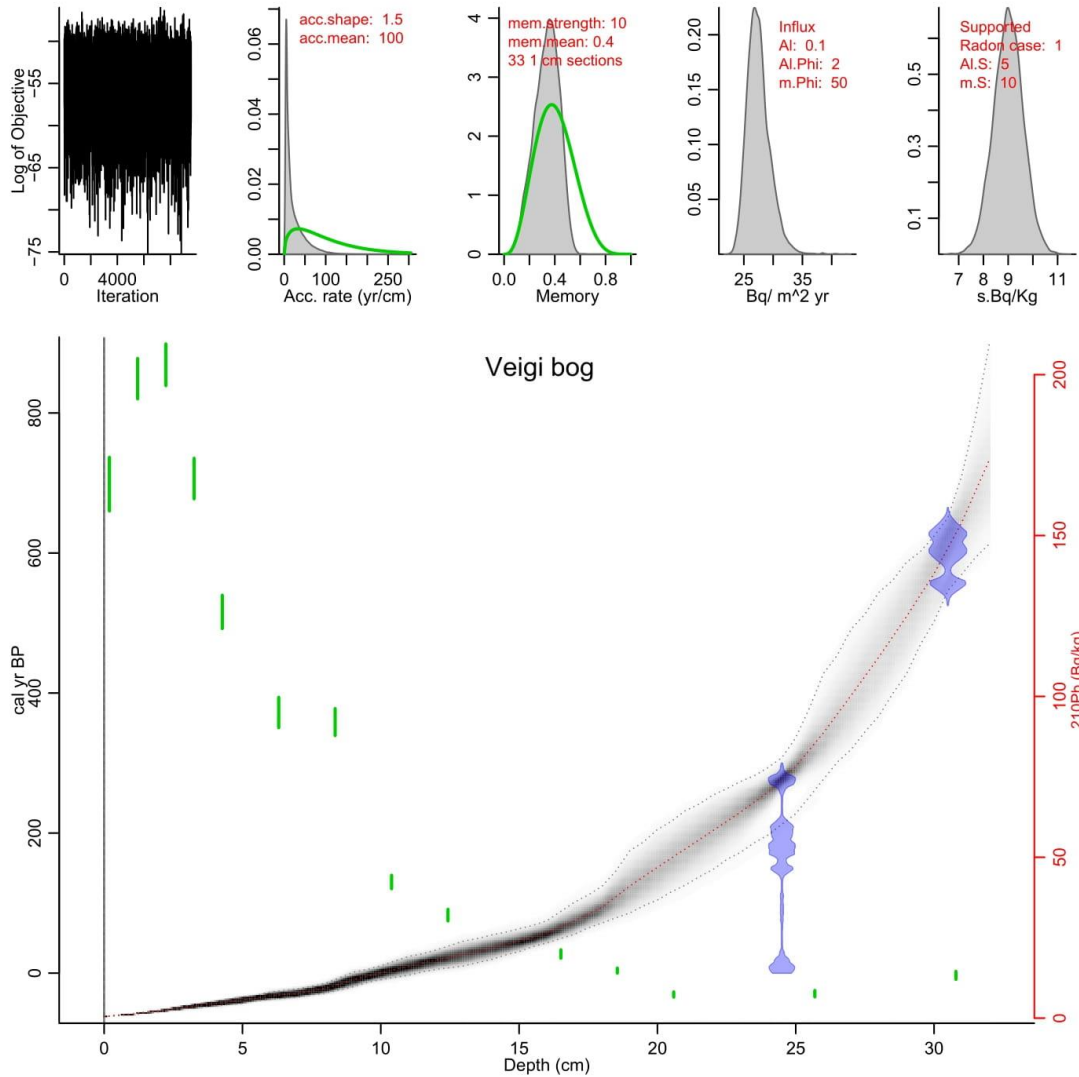


Figure B.30. Age-depth model for Veigi bog peat profile. Upper panels depicted from left to right: the log of the objective function of the MCMC iterations, accumulation rate (yr cm^{-1}), Memory, influx of ^{210}Pb ($\text{Bq cm}^{-2} \text{ yr}^{-1}$) and supported ^{210}Pb (Bq kg^{-1}). The log of the objective function panel is used for interpreting the convergence of the MCMC model: good runs show a stationary distribution with little structure among neighbouring iterations. Bottom panel shows the calibrated ^{14}C dates (transparent blue), ^{210}Pb (Bq/kg) concentrations (green lines with reference to the red scale on the right) and the age-depth model (darker greys indicate more likely calendar ages; grey stippled lines show 95% confidence intervals; red stippled line shows single 'best' model based on the mean age for each depth).

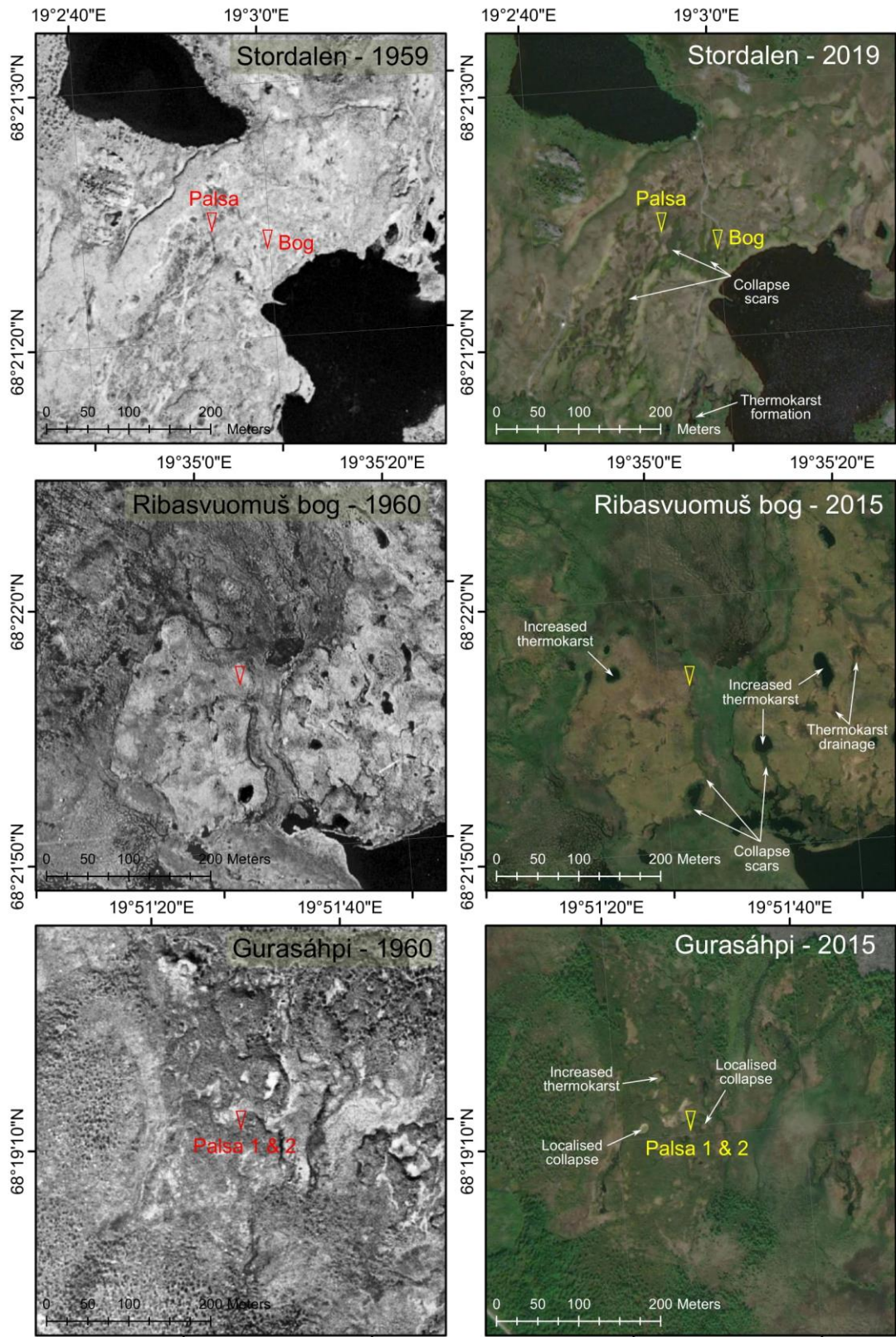


Figure B.31. Comparative historic and recent imagery of the Stordalen, Ribasvuomuš bog and Gurasáhpi sites. Core locations are marked and clear changes in permafrost structure and drainage annotated. Historic orthophotos (geometrically corrected) from 1959-1960 are sourced from Lantmäteriet and contemporary satellite imagery (2012-2019) is from ArcGIS online (source: Esri, DigitalGlobe, GeoEye, Earthstar Geographics, CNES/Airbus DS, USDA, USGS, AeroGRID, IGN and the GIS User Community).

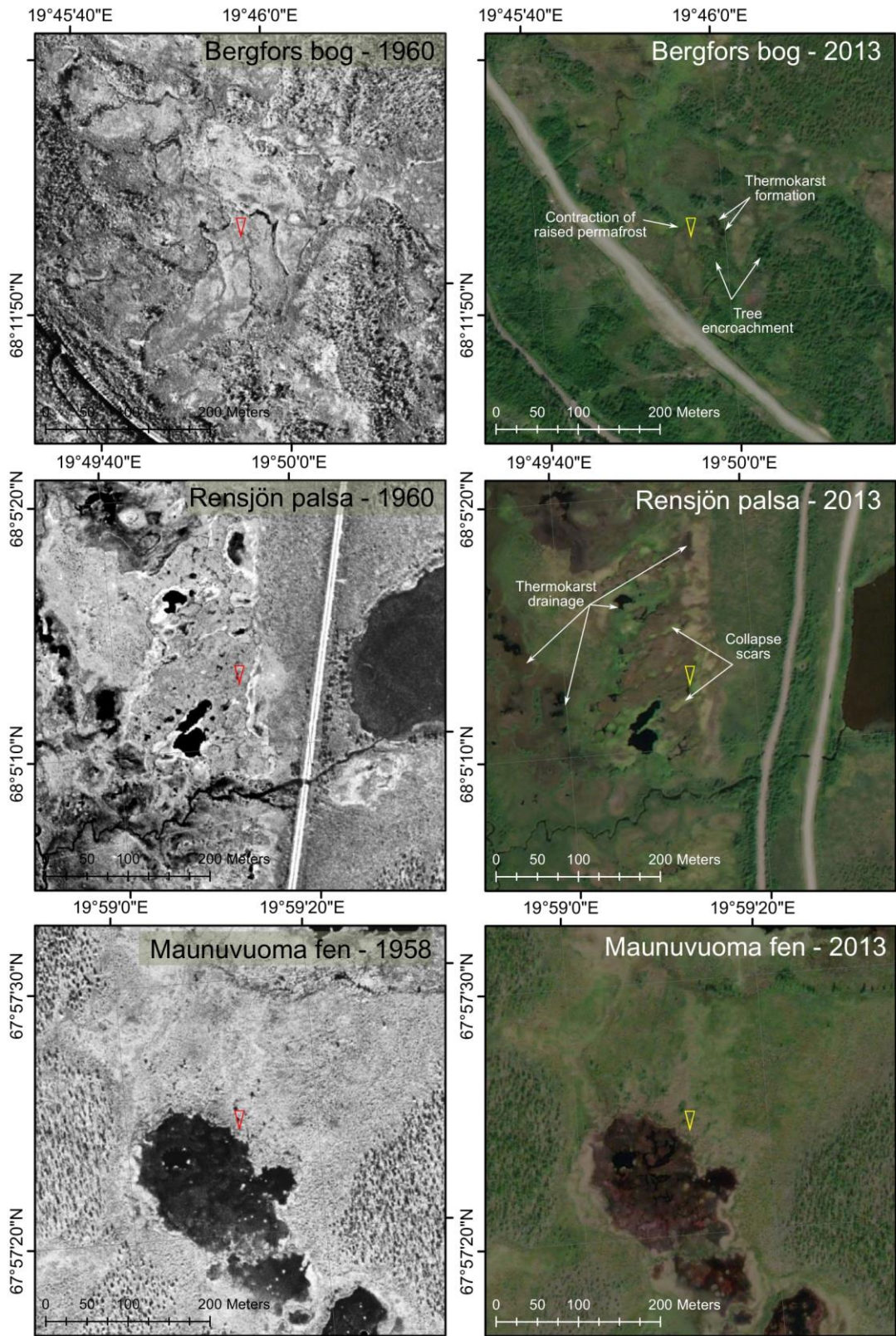


Figure B.32. Comparative historic and recent imagery of the Bergfors bog, Rensjön palsa and Maunuvuoma fen sites. Core locations are marked and clear changes in permafrost structure and drainage annotated. Historic orthophotos (geometrically corrected) from 1959-1960 are sourced from Lantmäteriet and contemporary satellite imagery (2012-2019) is from ArcGIS online (source: Esri, DigitalGlobe, GeoEye, Earthstar Geographics, CNES/Airbus DS, USDA, USGS, AeroGRID, IGN and the GIS User Community).

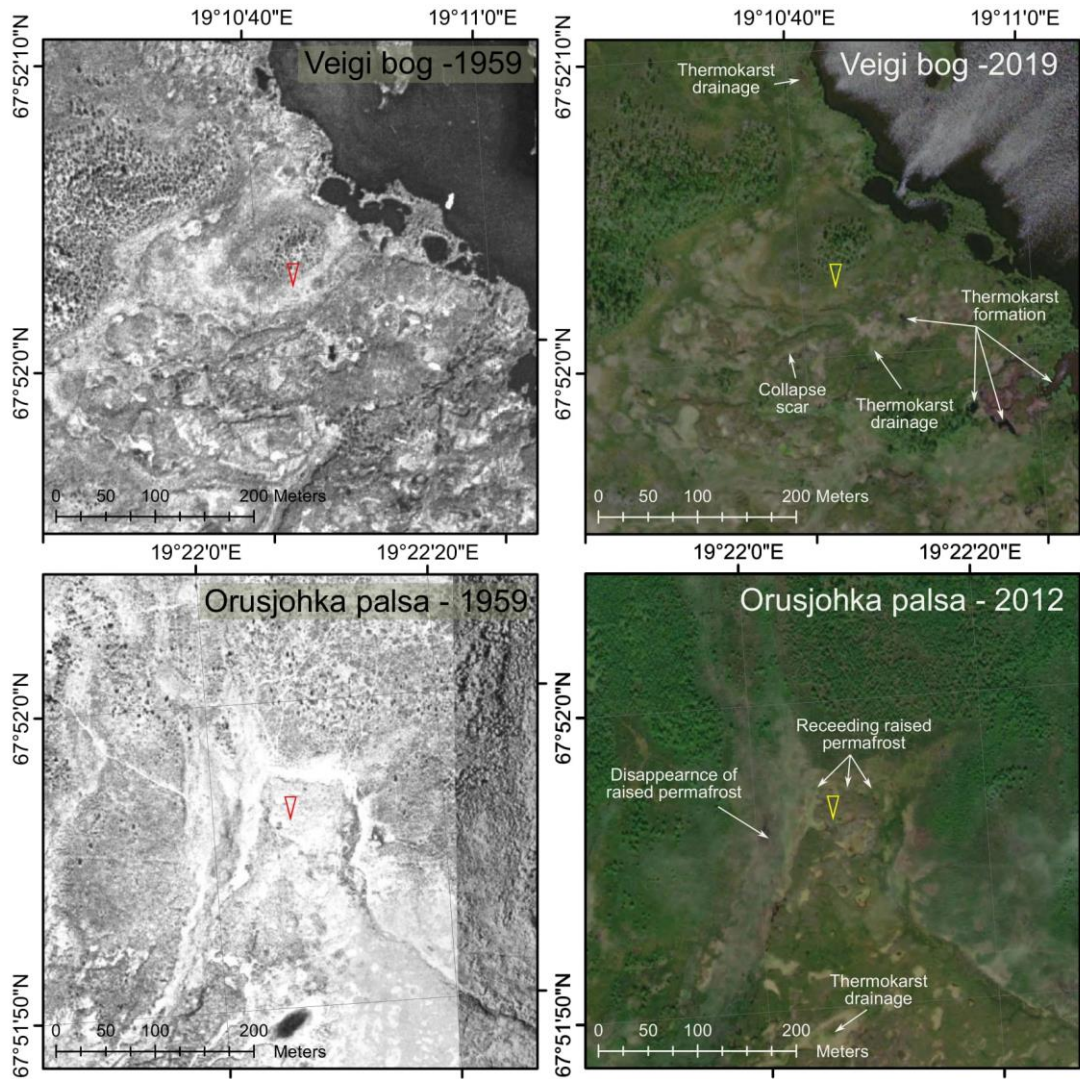


Figure B.33. Comparative historic and recent imagery of the Veigi bog and Orusjohka palsa sites. Core locations are marked and clear changes in permafrost structure and drainage annotated. Historic orthophotos (geometrically corrected) from 1959-1960 are sourced from Lantmäteriet and contemporary satellite imagery (2012-2019) is from ArcGIS online (source: Esri, DigitalGlobe, GeoEye, Earthstar Geographics, CNES/Airbus DS, USDA, USGS, AeroGRID, IGN and the GIS User Community).

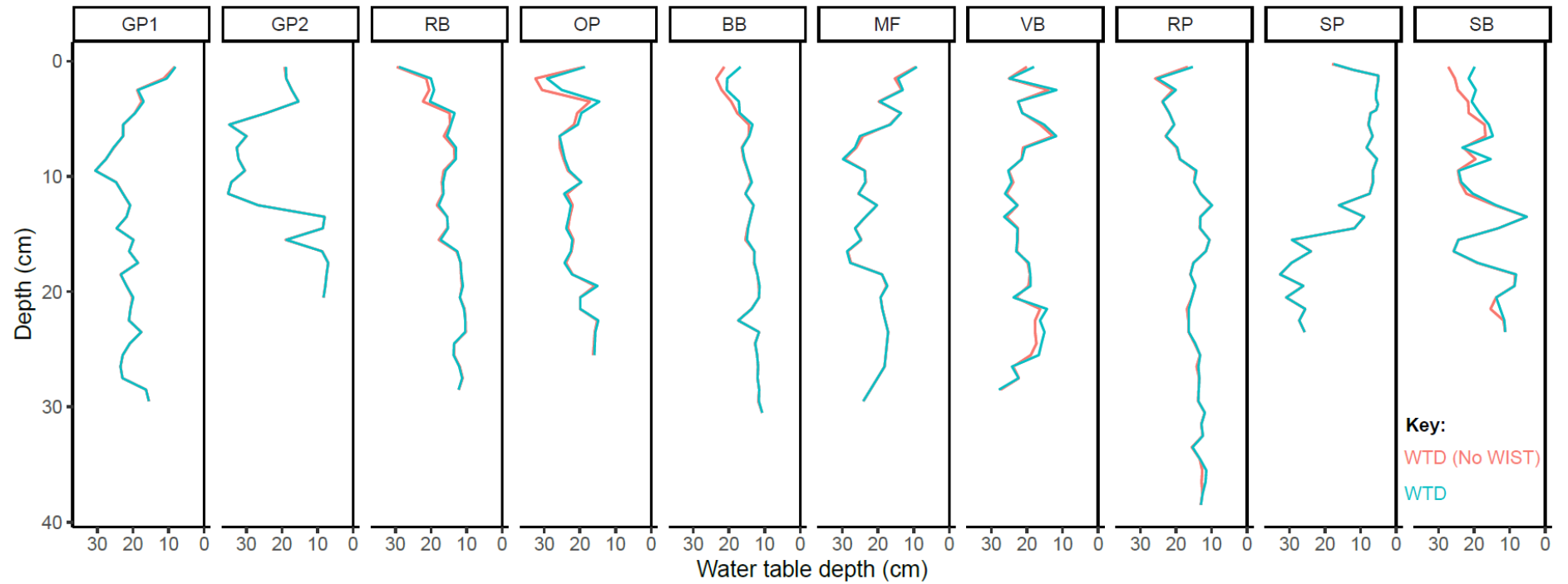


Figure B.34. Comparison of testate amoebae WTD (cm) reconstructions including and excluding WIST taxa for each site.= Gurasáhpí palsa 1, GP2= Gurasáhpí palsa 2, RB = Ribasvuomuš bog, OP = Orusjohka palsa, BB = Bergfors bog, MF = Maunuvuoma fen, VB = Veigi bog, RP = Rensjón palsa, SP = Stordalen palsa and SB = Stordalen bog.

Table B.1. Plant macrofossil taxa groupings used in Figure 3.2.

Grouping	Taxa or type included				
Brown moss spp.	<i>Aulacomnium turgidum</i>	Brown moss spp.	<i>Drepanocladus</i> sp.	<i>Scorpidium/Drepanocladus</i>	<i>Warnstorfia</i> cf. <i>fluitans</i>
Cyperaceae and herbs	Cyperaceae	<i>Eriophorum</i> sp.	<i>Eriophorum vaginatum</i>	Herbs	
<i>Dicranum</i> spp.	<i>Dicranum bergeri</i>	<i>Dicranum</i> cf. <i>elongatum</i>	<i>Dicranum elongatum</i>	<i>Dicranum</i> sp.	
Ericaceae	Ericaceae	Ericaceae and wood			
Liverworts	Liverworts				
Other	<i>Pohlia</i> sp.	<i>Pleurozium schreberi</i>	<i>Sphagnum</i> sp.	<i>Dicranaceae</i>	
<i>Polytrichum</i> spp.	<i>Polytrichum</i> sp.	<i>Polytrichum commune</i>	<i>Polytrichum strictum</i>		
<i>Sphagnum balticum</i>	<i>Sphagnum balticum</i>				
<i>Sphagnum fallax</i>	<i>Sphagnum fallax</i>	<i>Sphagnum angustifolium</i> / <i>fallax</i>			
<i>Sphagnum fuscum</i>	<i>Sphagnum fuscum</i>	<i>Sphagnum fuscum</i> / <i>capillifolium</i>			
<i>Sphagnum lindbergii</i>	<i>Sphagnum lindbergii</i>				
<i>Sphagnum magellanicum</i>	<i>Sphagnum magellanicum</i>				
<i>Sphagnum riparium</i>	<i>Sphagnum riparium</i>				
<i>Sphagnum russowii</i>	<i>Sphagnum russowii</i>	<i>Sphagnum russowii</i> / <i>warnstorfia</i>			
UOM	UOM				
Wood	Wood				

Appendix C. Supporting information for Chapter 4: Regional variability in peatland burning at mid- to high-latitudes during the Holocene

Contents of this section:

1. Figure C.1: Map of paleofire records representing burning in the wider landscape and their sub-region.
2. Table C.1: Metadata for all 221 peatland macrocharcoal records.
3. Table C.2: Metadata for wider landscape records from the Global Charcoal Database.
4. Figure C.2: Age-depth models for records 1-6.
5. Figure C.3: Age-depth models for records 7-12.
6. Figure C.4: Age-depth models for records 3-18.
7. Figure C.5: Age-depth models for records 19-24.
8. Figure C.6: Age-depth models for records 25-30.
9. Figure C.7: Age-depth models for records 31-36.
10. Figure C.8: Age-depth models for records 37-42.
11. Figure C.9: Age-depth models for records 43-48.
12. Figure C.10: Age-depth models for records 49-54.
13. Figure C.11: Age-depth models for records 55-60.
14. Figure C.12: Age-depth models for records 61-66.
15. Figure C.13: Age-depth models for records 67-72.
16. Figure C.14: Age-depth models for records 73-78.
17. Figure C.15: Age-depth models for records 79-84.
18. Figure C.16: Age-depth models for records 85-90.
19. Figure C.17: Age-depth models for records 91-96.
20. Figure C.18: Age-depth models for records 97-102.
21. Figure C.19: Age-depth models for records 103-108.
22. Figure C.20: Age-depth models for records 109-114.
23. Figure C.21: Age-depth models for records 115-120.
24. Figure C.22: Age-depth models for records 121-126.
25. Figure C.23: Age-depth models for records 127-132.
26. Figure C.24: Age-depth models for records 133-138.
27. Figure C.25: Age-depth models for records 139-144.
28. Figure C.26: Age-depth models for records 145-150.
29. Figure C.27: Age-depth models for records 151-156.
30. Figure C.28: Age-depth models for records 157-162.
31. Figure C.29: Age-depth models for records 163-168.
32. Figure C.30: Age-depth models for records 169-174.
33. Figure C.31: Age-depth models for records 175-180.
34. Figure C.32: Age-depth models for records 181-186.
35. Figure C.33: Age-depth models for records 187-192.
36. Figure C.34: Age-depth models for records 193-198.
37. Figure C.35: Age-depth models for records 199-204.
38. Figure C.36: Age-depth models for records 205-210.
39. Figure C.37: Age-depth models for records 211-216.
40. Figure C.38: Age-depth models for records 217-221.
41. Figure C.39: Conceptual diagram of the 50-year depth binning approach using example data.
42. Figure C.40: Influx values calculated for five example sites from the 50-year bin means method and 50-year depth binning method.

43. Figure C.41: The relationship between maximum resampled charcoal values (C_{\max}) and the proportion of resampled values containing charcoal within a record.

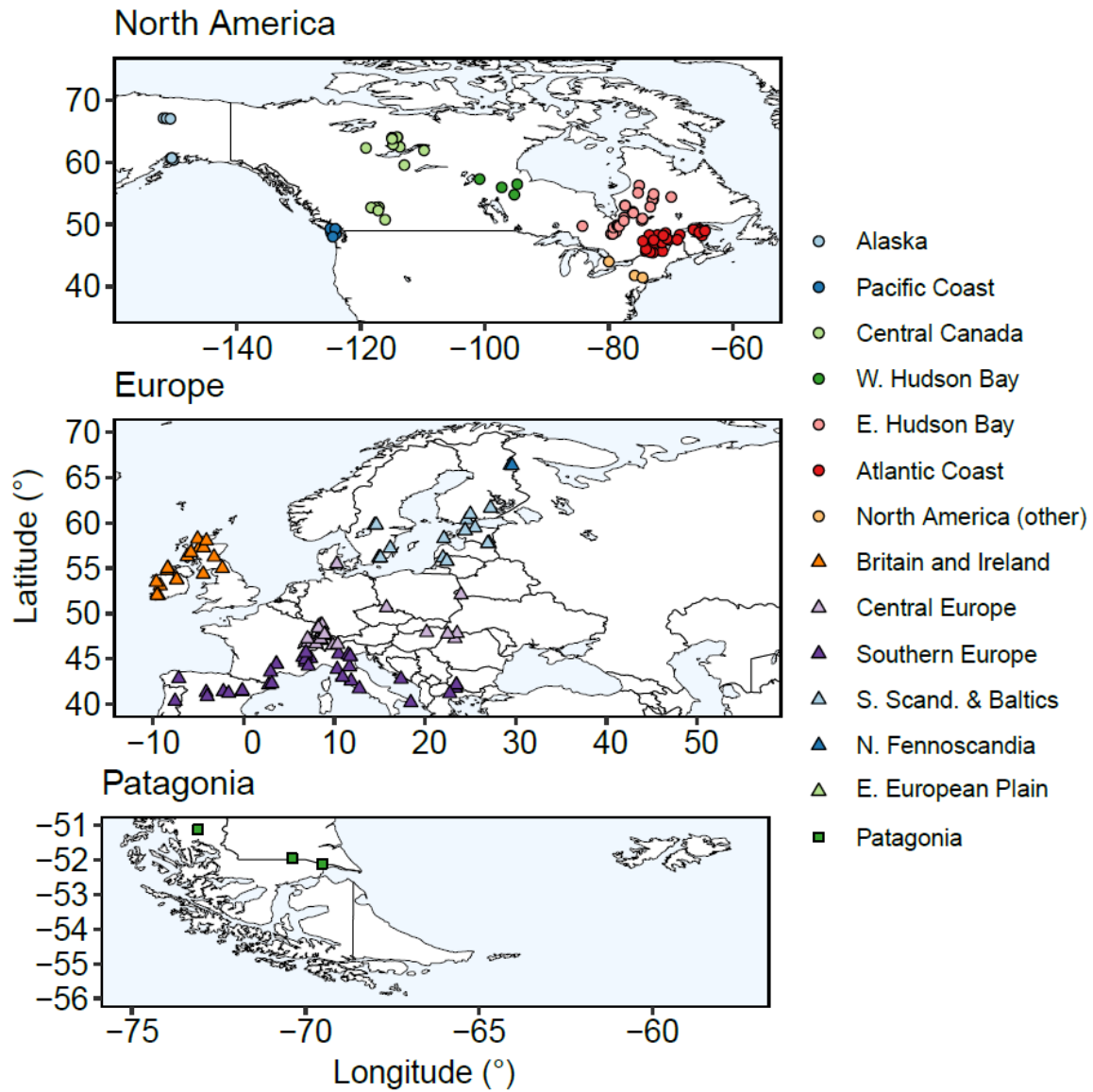


Figure C.1. Map of paleofire records representing burning in the wider landscape and their sub-region.

Table C.1. Metadata for all 221 macrocharcoal records. GCD = Global Charcoal Database.

#	Record	Charcoal size	Units	Lat (°N)	Long (°E)	Altitude (m)	Region	Sub-region	Country	Reference(s)	Contributor(s)
1	Horse Trail Fen	>250um	Particles cm-3	60.415	-150.902	101	North America	Alaska	USA	Jones, M.C., Wooller, M., Peteet, D.M., 2014. A deglacial and Holocene record of climate variability in south-central Alaska from stable oxygen isotopes and plant macrofossils in peat. <i>Quat. Sci. Rev.</i> 87, 1–11. https://doi.org/10.1016/J.QUASCIREV.2013.12.025	Miriam Jones
2	Toolik 1	>150um	Particles cm-3	68.62475	-149.596	715	North America	Alaska	USA	Galka, M., Swindles, G.T., Szal, M., Fulweber, R., Feurdean, A., 2018. Response of plant communities to climate change during the late Holocene: Palaeoecological insights from peatlands in the Alaskan Arctic. <i>Ecol. Indic.</i> 85, 525–536. https://doi.org/10.1016/J.ECOLIND.2017.10.062 ; Taylor, L.S., Swindles, G.T., Morris, P.J., Galka, M., Green, S.M., 2019. Evidence for ecosystem state shifts in Alaskan continuous permafrost peatlands in response to recent warming. <i>Quat. Sci. Rev.</i> 207, 134–144. https://doi.org/10.1016/j.quascirev.2019.02.001	Angelica Feurdean
3	Toolik 2	>150um	Particles cm-3	68.62276	-149.6	724	North America	Alaska	USA	Galka, M., Swindles, G.T., Szal, M., Fulweber, R., Feurdean, A., 2018. Response of plant communities to climate change during the late Holocene: Palaeoecological insights from peatlands in the Alaskan Arctic. <i>Ecol. Indic.</i> 85, 525–536. https://doi.org/10.1016/J.ECOLIND.2017.10.062 ; Taylor, L.S., Swindles, G.T., Morris, P.J., Galka, M., Green, S.M., 2019. Evidence for ecosystem state shifts in Alaskan continuous permafrost peatlands in response to recent warming. <i>Quat. Sci. Rev.</i> 207, 134–144. https://doi.org/10.1016/j.quascirev.2019.02.001	Angelica Feurdean
4	Auassat	>125um	Particles cm-3	51.8136	-63.6919	466	North America	Atlantic Coast	Canada	Primeau, G., Garneau, M., 2021. Carbon accumulation in peatlands along a boreal to subarctic transect in eastern Canada. <i>Holocene</i> 31, 858–869. https://doi.org/10.1177/0959683620988031	Guillaume Primeau, Michelle Garneau
5	Baie	>125um	Particles cm-3	49.0966	-68.25	17	North America	Atlantic Coast	Canada	Magnan, G., Garneau, M., Payette, S., 2014. Holocene development of maritime ombrotrophic peatlands of the St. Lawrence North Shore in eastern Canada. <i>Quat. Res. (United States)</i> 82, 96–106. https://doi.org/10.1016/j.yqres.2014.04.016	Gabriel Magnan, Michelle Garneau
6	Baltic Bog	>120um	Particles cm-3	46.4083	-61.85	44	North America	Atlantic Coast	Canada	Peros, M., Chan, K., Magnan, G., Ponsford, L., Carroll, J., McCloskey, T., 2016. A 9600-year record of water table depth, vegetation and fire inferred from a raised peat bog, Prince Edward Island, Canadian Maritimes. <i>J. Quat. Sci.</i> 31, 512–525. https://doi.org/10.1002/JQS.2875	Matthew Peros
7	Bouleau	>125um	Particles cm-3	50.5239	-63.2073	108	North America	Atlantic Coast	Canada	Primeau, G., Garneau, M., 2021. Carbon accumulation in peatlands along a boreal to subarctic transect in eastern Canada. <i>Holocene</i> 31, 858–869. https://doi.org/10.1177/0959683620988031	Guillaume Primeau, Michelle Garneau
8	Gaillard 1	>0.5mm	Particles cm-3	50.11327	-68.8088	392	North America	Atlantic Coast	Canada	Unpublished	Gabriel Magnan, Michelle Garneau
9	Innu	>0.5mm	Particles cm-3	50.06864	-68.8123	400	North America	Atlantic Coast	Canada	Remy, C.C., Fouquemberg, C., Asselin, H., Andrieux, B., Magnan, G., Brossier, B., Grondin, P., Bergeron, Y., Talon, B., Girardin, M.P., Blarquez, O., Bajolle, L., Ali, A.A., 2018. Guidelines for the use and interpretation of palaeofire reconstructions based on various archives and proxies. <i>Quat.</i>	Gabriel Magnan, Michelle Garneau

										Sci. Rev. 193, 312–322. https://doi.org/10.1016/j.quascirev.2018.06.010	
10	Lac des Ilets	>0.5mm	Particles cm-3	48.19	-71.24	358	North America	Atlantic Coast	Canada	Simard, I., Morin, H., Lavoie, C., 2006. A millennial-scale reconstruction of spruce budworm abundance in Saguenay, Québec, Canada. <i>The Holocene</i> 16, 31–37. https://doi.org/10.1191/0959683606HL904RP	GCD
11	Lac-à-la-Tortue 1	>150um	Particles cm-3	46.54288	-72.615	125	North America	Atlantic Coast	Canada	Pilote, L.M., Garneau, M., Van Bellen, S., Lamothe, M., 2018. Multiproxy analysis of inception and development of the Lac-à-la-Tortue peatland complex, St Lawrence Lowlands, eastern Canada. <i>Boreas</i> 47, 1084–1101. https://doi.org/10.1111/bor.12337	Louis-Martin Pilote, Michelle Garneau
12	Lac-à-la-Tortue 2	>150um	Particles cm-3	46.54239	-72.615	125	North America	Atlantic Coast	Canada	Pilote, L.M., Garneau, M., Van Bellen, S., Lamothe, M., 2018. Multiproxy analysis of inception and development of the Lac-à-la-Tortue peatland complex, St Lawrence Lowlands, eastern Canada. <i>Boreas</i> 47, 1084–1101. https://doi.org/10.1111/bor.12337	Louis-Martin Pilote, Michelle Garneau
13	Lac-à-la-Tortue 3	>150um	Particles cm-3	46.54245	-72.6155	125	North America	Atlantic Coast	Canada	Pilote, L.M., Garneau, M., Van Bellen, S., Lamothe, M., 2018. Multiproxy analysis of inception and development of the Lac-à-la-Tortue peatland complex, St Lawrence Lowlands, eastern Canada. <i>Boreas</i> 47, 1084–1101. https://doi.org/10.1111/bor.12337	Louis-Martin Pilote, Michelle Garneau
14	Lebel	>0.5mm	Particles cm-3	49.0983	-68.2216	22	North America	Atlantic Coast	Canada	Magnan, G., Garneau, M., Payette, S., 2014. Holocene development of maritime ombrotrophic peatlands of the St. Lawrence North Shore in eastern Canada. <i>Quat. Res. (United States)</i> 82, 96–106. https://doi.org/10.1016/j.yqres.2014.04.016	Gabriel Magnan, Michelle Garneau
15	Manic	>125um	Particles cm-3	49.1183	-68.305	22	North America	Atlantic Coast	Canada	Magnan, G., Garneau, M., Payette, S., 2014. Holocene development of maritime ombrotrophic peatlands of the St. Lawrence North Shore in eastern Canada. <i>Quat. Res. (United States)</i> 82, 96–106. https://doi.org/10.1016/j.yqres.2014.04.016	Gabriel Magnan, Michelle Garneau
16	Mista	>125um	Particles cm-3	50.8059	-63.3432	372	North America	Atlantic Coast	Canada	Primeau, G., Garneau, M., 2021. Carbon accumulation in peatlands along a boreal to subarctic transect in eastern Canada. <i>Holocene</i> 31, 858–869. https://doi.org/10.1177/0959683620988031	Guillaume Primeau, Michelle Garneau
17	Morts	>0.5mm	Particles cm-3	50.2633	-63.6683	14	North America	Atlantic Coast	Canada	Magnan, G., Garneau, M., Payette, S., 2014. Holocene development of maritime ombrotrophic peatlands of the St. Lawrence North Shore in eastern Canada. <i>Quat. Res. (United States)</i> 82, 96–106. https://doi.org/10.1016/j.yqres.2014.04.016	Gabriel Magnan, Michelle Garneau
18	Plaine	>0.5mm	Particles cm-3	50.275	-63.5383	34	North America	Atlantic Coast	Canada	Magnan, G., Garneau, M., Payette, S., 2014. Holocene development of maritime ombrotrophic peatlands of the St. Lawrence North Shore in eastern Canada. <i>Quat. Res. (United States)</i> 82, 96–106. https://doi.org/10.1016/j.yqres.2014.04.016	Gabriel Magnan, Michelle Garneau
19	Romaine	>0.5mm	Particles cm-3	50.2947	-63.7157	24	North America	Atlantic Coast	Canada	Magnan, G., Garneau, M., Payette, S., 2014. Holocene development of maritime ombrotrophic peatlands of the St. Lawrence North Shore in eastern Canada. <i>Quat. Res. (United States)</i> 82, 96–106. https://doi.org/10.1016/j.yqres.2014.04.016	Gabriel Magnan, Michelle Garneau
20	Anzac	>1mm	Particles cm-3	56.47194	-111.043	497	North America	Central Canada	Canada	Magnan, G., van Bellen, S., Davies, L., Froese, D., Garneau, M., Mullan-Boudreau, G., Zaccone, C., Shotyk, W., 2018. Impact of the Little Ice Age cooling and 20th century climate change on peatland vegetation dynamics in central and northern Alberta using a multi-proxy approach and high-	Gabriel Magnan, Michelle Garneau, Claudio Zaccone, William Shotyk, Simon van Bellen

21	Goldeye Lake Fen	>100um	Volume_%	52.45	-116.2	1390	North America	Central Canada	Canada	resolution peat chronologies. <i>Quat. Sci. Rev.</i> 185. https://doi.org/10.1016/j.quascirev.2018.01.015 Yu, Z., 2006. Holocene carbon accumulation of fen peatlands in boreal western Canada: A complex ecosystem response to climate variation and disturbance. <i>Ecosystems</i> 9, 1278–1288. https://doi.org/10.1007/s10021-006-0174-2	Zicheng Yu
22	Highway 3 peat	>100um	Particles cm-3	62.57795	-115.16	164	North America	Central Canada	Canada	Unpublished	Nicolas Pelletier
23	JPH4	>1mm	Particles cm-3	57.11222	-111.423	336	North America	Central Canada	Canada	Magnan, G., van Bellen, S., Davies, L., Froese, D., Garneau, M., Mullan-Boudreau, G., Zacccone, C., Shoty, W., 2018. Impact of the Little Ice Age cooling and 20th century climate change on peatland vegetation dynamics in central and northern Alberta using a multi-proxy approach and high-resolution peat chronologies. <i>Quat. Sci. Rev.</i> 185. https://doi.org/10.1016/j.quascirev.2018.01.015	Gabriel Magnan, Michelle Garneau, Claudio Zacccone, William Shoty, Simon van Bellen
24	Lutose MB-1	>1mm	Particles cm-3	59.48427	-117.177	303	North America	Central Canada	Canada	Heffernan, L., Estop-Aragonés, C., Knorr, K., Talbot, J., Olefeldt, D., 2020. Long-term impacts of permafrost thaw on carbon storage in peatlands: deep losses offset by surficial accumulation. <i>J. Geophys. Res. Biogeosciences</i> 125, e2019JG005501. https://doi.org/10.1029/2019JG005501	Liam Heffernan
25	Lutose P-1	>1mm	Particles cm-3	59.48449	-117.177	304	North America	Central Canada	Canada	Heffernan, L., Estop-Aragonés, C., Knorr, K., Talbot, J., Olefeldt, D., 2020. Long-term impacts of permafrost thaw on carbon storage in peatlands: deep losses offset by surficial accumulation. <i>J. Geophys. Res. Biogeosciences</i> 125, e2019JG005501. https://doi.org/10.1029/2019JG005501	Liam Heffernan
26	McKay	>1mm	Particles cm-3	57.22833	-111.7	302	North America	Central Canada	Canada	Magnan, G., van Bellen, S., Davies, L., Froese, D., Garneau, M., Mullan-Boudreau, G., Zacccone, C., Shoty, W., 2018. Impact of the Little Ice Age cooling and 20th century climate change on peatland vegetation dynamics in central and northern Alberta using a multi-proxy approach and high-resolution peat chronologies. <i>Quat. Sci. Rev.</i> 185. https://doi.org/10.1016/j.quascirev.2018.01.015	Gabriel Magnan, Michelle Garneau, Claudio Zacccone, William Shoty, Simon van Bellen
27	McMurray	>1mm	Particles cm-3	56.62778	-111.194	387	North America	Central Canada	Canada	Magnan, G., van Bellen, S., Davies, L., Froese, D., Garneau, M., Mullan-Boudreau, G., Zacccone, C., Shoty, W., 2018. Impact of the Little Ice Age cooling and 20th century climate change on peatland vegetation dynamics in central and northern Alberta using a multi-proxy approach and high-resolution peat chronologies. <i>Quat. Sci. Rev.</i> 185. https://doi.org/10.1016/j.quascirev.2018.01.015	Gabriel Magnan, Michelle Garneau, Claudio Zacccone, William Shoty, Simon van Bellen
28	Mildred	>1mm	Particles cm-3	56.93056	-111.475	334	North America	Central Canada	Canada	Magnan, G., van Bellen, S., Davies, L., Froese, D., Garneau, M., Mullan-Boudreau, G., Zacccone, C., Shoty, W., 2018. Impact of the Little Ice Age cooling and 20th century climate change on peatland vegetation dynamics in central and northern Alberta using a multi-proxy approach and high-resolution peat chronologies. <i>Quat. Sci. Rev.</i> 185. https://doi.org/10.1016/j.quascirev.2018.01.015	Gabriel Magnan, Michelle Garneau, Claudio Zacccone, William Shoty, Simon van Bellen
29	NWC1A	>140um	Particles cm-3	57.14778	-120.651	772	North America	Central Canada	Canada	Unpublished	Sanna Piilo, Minna Väiranta, Teemu Juselius
30	NWC2A	>140um	Particles cm-3	58.43194	-120.119	436	North America	Central Canada	Canada	Unpublished	Sanna Piilo, Minna Väiranta, Teemu Juselius
31	NWC2B	>140um	Particles cm-3	58.43194	-120.119	436	North America	Central Canada	Canada	Unpublished	Sanna Piilo, Minna Väiranta, Teemu Juselius

32	NWC4A	>140um	Particles cm-3	58.85222	-122.423	425	North America	Central Canada	Canada	Unpublished	Sanna Piilo, Minna Väiliranta, Teemu Juselius	
33	Scotty Creek	>100um	Particles cm-3	61.3053	-120.708	283	North America	Central Canada	Canada	Pelletier, N., Talbot, J., Olefeldt, D., Turetsky, M., Blodau, C., Sonnentag, O., Quinton, W.L., 2017. Influence of Holocene permafrost aggradation and thaw on the paleoecology and carbon storage of a peatland complex in northwestern Canada. <i>The Holocene</i> 27, 1391–1405. https://doi.org/10.1177/0959683617693899	Nicolas Pelletier	
34	Seba	>1mm	Particles cm-3	53.47611	-114.879	807	North America	Central Canada	Canada	Magnan, G., van Bellen, S., Davies, L., Froese, D., Garneau, M., Mullan-Boudreau, G., Zaccone, C., Shoty, W., 2018. Impact of the Little Ice Age cooling and 20th century climate change on peatland vegetation dynamics in central and northern Alberta using a multi-proxy approach and high-resolution peat chronologies. <i>Quat. Sci. Rev.</i> 185. https://doi.org/10.1016/j.quascirev.2018.01.015	Gabriel Magnan, Michelle Garneau, Claudio Zaccone, William Shoty, Simon van Bellen	
35	Tibbitt peatland	>100um	Particles cm-3	62.53652	-113.364	229	North America	Central Canada	Canada	Unpublished	Nicolas Pelletier	
36	Upper Pinto Fen	>100um	Volume_%	53.58333	-118.017	1310	North America	Central Canada	Canada	Yu, Z., Vitt, D.H., Campbell, I.D., Apps, M.J., 2003. Understanding Holocene peat accumulation pattern of continental fens in western Canada. <i>Can. J. Bot.</i> 81, 267–282. https://doi.org/10.1139/b03-016	Zicheng Yu	
37	Utikuma	>1mm	Particles cm-3	56.07639	-115.475	675	North America	Central Canada	Canada	Magnan, G., van Bellen, S., Davies, L., Froese, D., Garneau, M., Mullan-Boudreau, G., Zaccone, C., Shoty, W., 2018. Impact of the Little Ice Age cooling and 20th century climate change on peatland vegetation dynamics in central and northern Alberta using a multi-proxy approach and high-resolution peat chronologies. <i>Quat. Sci. Rev.</i> 185. https://doi.org/10.1016/j.quascirev.2018.01.015	Gabriel Magnan, Michelle Garneau, Claudio Zaccone, William Shoty, Simon van Bellen	
38	Abeille	>150um	Particles cm-3	54.1153	-72.5004	441	North America	East Bay	Hudson	Canada	van Bellen, S., Garneau, M., Ali, A.A., Lamarre, A., Robert, É.C., Magnan, G., Asnong, H., Pratte, S., 2013. Poor fen succession over ombrotrophic peat related to late Holocene increased surface wetness in subarctic Quebec, Canada. <i>J. Quat. Sci.</i> 28, 748–760. https://doi.org/10.1002/jqs.2670	Simon van Bellen, Michelle Garneau
39	Aéroport 1	>150um	Particles cm-3	54.10103	-72.5162	432	North America	East Bay	Hudson	Canada	van Bellen, S., Garneau, M., Ali, A.A., Lamarre, A., Robert, É.C., Magnan, G., Asnong, H., Pratte, S., 2013. Poor fen succession over ombrotrophic peat related to late Holocene increased surface wetness in subarctic Quebec, Canada. <i>J. Quat. Sci.</i> 28, 748–760. https://doi.org/10.1002/jqs.2670	Simon van Bellen, Michelle Garneau
40	Aéroport 2	>150um	Particles cm-3	54.10056	-72.5164	431	North America	East Bay	Hudson	Canada	van Bellen, S., Garneau, M., Ali, A.A., Lamarre, A., Robert, É.C., Magnan, G., Asnong, H., Pratte, S., 2013. Poor fen succession over ombrotrophic peat related to late Holocene increased surface wetness in subarctic Quebec, Canada. <i>J. Quat. Sci.</i> 28, 748–760. https://doi.org/10.1002/jqs.2670	Simon van Bellen, Michelle Garneau
41	Aéroport 1	>0.5mm	Particles cm-3	53.6535	-77.729	175	North America	East Bay	Hudson	Canada	Magnan, G., Lavoie, M., Payette, S., 2012. Impact of fire on long-term vegetation dynamics of ombrotrophic peatlands in northwestern Québec, Canada. <i>Quat. Res.</i> 77, 110–121. https://doi.org/10.1016/J.YQRES.2011.10.006	Gabriel Magnan, Michelle Garneau
42	Aéroport 2	>0.5mm	Particles cm-3	53.6536	-77.7263	175	North America	East Bay	Hudson	Canada	Magnan, G., Lavoie, M., Payette, S., 2012. Impact of fire on long-term vegetation dynamics of ombrotrophic peatlands in northwestern Québec, Canada. <i>Quat. Res.</i> 77, 110–121. https://doi.org/10.1016/J.YQRES.2011.10.006	Gabriel Magnan, Michelle Garneau
43	Amont	>180um	Particles cm-3	53.73	-74.38	289	North America	East Bay	Hudson	Canada	Paitre, C., 2008. Dynamique des marges forestières de milieux tourbeux du Haut-Boréal, Québec nordique. Université Laval. 1-131	GCD

44	Aval	>180um	Particles cm-3	53.41	-73.86	352	North America	East Bay	Hudson	Canada	Paitre, C., 2008. Dynamique des marges forestières de milieux tourbeux du Haut-Boréal, Québec nordique. Université Laval. 1-131	GCD
45	Casa 1	>0.5mm	Particles cm-3	49.55183	-78.9862	270	North America	East Bay	Hudson	Canada	Beaulne, J., Boucher, É., Garneau, M., Magnan, G., 2021a. Paludification reduces black spruce growth rate but does not alter tree water use efficiency in Canadian boreal forested peatlands. <i>For. Ecosyst.</i> 8. https://doi.org/10.1186/s40663-021-00307-x ; Beaulne, J., Garneau, M., Magnan, G., Boucher, É., 2021b. Peat deposits store more carbon than trees in forested peatlands of the boreal biome. <i>Sci. Rep.</i> 11, 1–11. https://doi.org/10.1038/s41598-021-82004-x	Joannie Beaulne, Michelle Garneau
46	Casa 2	>0.5mm	Particles cm-3	49.55201	-78.9867	270	North America	East Bay	Hudson	Canada	Beaulne, J., Boucher, É., Garneau, M., Magnan, G., 2021a. Paludification reduces black spruce growth rate but does not alter tree water use efficiency in Canadian boreal forested peatlands. <i>For. Ecosyst.</i> 8. https://doi.org/10.1186/s40663-021-00307-x ; Beaulne, J., Garneau, M., Magnan, G., Boucher, É., 2021b. Peat deposits store more carbon than trees in forested peatlands of the boreal biome. <i>Sci. Rep.</i> 11, 1–11. https://doi.org/10.1038/s41598-021-82004-x	Joannie Beaulne, Michelle Garneau
47	Casa 3	>0.5mm	Particles cm-3	49.55229	-78.9872	270	North America	East Bay	Hudson	Canada	Beaulne, J., Boucher, É., Garneau, M., Magnan, G., 2021a. Paludification reduces black spruce growth rate but does not alter tree water use efficiency in Canadian boreal forested peatlands. <i>For. Ecosyst.</i> 8. https://doi.org/10.1186/s40663-021-00307-x ; Beaulne, J., Garneau, M., Magnan, G., Boucher, É., 2021b. Peat deposits store more carbon than trees in forested peatlands of the boreal biome. <i>Sci. Rep.</i> 11, 1–11. https://doi.org/10.1038/s41598-021-82004-x	Joannie Beaulne, Michelle Garneau
48	Cheinu 1	>212um	Particles cm-3	52.647	-72.1926	462	North America	East Bay	Hudson	Canada	Robitaille, M., Garneau, M., Bellen, S. van, Sanderson, N.K., 2021. Long-term and recent ecohydrological dynamics of patterned peatlands in north-central Quebec (Canada). <i>Holocene</i> 31, 844–857. https://doi.org/10.1177/0959683620988051	Mylène Robitaille, Michelle Garneau
49	Cheinu 2	>212um	Particles cm-3	52.6458	-72.1912	462	North America	East Bay	Hudson	Canada	Robitaille, M., Garneau, M., Bellen, S. van, Sanderson, N.K., 2021. Long-term and recent ecohydrological dynamics of patterned peatlands in north-central Quebec (Canada). <i>Holocene</i> 31, 844–857. https://doi.org/10.1177/0959683620988051	Mylène Robitaille, Michelle Garneau
50	Cheinu 3	>212um	Particles cm-3	52.6477	-72.1932	462	North America	East Bay	Hudson	Canada	Robitaille, M., Garneau, M., Bellen, S. van, Sanderson, N.K., 2021. Long-term and recent ecohydrological dynamics of patterned peatlands in north-central Quebec (Canada). <i>Holocene</i> 31, 844–857. https://doi.org/10.1177/0959683620988051	Mylène Robitaille, Michelle Garneau
51	Kuujuarapik 2	>140um	Particles cm-3	55.22636	-77.6966	100	North America	East Bay	Hudson	Canada	Piilo, S.R., Zhang, H., Garneau, M., Gallego-Sala, A., Amesbury, M.J., Väiliranta, M.M., 2019. Recent peat and carbon accumulation following the Little Ice Age in northwestern Québec, Canada. <i>Environ. Res. Lett.</i> 14. https://doi.org/10.1088/1748-9326/ab11ec	Sanna Piilo
52	Lac Le Caron 1	>355um	Particles cm-3	52.29261	-75.8305	248	North America	East Bay	Hudson	Canada	van Bellen, S., Garneau, M., Ali, A.A., Bergeron, Y., 2012. Did fires drive Holocene carbon sequestration in boreal ombrotrophic peatlands of eastern Canada? <i>Quat. Res. (United States)</i> 78, 50–59. https://doi.org/10.1016/j.yqres.2012.03.009	Simon van Bellen, Michelle Garneau

53	Lac Le Caron 2	>355um	Particles cm-3	52.29453	-75.8408	254	North America	East Bay	Hudson	Canada	van Bellen, S., Garneau, M., Ali, A.A., Bergeron, Y., 2012. Did fires drive Holocene carbon sequestration in boreal ombrotrophic peatlands of eastern Canada? <i>Quat. Res. (United States)</i> 78, 50–59. https://doi.org/10.1016/j.yqres.2012.03.009	Simon van Bellen, Michelle Garneau
54	Lili 2	>0.5mm	Particles cm-3	49.172	-79.3695	317	North America	East Bay	Hudson	Canada	Magnan, G., Garneau, M., Le Stum-Boivin, É., Grondin, P., Bergeron, Y., 2020. Long-Term Carbon Sequestration in Boreal Forested Peatlands in Eastern Canada. <i>Ecosystems</i> 23. https://doi.org/10.1007/s10021-020-00483-x	Gabriel Magnan, Michelle Garneau
55	Lili 3	>0.5mm	Particles cm-3	49.1719	-79.3691	317	North America	East Bay	Hudson	Canada	Magnan, G., Garneau, M., Le Stum-Boivin, É., Grondin, P., Bergeron, Y., 2020. Long-Term Carbon Sequestration in Boreal Forested Peatlands in Eastern Canada. <i>Ecosystems</i> 23. https://doi.org/10.1007/s10021-020-00483-x	Gabriel Magnan, Michelle Garneau
56	Misask 1	>212um	Particles cm-3	52.7248	-72.2128	475	North America	East Bay	Hudson	Canada	Robitaille, M., Garneau, M., Bellen, S. van, Sanderson, N.K., 2021. Long-term and recent ecohydrological dynamics of patterned peatlands in north-central Quebec (Canada). <i>Holocene</i> 31, 844–857. https://doi.org/10.1177/0959683620988051	Mylène Robitaille, Michelle Garneau
57	Misask 2	>212um	Particles cm-3	52.7253	-72.2121	475	North America	East Bay	Hudson	Canada	Robitaille, M., Garneau, M., Bellen, S. van, Sanderson, N.K., 2021. Long-term and recent ecohydrological dynamics of patterned peatlands in north-central Quebec (Canada). <i>Holocene</i> 31, 844–857. https://doi.org/10.1177/0959683620988051	Mylène Robitaille, Michelle Garneau
58	Misask 3	>212um	Particles cm-3	52.7234	-72.2155	475	North America	East Bay	Hudson	Canada	Robitaille, M., Garneau, M., Bellen, S. van, Sanderson, N.K., 2021. Long-term and recent ecohydrological dynamics of patterned peatlands in north-central Quebec (Canada). <i>Holocene</i> 31, 844–857. https://doi.org/10.1177/0959683620988051	Mylène Robitaille, Michelle Garneau
59	Mosaik 1	>355um	Particles cm-3	51.98569	-75.3854	300	North America	East Bay	Hudson	Canada	van Bellen, S., Garneau, M., Ali, A.A., Bergeron, Y., 2012. Did fires drive Holocene carbon sequestration in boreal ombrotrophic peatlands of eastern Canada? <i>Quat. Res. (United States)</i> 78, 50–59. https://doi.org/10.1016/j.yqres.2012.03.009	Simon van Bellen, Michelle Garneau
60	Mosaik 2	>355um	Particles cm-3	51.98461	-75.4184	302	North America	East Bay	Hudson	Canada	van Bellen, S., Garneau, M., Ali, A.A., Bergeron, Y., 2012. Did fires drive Holocene carbon sequestration in boreal ombrotrophic peatlands of eastern Canada? <i>Quat. Res. (United States)</i> 78, 50–59. https://doi.org/10.1016/j.yqres.2012.03.009	Simon van Bellen, Michelle Garneau
61	Ours 1	>150um	Particles cm-3	54.04978	-72.4541	458	North America	East Bay	Hudson	Canada	van Bellen, S., Garneau, M., Ali, A.A., Lamarre, A., Robert, É.C., Magnan, G., Asnong, H., Pratte, S., 2013. Poor fen succession over ombrotrophic peat related to late Holocene increased surface wetness in subarctic Quebec, Canada. <i>J. Quat. Sci.</i> 28, 748–760. https://doi.org/10.1002/jqs.2670	Simon van Bellen, Michelle Garneau
62	Ours 4	>150um	Particles cm-3	54.04881	-72.456	459	North America	East Bay	Hudson	Canada	van Bellen, S., Garneau, M., Ali, A.A., Lamarre, A., Robert, É.C., Magnan, G., Asnong, H., Pratte, S., 2013. Poor fen succession over ombrotrophic peat related to late Holocene increased surface wetness in subarctic Quebec, Canada. <i>J. Quat. Sci.</i> 28, 748–760. https://doi.org/10.1002/jqs.2670	Simon van Bellen, Michelle Garneau
63	Radisson A	>0.5mm	Particles cm-3	53.7244	-77.7031	174	North America	East Bay	Hudson	Canada	Magnan, G., Lavoie, M., Payette, S., 2012. Impact of fire on long-term vegetation dynamics of ombrotrophic peatlands in northwestern Québec, Canada. <i>Quat. Res.</i> 77, 110–121. https://doi.org/10.1016/J.YQRES.2011.10.006	Gabriel Magnan, Michelle Garneau
64	Ring of Fire, Ontario	>150um	Particles cm-3	52.49597	-86.234	185	North America	East Bay	Hudson	Canada	Unpublished	Marissa Davies

65	Sterne 1	>355um	Particles cm-3	52.04539	-75.1589	308	North America	East Bay	Hudson	Canada	van Bellen, S., Garneau, M., Ali, A.A., Bergeron, Y., 2012. Did fires drive Holocene carbon sequestration in boreal ombrotrophic peatlands of eastern Canada? Quat. Res. (United States) 78, 50–59. https://doi.org/10.1016/j.yqres.2012.03.009	Simon van Bellen, Michelle Garneau
66	Sterne 2	>355um	Particles cm-3	52.04542	-75.1821	304	North America	East Bay	Hudson	Canada	van Bellen, S., Garneau, M., Ali, A.A., Bergeron, Y., 2012. Did fires drive Holocene carbon sequestration in boreal ombrotrophic peatlands of eastern Canada? Quat. Res. (United States) 78, 50–59. https://doi.org/10.1016/j.yqres.2012.03.009	Simon van Bellen, Michelle Garneau
67	Villebois 1	>0.5mm	Particles cm-3	49.4211	-79.003	272	North America	East Bay	Hudson	Canada	Magnan, G., Garneau, M., Le Stum-Boivin, É., Grondin, P., Bergeron, Y., 2020. Long-Term Carbon Sequestration in Boreal Forested Peatlands in Eastern Canada. Ecosystems 23. https://doi.org/10.1007/s10021-020-00483-x	Gabriel Magnan, Michelle Garneau
68	Villebois 3	>0.5mm	Particles cm-3	49.42	-79.0028	272	North America	East Bay	Hudson	Canada	Magnan, G., Garneau, M., Le Stum-Boivin, É., Grondin, P., Bergeron, Y., 2020. Long-Term Carbon Sequestration in Boreal Forested Peatlands in Eastern Canada. Ecosystems 23. https://doi.org/10.1007/s10021-020-00483-x	Gabriel Magnan, Michelle Garneau
69	Great Dismal Swamp 1	>125um	Particles cm-3	36.53593	-76.5241	15	North America	Other America	North	USA	Jones, M.C., Willard, D.A., and Hoefke, K.E., 2022, Charcoal data from four sites in Great Dismal Swamp National Wildlife Refuge - August 2022: U.S. Geological Survey data release, https://doi.org/10.5066/P9LYLGEF	Miriam Jones, Debra Willard
70	Great Dismal Swamp 2	>125um	Particles cm-3	36.56077	-76.4917	6	North America	Other America	North	USA	Jones, M.C., Willard, D.A., and Hoefke, K.E., 2022, Charcoal data from four sites in Great Dismal Swamp National Wildlife Refuge - August 2022: U.S. Geological Survey data release, https://doi.org/10.5066/P9LYLGEF	Miriam Jones, Debra Willard
71	Great Dismal Swamp 3	>150um	Particles cm-3	36.52924	-76.5256	23	North America	Other America	North	USA	Jones, M.C., Willard, D.A., and Hoefke, K.E., 2022, Charcoal data from four sites in Great Dismal Swamp National Wildlife Refuge - August 2022: U.S. Geological Survey data release, https://doi.org/10.5066/P9LYLGEF	Miriam Jones, Debra Willard
72	Great Dismal Swamp 4	>125um	Particles cm-3	36.58018	-76.4101	20	North America	Other America	North	USA	Jones, M.C., Willard, D.A., and Hoefke, K.E., 2022, Charcoal data from four sites in Great Dismal Swamp National Wildlife Refuge - August 2022: U.S. Geological Survey data release, https://doi.org/10.5066/P9LYLGEF	Miriam Jones, Debra Willard
73	Polygon mire trough	>1mm	Particles cm-3	74.459	-121.04	89	North America	Other America	North	Canada	Sim, T.G., Swindles, G.T., Morris, P.J., Galka, M., Mullan, D., Galloway, J.M., 2019. Pathways for Ecological Change in Canadian High Arctic Wetlands Under Rapid Twentieth Century Warming. Geophys. Res. Lett. 46, 4726–4737. https://doi.org/10.1029/2019GL082611	Thomas Sim, Mariusz Galka
74	Swan Lake	>125um	Particles cm-3	42.341	-112.043	1454	North America	Other America	North	USA	Bright, R.C., 1966. Pollen and seed stratigraphy of Swan Lake, southeastern Idaho: Its relation to regional vegetation history and to Lake Bonneville history. Tebiwa 9(2), 1–47.	Lysanna Anderson, David Wahl
75	Tannersville Bog	>100um	Volume_%	41.0382	-75.2658	277	North America	Other America	North	USA	Cai, S., Yu, Z., 2011. Response of a warm temperate peatland to Holocene climate change in northeastern Pennsylvania. Quat. Res. 75. https://doi.org/10.1016/j.yqres.2011.01.003	Zicheng Yu
76	Wylde Lake Bog	>100um	Particles cm-3	43.90497	-80.4072	481	North America	Other America	North	Canada	Shiller, J., 2012. Factors Affecting Holocene Carbon Accumulation in a Peatland in Southern Ontario. Unpublished MSc thesis, University of Toronto.	Jennifer Shiller, Sarah Finkelstein
77	Anderson Fen	>150um	Particles cm-3	49.735	-125.193	554	North America	Pacific Coast		Canada	Lacourse, T., Adeleye, M.A., Stewart, J.R., 2019. Peatland formation, succession and carbon accumulation at a mid-elevation poor fen in Pacific Canada. Holocene 29, 1694–1707. https://doi.org/10.1177/0959683619862041	Terri Lacourse
78	Grant's Bog	>150um	Particles cm-3	49.7883	-125.127	80	North America	Pacific Coast		Canada	Lacourse, T., Adeleye, M.A., Stewart, J.R., 2019. Peatland formation, succession and carbon accumulation at a mid-elevation poor fen in Pacific Canada. Holocene 29, 1694–1707. https://doi.org/10.1177/0959683619862041	Terri Lacourse

79	Port McNeill Bog	>150um	Particles cm-3	50.5725	-127.072	93	North America	Pacific Coast	Canada	Lacourse, T., Davies, M.A., 2015. A multi-proxy peat study of Holocene vegetation history, bog development, and carbon accumulation on northern Vancouver Island, Pacific coast of Canada. <i>Holocene</i> 25. https://doi.org/10.1177/0959683615580201	Terri Lacourse
80	111_1	>180um	mm2/cm3	59.91624	-96.9438	226	North America	West Hudson Bay	Canada	Camill, P., Umbanhowar, C.E., Geiss, C., Edlund, M.B., Hobbs, W.O., Dupont, A., Doyle-Capitman, C., Ramos, M., 2017. The initiation and development of small peat-forming ecosystems adjacent to lakes in the north central Canadian low arctic during the Holocene. <i>J. Geophys. Res. Biogeosciences</i> 122, 1672–1688. https://doi.org/10.1002/2016JG003662	Philip Camill
81	111_2	>180um	mm2/cm3	59.92032	-96.9606	228	North America	West Hudson Bay	Canada	Camill, P., Umbanhowar, C.E., Geiss, C., Edlund, M.B., Hobbs, W.O., Dupont, A., Doyle-Capitman, C., Ramos, M., 2017. The initiation and development of small peat-forming ecosystems adjacent to lakes in the north central Canadian low arctic during the Holocene. <i>J. Geophys. Res. Biogeosciences</i> 122, 1672–1688. https://doi.org/10.1002/2016JG003662	Philip Camill
82	150_1	>180um	mm2/cm3	59.87827	-98.1397	302	North America	West Hudson Bay	Canada	Camill, P., Umbanhowar, C.E., Geiss, C., Edlund, M.B., Hobbs, W.O., Dupont, A., Doyle-Capitman, C., Ramos, M., 2017. The initiation and development of small peat-forming ecosystems adjacent to lakes in the north central Canadian low arctic during the Holocene. <i>J. Geophys. Res. Biogeosciences</i> 122, 1672–1688. https://doi.org/10.1002/2016JG003662	Philip Camill
83	150_2	>180um	mm2/cm3	59.87862	-98.1413	306	North America	West Hudson Bay	Canada	Camill, P., Umbanhowar, C.E., Geiss, C., Edlund, M.B., Hobbs, W.O., Dupont, A., Doyle-Capitman, C., Ramos, M., 2017. The initiation and development of small peat-forming ecosystems adjacent to lakes in the north central Canadian low arctic during the Holocene. <i>J. Geophys. Res. Biogeosciences</i> 122, 1672–1688. https://doi.org/10.1002/2016JG003662	Philip Camill
84	150_3	>180um	mm2/cm3	59.88284	-98.1408	300	North America	West Hudson Bay	Canada	Camill, P., Umbanhowar, C.E., Geiss, C., Edlund, M.B., Hobbs, W.O., Dupont, A., Doyle-Capitman, C., Ramos, M., 2017. The initiation and development of small peat-forming ecosystems adjacent to lakes in the north central Canadian low arctic during the Holocene. <i>J. Geophys. Res. Biogeosciences</i> 122, 1672–1688. https://doi.org/10.1002/2016JG003662	Philip Camill
85	396_1	>180um	mm2/cm3	59.56897	-98.5578	318	North America	West Hudson Bay	Canada	Camill, P., Umbanhowar, C.E., Geiss, C., Edlund, M.B., Hobbs, W.O., Dupont, A., Doyle-Capitman, C., Ramos, M., 2017. The initiation and development of small peat-forming ecosystems adjacent to lakes in the north central Canadian low arctic during the Holocene. <i>J. Geophys. Res. Biogeosciences</i> 122, 1672–1688. https://doi.org/10.1002/2016JG003662	Philip Camill
86	396_2	>180um	mm2/cm3	59.57126	-98.55	318	North America	West Hudson Bay	Canada	Camill, P., Umbanhowar, C.E., Geiss, C., Edlund, M.B., Hobbs, W.O., Dupont, A., Doyle-Capitman, C., Ramos, M., 2017. The initiation and development of small peat-forming ecosystems adjacent to lakes in the north central Canadian low arctic during the Holocene. <i>J. Geophys. Res. Biogeosciences</i> 122, 1672–1688. https://doi.org/10.1002/2016JG003662	Philip Camill
87	396_3	>180um	mm2/cm3	59.57897	-98.5682	317	North America	West Hudson Bay	Canada	Camill, P., Umbanhowar, C.E., Geiss, C., Edlund, M.B., Hobbs, W.O., Dupont, A., Doyle-Capitman, C., Ramos, M., 2017. The initiation and development of small peat-forming ecosystems adjacent to lakes in the north central Canadian low arctic during the Holocene. <i>J. Geophys. Res. Biogeosciences</i> 122, 1672–1688. https://doi.org/10.1002/2016JG003662	Philip Camill

88	614_1	>180um	mm2/cm3	59.32425	-97.2909	271	North America	West Hudson Bay	Canada	2017. The initiation and development of small peat-forming ecosystems adjacent to lakes in the north central Canadian low arctic during the Holocene. <i>J. Geophys. Res. Biogeosciences</i> 122, 1672–1688. https://doi.org/10.1002/2016JG003662	Philip Camill
89	630_1	>180um	mm2/cm3	59.31213	-98.0883	273	North America	West Hudson Bay	Canada	Camill, P., Umbanhowar, C.E., Geiss, C., Edlund, M.B., Hobbs, W.O., Dupont, A., Doyle-Capitman, C., Ramos, M., 2017. The initiation and development of small peat-forming ecosystems adjacent to lakes in the north central Canadian low arctic during the Holocene. <i>J. Geophys. Res. Biogeosciences</i> 122, 1672–1688. https://doi.org/10.1002/2016JG003662	Philip Camill
90	630_2	>180um	mm2/cm3	59.31198	-98.0922	288	North America	West Hudson Bay	Canada	Camill, P., Umbanhowar, C.E., Geiss, C., Edlund, M.B., Hobbs, W.O., Dupont, A., Doyle-Capitman, C., Ramos, M., 2017. The initiation and development of small peat-forming ecosystems adjacent to lakes in the north central Canadian low arctic during the Holocene. <i>J. Geophys. Res. Biogeosciences</i> 122, 1672–1688. https://doi.org/10.1002/2016JG003662	Philip Camill
91	785_3	>180um	mm2/cm3	59.11116	-97.3935	235	North America	West Hudson Bay	Canada	Camill, P., Umbanhowar, C.E., Geiss, C., Edlund, M.B., Hobbs, W.O., Dupont, A., Doyle-Capitman, C., Ramos, M., 2017. The initiation and development of small peat-forming ecosystems adjacent to lakes in the north central Canadian low arctic during the Holocene. <i>J. Geophys. Res. Biogeosciences</i> 122, 1672–1688. https://doi.org/10.1002/2016JG003662	Philip Camill
92	785_4	>180um	mm2/cm3	59.10815	-97.3961	234	North America	West Hudson Bay	Canada	Camill, P., Umbanhowar, C.E., Geiss, C., Edlund, M.B., Hobbs, W.O., Dupont, A., Doyle-Capitman, C., Ramos, M., 2017. The initiation and development of small peat-forming ecosystems adjacent to lakes in the north central Canadian low arctic during the Holocene. <i>J. Geophys. Res. Biogeosciences</i> 122, 1672–1688. https://doi.org/10.1002/2016JG003662	Philip Camill
93	Ennadai Lake	>125um	Volume_%	60.83333	-101.55	320	North America	West Hudson Bay	Canada	Sannel, A.B.K., Kuhry, P., 2008. Long-term stability of permafrost in subarctic peat plateaus, west-central Canada. <i>The Holocene</i> 18, 589–601. https://doi.org/10.1177/0959683608089658	A. Britta K. Sannel
94	Joey Lake Core 12	>180um	mm2/cm3	55.47	-98.15	214	North America	West Hudson Bay	Canada	Camill, P., Barry, A., Williams, E., Andreassi, C., Limmer, J., Solick, D., 2009. Climate-vegetation-fire interactions and their impact on long-term carbon dynamics in a boreal peatland landscape in northern Manitoba, Canada. <i>J. Geophys. Res.</i> 114, G04017. https://doi.org/10.1029/2009JG001071	Philip Camill
95	Joey Lake Core 15	>180um	mm2/cm3	55.47	-98.15	215	North America	West Hudson Bay	Canada	Camill, P., Barry, A., Williams, E., Andreassi, C., Limmer, J., Solick, D., 2009. Climate-vegetation-fire interactions and their impact on long-term carbon dynamics in a boreal peatland landscape in northern Manitoba, Canada. <i>J. Geophys. Res.</i> 114, G04017. https://doi.org/10.1029/2009JG001071	Philip Camill
96	Joey Lake Core 17	>180um	mm2/cm3	55.47	-98.16	219	North America	West Hudson Bay	Canada	Camill, P., Barry, A., Williams, E., Andreassi, C., Limmer, J., Solick, D., 2009. Climate-vegetation-fire interactions and their	Philip Camill

97	Joey Lake Core 2	>180um	mm2/cm3	55.47	-98.16	219	North America	West Hudson Bay	Canada	Camill, P., Barry, A., Williams, E., Andreassi, C., Limmer, J., Solick, D., 2009. Climate-vegetation-fire interactions and their impact on long-term carbon dynamics in a boreal peatland landscape in northern Manitoba, Canada. J. Geophys. Res. 114, G04017. https://doi.org/10.1029/2009JG001071	Philip Camill
98	Joey Lake Core 5	>180um	mm2/cm3	55.46	-98.16	216	North America	West Hudson Bay	Canada	Camill, P., Barry, A., Williams, E., Andreassi, C., Limmer, J., Solick, D., 2009. Climate-vegetation-fire interactions and their impact on long-term carbon dynamics in a boreal peatland landscape in northern Manitoba, Canada. J. Geophys. Res. 114, G04017. https://doi.org/10.1029/2009JG001071	Philip Camill
99	Joey Lake Core 7	>180um	mm2/cm3	55.46	-98.16	215	North America	West Hudson Bay	Canada	Camill, P., Barry, A., Williams, E., Andreassi, C., Limmer, J., Solick, D., 2009. Climate-vegetation-fire interactions and their impact on long-term carbon dynamics in a boreal peatland landscape in northern Manitoba, Canada. J. Geophys. Res. 114, G04017. https://doi.org/10.1029/2009JG001071	Philip Camill
100	Selwyn Lake	>125um	Volume_%	59.88333	-104.2	400	North America	West Hudson Bay	Canada	Sannel, A.B.K., Kuhry, P., 2008. Long-term stability of permafrost in subarctic peat plateaus, west-central Canada. The Holocene 18, 589–601. https://doi.org/10.1177/0959683608089658	A. Britta K. Sannel
101	Shuttle 1	>180um	mm2/cm3	59.85905	-97.6408	276	North America	West Hudson Bay	Canada	Camill, P., Umbanhowar, C.E., Geiss, C., Edlund, M.B., Hobbs, W.O., Dupont, A., Doyle-Capitman, C., Ramos, M., 2017. The initiation and development of small peat-forming ecosystems adjacent to lakes in the north central Canadian low arctic during the Holocene. J. Geophys. Res. Biogeosciences 122, 1672–1688. https://doi.org/10.1002/2016JG003662	Philip Camill
102	Shuttle 2	>180um	mm2/cm3	59.86132	-97.6425	278	North America	West Hudson Bay	Canada	Camill, P., Umbanhowar, C.E., Geiss, C., Edlund, M.B., Hobbs, W.O., Dupont, A., Doyle-Capitman, C., Ramos, M., 2017. The initiation and development of small peat-forming ecosystems adjacent to lakes in the north central Canadian low arctic during the Holocene. J. Geophys. Res. Biogeosciences 122, 1672–1688. https://doi.org/10.1002/2016JG003662	Philip Camill
103	Shuttle 3	>180um	mm2/cm3	59.85978	-97.6388	276	North America	West Hudson Bay	Canada	Camill, P., Umbanhowar, C.E., Geiss, C., Edlund, M.B., Hobbs, W.O., Dupont, A., Doyle-Capitman, C., Ramos, M., 2017. The initiation and development of small peat-forming ecosystems adjacent to lakes in the north central Canadian low arctic during the Holocene. J. Geophys. Res. Biogeosciences 122, 1672–1688. https://doi.org/10.1002/2016JG003662	Philip Camill
104	Shuttle 4	>180um	mm2/cm3	59.85984	-97.6402	276	North America	West Hudson Bay	Canada	Camill, P., Umbanhowar, C.E., Geiss, C., Edlund, M.B., Hobbs, W.O., Dupont, A., Doyle-Capitman, C., Ramos, M., 2017. The initiation and development of small peat-forming ecosystems adjacent to lakes in the north central Canadian low arctic during the Holocene. J. Geophys. Res. Biogeosciences 122, 1672–1688. https://doi.org/10.1002/2016JG003662	Philip Camill
105	Unit 1	>180um	mm2/cm3	59.41562	-97.4839	293	North America	West Hudson Bay	Canada	Camill, P., Umbanhowar, C.E., Geiss, C., Edlund, M.B., Hobbs, W.O., Dupont, A., Doyle-Capitman, C., Ramos, M., 2017. The initiation and development of small peat-forming ecosystems adjacent to lakes in the north central Canadian low arctic during the Holocene. J. Geophys. Res.	Philip Camill

106	Unit 2	>180um	mm2/cm3	59.41594	-97.4839	293	North America	West Hudson Bay	Canada	Biogeosciences 122, 1672–1688. https://doi.org/10.1002/2016JG003662	Philip Camill
107	Unit 3	>180um	mm2/cm3	59.41553	-97.4841	294	North America	West Hudson Bay	Canada	Camill, P., Umbanhowar, C.E., Geiss, C., Edlund, M.B., Hobbs, W.O., Dupont, A., Doyle-Capitman, C., Ramos, M., 2017. The initiation and development of small peat-forming ecosystems adjacent to lakes in the north central Canadian low arctic during the Holocene. <i>J. Geophys. Res. Biogeosciences</i> 122, 1672–1688. https://doi.org/10.1002/2016JG003662	Philip Camill
108	Unit 4	>180um	mm2/cm3	59.41863	-97.4834	295	North America	West Hudson Bay	Canada	Camill, P., Umbanhowar, C.E., Geiss, C., Edlund, M.B., Hobbs, W.O., Dupont, A., Doyle-Capitman, C., Ramos, M., 2017. The initiation and development of small peat-forming ecosystems adjacent to lakes in the north central Canadian low arctic during the Holocene. <i>J. Geophys. Res. Biogeosciences</i> 122, 1672–1688. https://doi.org/10.1002/2016JG003662	Philip Camill
109	Abbeyknockmoy Bog	>125um	Macrofossil_%	53.44	-8.76	35	Europe	Britain and Ireland	Ireland	Barber, K.E., Chambers, F.M., Maddy, D., 2003. Holocene palaeoclimates from peat stratigraphy: macrofossil proxy climate records from three oceanic raised bogs in England and Ireland. <i>Quat. Sci. Rev.</i> 22, 521–539. https://doi.org/10.1016/S0277-3791(02)00185-3	GCD
110	Allt Connie	>125um	Particles cm-3	56.95049	-3.53695	474	Europe	Britain and Ireland	UK	Meewis P., Broothaerts N., Verstraeten G., 2018. Reconstructie van Holocene branden in de bovenloop van de Dee (Schotland). BSc thesis. KU Leuven (Department of Earth and Environmental Sciences)	Nils Broothaerts, Gert Verstraeten, Ward Swinnen
111	Ballyduff	>125um	mm2/cm3	53.08583	-7.99306	60	Europe	Britain and Ireland	Ireland	Unpublished	Fraser Mitchell
112	Cappanawalla	>100um	5-grade scale	53.1177	-9.19687	296	Europe	Britain and Ireland	Ireland	Feeser, I., O'Connell, M., 2009. Fresh insights into long-term changes in flora, vegetation, land use and soil erosion in the karstic environment of the Burren, western Ireland. <i>J. Ecol.</i> 97, 1083–1100. https://doi.org/10.1111/J.1365-2745.2009.01533.X	Ingo Feeser
113	Crawshaw Moss	>1mm	Count	53.91028	-1.8625	361	Europe	Britain and Ireland	UK	Unpublished	Graeme Swindles
114	Ellerside Moss	>1mm	Particles cm-3	54.2131	-2.9981	9	Europe	Britain and Ireland	UK	Unpublished	Gareth Thompson
115	Fallahogy	>100um	Macrofossil_%	54.91167	-6.56111	43	Europe	Britain and Ireland	UK	Roland, T.P., Caseldine, C.J., Charman, D.J., Turney, C.S.M., Amesbury, M.J., 2014. Was there a '4.2 ka event' in Great Britain and Ireland? Evidence from the peatland record. <i>Quat. Sci. Rev.</i> 83, 11–27. https://doi.org/https://doi.org/10.1016/j.quascirev.2013.10.024	Thomas Roland
116	Gortaclare	>100um	5-grade scale	53.07743	-9.04418	272	Europe	Britain and Ireland	Ireland	Feeser, I., O'Connell, M., 2009. Fresh insights into long-term changes in flora, vegetation, land use and soil erosion in the karstic environment of the Burren, western Ireland. <i>J. Ecol.</i> 97, 1083–1100. https://doi.org/10.1111/J.1365-2745.2009.01533.X	Ingo Feeser
117	Malham Tarn Moss	>125um	Particles cm-3	54.09639	-2.175	380	Europe	Britain and Ireland	UK	Turner, T.E., Swindles, G.T., Roucoux, K.H., 2014. Late Holocene ecohydrological and carbon dynamics of a UK raised bog: Impact of human activity and climate change.	Graeme Swindles

											Quat.	Sci.	Rev.	84.
118	Migneint A	>300um	Macrofossil_%	52.82	-3.82	457	Europe	Britain and Ireland	UK		https://doi.org/10.1016/j.quascirev.2013.10.030			GCD
119	Mongan Bog	>125um	Macrofossil_%	53.33	-7.93	42	Europe	Britain and Ireland	Ireland		Ellis, C.J., Tallis, J.H., 2001. Climatic Control of Peat Erosion in a North Wales Blanket Mire. <i>New Phytol.</i> 152, 313–324.			GCD
120	Mossdale Moor	>125um	Particles cm-3	54.30029	-2.31551	550	Europe	Britain and Ireland	UK		Barber, K.E., Chambers, F.M., Maddy, D., 2003. Holocene palaeoclimates from peat stratigraphy: macrofossil proxy climate records from three oceanic raised bogs in England and Ireland. <i>Quat. Sci. Rev.</i> 22, 521–539.			Julia Webb
121	Nichols Moss	>1mm	Particles cm-3	54.2351	-2.8741	20	Europe	Britain and Ireland	UK		https://doi.org/10.1016/S0277-3791(02)00185-3			Gareth Thompson
122	Oxenhope Moor	>125um	Particles cm-3	53.79376	-1.97795	430	Europe	Britain and Ireland	UK		McCarroll, J., Chambers, F.M., Webb, J.C., Thom, T., 2017. Application of palaeoecology for peatland conservation at Mossdale Moor, UK. <i>Quat. Int.</i> 432, 39–47.			Julia McCarroll
123	Rusland Moss	>1mm	Particles cm-3	54.2888	-3.0239	12	Europe	Britain and Ireland	UK		https://doi.org/10.1016/j.quaint.2014.12.068			Gareth Thompson
124	Sluggan	>100um	Macrofossil_%	54.76556	-6.29361	42	Europe	Britain and Ireland	UK		Unpublished			Thomas Roland
125	Bagno Kusowo	>100um	Particles cm-3	53.81639	16.58889	147	Europe	Central Europe	Poland		Roland, T.P., Caseldine, C.J., Charman, D.J., Turney, C.S.M., Amesbury, M.J., 2014. Was there a '4.2 ka event' in Great Britain and Ireland? Evidence from the peatland record. <i>Quat. Sci. Rev.</i> 83, 11–27.			Katarzyna Marcisz
126	Bagno Serebryskie	>1mm	Count	52.1244	23.526	173	Europe	Central Europe	Poland		https://doi.org/10.1016/j.quascirev.2013.10.024			Mariusz Gałka, Liene Aunina
127	Brockenbettmoor	>200um	Particles cm-3	51.78472	10.63361	930	Europe	Central Europe	Germany		Marcisz, K., Lamentowicz, M., Gałka, M., Colombaroli, D., Adolf, C., Tinner, W., 2019. Responses of vegetation and testate amoeba trait composition to fire disturbances in and around a bog in central European lowlands (northern Poland). <i>Quat. Sci. Rev.</i> 208, 129–139.			Vincent Robin
128	Eustach	>125um	Particles cm-3	50.89067	14.42843	387	Europe	Central Europe	Czech Republic		https://doi.org/10.1016/J.QUASCIREV.2019.02.003			Přemysl Bobek
129	Gazwa bog	>1mm	Particles cm-3	53.87256	21.21992	153.4	Europe	Central Europe	Poland		Gałka, M., Aunina, L., Feurdean, A., Hutchinson, S., Kołaczek, P., Apolinarska, K., 2017a. Rich fen development in CE Europe, resilience to climate change and human impact over the last ca. 3500 years. <i>Palaeogeogr. Palaeoclimatol. Palaeoecol.</i> 473, 57–72.			Mariusz Gałka
130	Jaczno Bog	>100um	Particles cm-3	54.27692	22.87631	177	Europe	Central Europe	Poland		Robinson, V., Knapp, H., Bork, H.R., Nelle, O., 2013. Complementary use of pedoanthracology and peat macro-charcoal analysis for fire history assessment: Illustration from Central Germany. <i>Quat. Int.</i> 289, 78–87.			Katarzyna Marcisz
											https://doi.org/10.1016/j.quaint.2012.03.031			
											Bobek, P., Svobodová, H.S., Werchan, B., Švarcová, M.G., Kuneš, P., 2018b. Human-induced changes in fire regime and subsequent alteration of the sandstone landscape of Northern Bohemia (Czech Republic). <i>Holocene</i> 28.			
											https://doi.org/10.1177/0959683617729443			
											Gałka, M., Lamentowicz, M., 2014. Sphagnum succession in a Baltic bog in central-eastern Europe over the last 6200 years and paleoecology of <i>Sphagnum contortum</i> . <i>Bryologist</i> 117, 22–36.			
											https://doi.org/10.1639/0007-2745-117.1.022			
											Marcisz, K., Kołaczek, P., Gałka, M., Diaconu, A.C., Lamentowicz, M., 2020. Exceptional hydrological stability of a Sphagnum-dominated peatland over the late Holocene. <i>Quat.</i>			

131	Kobert-Haut	>200um	Particles cm-3	49.05194	7.616667	930	Europe	Central Europe	France	Sci. Rev. 231, 106180. https://doi.org/10.1016/J.QUASCIREV.2020.106180	Vincent Robin
132	Machais	>200um	Particles cm-3	48.00608	6.963431	900	Europe	Central Europe	France	Gouriveau, E., Ruffaldi, P., Duchamp, L., Robin, V., Schnitzler, A., Walter-Simonnet, A.V., 2020. Holocene vegetation history in the Northern Vosges Mountains (NE France): Palynological, geochemical and sedimentological data. <i>Holocene</i> 30, 888–904. https://doi.org/10.1177/0959683620902229	Vincent Robin
133	Malá niva	>125um	Particles cm-3	48.91376	13.81606	753	Europe	Central Europe	Czech Republic	Unpublished	Přemysl Bobek
134	Mechacz Wielki bog	>1mm	Particles cm-3	54.33106	22.44203	187	Europe	Central Europe	Poland	Bobek, P., Svobodová-Svitavská, H., Pokorný, P., Šamonil, P., Kuneš, P., Kozáková, R., Abraham, V., Klínerová, T., Švarcová, M.G., Jamrichová, E., Krauseová, E., Wild, J., 2019. Divergent fire history trajectories in Central European temperate forests revealed a pronounced influence of broadleaved trees on fire dynamics. <i>Quat. Sci. Rev.</i> 222. https://doi.org/10.1016/j.quascirev.2019.105865	Mariusz Gałka
135	Molhasul Mare	>150um	Particles cm-3	46.59	22.76	1124	Europe	Central Europe	Romania	Gałka, M., Tobolski, K., Lamentowicz, Ł., Ersek, V., Jassey, V.E.J., van der Knaap, W.O., Lamentowicz, M., 2017b. Unveiling exceptional Baltic bog ecohydrology, autogenic succession and climate change during the last 2000 years in CE Europe using replicate cores, multi-proxy data and functional traits of testate amoebae. <i>Quat. Sci. Rev.</i> 156, 90–106. https://doi.org/10.1016/J.QUASCIREV.2016.11.034	Angelica Feurdean
136	Odersprungmoor	>1mm	Particles cm-3	51.8049	10.5679	810	Europe	Central Europe	Germany	Feurdean, A., Willis, K.J., 2008. The usefulness of a long-term perspective in assessing current forest conservation management in the Apuseni Natural Park, Romania. <i>For. Ecol. Manage.</i> 256, 421–430. https://doi.org/10.1016/j.foreco.2008.04.050	Mariusz Gałka, Klaus-Holger Knorr
137	Okna	>125um	Particles cm-3	50.53207	14.67593	277	Europe	Central Europe	Czech Republic	Gałka, M., Szal, M., Broder, T., Loisel, J., Knorr, K.H., 2019. Peatbog resilience to pollution and climate change over the past 2700 years in the Harz Mountains, Germany. <i>Ecol. Indic.</i> 97, 183–193. https://doi.org/10.1016/j.ecolind.2018.10.015	Přemysl Bobek
138	Orlovske vrsky	>125um	Particles cm-3	48.4693	17.06253	184	Europe	Central Europe	Slovakia	Bobek, P., Svobodová-Svitavská, H., Pokorný, P., Šamonil, P., Kuneš, P., Kozáková, R., Abraham, V., Klínerová, T., Švarcová, M.G., Jamrichová, E., Krauseová, E., Wild, J., 2019. Divergent fire history trajectories in Central European temperate forests revealed a pronounced influence of broadleaved trees on fire dynamics. <i>Quat. Sci. Rev.</i> 222. https://doi.org/10.1016/j.quascirev.2019.105865	Přemysl Bobek
139	Poiana Stiol	>150um	Particles cm-3	47.59	24.81	1520	Europe	Central Europe	Romania	Jamrichová, E., Bobek, P., Šolcová, A., Tkáč, P., Hédli, R., Valachovič, M., 2019. Lowland pine forests in the northwestern Pannonian Basin: between natural vegetation and modern plantations. <i>Reg. Environ. Chang.</i> 19, 2395–2409. https://doi.org/10.1007/s10113-019-01555-y	Angelica Feurdean
140	Polomovy dul	>125um	Particles cm-3	50.88287	14.3175	313	Europe	Central Europe	Czech Republic	Feurdean, A., Florescu, G., Vannièrè, B., Tanțău, I., O'Hara, R.B., Pfeiffer, M., Hutchinson, S.M., Gałka, M., Moskal-del Hoyo, M., Hickler, T., 2017. Fire has been an important driver of forest dynamics in the Carpathian Mountains during the Holocene. <i>For. Ecol. Manage.</i> 389, 15–26. https://doi.org/10.1016/j.foreco.2016.11.046	Přemysl Bobek
										Bobek, P., Svobodová-Svitavská, H., Pokorný, P., Šamonil, P., Kuneš, P., Kozáková, R., Abraham, V., Klínerová, T., Švarcová, M.G., Jamrichová, E., Krauseová, E., Wild, J., 2019. Divergent fire history trajectories in Central European temperate forests revealed a pronounced influence of	

141	Poselský rybník	>125um	Particles cm-3	50.5444	14.67537	274	Europe	Central Europe	Czech Republic	broadleaved trees on fire dynamics. Quat. Sci. Rev. 222. https://doi.org/10.1016/j.quascirev.2019.105865 Bobek, P., Svobodová-Svitavská, H., Pokorný, P., Šamonil, P., Kuneš, P., Kozáková, R., Abraham, V., Klínerová, T., Švarcová, M.G., Jamrichová, E., Krauseová, E., Wild, J., 2019. Divergent fire history trajectories in Central European temperate forests revealed a pronounced influence of broadleaved trees on fire dynamics. Quat. Sci. Rev. 222. https://doi.org/10.1016/j.quascirev.2019.105865	Přemysl Bobek
142	Pravčický dul	>125um	Particles cm-3	50.88424	14.29683	382	Europe	Central Europe	Czech Republic	Bobek, P., Svobodová-Svitavská, H., Pokorný, P., Šamonil, P., Kuneš, P., Kozáková, R., Abraham, V., Klínerová, T., Švarcová, M.G., Jamrichová, E., Krauseová, E., Wild, J., 2019. Divergent fire history trajectories in Central European temperate forests revealed a pronounced influence of broadleaved trees on fire dynamics. Quat. Sci. Rev. 222. https://doi.org/10.1016/j.quascirev.2019.105865	Přemysl Bobek
143	Puklina	>125um	Particles cm-3	50.93239	14.43977	386	Europe	Central Europe	Czech Republic	Bobek, P., Svobodová-Svitavská, H., Pokorný, P., Šamonil, P., Kuneš, P., Kozáková, R., Abraham, V., Klínerová, T., Švarcová, M.G., Jamrichová, E., Krauseová, E., Wild, J., 2019. Divergent fire history trajectories in Central European temperate forests revealed a pronounced influence of broadleaved trees on fire dynamics. Quat. Sci. Rev. 222. https://doi.org/10.1016/j.quascirev.2019.105865	Přemysl Bobek
144	Raseliniste Jizery	>125um	Particles cm-3	50.86171	15.30188	843	Europe	Central Europe	Czech Republic	Bobek, P., Svobodová-Svitavská, H., Pokorný, P., Šamonil, P., Kuneš, P., Kozáková, R., Abraham, V., Klínerová, T., Švarcová, M.G., Jamrichová, E., Krauseová, E., Wild, J., 2019. Divergent fire history trajectories in Central European temperate forests revealed a pronounced influence of broadleaved trees on fire dynamics. Quat. Sci. Rev. 222. https://doi.org/10.1016/j.quascirev.2019.105865	Přemysl Bobek
145	Riffelsbruch mire	>250um	Count	50.51667	6.3	596	Europe	Central Europe	Germany	Unpublished	Karsten Schitteck
146	Romincka Forest	>1mm	Particles cm-3	54.39028	22.705	153	Europe	Central Europe	Poland	Unpublished	Karina Apolinarska
147	Sint Agatha Rode-400	>0.5mm	Particles cm-3	50.78889	4.619444	30	Europe	Central Europe	Belgium	Broothaerts, N., Verstraeten, G., Kasse, C., Bohncke, S., Notebaert, B., Vandenberghe, J., 2014. Reconstruction and semi-quantification of human impact in the Dijle catchment, central Belgium: a palynological and statistical approach. Quat. Sci. Rev. 102, 96–110. https://doi.org/10.1016/J.QUASCIREV.2014.08.006	Renske Hoeyers, Gert Verstraeten
148	Sklarske udoli	>125um	Particles cm-3	49.14351	13.39533	810	Europe	Central Europe	Czech Republic	Kozáková, R., Bobek, P., Dreslerová, D., Abraham, V., Svobodová-Svitavská, H., 2021. The prehistory and early history of the Šumava Mountains (Czech Republic) as seen through anthropogenic pollen indicators and charcoal data. Holocene 31, 145–159. https://doi.org/10.1177/0959683620961484	Přemysl Bobek
149	Smauzy	>125um	Particles cm-3	49.19277	13.27098	1010	Europe	Central Europe	Czech Republic	Kozáková, R., Bobek, P., Dreslerová, D., Abraham, V., Svobodová-Svitavská, H., 2021. The prehistory and early history of the Šumava Mountains (Czech Republic) as seen through anthropogenic pollen indicators and charcoal data. Holocene 31, 145–159. https://doi.org/10.1177/0959683620961484	Přemysl Bobek
150	Stodthagen Forest	>200um	Particles cm-3	54.4197	10.0633	25	Europe	Central Europe	Germany	Robin, V., Rickert, B.-H., Nadeau, M.-J., Nelle, O., 2011. Assessing Holocene vegetation and fire history by a multiproxy approach: The case of Stodthagen Forest (northern	Vincent Robin

151	Tajga	>125um	Particles cm-3	50.0261	12.68036	817	Europe	Central Europe	Czech Republic	Germany). The Holocene 22, 337–346. https://doi.org/10.1177/0959683611423687 Bobek, P., Svobodová-Svitavská, H., Pokorný, P., Šamonil, P., Kuneš, P., Kozáková, R., Abraham, V., Klinerová, T., Švarcová, M.G., Jamrichová, E., Krauseová, E., Wild, J., 2019. Divergent fire history trajectories in Central European temperate forests revealed a pronounced influence of broadleaved trees on fire dynamics. Quat. Sci. Rev. 222. https://doi.org/10.1016/j.quascirev.2019.105865	Přemysl Bobek
152	Taul Muced	>150um	Particles cm-3	47.5739	25.7611	1340	Europe	Central Europe	Romania	Feurdean, A., Florescu, G., Vannièrè, B., Tanțău, I., O'Hara, R.B., Pfeiffer, M., Hutchinson, S.M., Gaika, M., Moskal-del Hoyo, M., Hickler, T., 2017. Fire has been an important driver of forest dynamics in the Carpathian Mountains during the Holocene. For. Ecol. Manage. 389, 15–26. https://doi.org/10.1016/j.foreco.2016.11.046	Angelica Feurdean
153	Turtul	>1mm	Particles cm-3	54.27917	23.07667	197	Europe	Central Europe	Poland	Unpublished	Karina Apolinarska
154	Velké ohbí	>125um	Particles cm-3	50.60406	16.12713	528	Europe	Central Europe	Czech Republic	Bobek, P., Svobodová-Svitavská, H., Pokorný, P., Šamonil, P., Kuneš, P., Kozáková, R., Abraham, V., Klinerová, T., Švarcová, M.G., Jamrichová, E., Krauseová, E., Wild, J., 2019. Divergent fire history trajectories in Central European temperate forests revealed a pronounced influence of broadleaved trees on fire dynamics. Quat. Sci. Rev. 222. https://doi.org/10.1016/j.quascirev.2019.105865	Přemysl Bobek
155	Vlcek	>125um	Particles cm-3	50.0398	12.73194	769	Europe	Central Europe	Czech Republic	Bobek, P., Svobodová-Svitavská, H., Pokorný, P., Šamonil, P., Kuneš, P., Kozáková, R., Abraham, V., Klinerová, T., Švarcová, M.G., Jamrichová, E., Krauseová, E., Wild, J., 2019. Divergent fire history trajectories in Central European temperate forests revealed a pronounced influence of broadleaved trees on fire dynamics. Quat. Sci. Rev. 222. https://doi.org/10.1016/j.quascirev.2019.105865	Přemysl Bobek
156	Zofinsky prales	>125um	Particles cm-3	48.66444	14.70535	785	Europe	Central Europe	Czech Republic	Bobek, P., Šamonil, P., Jamrichová, E., 2018a. Biotic controls on Holocene fire frequency in a temperate mountain forest, Czech Republic. J. Quat. Sci. 33, 892–904. https://doi.org/10.1002/JQS.3067	Přemysl Bobek
157	Holbicky	>125um	Particles cm-3	48.5112	17.10917	185	Europe	Central Europe	Slovakia	Jamrichová, E., Bobek, P., Šolcová, A., Tkáč, P., Hédl, R., Valachovič, M., 2019. Lowland pine forests in the northwestern Pannonian Basin: between natural vegetation and modern plantations. Reg. Environ. Chang. 19, 2395–2409. https://doi.org/10.1007/s10113-019-01555-y	Přemysl Bobek
158	Agrafenino	>125um	Particles cm-3	55.2341	36.3361	175	Europe	Eastern European Plain	Russia	Nizovtsev V.A., Novenko E.Yu., Erman N.M. et al., 2019. Holocene evolution of landscapes in the middle Protva River basin. Vestnik Moskovskogo universiteta. Seriya 5, Geografiya. Vol.1, 73-86.	Elena Novenko
159	Indico	>1mm	Particles cm-3	67.26694	49.88331	41	Europe	Eastern European Plain	Russia	Zhang, H., Gallego-Sala, A. V., Amesbury, M.J., Charman, D.J., Piilo, S.R., Väliranta, M.M., 2018. Inconsistent response of Arctic permafrost peatland carbon accumulation to warm climate phases. Global Biogeochem. Cycles 32, 1605–1620. https://doi.org/10.1029/2018GB005980	Hui Zhang, Minna Väliranta
160	Krivetsky Mokh	>125um	Particles cm-3	57.1046	32.35895	247	Europe	Eastern European Plain	Russia	Mazei, Y.A., Tsyganov, A.N., Bobrovsky, M. V., Mazei, N.G., Kupriyanov, D.A., Gaika, M., Rostanets, D. V., Khazanova, K.P., Stoiko, T.G., Pastukhova, Y.A., Fatynina, Y.A., Komarov, A.A., Babeshko, K. V., Makarova, A.D., Saldaev, D.A., Zazovskaya, E.P., Dobrovolskaya, M. V., Tiunov, A. V., 2020. Peatland development, vegetation history, climate change and human activity in the valdai uplands (Central european	Yuri Mazei, Dmitri Kupriyanov, Alexey Tiunov, Andrey Tsyganov, Natalia Mazei

161	Mostovoye	>125um	Particles cm-3	55.1419	40.9386	102	Europe	Eastern European Plain	Russia	Russia) during the holocene: A multi-proxy palaeoecological study. <i>Diversity</i> 12, 1–25. https://doi.org/10.3390/d12120462	Unpublished	Elena Novenko
162	Selikhovo	>250um	Particles cm-3	53.23	35.77	209	Europe	Eastern European Plain	Russia	Novenko, E.Y., Tsyganov, A.N., Rudenko, O. V., Volkova, E. V., Zuyganova, I.S., Babeshko, K. V., Olchev, A. V., Losbenev, N.I., Payne, R.J., Mazei, Y.A., 2016. Mid- and late-Holocene vegetation history, climate and human impact in the forest-steppe ecotone of European Russia: new data and a regional synthesis. <i>Biodivers. Conserv.</i> 25, 2453–2472. https://doi.org/10.1007/s10531-016-1051-8	Unpublished	Elena Novenko
163	Ustyany	>125um	Particles cm-3	60.85911	43.26733	150	Europe	Eastern European Plain	Russia	Unpublished	Unpublished	Elena Novenko
164	Yak2-A	>160um	Particles cm-3	61.69619	55.57433	140	Europe	Eastern European Plain	Russia	Barhoumi, C., Peyron, O., Joannin, S., Subetto, D., Kryshen, A., Drobyshev, I., Girardin, M.P., Brossier, B., Paradis, L., Pastor, T., Alleaume, S., Ali, A.A., 2019. Gradually increasing forest fire activity during the Holocene in the northern Ural region (Komi Republic, Russia): The Holocene 29, 1906–1920. https://doi.org/10.1177/0959683619865593	Unpublished	GCD
165	Gurasáhpi palsa 2	>1mm	Particles cm-3	68.3195	19.8576	379	Europe	Northern Fennoscandia	Sweden	Sim, T.G., Swindles, G.T., Morris, P.J., Baird, A.J., Cooper, C.L., Gallego-Sala, A. V., Charman, D.J., Roland, T.P., Borken, W., Mullan, D.J., Aquino-López, M.A., Gałka, M., 2021. Divergent responses of permafrost peatlands to recent climate change. <i>Environ. Res. Lett.</i> 16, 034001. https://doi.org/10.1088/1748-9326/abe00b	Unpublished	Thomas Sim, Mariusz Gałka
166	Lovozero	>140um	Particles cm-3	67.97939	35.06378	158	Europe	Northern Fennoscandia	Russia	Unpublished	Unpublished	Sanna Piilo
167	Maunuvuoma fen	>1mm	Particles cm-3	67.9567	19.9865	476	Europe	Northern Fennoscandia	Sweden	Sim, T.G., Swindles, G.T., Morris, P.J., Baird, A.J., Cooper, C.L., Gallego-Sala, A. V., Charman, D.J., Roland, T.P., Borken, W., Mullan, D.J., Aquino-López, M.A., Gałka, M., 2021. Divergent responses of permafrost peatlands to recent climate change. <i>Environ. Res. Lett.</i> 16, 034001. https://doi.org/10.1088/1748-9326/abe00b ; Gałka, M., Szal, M., Watson, E.J., Gallego-Sala, A., Amesbury, M.J., Charman, D.J., Roland, T.P., Edward Turner, T., Swindles, G.T., 2017b. Vegetation Succession, Carbon Accumulation and Hydrological Change in Subarctic Peatlands, Abisko, Northern Sweden. <i>Permafr. Periglac. Process.</i> 28, 589–604. https://doi.org/10.1002/ppp.1945	Unpublished	Thomas Sim, Mariusz Gałka
168	Rensjön palsa	>1mm	Particles cm-3	68.0868	19.8314	488	Europe	Northern Fennoscandia	Sweden	Sim, T.G., Swindles, G.T., Morris, P.J., Baird, A.J., Cooper, C.L., Gallego-Sala, A. V., Charman, D.J., Roland, T.P., Borken, W., Mullan, D.J., Aquino-López, M.A., Gałka, M., 2021. Divergent responses of permafrost peatlands to recent climate change. <i>Environ. Res. Lett.</i> 16, 034001. https://doi.org/10.1088/1748-9326/abe00b	Unpublished	Thomas Sim, Mariusz Gałka
169	Ribasvuomuš bog	>1mm	Particles cm-3	68.3657	19.5841	379	Europe	Northern Fennoscandia	Sweden	Sim, T.G., Swindles, G.T., Morris, P.J., Baird, A.J., Cooper, C.L., Gallego-Sala, A. V., Charman, D.J., Roland, T.P., Borken, W., Mullan, D.J., Aquino-López, M.A., Gałka, M., 2021. Divergent responses of permafrost peatlands to recent climate change. <i>Environ. Res. Lett.</i> 16, 034001. https://doi.org/10.1088/1748-9326/abe00b	Unpublished	Thomas Sim, Mariusz Gałka
170	River Levigus 1	>100um	Particles cm-3	66.35333	30.50111	150	Europe	Northern Fennoscandia	Russia	Wallenius, T.H., Pitkänen, A., Kuuluvainen, T., Pennanen, J., Karttunen, H., 2005. Fire history and forest age distribution of	Unpublished	T. H. Wallenius, Teemu Juselius

171	Stordalen bog	>1mm	Particles cm-3	68.35652	19.0498	351	Europe	Northern Fennoscandia	Sweden	an unmanaged <i>Picea abies</i> dominated landscape. Can. J. For. Res. 35, 1540–1552. https://doi.org/10.1139/x05-050 Sim, T.G., Swindles, G.T., Morris, P.J., Baird, A.J., Cooper, C.L., Gallego-Sala, A. V, Charman, D.J., Roland, T.P., Borken, W., Mullan, D.J., Aquino-López, M.A., Gaika, M., 2021. Divergent responses of permafrost peatlands to recent climate change. Environ. Res. Lett. 16, 034001. https://doi.org/10.1088/1748-9326/abe00b	Thomas Sim, Mariusz Gaika
172	Stordalen palsa	>1mm	Particles cm-3	68.35675	19.04819	351	Europe	Northern Fennoscandia	Sweden	Sim, T.G., Swindles, G.T., Morris, P.J., Baird, A.J., Cooper, C.L., Gallego-Sala, A. V, Charman, D.J., Roland, T.P., Borken, W., Mullan, D.J., Aquino-López, M.A., Gaika, M., 2021. Divergent responses of permafrost peatlands to recent climate change. Environ. Res. Lett. 16, 034001. https://doi.org/10.1088/1748-9326/abe00b ; Gaika, M., Szal, M., Watson, E.J., Gallego-Sala, A., Amesbury, M.J., Charman, D.J., Roland, T.P., Edward Turner, T., Swindles, G.T., 2017b. Vegetation Succession, Carbon Accumulation and Hydrological Change in Subarctic Peatlands, Abisko, Northern Sweden. Permafr. Periglac. Process. 28, 589–604. https://doi.org/10.1002/ppp.1945	Thomas Sim, Mariusz Gaika
173	Ulvinsalo 1	>200um	Particles cm-3	63.96667	30.36667	250	Europe	Northern Fennoscandia	Finland	Pitkänen, A., Huttunen, P., Tolonen, K., Jungner, H., 2003. Long-term fire frequency in the spruce-dominated forests of the Ulvinsalo strict nature reserve, Finland. For. Ecol. Manage. 176, 305–319. https://doi.org/10.1016/S0378-1127(02)00291-8	A. Pitkänen, Teemu Juselius
174	Ulvinsalo 2	>200um	Particles cm-3	63.96667	30.36667	282	Europe	Northern Fennoscandia	Finland	Pitkänen, A., Huttunen, P., Tolonen, K., Jungner, H., 2003. Long-term fire frequency in the spruce-dominated forests of the Ulvinsalo strict nature reserve, Finland. For. Ecol. Manage. 176, 305–319. https://doi.org/10.1016/S0378-1127(02)00291-8	A. Pitkänen, Teemu Juselius
175	Veigi bog	>1mm	Particles cm-3	67.8673	19.1785	477	Europe	Northern Fennoscandia	Sweden	Sim, T.G., Swindles, G.T., Morris, P.J., Baird, A.J., Cooper, C.L., Gallego-Sala, A. V, Charman, D.J., Roland, T.P., Borken, W., Mullan, D.J., Aquino-López, M.A., Gaika, M., 2021. Divergent responses of permafrost peatlands to recent climate change. Environ. Res. Lett. 16, 034001. https://doi.org/10.1088/1748-9326/abe00b	Thomas Sim, Mariusz Gaika
176	Vodoprovodnoe	>1mm	Particles cm-3	66.54347	33.10761	78	Europe	Northern Fennoscandia	Russia	Babeshko, K. V, Shkurko, A., Tsyganov, A.N., Severova, E.E., Gaika, M., Payne, R.J., Mauquoy, D., Mazei, N.G., Fatynina, Y.A., Krasnova, E.D., Saldaev, D.A., Voronov, D.A., Zazovskaya, E., Mazei, Y.A., 2021. A multi-proxy reconstruction of peatland development and regional vegetation changes in subarctic NE Fennoscandia (the Republic of Karelia, Russia) during the Holocene. The Holocene 31, 421–432. https://doi.org/10.1177/0959683620972795	Yuri Mazei, Mariusz Gaika, Andrey Tsyganov, Natalia Mazei
177	Amourous	>200um	Particles cm-3	44.43472	3.663333	1550	Europe	Southern Europe	France	Servera-Vives, G., 2014. Dynamique holocène du paysage et mobilités des pratiques territoriales au mont Lozère (Massif central, France) : Approche paléoenvironnementale multi-indicateurs à haute résolution spatio-temporelle. Géographie. Université de Limoges; Universitat de Barcelona.	Gabriel Servera-Vives
178	Bosc dels Estanyons fen	>150um	Count	42.48046	1.629156	2180	Europe	Southern Europe	Andorra	Miras, Y., Ejarque, A., Riera, S., Palet, J.M., Orenco, H., Euba, I., 2007. Dynamique holocène de la végétation et occupation des Pyrénées andorranes depuis le Néolithique ancien, d'après l'analyse pollinique de la tourbière de Bosc dels Estanyons (2180 m, Vall del Madriu, Andorre). Comptes	Yannick Miras

179	Chao de Lamoso	>125um	mm2/cm3	43.5025	-7.55028	1020	Europe	Southern Europe	Spain	Rendus Palevol 6, 291–300. https://doi.org/10.1016/J.CRPV.2007.02.005 Corcoran J.P., 2007. Impact of Climate Change on Fire Regime in North-west Spain. MSc Thesis, Centre for the Environment, Trinity College Dublin.	Fraser Mitchell
180	Countrasts	>200um	Particles cm-3	44.46111	3.613333	1400	Europe	Southern Europe	France	Servera-Vives, G., 2014. Dynamique holocène du paysage et mobilités des pratiques territoriales au mont Lozère (Massif central, France) : Approche paléoenvironnementale multi-indicateurs à haute résolution spatio-temporelle. Géographie. Université de Limoges; Universitat de Barcelona.	Gabriel Servera-Vives
181	Ech	>150um	Particles cm-3	43.08298	-0.09404	710	Europe	Southern Europe	France	Rius, D., Vannière, B., Galop, D., 2012. Holocene history of fire, vegetation and land use from the central Pyrenees (France). Quat. Res. 77, 54–64. https://doi.org/10.1016/J.YQRES.2011.09.009	Damien Rius
182	El Tiemblo	>150um	Particles cm-3	40.3575	-4.5263	1242	Europe	Southern Europe	Spain	López-Sáez, J.A., Vargas, G., Ruiz-Fernández, J., Blarquez, O., Alba-Sánchez, F., Oliva, M., Pérez-Díaz, S., Robles-López, S., Abel-Schaad, D., 2018. Paleofire Dynamics in Central Spain during the Late Holocene: The Role of Climatic and Anthropogenic Forcing. L. Degrad. Dev. 29, 2045–2059. https://doi.org/10.1002/LDR.2751	GCD
183	Font Bernard	>200um	Particles cm-3	44.41472	3.670278	1350	Europe	Southern Europe	France	Servera-Vives, G., 2014. Dynamique holocène du paysage et mobilités des pratiques territoriales au mont Lozère (Massif central, France) : Approche paléoenvironnementale multi-indicateurs à haute résolution spatio-temporelle. Géographie. Université de Limoges; Universitat de Barcelona.	Gabriel Servera-Vives
184	Gabarn	>150um	Particles cm-3	43.1717	-0.5555	310	Europe	Southern Europe	France	Rius, D., Vannière, B., Galop, D., 2009. Fire frequency and landscape management in the northwestern Pyrenean piedmont, France, since the early Neolithic (8000 cal. BP). Holocene 19, 847–859. https://doi.org/10.1177/0959683609105299	Damien Rius
185	La Veyssière	>200um	Particles cm-3	44.40306	3.653889	1150	Europe	Southern Europe	France	Servera-Vives, G., 2014. Dynamique holocène du paysage et mobilités des pratiques territoriales au mont Lozère (Massif central, France) : Approche paléoenvironnementale multi-indicateurs à haute résolution spatio-temporelle. Géographie. Université de Limoges; Universitat de Barcelona.	Gabriel Servera-Vives
186	Lanzahita	>150um	Particles cm-3	40.272	-4.935	1270	Europe	Southern Europe	Spain	López-Sáez, J.A., Vargas, G., Ruiz-Fernández, J., Blarquez, O., Alba-Sánchez, F., Oliva, M., Pérez-Díaz, S., Robles-López, S., Abel-Schaad, D., 2018. Paleofire Dynamics in Central Spain during the Late Holocene: The Role of Climatic and Anthropogenic Forcing. L. Degrad. Dev. 29, 2045–2059. https://doi.org/10.1002/LDR.2751	GCD
187	Les Laubies	>200um	Particles cm-3	44.43333	3.623889	1280	Europe	Southern Europe	France	Servera-Vives, G., 2014. Dynamique holocène du paysage et mobilités des pratiques territoriales au mont Lozère (Massif central, France) : Approche paléoenvironnementale multi-indicateurs à haute résolution spatio-temporelle. Géographie. Université de Limoges; Universitat de Barcelona.	Gabriel Servera-Vives
188	Lourdes	>150um	Particles cm-3	43.10778	-0.08361	430	Europe	Southern Europe	France	Rius, D., Vannière, B., Galop, D., Richard, H., 2011. Holocene fire regime changes from multiple-site sedimentary charcoal analyses in the Lourdes basin (Pyrenees, France). Quat. Sci. Rev. 30, 1696–1709. https://doi.org/10.1016/j.quascirev.2011.03.014	Damien Rius
189	Orris de Setut	>200um	Particles cm-3	42.483	1.65	2300	Europe	Southern Europe	Andorra	Ejarque, A., Miras, Y., Riera, S., Palet, J.M., Orongo, H.A., 2010. Testing micro-regional variability in the Holocene shaping of high mountain cultural landscapes: a palaeoenvironmental case-study in the eastern Pyrenees. J.	Ana Ejarque

190	Pedrido	>125um	mm2/cm3	43.45028	-7.52917	770	Europe	Southern Europe	Spain	Archaeol. Sci. 37, 1468–1479. https://doi.org/10.1016/J.JAS.2010.01.007 Stefanini, B.S., Oksanen, P.O., Corcoran, J.P., Mitchell, F.J.G., 2018. Appraising the cohesion of palaeoenvironmental reconstructions in north-west Spain since the mid-Holocene from a high temporal resolution multi-proxy peat record. <i>Holocene</i> 28, 681–694. https://doi.org/10.1177/0959683617744258	Fraser Mitchell
191	Posta Fibreno	>1mm	Particles cm-3	41.69494	13.69175	290	Europe	Southern Europe	Italy	Zacccone, C., Lobianco, D., Shoty, W., Ciavatta, C., Appleby, P.G., Brugiapaglia, E., Casella, L., Miano, T.M., D'Orazio, V., 2017. Highly anomalous accumulation rates of C and N recorded by a relic, free-floating peatland in Central Italy. <i>Sci. Rep.</i> 7, 1–10. https://doi.org/10.1038/srep43040 ; Concheri, G., Stevanato, P., Zacccone, C., Shoty, W., D'Orazio, V., Miano, T., Piffanelli, P., Rizzi, V., Ferrandi, C., Squartini, A., 2017. Rapid peat accumulation favours the occurrence of both fen and bog microbial communities within a Mediterranean, free-floating peat island. <i>Sci. Rep.</i> 7, 1–10. https://doi.org/10.1038/s41598-017-08662-y ; Zacccone, C., Lobianco, D., Raber, G., D'Orazio, V., Shoty, W., Miano, T.M., Francesconi, K., 2018. Methylated arsenic species throughout a 4-m deep core from a free-floating peat island. <i>Sci. Total Environ.</i> 621, 67–74. https://doi.org/10.1016/j.scitotenv.2017.11.152	Claudio Zacccone
192	Pradell	>200um	Count	42.289	1.548	1975	Europe	Southern Europe	Spain	Ejarque, A., Julià, R., Riera, S., Palet, J.M., Orengo, H.A., Miras, Y., Gascón, C., 2009. Tracing the history of highland human management in the eastern Pre-Pyrenees: An interdisciplinary palaeoenvironmental study at the Pradell fen, Spain. <i>Holocene</i> 19, 1241–1255. https://doi.org/10.1177/0959683609345084	Ana Ejarque
193	Riu dels Orris	>200um	Particles cm-3	42.489	1.637	2390	Europe	Southern Europe	Andorra	Ejarque, A., Miras, Y., Riera, S., Palet, J.M., Orengo, H.A., 2010. Testing micro-regional variability in the Holocene shaping of high mountain cultural landscapes: a palaeoenvironmental case-study in the eastern Pyrenees. <i>J. Archaeol. Sci.</i> 37, 1468–1479. https://doi.org/10.1016/J.JAS.2010.01.007	Ana Ejarque
194	Serranillos	>150um	Particles cm-3	40.372	-4.941	1281	Europe	Southern Europe	Spain	López-Sáez, J.A., Vargas, G., Ruiz-Fernández, J., Blarquez, O., Alba-Sánchez, F., Oliva, M., Pérez-Díaz, S., Robles-López, S., Abel-Schaad, D., 2018. Paleofire Dynamics in Central Spain during the Late Holocene: The Role of Climatic and Anthropogenic Forcing. <i>L. Degrad. Dev.</i> 29, 2045–2059. https://doi.org/10.1002/LDR.2751	GCD
195	Vapsko 1	>0.5mm	Particles cm-3	42.07612	23.52384	2143	Europe	Southern Europe	Bulgaria	Hoovers R., Van Neer W, Marinova E., 2017. Plant macrofossils as proxy for Holocene tree-line changes in Southeastern Europe - a case study of the Rila Mountains, Bulgaria. MSc thesis. KU Leuven (Department of Biology).	Renske Hoovers, Elena Marinova
196	Vapsko 2	>150um	Particles cm-3	42.0739	23.5242	2120	Europe	Southern Europe	Bulgaria	Feurdean, A., Tonkov, S., Pfeiffer, M., Panait, A., Warren, D., Vannière, B., Marinova, E., 2019. Fire frequency and intensity associated with functional traits of dominant forest type in the Balkans during the Holocene. <i>Eur. J. For. Res.</i> 138, 1049–1066. https://doi.org/10.1007/s10342-019-01223-0	Angelica Feurdean
197	Biscaye	>150um	Particles cm-3	43.11917	-0.07111	410	Europe	Southern Europe	France	Rius, D., Vannière, B., Galop, D., Richard, H., 2011. Holocene fire regime changes from multiple-site sedimentary charcoal analyses in the Lourdes basin (Pyrenees, France). <i>Quat. Sci.</i>	Damien Rius

198	Apsuciems Mire	>1mm	Count	57.0521	23.3189	6.6	Europe	Southern Scandinavia and the Baltics	Latvia	Rev. 30, 1696–1709. https://doi.org/10.1016/j.quascirev.2011.03.014 Galka, M., Aunina, L., Tobolski, K., Feurdean, A., 2016. Development of Rich Fen on the SE Baltic Coast, Latvia, during the Last 7500 Years, Using Paleoecological Proxies: Implications for Plant Community Development and Paleoclimatic Research. <i>Wetlands</i> 36, 689–703. https://doi.org/10.1007/s13157-016-0779-y	Mariusz Galka, Liene Aunina
199	Bažu Bog	>160um	Particles cm-3	57.69436	22.44414	15	Europe	Southern Scandinavia and the Baltics	Latvia	Unpublished	Normunds Stivrins, Alekss Maksims
200	Kalevansuo 3	>140um	Particles cm-3	60.64745	24.35795	123	Europe	Southern Scandinavia and the Baltics	Finland	Mathijssen, P.J.H., Kähkölä, N., Tuovinen, J.P., Lohila, A., Minkkinen, K., Laurila, T., Väiliranta, M., 2017. Lateral expansion and carbon exchange of a boreal peatland in Finland resulting in 7000 years of positive radiative forcing. <i>J. Geophys. Res. Biogeosciences</i> 122, 562–577. https://doi.org/10.1002/2016JG003749	Paul J.H. Mathijssen, Minna Väiliranta
201	Kalevansuo 7	>140um	Particles cm-3	60.6502	24.35996	123	Europe	Southern Scandinavia and the Baltics	Finland	Mathijssen, P.J.H., Kähkölä, N., Tuovinen, J.P., Lohila, A., Minkkinen, K., Laurila, T., Väiliranta, M., 2017. Lateral expansion and carbon exchange of a boreal peatland in Finland resulting in 7000 years of positive radiative forcing. <i>J. Geophys. Res. Biogeosciences</i> 122, 562–577. https://doi.org/10.1002/2016JG003749	Paul J.H. Mathijssen, Minna Väiliranta
202	Kontolanrahka	>100um	Particles cm-3	60.78333	22.78333	88	Europe	Southern Scandinavia and the Baltics	Finland	Väiliranta, M., Korhola, A., Seppä, H., Tuittila, E.S., Sarmaja-Korjonen, K., Laine, J., Alm, J., 2007. High-resolution reconstruction of wetness dynamics in a southern boreal raised bog, Finland, during the late Holocene: A quantitative approach. <i>Holocene</i> 17, 1093–1107. https://doi.org/10.1177/0959683607082550 ; Morris, J.L., Väiliranta, M., Sillasoo, Ü., Tuittila, E.S., Korhola, A., 2015. Re-evaluation of late Holocene fire histories of three boreal bogs suggest a link between bog fire and climate. <i>Boreas</i> 44. https://doi.org/10.1111/bor.12086	Eeva-Stiina Tuittila, Minna Väiliranta, Atte Korhola, Teemu Juselius
203	Lakkasuo 1	>125um	Particles cm-3	61.78333	24.3	150	Europe	Southern Scandinavia and the Baltics	Finland	Tuittila, E.-S., Väiliranta, M., Laine, J., Korhola, A., 2007. Quantifying patterns and controls of mire vegetation succession in a southern boreal bog in Finland using partial ordinations. <i>J. Veg. Sci.</i> 18, 891. https://doi.org/10.1658/1100-9233(2007)18[891:qpacom]2.0.co;2 ; Morris, J.L., Väiliranta, M., Sillasoo, Ü., Tuittila, E.S., Korhola, A., 2015. Re-evaluation of late Holocene fire histories of three boreal bogs suggest a link between bog fire and climate. <i>Boreas</i> 44. https://doi.org/10.1111/bor.12086	Eeva-Stiina Tuittila
204	Lakkasuo 2	>125um	Particles cm-3	61.78333	24.3	150	Europe	Southern Scandinavia and the Baltics	Finland	Tuittila, E.-S., Väiliranta, M., Laine, J., Korhola, A., 2007. Quantifying patterns and controls of mire vegetation succession in a southern boreal bog in Finland using partial ordinations. <i>J. Veg. Sci.</i> 18, 891. https://doi.org/10.1658/1100-9233(2007)18[891:qpacom]2.0.co;2 ; Morris, J.L., Väiliranta, M., Sillasoo, Ü., Tuittila, E.S., Korhola, A., 2015. Re-evaluation of late Holocene fire histories of three boreal bogs suggest a link between bog fire and climate. <i>Boreas</i> 44. https://doi.org/10.1111/bor.12086	Eeva-Stiina Tuittila
205	Männikjärve	>100um	Particles cm-3	58.86667	26.25	82	Europe	Southern Scandinavia and the Baltics	Estonia	Sillasoo, Ü., Mauquoy, D., Blundell, A., Charman, D., Blaauw, M., Daniell, J., Toms, P., Newberry, J., Chambers, F., Karofeld, E., 2007. Peat multi-proxy data from Männikjärve bog as indicators of late Holocene climate changes in Estonia.	Eeva-Stiina Tuittila

										Boreas	36,	20–37.	
206	Notteryd	>250um	Particles cm-3	56.91306	14.88556	186	Europe	Southern Scandinavia and the Baltics	Sweden	Cui, Q.-Y., Gaillard, M.-J., Vanni�re, B., Colombaroli, D., Lemdahl, G., Olsson, F., Benito, B., Zhao, Y., 2020. Evaluating fossil charcoal representation in small peat bogs: Detailed Holocene fire records from southern Sweden. <i>Holocene</i> 30, 1540–1551. https://doi.org/10.1177/0959683620941069			Qiao-Yu Cui, M.J. Gaillard, Geoffrey Lemdahl, Fredrik Olsson
207	Siikaneva B	>140um	Particles cm-3	61.83733	24.16912	160	Europe	Southern Scandinavia and the Baltics	Finland	Mathijssen, P.J.H., V�liranta, M., Korrensalo, A., Alekseychik, P., Vesala, T., Rinne, J., Tuittila, E.S., 2016. Reconstruction of Holocene carbon dynamics in a large boreal peatland complex, southern Finland. <i>Quat. Sci. Rev.</i> 142. https://doi.org/10.1016/j.quascirev.2016.04.013			Paul J.H. Mathijssen, Minna V�liranta
208	Siikaneva F	>140um	Particles cm-3	61.83237	24.19296	160	Europe	Southern Scandinavia and the Baltics	Finland	Mathijssen, P.J.H., V�liranta, M., Korrensalo, A., Alekseychik, P., Vesala, T., Rinne, J., Tuittila, E.S., 2016. Reconstruction of Holocene carbon dynamics in a large boreal peatland complex, southern Finland. <i>Quat. Sci. Rev.</i> 142. https://doi.org/10.1016/j.quascirev.2016.04.013			Paul J.H. Mathijssen, Minna V�liranta
209	Stavs�kra-09	>250um	Particles cm-3	57.02417	14.81306	187	Europe	Southern Scandinavia and the Baltics	Sweden	Cui, Q.-Y., Gaillard, M.-J., Vanni�re, B., Colombaroli, D., Lemdahl, G., Olsson, F., Benito, B., Zhao, Y., 2020. Evaluating fossil charcoal representation in small peat bogs: Detailed Holocene fire records from southern Sweden. <i>Holocene</i> 30, 1540–1551. https://doi.org/10.1177/0959683620941069			Qiao-Yu Cui, M.J. Gaillard, Geoffrey Lemdahl, Fredrik Olsson
210	Storasj�	>250um	Particles cm-3	56.93333	15.26667	255	Europe	Southern Scandinavia and the Baltics	Sweden	Olsson, F., Gaillard, M.J., Lemdahl, G., Greisman, A., Lanos, P., Marguerie, D., Marcoux, N., Skoglund, P., W�glind, J., 2010. A continuous record of fire covering the last 10,500 calendar years from southern Sweden - The role of climate and human activities. <i>Palaeogeogr. Palaeoclimatol. Palaeoecol.</i> 291, 128–141. https://doi.org/10.1016/j.palaeo.2009.07.013 ; Olsson, F., Lemdahl, G., 2010. A forest history for the last 10 900 years at the site Storasj�, southern Sweden: implications from beetle assemblages. <i>J. Quat. Sci.</i> 25, 1211–1221. https://doi.org/10.1002/JQS.1400			M.J. Gaillard, Annica Greisman, Geoffrey Lemdahl, Fredrik Olsson
211	Store Mosse	>120um	Particles cm-3	57.22728	13.91968	160	Europe	Southern Scandinavia and the Baltics	Sweden	Ryberg, E.E., V�liranta, M., Martinez-Cortizas, A., Ehrl�n, J., Sj�str�m, J.K., Kylander, M.E., 2022. Postglacial peatland vegetation succession in Store Mosse bog, south-central Sweden: An exploration of factors driving species change. <i>Boreas</i> . https://doi.org/10.1111/BOR.12580			Eleonor Eva Stina Ryberg, Malin Kylander
212	Caleta Eugenia	>100um	Particles cm-3	-54.9291	-67.3457	3.7	Patagonia	Patagonia	Chile	McCulloch, R.D., Mansilla, C.A., Morello, F., De Pol-Holz, R., San Rom�n, M., Tisdall, E., Torres, J., 2019. Late glacial and Holocene landscape change and rapid climate and coastal impacts in the Canal Beagle, southernmost Patagonia. <i>J. Quat. Sci.</i> 34, 674–684. https://doi.org/10.1002/jqs.3167			Robert D. McCulloch
213	Cerro Fox	>100um	Particles cm-3	-52.1315	-69.5535	46	Patagonia	Patagonia	Chile	Unpublished			Claudia A. Mansilla
214	Lago Lynch	>100um	Particles cm-3	-53.0944	-68.5614	165	Patagonia	Patagonia	Chile	Mansilla, C.A., McCulloch, R.D., Morello, F., 2018. The vulnerability of the <i>Nothofagus</i> forest-steppe ecotone to climate change: Palaeoecological evidence from Tierra del Fuego (~53�S). <i>Palaeogeogr. Palaeoclimatol. Palaeoecol.</i> 508, 59–70. https://doi.org/10.1016/J.PALAEO.2018.07.014			Claudia A. Mansilla
215	Punta Arenas	>100um	Particles cm-3	-53.1457	-70.9518	80	Patagonia	Patagonia	Chile	Unpublished			Robert D. McCulloch
216	Punta Burslem	>100um	Particles cm-3	-54.1916	-67.9532	54	Patagonia	Patagonia	Chile	McCulloch, R.D., Blaikie, J., Jacob, B., Mansilla, C.A., Morello, F., De Pol-Holz, R., San Rom�n, M., Tisdall, E., Torres, J., 2020. Late glacial and Holocene climate variability,			Robert D. McCulloch

217	Punta Yartou	>100um	Particles cm-3	-52.1386	-69.8611	51	Patagonia	Patagonia	Chile	southernmost Patagonia. <i>Quat. Sci. Rev.</i> 229, 106131. https://doi.org/10.1016/J.QUASCIREV.2019.106131 Mansilla, C.A., McCulloch, R.D., Morello, F., 2016. Palaeoenvironmental change in Southern Patagonia during the Lateglacial and Holocene: Implications for forest refugia and climate reconstructions. <i>Palaeogeogr. Palaeoclimatol. Palaeoecol.</i> 447, 1–11. https://doi.org/10.1016/J.PALAEO.2016.01.041	Claudia Mansilla	A.
218	Rio Grande	>100um	Particles cm-3	-52.3397	-69.4925	79	Patagonia	Patagonia	Chile	Unpublished	Claudia Mansilla	A.
219	Skyring 1	>1mm	Particles cm-3	-52.5087	-72.1273	40	Patagonia	Patagonia	Chile	Mathijssen, P.J.H., Gaika, M., Borken, W., Knorr, K.H., 2019. Plant communities control long term carbon accumulation and biogeochemical gradients in a Patagonian bog. <i>Sci. Total Environ.</i> 684, 670–681. https://doi.org/10.1016/j.scitotenv.2019.05.310	Paul Mathijssen, Mariusz Gaika, Werner Borken, Klaus-Holger Knorr	J.H.
220	Skyring 2	>1mm	Particles cm-3	-52.5146	-72.1238	16	Patagonia	Patagonia	Chile	Mathijssen, P.J.H., Gaika, M., Borken, W., Knorr, K.H., 2019. Plant communities control long term carbon accumulation and biogeochemical gradients in a Patagonian bog. <i>Sci. Total Environ.</i> 684, 670–681. https://doi.org/10.1016/j.scitotenv.2019.05.310	Paul Mathijssen, Mariusz Gaika, Werner Borken, Klaus-Holger Knorr	J.H.
221	Sussex Mountains	>180um	Particles cm-3	-51.6328	-58.9965	233	Patagonia	Patagonia	Falkland Islands	Mauquoy, D., Payne, R.J., Babeshko, K. V., Bartlett, R., Boomer, I., Bowey, H., Evans, C.D., Ring-Hrubesh, F., Muirhead, D., O'Callaghan, M., Piotrowska, N., Rush, G., Sloan, T., Smeaton, C., Tsyganov, A.N., Mazei, Y.A., 2020. Falkland Island peatland development processes and the pervasive presence of fire. <i>Quat. Sci. Rev.</i> 240, 106391.	Dmitri Mauquoy	

Table C.2. Metadata for wider landscape records from the Global Charcoal Database (GCD). See <https://paleofire.org/index.php> for more information on the GCD (e.g. unit/site type classifications) and data access.

Site Name	Paleofire site ID	Units	Lat (°N)	Lon (°E)	Altitude (m)	ID_Site_Type	Continent	GCD version
Loch an Amair	163	XCOP	57.28	-4.89	315	LGLA	Europe	GCD1
Dubh-Lochan	164	XCOP	57.29	-4.43	150	LGLA	Europe	GCD1
Lochan na h-Inghinn	165	XCOP	58.25	-5.09	65	LGLA	Europe	GCD1
Reidh-lochan	166	XCOP	58.03	-4.12	160	LGLA	Europe	GCD1
Lough Mullaghlahan	557	PTC0	54.76	-8.46	40	NOTK	Europe	GCD3
Lough Nabraddan	558	PTC0	55.01	-8.35	20	NOTK	Europe	GCD3
Altar Lough	559	PTC0	55.01	-8.4	30	NOTK	Europe	GCD3
Lios Lairthin Mor	560	X37P	53.08	-9.21	270	NOTK	Europe	GCD3
Lough Maumeen	643	PPOL	53.48	-9.65	250	LGLA	Europe	GCD2
Derrycunihy Wood	644	XCM3	52.01	-9.41	75	HOLL	Europe	GCD2
Camillan Wood	645	XCM3	52.03	-9.56	17	HOLL	Europe	GCD2
Loch an t'Suidhe	648	XFRP	56.3	-6.24	85	LACU	Europe	GCD2
Crag Lough	651	CMGR	55	-2.36	250	LGLA	Europe	GCD4
Balywillin Crannog	956	GT5C	54.37	-4.47	20	NULL	Europe	GCD4
Derragh Bog	958	GT5C	53.76	-7.4	70	NULL	Europe	GCD4
Derragh Lough	959	GT5C	53.76	-7.4	62	NULL	Europe	GCD4
Kentra Moss	962	PCMY	56.75	-5.83	10	NULL	Europe	GCD4
West Lomond	969	SQCU	56.25	-3.28	522	NULL	Europe	GCD4
Soppensee	230	CARE	47.08	8.08	596	LGLA	Europe	GCD1
Lobsigensee	231	CARE	47.03	7.29	514	LGLA	Europe	GCD1
Lej da San Murrezzan	374	C010	46.49	9.84	1768	LNAT	Europe	GCD1
Turbuta	515	XFRG	47.25	23.3	275	NOTK	Europe	GCD4
Nussbaumersee	601	X125	47.6	8.81	450	LACU	Europe	GCD2
Seedorf	603	X125	46.79	7.04	609	LACU	Europe	GCD2
Lake Lucerne	605	GT38	47.05	8.59	434	LACU	Europe	GCD2
Dallund So North Funen	937	PCMY	55.48	10.26	12	NULL	Europe	GCD4
Cerna Horna	942	X100	50.66	15.75	1190	NULL	Europe	GCD4
Sirok Nyiries To	946	SQC0	47.93	20.18	200	NULL	Europe	GCD4
Fuldera-Palu	949	PCMY	46.61	10.36	1822	NULL	Europe	GCD4
Wildseemoor	970	XCM3	48.71	8.45	909	NULL	Europe	GCD4
Wilder See	971	XCM3	48.56	8.23	910	NULL	Europe	GCD4

Steregoiu	978	XCM3	47.81	23.54	790	NULL	Europe	GCD4
Sagistalsee	979	XCM3	46.68	7.98	1953	NULL	Europe	GCD4
Bibersee	982	XCM3	47.21	8.47	429	NULL	Europe	GCD4
Bruckmisse	983	XCM3	48.73	8.64	670	NULL	Europe	GCD4
Durchenbergried core 1	986	XCM3	47.78	8.98	432	NULL	Europe	GCD4
Etang de la Gruere	987	XCM3	47.23	7.04	1005	NULL	Europe	GCD4
Glaswaldsee	989	XCM3	48.42	8.24	839	NULL	Europe	GCD4
Batorliget	990	SQCU	47.75	22.5	130	NULL	Europe	GCD4
Bialoweiza forest I	991	XCM3	52.08	23.97	165	NULL	Europe	GCD4
Hornstaad	992	PCMY	47.69	8.9	393	NULL	Europe	GCD4
Putaanlampi	260	C010	66.38	29.41	230	LNAT	Europe	GCD1
Ylimmainen Kuivajarvi	284	GT05	66.35	29.61	255	LNAT	Europe	GCD1
Lake Suho Breznishko	63	OTHE	41.81	23.35	1963	LCIR	Europe	GCD1
Lake Okadensko	64	OTHE	41.78	23.35	2475	LCIR	Europe	GCD1
Lago di Massaciuccoli	118	X010	43.85	10.31	1	COAS	Europe	GCD1
Lago Piccolo di Avigliana	332	XPEE	45.05	7.38	356	LMOR	Europe	GCD1
Lago della Costa AP1	395	C010	45.27	11.74	7	LACU	Europe	GCD3
Lago del Greppo	436	C010	44.11	11.66	1442	LACU	Europe	GCD1
El Carrizal	517	CARE	41.31	-4.14	860	LACU	Europe	GCD3
Lac du Lait	548	XARE	45.31	6.81	2180	LACU	Europe	GCD2
Lac Miroir	551	XARE	44.63	6.79	2214	LACU	Europe	GCD4
Guallar	668	MMDW	41.4	-0.22	336	LACU	Europe	GCD2
Lago Lucone	704	PTC3	45.55	10.48	249	LACU	Europe	GCD2
Lago di Fimon	706	PCMY	45.46	11.53	23	LACU	Europe	GCD2
Hoya del Castillo	717	MMDW	41.48	-0.15	258	LACU	Europe	GCD2
Lagaccione	718	CMGR	42.56	11.85	355	LACU	Europe	GCD2
Valle di Castiglione	719	SQC0	41.72	12.75	44	OTHE	Europe	GCD2
Lac du Loup	720	XARE	45.18	6.53	2032	LNAT	Europe	GCD2
Lake Ostrezko-2	734	PRAB	42.13	23.46	2320	LACU	Europe	GCD2
Lake Ostrezko-3	735	PRAB	42.13	23.46	2340	LACU	Europe	GCD2
Malo Jezero	737	XCM3	42.78	17.35	24	LACU	Europe	GCD2
Lago Dell'Accesa	815	C125	42.98793	10.89512	155	LACU	Europe	GCD2
Lago della Costa AP2	844	C010	45.27	11.74	7	LACU	Europe	GCD3
Lago Perso	872	XARE	44.92	6.8	1801	LACU	Europe	GCD4
Besos	941	PPOL	41.4	-2.25	7	NULL	Europe	GCD4

Cubelles	943	C150	41.2	-1.67	2	NULL	Europe	GCD4
Lago Alimini Piccolo	945	CMGR	40.18	18.43	1	NULL	Europe	GCD4
Pena da Cadela	948	SQC0	42.83	-7.17	970	NULL	Europe	GCD4
Tourbiere du Peschio	974	XCM3	44.45	3.6	1370	NULL	Europe	GCD4
Tourbiere des Narses Morte	975	XCM3	44.43	3.6	1400	NULL	Europe	GCD4
Tourbiere de La Lande	976	XCM3	43.56	2.96	1040	NULL	Europe	GCD4
Torveraz core 2	977	XCM3	45.69	6.86	2415	NULL	Europe	GCD4
Laghi dell'Orgials	981	XCM3	44.23	7.13	2240	NULL	Europe	GCD4
Candieira (Charco da Candieira)	1146	MCM3	40.34361	-7.57806	1400	LCIR	Europe	GCD4
Banyoles	1147	C150	42.12908	2.751844	174	LNAT	Europe	GCD4
Castello Lagoon	1149	XFRG	42.28156	3.099528	2	CSLT	Europe	GCD4
Lake Dojran	1161	XFRP	41.19123	22.73264	144	LACU	Europe	GCD4
Arroyo de las Carcavas	1165	XFRP	40.84192	-4.03139	1300	HOLL	Europe	GCD4
Iso Lehmalmampi	252	GT05	60.35	24.6	106	LNAT	Europe	GCD1
Etu-Mustajarvi	268	GT05	60.98	25	157	LNAT	Europe	GCD1
Ljustjarnen	321	X250	59.75	14.43	183	LACU	Europe	GCD1
Lilla Glopssjon	323	X250	59.8	14.62	198	LACU	Europe	GCD1
Bohult Hollow	468	C250	57.23	16.16	77	HOLL	Europe	GCD1
Hunnemara Lake Blekinge coast	898	X05C	56.16	14.89	3	NULL	Europe	GCD4
Lake Orjarvi	933	X010	61.66	27.23	90	NULL	Europe	GCD4
Zadeikiai Bog	939	PPOL	56.17	21.98	120	NULL	Europe	GCD4
Lake Farskjon	954	X05C	56.17	14.99	7	NULL	Europe	GCD4
Lake Ryssjon	955	X05C	56.17	15.08	5	NULL	Europe	GCD4
Birzulio Sasmauka	993	PCMY	55.78	22.43	148	NULL	Europe	GCD4
Vedruka	994	PCMY	58.29	22.08	21	NULL	Europe	GCD4
Daktariske	996	PPOL	55.8	22.4	148	NULL	Europe	GCD4
Lake Verijarv	998	XCM3	57.81	27.06	88	NULL	Europe	GCD4
Lake Kahala	999	XCM3	59.48	25.52	33	NULL	Europe	GCD4
Lake Rouge Tourgjav micro	1000	XCM3	57.73	26.92	114	NULL	Europe	GCD4
Lake Ruila micro	1001	XCM3	59.17	24.43	43	NULL	Europe	GCD4
Lake Ruila macro	1002	XCM3	59.17	24.43	43	NULL	Europe	GCD4
Lake Rouge Tourgjav macro	1003	XCM3	57.73	26.92	114	NULL	Europe	GCD4
Paradox Lake	125	X125	60.62	-150.75	68	LACU	North America	GCD1
Code	200	X125	67.15	-151.86	250	LTHK	North America	GCD1
Wild Tussock	201	X125	67.12	-151.38	290	LGLA	North America	GCD1

Last Chance	202	X125	67.07	-150.75	250	LTHK	North America	GCD1
Arrow	204	XARE	60.75	-150.51	90	COAS	North America	GCD1
Rock	205	XARE	60.41	-150.25	285	COAS	North America	GCD1
Portage	207	XARE	60.71	-150.53	75	COAS	North America	GCD1
Albion	183	XARP	45.67	-71.32	320	LACU	North America	GCD1
Castor	184	XARP	46.61	-72.99	220	LACU	North America	GCD1
Dolbeau	186	XARP	48.96	-65.95	965	LACU	North America	GCD1
J'Arrive	187	XARP	49.24	-65.37	56	LACU	North America	GCD1
Madeleine	188	XARP	47.66	-70.71	800	LACU	North America	GCD1
Yamaska	191	XARE	45.45	-72.87	265	LACU	North America	GCD1
Lac Hertel	270	XARP	45.68	-74.05	75	NOTK	North America	GCD1
Lac a l'Ange	318	XARE	47.46	-70.4	648	LACU	North America	GCD1
Lac Marcotte	320	XARE	47.07	-71.42	503	LACU	North America	GCD1
St Francois	322	XARE	48.29	-72.14	358	LACU	North America	GCD1
Mont Valin	324	XARE	48.61	-70.83	356	LACU	North America	GCD1
Lac Rond	334	XARE	46	-74	360	LACU	North America	GCD1
Petit Bouchard	349	CARE	48.85	-64.6	145	LACU	North America	GCD1
Lac aux Atocas	350	XARP	45.53	-73.31	114	LACU	North America	GCD1
Lac Caribou	351	XARP	48.19	-64.94	116	LACU	North America	GCD1
Lac a Euloge	355	XARP	49.24	-65.37	83	LACU	North America	GCD1
Lac Gabriel	356	XARP	48.28	-73.47	250	LACU	North America	GCD1
Lac a Leonard	357	XARP	49.2	-65.81	17	LACU	North America	GCD1
Lac a la Main	358	XARP	47.7	-70.62	730	LACU	North America	GCD1
Lac Martini	359	XARP	47.47	-72.76	242	LACU	North America	GCD1
Lac a la Montagne Ronde	360	XARP	48.32	-68.56	150	LACU	North America	GCD1
Lac Ouellet	361	XARP	47.53	-68.94	300	LACU	North America	GCD1
Lac Perdu	362	XARP	49.17	-66.32	152	LACU	North America	GCD1
Triangle	364	XARP	48.71	-65.41	465	LACU	North America	GCD1
Lac Flevy	365	XARP	48.21	-71.21	381	LACU	North America	GCD1
Lac Geai SBL	1169	SQCU	45.99588	-73.9932	365	NULL	North America	GCD4
Lac a Jean-Marie Boulay	1177	CARE	48.9698	-64.4861	276	NULL	North America	GCD4
Lac Bride	1178	CARE	47.3136	-74.5046	437	NULL	North America	GCD4
Excelsior Basin	22	1424	52.78	-117.11	2631	LACU	North America	GCD1
Maligne Lake	29	1424	52.73	-117.61	1675	LACU	North America	GCD1
Ninisith Lake	31	XFRS	59.58	-113	225	LACU	North America	GCD1

Tonquin Creek	40	1424	52.73	-118.36	1935	LACU	North America	GCD1
Wilcox Pass	41	1220	52.24	-117.21	2355	LACU	North America	GCD1
Dog Lake	43	C250	50.76	-116.1	1183	LACU	North America	GCD1
7-M	203	XARE	62.5	-113.72	213	LACU	North America	GCD1
Nicole Lake	293	XARE	62.9	-114.81	300	NOTK	North America	GCD1
Brenda Lake	437	XARE	62.35	-119.19	207	LACU	North America	GCD1
Andy Lake	438	XARE	61.95	-109.81	360	LACU	North America	GCD1
Emile_Lake	1238	XARS	64.0544	-114.106	393	LACU	North America	GCD4
Izaak_Lake	1239	XARS	64.0988	-114.176	394	LACU	North America	GCD4
Paradis_Lake	1240	XARS	64.00639	-114.989	347	LACU	North America	GCD4
Saxon_Lake	1241	XARS	63.80722	-114.976	392	LACU	North America	GCD4
Lac Francis	109	XARE	48.52	-79.47	305	LKET	North America	GCD1
Pas-de-Fond	111	XARE	48.8	-78.83	290	LKET	North America	GCD1
EC1	160	XARP	56.28	-75.1	250	LNAT	North America	GCD1
GB2	161	XARP	55.1	-75.28	300	NOTK	North America	GCD1
Yelle	192	XARE	48.5	-79.63	356	LACU	North America	GCD1
Lac Clo	352	XARP	48.49	-79.35	280	LACU	North America	GCD1
Lac Delorme	354	XARP	54.43	-69.92	538	LACU	North America	GCD1
Lac Pessiere_B	363	XARS	49.5	-79.24	280	LACU	North America	GCD1
LG4-01	450	XARP	54.03	-72.87	470	LNAT	North America	GCD1
LG4-05	451	XARP	54.06	-72.91	350	LNAT	North America	GCD1
LG4-06	452	XARP	54.07	-72.94	365	LNAT	North America	GCD1
LG4-09	453	XARP	54.9	-72.77	442	LNAT	North America	GCD1
LG4-12	454	XARP	52.84	-73.31	534	LNAT	North America	GCD1
Lac aux Geais	503	X160	49.89	-78.65	280	LACU	North America	GCD1
Lac Profond	504	X160	49.86	-78.61	270	LACU	North America	GCD1
Lac Raynald	505	X160	49.8	-78.53	250	LACU	North America	GCD1
Lac a la Loutre	506	X160	49.71	-78.33	274	LACU	North America	GCD1
Lac Christelle	1117	XARE	49.73214	-84.2545	291	LACU	North America	GCD4
Lac Garot	1120	XARE	51.09964	-77.5536	291	LACU	North America	GCD4
Lac du Loup II	1123	XARE	53.05503	-77.4005	206	NULL	North America	GCD4
Lac Marie-Eve	1124	XARE	52.06169	-76.1523	296	LACU	North America	GCD4
Lac Nano	1125	XARE	53.02375	-77.3643	206	LACU	North America	GCD4
Lac Richard	1126	XARE	50.65274	-74.6861	432	LACU	North America	GCD4
Lac Schon	1127	XARE	50.59492	-77.5684	248	LACU	North America	GCD4

Lac Trefle	1130	XARE	51.85014	-76.0451	270	LACU	North America	GCD4
Twin Lake	1131	XARE	50.95247	-74.5753	376	LACU	North America	GCD4
Ely	333	XARE	41.76	-75.83	384	LACU	North America	GCD1
Crawford	338	XARE	44	-80	279	LACU	North America	GCD1
Binnewater	829	TOMX	41.41	-74.55	256	LACU	North America	GCD2
Pixie	178	X150	48.59	-124.19	70	LKET	North America	GCD1
Whyac	179	X150	48.67	-124.84	15	LKET	North America	GCD1
Walker	181	C125	48.52	-124	950	LACU	North America	GCD2
Turtle	315	C125	49.32	-124.95	80	LNAT	North America	GCD2
Enos	317	C125	49.28	-124.15	50	LNAT	North America	GCD3
Wentworth Lake	1014	C125	48	-124.53	47	LACU	North America	GCD4
Sky Lake	296	XARE	56.48	-94.78	145	NOTK	North America	GCD1
Corral Lake	440	XARE	57.32	-100.85	75	LACU	North America	GCD1
Two Hill Lake	441	XARE	55.98	-97.28	200	LACU	North America	GCD1
OK Lake	442	XARE	54.8	-95.25	108	LACU	North America	GCD1
Lago Guanaco	140	C125	-51.13	-73.1	60	LKET	South America	GCD1
Potrok Aike	142	X01K	-51.96	-70.38	100	LVOL	South America	GCD2
Laguna Azul	539	X01K	-52.12	-69.52	100	LEXP	South America	GCD2

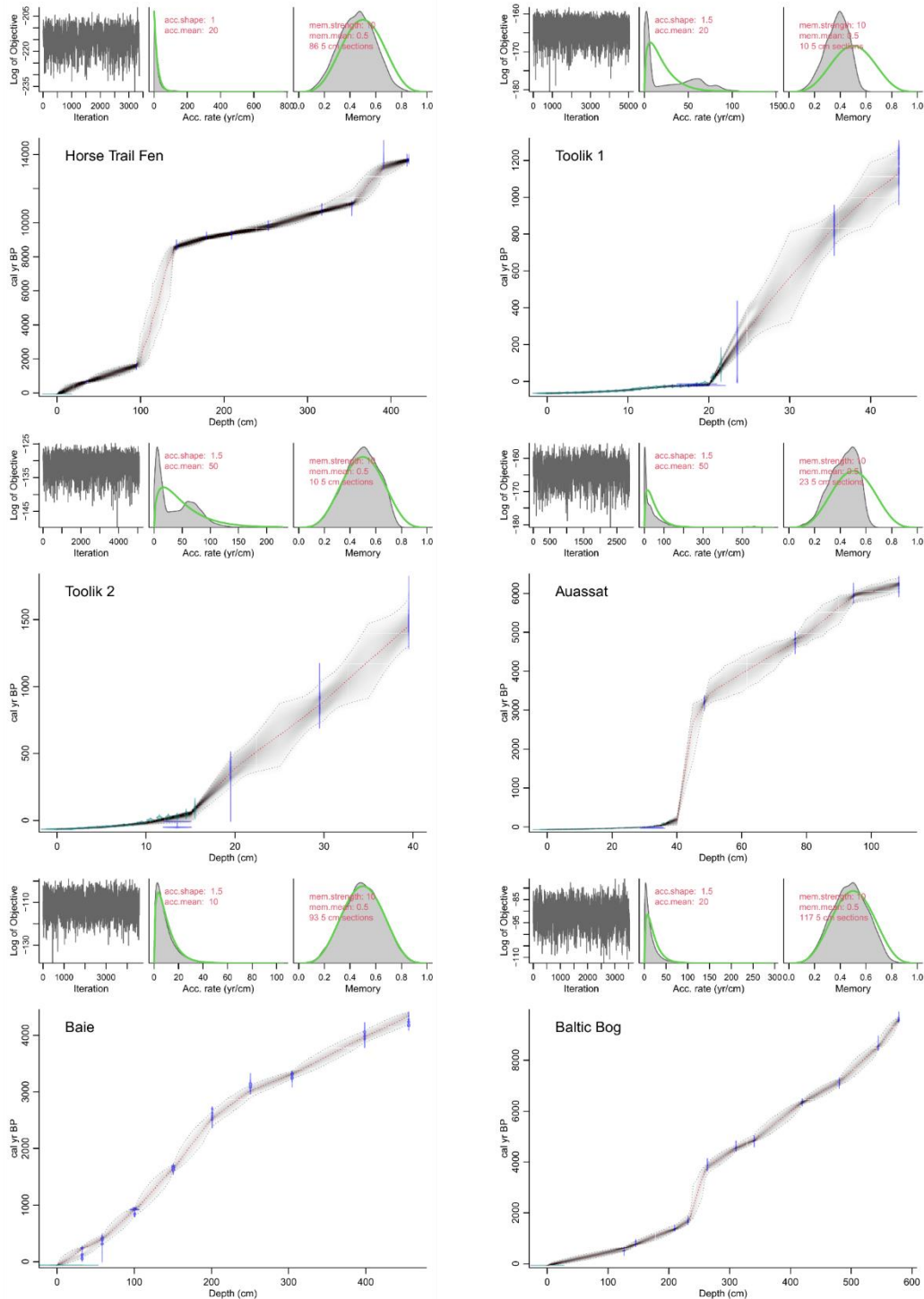


Figure C.2. Age-depth models for records 1-6. For each age-depth model upper panels depict the MCMC iterations (left; good runs show a stationary distribution with little structure among neighbouring iterations), the prior (green curves) and posterior (grey histograms) distributions for the accumulation rate (middle panel) and memory (right panel). Bottom panel shows the calibrated ^{14}C dates (transparent blue) and the age-depth model (darker greys indicate more likely calendar ages; grey stippled lines show 95% confidence intervals; red curve shows single 'best' model based on the median age for each depth). Prior information for accumulation rate and its memory or variability are shown as red text.

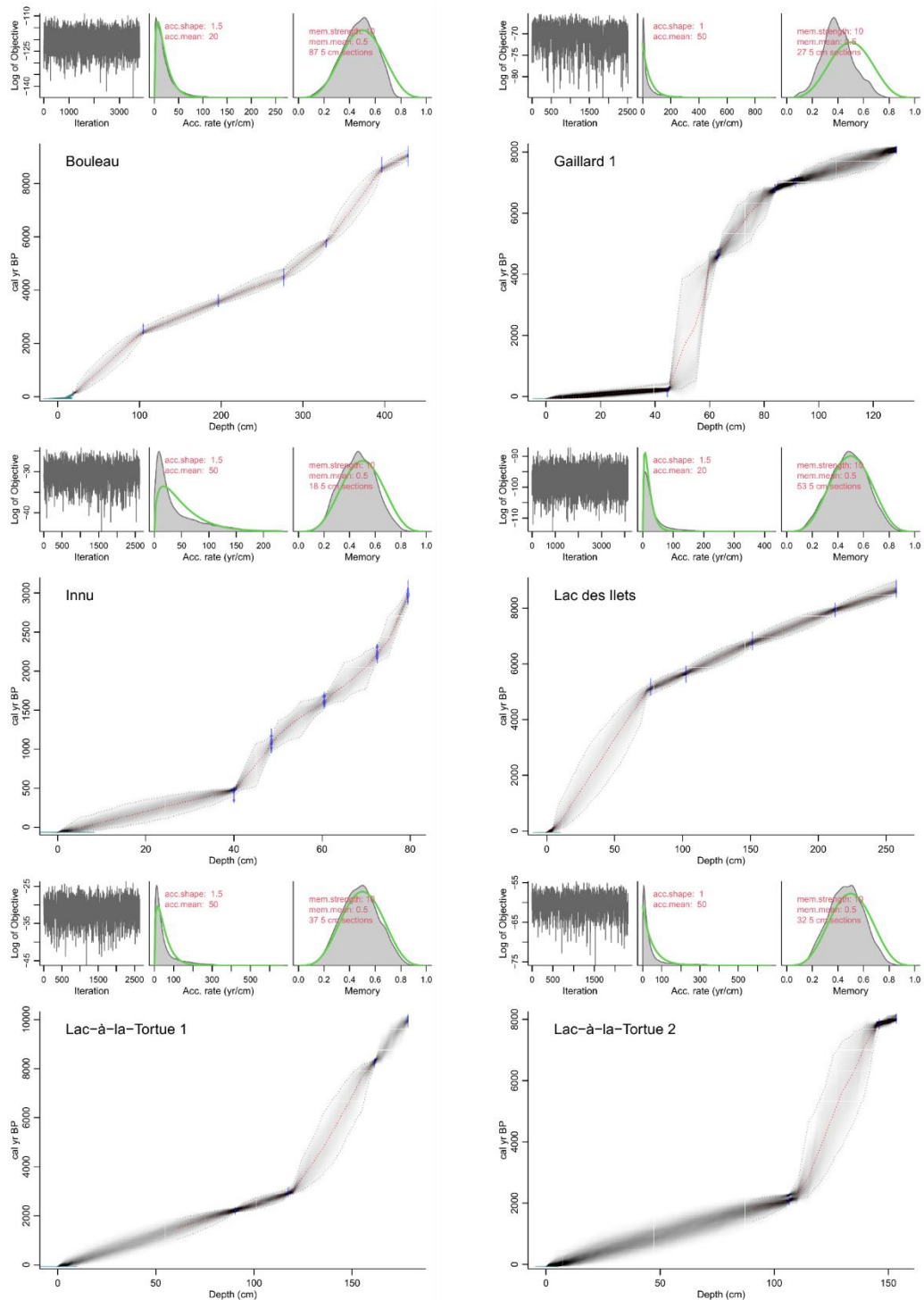


Figure C.3. Age-depth models for records 7-12. For each age-depth model upper panels depict the MCMC iterations (left; good runs show a stationary distribution with little structure among neighbouring iterations), the prior (green curves) and posterior (grey histograms) distributions for the accumulation rate (middle panel) and memory (right panel). Bottom panel shows the calibrated ^{14}C dates (transparent blue) and the age-depth model (darker greys indicate more likely calendar ages; grey stippled lines show 95% confidence intervals; red curve shows single 'best' model based on the median age for each depth). Prior information for accumulation rate and its memory or variability are shown as red text.

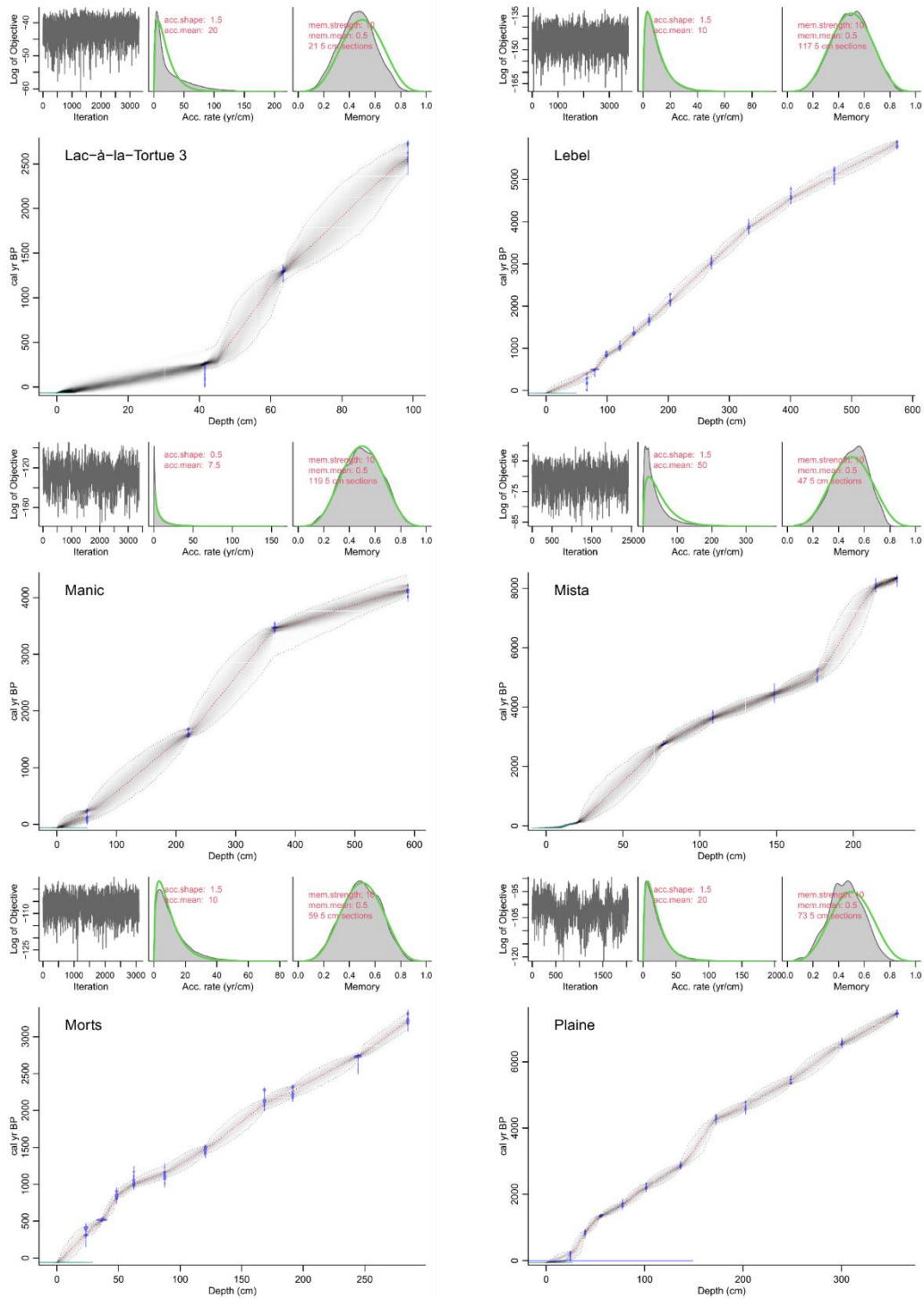


Figure C.4. Age-depth models for records 3-18. For each age-depth model upper panels depict the MCMC iterations (left; good runs show a stationary distribution with little structure among neighbouring iterations), the prior (green curves) and posterior (grey histograms) distributions for the accumulation rate (middle panel) and memory (right panel). Bottom panel shows the calibrated ^{14}C dates (transparent blue) and the age-depth model (darker greys indicate more likely calendar ages; grey stippled lines show 95% confidence intervals; red curve shows single 'best' model based on the median age for each depth). Prior information for accumulation rate and its memory or variability are shown as red text.

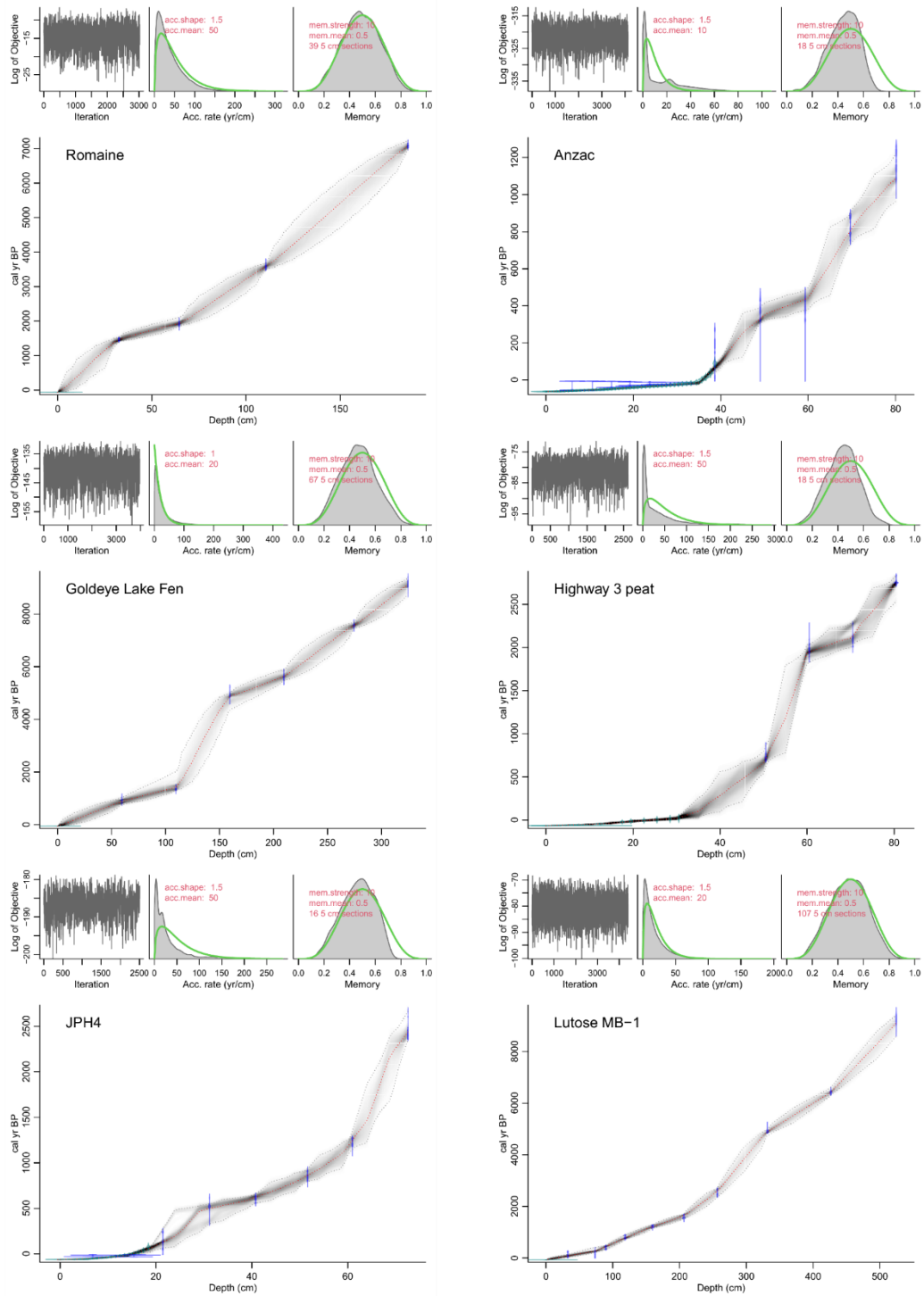


Figure C.5. Age-depth models for records 19-24. For each age-depth model upper panels depict the MCMC iterations (left; good runs show a stationary distribution with little structure among neighbouring iterations), the prior (green curves) and posterior (grey histograms) distributions for the accumulation rate (middle panel) and memory (right panel). Bottom panel shows the calibrated ^{14}C dates (transparent blue) and the age-depth model (darker greys indicate more likely calendar ages; grey stippled lines show 95% confidence intervals; red curve shows single 'best' model based on the median age for each depth). Prior information for accumulation rate and its memory or variability are shown as red text.

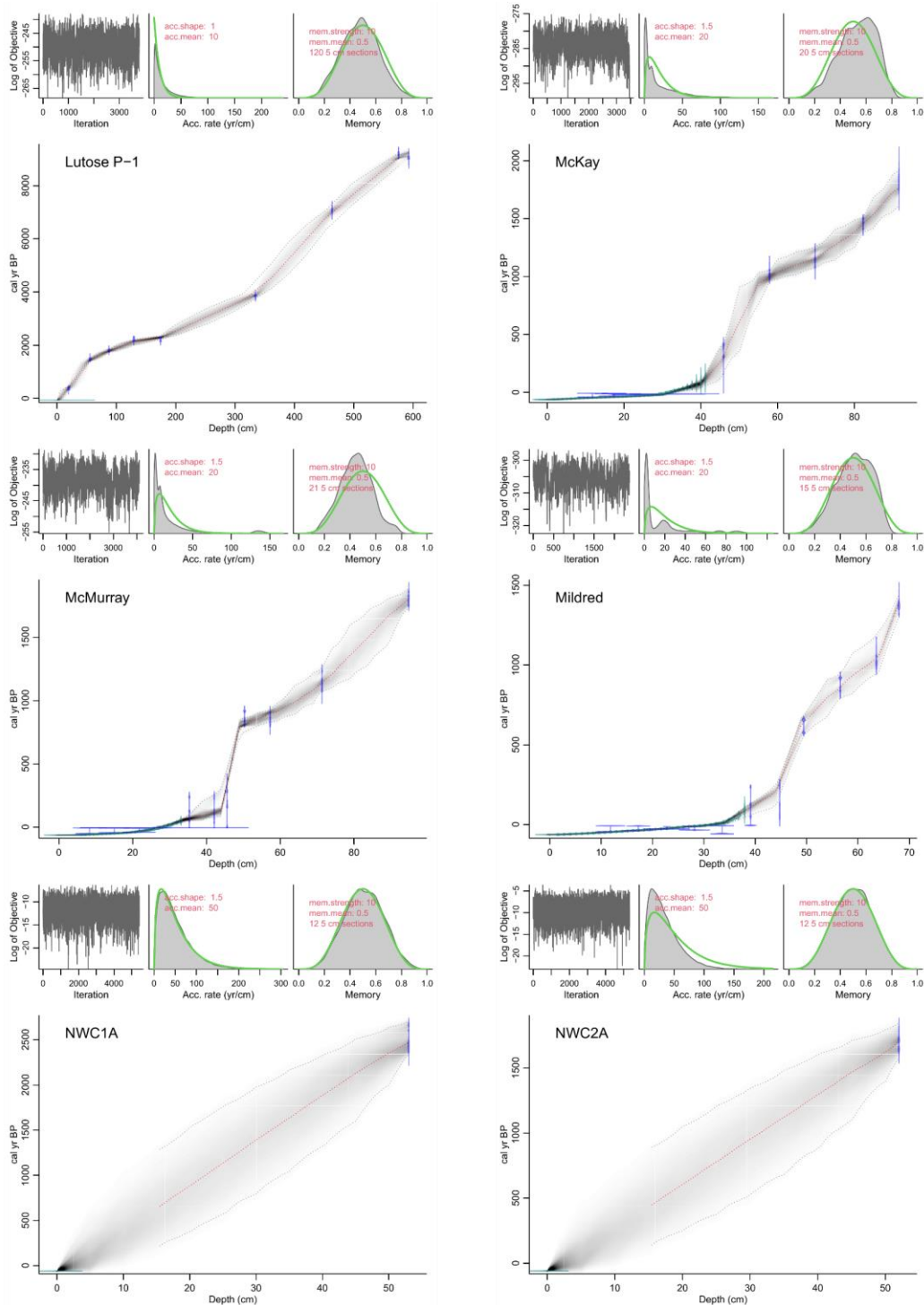


Figure C.6. Age-depth models for records 25-30. For each age-depth model upper panels depict the MCMC iterations (left; good runs show a stationary distribution with little structure among neighbouring iterations), the prior (green curves) and posterior (grey histograms) distributions for the accumulation rate (middle panel) and memory (right panel). Bottom panel shows the calibrated ^{14}C dates (transparent blue) and the age-depth model (darker greys indicate more likely calendar ages; grey stippled lines show 95% confidence intervals; red curve shows single 'best' model based on the median age for each depth). Prior information for accumulation rate and its memory or variability are shown as red text.

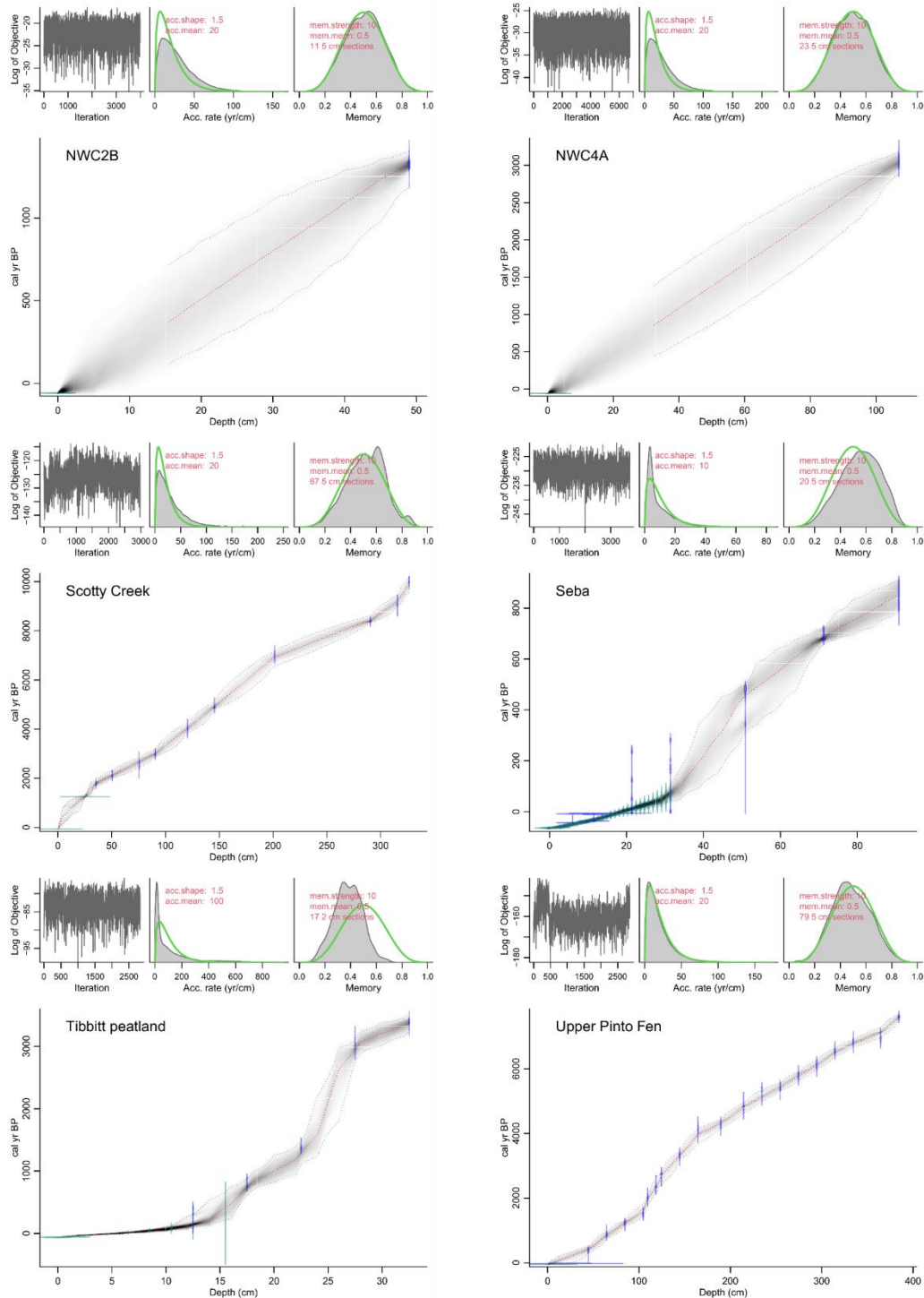


Figure C.7. Age-depth models for records 31-36. For each age-depth model upper panels depict the MCMC iterations (left; good runs show a stationary distribution with little structure among neighbouring iterations), the prior (green curves) and posterior (grey histograms) distributions for the accumulation rate (middle panel) and memory (right panel). Bottom panel shows the calibrated ^{14}C dates (transparent blue) and the age-depth model (darker greys indicate more likely calendar ages; grey stippled lines show 95% confidence intervals; red curve shows single 'best' model based on the median age for each depth). Prior information for accumulation rate and its memory or variability are shown as red text.

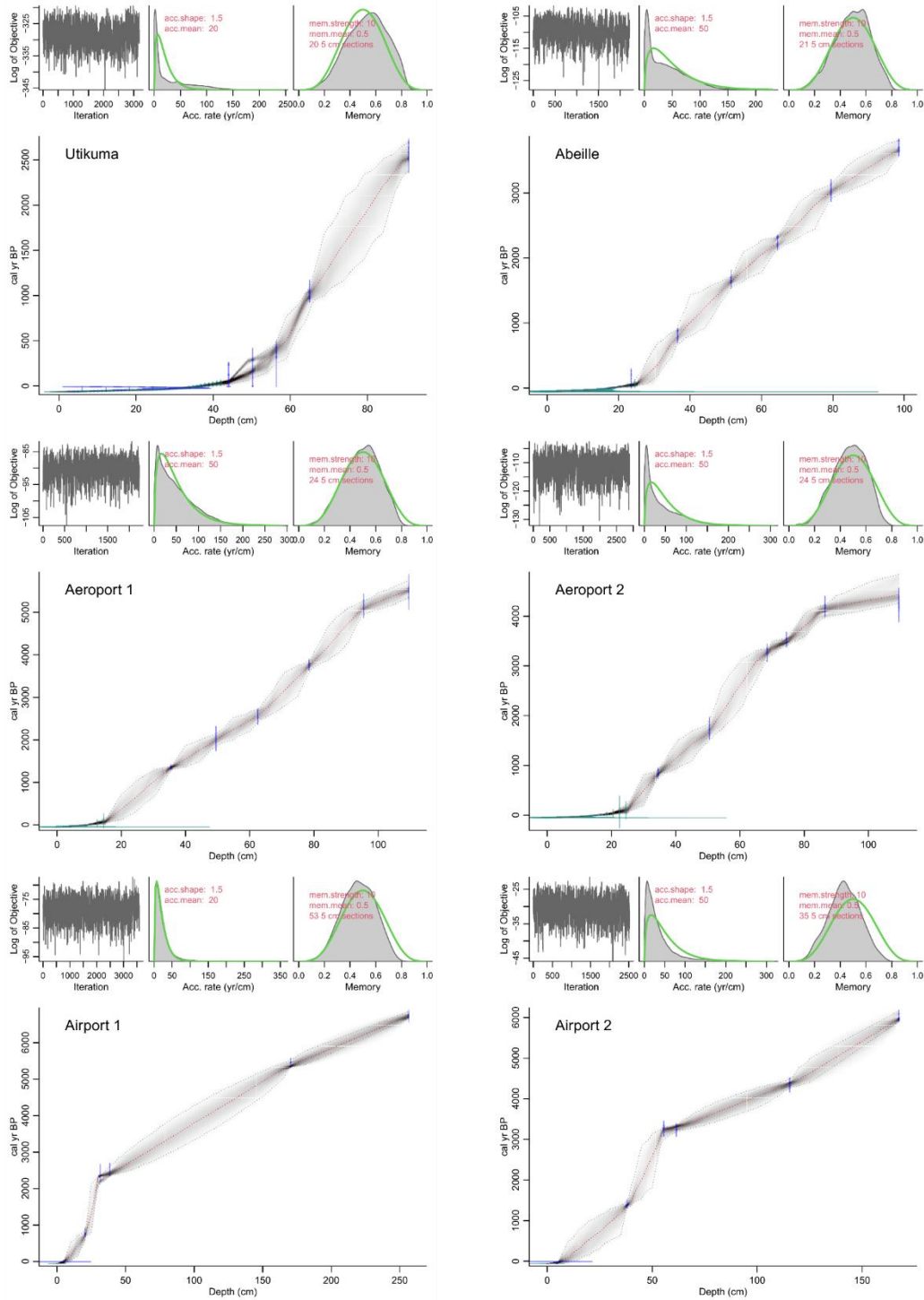


Figure C.8. Age-depth models for records 37-42. For each age-depth model upper panels depict the MCMC iterations (left; good runs show a stationary distribution with little structure among neighbouring iterations), the prior (green curves) and posterior (grey histograms) distributions for the accumulation rate (middle panel) and memory (right panel). Bottom panel shows the calibrated ^{14}C dates (transparent blue) and the age-depth model (darker greys indicate more likely calendar ages; grey stippled lines show 95% confidence intervals; red curve shows single 'best' model based on the median age for each depth). Prior information for accumulation rate and its memory or variability are shown as red text.

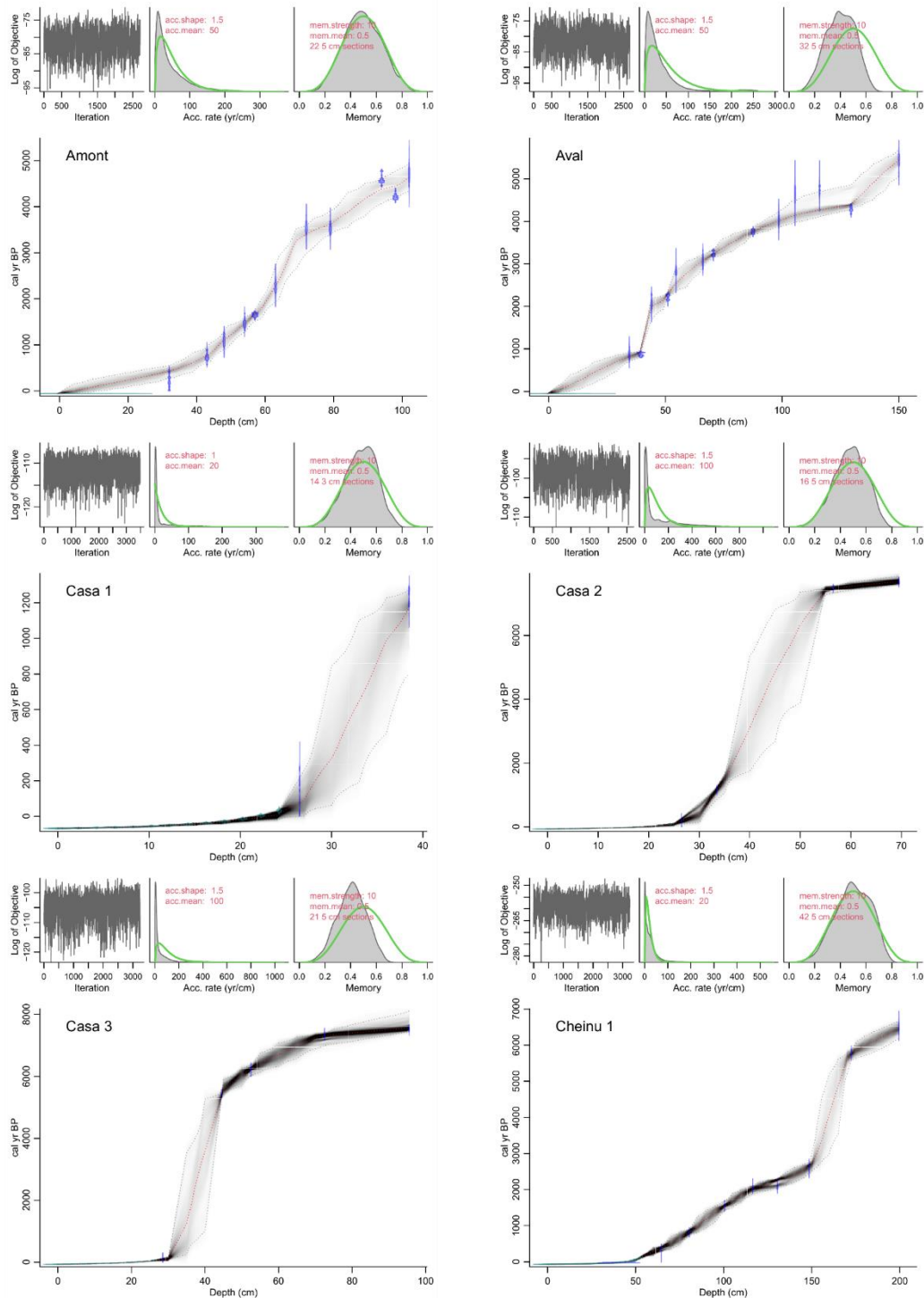


Figure C.9. Age-depth models for records 43-48. For each age-depth model upper panels depict the MCMC iterations (left; good runs show a stationary distribution with little structure among neighbouring iterations), the prior (green curves) and posterior (grey histograms) distributions for the accumulation rate (middle panel) and memory (right panel). Bottom panel shows the calibrated ^{14}C dates (transparent blue) and the age-depth model (darker greys indicate more likely calendar ages; grey stippled lines show 95% confidence intervals; red curve shows single 'best' model based on the median age for each depth). Prior information for accumulation rate and its memory or variability are shown as red text.

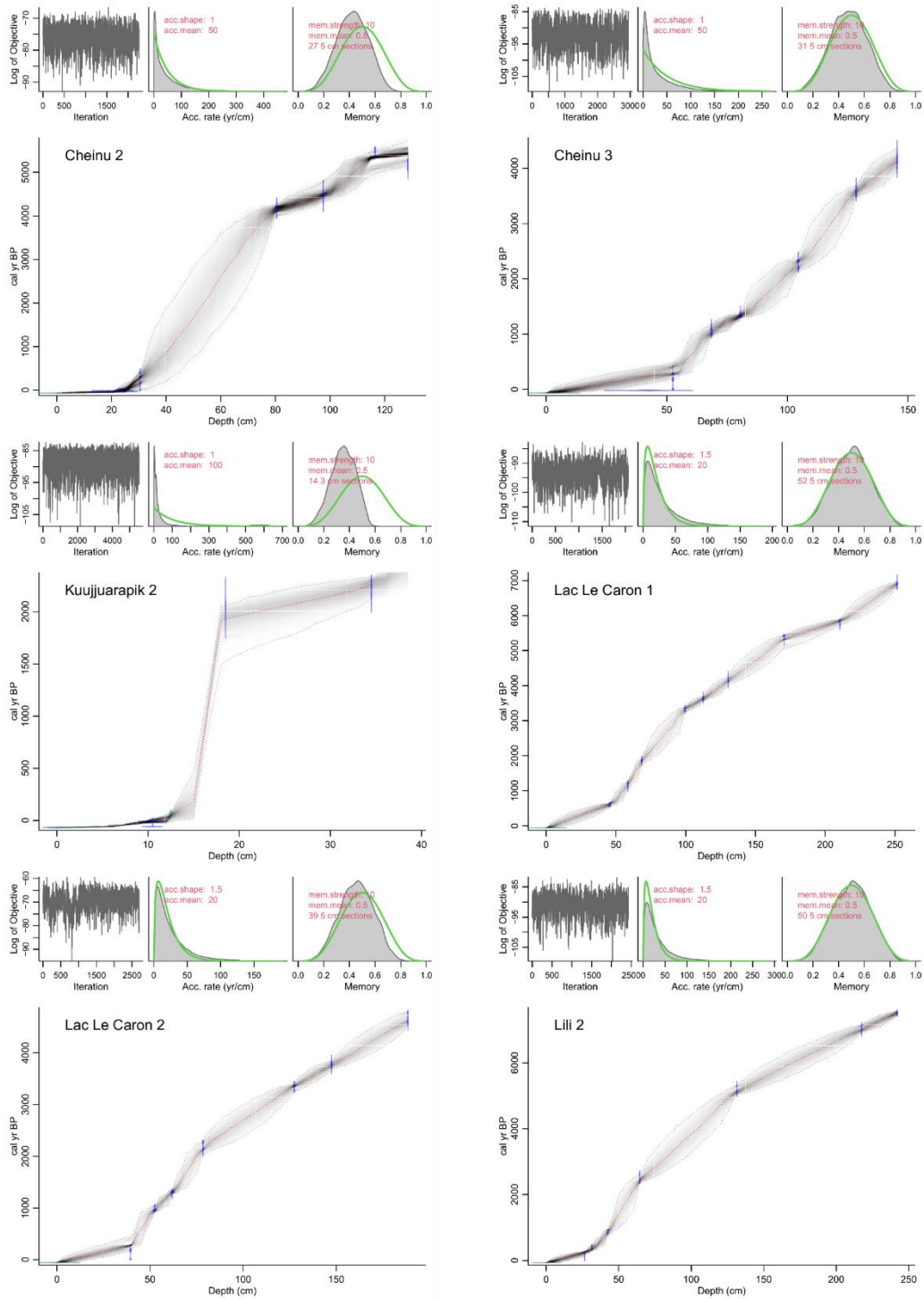


Figure C.10. Age-depth models for records 49-54. For each age-depth model upper panels depict the MCMC iterations (left; good runs show a stationary distribution with little structure among neighbouring iterations), the prior (green curves) and posterior (grey histograms) distributions for the accumulation rate (middle panel) and memory (right panel). Bottom panel shows the calibrated ¹⁴C dates (transparent blue) and the age-depth model (darker greys indicate more likely calendar ages; grey stippled lines show 95% confidence intervals; red curve shows single 'best' model based on the median age for each depth). Prior information for accumulation rate and its memory or variability are shown as red text.

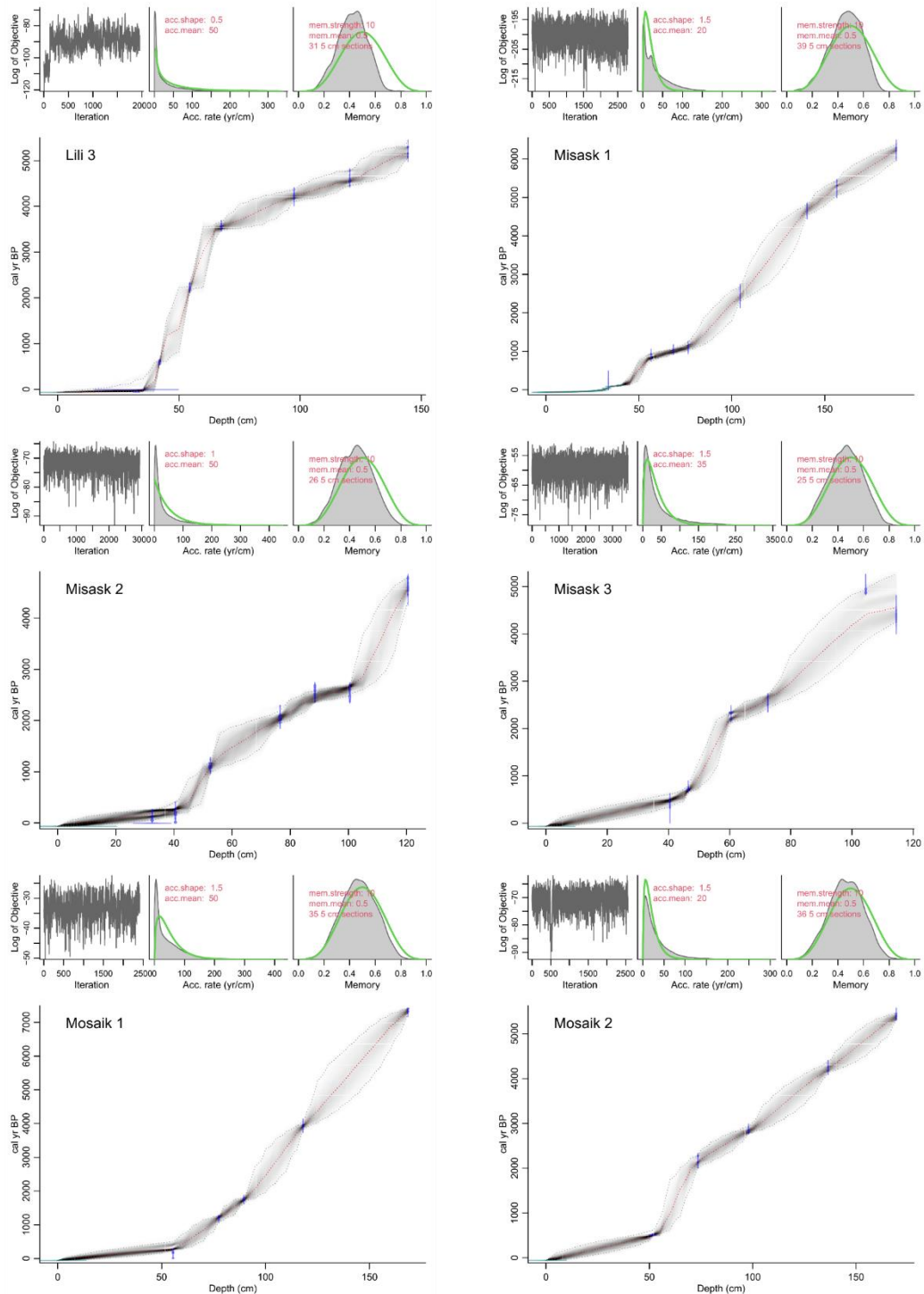


Figure C.11. Age-depth models for records 55-60. For each age-depth model upper panels depict the MCMC iterations (left; good runs show a stationary distribution with little structure among neighbouring iterations), the prior (green curves) and posterior (grey histograms) distributions for the accumulation rate (middle panel) and memory (right panel). Bottom panel shows the calibrated ^{14}C dates (transparent blue) and the age-depth model (darker greys indicate more likely calendar ages; grey stippled lines show 95% confidence intervals; red curve shows single 'best' model based on the median age for each depth). Prior information for accumulation rate and its memory or variability are shown as red text.

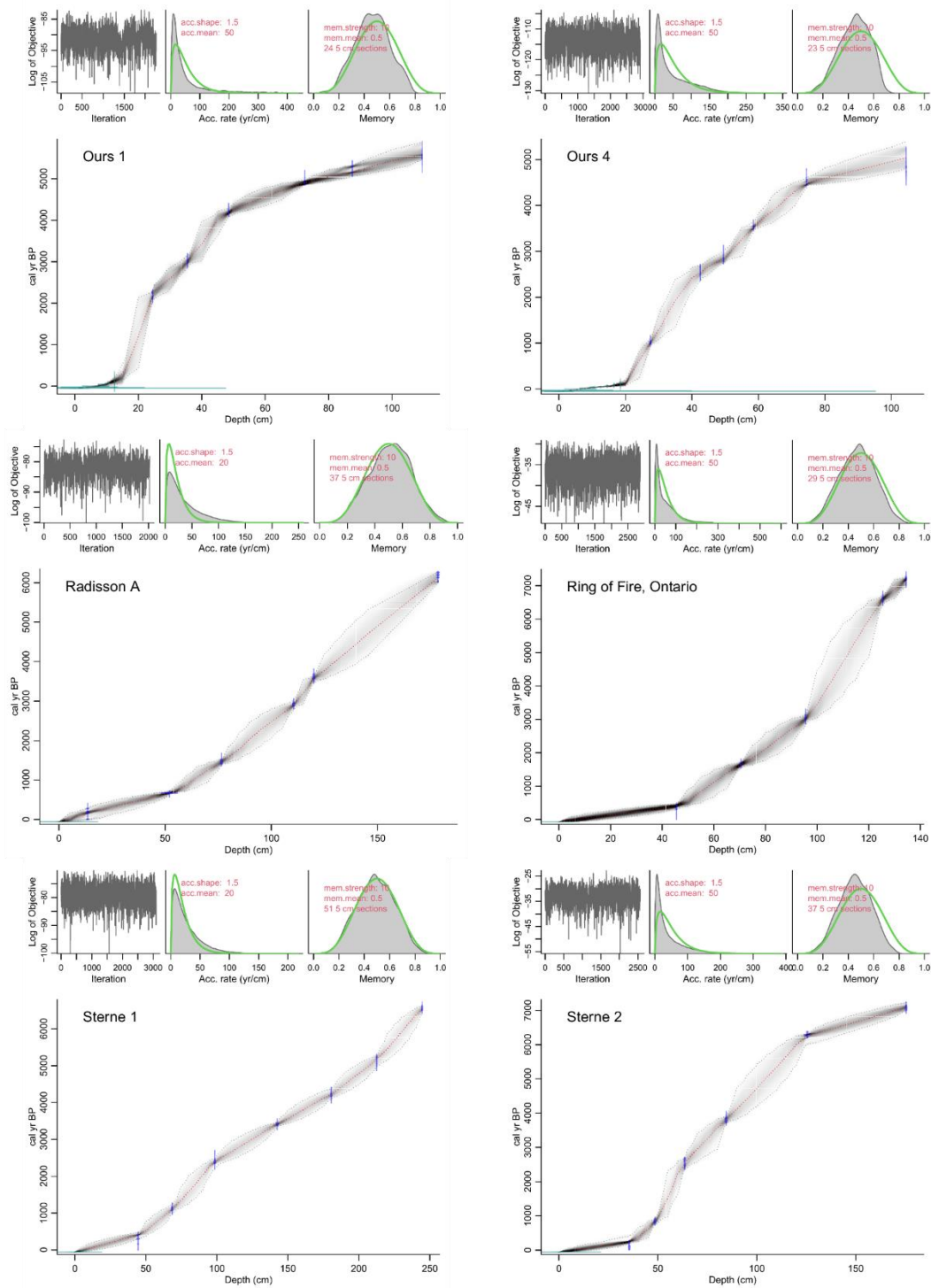


Figure C.12. Age-depth models for records 61-66. For each age-depth model upper panels depict the MCMC iterations (left; good runs show a stationary distribution with little structure among neighbouring iterations), the prior (green curves) and posterior (grey histograms) distributions for the accumulation rate (middle panel) and memory (right panel). Bottom panel shows the calibrated ^{14}C dates (transparent blue) and the age-depth model (darker greys indicate more likely calendar ages; grey stippled lines show 95% confidence intervals; red curve shows single 'best' model based on the median age for each depth). Prior information for accumulation rate and its memory or variability are shown as red text.

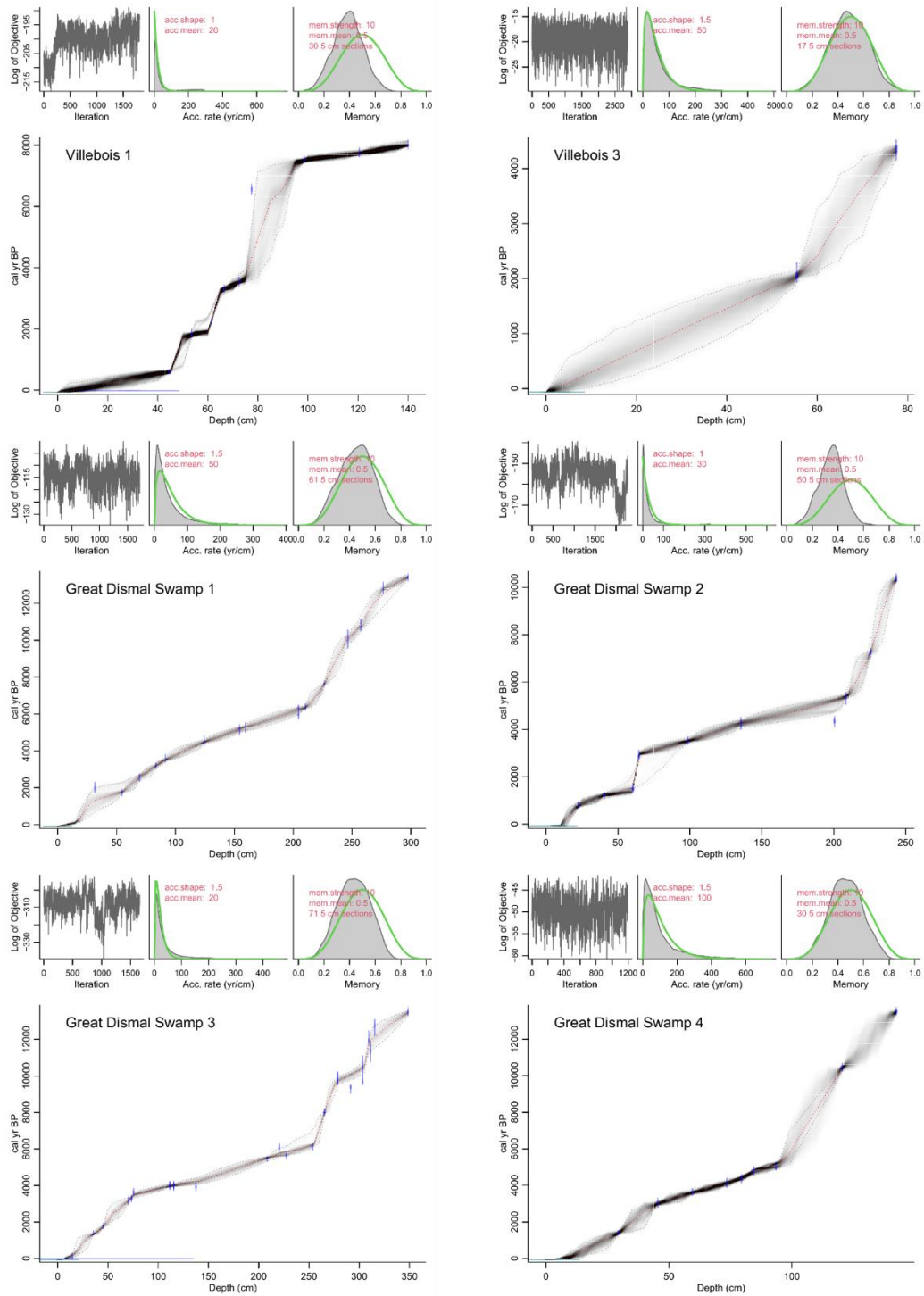


Figure C.13. Age-depth models for records 67-72. For each age-depth model upper panels depict the MCMC iterations (left; good runs show a stationary distribution with little structure among neighbouring iterations), the prior (green curves) and posterior (grey histograms) distributions for the accumulation rate (middle panel) and memory (right panel). Bottom panel shows the calibrated ^{14}C dates (transparent blue) and the age-depth model (darker greys indicate more likely calendar ages; grey stippled lines show 95% confidence intervals; red curve shows single 'best' model based on the median age for each depth). Prior information for accumulation rate and its memory or variability are shown as red text.

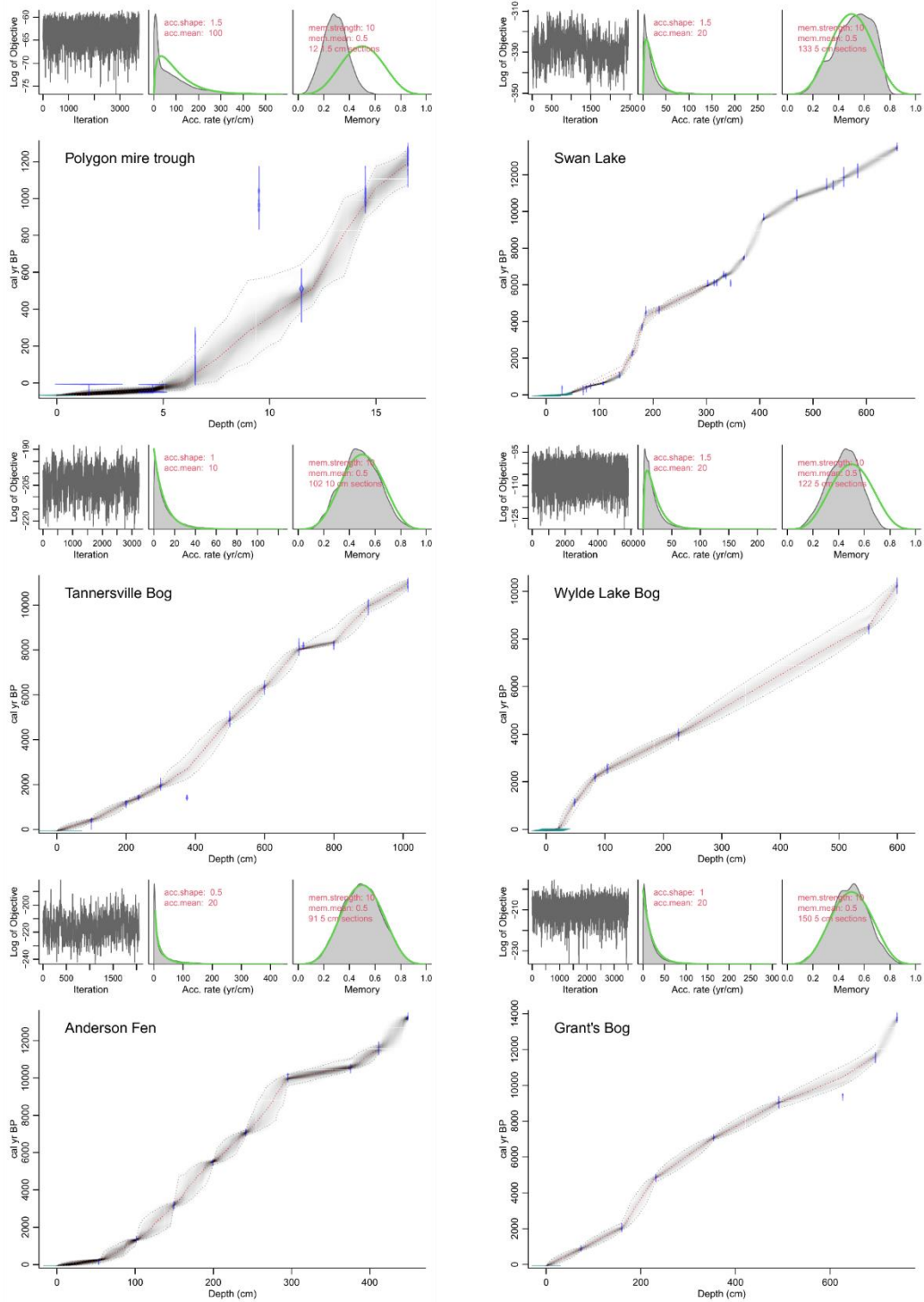


Figure C.14. Age-depth models for records 73-78. For each age-depth model upper panels depict the MCMC iterations (left; good runs show a stationary distribution with little structure among neighbouring iterations), the prior (green curves) and posterior (grey histograms) distributions for the accumulation rate (middle panel) and memory (right panel). Bottom panel shows the calibrated ^{14}C dates (transparent blue) and the age-depth model (darker greys indicate more likely calendar ages; grey stippled lines show 95% confidence intervals; red curve shows single 'best' model based on the median age for each depth). Prior information for accumulation rate and its memory or variability are shown as red text.

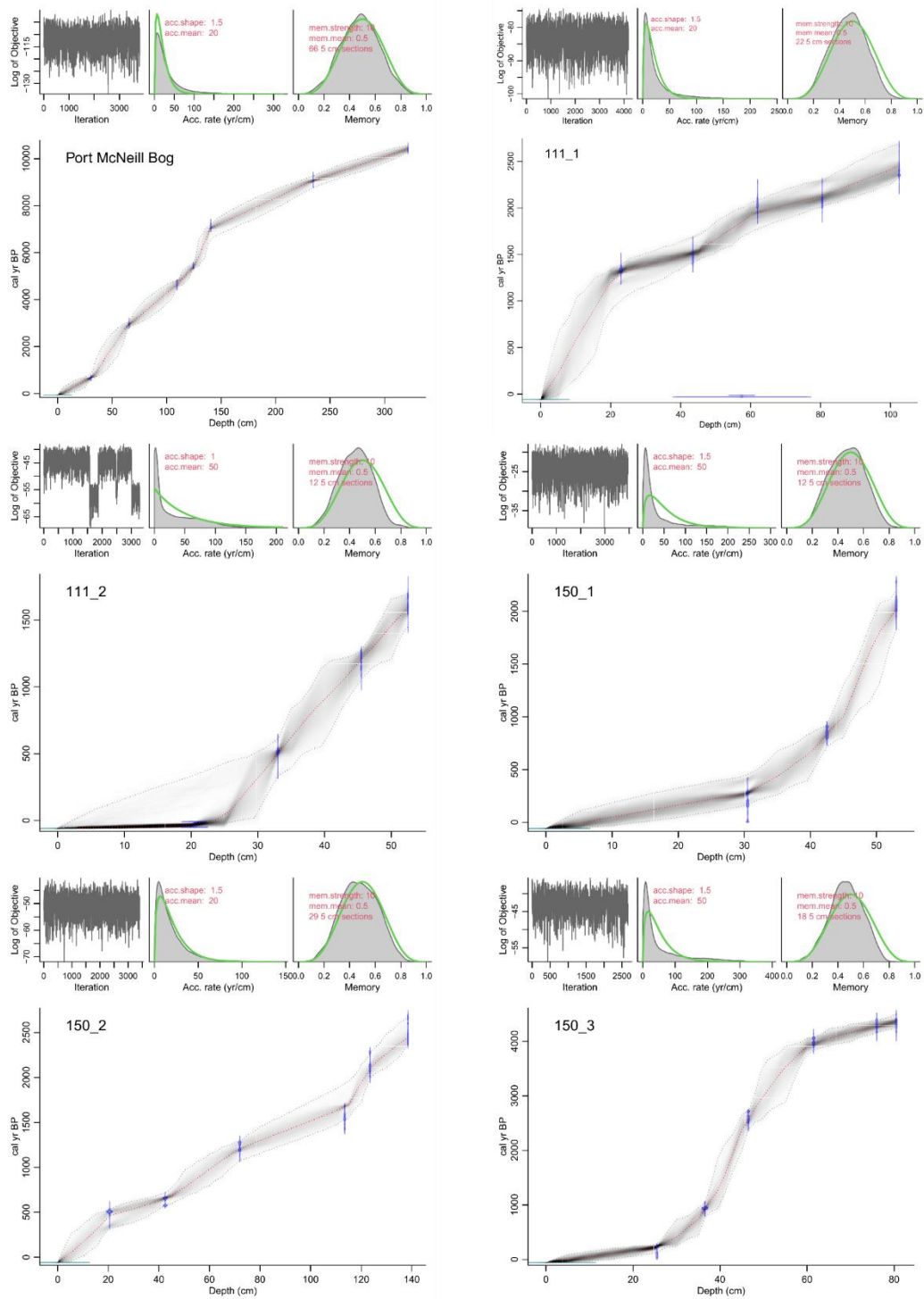


Figure C.15. Age-depth models for records 79-84. For each age-depth model upper panels depict the MCMC iterations (left; good runs show a stationary distribution with little structure among neighbouring iterations), the prior (green curves) and posterior (grey histograms) distributions for the accumulation rate (middle panel) and memory (right panel). Bottom panel shows the calibrated ^{14}C dates (transparent blue) and the age-depth model (darker greys indicate more likely calendar ages; grey stippled lines show 95% confidence intervals; red curve shows single 'best' model based on the median age for each depth). Prior information for accumulation rate and its memory or variability are shown as red text.

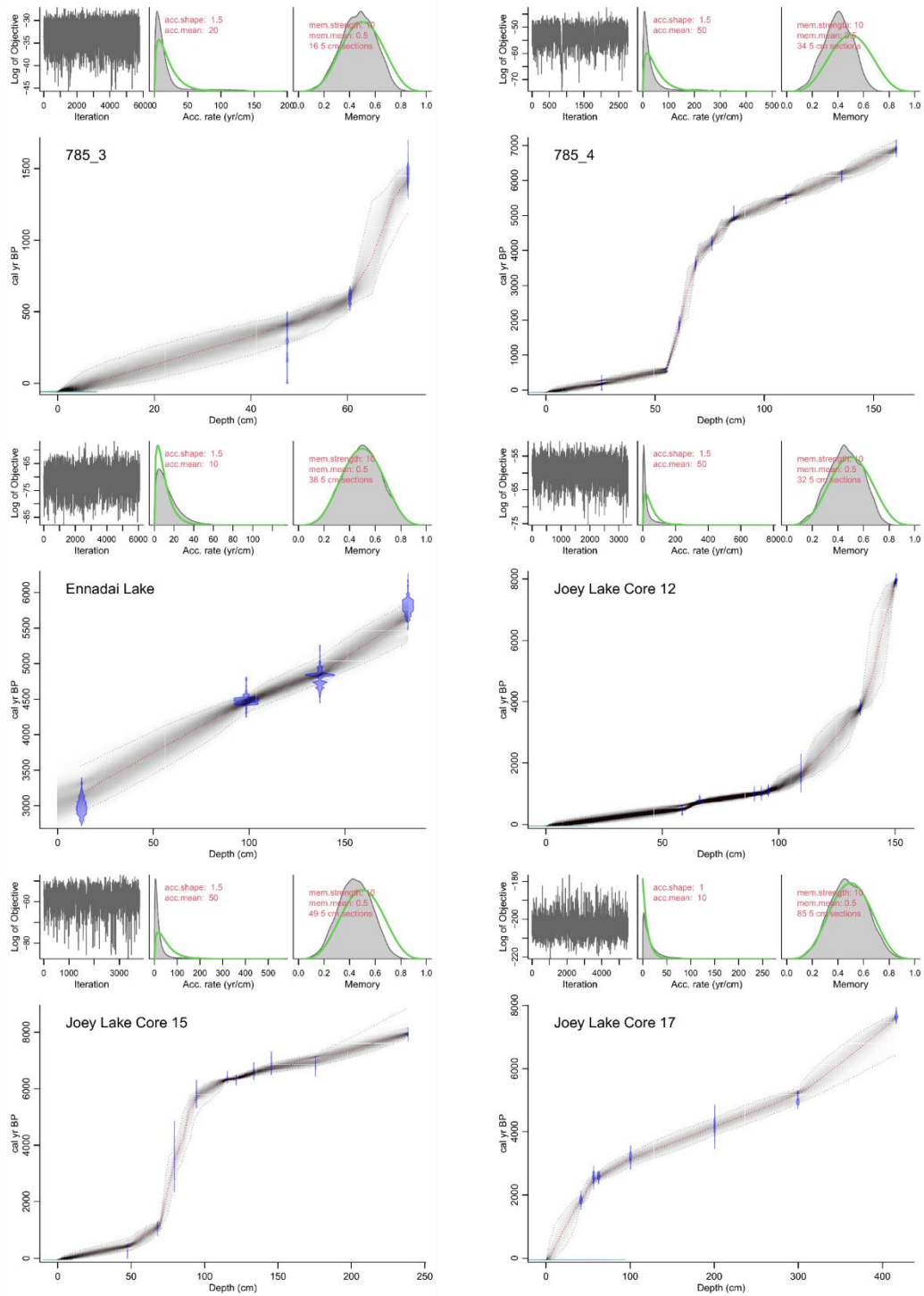


Figure C.17. Age-depth models for records 91-96. For each age-depth model upper panels depict the MCMC iterations (left; good runs show a stationary distribution with little structure among neighbouring iterations), the prior (green curves) and posterior (grey histograms) distributions for the accumulation rate (middle panel) and memory (right panel). Bottom panel shows the calibrated ^{14}C dates (transparent blue) and the age-depth model (darker greys indicate more likely calendar ages; grey stippled lines show 95% confidence intervals; red curve shows single 'best' model based on the median age for each depth). Prior information for accumulation rate and its memory or variability are shown as red text.

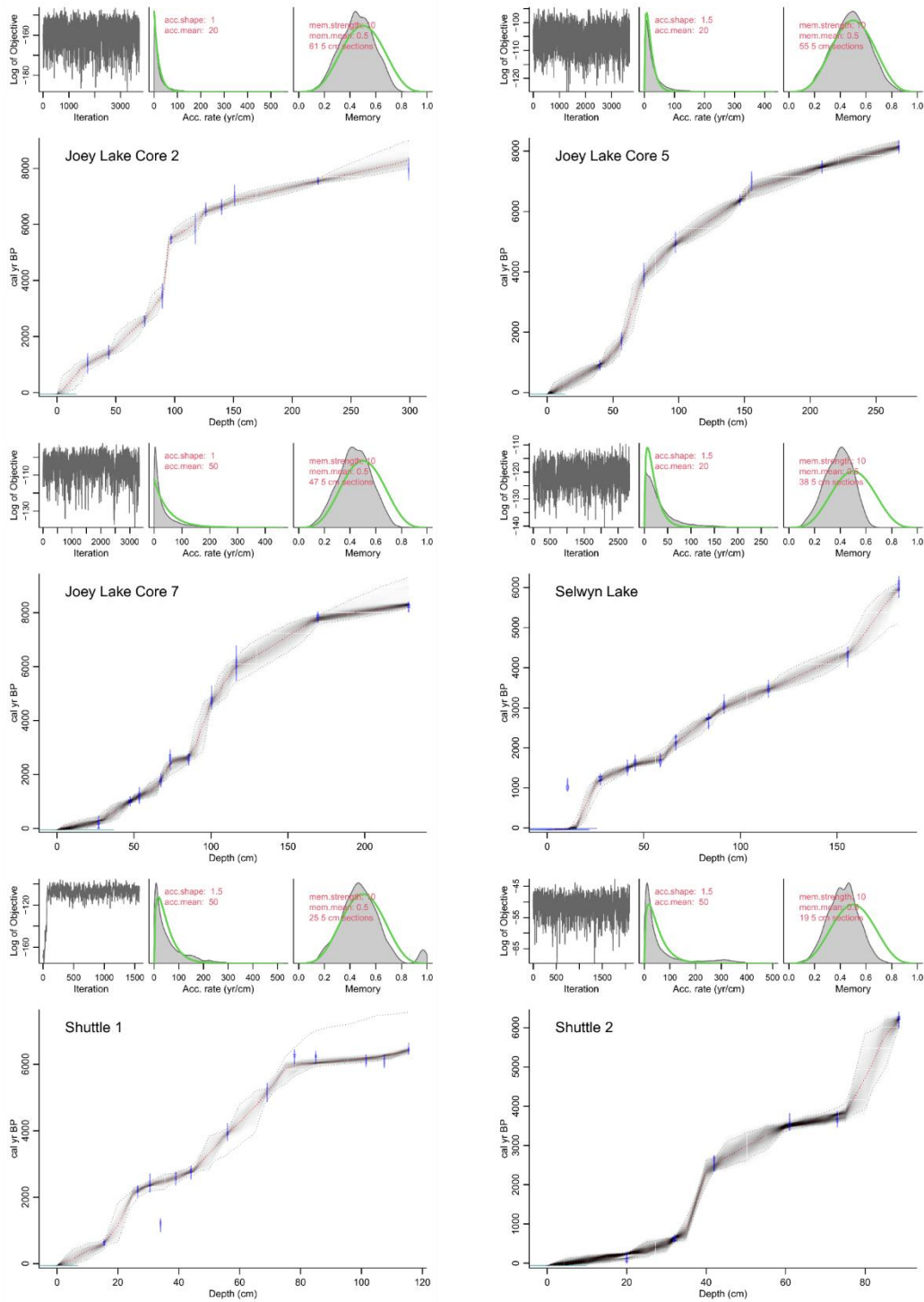


Figure C.18. Age-depth models for records 97-102. For each age-depth model upper panels depict the MCMC iterations (left; good runs show a stationary distribution with little structure among neighbouring iterations), the prior (green curves) and posterior (grey histograms) distributions for the accumulation rate (middle panel) and memory (right panel). Bottom panel shows the calibrated ^{14}C dates (transparent blue) and the age-depth model (darker greys indicate more likely calendar ages; grey stippled lines show 95% confidence intervals; red curve shows single 'best' model based on the median age for each depth). Prior information for accumulation rate and its memory or variability are shown as red text.

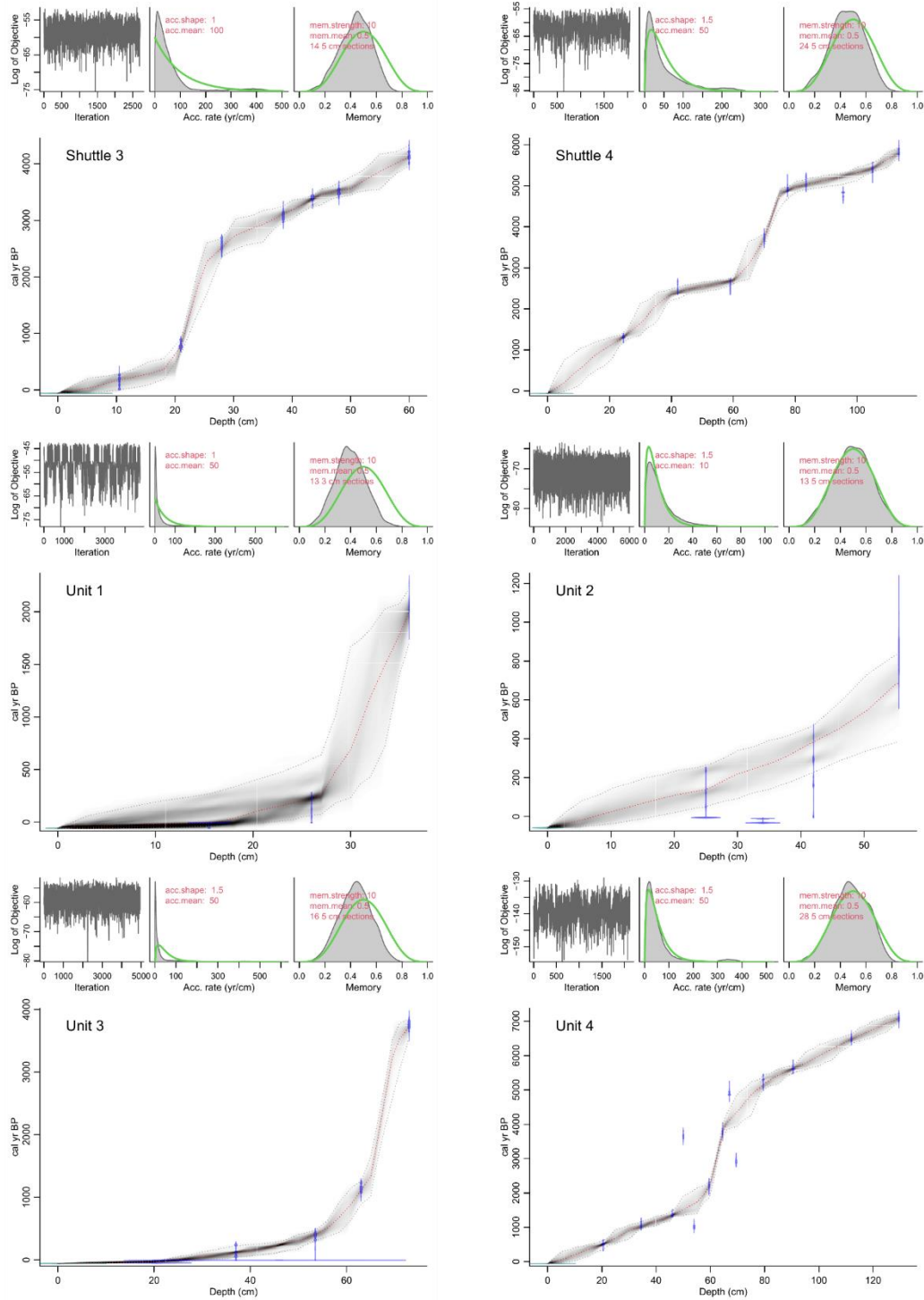


Figure C.19. Age-depth models for records 103-108. For each age-depth model upper panels depict the MCMC iterations (left; good runs show a stationary distribution with little structure among neighbouring iterations), the prior (green curves) and posterior (grey histograms) distributions for the accumulation rate (middle panel) and memory (right panel). Bottom panel shows the calibrated ^{14}C dates (transparent blue) and the age-depth model (darker greys indicate more likely calendar ages; grey stippled lines show 95% confidence intervals; red curve shows single 'best' model based on the median age for each depth). Prior information for accumulation rate and its memory or variability are shown as red text.

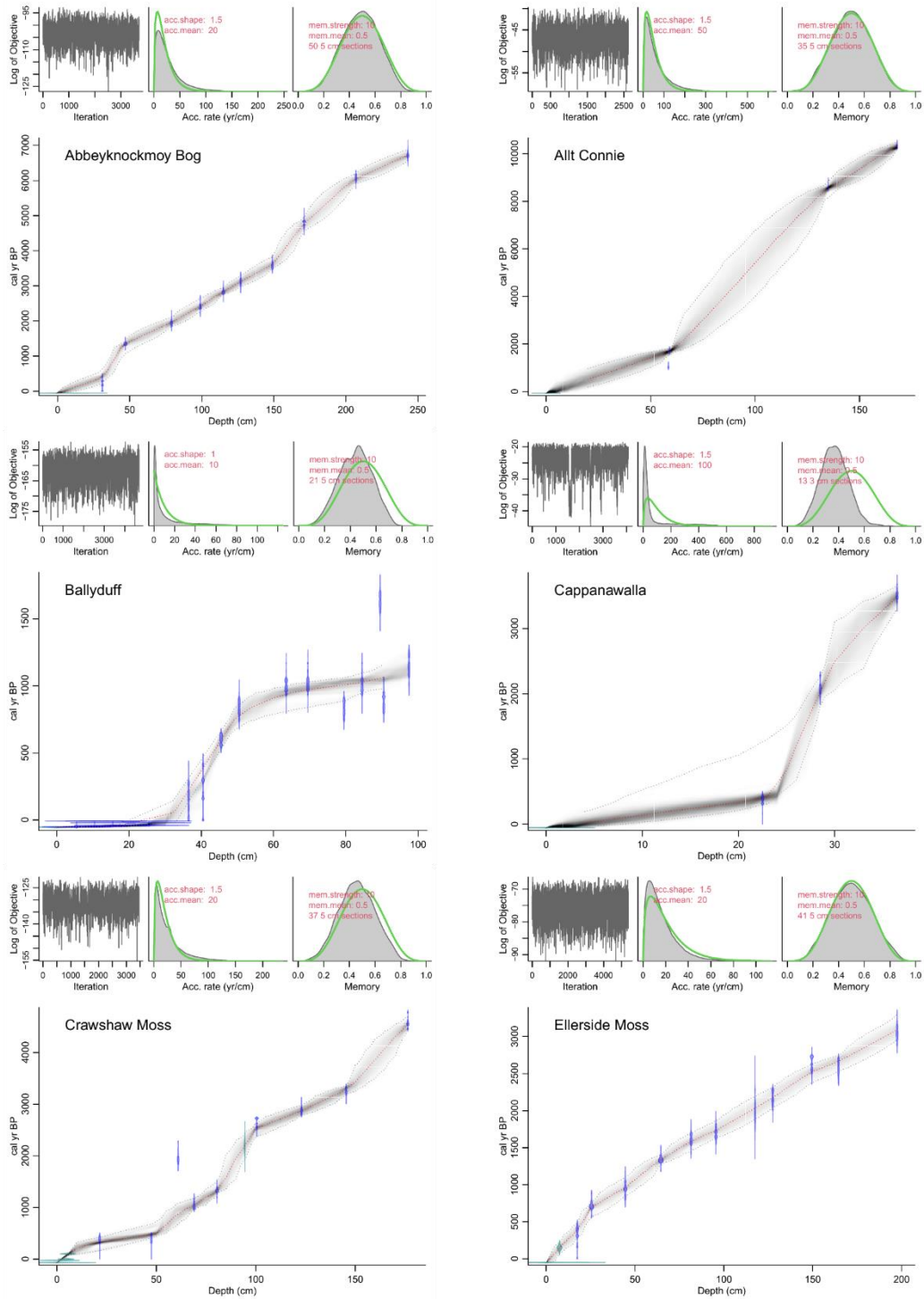


Figure C.20. Age-depth models for records 109-114. For each age-depth model upper panels depict the MCMC iterations (left; good runs show a stationary distribution with little structure among neighbouring iterations), the prior (green curves) and posterior (grey histograms) distributions for the accumulation rate (middle panel) and memory (right panel). Bottom panel shows the calibrated ^{14}C dates (transparent blue) and the age-depth model (darker greys indicate more likely calendar ages; grey stippled lines show 95% confidence intervals; red curve shows single 'best' model based on the median age for each depth). Prior information for accumulation rate and its memory or variability are shown as red text.

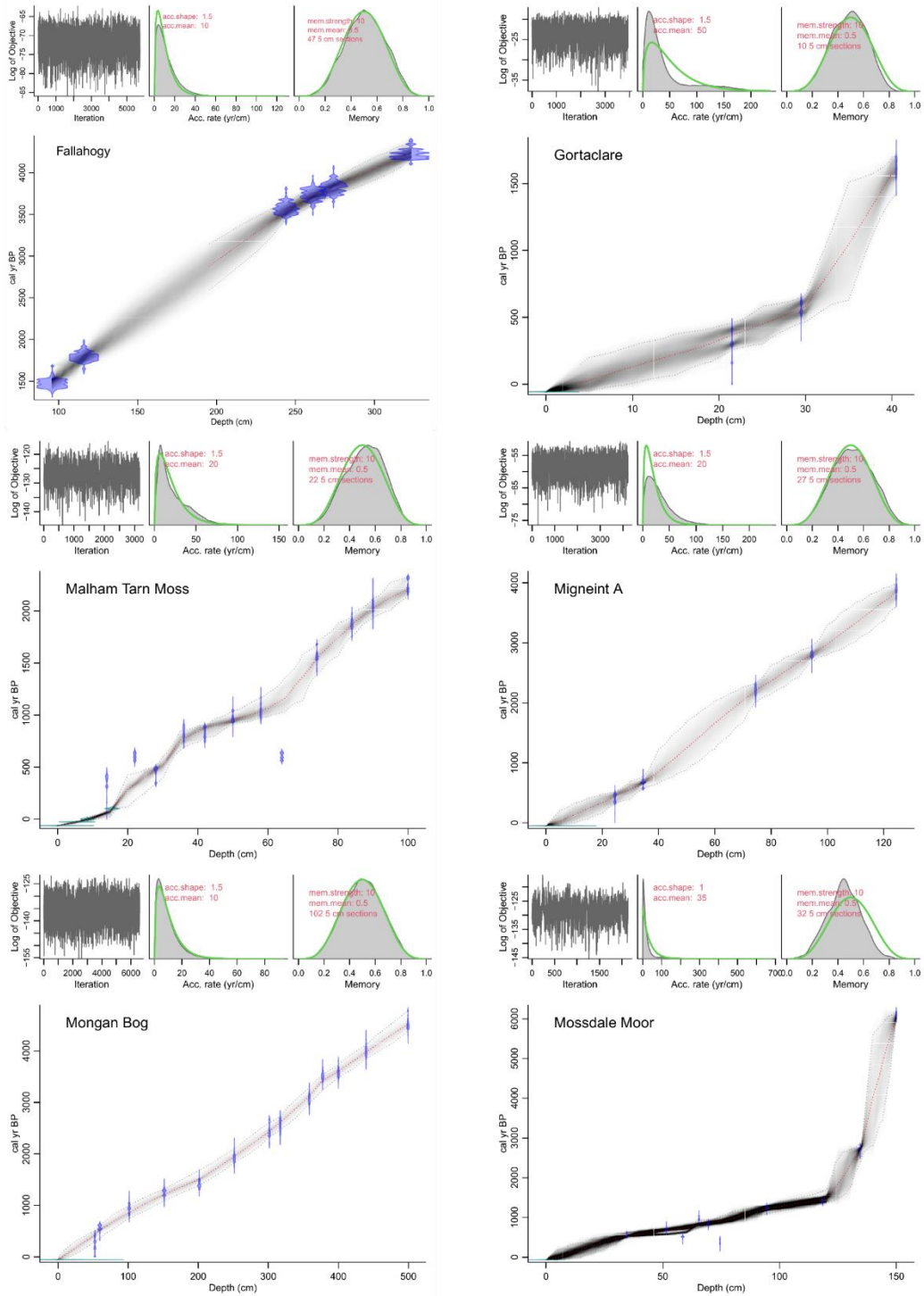


Figure C.21. Age-depth models for records 115-120. For each age-depth model upper panels depict the MCMC iterations (left; good runs show a stationary distribution with little structure among neighbouring iterations), the prior (green curves) and posterior (grey histograms) distributions for the accumulation rate (middle panel) and memory (right panel). Bottom panel shows the calibrated ^{14}C dates (transparent blue) and the age-depth model (darker greys indicate more likely calendar ages; grey stippled lines show 95% confidence intervals; red curve shows single 'best' model based on the median age for each depth). Prior information for accumulation rate and its memory or variability are shown as red text.

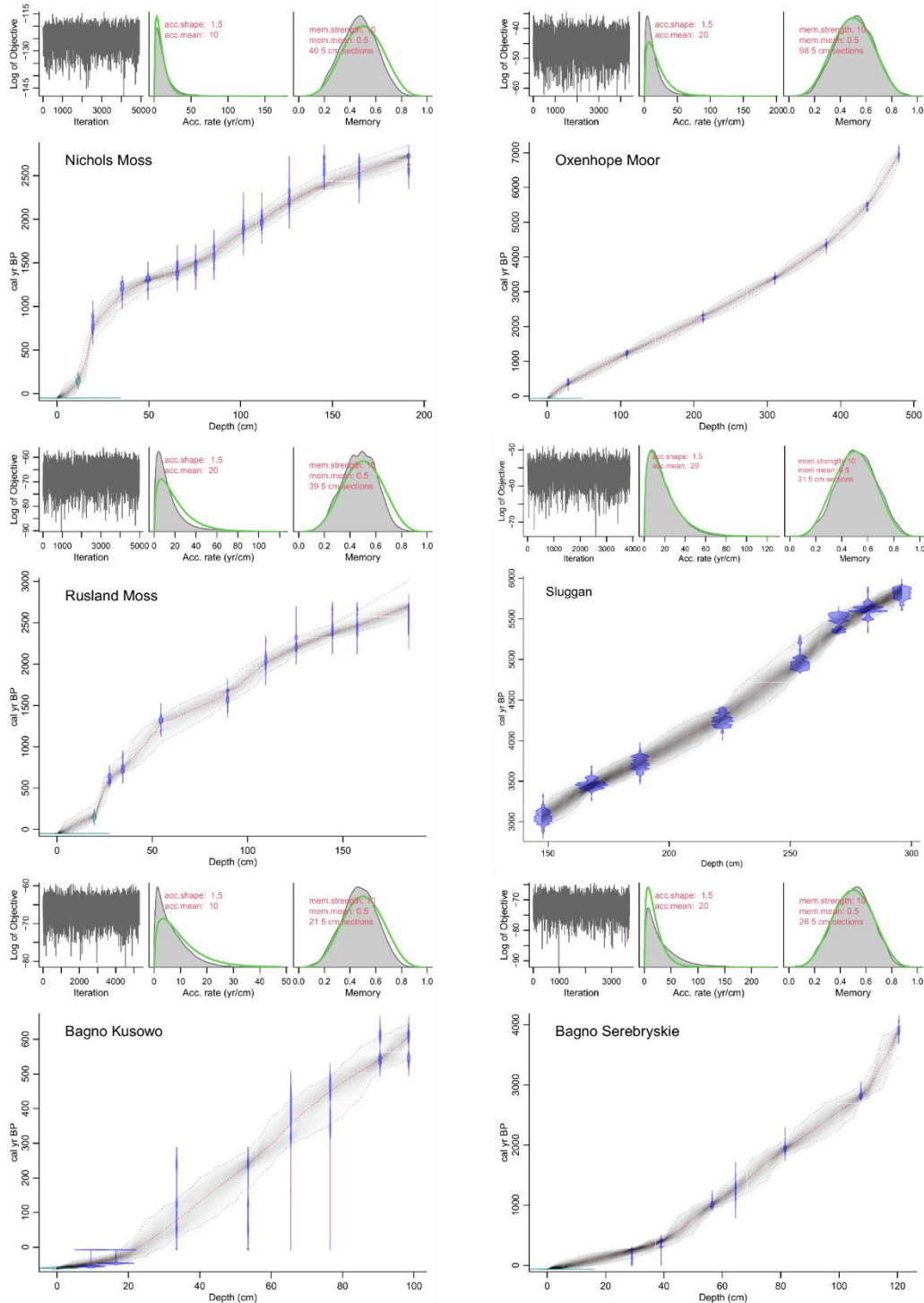


Figure C.22. Age-depth models for records 121-126. For each age-depth model upper panels depict the MCMC iterations (left; good runs show a stationary distribution with little structure among neighbouring iterations), the prior (green curves) and posterior (grey histograms) distributions for the accumulation rate (middle panel) and memory (right panel). Bottom panel shows the calibrated ^{14}C dates (transparent blue) and the age-depth model (darker greys indicate more likely calendar ages; grey stippled lines show 95% confidence intervals; red curve shows single 'best' model based on the median age for each depth). Prior information for accumulation rate and its memory or variability are shown as red text.

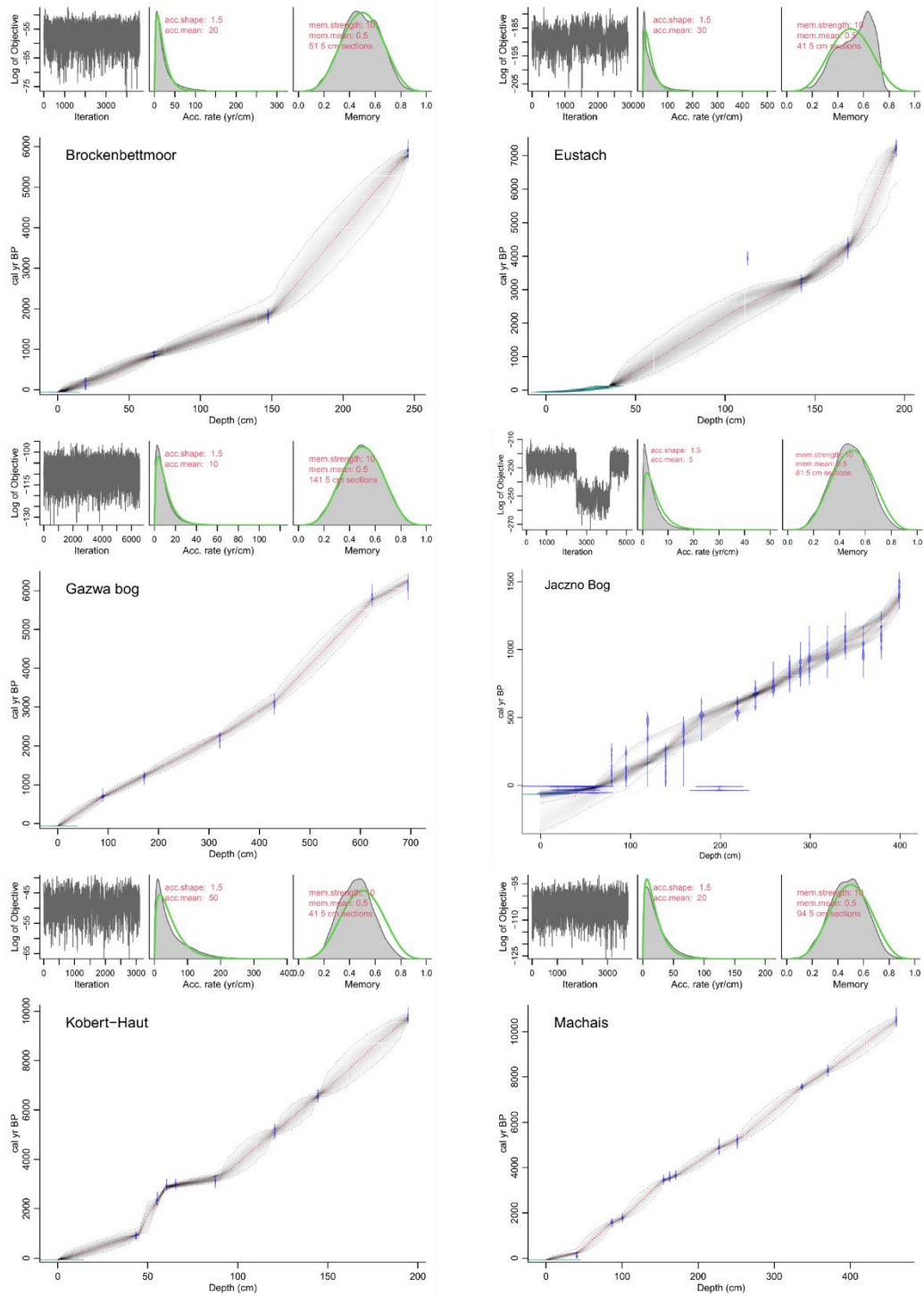


Figure C.23. Age-depth models for records 127-132. For each age-depth model upper panels depict the MCMC iterations (left; good runs show a stationary distribution with little structure among neighbouring iterations), the prior (green curves) and posterior (grey histograms) distributions for the accumulation rate (middle panel) and memory (right panel). Bottom panel shows the calibrated ^{14}C dates (transparent blue) and the age-depth model (darker greys indicate more likely calendar ages; grey stippled lines show 95% confidence intervals; red curve shows single 'best' model based on the median age for each depth). Prior information for accumulation rate and its memory or variability are shown as red text.

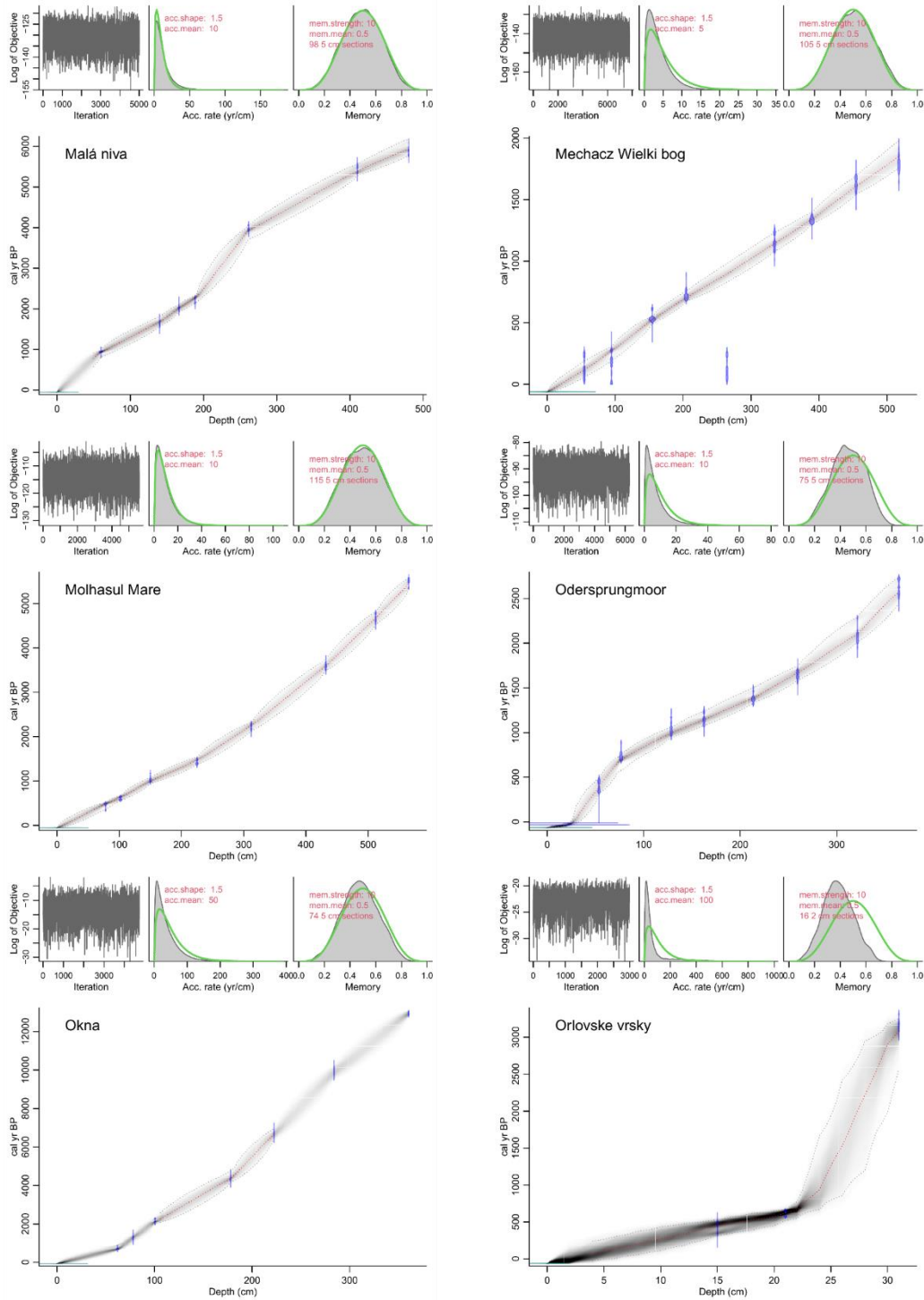


Figure C.24. Age-depth models for records 133-138. For each age-depth model upper panels depict the MCMC iterations (left; good runs show a stationary distribution with little structure among neighbouring iterations), the prior (green curves) and posterior (grey histograms) distributions for the accumulation rate (middle panel) and memory (right panel). Bottom panel shows the calibrated ^{14}C dates (transparent blue) and the age-depth model (darker greys indicate more likely calendar ages; grey stippled lines show 95% confidence intervals; red curve shows single 'best' model based on the median age for each depth). Prior information for accumulation rate and its memory or variability are shown as red text.

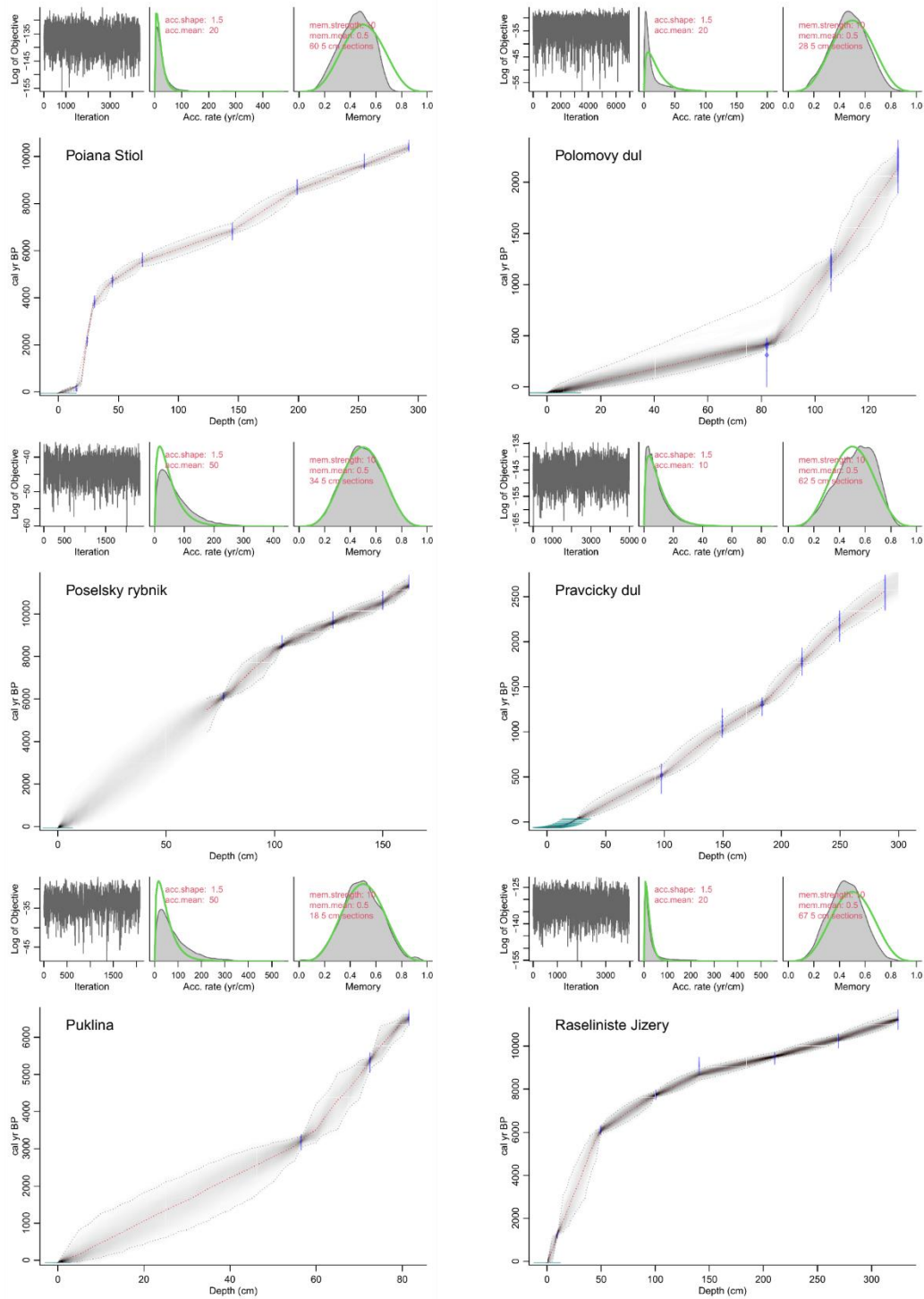


Figure C.25. Age-depth models for records 139-144. For each age-depth model upper panels depict the MCMC iterations (left; good runs show a stationary distribution with little structure among neighbouring iterations), the prior (green curves) and posterior (grey histograms) distributions for the accumulation rate (middle panel) and memory (right panel). Bottom panel shows the calibrated ^{14}C dates (transparent blue) and the age-depth model (darker greys indicate more likely calendar ages; grey stippled lines show 95% confidence intervals; red curve shows single 'best' model based on the median age for each depth). Prior information for accumulation rate and its memory or variability are shown as red text.

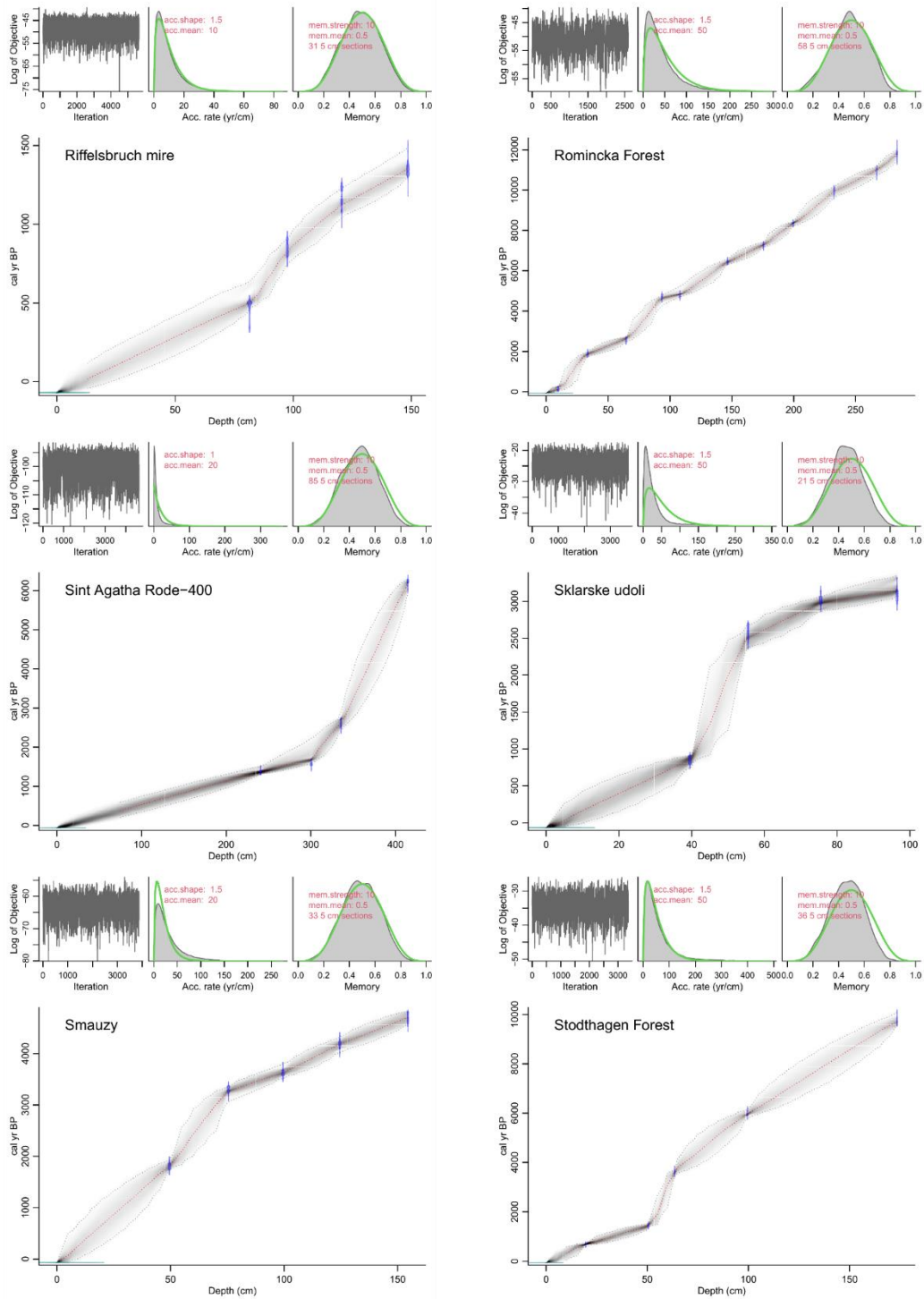


Figure C.26. Age-depth models for records 145-150. For each age-depth model upper panels depict the MCMC iterations (left; good runs show a stationary distribution with little structure among neighbouring iterations), the prior (green curves) and posterior (grey histograms) distributions for the accumulation rate (middle panel) and memory (right panel). Bottom panel shows the calibrated ^{14}C dates (transparent blue) and the age-depth model (darker greys indicate more likely calendar ages; grey stippled lines show 95% confidence intervals; red curve shows single 'best' model based on the median age for each depth). Prior information for accumulation rate and its memory or variability are shown as red text.

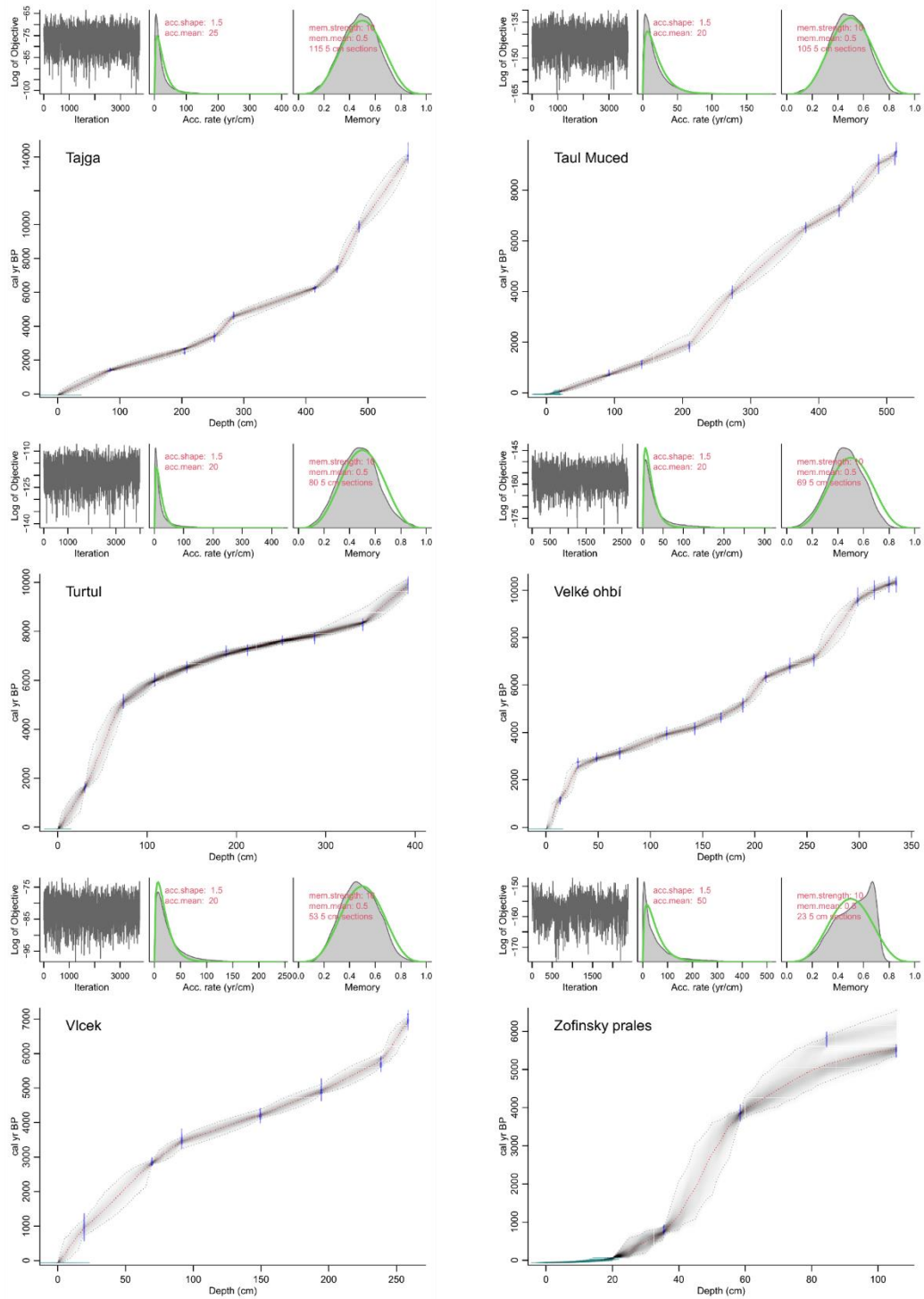


Figure C.27. Age-depth models for records 151-156. For each age-depth model upper panels depict the MCMC iterations (left; good runs show a stationary distribution with little structure among neighbouring iterations), the prior (green curves) and posterior (grey histograms) distributions for the accumulation rate (middle panel) and memory (right panel). Bottom panel shows the calibrated ^{14}C dates (transparent blue) and the age-depth model (darker greys indicate more likely calendar ages; grey stippled lines show 95% confidence intervals; red curve shows single 'best' model based on the median age for each depth). Prior information for accumulation rate and its memory or variability are shown as red text.

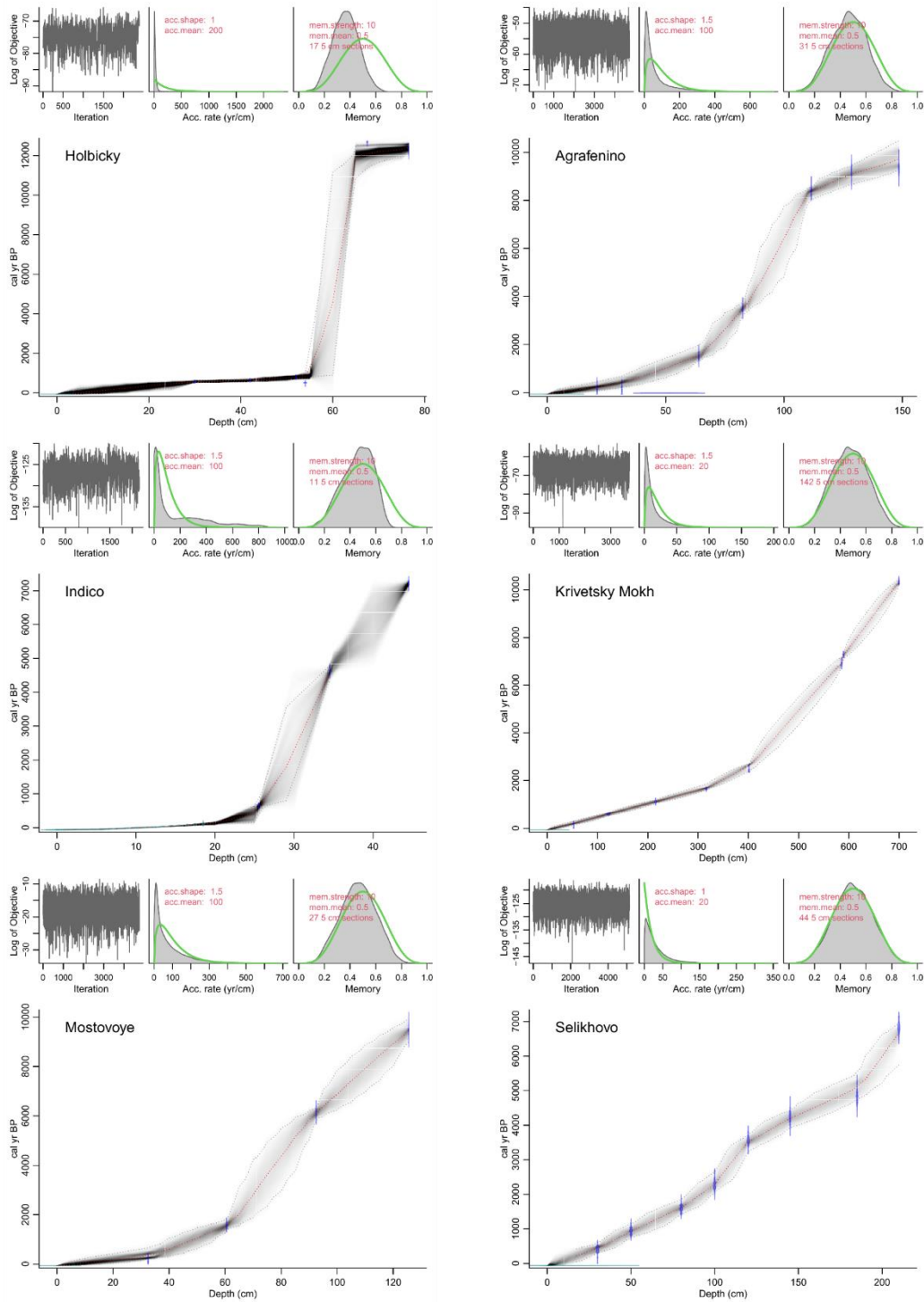


Figure C.28. Age-depth models for records 157-162. For each age-depth model upper panels depict the MCMC iterations (left; good runs show a stationary distribution with little structure among neighbouring iterations), the prior (green curves) and posterior (grey histograms) distributions for the accumulation rate (middle panel) and memory (right panel). Bottom panel shows the calibrated ^{14}C dates (transparent blue) and the age-depth model (darker greys indicate more likely calendar ages; grey stippled lines show 95% confidence intervals; red curve shows single 'best' model based on the median age for each depth). Prior information for accumulation rate and its memory or variability are shown as red text.

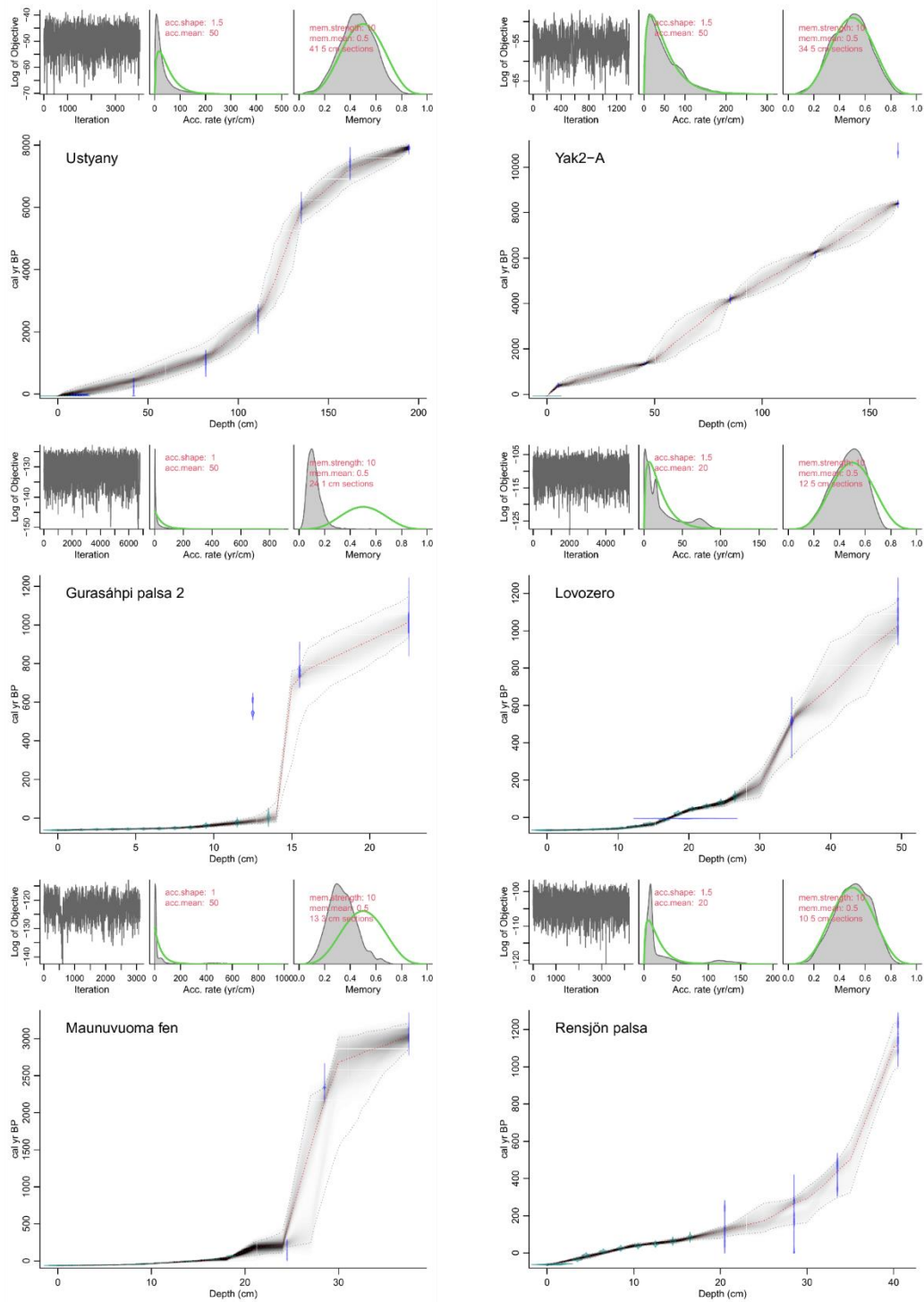


Figure C.29. Age-depth models for records 163-168. For each age-depth model upper panels depict the MCMC iterations (left; good runs show a stationary distribution with little structure among neighbouring iterations), the prior (green curves) and posterior (grey histograms) distributions for the accumulation rate (middle panel) and memory (right panel). Bottom panel shows the calibrated ^{14}C dates (transparent blue) and the age-depth model (darker greys indicate more likely calendar ages; grey stippled lines show 95% confidence intervals; red curve shows single 'best' model based on the median age for each depth). Prior information for accumulation rate and its memory or variability are shown as red text.

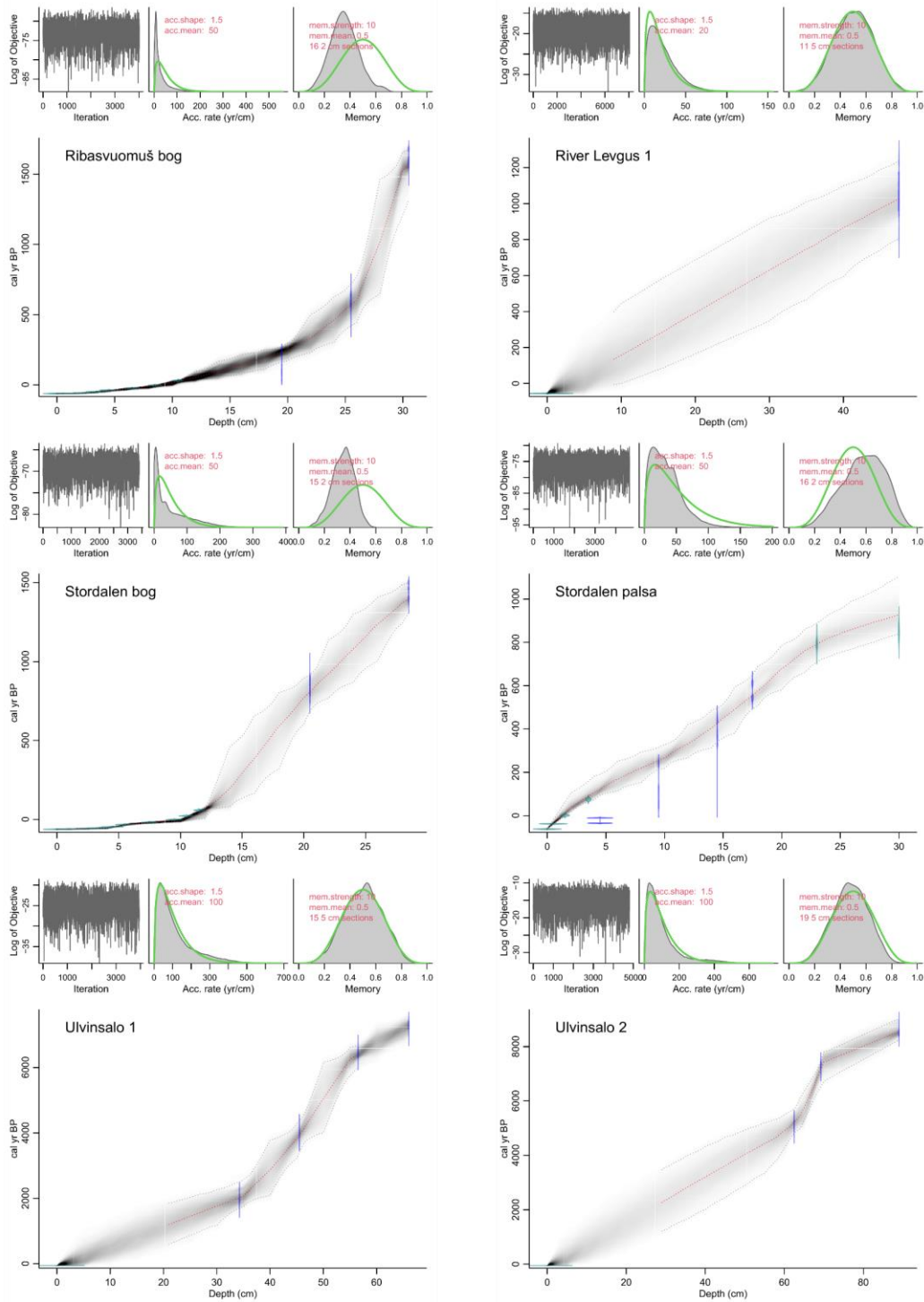


Figure C.30. Age-depth models for records 169-174. For each age-depth model upper panels depict the MCMC iterations (left; good runs show a stationary distribution with little structure among neighbouring iterations), the prior (green curves) and posterior (grey histograms) distributions for the accumulation rate (middle panel) and memory (right panel). Bottom panel shows the calibrated ^{14}C dates (transparent blue) and the age-depth model (darker greys indicate more likely calendar ages; grey stippled lines show 95% confidence intervals; red curve shows single 'best' model based on the median age for each depth). Prior information for accumulation rate and its memory or variability are shown as red text.

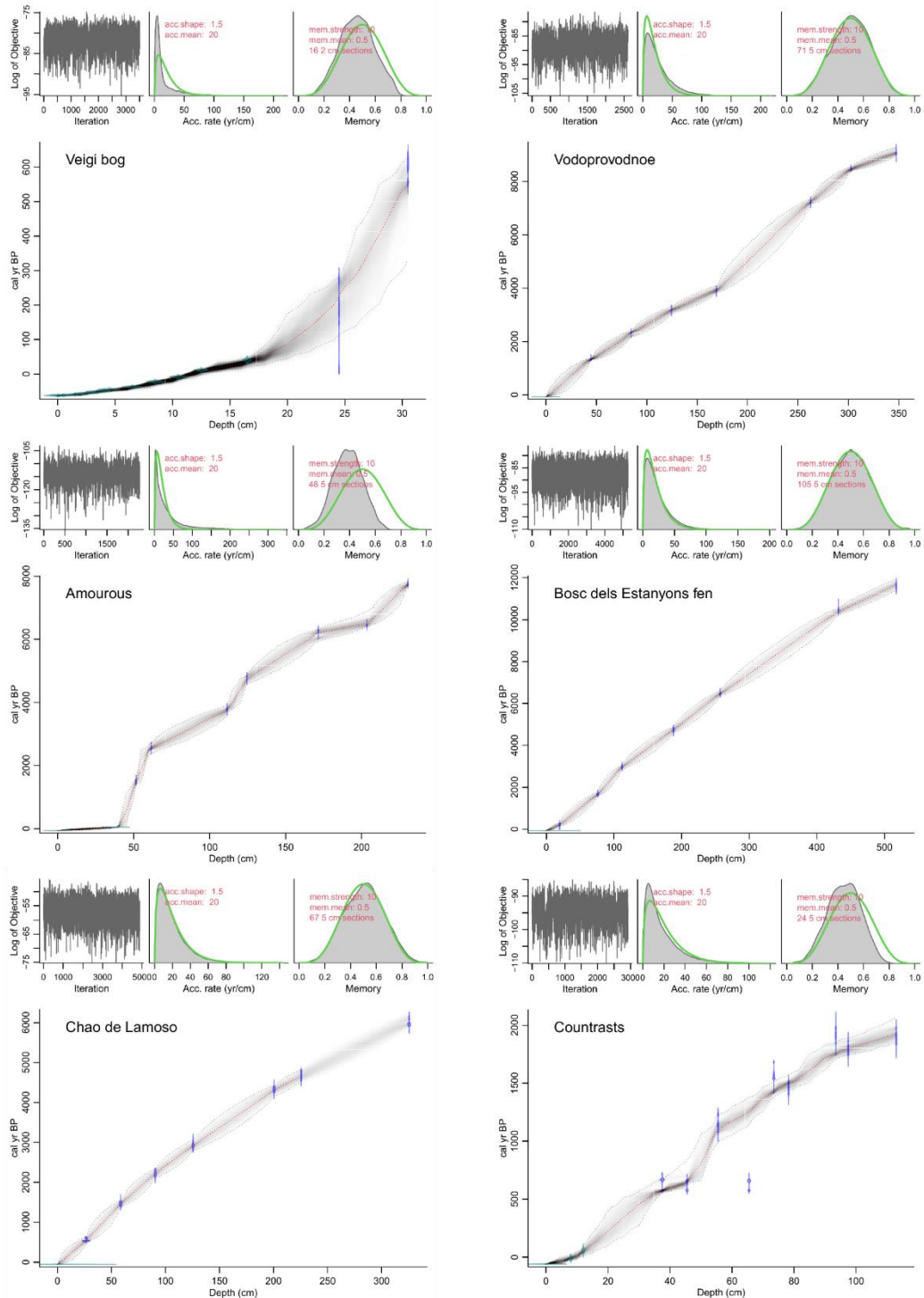


Figure C.31. Age-depth models for records 175-180. For each age-depth model upper panels depict the MCMC iterations (left; good runs show a stationary distribution with little structure among neighbouring iterations), the prior (green curves) and posterior (grey histograms) distributions for the accumulation rate (middle panel) and memory (right panel). Bottom panel shows the calibrated ^{14}C dates (transparent blue) and the age-depth model (darker greys indicate more likely calendar ages; grey stippled lines show 95% confidence intervals; red curve shows single 'best' model based on the median age for each depth). Prior information for accumulation rate and its memory or variability are shown as red text.

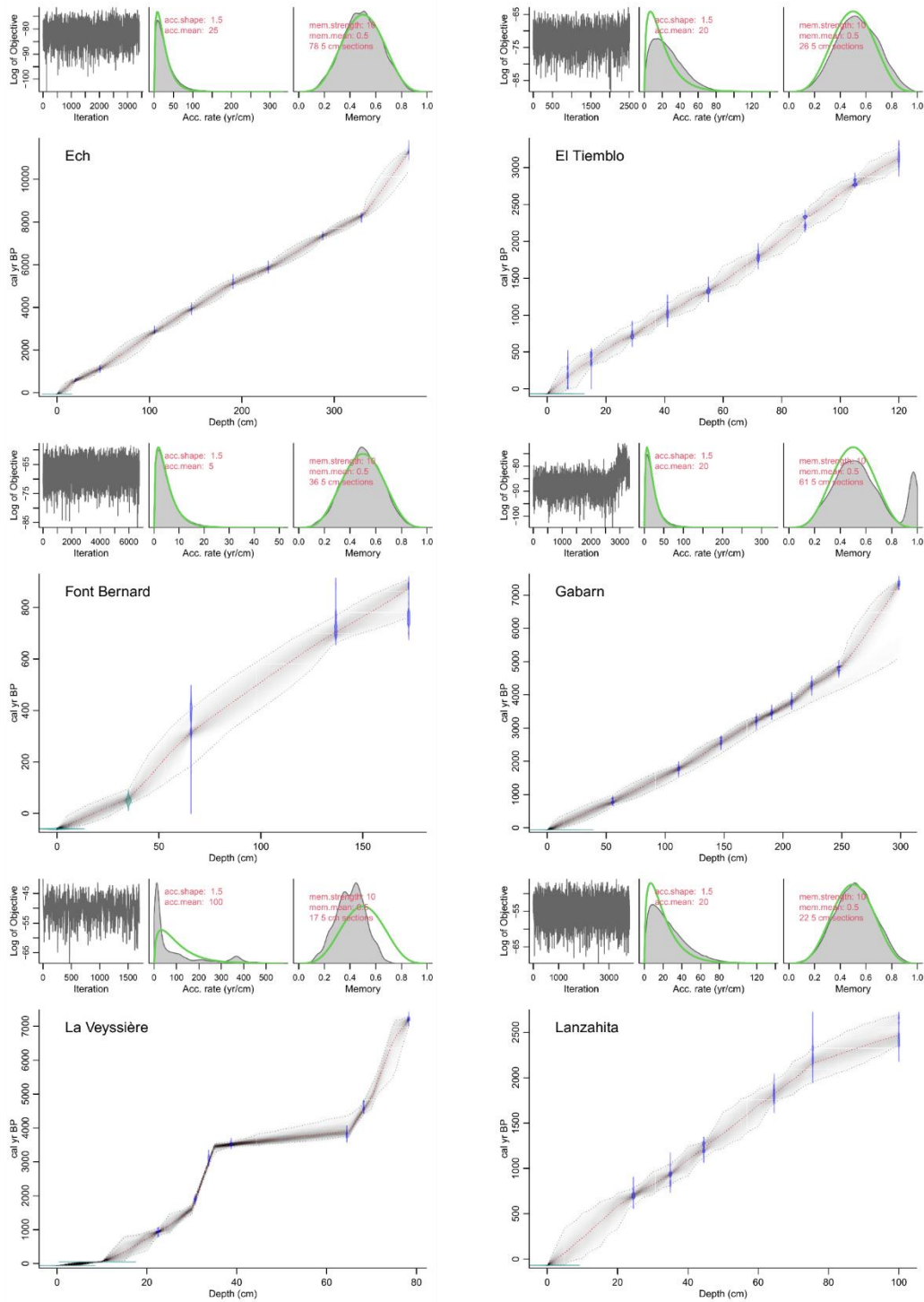


Figure C.32. Age-depth models for records 181-186. For each age-depth model upper panels depict the MCMC iterations (left; good runs show a stationary distribution with little structure among neighbouring iterations), the prior (green curves) and posterior (grey histograms) distributions for the accumulation rate (middle panel) and memory (right panel). Bottom panel shows the calibrated ^{14}C dates (transparent blue) and the age-depth model (darker greys indicate more likely calendar ages; grey stippled lines show 95% confidence intervals; red curve shows single 'best' model based on the median age for each depth). Prior information for accumulation rate and its memory or variability are shown as red text.

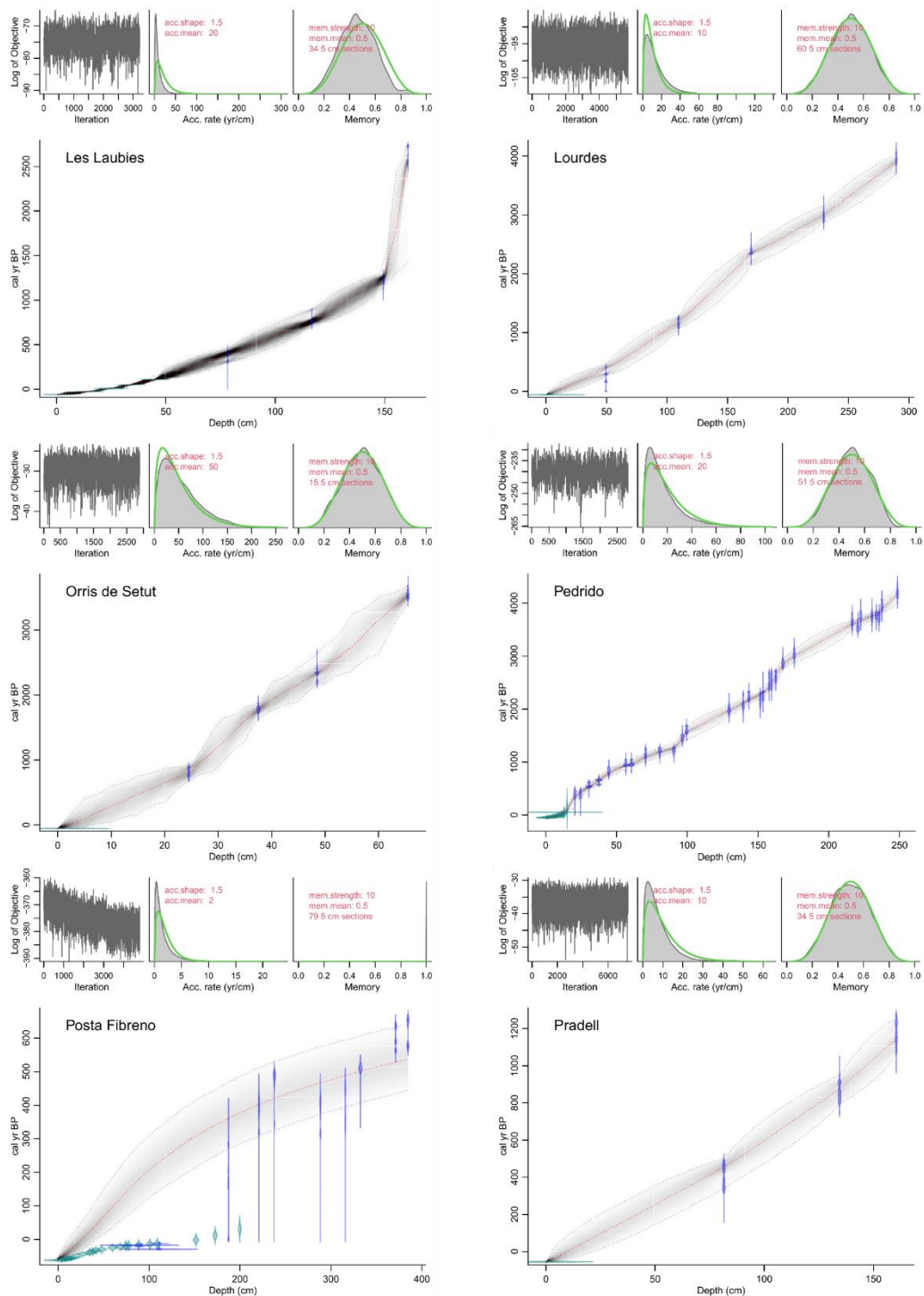


Figure C.33. Age-depth models for records 187-192. For each age-depth model upper panels depict the MCMC iterations (left; good runs show a stationary distribution with little structure among neighbouring iterations), the prior (green curves) and posterior (grey histograms) distributions for the accumulation rate (middle panel) and memory (right panel). Bottom panel shows the calibrated ^{14}C dates (transparent blue) and the age-depth model (darker greys indicate more likely calendar ages; grey stippled lines show 95% confidence intervals; red curve shows single 'best' model based on the median age for each depth). Prior information for accumulation rate and its memory or variability are shown as red text.

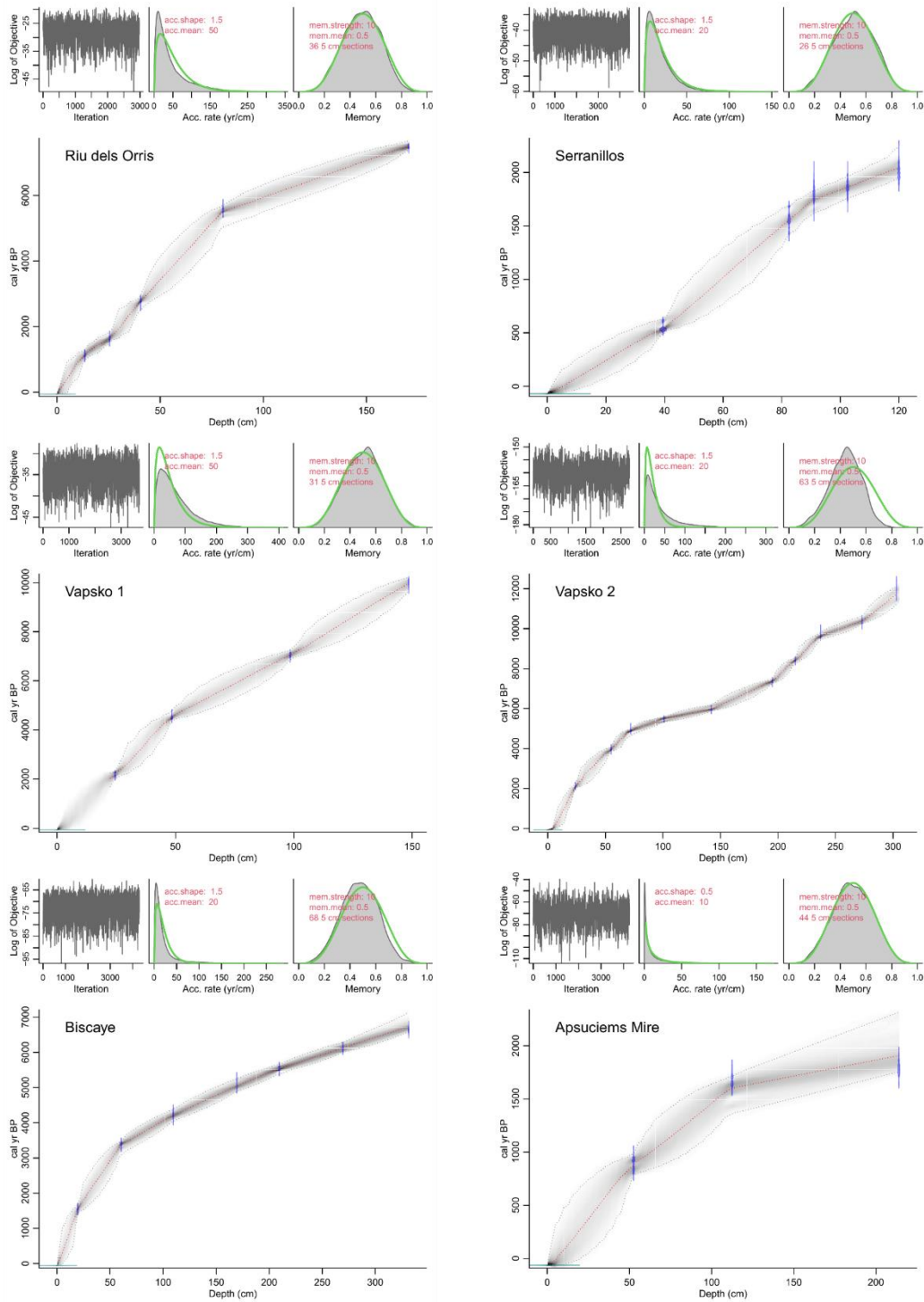


Figure C.34. Age-depth models for records 193-198. For each age-depth model upper panels depict the MCMC iterations (left; good runs show a stationary distribution with little structure among neighbouring iterations), the prior (green curves) and posterior (grey histograms) distributions for the accumulation rate (middle panel) and memory (right panel). Bottom panel shows the calibrated ^{14}C dates (transparent blue) and the age-depth model (darker greys indicate more likely calendar ages; grey stippled lines show 95% confidence intervals; red curve shows single 'best' model based on the median age for each depth). Prior information for accumulation rate and its memory or variability are shown as red text.

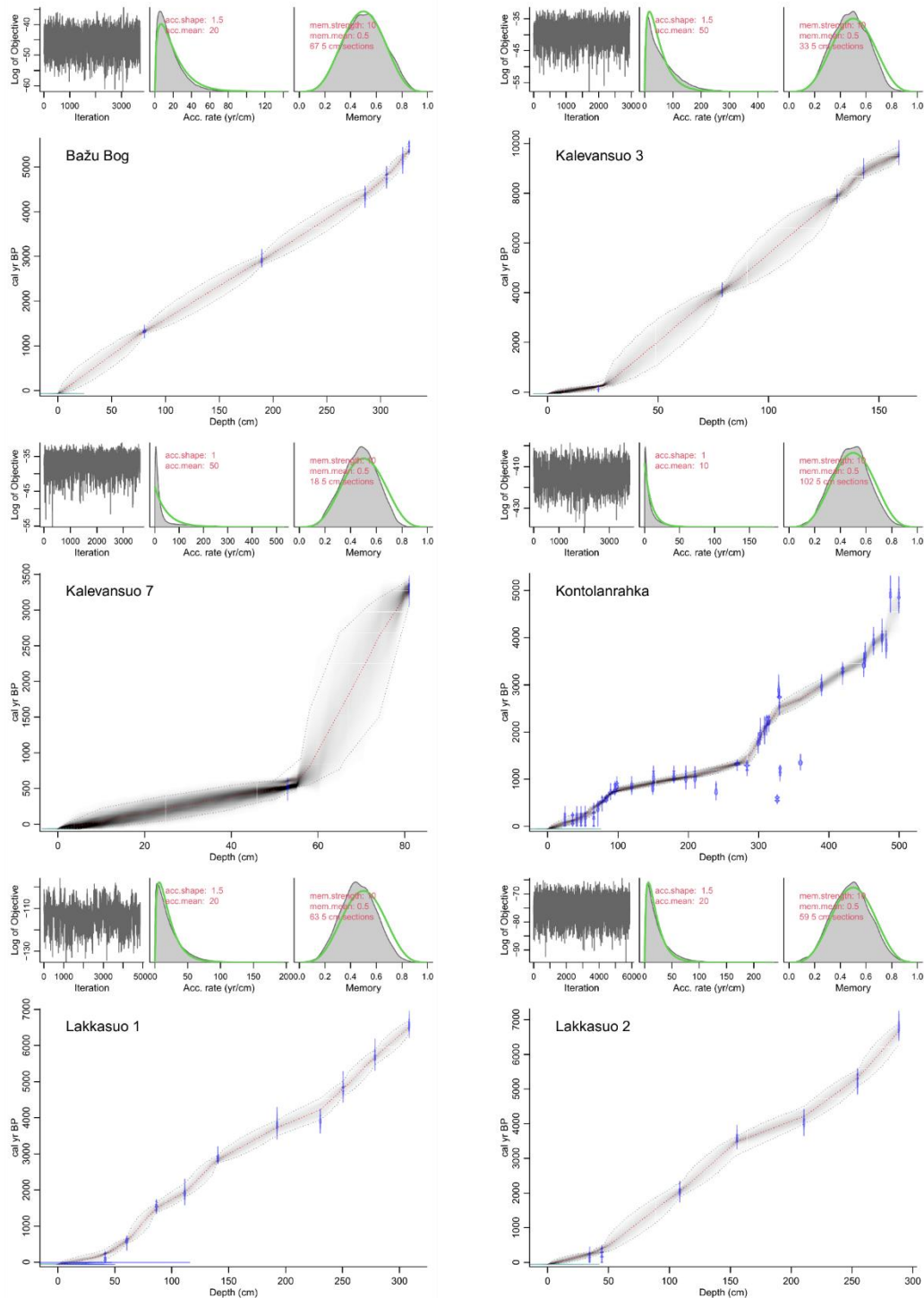


Figure C.35. Age-depth models for records 199-204. For each age-depth model upper panels depict the MCMC iterations (left; good runs show a stationary distribution with little structure among neighbouring iterations), the prior (green curves) and posterior (grey histograms) distributions for the accumulation rate (middle panel) and memory (right panel). Bottom panel shows the calibrated ^{14}C dates (transparent blue) and the age-depth model (darker greys indicate more likely calendar ages; grey stippled lines show 95% confidence intervals; red curve shows single 'best' model based on the median age for each depth). Prior information for accumulation rate and its memory or variability are shown as red text.

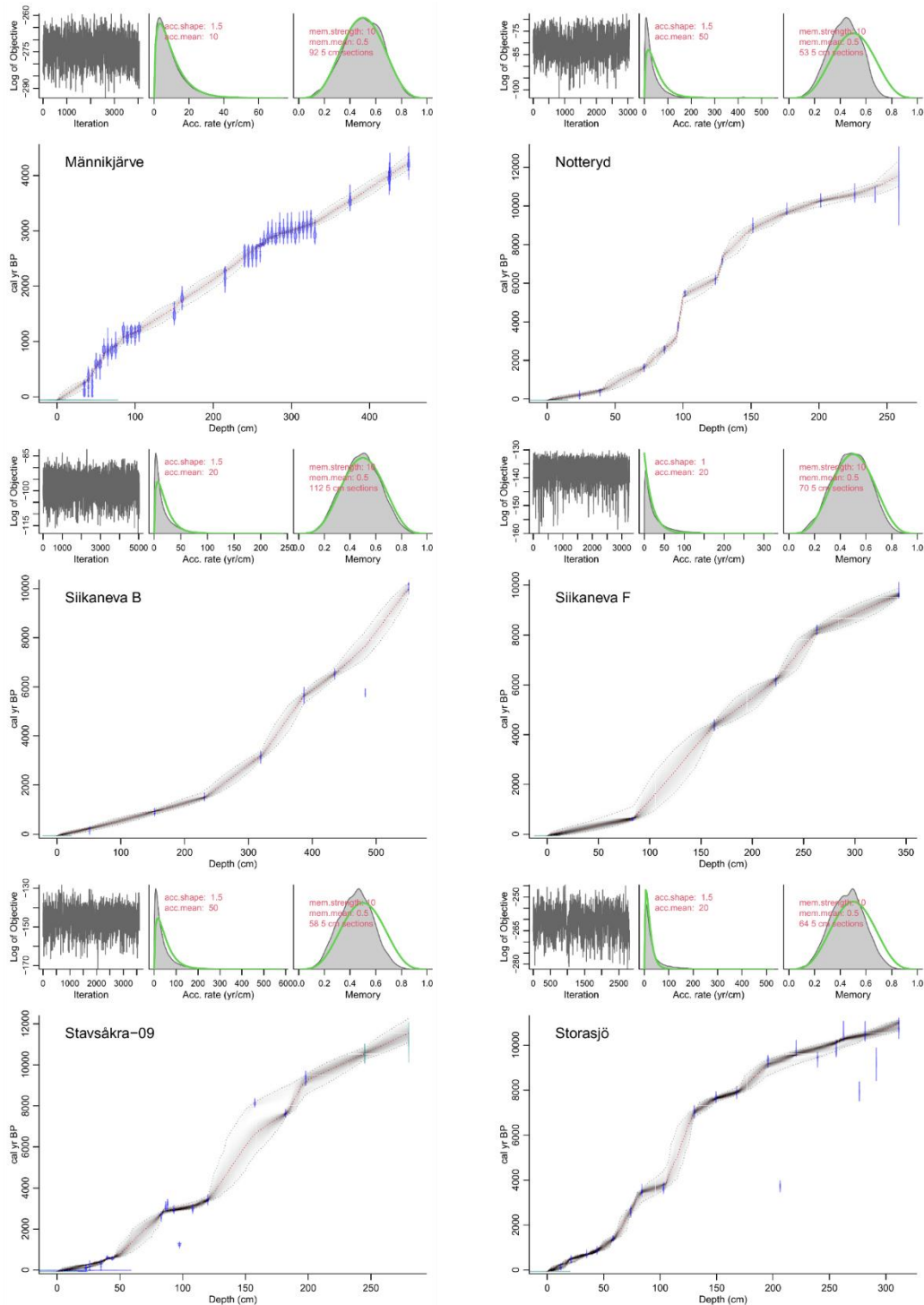


Figure C.36. Age-depth models for records 205-210. For each age-depth model upper panels depict the MCMC iterations (left; good runs show a stationary distribution with little structure among neighbouring iterations), the prior (green curves) and posterior (grey histograms) distributions for the accumulation rate (middle panel) and memory (right panel). Bottom panel shows the calibrated ^{14}C dates (transparent blue) and the age-depth model (darker greys indicate more likely calendar ages; grey stippled lines show 95% confidence intervals; red curve shows single 'best' model based on the median age for each depth). Prior information for accumulation rate and its memory or variability are shown as red text.

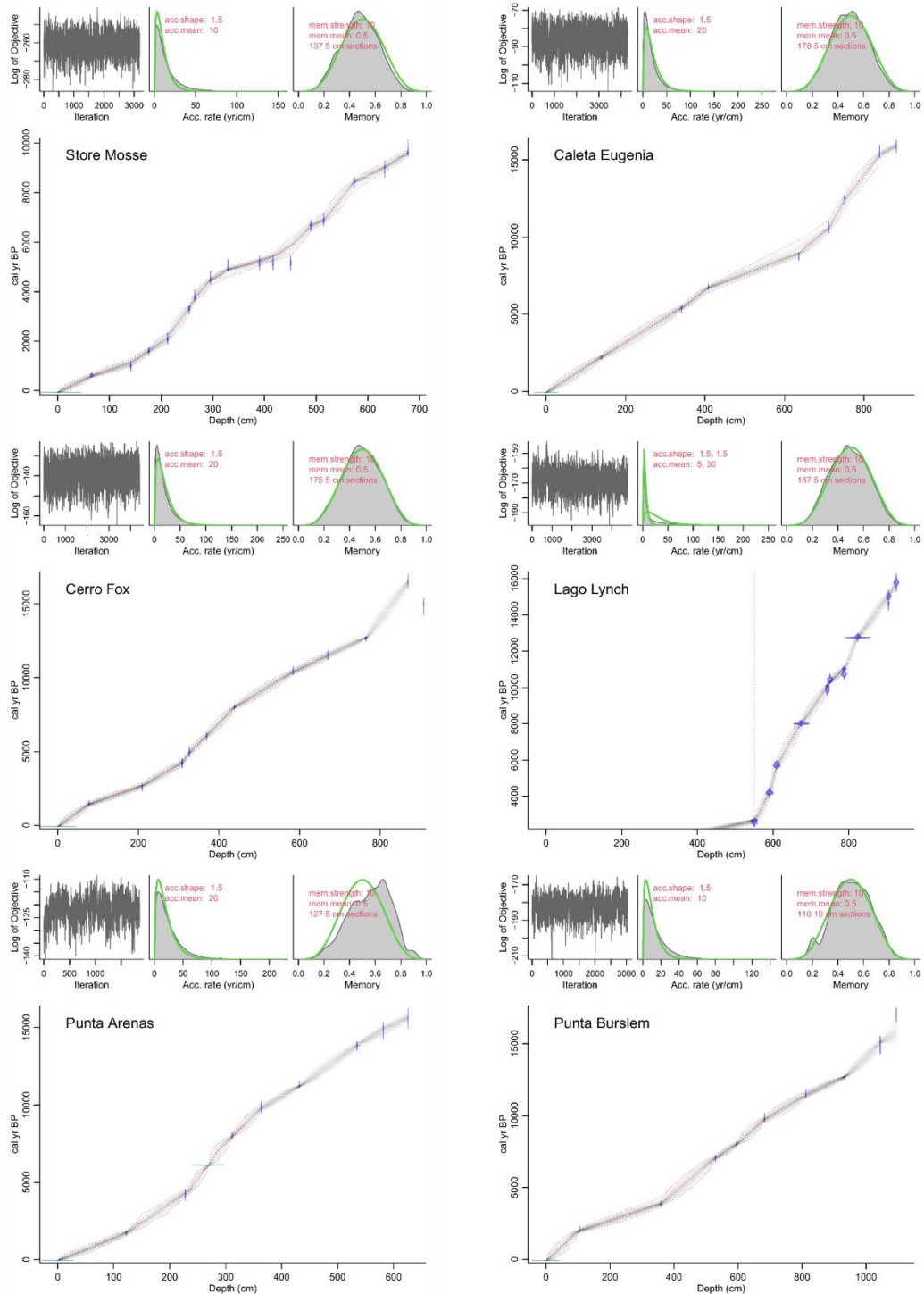


Figure C.37. Age-depth models for records 211-216. For each age-depth model upper panels depict the MCMC iterations (left; good runs show a stationary distribution with little structure among neighbouring iterations), the prior (green curves) and posterior (grey histograms) distributions for the accumulation rate (middle panel) and memory (right panel). Bottom panel shows the calibrated ^{14}C dates (transparent blue) and the age-depth model (darker greys indicate more likely calendar ages; grey stippled lines show 95% confidence intervals; red curve shows single 'best' model based on the median age for each depth). Prior information for accumulation rate and its memory or variability are shown as red text.

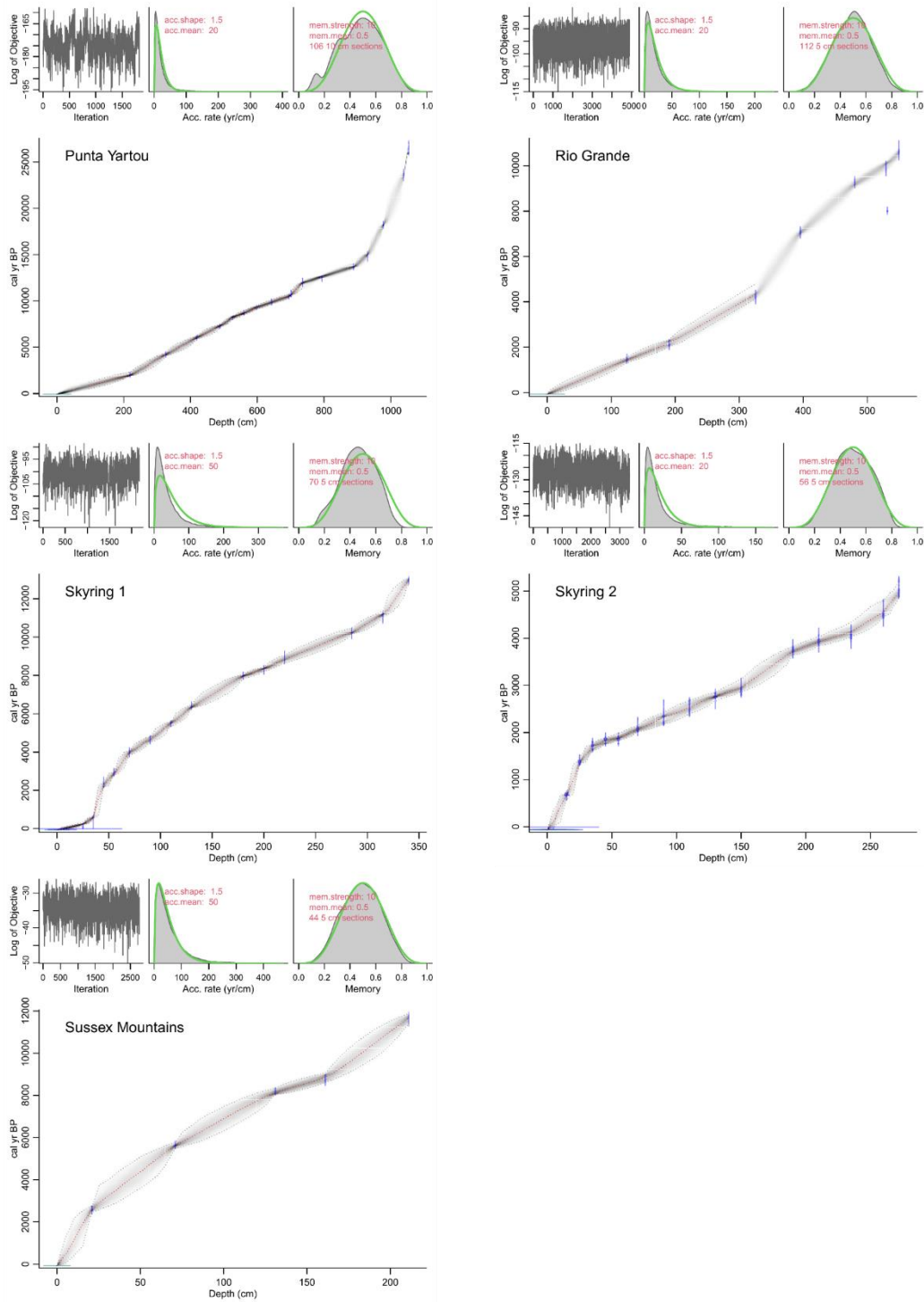


Figure C.38. Age-depth models for records 217-221. For each age-depth model upper panels depict the MCMC iterations (left; good runs show a stationary distribution with little structure among neighbouring iterations), the prior (green curves) and posterior (grey histograms) distributions for the accumulation rate (middle panel) and memory (right panel). Bottom panel shows the calibrated ^{14}C dates (transparent blue) and the age-depth model (darker greys indicate more likely calendar ages; grey stippled lines show 95% confidence intervals; red curve shows single 'best' model based on the median age for each depth). Prior information for accumulation rate and its memory or variability are shown as red text.

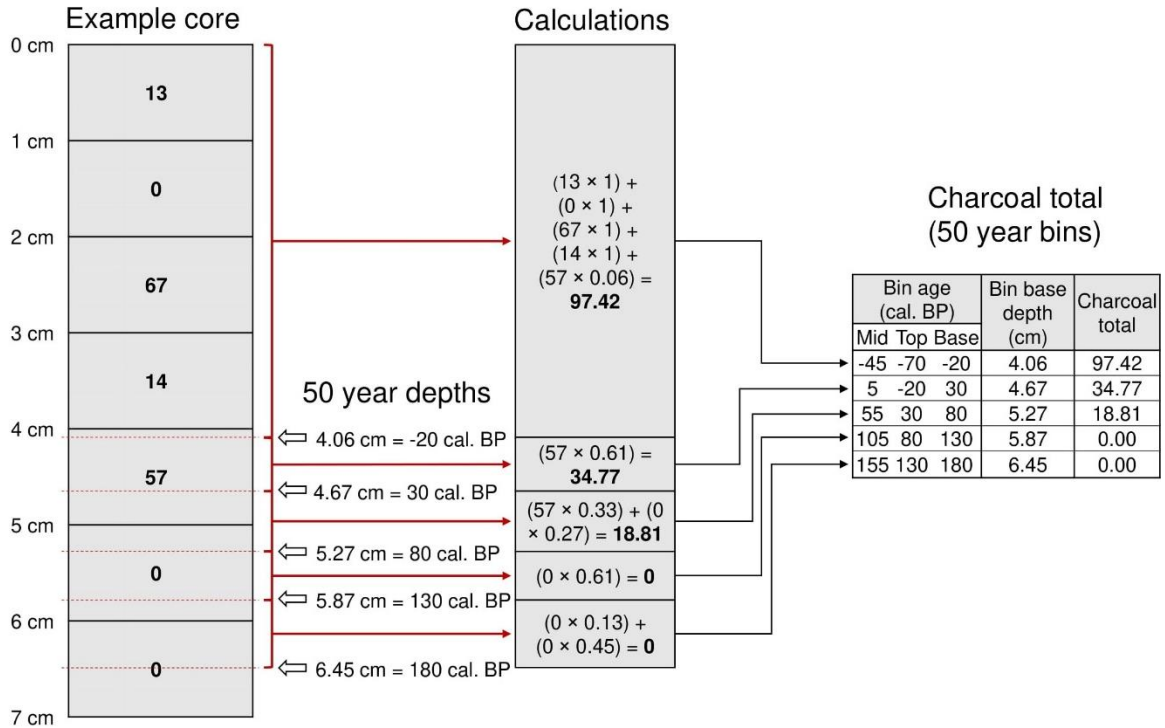


Figure C.39. Conceptual diagram of the 50-year depth binning approach using example data. Bold numbers in each sample for the example core represent the original charcoal quantity. The depths (cm) of each 50 year interval (cal. BP) are shown. The calculations section shows the multiplication of the original charcoal quantity by the proportion of the sample within each 50-year bin – assuming charcoal particles are distributed evenly within a sample.

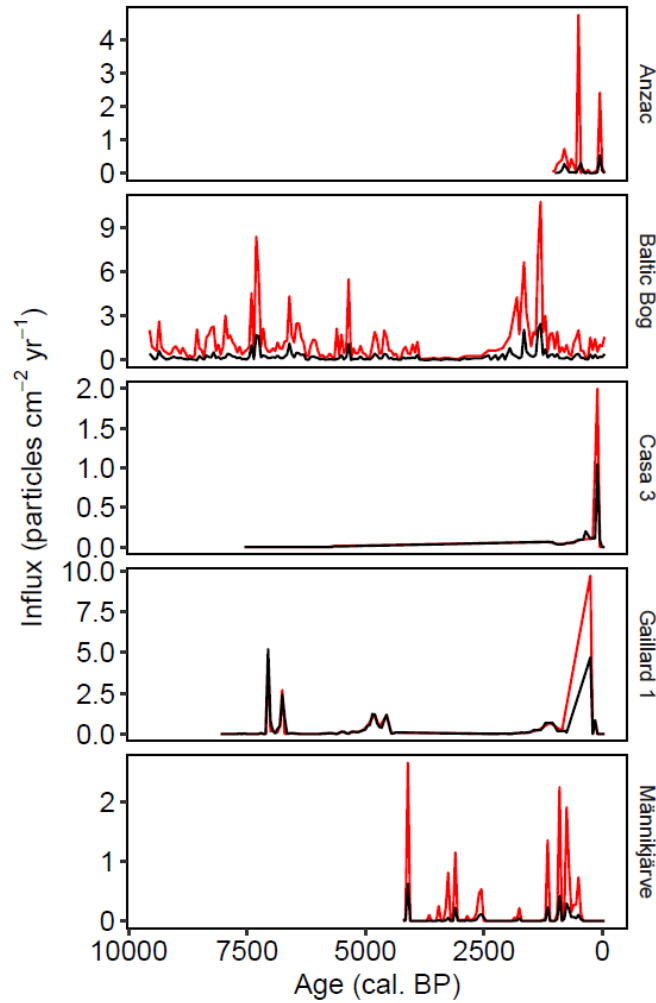


Figure C.40. Influx values calculated for five example sites from the 50-year bin means method (red) and 50-year depth binning method (black).

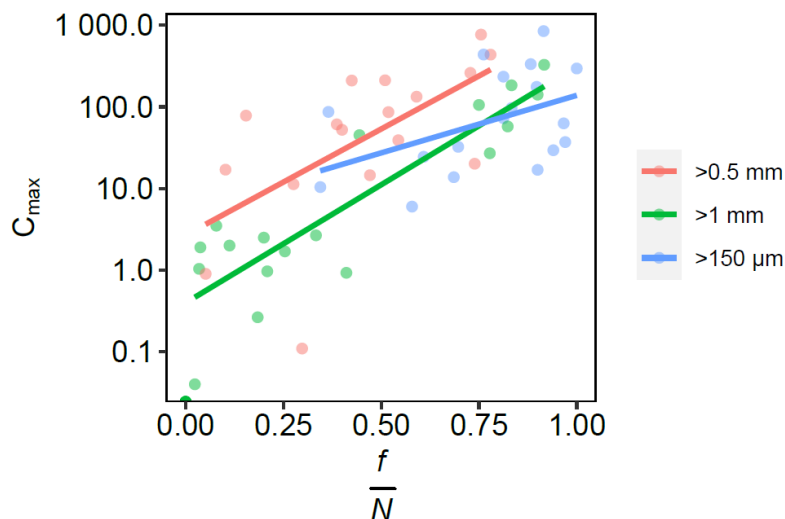


Figure C.41. The relationship between maximum resampled charcoal values (C_{\max}) and the proportion of resampled values containing charcoal within a record – frequency (f) divided by total number (N) - for the three most common particle sizes ($>150 \mu\text{m}$, $>0.5 \text{ mm}$ and $>1 \text{ mm}$) expressing charcoal quantity as a concentration (particles cm^{-3}) within our dataset.